Marina Mendes Sargento Domingues Perdigão

Research and Development on New Control Techniques for Electronic Ballasts based on Magnetic Regulators

Ph. D. Thesis

Dissertação submetida para obtenção do grau de Doutor em Engenharia Electrotécnica, na especialidade Sistemas de Energia, elaborada sob a orientação do Professor Eduardo de Sousa Saraiva, Professor Catedrático do Departamento de Engenharia Electrotécnica e de Computadores da Faculdade de Ciências e Tecnologia da Universidade de Coimbra, e do Professor José Marcos Alonso Álvarez, Professor Catedrático do Departamento de Ingeniería Eléctrica, Electrónica, de Computadores y de Sistemas da Universidade de Oviedo.

September 2011

POPH
POTENCIAL HUMANO
QREN
QUADRO DE REFERÊNCIA ESTRATÉGICO NACIONAL
UNIÃO EUROPEIA
Fundo Social Europeu
U C

To my father

ACKNOWLEDGEMENTS

It is with my deepest gratitude that I acknowledge the support and help of my supervisors. This work would not have been possible without the guidance and support of Professor Eduardo Saraiva and Professor J. Marcos Alonso. I wish to thank to Professor Marcos for his positive thinking, and for making everything seem simple, especially when it was not. I am indebted to Professor Eduardo who shared with me the value of tenacity and discipline in pursuing the research objectives. To both of them I express my sincere gratitude.

I wish to thank my colleagues from the group GEDRE, Federal University of Santa Maria, particularly to Marco Dalla Costa and Alysson Seidel, who supported me in my research.

I also would like to thank the support from all the Professors of the Industrial Electronics and Lighting Group, University of Oviedo. I was welcomed and I felt as if I was a member of their excellent research group since the very beginning. I am grateful to them for all their help, support, interest and valuable hints.

In addition, I would like to thank Bruno Baptista and Heitor Marques, for their help and contributions as members of the research team at the Instituto de Telecomunicações, and to many of my colleagues from the Department of Electrical Engineering, ISEC, for their words of encouragement.

My special gratitude is due to my mother, Isabel, and to Vasco for their patience and support, but especially to my father, João, for his strength and belief. Finally, I would like to thank my closest friends, for their support and encouragement.

The financial support from the Instituto de Telecomunicações and the doctoral degree grant from the Fundação para a Ciência e Tecnologia are gratefully acknowledged.

ABSTRACT

Current lighting trends indicate the urgency for more efficient, flexible and controllable systems. Highly-efficient fluorescent lamps are still expected to be a dominant, cost-effective lighting solution in the following years and therefore, there is a clear opportunity to invest in the development of new control techniques in this domain. The flexibility expected from modern fluorescent lighting systems requires an intensive use of electronic ballasts, since this type of electronic control offers higher levels of adaptability, not viable with traditional magnetic ballasts. The purpose of the work presented in this Ph. D. Thesis is to propose and develop a new control technique for fluorescent lamps based on a specific magnetic device known as magnetic regulator.

Two different areas are explored: luminous flux regulation and multi-Watt operation. This new control technique, whether specifically used for dimming purposes or for multiple lamp operation, is based on a simple principle: controlling the electronic ballast circuit through the variation of the resonant frequency, instead of varying the operating frequency of the inverter. The technique is implemented by means of a dc-controlled magnetic element, which can be simply described as a variable inductor or as a variable transformer. These devices have been known from several decades; however, advances in the magnetic properties of the core materials and a new interpretation of the already known former applications lead to this innovative and useful technique for fluorescent lighting control.

In commercial dimmable electronic ballasts as well as in multi-Watt electronic ballasts, some negative aspects may emerge, mainly related to the non-constant frequency operation. Not only to avoid this drawback, but also due to some other limitations and shortcomings presented by current dimming and universal control techniques, a research is carried out to validate the effectiveness of using this novel magnetic control technique for similar purposes. Throughout this Ph. D. Thesis several aspects related to this research will be presented and analysed. The work will describe the theoretical development and practical implementation of magnetic control techniques in prototype versions of magnetically-controlled electronic ballasts, as well as the research steps involving these variable magnetic devices, from initial project and design, to theoretical and behavioural analysis, and finally, simulation and prototype implementation. Experimental results, retrieved from these proposals which validate the effectiveness and the efficiency of this type of control, will be delivered throughout the thesis.

Key words: *lighting, electronic ballast, fluorescent lamp, magnetic regulator, variable inductance, resonant circuit.*

RESUMO

A tendência actual na iluminação indica urgência na utilização de sistemas mais eficientes, mais flexíveis e mais controláveis. Num futuro próximo é previsível que as lâmpadas fluorescentes de alta eficiência sejam a solução dominante em iluminação, devido à sua relação custo-benefício antevendo-se uma oportunidade clara para o investimento no desenvolvimento de novas formas de controlo neste domínio. A flexibilidade expectável dos sistemas modernos de iluminação fluorescente requer o uso intensivo de balastros electrónicos, porque este tipo de controlo electrónico oferece níveis mais elevados de adaptabilidade, que não são viáveis em balastros magnéticos. O objectivo do trabalho apresentado nesta tese de doutoramento é propor e desenvolver uma nova técnica de controlo para lâmpadas fluorescentes baseada num dispositivo magnético específico, conhecido como regulador magnético.

São exploradas duas áreas diferentes: regulação de fluxo luminoso e funcionamento com lâmpadas com diferentes valores de potência nominal (balastro multi-Watt ou universal). Esta nova técnica de controlo, quer seja usada na regulação de fluxo luminoso quer no funcionamento com lâmpadas com diferentes valores de potência nominal, é baseada num princípio simples: o controlo do circuito do balastro electrónico usando a variação da frequência de ressonância, em vez da variação da frequência de comutação do inversor. A técnica é implementada usando um elemento magnético controlado por uma corrente contínua, que pode ser descrito, em termos simples, como sendo uma indutância variável ou um transformador variável. Estes dispositivos são conhecidos desde há algumas décadas; porém os avanços nas propriedades magnéticas dos materiais magnéticos usados nos núcleos e uma nova interpretação das aplicações previamente desenvolvidas, conduziram a esta nova e útil técnica para o controlo de lâmpadas fluorescentes.

Nos balastros electrónicos comerciais com capacidade de regulação do fluxo luminoso e também em balastros electrónicos universais, podem surgir alguns aspectos negativos, a maioria relacionada com o facto de se usar frequência de comutação variável. Não só para evitar esta desvantagem, mas também algumas outras limitações das actuais técnicas comerciais de controlo de fluxo luminoso e de controlo de balastros universais, foi desenvolvida investigação com o objectivo de validar o uso desta nova técnica de controlo magnético em aplicações similares. Ao longo desta tese de doutoramento são apresentados e analisados alguns aspectos relacionados com esta investigação. O trabalho apresentado descreve o desenvolvimento teórico e a realização experimental de técnicas de controlo magnético em versões protótipo de balastros

electrónicos, bem como os passos de investigação relativos a estes dispositivos magnéticos, desde a fase inicial de projecto, até à análise teórica e funcional e finalmente a realização de protótipos.

Ao longo da tese são apresentados resultados experimentais que validam a adequação e eficiência deste tipo de controlo.

Palavras chave: *iluminação, balastro electrónico, lâmpada fluorescente, regulador magnético, indutância variável, circuito ressonante.*

ACRONYMS

ANSI	*American National Standards Institute*
BLU	*Back-Light Unit*
CCFL	*Cold-Cathode Fluorescent Lamp*
CCM	*Continuous-Current Conduction Mode*
CCT	*Correlated Colour Temperature,*
CFL	*Compact Fluorescent Lamp*
CIE	*Comission Internationale de l'Eclairage*
CRI	*Colour Rendering Index*
DALI	*Digitally Addressable Lighting Interface*
DCM	*Discontinuous-Current Conduction Mode*
EMC	*Electromagnetic Compatibility*
EMI	*Electromagnetic Interference*
HBLED	*High-Brightness Light Emitting Diode*
HID	*High-Intensity Discharge Lamp,*
HPMV	*High-Pressure Mercury Vapour Discharge Lamp*
HPS	*High-Pressure Sodium Discharge Lamp*
IC	*Integrated Circuit*
IPT	*Inductive-Coupled Power Transfer*
LCD	*Liquid-Crystal Display*
LED	*Light Emitting Diode*
LVI	*Linear Variable Inductor*
MFFFL	*Mercury-Free Flat Fluorescent Lamp*
PFC	*Power-Factor Correction*
PNAC	*Portuguese National Programme for Climate Change*
PNAEE	*Portuguese National Action Plan for Energy Efficiency*
PNALE	*Portuguese National Action Plan for Allocation of CO2 Emissions*
PWM	*Pulse-Width Modulation*
SVC	*Static VAR Compensator*
THD	*Total Harmonic Distortion*
VCO	*Voltage-Controlled Oscillator*
VSI	*Voltage-Source Inverter*
SoS	*Sum of the Squares*
μC	*Microcontroller*

GLOSSARY

Luminous flux	*Quantity derived from radiant flux by evaluating the radiation according to its action upon the Comission Internationale de l'Eclairage (CIE) standard, expressed in lumen [lm].*
Luminous efficacy	*Luminous flux emitted by a light source divided by the electric power consumed by the same light source, expressed in lumen per watt [lm/W].*
Colour rendering index, CRI	*Degree to which the colour of an object illuminated by the light source conforms to that of the same object illuminated by a reference light source.*
Correlated colour temperature, CCT	*Temperature of the blackbody radiator whose colour, according to the human perception, most closely resembles to the considered light source, expressed in Kelvin [K].*
Colour temperature	*Temperature of the blackbody which emits radiation of the same chromaticity of the light source, expressed in Kelvin [K].*
Dimming	*Regulation of the luminous flux level.*
Blackbody	*Idealized body that absorbs all electromagnetic radiation falling upon it and that is also capable of re-emitting.*
Sputtering	*Ejection of atoms by ionic impact on the cathode.*
Positive column	*The region in an electric discharge that extends from the anode to the Faraday dark space.*
Universal, multi-Watt ballast	*Ballast capable of operating several lamps of different power ratings.*
Current crest factor	*Ratio of the peak value to the rms value of the lamp current.*
Electrophoresis	*Motion of charged dispersed particles relative to a fluid in a uniform electric field.*
Permeability	*Measure of the magnetic conductivity of a substance [H/m].*
Reluctance	*Resistance or opposition a material offers to the lines of flux in a portion or in an entire magnetic circuit.*
Striations	*Visual phenomenon determined by the lamp physics. Series of bright and dim areas in a fluorescent lamp, sometimes moving down the length of the lamp and sometimes taking the appearance of a standing wave.*

SYMBOLS

A	*Cross-sectional area [m^2]*
$B(H)$	*Magnetization curve*
$B; \vec{B}$	*Magnetic flux density [T]; magnetic flux density vector or surface density of the magnetic flux*
B_r	*Residual flux density [T]*
B_{sat}	*Saturation flux density [T]*
C	*Proportionality constant*
C_P	*Parallel capacitor [F]*
C_S	*Series capacitor [F]*
$C_b, C \sim \infty$	*DC-blocking capacitance [F]*
C_r	*Resonant capacitance [F]*
$dS;\ d\vec{S}$	*Surface element; vector with magnitude dS and direction normal to surface element dS [m^2]*
$dl;\ d\vec{l}$	*Element of path length; vector with magnitude dl and direction of element of path of length [m]*
D	*Duty-cycle of the switches of the half-bridge inverter*
$D_1;\ D_2$	*Inverter- switches anti-parallel diodes*
f_{ig}	*Ignition frequency of the half-bridge inverter [Hz]*
f_o	*Natural frequency [Hz]*
f_{ph}	*Preheat frequency of the half-bridge inverter [Hz]*
f_r	*Resonant frequency [Hz]*
$f_s;\ f_{run}$	*Switching frequency, operating frequency; running frequency of the half-bridge inverter [Hz]*
$\underline{G}(j\omega)$	*Resonant circuit voltage gain*
$H; \vec{H}$	*Magnetic field intensity [A/m]; magnetic field vector*
H_c	*Coercive force [A/m]*
$I_{in}; i_{in}$	*Resonant current of the half-bridge inverter [V]- rms value; instantaneous value*
$\hat{\imath}$	*Small-signal lamp current perturbation [A] – rms value*
$i_{M1};\ i_{M2}$	*Inverter-switches current [A] – instantaneous values*
I_D	*Discharge current [A] - rms value*
I_H	*Heating current [A] – rms value*
I_{LH}	*Higher lead wire current [A] – rms value*
I_{LL}	*Lower lead wire current [A] – rms value*
I_{arc}	*Arc current [A] - rms value; also referred as I_D*
I_{dc}	*DC control current [A]*
$I_{lamp};\ i_{lamp}$	*Lamp current [A] – rms value; also referred as I_{res}; instantaneous value*
I_{res}	*Resonant current [A]- rms value*
$l; l_i$	*Magnetic path length [m]*
L	*Inductance, inductor, inductive filter [H]*
L_{ac}	*Variable inductor inductance; variable inductor differential inductance [H]*
$L_{ac}(I_{dc})$	*Small-signal characteristic of the variable inductor*
L_{dif}	*Differential inductance [H]*
L_r	*Resonant inductance [H]*
L_s	*Saturable inductance [H]*

M_1; M_2	*Half-bridge resonant inverter switches (MOSFETs)*
N	*Number of turns of a winding*
N_{ac}	*Number of turns of the main winding of the variable inductor*
N_{dc}	*Number of turns of each control winding of the variable inductor*
P_{arc}	*Arc power [W] - average value*
P_{electr}	*Single-electrode power [W] - average value*
$P_{lamp}(L_{ac})$	*Dimming curve*
P_{lamp}; p_{lamp}	*Lamp power [W]- average value; instantaneous value*
P_{lamp_avg}	*Low-pass-filtered version of the instantaneous lamp power [W]*
P_{lamp0}	*Average power offset (lamp model)[W]*
$\hat{P}_{lamp}$	*Small-signal lamp power perturbation [W]*
$\mathcal{P}$	*Permeance [Wb/A]*
Q	*Quality factor*
$\hat{R}_{lamp}$	*Small-signal lamp resistance perturbation [Ω]*
R	*Resistance, Resistor, Load [Ω]*
R_{electr}	*Single-electrode resistance [Ω]*
R_{lamp}	*Lamp resistance [Ω]*
R_s	*Slope of the line fitted to the rms $V(I)$ characteristic of a tubular fluorescent lamp[Ω]*
$\mathcal{R}$	*Reluctance [A/Wb]*
V_{AB}	*Inverter output voltage [V] – rms value*
V_H	*Voltage at the intersection of the line fitted to the rms $V(I)$ characteristic of a tubular fluorescent lamp, with the voltage axis [V]*
V_{dc}	*DC input voltage of the half-bridge inverter [V]*
$V_{in,n}$	*Input resonant circuit voltage – rms value of the harmonic component n*
$\underline{V}_{in}$	*Input voltage of the resonant circuit [V]*
$\underline{V}_o$	*Output voltage of the resonant circuit [V]*
V_{in}; v_{in}	*Output voltage of the half-bridge inverter [V]- rms value; instantaneous value*
V_{lamp}; v_{lamp}	*Lamp voltage [V] – rms value; instantaneous value*
V_{lampDC}	*DC lamp voltage (lamp model)[V]*
V_{ph}; V_{ig}	*Lamp heating voltage [V]; lamp ignition voltage[V] – rms value*
$v_{L_{ac}}$	*Variable-inductor voltage [V] – instantaneous value*
$\hat{v}$	*Small-signal lamp voltage perturbation [V] – rms value*
v_{AB}	*Inverter output voltage [V]– instantaneous value*
v_C	*Integrator-capacitor voltage [V]– instantaneous value*
v_{DM1}; v_{DM2}	*Anti-parallel diode voltage [V] - instantaneous values*
v_{GM1}; v_{GM2}	*Rectangular-wave voltage sources*
$v_i(t)$	*Inductive voltage [V]*
$\underline{Z}_{in}$	*Impedance of the resonant circuit [Ω]*
$\underline{Z}_l$	*Incremental impedance [Ω]*
$\Psi(t)$	*Totalized flux or total ac flux linkage [Wb]*
$\phi(t)$	*Time-changing magnetic flux [Wb]*
ϕ_{in}	*Input current phase of the resonant circuit [º]*
μ_0	*Air permeability [H/m]*
μ_{dif}	*Differential permeability [H/m]*

$\boldsymbol{\mu}$	*Permeability [H/m]*
$\boldsymbol{\mu_i}$	*Initial permeability [H/m]*
$\boldsymbol{\mu_r}$	*Relative permeability - dimensionless*
$\boldsymbol{\omega}$	*Angular frequency [rad/s]*
$\boldsymbol{\omega_m}$	*Small-signal modulating angular frequency[rad/s]*
$\boldsymbol{\eta}$	*Efficiency [%]*
$\boldsymbol{\rho}$	*Ionization density the number of ion pairs per unit volume)*
$\boldsymbol{\tau}$	*Ionization recombination time constant [s]*
$\boldsymbol{\varphi}$	*Impedance phase of the resonant circuit [°]*

CONTENTS

LIST OF FIGURES

LIST OF TABLES

1 INTRODUCTION TO LIGHTING SYSTEMS. MOTIVATION AND MAIN OBJECTIVES OF THE WORK

In the present chapter, a succinct introduction to lamps and lighting is presented. Some general considerations on lighting efficiency, essential light properties and definitions are introduced. Due to the purpose of the developed work, the subject of fluorescent-lamp operation and control is addressed along with a short introduction to conventional ballasts, electronic ballasts and fluorescent-lamp models. The replacement of conventional ballasts by electronic ballasts has come to confirm that the latter are effectively an efficient way of saving energy in lighting systems. The fundamental requirements of typical fluorescent lighting systems controlled by electronic ballasts are described. However, there are always new demands with respect to their working possibilities. Electronic ballasts with additional control circuitry can provide multi-lamp operation and dimming. This important feature allows the ballast to control the lamp power and thereby the light output. The state of the art in fluorescent-lamp dimming techniques is presented. Other features related to remote control of the lighting system are also referred. Magnetic regulators are introduced as a new concept related to magnetic control in electronic ballasts, for dimming and multi-Watt operation. The chapter ends with a brief description of this type of control and sets the directions for the remaining chapters.

1.1 LAMPS AND LIGHTING

1.1.1 RADIATION AND LIGHT

Radiation describes any process in which energy travels through a medium or through space, eventually being absorbed by another body. Light is considered to be a particular form of

radiation, better described in terms of waves travelling in one specific direction, dictated by the light ray. These waves are electromagnetic in character, occupying only a very small portion of the electromagnetic spectrum, in a range from approximately 380 nm to 780 nm, perceptible to the human eye.

Visible light is measured in lumen [lm], the SI unit of *luminous flux*, which is a quantity derived from radiant flux by evaluating the radiation according to its action as described by the Commission Internationale de l'Eclairage standard photometric observer, CIE 084-1989. This luminous flux is correlated to the differing sensitivity of the human eye to light with different wavelengths [1.1].

A monochromatic light has a single wavelength. If lights with different wavelengths are combined, less strong colours are obtained. The eye discriminates between these different wavelengths by the sensation of colour; blue and violet correspond to the short wavelengths, yellow and green to the middle wavelengths, and finally, red to the long wavelengths. For a mixed radiation, the eye is unable to accurately detect the different components. In addition, the sensitivity of the human eye is not uniform over the visible spectrum and the maximum visual response is obtained in the yellow-green area [1.2].

The visible portion of the electromagnetic spectrum is represented in Fig.1.1. Electromagnetic radiations beyond the violet barrier are known as ultraviolet, x-rays and gamma-rays. Beyond the red barrier are infrared and radio radiations.

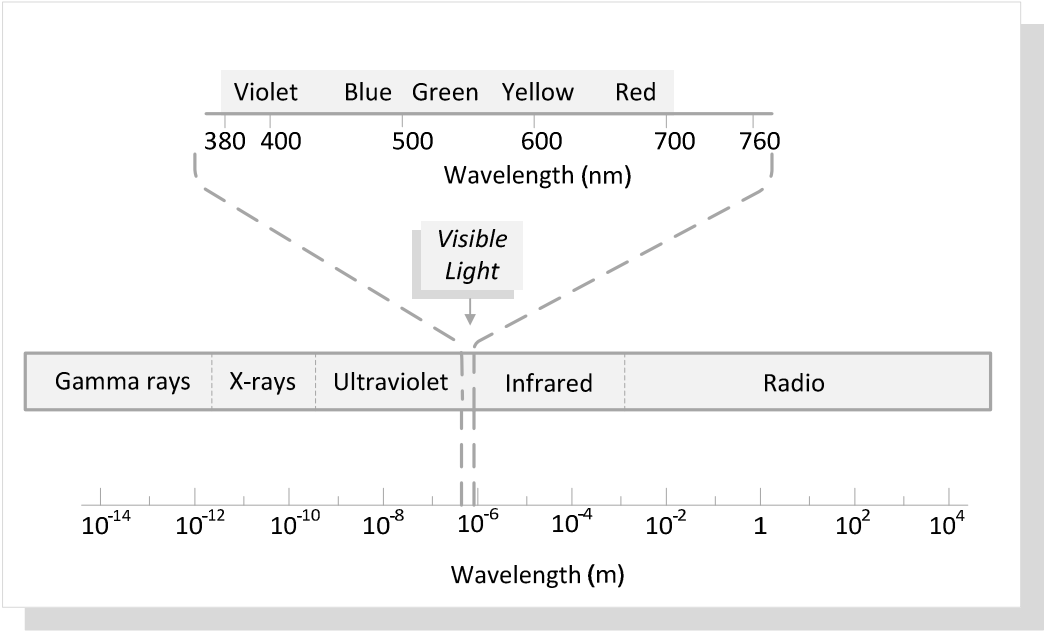

Fig.1.1. The electromagnetic spectrum.

From an historical point of view, artificial light sources are typically classified according to the mechanism which is used to produce light, the most common being incandescence and luminescence.

Both mechanisms are the result of the same process: transitions between energy levels of atoms, ions, molecules and solids. Whereas incandescence is the emission of light by a hot body, especially solids, luminescence is used to describe the general process by which an excited material emits light, not by a rise of temperature of the emitting body, but by the intervention of an external agent. This excitation may usually be achieved with ultraviolet radiation, x-rays, electrons, electric fields, or chemical energy. The colour or wavelength of the emitted light is determined by the material, while the intensity depends on both the material and the input energy [1.2], [1.3].

1.1.2 INCANDESCENCE

One of the first well-known examples of artificial light sources is the incandescent lamp. On January 27, 1880, Thomas Edison received the historic patent claiming the principles of his incandescent lamp, based on a filament of carbon of high resistance, which then led the way for the universal domestic use of electric light [1.3].

Today's typical incandescence mechanism can be simply described by an electric current passing through a thin filament of solid tungsten or carbon, heating it to a temperature that produces light. Even if incandescent lamps are still very common in daily life, their application is limited according to their low luminous efficacy and rated lamp life. The *luminous efficacy* is the quotient between the luminous flux emitted and the power consumed by the source, expressed in lumen per watt [lm/W] [1.1].

Typically, larger wattage incandescent bulbs have a higher efficacy than smaller wattage bulbs, around 20 lm/W; still most of the energy consumed is emitted and lost in heat, rather than as visible light. Moreover, the estimated lamp life, around 1000 burning hours, is well below other common light sources. Incandescent lamps are also limited by the rate of evaporation of the tungsten filament. In conventional lamps, the bulb is normally filled with an inert gas such as argon to reduce this evaporation.

In 1959, a special type of incandescent lamp became commercially available: halogen lamps. In this type of lamps, the tungsten filament is sealed into a compact transparent envelope filled with an inert gas and a small amount of a halogen. The purpose of the halogen is to prevent

evaporating tungsten from settling on the bulb wall. The life of a lamp is inversely proportional to the tungsten transportation rate. Any variation on the composition or geometry of the filament causes hot spots. The end-of-life of incandescent lamps, with or without halogen addition, occurs when these hot spots fuse. Halogen and particular temperature regimes, establish a chemical cycle which transports tungsten from the cooler regions near the bulb wall, to higher temperature zones surrounding the incandescent filament, regenerating it. The thermal regimes required to slow down the tungsten transportation rate require a smaller bulb, which then allows a higher operating pressure and slows down the tungsten transportation rate and increases the lamp life. For this reason, and the fact that these lamps operate at a higher temperature than a standard gas-filled lamp of similar power, without loss of operating life, they exhibit a higher efficacy. Examples of both incandescent and halogen lamps are presented in Fig.1.2 [1.2], [1.3].

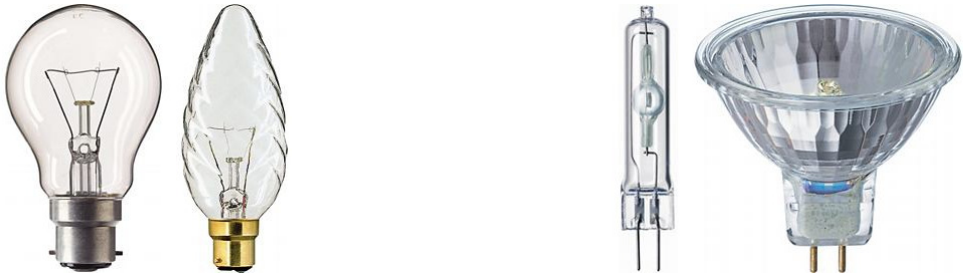

a. Conventional pear and candle shaped incandescent lamps b. Halogen lamps

Fig.1.2. Incandescent and halogen lamps retrieved from the Philips Product Catalogue 2010 [1.4].

1.1.3 LUMINESCENCE

Luminescence is the mechanism by which an excited material emits luminous radiation in a process not solely caused by a rise in temperature. The excitation is usually achieved with ultraviolet radiation, X-rays, electrons, electric fields, or chemical energy. The colour, or wavelength, of the light emitted is determined by the material, while the intensity depends on both the material and the input energy.

The most important well-known forms of luminescence are: low and high-pressure discharges, electroluminescence, fluorescence, which is a specific type of low-pressure discharge, and finally phosphorescence. These last two are distinguished by the delay between excitation and emission. Processes involving delay times longer than 10 ns are usually referred to as phosphorescence.

In fluorescence, the radiation which produces excitation is ultraviolet and the visible radiation colour depends upon the phosphor material which is used. A typical example of this luminescence mechanism is the tubular-shaped fluorescent lamp presented in Fig.1.3a.

Standard low-pressure discharge lamps are mainly based in mercury and sodium discharges. These lamps usually operate with pressures lower than 1 Pa. Typical features are low current density inside the discharge and low power per unit of discharge length. Therefore, they normally present a quite large discharge volume with a low power rating [1.3], [1.8].

The fluorescent lamp works on the low-pressure mercury discharge principle [1.2]. The discharge tube is typically made of a transparent or translucent material, filled with an inert gas, typically argon, and a metal vapour, mercury, with two sealed-in electrodes placed at both ends. The fluorescent powder placed on the inside wall of the discharge tube converts the ultraviolet radiation into visible radiation: the heated electrodes generate free electrons which will be accelerated by the electrical field existing in the discharge with the purpose of colliding with the mercury atoms. These excited mercury atoms will then emit ultraviolet radiation causing the fluorescent material to fluoresce, producing visible light.

Fluorescent lamps were first introduced around 1940 and by 1970 they had become the most dominant artificial light source, particularly in the industrial and service buildings. Generally, these lamps present a high luminous efficacy, around 60-80 lm/W, good light output, a wide choice of colour and long burning hours, around 12000. Depending on each specific lamp, some of these characteristics can be further enhanced. They are typically identified by their diameter in mm or by the letter T followed by a number, T12, T8 or T5. The T represents the shape of the lamp, tubular. The number following the T represents the diameter of the lamp in eighths of an inch. Similarly to other discharge lamps, it is necessary to use a current-limiting device, the ballast, typically a simple inductor, in order to stabilize the lamp at the required operating point, by limiting the discharge current.

Compact Fluorescent Lamps, CFLs, were first introduced in the 1980's. With integrated ballasts, these lamps were specially designed to be an effective replacement for incandescent lamps. They are produced using very small diameter glass tubing, of around 10-16mm, which may be bent, fused and joined to form a very compact unit, as the ones shown in Fig.1.3b. They sometimes come with an external envelope which hides the tube and make them even more similar to light bulbs. This envelope also mitigates the risks connected to mercury emissions because of lamp breakage [1.5]. Similar to common fluorescent lamps, they exhibit a long lamp life, between 8000 and 15000 hours, depending on the type and application, and present a higher luminous efficacy.

a. Tubular and circular shaped fluorescent lamps b. Compact fluorescent lamps

Fig.1.3. Fluorescent lamps retrieved from the Philips Product Catalogue 2010 [1.4].

The other typical example of a low-pressure discharge lamp is the low-pressure sodium lamp, with an average life time between 16000 and 18000 hours. Since the melting point of sodium is higher than that of mercury, the sodium arc tube must operate at a higher temperature than a fluorescent tube, so, for energy conservation purposes, it must be insulated from its surroundings with an extra bulb as shown in Fig.1.4 [1.2]. After ignition, the sodium vapour in the glass tube emits a monochromatic yellow light.

They are considered to be the most efficient lamp available since the emitted radiation has a wavelength close to the peak sensitivity of the human eye around 590 nm, leading to a higher luminous efficacy, which in particular cases may reach 200 lm/W. Due to this monochromatic character, these lamps can only be used where natural colour rendering is not required. This colour rendering is directly related to the ability of a light source to reproduce the colours of different objects. Nevertheless, they offer high-contrast visibility in mist and fog. This is the main reason why they are used in situations where high levels of safety and reliability are needed, for example for arterial roads, highways, tunnels, canals, harbors, water gates and locks [1.6].

Fig.1.4. Low-pressure Sodium Lamp from the Osram Sylvania Product Catalogue [1.6]: SOX or SOX-E.

As previously referred, other known forms of luminescence result from high-pressure discharges. High Intensity Discharge lamps, HID, include High-Pressure Sodium discharge lamps, HPS, High-Pressure Mercury Vapour discharge lamps, HPMV, and Metal Halide lamps.

The elements added to the gases, mercury, sodium or metal halide, cause each type of lamp to have different colour characteristics and different efficiencies. The discharge principle is similar to the previous examples: an arc is established between two electrodes, which in this case are only a few centimetres apart, in a gas-filled tube which causes a metallic vapour to produce radiant energy. The gases in the tube are highly pressurized, with values around 10^5 Pa or higher, and in contrast to low-pressure lamps, their typical operating temperature is significantly higher. These lamps present a high-current density in the discharge and a high power per discharge-length ratio, which means that much smaller tubes can be used [1.8]. Typical examples are presented in Fig.1.5.

High-Pressure Mercury Vapour lamps are the oldest HID technology. The effect of increasing the vapour pressure can be seen from ignition to steady-state operation. When first ignited, the lamp voltage is low and the discharge fills the tube and appears blue, similarly to a low-pressure fluorescent tube, emitting mainly in the ultraviolet region. This bluish light renders colours feebly. Thus, most mercury vapour lamps have a phosphor coating that alters the colour temperature and improves colour rendering. Yet, due to the high vapour pressure and the rise in temperature, more mercury is evaporated and progressively the spectral lines move towards regions of longer wavelengths, and the light becomes whiter.

The luminous efficacy of a HPMV phosphor-coated lamp increases with wattage, ranging from about 40 to 60 lm/W at 1 kW. Their colour characteristics and poor rendering, easily surpassed by other HID technologies, has narrowed the practical use of these lamps to street lighting, highway lighting and some commercial interiors [1.2], [1.3], [1.6], [1.8].

The High-Pressure Sodium lamp is different from the low-pressure version and has only appeared after the development of a specialized ceramic material that forms the arc tube. This translucent material is able to resist the attack of sodium vapour at the temperature and pressure values attained in these high-pressure lamps. They are especially popular due to high luminous efficacy and exceptionally long lamp life, up to 40000 hours. They emit a characteristically yellow/orange light but they also render colours poorly. This tends to limit their use to outdoor and industrial applications where high efficacy and long life are priorities [1.2], [1.3], [1.6], [1.8].

Amongst all HID lamps, Metal Halide lamps exhibit the best colour properties and an excellent market penetration. Intensive research on high-pressure mercury lamps and the attempt to improve their rendering properties, led the way to a full spectrum light source. In the early

1960s it was found that, the addition of specific amounts of certain metal halides improved the spectral balance and therefore the colour properties of the lamp.

The development of this specific technology allowed engineers to finally manufacture white light sources. Not only were developed a variety of lamps with a daylight colour appearance, which eases the change from daylight to artificial light, but also UV sources for reprographic and industrial processes such as curing applications, all from a few tens of watts, up to several kilowatts, packaged in a variety of formats, depending on the specific application. Nowadays, they offer high efficacy, 80 to 125 lm/W, excellent colour rendition, long service life, around 10000 hours life time, and good lumen maintenance. Because of these numerous advantages, metal halide lamps are used extensively in outdoor applications, especially in sports lighting, and in commercial interiors. There is also an entire group of metal halide lamps that employ ceramic arc tube technology to improve colour uniformity and colour stability [1.2], [1.3], [1.6], [1.8].

Low-pressure or high-pressure discharge lamps can be operated both at low or high-frequency with advantages and disadvantages, which will be further discussed, particularly in the case of fluorescent lamps. In the case of metal halide lamps, electronic ballasts may provide a better colour control; there is however a main technical problem. An undesirable effect related to acoustic resonances, which appears due to high frequency excitation that can cause movement of the discharge [1.10]. Detection and elimination of these acoustic resonances has also been an intensive field of research [1.12]-[1.14].

a. HPS lamps Lumalux Ecologic

b. HPMV lamps

c. Metal Halide lamps

Fig.1.5. High Discharge Lamps from the Osram Sylvania Product Catalogue [1.6].

Another important form of luminescence is electroluminescence, a process by which a material emits light in response to an electric current passing through it. Perfect examples of electroluminescence are light emitting diodes, commonly known as LEDs. By adding selective impurity atoms to a crystalline semiconductor, an excess of free electrons is produced in the conduction band. These are classified as n-type semiconductors. By adding other impurities a p-

type material can be formed, where electrons are minority charge carriers and holes majority carriers. Electroluminescent p-n junctions are identical in terms of electrical characteristics when compared to conventional silicon diodes. When a light-emitting diode is forward biased, electrons are able to recombine with holes within the device, releasing energy in the form of photons and heat. In order to produce sufficient quantities of visible light, complex physical structures and materials had to be developed. Nowadays, the most important commercially available LEDs are based on aluminium gallium indium phosphide alloys for red, orange and yellow LEDs; and indium gallium nitride alloys for green, blue and white LEDs. Small changes in the composition of these alloys can alter the colour of the emitted light [1.15].

One of the first LEDs with practical electronic use, the red LED, was invented at General Electric in the 1960s and was typically used as an indicator. Following, in the 1970s, were developed the green, orange, and yellow LEDs. A major breakthrough in the 1990s, which revolutionized the LED industry, was the invention of the high-brightness blue LED by S. Nakamura [1.16]. With high-brightness LEDs, red, green and blue, white light was finally possible. Unlike other lights, LEDs are not inherently white light sources. They are nearly monochromatic with a narrow range of wavelengths. This means that light from several coloured LEDs must be mixed in order to create a spectral power distribution that appears white. Colour mixing techniques and human response in terms of colour perception, are quite complex subjects behind the development of these light sources.

Fig.1.6 and Fig.1.7 show commercial examples of high-brightness LEDs (HBLEDs) and LED lamps for a variety of applications. From automotive and aviation lighting, displays, traffic signals, floodlighting, street lighting, to medical applications and domestic use, everything is available. Infrared LEDs are also used in the remote control units of many commercial products including televisions, DVD players, and other domestic appliances. One of their major advantages is their rated life time, estimated to be over 50000 hours. Other key advantages of LED-based lighting are low-voltage and low-current requirements, high switching speed, high reliability, robustness, absence of mercury, compact size, lower maintenance costs and high efficacy, around 60 lm/W for a common bulb or higher, around 150 lm/W for a LED chip only [1.2], [1.16], [1.17].

a. CREE XLamp 4550 LED [1.16]

b. Philips Lumileds' SnapLED automotive LED [1.17]

c. NICHIA LED with high luminous efficacy [1.18]

Fig.1.6. LED lamps and High Brightness Power LEDs from large manufacturers: CREE, Philips and NICHIA.

d. Master LEDbulb

e. Master LEDspot

f. DecoLed lamp

Fig.1.7. LED lamps retrieved from the Philips Product Catalogue 2010 [1.4].

Like other light sources there are still many technical aspects that must or can be improved. A major issue is related to the heat dissipation and thermal degradation of efficacy. This degradation is due to the reduction of lumen per Watt due to the increasing junction temperature [1.21]. HBLEDs are typically classified as a high-efficacy light source. However, this is only true at low junction temperatures, and the usually presented values are not sustainable at higher temperatures. But, these higher temperatures are inevitable, since most of the delivered energy is delivered in the form of heat. There is a known problem regarding the quantum efficiency, which is the rate of emitted photons with respect to electron-hole recombination [1.22]. Unless expensive heat sinks or cooling systems are used, this heat dissipation will have a negative effect on the light output. A concentration of LED lights can have a negative impact on the air-conditioning bill. This is a well-known effect which caught the scientists and designer's attention. Yet, it is consensual among experts that this technology is moving extremely fast and that these limitations will be eventually overcome.

Lighting represents a significant part of energy consumption in domestic and services areas. Engineers and lighting corporations around the world are constantly seeking for better, cheaper and more efficient luminescent-based light sources, as progressively, incandescent lamps are set aside. Though not forgetting market rules, competition and profits, there is now a commitment to

the search and development of a greener future. Promoting better energy efficiency in the lighting field implies higher demands concerning energy efficiency requirements, particularly of building regulations in the illumination domain. For the past years, regulations, standards, taxes, energy labels, and other product-related measures are constantly being deliberated to ensure and deliver a market transformation in lighting efficiency, thus contributing to a rapid transition to a clean energy economy.

1.1.4 GENERAL CONSIDERATIONS ON LIGHTING EFFICIENCY

In December 2008, European Union leaders adopted a comprehensive package of measures to reduce the EU's contribution to global warming and ensure reliable and sufficient supplies of energy. The Commission has adopted an Action Plan, which aimed at achieving a 20% reduction in energy consumption by 2020. It includes measures to improve the energy performance of products, buildings and services, to improve the yield of energy production and distribution, to reduce the impact of transport on energy consumption, to facilitate financing and investments in the sector, to encourage and consolidate rational energy consumption behaviour and to step up international action on energy efficiency [1.5]. Several other countries not belonging to the EU, are also implementing action plans for energy efficiency with an agenda depending on the technological evolution, the evolution of the energy consumption and the development of the economy. So in fact this is a world-wide trend.

In Portugal, since the entry into force of the Kyoto Protocol, legislation has been adopted ensuring compliance with the commitments undertaken at international level. Both the PNAC (Portuguese National Plan for Climate Change) and the PNALE (National Plan for the Allocation of Emission Allowances) have as their object to implement the Kyoto target. More recently, and also as a result of a European initiative, the PNAEE (National Action Plan for Energy Efficiency) was approved, envisaging to reduce energy consumption through an annual increase of 1.1% in energy efficiency until 2012, taking as reference the average final energy consumption between 2001 and 2005.

One of the measures, common to all European countries, consists on the ambitious program to phase out low-efficiency incandescent lamps between September 2009 and the end of 2016. The aim is to encourage the use of more energy efficient lighting alternatives in order to reduce the primary energy consumption. This means using mainly luminescence-based light sources such as

CFLs and LEDs. Nonetheless, and in spite of all the measurements and information campaigns, the general population is somewhat sceptical to the phase-out of incandescent lamps.

One of the reasons why this occurs is directly related to the inscriptions present in the more efficient light source alternative. Traditionally, with incandescent lamps, more light would mean more watts. Nowadays the same quantity of light, for instance 750 lumens, can be produced by an incandescent bulb using 60W, a halogen bulb using 42W, or a compact fluorescent lamp using 15W. This causes some confusion to the consumers, which manufacturers try to solve by giving equivalence with incandescent bulbs, which in fact has become an unreliable and complicated method of comparison between lamps having different energy efficiency. Since 2010 manufacturers are obligated to display the lumens offered by the light source at a larger font than the display of watts. This is an attempt to familiarized people with lamp comparisons based on their real performance and not their wattage.

Also, the purchase price difference between incandescent lamps and more efficient alternatives constitutes a psychological barrier, even if the higher initial investment will be retrieved due to long burning hours and higher luminous efficacy. Another discouraging factor has been the somehow poor quality of the so-called economic lamps placed on the market without being subject to quality requirements [1.5].

Another reason is related to the light source colour properties and consumers perception to these properties. The lighting industry predominantly uses the *colour rendering index* (CRI). This index measures the degree to which the colour of an object illuminated by the light source conforms to that of the same object illuminated by a reference light source. In basic terms, it gives an indication of the light source's ability to make illuminated objects appear natural.

Another common index is the *correlated colour temperature* (CCT), often confused with the *colour temperature*. Whereas the CCT is defined as the temperature of the blackbody radiator whose colour, according to human perception, most closely resembles to the considered light source; the colour temperature is simply the temperature of the blackbody which emits radiation of the same chromaticity of the light source, technically according to the *Colour Appearance Modeling for Colour Management* ratified by the CIE. Both terms are referred to in units of absolute temperature, Kelvin [K]. A *blackbody* or a full radiator is defined as an idealized body that absorbs all electromagnetic radiation falling upon it and is also capable of re-emitting. At zero K, the blackbody emits no radiation. At room temperature, black bodies emit mostly at infrared wavelengths, but as the temperature increases past a few hundred degrees, blackbodies

start to emit at visible wavelengths, appearing red, orange, yellow, white, and blue with increasing temperature, under a continuous spectral distribution. The CCT index is in fact a physiological response, commonly used as an indication of the apparent "warmth" or "coolness" of the light emitted by the source. Thus, a luminescence-based light source such as a cool white fluorescent lamp, which emits radiation of a specific wavelength, has a CCT around 3500K and it is perceived as a white source of light, whereas a HPS lamp, which presents a CCT of about 2000K appears yellow, and is perceived as a warmer light source.

These two metrics, CCT and CRI, are facing increased challenges and criticisms as new types of light sources appear, particularly since LEDs are becoming more prevalent in the market [1.1], [1.2], [1.7], [1.15].

These measures along with increasingly higher energy conservation concerns just confirm that the money invested in this field of research has not stopped growing during the past-years. Lighting companies are strongly encouraged and committed to develop efficient, cost-effective and ecologically aware solutions in all the lighting domains. One of the most active fields of research, besides LEDs and high-efficiency discharge lamps, is related to the efficient control of operation of light sources.

Although LED technology caught the attention of scientists and of the general population, with promising results regarding efficiency and rated lamp life, there are still large investments in fluorescent lighting systems. High-frequency operated fluorescent tubes represent an alternative cost-effective technology, with a widespread use in industrial and commercial buildings which is still expected to prevail in the near future. One of the most obvious reasons corresponds to the broader range of commercially-existing solutions, which fulfil the need of creating adaptable and flexible environments. Currently, electronic ballasts are becoming inevitable in systems where rational rules of energy utilization are to be implemented, and viewed as crucial elements in economical and energy-efficient fluorescent lighting systems. With energy conservation concerns becoming increasingly high, electronic ballast consumption has intensified. A number of factors are contributing to this growth rate, including government regulations, lower prices and innovative technologies, but mainly due to a set of specifications and additional functions which are responsible for a more efficient electronic and digital control of the system, and particularly of the lamp operation.

Until ten or fifteen years ago, the standard type of ballast used for office or industrial fluorescent lighting systems was still the electromagnetic type, obviously with several well-

known drawbacks, mainly related to low-frequency lamp operation. Typically, the overall achievement in a suitable luminaire represents an energy reduction around 20-30% due to two main factors: improved light output at high frequency operation, also eliminating visible flicker and audible noise, and reduced power losses when compared to conventional electromagnetic ballasts. These two factors, coupled with government policies, makes the upgrading of all ballasts a cost-effective move, simultaneously pointing the solutions that could be adopted society-wide to secure a swift transition to a clean energy economy, and lead the way to a better use of the world finite, non-renewable natural resources.

1.2 FLUORESCENT LIGHTING SYSTEMS

1.2.1 FLUORESCENT LAMPS

Discharge lamps are usually more efficient than incandescent lamps because they radiate from regions of higher temperature that can be reached with tungsten filaments. Discharges are also more selective emitters than incandescent lamps, so less energy will be wasted in IR emission. As previously stated, the tubular fluorescent lamp is a common example of a luminescent-based light source and works on the low-pressure mercury discharge principle.

Like all discharges, the fluorescent lamp requires plasma which is a substance similar to gas in which a certain portion of the particles are ionized. In fact, plasma can also be described as a mixture of ions and electrons, electrically neutral on average together with another variety of neutral or excited particles. This plasma is also referred to, as the *positive column*. The fluorescent tube typically contains a mercury vapour at about 0.8 Pa and a rare gas, such as argon at a pressure of typically 266 Pa or higher [1.2]. Two sealed-in electrodes are also placed at both ends in order to provide an electrical connection to the plasma. Electrodeless connections are possible and will be further discussed. The fluorescent material that covers the inside wall of the tube, phosphor, is responsible for converting the UV radiation obtained from the discharge, into visible radiation. The basic processes inside the tube can be observed in Fig.1.8 and can be described as follows [1.2], [1.8]:

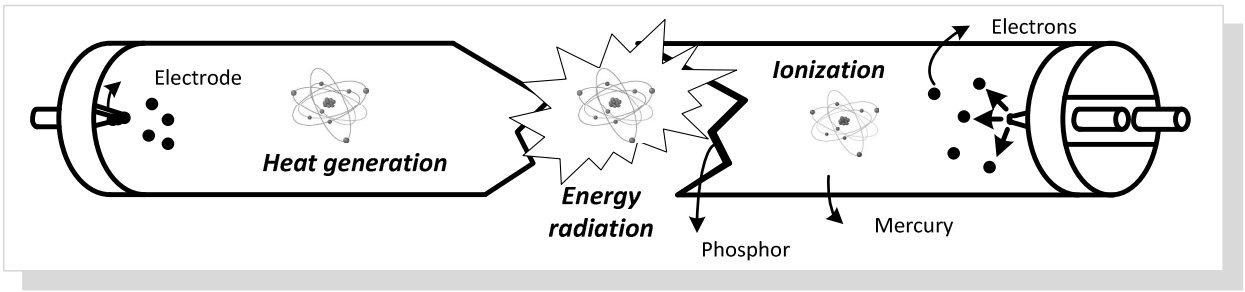

Fig.1.8. Basic processes in the fluorescent lamp tube.

- *Heat generation:* if a high enough electric field is applied to the plasma or gas, the gas breaks down and becomes conducting. Breakdown initially occurs because there is always a small amount of ionization due to the constant generation and emission of free electrons by the electrodes. The applied electric field heats and accelerates these electrons, and some may become sufficiently energetic to ionize more gas atoms. If the kinetic energy of the electrons is low, elastic collisions take place and energy is transferred to the atoms. The consequence of these collisions is an increase of the gas temperature, which means more heated electrons.

  One of the main differences between low and high-pressure discharges is related to the difference between the gas and electrons temperature. Contrary to high-pressure discharge lamps, where the collision rate is high enough for the gas temperature to be similar to the electron temperature, in low-pressure discharge lamps, gases of atoms and electrons exhibit different temperatures. Though it might seem strange, since they occupy the same space, there is little interaction between them. Therefore, hot electrons will continuously make elastic collisions with atoms at high frequency, transferring very small amounts of energy, due to their different masses, and with no significant losses in velocity.

- *Ionization:* If an electron has sufficient energy, it is capable of ionizing a gas atom, which means sending an electron of the gas atom to a higher orbit. So, if an electron belonging to the atom is freed, this will result also in a positive charged ion. These freed electrons can play the same role as those generated by the electrodes.

  Electrons and ions in the discharge will likely diffuse towards the wall of the tube and because of their mutual electrostatic attractions they will tend to recombine again into atoms. During this process, energy will be delivered to the wall in the form of heat. By increasing the pressure of the rare gas, this recombination rate may be reduced. It also reduces the electron temperature and in this way the number of collisions which excite the atoms may be controlled.

In order to maintain the discharge, the applied electric field must also be adequate so that the electron temperature is high enough to provide sufficient ionizing collisions to replace the electrons and ion losses. So, this whole process is very crucial, whether during discharge ignition or normal running, because ionized atoms and electrons are necessary to maintain the electrical current through the lamp.

- *Energy radiation:* After collision, the freed electron of the gas atom which remains in a higher orbit stays in an unstable condition. It tends to recover its original level, and during this process it emits the absorbed energy primarily in the form of electromagnetic radiation, mainly in the ultraviolet region, at the wavelengths of 254nm and 185nm, which are both resonance radiation lines in the atomic spectrum of mercury. Only a very small part of energy is directly converted into visible radiation. The remainder energy is dissipated as heat in the form of losses in the plasma and in the electrodes.

  There is an optimum mercury pressure for the operation of fluorescent lamps. The mercury pressure has a strong influence in the electric arc. As the pressure is increased from a low value, the efficiency increases because there is an increasing number of mercury atoms that radiate. This electromagnetic radiation is then transformed into visible light due to the phosphor coating existing in the inside wall of the tube. However not all UV photons are converted into visible radiation. In a common T8 or T12 lamp the overall conversion efficiency is about 40%.

Most of the gases, like air, are very good insulators at normal pressure and temperature. If however, the voltage stress is sufficiently high, it may become partially conductive, which means that a sufficient concentration of charged particles is present. If the voltage is sufficiently high, complete electrical breakdown of the air will culminate in an electrical spark or arc. In fluorescent tubes, this voltage stress or starting voltage is translated into an electric field strength around 10V/cm, considering an optimum mercury pressure. This means 1000V for 1 meter of tube, approximately. The auxiliary inert gases are also used to decrease this starting voltage. Penning mixtures are special inert gas mixtures capable of providing very low starting voltages. Narrower tubes have higher fields so the discharge length is shorter, but yet, CFLs tubes must be folded to attain the recommended levels. In electrodeless lamps the constraint on lamp voltage no longer applies, and this is the reason why they can be built in similar shapes to incandescent lamps [1.2] [1.8].

The efficiency of the fluorescent lamp depends on two processes: the conversion of the electrical energy from the supply into UV radiation and the conversion of this UV radiation into visible light. While the first is directly related to the discharge arc length, tube diameter, gas mixture and pressure, mercury pressure and power loading of the tube (in watts per unit area of discharge surface), the second one is related to the emission spectrum of the lamp, phosphor or phosphor mixture used to obtain that spectrum and the efficiency of these phosphors.

Other aspects that contribute to lower efficiency and diminish the rated lamp life are related to ambient temperature and cathodes operation.

The luminous flux of a low-pressure mercury lamp is determined by the mercury vapour pressure, which in its turn is dependent on the temperature of the coldest spot in the lamp. During the initial running of the lamp, the mercury vapour will re-condense at that coolest spot of the tube as excess liquid mercury. For T12 and T8 the optimum cold spot temperature for maximum efficiency or maximum light output is about 40º-45º C. For linear lamps operated horizontally the coolest spot coincides with the bottom centre of the tube and the optimum temperature is achieved when ambient air temperature is between 20º and 30º C. So, it is clear that ambient temperature plays an important role in the lamp performance.

The design of the luminaire will also determine the actual air temperature adjacent to the tube and therefore influences the temperature of the coolest region of the tube. CFLs typically run hotter than linear tubes due to their higher wattage per unit area of the tube, so, they have a tendency to operate at higher temperatures than the optimum ones. In these cases, an artificial cool spot may be created, by having an extension of the tube away from the heat sources, the electrodes or the discharge itself [1.2].

The TL5 lamp from Philips was also designed to reach its maximum flux at 35º C ambient temperature in draught-free air when operated with an electronic ballast without additional heating of the electrodes. Such ballast is called cut-off ballast. The temperature of 35º C is considered to be the common ambient temperature inside the luminaire. The cold spot in these lamps is situated behind the electrode at the stamp side: the so-called cold chamber. There will be an evident depreciation of the luminous flux if the air temperature is higher than the recommended value. For values higher than 70º C, the electric characteristics of the lamp will change sharply which may have a damaging effect on the system lamp plus ballast. So, for those reasons, the cold-spot temperature should not exceed 100º C. If however, high ambient temperatures are impossible to avoid, a physical contact with the luminaire can create a second

cold spot, turning the cold chamber obsolete. With this new cold spot the lamp can be brought to optimum conditions. If however the opposite occurs, the ambient temperature is too low, a standard solution is to cover the cold spot with an insulating material, thereby guaranteeing that the optimum cold spot temperature is reached [1.19].

In order to maintain the discharge current, the electrons which return to the external circuit at the anode must be replaced by electrons emitted by the cathode. The electrodes are also responsible for replacing the electrons lost during the recombination process. So, they play a crucial role in the lamp operation. The electrodes, usually small tungsten wires structures, are heated by ion bombardment, and the probability that an electron will escape from the cathode depends exponentially on its temperature and on its surface barrier which is called the work function material. They are typically covered with low-work-function materials such as barium oxide so that they can emit at relatively low temperatures with low evaporation rates. It is a fact that high temperatures and low work function materials favour the thermionic emission [1.2].

The ignition process is a decisive factor in terms of electrode preservation with an immediate effect on the lamp life. Before reaching the thermionic state, the electrons have to be extracted by field emission. This means that initially the electric field must be very high for electrons to escape. This high electric field causes ions to be accelerated towards the cathode, hitting it with very high energy. This leads to loss of emitter material due to *sputtering*: ejection of atoms by ion impact. In order to limit this effect and its impact on the average lamp life, the electrodes must be pre-heated. For the same reason, repeated switching evidently shortens the lamp and these are the reasons why the preheating process is extremely important to ensure a longer lamp life [1.9].

1.2.2 LOW-FREQUENCY AND HIGH-FREQUENCY OPERATION

Contrary to incandescent lamps, which can be directly connected to an appropriate power supply, discharge lamps require a control circuit or ballast in order to insure proper starting and stable operation. Fluorescent lamps can be operated on mains frequency, 50Hz or 60Hz or at high-frequency, over 40kHz. In both situations, ballasts are used to limit the discharge current. Plus, a high voltage is generally required to initiate the ionization process. If the supply voltage is insufficient to provide ignition, some auxiliary circuits must be added to the system.

Prior to ignition, fluorescent lamps are typically characterized by almost infinite impedance. After the gas breakdown, and when the rate of ionization exceeds the rate of loss of ions and electrons due to the recombination process, the discharge current tends to grow rapidly. An

immediate effect is the drop in the electric field and discharge voltage. At steady-state, the lamp typically behaves like a power-dependant resistance. Fig.1.9 shows the rms voltage-current characteristics of a TL5 14W fluorescent lamp from Philips, operated at high–frequency. It exhibits the characteristic negative differential resistance behaviour common to all fluorescent lamps. However, due to this negative characteristic, a stable operating point is not viable unless a current-limiting device is used. Without this device and with the continuous presence of an applied electric field, the current would rise indefinitely culminating into an almost short-circuit and obvious lamp failure.

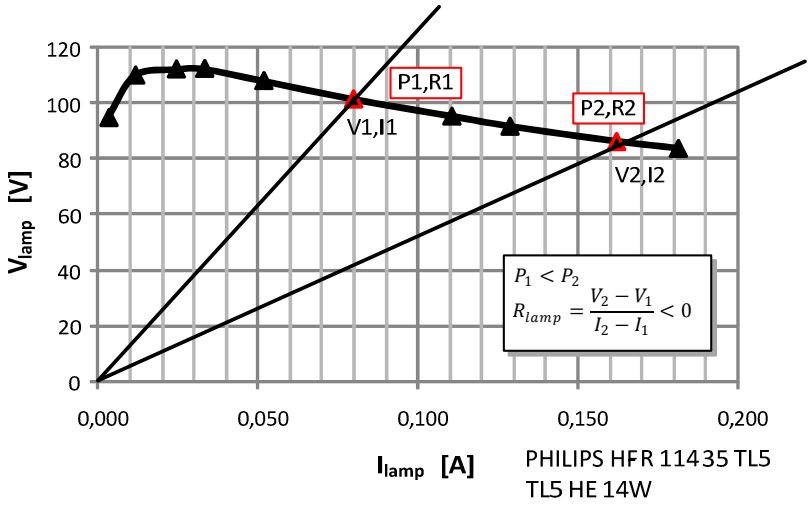

Fig.1.9. Negative differential or incremental resistance of a fluorescent lamp.

When the lamp is operated at low-frequency this limiting device is commonly referred to as conventional ballast or electromagnetic ballast. The key function of the device, usually a series connected inductor, is to prevent current runaway while stabilizing the lamp, without adverse effect on lamp life. It should be efficient, simple and ensure proper lamp starting and operation [1.2]. Resistive ballasts could also be used, but the associated losses would be higher, decreasing the overall efficiency of the system.

High-frequency operation can be implemented using electronic ballasts. For fluorescent lamps, operation at 20kHz or higher reduces the electrodes losses substantially and eliminates the modulation of light output which normally has some undesirable effects on the users. The use of electronics also allows more complicated functions, such as user control of the luminous flux level. The key function of the ballast is similar to the previous one. Enough positive impedance must be in series with the lamp to overcome the negative resistance characteristic [1.2]. Standard and simple connection circuits using electromagnetic or electronic ballasts, for low and high-frequency operation respectively can be observed in Fig.1.10.

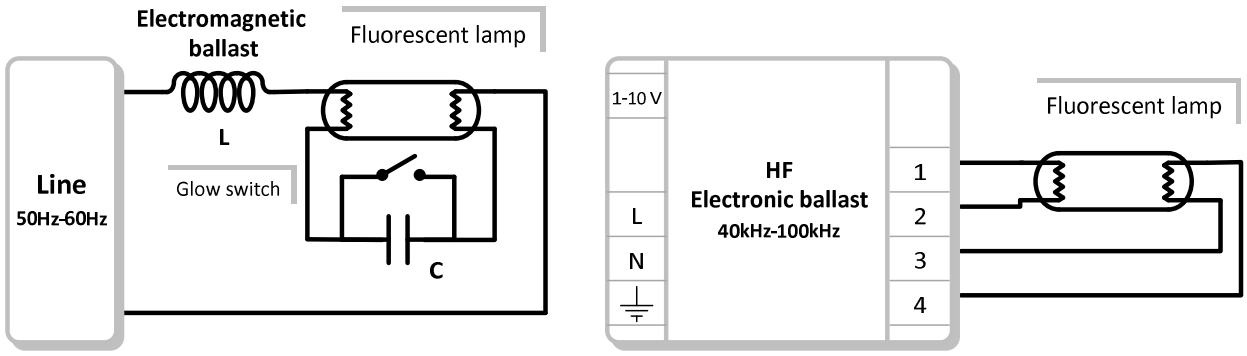

a. Electromagnetic ballast b. Electronic ballast

Fig.1.10. Low-frequency and high-frequency operation.

In the case of Fig.1.10a., the inductor is connected in series with the lamp and a glow-switch is used to provide the required starting voltage to produce the discharge breakdown. This represents the simplest possible connection. Glow-switches are inexpensive and simple. Normally they are made of two bi-metal contacts inside a small tube filled with an inert gas. Before switching on, the contacts are separated by a small gap. When the circuit is energized, the supply voltage is sufficient to initiate a glow discharge inside the switch, which slowly heats the contacts and bends them towards each other. Then, the switch closes and a short-circuit current flows through the circuit, heating the electrodes of the main lamp. When the switch closes, the glow discharge is extinguished, the contacts begin to cool and they will eventually spread, opening the switch. At this moment, the energy stored in the inductor causes a voltage pulse across the lamp terminals and the lamp ignites. In normal operating condition, the lamp voltage, which is lower than the line voltage, is not sufficient to reignite the switch [1.2], [1.22]. At these low frequencies, electrons and ionized atoms have enough time to recombine at each current reversal, thus, in order to maintain the lamp running, the discharge must occur twice within each line period. Sometimes, when the lamp fails and the electrodes are still operating but not capable of maintaining the arc current, the switch continuously attempts to start the lamp, causing flashing and blinking.

Electronic ballasts are essentially power converter circuits with three major functions, such as lamp ignition, lamp operation and suppression of electromagnetic interference. Usually, as represented in Fig.1.10b., they are directly supplied by the mains voltage. The drawn current is then changed in terms of frequency, waveform and magnitude in order to supply the lamp adequately. As well as acting as power source for the lamp, the ballast generally performs some additional functions. Power factor correction, lamp failure detection or luminous flux regulation, commonly referred to as *dimming*, are some of these functions. Particularly, dimming is one of

the most important features giving the ability to control the light output. Commercially, electronic ballasts present two different solutions in terms of dimming control: analogue control with 1-10V DC systems as shown in Fig.1.10b., or digital control systems, which will be further discussed.

The electric properties of the fluorescent lamp will depend on the operating frequency and the selected ballast, but whatever the chosen operating conditions, an increase in current does not change the gas conductivity immediately. A short time is required before the lamp reaches equilibrium at the new value. At low frequency it is possible for the lamp to follow these variations and the lamp impedance changes continuously during each cycle. This results in a non-sinusoidal voltage waveform. As the frequency increases, the ionization state no longer follows the rapid changes in current, which results in a near-constant plasma density and an almost constant impedance throughout the cycle. This means that the dynamic voltage-current characteristic of the lamp, tends to become linear and the voltage waveform distortion is reduced [1.2]. Fig.1.11 presents some simulation results which exemplify the evolution of the fluorescent-lamp voltage-current characteristics with increasing frequency values [1.31].

A more accurate description of this behaviour can be observed in Fig.1.12. It shows typical fluorescent-lamp waveforms, lamp voltage and arc current, for low-frequency and high-frequency operations, retrieved from a 20W tubular lamp from Osram. The corresponding dynamic voltage-current characteristics can also be observed.

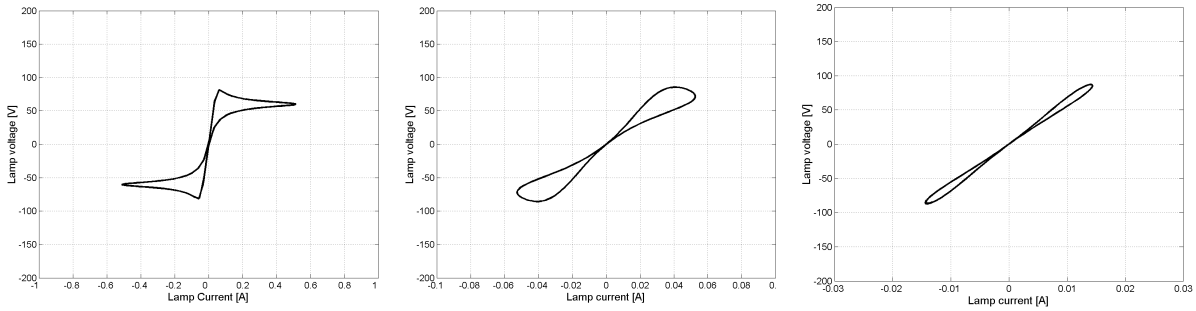

a. 50 Hz b. 500 Hz c. 2000 Hz

Fig.1.11. Dynamic voltage-current characteristics of a fluorescent lamp operated at various frequencies.

In both cases, the lamp voltage and arc current are in phase, confirming the lamp's resistive behaviour. However, at low frequency, the lamp voltage is distorted, presenting a quasi-rectangular waveform with characteristic voltage spikes at each current reversal, due to re-ignitions. As expected, the arc current is almost sinusoidal. At high frequencies, electrons and ionized atoms do not have enough time to recombine at each current reversal, which means that

the charge-carrier density is sufficiently high and there is no need for extra power to reignite the lamp. So, in this case, both arc current and lamp voltage are almost sinusoidal.

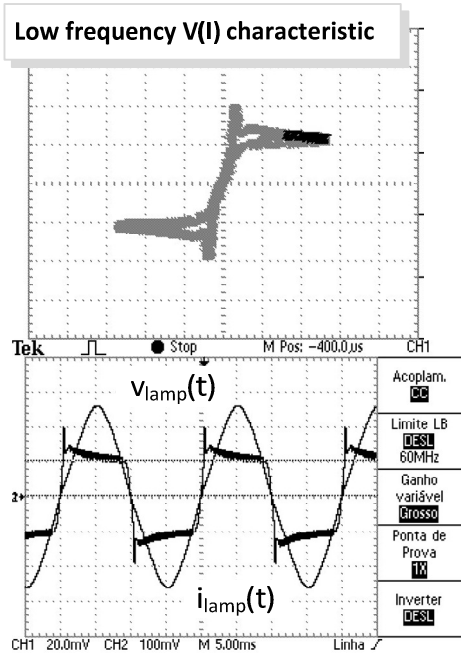

a. Low-frequency, 50 Hz - electromagnetic ballast
18 W L18.706 VOSSLOH SCHWABE

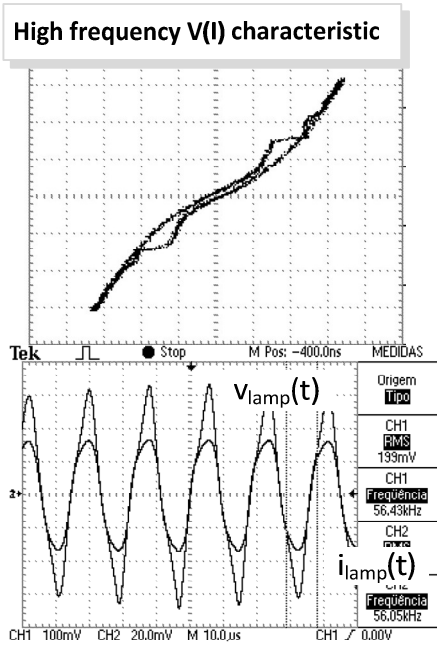

b. High-frequency - electronic ballast
Osram Quicktronic Instant Start QTIS B 1× 58/230-240, 50 kHz

Fig.1.12. Fluorescent-lamp typical waveforms and voltage-current characteristics: TL 20 W Osram.

High-frequency operation is normally preferred due to several reasons. High-frequency operation reduces the electrodes losses and there may be a small gain in the positive column. Overall lamp efficiency is improved by 20% in terms of lumen output, at frequencies above 20kHz. Unpleasant effects related to the lamp normal behaviour at low-frequency can also be avoided, such as flickering and stroboscopic effect. The luminous flux is a function of the instantaneous lamp power. Therefore, when operated at line frequency, the light output fluctuates. This is called flicker. This variation is however too fast to be perceived by the human eye. However, when rapidly moving objects are exposed under such light sources, the objects may seem to move slowly, like flashing film frames. This is called stroboscopic effect and can be very dangerous in the industrial environment [1.8].

1.2.3 ELECTROMAGNETIC BALLASTS

The main advantage of the electromagnetic ballast still is its simplicity, which in turn provides low cost and high reliability. The power losses in the electromagnetic ballast can also be relatively low. Losses occur in the copper winding due to the resistance of the wire, and in the

iron core due to hysteresis, eddy currents and gap fringing losses, and increase with temperature. This means that the design of the inductor will always be a compromise between size, shape, performance and cost [1.2]. Naturally, other aspects and technical issues must be considered.

For instance, the reliability can be compromised if the matching between the supply voltage and the lamp voltage is not carefully made. The dynamic sustaining voltage from the supply throughout the cycle must exceed the instantaneous lamp voltage, guaranteeing re-ignition. A supply voltage in the range of 100-120V restricts the use of the series inductor to lamps exhibiting nominal voltages around 55V. For 220-240V supplies, a nominal lamp voltage in the range of 70-145V generally gives satisfactory operation. In addition, all discharge lamps can only withstand a limited drop in supply voltage, between 10-15%, before unstable operation and extinction occurs [1.2].

Operation at line frequency, 50Hz or 60Hz, also means high size and weight for the passive element, and susceptibility to light flickering and to the stroboscopic effect. This inductor also produces a phase displacement between the supply voltage and the lamp current. Even if this allows a higher sustaining voltage to be available at the start of each half-cycle, when compared to resistive ballasts, it reduces the input power factor. Increasing the power factor implies using large capacitors across the line input. In addition, the lamp voltage presents a high level of harmonic distortion.

A simple ignition system based in glow-switches is not possible for lamps presenting higher starting voltages. In these cases, the series inductor used to limit the discharge current can be incorporated into an autotransformer to attain higher voltage pulses for lamp ignition. This solution is very common in 120V-60Hz systems. In other cases, separate igniting transformers are needed, offering electrical isolation and safety. The use of glow-switches also makes the life of the lamp very dependent on the switching frequency. Electronic starters with controlled electrode preheating are now more common [1.22]. This has a positive effect on lamp life, since the ignition voltage pulse is only applied when the electrodes have reached the emission temperature. This results in a more reliable lamp starting and minimizes the damages to the electrodes, making the lamp less dependent on the switching cycle. There are also other cases where the necessary preheat current and lamp starting voltage can be obtained from circuits using resonant combinations of inductance and capacitance. Such circuits do not require starter switches or power factor correction (PFC) [1.2].

Fluorescent lamps characteristics also change throughout the lamp life, due to the natural aging process. The initial matching between the ballast and the lamp may diverge from the original optimum operating point. A latest aspect is related to the fact that electromagnetic ballasts are unsuitable for emergency and automotive lighting, traditionally supplied in dc [1.8].

Since the development, and widespread commercialization and acceptance of electronic ballasts, low-frequency operation has been slowly discarded. The large multiplicity of new and practical functions proposed by electronic ballasts made conventional ballasts quite old-fashioned. However, their simplicity, low-cost, recyclability, and long life may be hard to beat in some applications, even considering all the benefits proposed by electronic ballasts. In [1.32] and [1.33] low-loss magnetic ballasts for T5 fluorescent lamps are proposed. These lamps are characterized by a high lamp voltage, and in some particular cases, low current. This is the reason why they were conventionally manufactured for high-frequency operation. But the fact is that these lamps present higher average life time than electronic ballasts, which are limited by the present short lifetime of electrolytic capacitors, around 8 years. At a first glance, electromagnetic ballasts were thought to be unsuitable. But in applications were concerns with energy saving, maintenance, long life-time and recyclability are mandatory; they stand as a cost-effective alternative. This is the case in systems were lower power versions of T5 lamps are used. These lamps require a smaller ignition voltage, which can be easily solved through adequate electronic starters. Besides, due to the low current, the magnetic conduction and core losses of the ballast are greatly reduced. In addition, magnetic ballasts can last for tens of years and can be recycled without creating the same amount of toxic and electronic waste as electronic ballasts do.

In particular cases, selecting electronic ballasts for replacing conventional ballasts may not be a simple decision, even if high-frequency operation clearly gives higher values of luminous output, eliminates flickering and overcomes the stroboscopic effect. The whole scenario must be analysed, namely issues like losses, longevity, replacement and maintenance costs. Using electronic ballasts in cases where there is no need for complicated additional features could lead to an erroneous choice.

1.2.4 ELECTRONIC BALLASTS

In terms of lamp operation, electronic ballasts will naturally offer higher levels of controllability due to the inclusion of different power converters in their configuration. There are

numerous possible electronic ballast topologies, depending on the type of power converters used. They can be divided into two main groups: non-resonant ballasts and resonant ballasts.

Non-resonant ballasts are generally less efficient due to high switching losses, and are also responsible for an early aging of the lamp. With these ballasts, the lamp is typically supplied by a non-sinusoidal voltage. For these reasons they are generally used in dc emergency lighting and low-power applications [1.34]. Resonant ballasts are characterized by the resonant circuits supplying the lamp. They can be classified into two categories: current-fed resonant ballasts or voltage-fed resonant ballasts. In fluorescent lighting, commercial and prototype versions of electronic ballasts are mostly based on voltage-fed resonant inverters, and if directly supplied by the grid, they generally obey to a simple schematic, similar to the one presented in Fig.1.13.

Some of the shown blocks or stages are easily justified and understood. If directly supplied by the grid, an EMI filter followed by a rectifier and a power factor correction stage are mandatory. Then, in order to properly ignite and operate the lamp at high-frequency, the standard choice is the half-bridge resonant inverter. Depending on the complexity of the ballast and provided additional features, some kind of control circuitry and user interface is also included in the configuration. Some particular considerations and remarks on each one of these stages are now presented:

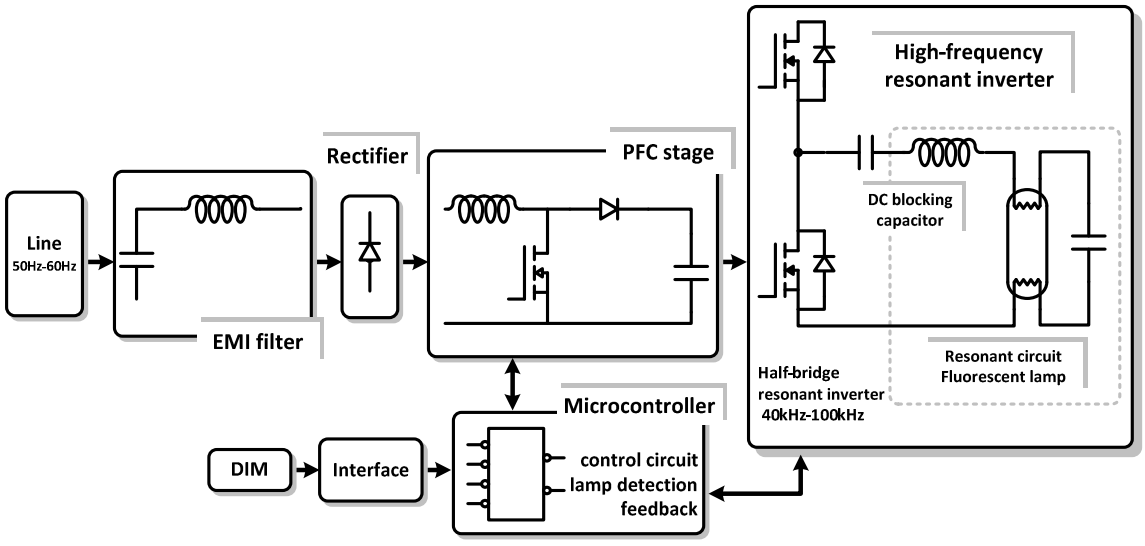

Fig.1.13. Electronic ballast schematic.

- *EMI filter.* EMI is a major concern with respect to the operation of all electrical equipment as it can affect its normal operation. Equipment containing high-speed processors, if not carefully designed and built, is notorious for emitting wide-band

electrical noise. On the other hand, it is also vulnerable to transient and surge voltages in the mains network. There are similar concerns regarding high-frequency lighting. In this case, there is a special concern regarding not only the electronic ballast, but the entire system, ballast, wiring, lamp and luminaire. In order to ensure that all electric and electronic equipment work correctly, the European Union has established some regulatory standards regarding electromagnetic compatibility (EMC), and manufacturers have a duty to provide equipment that does not cause undue interference and that is not unduly affected by it. EMI filters must not only protect against mains transients, but also comply with standards for harmonic currents emissions, and radiated and conducted interference [1.22].

- *Rectifier and PFC stage.* Electronic ballasts commonly use a full-bridge rectifier followed by a filter capacitor to generate an adequate dc voltage for the inverter. This first stage leads to high harmonics in the line current, low input power factor, and poor regulation. In order to improve the consumption of electrical energy and to provide agreement with power quality standards [1.35], electronic ballasts incorporate PFC techniques. An ideal power-factor corrector stage should emulate a resistor on the supply side while maintaining a fairly regulated output voltage. PFC techniques can be implemented using a two-stage or single-stage approach [1.36].

  Typically, in the two-stage approach, a switching-mode dc-dc converter precedes the resonant inverter. The dc-dc converter can be operated in CCM (continuous current mode), DCM (discontinuous current mode) or in the boundary of the two modes, depending on the chosen control technique: peak current control, average current control, hysteresis or borderline control [1.37]. Several topologies can be used, buck, buck-boost, flyback (allows high-frequency electrical isolation) or boost converter; however this last one is the most common adopted solution. This simple approach generally exhibits a near-unit PF and may deal with a wide range of line input voltage variations. Nonetheless, the main problem of the two-stage approach is the cost of the additional power stage. In the single-stage approach, the PFC stage is combined with the high-frequency resonant inverter, which means that one or more active power switches are shared by both converters, leading to a lower component count and reduced cost. In [1.36] and [1.65] distinctive integrated solutions are presented; the first one, an integrated boost, half-bridge resonant inverter for multiple fluorescent lamps operation, and in the second one, an integrated buck-boost current-fed resonant inverter for a CFL.

- *High-frequency inverter and resonant circuit.* These two stages are responsible for transforming the switching converter characteristics from a voltage source into a current source in order to ensure stable lamp operation at high frequency. As previously referred, the standard choice is the parallel-loaded half-bridge resonant inverter. To benefit the most of high-frequency operation, several aspects and technical issues must be considered during the design project of the entire ballast and especially of the inverter. The first, obviously, is the selection of the operating frequency. A high frequency will guarantee higher levels of luminous output and lower size and weight of the resonant elements used to stabilize the discharge. An initial lower boundary would be 20kHz, in order to avoid audible frequencies. But, video, audio apparatus, computers, and lighting installations are increasingly being operated with IR remote controls, using frequencies in the range of 30-40kHz. This fact will increase this lower boundary. So, in effect, commercial ballasts for fluorescent lamps typically operate between 40-100kHz. Higher levels of operating frequencies would lead to higher switching losses in the power MOSFETs, decreasing the overall efficiency of the ballast. Another important issue in the power control of the inverter is the study of the phase angle of the input current of the resonant circuit. A delayed current must be used in order to achieve zero voltage switching (ZVS) in the bridge MOSFETs.

  Other aspects directly related with these two stages are the control over the lamp or discharge current waveforms and the lamp starting procedure. In order to ensure maximum lamp life, it is important to drive the lamp with symmetrical alternating currents, thus making use of both electrodes alternatively. A related important parameter is the *current crest factor*, which is the ratio of the peak value to the rms value of the lamp current. A value close to $\sqrt{2}$ implies that the lamp current waveform is equivalent to a sine wave, which would correspond to the ideal situation. In order to avoid early aging of the lamp it is usually recommended a lamp current crest factor lower than 1.7.

  The starting procedure is typically controlled by the inverter. During the description of the basic fluorescent lamp mechanisms it was referred the importance of the ignition process. In classical fluorescent lamp tubes, the electrodes must be warmed up to the emission temperature and no high-voltage should be applied until they reach the right temperature level, thus avoiding sputtering damage. Once they reach that level, the starting voltage can be applied to ignite the lamp [1.8]. Considering the half-bridge parallel-loaded resonant inverter, the heating procedure and lamp voltage can both be

controlled by slightly changing the operating frequency. If the circuit is operated in inductive mode, thus ensuring soft-switching, a higher frequency results in a lower voltage applied to the lamp, enough to pre-heat the electrodes when the lamp is still off. If the frequency is then decreased from this higher value, resonance can be reached and a high voltage can be applied to the lamp, guaranteeing its ignition [1.66]. To avoid undesirable starting conditions, this voltage must also be limited to its minimum value. This process, normally implemented with a closed-loop system, will further be addressed in future chapters.

- *User interface, control and protection circuit.* These stages contain all the necessary sensors and intelligence to manage the mains input and lamp output functions of the electronic ballast, such as the preheating and ignition process, lamp power control or other additional control features, stop circuit or safety switch-off, output over-voltage or over-current protection, end-of-life detection and lamp failure protection. Depending on the complexity of the ballast or the pretended installed system, it can vary from very simple circuits to more complex circuits involving microprocessors, which is now common in most of the commercial solutions.

In the case of CFLs, the electronic ballast is retrofitted into the existing lamp socket. These ballasts are similar to the previous ones but generally, in low-power versions, the PFC stage is excluded from the ballast configuration, which results in a non-sinusoidal ballast current [1.2]. Electronic ballasts for multiple lamp operation can also be designed, by replicating the combination resonant inductor plus lamp, and connecting them in parallel. Each lamp is controlled separately, and failure of any one lamp will not affect the operation of others. There are other solutions which replicate not only the resonant circuit but also the high-frequency inverter [1.36]. Commercial ballasts typically present solutions for the simultaneous control of two or four lamps.

1.2.5 CONTROL SYSTEMS

At the present time, lighting projects should be designed according to the worlds' economic circumstances, increasing budget limitations and increasing efficiency demands. In addition, there is growing evidence that personal control over lighting is a key determinant for office-workers environmental satisfaction and productivity. It is also clear that lighting requirements in public, commercial, office buildings and even in residential houses change constantly. In fact,

there is a real commercial need for safe, reliable, versatile equipment which simultaneously avoids future costs and offers flexibility to the worker or consumer, and this is difficult to be provided by conventional ballasts.

In most cases, the key for an intelligent, high-performance, light management in a local zone, is the use of a more or less sophisticated control system. For an adequate task lighting or visual comfort, messages for lamps switching and dimming must be transmitted from the user to the electronic ballasts. These messages can be generated manually, through switches or transmitters, or automatically, through light sensors, movement detectors or computer programs. Presently, there are several options which make it possible to regulate more than fifty ballasts simultaneously [1.4], [1.6].

The most common interface on the market is the analogue 1-10V DC dimming interface. In this control system, the communication is unidirectional. The system tells, each ballast, what to do, using the dc level imposed on the control circuit. This analogue interface, although sufficient in most applications, has some major drawbacks: ballast feedback is not possible, there is a signal degradation on long lines, the control only sets the lamp power level (switching must be done by a separate control circuit) and there is a poor definition at minimum light levels (different ballasts can give different light levels at the same control voltage).

In order to avoid some of these drawbacks and establish a new and simple alternative, some of the leading European lighting companies started, almost two decades ago, to work on a new digital interface. These companies were then followed by other lighting manufacturers and an international standard for digital communication in lighting was developed: the DALI protocol. This Digital Addressable Lighting Interface is now available for all T5 lamps and CFLs. The key feature of this interface is the possibility to individually address all ballasts included in a lighting system, by connecting them in parallel to a two wire control line. Since it is an open protocol, it is also possible to interconnect ballasts from different manufacturers.

The DALI protocol supports a variety of commands, namely: light level setting (dimming), remote switching (on/off), storing and recalling pre-set light levels (light scenes). These commands can be addressed to a single ballast, to a group of ballasts or to all the ballasts connected to the two mandatory control lines, to a maximum of 64 individual addresses, as shown in Fig.1.14. Besides these commands, there are also query modes for problem diagnosis, such as query status and query lamp failure. Additional commands are used for assigning addresses and group numbers and there is also a category of reserved codes for future extensions

to the command set. Considering a single DALI interface, the maximum number of ballasts which can be controlled is 125. This is only possible if they do not all require different addresses. These ballasts can also be distributed into a maximum of 16 groups for independent control. So this means that lighting scenarios can be programmed, either individually or by groups.

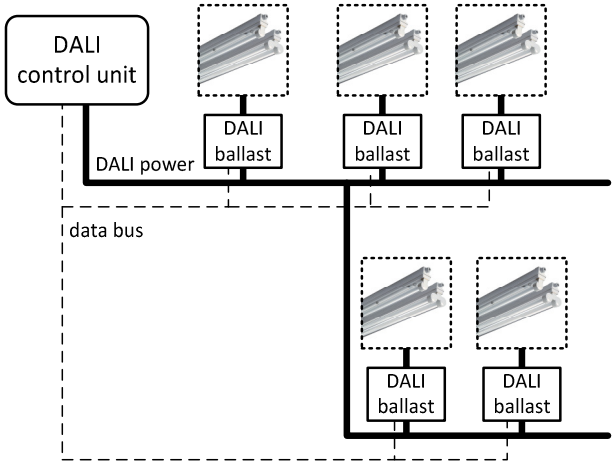

Fig.1.14. Installation of a **D**igital **A**ddressable **L**ighting **I**nterface (DALI) system.

A typical architecture of a digital ballast is presented in Fig.1.15 [1.23]. The microcontroller is the central unit of the digital ballast. It receives commands from the DALI control lines via a transceiver unit, which is typically a voltage scaling and protection unit. Two separate converters are used to control the lamp; the first one to drive the lamp with a sinusoidal current and the second one to drive the electrodes. Both converters receive their drive signals directly from the microcontroller, which in turn receives signals from the sensors in the power circuit regarding the lamp current and lamp voltage. Since both arc and electrode currents are uncoupled, they can be controlled separately, improving lamp and electrode efficiency. The microcontroller is also responsible for storing specific data if the ballast is disconnected from the mains.

Summarizing, some of the main advantages of these digital ballasts are:

- *Feedback signals.* Ballasts can report any problems such as lamp failure on request.
- *Flexibility and simplicity.* Changes often require only software adjustments. All ballasts can be controlled individually, by the same two-wire control connection. In terms of ballast design, all control loops and signal processing are performed by the microcontroller, implying a reduced component count, better accuracy and miniaturization.
- *Controllability.* Users can pre-set a light scene, dim, switch on or off lamps or groups of lamps, using additional software via remote control. Since the DALI interface is

integrated into the ballast, this action can be done with a high-level performance rate. Since it is an open protocol, different company ballasts can be controlled and co-exist on a DALI network.

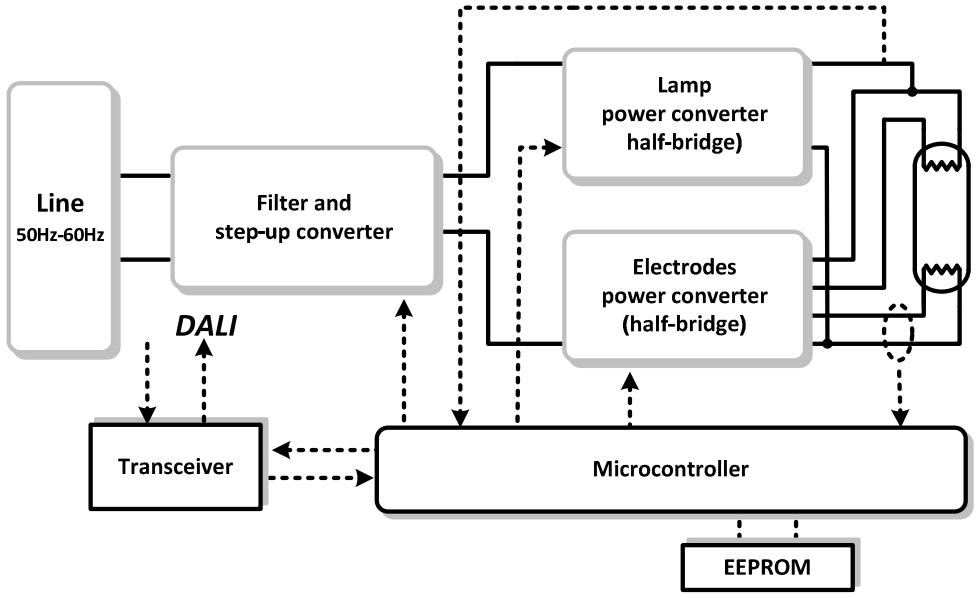

Fig.1.15. Architecture of an electronic ballast with DALI [1.23].

There is another protocol for digital communication between controllers and dimmers: the DMX protocol. DMX is typically used in theatres and show rooms and it was initially specialized in creating and controlling lighting scenes by allowing lighting equipment, from different manufacturers, to be used together. However, it soon became the primary method for connecting not only controllers and dimmers, but also more advanced fixtures and special effects devices such as fog machines and moving lights. More specifically the DMX512 protocol was initially developed by the Engineering Commission of United States Institute for Theatre Technology and was then revised by the Entertainment Services and Technology Association in order to provide the current ANSI standard. Physically, the DMX512 is a bus network with no more than 1200 meters long, and no more than 32 devices on a single bus. If more than 32 devices need to communicate, the network may be expanded across parallel buses using DMX splitters [1.24].

1.2.6 SPECIAL TYPES OF FLUORESCENT LAMPS

There are also several special types of fluorescent lamps, for instance the electrodeless lamp, the cold cathode fluorescent lamp, CCFL, and more recently some new mercury-free fluorescent lamps.

The earliest electrodeless lamps were invented over 100 years ago by J. J. Thomson, Tesla and others. However, the single commercially available electrodeless fluorescent lamp is based on an induction discharge, which implies a magnetic coupling between the circuit and the plasma. This is the reason why this lamp is commonly known as the induction lamp. Typically, a coil is superposed on a tube with fluorescent coatings to convert the UV radiation into visible light. An alternating current through that coil produces a magnetic field in the discharge space which then produces an electric field, ultimately responsible for the discharge. The optimum operating frequency of the system is in part determined by the efficiency of coupling energy from the coil into the plasma and the EMI regulations [1.2], [1.25]. These lamps operate at very high frequency, reaching even values of 1MHz, meaning that only over the past two decades, with the advances in high-frequency power converters, was it possible for them to be a real cost-effective alternative [1.27].

In fact, one of the main advantages of the electrodeless lamps is that all the problems associated with electrodes are avoided. Starting can be instantaneous, therefore they can be switched any number of times. They also have the possibility of providing higher power, since there are no constraints regarding maximum electrode current and electrode losses. These factors clearly increase their average lamp life, rated over 60000 hours. They can also work at lower pressure levels, not recommended for regular fluorescent lamps since internal pressure reduction results in high evaporation of the emissive material [1.26]. In terms of environmental related issues, there are other advantages: easily recycled, less pollution, because instead of using liquid mercury they use amalgam (solid mercury composition with other metals), easy to remove if the lamp is recycled and finally a high average lamp life due to the absence of electrodes, which in turn decreases maintenance and replacement costs.

Cold-cathode fluorescent lamps, CCFLs, whose electrodes are not preheated, are also available and commonly used in backlight liquid crystal displays (LCDs) in TV and PC monitor applications. Besides straight tubes, there are also U-tubes and L-tubes, for other different applications. Cold-start ignition is obtained by applying an especially high initial voltage to the lamp electrodes, which in turn must be very robust [1.22]. The cold-start lamp will ignite the moment that this voltage is applied, and for this reason they are also referred to as instant start lamps. In order to reduce, as much as possible, the ignition voltage, the two electrodes are brought closer together by special construction features. Usually, a conductive strip connects both electrodes, creating a local high electric-field strength for breakdown. Since these lamps operate at lower current levels, it is possible to reduce the electrode heating losses in order to extend the

life of the electrodes, so normally they have a higher average lamp life [1.28]. Typically CCFLs are more efficient than comparable hot cathode fluorescent lamps. A disadvantage is related to the eventual user exposition to the mains voltage: if one lamp end has already made contact during the lamp insertion and the user touches the other end. For this reason, these lamps are fitted with special caps. Even if high brightness LEDs are currently considered as an effective alternative for backlight sources, CCFLs are still the main stream in large size LCDs. The key reason is the manufacturing process of LEDs, which until now is not capable of producing completely identical HBLEDs [1.29].

Environmental awareness intensified the development of new mercury-free fluorescent lamps. Although the Xenon is one of the most promising candidates for mercury substitution, its discharge tends to constrict, which drastically drops the lamp efficacy at high power [1.30]. Examples are mercury-free flat fluorescent lamps, MFFFL. These lamps are suitable for backlight source applications. They present high colour saturation and contrast which improves the image quality of LCDs. This technology however is still in the development stage [1.29].

1.2.7 FLUORESCENT-LAMP MODELS

Discharge-lamp modelling is an important domain in lighting related research. Numerical low-pressure-discharge-lamp models, which accurately simulate the real behaviour of fluorescent lamps, are extremely necessary from two points of view. Firstly it is important to translate the physical mechanisms which occur inside the glass tube, in order to guide lamp manufacturers in the search for more efficient light sources, and secondly it is also important to describe the electrical terminal characteristics of these lamps in order to use this behaviour in the design and conception of electronic control gear.

A wide literature search reveals that there are several types of fluorescent-lamp models. Examples of models which are representative of the physical behaviour of the lamp can be found in [1.39], [1.40] and [1.41]. These physical models generally involve the rate equations and simplified assumptions on the electron energy distribution function [1.38]. They are usually quite complex due to the complicated nature of the physical process itself. In [1.39], the proposed physical model can be used to simulate any low-pressure mercury-buffer gas fluorescent lamp, over a wide range of operating frequencies, by entering key lamp parameters. These parameters are: length, radius, cold-spot temperature and buffer gas fill pressure. If this pressure is unknown, a default value dependent on the lamp radius can be used. Even if the model can describe the

lamp behaviour under transient conditions, it cannot correctly predict the breakdown stage. Moreover, the model only considers the positive column, ignoring the electrodes behaviour. From the electrical research engineer point of view, it is more attractive, or even simpler, to use fluorescent-lamp models which are able to predict the electrical characteristics at the lamp terminals, without entering the subject of complex physical equations. Such models are preferably used to perform optimization studies in the design of electronic ballasts. Despite the selected models, circuit-simulation programs such as SPICE or MATLAB-Simulink are the commonly chosen implementation environments [1.39], [1.45], [1.56].

As previously described, fluorescent lamps are nonlinear light sources that in parts of the $V(I)$ characteristic exhibit a dynamic negative differential resistance behaviour: the rms value of the lamp current increases with a slight decrease in rms value of the lamp voltage. This is the reason why some researchers have used a fixed resistance model for simulating the fluorescent-lamp behaviour. These models are based on the static characteristics of the lamp and they typically use linear approximations. This is one of the simplest ways to model the lamp, but it has a clear disadvantage, it can only be used to design electronic control gear at specific conditions, for example at nominal power. In fact, in the normal operating range, the negative dynamic resistance of the lamp is dependent on the average lamp power. Therefore, specific models which vary the lamp resistance with the average lamp power are in fact the most suitable for the majority of studies. It is a fact, however, that these models are purely based on the empirical behaviour of the lamp, which means that they are only applicable over a narrow range of operating conditions, centred mainly on the characteristics which are easily identified when collecting the necessary data [1.39]. Consequently, most of these models are power-dependent models, generally based on polynomial or exponential functions, applied using curve-fitting techniques, which describe the lamp impedance or conductance behaviour of the lamp [1.42]-[1.48]. A main goal should be the definition of a dynamic model capable of describing the lamp behaviour at different frequencies, at different dimming levels and eventually under transient conditions.

1.2.7.1 LARGE-SIGNAL DYNAMIC MODELS

One of the earliest models was proposed by U. Mader and P. Horn in 1992, and is commonly known as the Mader-Horn model [1.42]. The model is based on the observation that in the full process of creating visible light, the mechanisms occurring inside the tube are very fast except for the generation of the ionized mercury atoms from the applied electric power. This mechanism has

a conversion rate of approximately 1ms. So, in the model, the ionization density, ρ, is assumed to be related to the instantaneous lamp power, p_{lamp}, by a so-called "recent running average". In terms of the Laplace transform, this relation can be defined using a first-order low-pass filter:

$$\rho(s) = C\frac{1}{1+\tau s}p_{lamp}(s) \tag{1.1}$$

where C is a proportionality constant and τ is the ionization recombination time constant. The previous equation can also be defined as follows:

$$p_{lamp}(t) = \frac{1}{C}\left(\rho(t) + \tau\frac{d\rho(t)}{dt}\right) \tag{1.2}$$

In order to simplify this equation, the constant C and the ionization density ρ are replaced by an average lamp power, P_{lamp_avg}, which in fact is the low-pass-filtered version of the instantaneous lamp power, p_{lamp}:

$$P_{lamp\_avg}(s) = \frac{1}{1+\tau s}\left(p_{lamp}(s)\right) \tag{1.3}$$

So, by measuring the $v(i)$ characteristics of the lamp, at dc and at several high-frequency values, using for instance, a commercial dimmable electronic ballast, it is possible to model these curves trough a function describing the dependence of the lamp voltage to the lamp current (more specifically the arc current), with the average lamp power as parameter, $v = f(i, P_{lamp\_avg})$. An example of theses curves can be seen in Fig.1.16. The analysis of these curves clearly reveals that a different average lamp power will correspond to a different lamp resistance value. Besides, it is also clear, that the high-frequency lamp characteristics are non-linear. The dc characteristic of the lamp can be measured using a large variable resistor in series with the lamp supplied by a dc voltage source with a voltage level which doubles the lamp voltage.

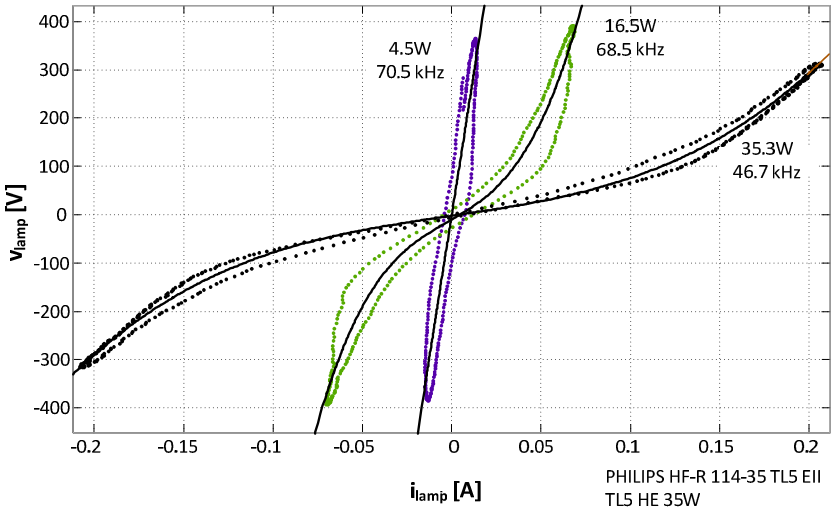

Fig.1.16. High-frequency $v(i)$ characteristics of a TL5 HE 35W fluorescent lamp at different power levels.

So finally, the model is based on the following equations:

$$p_{lamp}(t) = v_{lamp}(t) \cdot i_{lamp}(t) \tag{1.4}$$

$$p_{lamp}(t) = P_{lamp_{avg}}(t) + \tau \frac{dP_{lamp_{avg}}(t)}{dt} \tag{1.5}$$

$$v_{lamp}(t) = f(i_{lamp}(t), P_{lamp_{avg}}(t)) \tag{1.6}$$

The purpose is then to find out the function f. Mader and Horn proposed two different approaches. The simplest version is to use a first-order linear resistance model and the second approach is to use a third-order polynomial resistance model:

$$v_{lamp}(t) = R(P_{lamp_{avg}}(t)) \cdot i_{lamp}(t) \tag{1.7}$$

Accordingly, the simplest version states that at high frequency, the lamp impedance can be estimated in steady-state as:

$$R(P_{lamp_{avg}}(t)) = \frac{V_{lampDC}^2}{P_{lamp_{avg}}(t)} \tag{1.8}$$

If dynamic studies are intended the following adjustment must be done:

$$v_{lamp}(t) = f\left(i_{lamp}(t), P_{lamp_{avg}}(t)\right) = \frac{V_{lampDC}^2}{P_{lamp_{avg}}(t) + P_{lamp0}} \cdot i_{lamp}(t) \tag{1.9}$$

where V_{lampDC}^2 represents the dc lamp voltage and P_{lamp0} is an average power offset. The reason why P_{lamp0} is included in (1.9) results from the fact that the resistance of the lamp is infinite when the lamp power is zero. Due to possible convergence problems in terms of numerical simulations, an average power offset must be included in the denominator. In the cubic version of the model, expression (1.9) assumes the following form:

$$\begin{aligned} v_{lamp}(t) &= f\left(i_{lamp}(t), P_{lamp_{avg}}(t)\right) \\ &= A\left(P_{lamp_{avg}}\right) \cdot i_{lamp}(t) + B\left(P_{lamp_{avg}}\right) \cdot i_{lamp}^3(t) \end{aligned} \tag{1.10}$$

where functions A and B are empirically determined using specific points of the experimental high-frequency $v(i)$ characteristics of the lamp. A is the slope of the high-frequency characteristic at the origin, and B adjusts the nonlinear upward bend. The main disadvantage of this model is the fact that different coefficients are needed if the model is planned to simulate the high or low-frequency behaviour [1.39], [1.3]. The model parameters can be adjusted so that the dc characteristics are better modelled, but the high frequency characteristics are then no longer well modelled, since the fluorescent lamp does not follow the same function independent of frequency [1.42]. In [1.44] M. Sun and B. Hesterman suggest an alternative approximation to functions A and B in order to avoid convergence problems found when using the Mader–Horn lamp model.

T. F. Wu proposed in 1995 another fluorescent-lamp model [1.43]. The so-called plasma model was expected to simulate the lamp behaviour at high frequencies. It is based on the observation that, for a given high-frequency rms current, the lamp behaves, to a first approximation, as a pure resistor. The model is easily obtained from a two parameter equation:

$$v_{lamp}(t) = R_{lamp}(t) \cdot i_{lamp}(t) = \left(R_s + \frac{V_H}{I_{arc}}\right) i_{lamp}(t) \tag{1.11}$$

where R_s and V_H are lamp constants and I_{arc} is the rms current through the lamp. The first two parameters can be measured from experimental data, using the rms $V(I)$ characteristic of the lamp as previously shown in Fig.1.9. These measurements are approximately distributed along a line. Thus, a line equation can be used to model the lamp. The lamp constants, R_s and V_H are

respectively the slope of the line and the intersection of the line with the voltage axis. A convergence problem is also present because the resistance of the lamp is infinite when the lamp current is zero. Therefore, it is necessary to set an initial condition for the lamp current. In [1.45], Ben- Yaakov states that this model cannot cope with a change of operating conditions, such as a power level variation, during a given simulation run. In fact, the main problem of this model is the fact that it only works in steady-state conditions and within a certain frequency range.

Evidently, there are multiple options for fluorescent-lamp models, all based in similar observations but using better or more advanced curve fitting techniques. In [1.46], C. S. Moo proposes a model with power and temperature dependence for high-frequency operation. As previously referred, the electrical characteristics of the lamp are sensitive to temperature variations. Considering an electronic ballast designed to operate in a wide temperature range, having a model capable of coping with these changes is obviously an advantage. In [1.49], the model presented by H. Cheng also includes the electrodes resistance. Models using the lamp conductance are also extremely popular [1.47]. In [1.50] a cubic-spline interpolation-based method for modelling the lamp dynamic conductance is proposed. This method is based on a spline constructed of piecewise third-order polynomial which passes through a set of data points without knowing the slopes. In [1.48] a comparison is proposed between different physical models also based on the lamp dynamic conductance, by referring to theoretical exponential and polynomial models. More recently, it is also possible to identify models which simultaneously include physical and circuit equations. In [1.51] several equations are proposed which model the thermal conduction and radiation losses, the electron temperature, the lamp resistance (as a function of the electron temperature and the Boltzmann constant). A final circuit equation considering a 50 Hz driving circuit (series electromagnetic ballast) is also proposed. After the adjustable model constants are determined at 50 Hz, using a genetic algorithm, the model is then applied to high-frequency operation with agreeing results.

In the case of CFLs similar techniques may be applied. The terminal electrical characteristics of the lamp are measured and curve fitting techniques are used to process the data. The implementation and verification of different CFL models can be found in [1.52]. An exponential model which characterizes the rms $V(I)$ characteristic of a 42W CFL lamp and two physically-based models, Mayr and Cassie models, are analysed. However, if the purpose is to conduct performance analyses, the main concern is the behavioural impact of the widespread utilization of such light sources on the grid. CFLs are considered to be harmonic sources due to the high level of THD in the ac current. A typical electronic ballast circuit is the single-phase capacitor-filtered

uncontrolled ac-dc converter, followed by a high-frequency inverter. So, the goal is not to model the lamp itself but to provide a CFL harmonic model capable of simulating the power-quality impact of these lamps in order to perform large-scale harmonic penetration impacts. Such models can be found in [1.53], [1.54].

Modelling CCFLs is a different challenge. Physical and circuit models are also available. Circuit models are normally preferred for steady-state analysis due to their simplicity. In [1.55], a simple exponential model is used to characterize the rms $V(I)$ characteristic of the lamp. However, these lamps are somehow different from tubular fluorescent lamps since the mechanism of electron emission is different and since they operate at much higher voltage and much lower current. This lower current, translated into low heating losses in the electrodes, is the reason why it is possible to extend their life making them suitable for LCD devices. The required high electrode voltage to cause breakdown is the key issue in some of these models and the accuracy in predicting the electrode voltage drop will influence the model precision. As mentioned in [1.56], the electrode voltage drop may be experimentally determined or theoretically derived. D. Lin and W. Yan propose a simple, non-intrusive method to identify the electrode voltage drop inside the CCFL, using the so-called lamp operating voltage method. The measured lamp operating voltage is the sum of the electrodes voltages and the positive column voltage. A genetic algorithm and a piecewise function are then used to estimate and to model the optimal electrode voltage drop. The following assumptions are considered: contrary to the hot cathode fluorescent lamp, where the electrode voltage is assumed as a constant value, the CCFL shows a voltage which is a function of the discharge current, and that presents a specific shape (combination of two parabola curves and one straight line). Finally, as in [1.51], the same authors use physical and circuit equations to model the whole system, including now the modelling function of the electrode voltage.

A distributed-circuit model of a CCFL back-light unit (BLU), for an LCD device, is proposed in [1.57]. Simulation results are compared to a set of experimental results retrieved from a physical system consisting of a CCFL BLU for a 42 inches LCD. The model consists of a circuit model for the lamp itself, and uses capacitors and inductors to represent the parasitic elements of the lamp, the coupling between the lamps and the coupling between the lamp and the frame of the back-light unit. The lamp model is obtained using two current-controlled current sources. These current sources are controlled by two additional sub-circuits, responsible for modelling the heating and ignition effects, and three voltage-controlled variable resistors, responsible for implementing the dc $V(I)$ characteristics of the lamp. The lamp model parameters are obtained

through laboratory tests and the parasitic inductances and capacitances are calculated using a three-dimensional electromagnetic solver.

1.2.7.2 SMALL-SIGNAL DYNAMIC MODELS

Small-signal models are normally used in analytical and simulation studies where the main concern is the dynamic response and stability of the lamp-ballast system. With these models it is possible to use the classical control theory and to apply stability criteria to verify whether the system is stable or not. These models are focused in the characterization of the lamp small-signal dynamic impedance, or more specifically, they are focused on the change of the lamp's operating point or on its negative incremental impedance.

The origin of these small-signal dynamic models relies on the model proposed by E. Deng and S. Cuk in 1997 [1.58]. Deng and Cuk proposed to study the incremental impedance of fluorescent lamps, in the frequency domain. As represented in Fig.1.17, the steady-state behaviour of the lamp can be modelled by a linear resistance, represented by the straight lines A-O or B-O through the origin which have a positive $V(I)$ slope. As observed by Ben-Yaakov *et al* in [1.59], for a fast current change the resistance will remain the same. Fast current changes do not significantly alter the density of carriers in the plasma and the resistance of the lamp remains constant. However if a slow current change is considered, the density of the carriers changes and the resistance shifts: the rms operating point will then move along the A-B line. The A-B curve, which has a negative dV/dI slope, helps to describe the small-signal change of an operating point or its incremental behaviour. The response to this change is associated with a low-frequency time constant that controls the rate at which the incremental impedance of the lamp is varying [1.59]. So, instead of characterizing only the lamp steady-state behaviour, its slow dynamics may also be characterized through its negative incremental impedance.

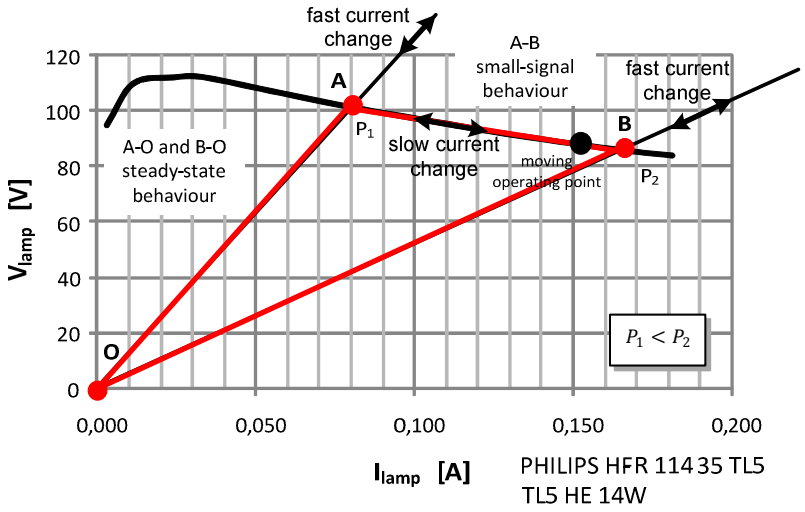

Fig.1.17. Steady-state and small-signal behaviour: negative incremental impedance definition [1.58], [1.59].

To study this behaviour, a sufficiently small perturbation may be applied around the lamp operating point. Deng and Cuk notice that, if the lamp is driven with a high-frequency sine wave, and then exposed to slow-varying perturbation signals, the amplitude of the lamp voltage and lamp current may both be modulated by the small-signal modulating angular frequency, ω_m. Thus, the incremental impedance of the lamp may be defined as the ratio of the slow-varying signals which modulate the lamp voltage and the lamp current, respectively. The applied small-signal perturbation will also result in a phase difference between the voltage and current envelopes. So typically, the incremental impedance $\underline{Z_l}$ is defined as:

$$\underline{Z_l}\,(j\omega_m) = \frac{|\hat{v}|}{|\hat{\imath}|}\,\angle\phi \tag{1.12}$$

where $\hat{v}$ and $\hat{\imath}$ are respectively rms values of the small-signal lamp voltage and lamp current perturbations [1.58], [1.3]. By varying the perturbation frequency it is also possible to experimentally determine a *Bode* plot, representing the magnitude and phase of $\underline{Z_l}$ as a function of frequency, or the *Nyquist* plot, as shown in Fig.1.18, representing the frequency response of the magnitude and phase of $\underline{Z_l}$ in polar coordinates. The typical *Nyquist* plot of the discharge lamp reveals that when $\omega_m = {}^{s}/_{j}$ is close to zero, $\underline{Z_l}\,(j\omega_m)$ or $Z_l(s)$, has a negative value, with a phase of 180º. As the modulating frequency increases, the magnitude of $Z_l(s)$ increases but its phase decreases. When ω_m approaches the lamp operating frequency, $Z_l(s)$ is close to a positive value and its phase near 0º. The slope of the A-B line previously represented in Fig.1.17 corresponds to the dc value of the incremental impedance, $Z_l(s)|_{s=0}$. This implies that

$Z_l(s)|_{s=0} < 0$ since the slope in the $v-i$ plane is negative. When ω_m approaches the lamp operating frequency, $Z_l(s)$ is close to the positive slope of the A-O line, so $Z_l(s)|_{s=j\omega_s} > 0$

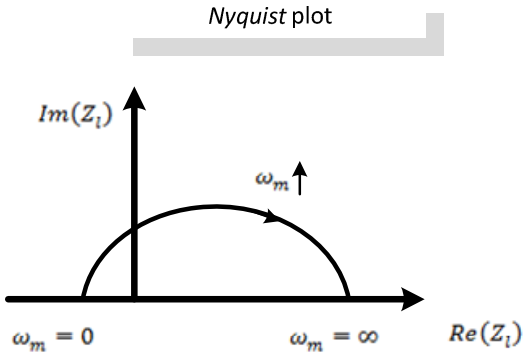

Fig.1.18. Typical plot of the lamp incremental impedance in the complex plane [1.58].

Experimentally, Deng and Cuk also proposed to model the incremental impedance behaviour using a simple single-pole, single-zero transfer function:

$$Z_l(s) = k_1 \frac{\frac{s}{z}+1}{\frac{s}{p}+1} \tag{1.13}$$

where k_1 and z are negative constants and p a positive constant. This function is considered appropriate for fitting the experimental measurements retrieved from most of the selected discharge lamps. According to traditional control theory, if an impedance has a zero in the positive half plane it cannot be driven directly by a voltage source. This agrees with the fact that the discharge lamp can be directly driven by a current source and not by a voltage source [1.60]. The constant k_1 should coincide with the slope of the steady-state behaviour of the lamp. Then, with both small-signal models, of the lamp and of the ballast equivalent circuit, the stability and interaction of the lamp-ballast system may be analysed. The stability analysis is performed applying the *Nyquist* criteria.

In [1.61], the stability of a CCFL LCD backlight inverter system is discussed. As suggested by Deng and Cuk, the authors study the CCFL incremental impedance by applying a perturbation which is sufficiently small in magnitude, around its operating point. As usual, the incremental impedance is defined as the ratio of the slow varying signals which modulate the lamp voltage and the lamp current, respectively. After several experimental acquisitions, it is noticed that, at a certain modulation frequency, the lamp voltage responds to the lamp current not instantly, but after some time delay. At several operating conditions, this time delay was observed to be almost

constant. Therefore, the authors concluded that this time delay is one of the characteristics of the lamp and would be noticed on its incremental impedance at high frequencies. By studying the phase of the incremental impedance, which is directly obtained from the observed time delay, and the output impedance of the inverter, the authors verify the stability of the system. This study is conducted at different operating frequencies, and with different resonant inverter parameters. Similarly, in [1.62] and in [1.63] a small-signal stability analysis of CCFL systems is also performed. The type of ballast is however different. In recent years, CCFL-ballast systems normally include a piezoelectric transformer instead of a magnetic transformer (typically used for isolation purposes and voltage matching). Particularly, in [1.62], it is analysed the implications of the thermal operating conditions on the stability of such systems. In this case, the so-called incremental impedance of the lamp is defined as the envelope impedance, which is also the ratio of the envelope of the lamp voltage to the envelope of the lamp current, when the system is driven by an AM modulated signal.

In [1.64] a method is proposed to characterize and evaluate the stability of a CFL-ballast system in dimmed operation. Most of the models are only focused on the lamp small-signal dynamic behaviour at nominal power level. This implies that the incremental impedance can only be used to analyse the lamp-ballast interaction at nominal power. However, in dimming ballasts, the interaction between lamp and ballast can also lead to system instability at reduced power operation. So, it is also important to observe and verify eventual non-stable conditions at all power levels. This is obviously an important application for these small-signal modelling systems. This is the main concern in [1.64]. At each power level, the parameters of the single-pole, single-zero model are obtained. The static gain, pole and zero values of the model are calculated and fitted to a power dependent polynomial expression. In this case, instead of using directly the small-signal impedance, a function of the small-signal variation of the lamp equivalent resistance, $\hat{R}_{lamp}$, against the lamp power perturbation is used, $\hat{P}_{lamp}$. Through the combination of the small-signal models of the lamp and ballast circuit, the small-signal lamp-ballast system transfer function and corresponding loop gain are obtained. The stability analysis is also performed applying the *Nyquist* criteria.

1.3 DIMMING IN FLUORESCENT LIGHTING SYSTEMS

Naturally, one of the most important features in modern lighting systems is the capability of controlling the luminous flux level of a light source. It is now obvious that for an intelligent and

cost-effective light-management system, a reduction of the power consumption is not synonym of turning off the lights completely. Developing an efficient dimming technology, while guaranteeing adequate task lighting and visual comfort, has been a determinant goal over the last two decades for the lighting industry, especially in fluorescent lighting systems.

1.3.1 STEP DIMMING AND CONTINUOUS DIMMING

From the start, dimming was divided into two categories: continuous dimming and step dimming. While the first is generally understood as a technology capable of dimming the lamp from 100% of light output down to approximately 1%, without interruptions, the second one provides a discrete reduction of the light output level according to some predetermined levels.

Typically step dimming systems are based on bi-level switching: 100% or 50% of light output, with also the possibility of shutting down the lamp. Usually the control is provided by two switches connected between the input mains and the ballast. Both switches must be on the same phase for proper application of step functionality. In these applications, the lamp must be ignited to either 100% output level or 50% output level without going first to the nominal power. These ballasts generally have programmed-start circuitry to guarantee extended lamp life in frequent switching applications, like those associated with the use of occupancy sensors or motion detectors. It is clearly a system that provides specific light control and some energy savings, but does not offer the same freedom that continuous dimming offers. Even if there is some research on step-dimming, [1.68], and there are some specific products on the market for fluorescent lighting systems [1.69], similar types of discrete dimming are more popular for HPS lamps for street lighting and outdoor operation. So, in terms of fluorescent lighting and from the market point of view, there is a clear preference for products allowing a broad range of control, and smooth continuous dimming.

1.3.2 DIMMING TECHNIQUES

Except for very-low-power dimming levels, the lamp voltage does not change significantly. This is a common behaviour to all fluorescent lamps. An obvious conclusion is the fact that the lamp power, and consequently the luminous flux level, can simply be varied by controlling the lamp current. So, up to now, the proposed dimming techniques use different control parameters which have an immediate effect on the lamp current.

As stated earlier, in order to comply with international standards such as the IEC 1000-3-2, most of the existing ballasts usually exhibit a PFC stage followed by a high-frequency resonant inverter as the one represented in Fig.1.19. In some occasions, a single-stage approach is implemented, but the two-stage approach presented in Fig.1.13 is also common. In that case, the connection between the two stages is made by a dc-voltage bus, using for instance a simple electrolytic capacitor. Typically, there are three different techniques for adjusting the lamp current and consequently the luminous flux level [1.67]-[1.73]. The first one is to control the value of the dc voltage applied to the inverter, V_{dc}. The others are: to control the inverter operating or switching frequency, f_s, or to control the duty-cycle of the inverter switches, D.

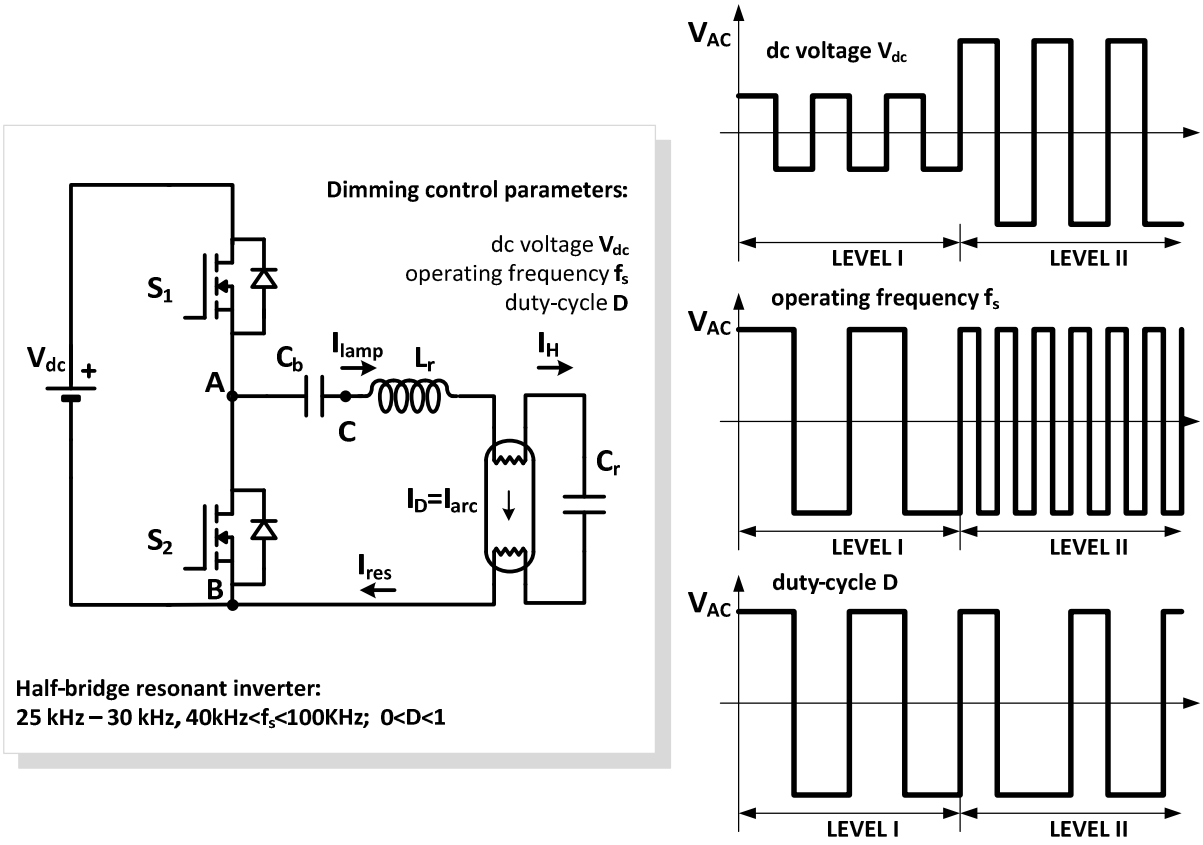

Fig.1.19. Dimming control parameters: dc voltage, operating frequency and duty-cycle.

These dimming techniques have obviously specific technical and implementation issues, some advantages and disadvantages:

- *Dc voltage control.* This first dimming technique is capable of providing a smooth and broad range of dimming control, by using an additional power stage which is capable of supplying the inverter with a variable dc voltage. As an example, the patented scheme described in [1.70], uses an ac-dc converter with power factor correction, capable of

producing a variable dc output between 20V and 300V which is then applied to the inverter. As stated, this converter may comprise a diode-bridge rectifier, followed by a flyback converter or some similar solution which also enables PFC. A decreasing dc voltage will result in a decreasing inverter output voltage, decreasing the lamp current, and consequently, also decreasing the lamp power.

A major characteristic of this technique is the fact that the lamp current is roughly proportional to the dc voltage, which gives an almost linear control over a wide lamp power range. Also, the half-bridge inverter is operated at constant frequency and the switches are operated at constant duty-cycle, around 0.5. The constant-frequency operation makes the switching control and the EMI filter design easier, and the resonant circuit can be optimized for a given type of lamp.

In addition, as stated in [1.67], the resonant circuit can be designed to operate with zero-voltage switching (ZVS) under a fixed frequency, over a wide dimming range. ZVS is desirable because it reduces the turn-on switching losses and minimizes the electromagnetic interference from the power switches. The operating frequency is set at a slightly higher value than the circuit resonant frequency, also minimizing the consumption of reactive power.

A known limitation is the fact that it can be difficult to ensure good lamp soft-starting by using only this control variable, if the electrodes are not separately heated. So, this method can be, in some cases, an impractical commercial solution. Another observation is the fact that, at low dimming levels, the voltage across the lamp will raise. So, low operating dc voltages will correspond to a higher voltage at the lamp terminals. Since the lamp will be operated near resonance the losses will be higher [1.72].

- *Duty-cycle control.* The ideal duty-cycle of the switches S_1 and S_2, should be slightly less than 0.5 so that a small dead time (off-time for both switches) is available to avoid short-circuiting the input [1.67], [1.70]. But, varying the duty-cycle of the switches allows controlling the pulse width of the voltage waveform at the output of the inverter, which means controlling its rms value and consequently providing a variable rms current through the lamp. The advantage of this technique is the constant-frequency operation. However it also presents some major drawbacks, one is the non-sinusoidal, asymmetrical lamp current waveform [1.71]. Another drawback is the high harmonic content of the modulated square waveform, which can also produce high EMI.

This can be implemented in two different ways [1.72]. One is to vary the on-time of the switches in the same manner. This means equal dead-time for both switches and makes it impossible to realize ZVS for all the dimming levels. If the duty cycle is too small, the inductor current becomes discontinuous, ZVS conditions will be lost and the switches will suffer high switching stress due to the high value of the dc bus voltage (in commercial ballasts around 400 V). This could lead to reduced reliability and increased EMI emission [1.67]. If ZVS conditions are not implemented, the practical minimum duty cycle also restricts the dimming range of the fluorescent lamps. The other way is to vary the on-time in different manners, ensuring a minor variation of dead-time for all the pulse width settings. This solution could guarantee more ZVS. However, for both options, the asymmetrical lamp current waveform in conjunction with low room temperatures, cause the premature aging of the lamp due to a mechanism called nonlinear *electrophoresis*, as explained in [1.72]. This mechanism can be avoided by using a modified duty-cycle variation scheme, called toggled duty-cycle operation [1.72]. It can also produce some flickering, if the operating frequency is not adequately chosen.

A similar method called group-asymmetrical PWM control (GAPWM), capable of operating at ZVS conditions, is proposed in [1.73]. This method will work in conjunction with symmetrical PWM, in order to avoid striations, and is activated only at low dimming levels, below 35% of the nominal lamp power.

Although theoretically quite simple, these methods are quite complex to implement and the use of microcontrollers is indispensable. So, this dimming technique has not been an option for commercial electronic ballasts.

- *Frequency control.* Among these three techniques, the frequency control has a wide dimming range and can be easily implemented. It is the standard control method adopted by the lighting industry. If the switching frequency of the inverter is increased, the impedance of the resonant inductor, L_r, increases, and the impedance of the resonant capacitor, C_r, decreases. At this point, it is important to recall, that the lamp resistance, R_{lamp}, increases as the lamp power decreases. So, as a result of the reduction of the capacitor impedance and the rise of R_{lamp}, the lamp current will be diverted to the capacitor, and the lamp power will be reduced. The lamp current is roughly inversely proportional to the operating frequency of the inverter, implying a non-linear dimming control [1.67].

A major drawback is obviously the non-constant frequency operation. In order to achieve low dimming levels, a wide frequency range is necessary (for commercial ballasts, generally between 40kHz and 100kHz). This means that soft-switching is not easily achieved over the entire switching range, particularly at low power levels. The switching transients due to hard-switching will be responsible for high EMI. In these conditions, the switching losses of the inverter will increase; which will have a negative effect on the efficiency of the system [1.70]. So, compared to the dc voltage control, the global efficiency of the ballast is typically lower [1.67], [1.71].

As already referred, a common concern regarding the application of these techniques is the electrodes preheating process and their behaviour during the dimming operation. During the preheating process, the voltage applied across the lamp must remain below a certain value, in order to prevent the lamp to ignite prematurely [1.76]. If the ballast circuit is similar to the one presented in Fig.1.19, the best method for soft-starting the lamp is to control the resonant-inverter switching frequency. Initially, the frequency is set to a value higher than the natural-resonance frequency of the tank; the electrodes heating current is then adjusted to the necessary value, maintaining a lamp voltage much lower than the starting voltage. After a short period, for example above 0.4s for TL5 lamps, the frequency is reduced until the starting voltage is obtained, igniting the lamp [1.19].

There are several commercial IC's which are designed to drive almost all types of fluorescent-lamp ballasts. Most of them have externally programmable features such as preheat time and frequency, controlled ignition and the so-called running mode operating frequency, which provides a high degree of flexibility for the ballast design engineer. As examples two controllers will be referred: the IR21571 and the IR21592, [1.74], [1.75]. The first one is not a dimming ballast controller but it serves as an example of the available features which are common in a dimming controller. They normally include protection features such as protection from failure of a lamp to ignite, filament failures, low dc bus voltage, thermal overload, or lamp failure during normal operation. As example, in Fig.1.20, it is presented the control sequence to drive rapid start fluorescent lamps in the IR21571. The control sequence allows the run mode operating frequency of the ballast to be higher than the ignition frequency. This control sequence is recommended for lamp types where the ignition frequency is too close to the running frequency to ensure proper lamp ignition for all production resonant LC component tolerances.

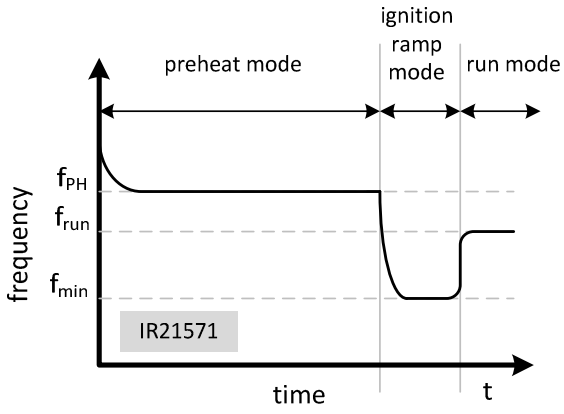

Fig.1.20. Frequency control with IC IR21571.

During the start mode, before the preheat mode, a frequency value is selected in order to ensure that the instantaneous voltage across the lamp during the first few cycles of operation does not exceed the ignition voltage. This frequency is then decreased exponentially to the preheat frequency, f_{ph}. According to [1.74], this frequency and the preheat time are typically chosen to ensure an adequate heating of the lamps electrodes, typically a ratio of the hot filament-to-cold filament resistance of 4.5:1 must be used. At the end of the preheat mode, the frequency falls exponentially to a minimum value, f_{min}. Afterwards the operating frequency is set to a running frequency value, f_{run}. These actions are performed by external resistors and capacitors connected to specific pins.

The IR21592 provides simultaneously ballast control and 600V half-bridge drivers, together with a 0.5-5V DC dimming control input. It also provides closed-loop power control and pre-heat current control. Some of the features are externally programmable such as pre-heat time and current, ignition-to-dim time and minimum and maximum settings for the dimming interface. The heart of the controller is a voltage controlled oscillator with externally programmable minimum frequency. To regulate the power, the error between the reference phase (the output inverter voltage phase) and the phase of the output current forces the VCO to steer the frequency in the proper direction. A 5V DC at the external DIM pin input corresponds to a minimum phase shift and maximum lamp power [1.75].

After ignition, all linear fluorescent tubes can be properly dimmed without a negative impact on the lifetime of the lamps if the electrodes are also heated to the proper level, whatever the operating power level. For T5 lamps or other fluorescent-lamp types, some pre-heating and heating limits are given by manufacturers which should be respected, in order to avoid end-blackening of the tube in the electrode region, the so-called SoS limits. Despite of the selected

dimming technique, the necessity of fulfilment of these limits may require separate electrode pre-heating, using external voltage sources [1.78]. The value of the required additional heating is a function of the discharge current, but it also depends on the ballast topology.

Apart from these dimming techniques, other solutions are now being proposed, particularly for CFLs. With the replacement of incandescent lamps by CFLs in domestic houses, it is important to adapt the existing dimmers, originally designed for incandescent lamps, for these light sources. Most of these dimmers are phase-cut dimmers. The average lamp power is dimmed by decreasing the conduction time during each half period of the line voltage. If the load has a resistive behaviour like incandescent lamps, the line current will be essentially in phase with the line voltage. But the fact is that CFLs do not behave in the same way. So in order to benefit from these existing dimmers, one possible solution is to include a PFC stage into the retrofitted electronic ballast in order to simulate the incandescent lamp behaviour as shown in Fig.1.21. Normally, for low-power CFLs, the PFC stage would be excluded from the ballast configuration. An example of this approach can be observed in [1.79] or in [1.80], where it is also proposed a standard for fluorescent tubes.

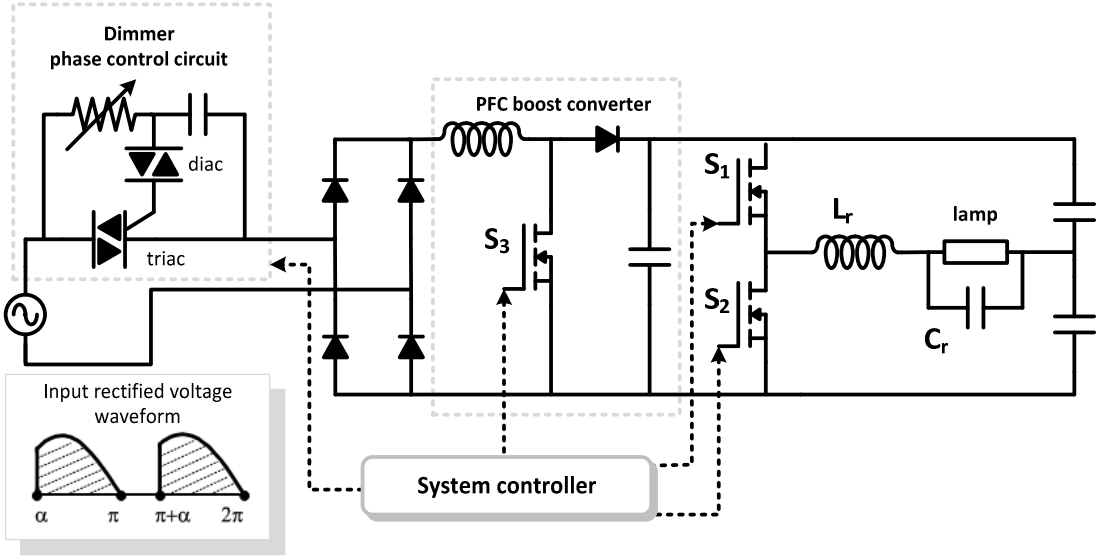

Fig.1.21. Dimming with Triac Phase Control.

1.4 MOTIVATION AND MAIN OBJECTIVES OF THE WORK

In this first chapter, after a short presentation of the main aspects concerning general lighting and specifically the ones regarding fluorescent lighting, it is important to establish the motivation

and main goals of the work presented in this thesis and finally introduce the magnetic control in electronic ballasts.

The title of this work, *Research and Development on New Control Techniques for Electronic Ballasts based on Magnetic Regulators*, summarizes the key subject. An initial goal was set to investigate magnetic-control based techniques for luminous flux regulation. The objective was to implement a new dimming technique based on a variable magnetic device. This preliminary work only served as an encouragement to follow other lines of research, and, after studying several possibilities or solutions regarding the implementation of the magnetic device, other applications and control techniques were developed, namely, in *universal* or *multi-Watt* electronic ballasts.

The term *universal ballast* was recently introduced as reference to a different type of electronic ballasts which are able to supply different lamps without requiring any physical change in the hardware. In such cases, the ballasts must incorporate the necessary intelligence to measure the electrical characteristics of the lamps wired to their output, and be able to adjust their internal operation in order to correctly ignite and supply these lamps. Similarly to dimmable electronic ballasts, there are several control parameters which can be used to adjust the lamp operation in universal ballasts; however, at the present time, a common solution is to use the operating frequency of the inverter as control parameter. This means that these ballasts will typically work at several different frequencies depending on the attached lamp.

In commercial dimmable electronic ballasts as well as in universal electronic ballasts, some negative aspects may emerge, mainly related to the non-constant frequency operation, as previously described. Not only to avoid this drawback, but also some other limitations and shortcomings presented by current dimming and universal control techniques, a research was carried out to validate the effectiveness of using novel magnetic control techniques for similar purposes.

1.4.1 MAGNETIC CONTROL IN ELECTRONIC BALLASTS

As previously referred, high-frequency operation of tubular fluorescent lamps is typically controlled by voltage-fed resonant inverters and among them, the most popular, the half-bridge inverter connected to a parallel-loaded resonant tank. This topology together with an adequate control circuit is able to guarantee soft-starting and safe lamp operation until lamp failure. The proposed magnetic-control technique, whether specifically used for dimming purposes or for other applications, is based on a simple premise: controlling the circuit through the variation of

the resonant frequency, instead of varying the inverter operating frequency. The technique is implemented by means of a dc-controlled magnetic element, the magnetic regulator.

In Fig.1.22 a schematic version of a magnetically-controlled electronic ballast is presented. The configuration of this ballast is very similar to the one presented by a standard electronic ballast. The only difference is the presence of the magnetic regulator, which takes the place of the classical resonant inductor, and provides similar basic functions, namely the stabilization of the discharge. However, the nature of this device is rather different because it is a variable magnetic element [1.81], [1.82]. Its philosophy is based on the possibility of controlling an ac output voltage, at a pre-set frequency, in response to a dc-controlled current source, which will provide immediate control over the resonant characteristics of the half-bridge resonant inverter.

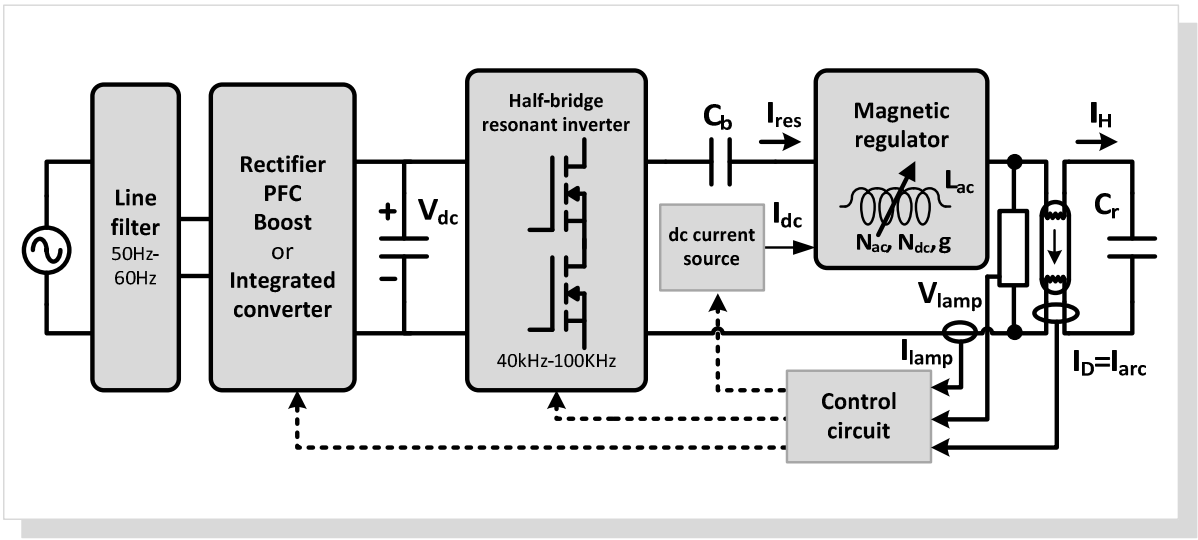

Fig.1.22. Magnetically-controlled electronic ballast schematic.

Fig.1.23 presents two different options for the implementation of this control technique. Both options are inspired on the voltage-fed, parallel-loaded, half-bridge resonant inverter. Since the magnetic regulator only affects the resonant inverter, from now on, the previous stages will be disregarded. Similarly to the classical LC circuit, both resonant circuits are constituted by the parallel resonant capacitor, C_r, and the magnetic regulator, which may be a variable inductor, as in Fig.1.23a., or a variable transformer, as in Fig.1.23b., [1.81], [1.82]. This variable behaviour is obtained through the modulation of the permeance of the ferromagnetic core, as a result of using a polarizing magnetic field imposed by the dc-controlled auxiliary windings. As described in future chapters, these windings can be disposed differently depending on the chosen regulator, core structure and topology. Whatever the selected regulator, the device will integrate the inductive element required to limit the lamp current. It is also important to avoid the dc

component of the output voltage that is delivered by the inverter, avoiding any dc current component to flow through the lamp. This task can easily be accomplished by a capacitor connected in series to the lamp, referred to as the dc-blocking capacitor, C_b. It is important to guarantee that its capacitance is high enough in order to consider the capacitor voltage ripple negligible.

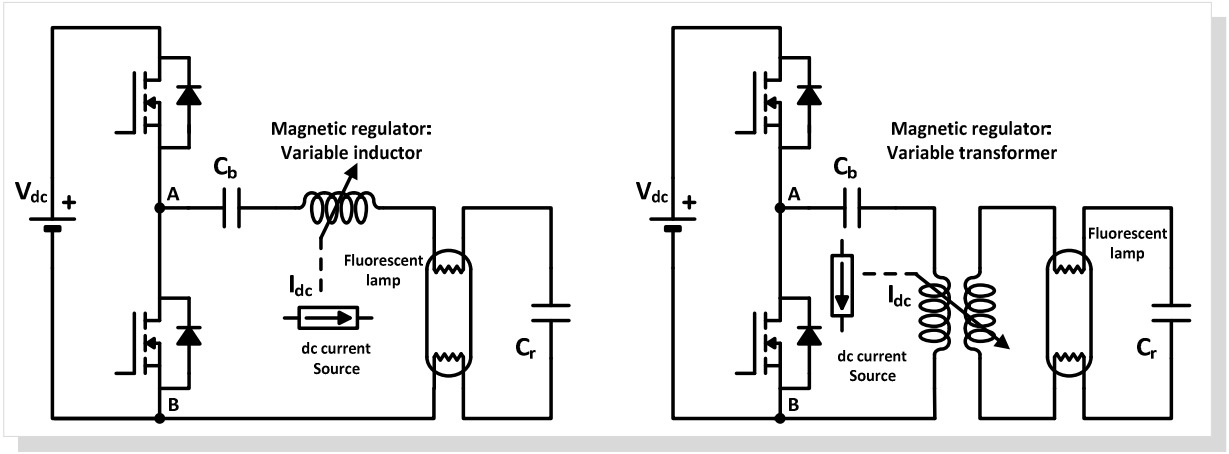

a. Variable-inductor option b. Variable-transformer option

Fig.1.23. Magnetically-controlled electronic ballasts.

In the variable inductor version presented in Fig.1.23a., the regulator control windings are used to modify the inductance of the ac winding, represented in series with the lamp. So, the inductance value in the resonant circuit may be adjusted as desired, depending on the dc current level circulating through those control windings. If the impedance of the resonant circuit is changed, it is possible to control the operating point of the lamp as well as its power. Therefore, it is possible to control the light output of the system. The lamp can also be isolated from the mains voltage with the inclusion of a variable transformer in the half-bridge inverter, as presented in Fig.1.23b. The variable behaviour of the resonant circuit will now depend on the transformer equivalent circuit model together with the resonant capacitor. This behaviour will also be dictated by the dc control windings included in the regulator structure. With this solution, it is possible to provide electrical isolation in addition to the control of the lamp's operating point. This can be a useful combination for applications with CCFLs in LCD backlighting applications.

The magnetic regulator concept is not new, however applying the concept to electronic ballasts is considered to be an innovative and promising technique. The work presented in this thesis describes the theoretical development and practical implementation of magnetic control techniques in prototype versions of magnetically-controlled electronic ballasts, as well as the

research steps involving these variable magnetic devices, from initial project and design, to theoretical and behavioural analysis, and finally, simulation and prototype implementation.

1.4.2 OUTLINE OF THE WORK

This Ph. D. Thesis is divided in five chapters. The first chapter provides an overview of the lighting domain, namely the current state of the art of fluorescent lighting. The fundamental requirements of typical fluorescent lighting systems controlled by electronic ballasts are described. Additional features related to remote control of the lighting system are also referred. The motivation of this research is then exposed and magnetic regulators are introduced as a new concept related to magnetic control in electronic ballasts, for dimming and multi-Watt operation.

Chapter 2 starts with a succinct introduction to saturable-core reactors and magnetic amplifiers. Some general considerations on different topologies and their behaviour are presented together with some fundamental notions on magnetic material behaviour, mainly related to the magnetization curve of the materials and hysteresis loop. Magnetic regulators are then introduced. The fundamental principles of operation of variable inductors and variable transformers are described while the basic laws of magnetism are recalled. The use of variable inductors or variable transformers in resonant power converters is addressed in detail. The chapter ends with a brief description of the proposed control techniques, for dimmable or universal ballasts, and top advantages are pointed out.

The next two chapters are the core of this Ph. D. Thesis and are divided in variable inductor ballast applications and variable transformer ballast applications.

Chapter 3 starts by describing the variable inductor modelling and design. It moves on to the description of the flux regulation technique. A comparative analysis between resonant circuits, different regulators structures, topologies and their effects on lamp operation is carried out. Finally, the chapter describes the other proposed technique: magnetically-controlled universal ballasts. The technique is explained and two different prototype versions are presented, the last one with constant-frequency operation. A special attention regarding some critical issues related to electrodes operation with these control techniques is also presented.

In Chapter 4 the variable transformer solution is presented as a step forward in magnetically-controlled electronic ballasts. It is shown how the proposed technique takes advantage of the magnetic behaviour of the device by integrating the magnetic component necessary to control the lamp current while guaranteeing electrical isolation and constant-frequency operation. Two

different variable transformer topologies are suggested, five-leg and three-leg, and a comprehensive description of their behaviour, modelling and characterization, using a simple methodology is also presented. The large-signal characterization of the three-leg variable transformer is also presented.

Both Chapter 3 and Chapter 4 present a vast set of experimental results which validate the proposed techniques. Prototype versions of magnetically-controlled electronic ballasts are presented and the collected experimental results clearly show the adequate behaviour of the selected fluorescent lamps under this type of magnetic control. Most of these results are based on modern T5 lamps.

Finally, Chapter 5 presents the conclusions and main contributions related to the application of magnetic regulators in electronic ballasts. The main achieved goals are emphasized, optimizations issues are raised as future work and a special attention is paid on future lines of research which includes other fields of applications.

REFERENCES

[1.1] CIE, Commission Internationale de l´Eclairage, http://www.cie.co.at.

[1.2] J. R. Coaton and A. M. Marsden, "Lamps and Lighting", 4th Edition, Arnold and Contributors 1997, ISBN: 0340646187.

[1.3] Javier Ribas Bueno, "Control optimizado de balastos electrónicos. Modelado estático y dinámico de inversores resonantes y lámparas de descarga", University of Oviedo, September 2001.

[1.4] Thomas Edison's Patent Application for the Light Bulb 1880, http://www.ourdocuments.gov/doc.php?doc=46.

[1.5] Philips Product Catalogue 2010, http://www.lighting.philips.com.

[1.6] European Union portal, http://europa.eu/pol/ener/index_en.htm.

[1.7] Osram Sylvania Product Catalogue, http://www.osram.com.

[1.8] Lighting Research Center, http://www.lrc.rpi.edu/.

[1.9] Alonso, J. M., Rashid, Muhammad H., "Power Electronics Handbook, Chapter 22 Electronic Ballasts", Academic Press, Inc., 2001, ISBN: 978-0-12-581650-2.

[1.10] Buso, D.; Bhosle, S.; Zissis, G.; Mayhrofer, M.; Zudrell-Koch, S.; Severinsson, M.; Rydhem, A.; Ruscassie, R.; "Predictive Evaluation of Fluorescent Lamp Lifetime," Industry Applications Society Annual Meeting, 2009. IAS 2009. IEEE, vol., no., pp.1-7, 4-8 Oct. 2009.

[1.11] Maussion, P.; Chhun, L.; Bhosle, S.; Zissis, G.; "Acoustic Resonance Characteristics in a High Pressure Sodium Lamp," Industry Applications Society Annual Meeting, 2008. IAS '08. IEEE, vol., no., pp.1-4, 5-9 Oct. 2008.

[1.12] Kaiser, W.; Marques, R.P.; Correa, A.F.; "An Alternative Optical Method for Acoustic Resonance Detection in HID Lamps," Industry Applications Society Annual Meeting, 2009. IAS 2009. IEEE, vol., no., pp.1-6, 4-8 Oct. 2009.

[1.13] Cheng, C.-A.; Lin, K.-J.; Kao, Y.-M.; "Acoustic-resonance-free electronic ballast for automotive HID lamps," Electronics Letters, vol.44, no.17, pp.1027-1029, Aug. 14 2008.

[1.14] Garcia-Garcia, J.; Cardesin, J.; Ribas, J.; Calleja, A.J.; Rico-Secades, M.; Alonso, J.M.; Corominas, E.L.; "Minimization of acoustic resonances in HID lamps: analysis and comparison of power harmonics content in high frequency non-resonant inverters," Power Electronics, IEEE Transactions on , vol.20, no.6, pp. 1467-1479, Nov. 2005.

[1.15] Lehman, Brad; "Introduction to LED Lighting Systems", IEEE Energy Conversion Congress and Exposition, ECCE 2010, Atlanta, Georgia, September, 2010.

[1.16] S. Nakamura, T. Mukai, M. Sengh, "Candela-class high-brightness InGan-AlGan double heterostructure blue light-emitting diodes," Appl. Phys. Lett., 64(13):1687-9, 1994.

[1.17] CREE, http://www.cree.com.

[1.18] Philips Lumileds Products, http://www.philipslumileds.com.

[1.19] NICHIA LED Catalogue 2010, http://www.nichia.co.jp.

[1.20] Philips MASTER TL5 lamps, Philips 2006, Access in: Jan. 2011, http://www.lighting.philips.com.

[1.21] Qin, Y.X.; Lin, D.Y.; Hui, S.Y.R.; "A Simple Method for Comparative Study on the Thermal Performance of Light Emitting Diodes (LED) and Fluorescent Lamps," Applied Power Electronics Conference and Exposition, 2009. APEC 2009. Twenty-Fourth Annual IEEE, vol., no., pp.152-158, 15-19 Feb. 2009.

[1.22] Buso, S.; Spiazzi, G.; Meneghini, M.; Meneghesso, G.; "Performance Degradation of High-Brightness Light Emitting Diodes Under DC and Pulsed Bias," Device and Materials Reliability, IEEE Transactions on, vol.8, no.2, pp.312-322, June 2008.

[1.23] Application guide to fluorescent gear, http://www.lighting.philips.com.

[1.24] ANSI E1.11-2008, Entertainment Technology - USITT DMX512-A - Asynchronous Serial Digital Data Transmission Standard for Controlling Lighting Equipment and Accessories, http://webstore.ansi.org/RecordDetail.aspx?sku=ANSI+E1.11-2008

[1.25] Tae-Eun Jang; Hee-Jun Kim; Hoon Kim; "Dimming Control Characteristics of Electrodeless Fluorescent Lamps," Industrial Electronics, IEEE Transactions on , vol.56, no.1, pp.93-100, Jan. 2009.

[1.26] da Silva, M.F.; de P Lopes, J.; Chagas, N.B.; Seidel, A.R.; Costa, M.A.D.; do Prado, R.N.; "High power factor dimmable lighting system for electrodeless fluorescent lamp," Power Electronics Electrical Drives Automation and Motion (SPEEDAM), 2010 International Symposium on , vol., no., pp.379-384, 14-16 June 2010.

[1.27] Wonseok Oh; Kyumin Cho; Jaeeul Yeon; Kyungsang Yoo; "Fully digital controlled electronic ballast for electrode-less lamps," Power Electronics Electrical Drives Automation and Motion (SPEEDAM), 2010 International Symposium on , vol., no., pp.363-367, 14-16 June 2010.

[1.28] Lin, D.Y.; Yan, W.; "Study and Modeling of Cold Cathode Fluorescent Lamps (CCFL)," Applied Power Electronics Conference and Exposition, 2009. APEC 2009. Twenty-Fourth Annual IEEE, vol., no., pp.812-818, 15-19 Feb. 2009.

[1.29] Ke, Yu-Lung; Chuang, Ying-Chun; Chuang, Hung-Shiang; Wu, Yuan-Kang; Chang, Chun-Chih; "Self-excited electronic ballast for cold cathode fluorescent lamps," Industrial and Commercial Power Systems Technical Conference (I&CPS), 2010 IEEE , vol., no., pp.1-6, 9-13 May 2010.

[1.30] Hirahaya, M.; Takeda, M.; Oka, K.; Toda, Y.; Motomura, H.; Jinno, M.; "Effect of the auxiliary external electrode on xenon fluorescent lamp depending on its diameter," Plasma Science - Abstracts, 2009. ICOPS 2009. IEEE International Conference on, vol., no., pp.1-1, 1-5 June 2009.

[1.31] Perdigão, M.; Saraiva, E.S.; "Matlab-Simulink implementation of the Mader-Horn fluorescent-lamp model: permissible range of the resistive lamp model," Industrial Technology, 2004. IEEE ICIT '04. 2004 IEEE International Conference on, vol.1, no., pp. 492- 497 Vol. 1, 8-10 Dec. 2004

[1.32] Hui, S.Y.R.; Lin, D.Y.; Ng, W.M.; Yan, W.; "A "Class-A2" ultra-low-loss magnetic ballast for T5 fluorescent lamps," Applied Power Electronics Conference and Exposition (APEC), 2010 Twenty-Fifth Annual IEEE, vol., no., pp.1346-1351, 21-25 Feb. 2010.

[1.33] Wai Man Ng, Deyan Lin and S.Y.R. Hui; "A Single Eco-Friendly Ultra-Low-Loss Magnetic Ballast Design for a Wide Range of T5 High-Efficient Fluorescent Lamps", Energy Conversion Congress & Exposition (ECCE), IEEE, September 2010.

[1.34] Simões, A.S.; Silva, M.M.; Anunciada, A.V.; "A boost-type converter for DC-supply of fluorescent lamps," Industrial Electronics, IEEE Transactions on , vol.41, no.2, pp. 251- 255, Apr 1994

[1.35] IEC 1000-3-2 (1995-03) standards on EMC, Part 3, Section 2: Limits for harmonic current emissions. International Electrotechnical Commission, Geneva, Switzerland, April 1995.

[1.36] Ying-Chun Chuang; Chin-Sien Moo; Hsien-Wen Chen; Tsai-Fu Lin; "A Novel Single-Stage High-Power-Factor Electronic Ballast With Boost Topology for Multiple Fluorescent Lamps," Industry Applications, IEEE Transactions on , vol.45, no.1, pp.323-331, Jan.-Feb. 2009

[1.37] L. Rossetto, G. Spiazzi, P. Tenti, "Control techniques for power factor correction converters", Proc. of Power Electronics, Motion Control (PEMC), 1310-1318, September 1994.

[1.38] Deyan Lin; Wei Yan; Zissis, G.; Hui, S.; "A simple physical low pressure discharge lamp model," Energy Conversion Congress and Exposition, 2009. ECCE 2009. IEEE, vol., no., pp.2051-2058, 20-24 Sept. 2009.

[1.39] Holloway, A.J.; Tozer, R.C.; Stone, D.A.; "A Physically Based Fluorescent Lamp Model for a SPICE or a Simulink Environment," Power Electronics, IEEE Transactions on, vol.24, no.9, pp.2101-2110, Sept. 2009.

[1.40] Ka Hong Loo; Moss, G.J.; Tozer, R.C.; Stone, D.A.; Jinno, M.; Devonshire, R.; "A dynamic collisional-radiative model of a low-pressure mercury-argon discharge lamp: a physical approach to modeling fluorescent lamps for circuit simulations," Power Electronics, IEEE Transactions on , vol.19, no.4, pp. 1117-1129, July 2004.

[1.41] Zissis, G.; Buso, D.; "Using full physical model for fluorescent lamps in ballast engineering," Industry Applications Conference, 2003. 38th IAS Annual Meeting. Conference Record of the, vol.1, no., pp. 537-541 vol.1, 12-16 Oct. 2003.

[1.42] Mader, U.; Horn, P.; "A dynamic model for the electrical characteristics of fluorescent lamps," Industry Applications Society Annual Meeting, 1992., Conference Record of the 1992 IEEE , vol., no., pp.1928-1934 vol.2, 4-9 Oct 1992.

[1.43] Wu, T.-F.; Hung, J.-C.; Yu, T.-H.; "A PSpice model for fluorescent lamps operated at high frequencies," Industrial Electronics, Control, and Instrumentation, 1995., Proceedings of the 1995 IEEE IECON 21st International Conference on , vol.1, no., pp.359-364 vol.1, 6-10 Nov 1995.

[1.44] Sun, M.; Hesterman, B.L.; "PSpice high-frequency dynamic fluorescent lamp model," Power Electronics, IEEE Transactions on , vol.13, no.2, pp.261-272, Mar 1998.

[1.45] Ben-Yaakov, S.; "Modeling the high-frequency behavior of a fluorescent lamp: a comment on “a PSpice circuit model for low-pressure gaseous discharge lamps operating at high frequency”," Industrial Electronics, IEEE Transactions on , vol.45, no.6, pp.947-950, Dec 1998.

[1.46] Moo, C.S.; Hsieh, Y.C.; Yen, H.C.; Lee, C.R.; "Fluorescent lamp model with power and temperature dependence for high-frequency electronic ballasts," Industry Applications, IEEE Transactions on , vol.39, no.1, pp. 121- 127, Jan/Feb 2003.

[1.47] Blanco, C.; Anton, J.C.; Robles, A.; Ferrero, F.J.; Campo, J.C.; Gonzalez, M.; Zissis, G.; "A Discharge Lamp Model Based on Lamp Dynamic Conductance," Power Electronics, IEEE Transactions on , vol.22, no.3, pp.727-734, May 2007.

[1.48] Blanco, C.; Anton, J.C.; Robles, A.; Ferrero, F.; Viera, J.C.; Bhosle, S.; Zissis, G.; "Comparison between Different Discharge Lamp Models Based on Lamp Dynamic Conductance," Industry Applications Society Annual Meeting, 2008. IAS '08. IEEE, vol., no., pp.1-6, 5-9 Oct. 2008.

[1.49] Hung-Liang Cheng; Yung-Hsin Huang; "Design and Implementation of Dimmable Electronic Ballast for Fluorescent Lamps Based on Power-Dependent Lamp Model," Plasma Science, IEEE Transactions on, vol.38, no.7, pp.1644-1650, July 2010.

[1.50] Chang, G.W.; Liu, Y.J.; "A New Approach for Modeling Voltage–Current Characteristics of Fluorescent Lamps," Power Delivery, IEEE Transactions on, vol.23, no.3, pp.1682-1684, July 2008.

[1.51] Lin, D.; Yan, W.; Hui, S. Y. R.; "Modeling of Dimmable Fluorescent Lamp Including the Tube Temperature Effects," Industrial Electronics, IEEE Transactions on, vol., no.99, pp.1, 2011. (Early access)

[1.52] Shafi, M.A.; McMahon, R.A.; "Implementation and verification of CFL models for use in performance analysis in high frequency electronic ballasts," Power Electronics, Machines and Drives, 2006. PEMD 2006. The 3rd IET International Conference on, vol., no., pp.561-565, 4-6 April 2006.

[1.53] Wei, Z.; Watson, N.R.; Frater, L.P.; "Modelling of compact fluorescent lamps," Harmonics and Quality of Power, 2008. ICHQP 2008. 13th International Conference on, vol., no., pp.1-6, Sept. 28 2008-Oct. 1 2008.

[1.54] Jing Yong; Liang Chen; Nassif, A.B.; Wilsun Xu; "A Frequency-Domain Harmonic Model for Compact Fluorescent Lamps," Power Delivery, IEEE Transactions on, vol.25, no.2, pp.1182-1189, April 2010.

[1.55] Cherl-Jin, K.; Yoo Byeong-Kyu; Yoon Shin-Yong; Baek Soo-Hyun; "A Proper Impedance Model of CCFL (Cold Cathode Fluorescent Lamp) Applied to the Display Unit," Electrical Machines and Systems, 2005. ICEMS 2005. Proceedings of the Eighth International Conference on, vol.2, no., pp.1457-1460, 29-29 Sept. 2005.

[1.56] Deyan Lin; Wei Yan; "Modeling of Cold Cathode Fluorescent Lamps (CCFLs) With Realistic Electrode Profile," *Power Electronics, IEEE Transactions on*, vol.25, no.3, pp.699-709, March 2010.

[1.57] Min Sup Song, Yong Kyu Park, Jae Joong Yun, Young Ho Hwang, Bongkoo Kang; "Distributed circuit model for cold cathode fluorescent lamps in back-light unit of liquid crystal display," Elsévier Journal, Displays, vol. 31, issue 2, pp.104-110, April 2010.

[1.58] Deng, E.; Cuk, S.; "Negative incremental impedance and stability of fluorescent lamps," Applied Power Electronics Conference and Exposition, 1997. APEC '97 Conference Proceedings 1997, Twelfth Annual, vol.2, no., pp.1050-1056 vol.2, 23-27 Feb 1997.

[1.59] Ben-Yaakov, S.; Shvartsas, M.; Glozman, S.; "Statics and dynamics of fluorescent lamps operating at high frequency: modeling and simulation," Industry Applications, IEEE Transactions on , vol.38, no.6, pp. 1486-1492, Nov/Dec 2002.

[1.60] Glozman, S.; Ben-Yaakov, S.; "Dynamic interaction analysis of HF ballasts and fluorescent lamps based on envelope simulation," Industry Applications, IEEE Transactions on, vol.37, no.5, pp.1531-1536, Sep/Oct 2001.

[1.61] Chang-Gyum Kim; Kyu-Chan Lee; Cho, B.H.; "Modeling of CCFL using lamp delay and stability analysis of backlight inverter for large size LCD TV," Applied Power Electronics Conference and Exposition, 2005. APEC 2005.

[1.62] Ben-Yaakov, S.; Peretz, M.M.; "Cold Cathode Fluorescent Lamps Driven by Piezoelectric Transformers: Stability Conditions and Thermal Effect," Power Electronics, IEEE Transactions on, vol.22, no.3, pp.761-768, May 2007.

[1.63] Spiazzi, G.; Buso, S.; "Small-Signal Analysis of Cold Cathode Fluorescent Lamp Ballasts," Power Electronics, IEEE Transactions on, vol.22, no.3, pp.753-760, May 2007.

[1.64] Diaz, R.E.; Ribas, J.; Calleja, A.J.; Alonso, J.M.; Garcia-Garcia, J.; "Small signal characterization of fluorescent lamps in dimmed operation," Industrial Electronics, 2009. IECON '09. 35th Annual Conference of IEEE, vol., no., pp.3563-3568, 3-5 Nov. 2009.

[1.65] Lam, J.; Jain, Praveen K.; "A Novel Single-Stage Dimmable Electronic Ballast with High Efficiency and Unity Power Factor Using an Integrated Buck-boost Current Source Resonant Inverter," Applied Power Electronics Conference, APEC 2007 - Twenty Second Annual IEEE , vol., no., pp.1309-1315, Feb. 25 2007-March 1 2007.

[1.66] Zan Huang; Ribarich, T.; "A New Dimming Method for Highly Integrated Fluorescent Ballast," Applied Power Electronics Conference and Exposition, 2009. APEC 2009. Twenty-Fourth Annual IEEE, vol., no., pp.1553-1557, 15-19 Feb. 2009.

[1.67] Tam, P.W.; Lee, S.T.S.; Hui, S.Y.R.; Chung, H.S.-H.; "Practical Evaluation of Dimming Control Methods for Electronic Ballasts," Power Electronics, IEEE Transactions on, vol.21, no.6, pp.1769-1775, Nov. 2006.

[1.68] Haiyan Wang; Stankovic, A.V.; Nerone, L.; Kachmarik, D.; "A Novel Discrete Dimming Ballast for Linear Fluorescent Lamps," Power Electronics, IEEE Transactions on , vol.24, no.6, pp.1453-1462, June 2009.

[1.69] Philips Advance Optanium® high-efficiency ballasts with step-dim capability, http://www.lighting.philips.com.

[1.70] S. Y. R. Hui and H. S. H. Chung, "Dimming Control of Electronic Ballasts," U.S. Patent 6 486 615, Nov. 26, 2002.

[1.71] Alonso, J.M.; Dalla Costa, M.A.; Rico-Secades, M.; Cardesin, J.; Garcia, J.; "Investigation of a New Control Strategy for Electronic Ballasts Based on Variable Inductor," Industrial Electronics, IEEE Transactions on , vol.55, no.1, pp.3-10, Jan. 2008.

[1.72] Raiser, F.; "Dim the lights. Problems with lamp current control using a PWM signal," Industry Applications Magazine, IEEE, vol.8, no.6, pp. 54- 59, Nov/Dec 2002.

[1.73] Guan-Chyun Hsieh; "Group-Asymmetrical PWM Control for Dimmable Fluorescent Lamp Ballast Without Striation and Thermostat Effect," Power Electronics, IEEE Transactions on, vol.24, no.5, pp.1293-1303, May 2009.

[1.74] IR21571(S) Datasheet PD Nº 60179-I, International Rectifier, www.irf.com.

[1.75] IR21592(S) Datasheet PD Nº 60194 revD, International Rectifier, www.irf.com.

[1.76] Dorleijn, J.W.F.; Goud, L.H.; "Standardisation of the static resistances of fluorescent lamp cathodes and new data for preheating," Industry Applications Conference, 2002. 37th IAS Annual Meeting. Conference Record of the, vol.1, no., pp. 665- 672 vol.1, 2002.

[1.77] Goud, L.H.; Dorleijn, J.W.F.; "Standardized data for dimming of fluorescent lamps," Industry Applications Conference, 2002. 37th IAS Annual Meeting. Conference Record of the, vol.1, no., pp. 673- 679 vol.1, 2002.

[1.78] Ballasts for tubular fluorescent lamps – Performance requirements, IEC 60921, 2006.

[1.79] Lam, J.; Jain, P.K.; "A novel dimmable electronic ballast for compact fluorescent lamps using phase-cut incandescent lamp dimmers with wide dimming range and low dimming level lamp ignition capability," Applied Power Electronics Conference and Exposition (APEC), 2010 Twenty-Fifth Annual IEEE , vol., no., pp.2321-2327, 21-25 Feb. 2010.

[1.80] Yu-Kai Chen; Yung-Chun Wu; Chau-Chung Song; Li-June Liu; "Design and implementation of dimmable fluorescent lamps with TRIAC phase control," Industrial Technology, 2009. ICIT 2009. IEEE International Conference on, vol., no., pp.1-6, 10-13 Feb. 2009.

[1.81] Medini, D.; Ben-Yaakov, S.; "A current-controlled variable-inductor for high frequency resonant power circuits," Applied Power Electronics Conference and Exposition, 1994. APEC '94. Conference Proceedings 1994., Ninth Annual , vol., no., pp.219-225 vol.1, 13-17 Feb 1994

[1.82] Vollin, J.; Tan, F.D.; Cuk, S.M.; "Magnetic regulator modeling," Applied Power Electronics Conference and Exposition, 1993. APEC '93. Conference Proceedings 1993, Eighth Annual, vol., no., pp.604-611, 7-11 Mar 1993.

BIBLIOGRAPHY

[B1.1] J. R. Coaton and A. M. Marsden, "Lamps and Lighting", 4th Edition, Arnold and Contributors 1997, ISBN: 0340646187.

[B1.2] Alonso, J. M., Rashid, Muhammad H., "Power Electronics Handbook, Chapter 22 Electronic Ballasts", Academic Press, Inc., 2001, ISBN: 978-0-12-581650-2.

[B1.3] Application guide to fluorescent gear, http://www.lighting.philips.com

2 LITERATURE REVIEW ON MAGNETIC REGULATORS

In the present chapter, the state of the art on magnetic regulators is presented. The chapter starts with a succinct introduction to saturable-core reactors and magnetic amplifiers. Some general considerations on different topologies and their behaviour are presented together with some fundamental notions on magnetic material behaviour, mainly related to the magnetization curve of the material and hysteresis loop. Magnetic regulators are then introduced. The fundamental principles of operation of variable inductors and variable transformers are described while the basic laws of magnetism are recalled. Since magnetic regulators in the form of variable inductors or variable transformers have been the object of several patents and several scientific papers, a general overview is presented. Typically, they all refer the device, or the invention, as useful or industrially applicable. Due to the focus of the developed work, the subject of their application to resonant power converters is addressed in detail. The chapter ends with a brief description of magnetic control applied to electronic ballasts. Basic concepts behind the proposed control techniques are underlined, whether they refer to dimmable or universal ballasts, and leading advantages are pointed out.

2.1 SATURABLE REACTORS AND MAGNETIC AMPLIFIERS

A saturable reactor is an electromagnetic device which was invented late in the 19th century in the United States, and was initially used for theatre lighting control. A practical application related to radio telephone transmission, and some details on the device operating principle were firstly reported in a technical paper in 1916 [2.1]. Years later, mainly as a result of a German development program, it was used during and after the World War II, in the 1940's and 50's, as a controlled switch in a variety of applications, especially aboard ships and aircrafts. These applications included throttle controls on the main engines of ships; auxiliary equipments (current

and voltage control, temperature control), servomechanisms, stabilizers for guns, radar and sonar equipment [2.2], [2.7].The switch mechanism was based on the changing inductive impedance of a winding placed around a saturable magnetic core. This switch mechanism was then used to control the power delivered to a specific load [2.3]. Saturable reactors and magnetic amplifiers, which are a combination of a saturable reactor and a rectifying diode, were considered as reliable devices, with low maintenance costs, long life and a good tolerance to mechanical shock, vibration and moisture. With no moving parts, the devices could be hermetically sealed within a case, in order to resist the effects of adverse environmental conditions. They were traditionally used in high-power, low-frequency applications, 50 Hz or 60 Hz systems. In the 1980's and 90's these devices were also used in some specific low-power applications, mainly in switching power supplies, at higher frequency values [2.4], [2.2].

Recently, modern technology was capable of finding some new interesting applications for these magnetic devices, by adapting and changing topologies, core structures and materials, and most of all, by interpreting those former applications in a different way.

2.1.1 FUNDAMENTALS

The magnetic flux density or magnetic induction, B , in a magnetic material depends upon the magnetic conducting ability of the material, called *permeability*, μ, and the magnetic field intensity, H and the effect of any change in the flux density within the material can be observed by the magnetization curve of the material, the $B(H)$ curve:

$$B = \mu H = \mu_r \mu_0 H \tag{2.1}$$

Where μ_0 is the permeability of vacuum, a constant equal to $4\pi \times 10^{-7}$ H/m, and μ_r is the relative permeability of the magnetic material, which is a dimensionless ratio, $\mu_r = \mu/\mu_0$. The value for μ_r for air and electrical conductors is 1. For ferromagnetic materials this value is much higher and varies from several hundred to tens of thousands.

The relationship between B and H for ferromagnetic materials is usually non-linear. An example of this magnetization curve can be observed in Fig. 2.1. The $B(H)$ curve is characterized by three different regions: the unsaturated region, a, the transition region, also known as the knee of the curve, b, and the saturated region, c. In the first region, for very low values of H, the flux density increases at a very slow rate due to the initial inertia of the magnetic domains of the material. After this initial phase, the flux density increases much more quickly with increasing

values of H and the curve exhibits an almost linear behaviour. In the transition region, the rate of increase of the flux density drops until the saturation region is finally reached.

In this saturated region, all the magnetic domains are oriented in the same direction. The magnetization vector, $\vec{M}$, defined as the magnetic dipole moment per unit of volume, has reached its maximum value. For this reason, the slight increase shown by the magnetization curve is due only to the term $\mu_0\vec{H}$ as in (2.2). The material is said to be magnetized to a maximum extent or to be saturated [2.6], [2.7].

$$\vec{B} = \mu_0(\vec{H} + \vec{M}) \tag{2.2}$$

The magnetization curve differs in shape and characteristics with different magnetic materials: some may present large or smaller slopes; some may require a large amount of magnetomotive force to become saturated.

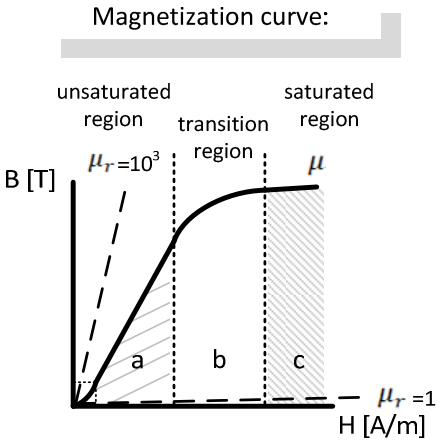

Fig. 2.1. Typical magnetization curve for a soft magnetic material.

Another important characteristic related to the magnetic properties of the materials is hysteresis. Hysteresis in a magnetic material means that the magnetic flux density lags the magnetic field intensity [2.7]. When a magnetic material is subjected to an increasing magnetic field until saturation is reached, and then this field is slowly decreased to zero and set into the opposite direction, until saturation is reached again, the material does not follow the initial magnetization curve which followed the path 1, 2 and 3. Instead, it follows the left side of the initial curve. This effect is shown in Fig. 2.2a. If this process is repeated until the cycle is completed, and again the magnetic field is set at its maximum positive value, a closed loop is obtained. This loop is called the hysteresis loop. The values B_{sat} and -B_{sat} correspond to the maximum positive and negative flux density. B_r corresponds to the residual flux density when the

magnetic field H is set back to zero. H_c is called the coercive force and corresponds to the necessary value of H at which B is set back to zero.

Similar to the initial magnetization curve, the shape of the hysteresis loop is also material dependant. Soft magnetic materials are characterized by an easy change of the magnetic domains and consequently present a low coercive force and a narrower hysteresis loop. Hard magnetic materials, also called permanent magnets, strongly resist to the influence of an external magnetic field and thereby the coercive force is much higher. The hysteresis loop is larger and they also present a high value of residual flux. There are also some core materials with rectangular hysteresis loops, where the B_{sat} is reached for smaller values of H. An example of this type of loop is presented in Fig. 2.2b. These are the type of materials typically used in magnetic amplifiers [2.5], [2.6], [2.7].

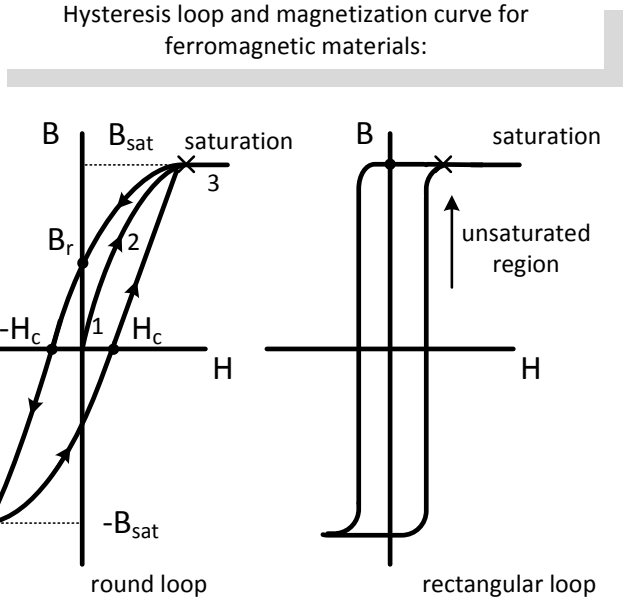

a. Soft magnetic material: less used in saturable reactors

b. Materials used in saturable reactors

Fig. 2.2. Hysteresis loop shapes for different magnetic materials.

2.1.2 OPERATING PRINCIPLE

The principle of operation of the saturable reactor can be simply described. According to the fundamental theory of transformers, a small amount of dc current flowing into the winding of a transformer, mounted on an ungapped core, causes the core to quickly saturate. So, this implies that the inductance of the transformer may be varied by a small amount of dc power. As a result, if one winding of this transformer is connected between an ac supply and a load, the amount of

power delivered to that load may be controlled by injecting a small amount of dc current in another winding. In such cases, this transformer may also be called a saturable inductor [2.5].

An example of a simple circuit containing this device can be observed in Fig. 2.3. Two types of magnetomotive forces will force a flux in the magnetic core: the dc magnetomotive force created by the dc control current, constant in magnitude and direction, and the ac magnetomotive force created by the ac voltage source which changes in magnitude and in direction. Due to its cyclical operation, the ac magnetomotive force contributes to the saturation or desaturation of the core. This results in a changing inductive reactance in the load winding. The dc magnetomotive force, according to its value, aids or opposes the ac magnetomotive force in this action [2.7].

However, if the core presents a relatively rectangular $B(H)$ loop, the change in the inductive reactance can be made quite large and abrupt, since the core is easily saturated. Therefore the device presents two operating modes: if the core is unsaturated, the ac winding inductance is extremely high, capable of supporting a high voltage with a small load current; if the core is saturated, the ac winding differential inductance will be low and the load current can easily flow [2.2], [2.4]. At this point the magnetization in the core is as high as it can be, meaning that only a residual amount of changing flux can be held by the core. So, in order to have an ideal switch, the desirable operating point should correspond to the one where a small increase in the control current causes a large increase in the output power, and a small decrease in the control current causes a large decrease in the output power. In such conditions the saturable reactor is said to present a bi-stable operation.

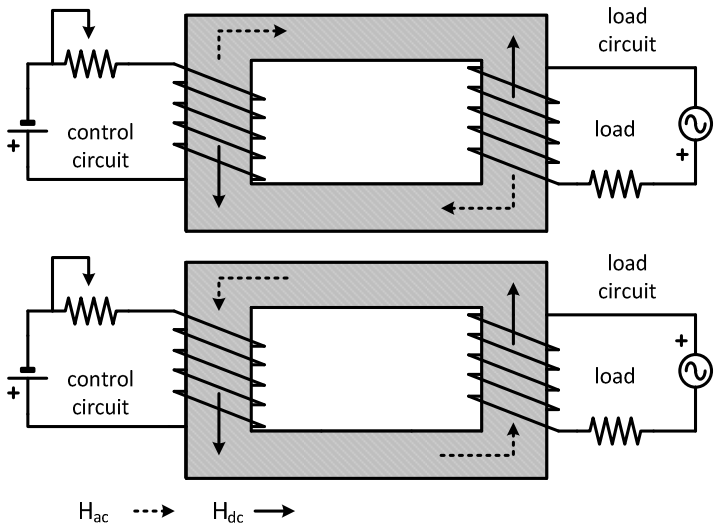

Fig. 2.3. Magnetic field paths in a saturable-core reactor.

As previously stated, and once again referring to Fig. 2.3, if a dc voltage is applied to the control winding and an ac voltage is applied to the load winding; the ac magnetic field will oppose the dc magnetic field on one half-cycle and aid the dc magnetic field on the other half-cycle. This means that an ac voltage would be induced in the dc control winding, due to the so-called transformer action. If this dc winding was closed only on the battery voltage source, it could short-circuit the ac voltage connected to the ac winding [2.2], [2.5]. This difficulty could be overcome using high impedance in the dc control circuit; a better option would be using a dc current source. This situation causes the operating point of the saturable inductor to shift with the applied ac voltage. It would be preferable if there was no influence of the ac flux on the control flux. This is the reason why most of the saturable inductors exhibit a configuration similar to the one presented in Fig. 2.4. In this case, for both half-cycles, the ac magnetic field almost cancels itself in the centre leg of the core. As a result there is almost no undesirable effect on the dc control flux.

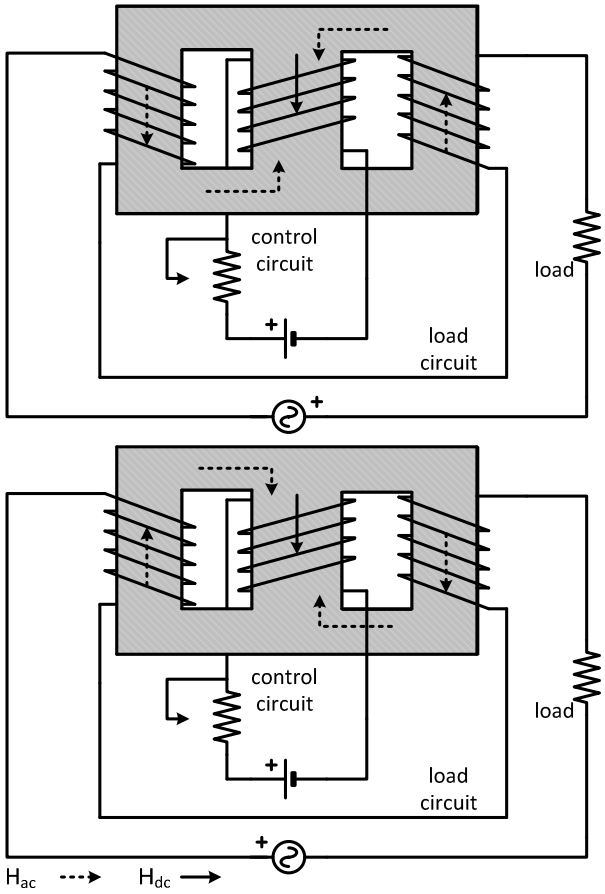

Fig. 2.4. Magnetic field paths in a three-legged saturable-core reactor.

Another approach is presented in Fig. 2.5. In this case a toroidal-shaped core is used. During the first half-cycle, the ac magnetic field aids the control magnetic field in the left core and

opposes it in the right core. During the second half-cycle, the situation is reversed. Regardless of the amount of the ac magnetic field or its direction, there is almost no net effect of the ac magnetic field intensity on the dc control winding.

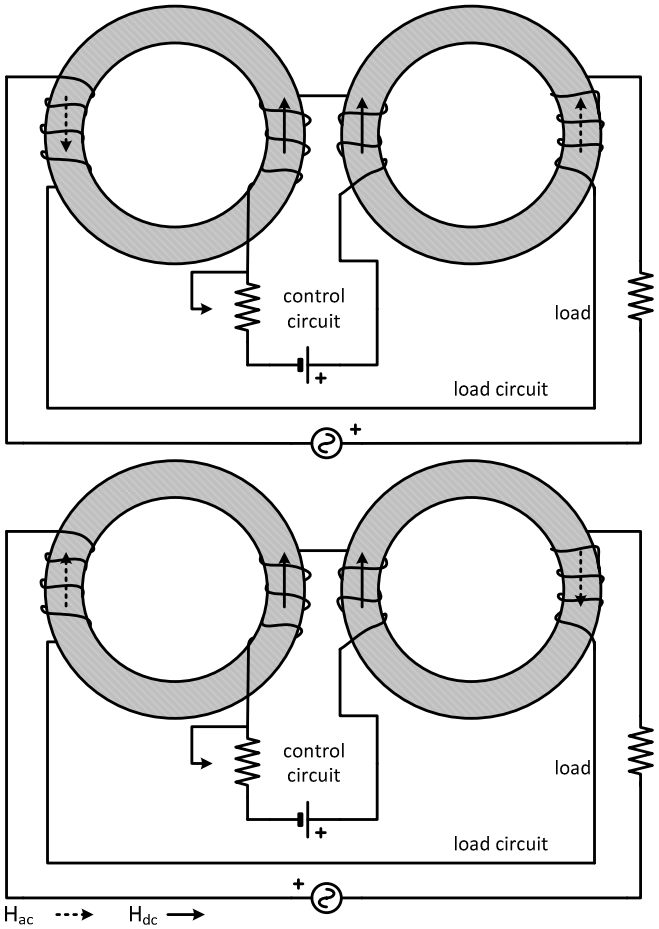

Fig. 2.5. Magnetic field paths in a toroidal saturable-core reactor.

A magnetic amplifier typically differs from a simple saturable inductor due to the inclusion of a rectifying diode in series with the load circuit.

When a periodic changing current is applied to a winding, there will be some hysteresis losses associated with this voltage. The hysteresis and eddy current losses are proportional to the area enclosed by the $B(H)$ loop, to frequency and core volume.

If a simple magnetic circuit, with only one winding, is considered, and if a sinusoidal current is flowing into this winding during one half-cycle of this alternating current, the resultant ac flux increases from zero to its maximum value and then collapses to zero. During the following half-cycle, it decreases from zero to its negative extreme and then goes to zero again. So, the magnetic flux created in the first half-cycle opposes the magnetic flux created in the second half-cycle. This implies that any attempt to saturate the core in the first half-cycle is accompanied by an

equal attempt to desaturate the core in the second half-cycle. Therefore, due to the nature of the supply current, the core is subjected to saturating and desaturating ac currents.

Considering a magnetic amplifier, the presence of the diode rectifier in the load circuit, imposes the load current to flow in only one direction [2.7], preferably to enhance the effect of the control winding current, towards saturation. As a consequence, the hysteresis losses will decrease. The saturation of the core leads to an increase of the load current, and in these conditions the saturable-core reactor is said to be amplifying the control current.

An example of this device can be observed in the half-wave magnetic amplifier circuit presented in Fig. 2.6 [2.3], [2.5]. In Fig. 2.6, N_p represents the winding in the device through which the current flows from the sinusoidal voltage source, E_s, to the load, R. The control is enforced by the second winding, N_c, which is also connected to another source, E_c. Due to the presence of the diode, D, in a simplified way, conduction is only permitted during the positive half-cycle of the ac voltage. If the reactor core presents a rectangular loop, the inductive impedance of the winding N_p will be extremely high for an unsatured core and extremely low for a saturated core. So, the power flow between E_s and R can be controlled by fixing the instant of saturation of the core during this positive half-cycle. This achievement must be enforced by the control loop during the preceding half-cycle [2.3].

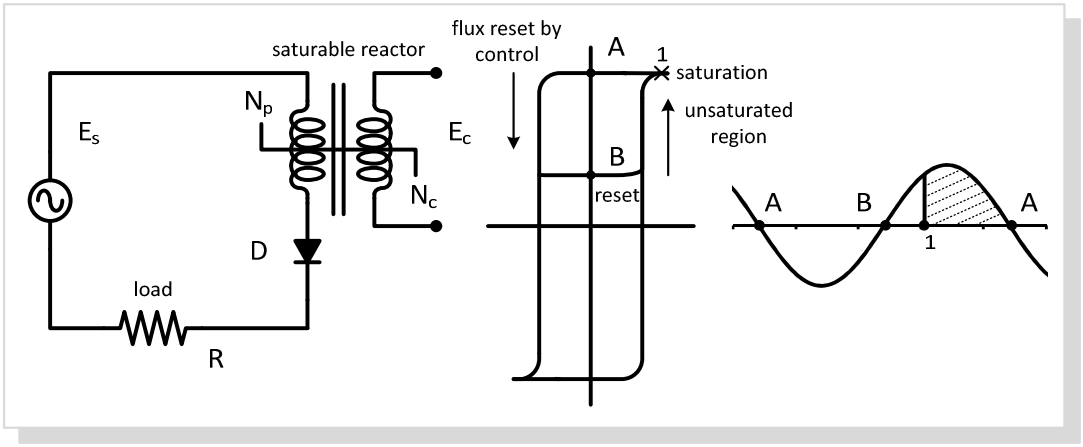

Fig. 2.6. Half-wave magnetic amplifier circuit: flux control and output waveform characteristics.

Taking into account the rectangular $B(H)$ loop and the sinusoidal waveform presented in Fig. 2.6, the half-wave magnetic amplifier operation can be described as follows: the reactor is driven into saturation, enabling the load current to flow, during the so-called conducting period. The reactor operating point is at the level of position 1. Then, at the beginning of the next half-cycle, the so-called control period, the reactor returns to its remanence position, near saturation, position

A, and the diode rectifier becomes reversed biased. At this moment, the control source must set a dc flux level capable of bringing the operating point from position A to position B. At the beginning of the following half-cycle, the diode is once again forward biased and the ac voltage source will cause the reactor to act in the same way, towards saturation.

2.1.3 GENERAL APPLICATIONS AND CONSTRUCTION

The half-wave magnetic amplifier circuit presented in Fig. 2.6 and much more complicated versions had a phenomenal widespread use in the 1950's. The magnetic amplifier or the simple saturable reactor was intensively used in several fields, such as control, regulation and instrumentation. This magnetic device was considered to be one of the most efficient and reliable methods of controlling large amounts of power. It was especially designed to operate from ac supply voltages, 50Hz or 60Hz and it was not expected to respond to frequencies higher than the line-voltage frequency.

It was considered as a long-life, low-maintenance, simple controlled-switch, with no moving-parts and contacts, which required only a very small amount of control power to actuate (high power gain). Input and output were electrically isolated, it presented low internal power losses (the only resistance present was the one associated to the windings), and could easily meet vibration, acceleration and most importantly high-shock requirements, which was mandatory for all equipment installed for the US Navy and other armed forces [2.3], [2.7].

In electric utilities, due to continuity of service requirements, the magnetic amplifier was popularly used in magnetic-amplifier voltage and frequency regulators. It was also used for power control in electric heaters, temperature-controlled ovens, overload detection systems, speed control of dc motors and some special low-power applications [2.4], [2.5], [2.7].

Main aspects regarding construction were strongly related to the selection of the core material. Examples of some of the required characteristics are as follows: minimum hysteresis and eddy current losses, which would mean low resistivity and low coercive force (a lower H_c implies less control power to reset the core); high peak saturation density for large power-handling capacity; quasi rectangular hysteresis loop for an improved switching action; and finally high stability of the magnetic characteristics. In terms of core structures, a large selection was available: toroidal or rectangular-laminated cores (U, E or I shape) were typically used.

Most of the previously referred applications are out-of-date. However, a clear understanding of the operational behaviour of the saturable reactor or the magnetic amplifier, is essential to

demonstrate the flexibility of these magnetic devices. Selecting core materials with different magnetic properties further increases this flexibility and other magnetic devices with different operating capabilities are obtained. So, some of the prior applications have evolved and were adapted to modern technology. New challenges and new control techniques have also appeared. In the following sections, magnetic regulators are presented and some of their current applications will be described.

2.2 MAGNETIC REGULATORS

The well-known bi-stable operation demands some special requirements regarding the selection of the core material, namely selecting a core with a relatively rectangular $B(H)$ loop. However there is another option: it is possible to operate the saturable core reactor in the whole range of the magnetization curve, using round loop, soft-saturation materials.

These regulators may be quite similar in terms of construction, but a different operating principle is established. If these regulators are operated in the knee of the magnetization curve, they may be referred to as one of two types: variable inductors or variable transformers, depending on the number of ac windings. As it will be revealed throughout the remaining sections, these regulators are quite similar to the classical saturable-core reactor, in terms of construction. They exhibit multiple topologies depending on the selected core structures and winding arrangements. The advantages related to the application of these regulators will be pointed out.

2.2.1 VARIABLE INDUCTORS

2.2.1.1 FUNDAMENTALS

In order to describe the operating principle of the variable inductor it is important to recall the fundamentals on inductance definition, as well as some of the basic laws of magnetic theory which are strongly related. An inductor is a device for storing energy in a magnetic field. A typical example is a loop or coil, while the inductance is the constant of the coil [2.6], [2.7].

A time-changing flux $\phi(t)$ passing through a closed loop of wire creates an inductive voltage across that wire. The relationship between the inductive voltage $v_i(t)$ and the magnetic flux $\phi(t)$ is given by *Faraday's law*. If this winding has multiple turns, and each turn links the same

amount of flux, the totalized flux or total *flux linkage*, $\Psi(t)$, may be considered. This statement is expressed in (2.3):

$$v_i(t) = N\frac{d\phi(t)}{dt} = \frac{d\Psi(t)}{dt} \tag{2.3}$$

where N equals the number of turns of wire and $d\Psi/dt$ the time derivative of the flux linkage. If the dc resistance of the winding is considered, (2.3) may be re-written:

$$v(t) = Ri(t) + \frac{d\Psi(t)}{dt} = Ri(t) + v_i(t) \tag{2.4}$$

The term inductance may be defined in different ways with respect to the $B(H)$ curve or loop. The first definition, which is also considered as the general definition, states that the inductance, L, is the ratio of the total flux linkage, to the current trough the winding:

$$L = \frac{\Psi(t)}{i(t)} \tag{2.5}$$

This definition is satisfactory for a medium with a constant permeability such as air. This is not the case for ferromagnetic materials. This is the reason why in such cases a differential inductance, L_{dif}, is also defined as in (2.6):

$$L_{dif} = \frac{d\Psi(t)}{di(t)} = N\frac{d\phi(t)}{di(t)} \tag{2.6}$$

In Fig. 2.7 these two definitions are graphically represented on the $\Psi(t) - i(t)$ plane.

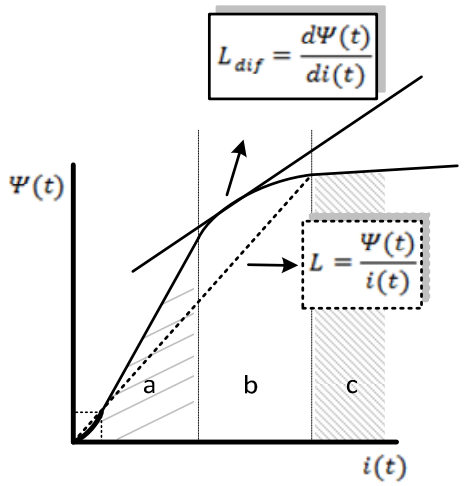

Fig. 2.7. Flux linkage as a function of current, and inductance definitions [2.6].

The magnetic field intensity, H, is defined by Ampère's law. This law states that the integral of the magnetic field intensity vector, $\vec{H}$, around a closed path of length, l, is equal to the total current passing through the interior of the path. If the currents are carried by a winding with N turns, this law can be simply described by:

$$\oint_l \vec{H} \cdot d\vec{l} = Ni \tag{2.7}$$

where i is the current in each turn and $d\vec{l}$ is the infinitesimal element of path length. Both terms in (2.7) are equivalent to a source called magnetomotive force (*mmf*), $\mathcal{F}$. If the magnetic path has *m* windings, (2.7) can be rewritten as:

$$\oint_l \vec{H} \cdot d\vec{l} = \sum_{k=1}^{m} N_k i_k \tag{2.8}$$

The scalar value of the magnetic flux ϕ passing trough a surface S, is related to the magnetic flux density by Gauss's Law (2.9):

$$\phi = \oint_S \vec{B} \cdot d\vec{S} \tag{2.9}$$

where the vector $\vec{B}$ is the surface density of the magnetic flux and $d\vec{S}$ is the vector with direction normal to surface element dS and magnitude equal to the area of dS. If the flux density is uniform and perpendicular to the whole surface area A, then (2.9) can be rewritten:

$$\phi = BA \tag{2.10}$$

The flux produced in a given material by a *mmf* also depends on the material's resistance to the flux, the reluctance of the material, $\mathcal{R}$, or on its permeance, $\mathcal{P}$, which is the inverse of the reluctance. The reluctance will depend on the composition of the material and its physical dimensions. A higher reluctance will imply a higher *mmf* in order to obtain a given magnetic field. The reluctance associated to a magnetic path, of constant cross-section A, considering an homogeneous magnetic material, can be obtained by:

$$\mathcal{R} = {}^{l}/_{\mu A} \tag{2.11}$$

where l is the magnetic path length and μ the permeability of the material.

If an air gap is included in a closed magnetic circuit, the total reluctance of the circuit is the sum of both reluctances. However, the reluctance of the air will obviously be much higher, since the relative permeability of the air is only 1. In those situations where the magnetic circuit is not homogeneous, the apparent total permeability of the circuit is called effective permeability, μ_e. This permeability depends on the initial permeability, μ_i, of the magnetic material, the dimensions of the magnetic path and the air gap.

These considerations and the reluctance and permeance definitions are very important for the description and understanding of the operating principle of the variable inductor. Taking into account these definitions and previous equations, (2.5) can be rewritten:

$$L = \frac{N\phi}{i} = \frac{NBA}{i} = \frac{N\mu HA}{Hl/N} = \frac{N^2\mu A}{l} = \frac{N^2}{\mathcal{R}} = N^2\mathcal{P} \tag{2.12}$$

2.2.1.2 OPERATING PRINCIPLE

It is important to relate the magnetization curve with the concept of variable inductance. Using (2.10), the totalized flux can be related with the magnetic flux density. Similarly, using (2.7) the current in each turn can be related with the magnetic field intensity, in a simplified version:

$$\begin{aligned} \Psi &= N\phi = NBA \\ i &= Hl/N \end{aligned} \tag{2.13}$$

Using a simple coordinate change, the graphic representation of the totalized flux versus current, $\Psi(i)$, may be superposed to the magnetization curve of the material. By recalling the inductance definition and particularly the differential inductance definition presented in (2.6), it is clear that operating the regulator in the different regions of the magnetization curve has a significant effect on the differential inductance of the ac winding placed on the magnetic core.

By using round loop, soft-saturation materials and operating the regulator on the transition region or in the knee of the $B(H)$ curve, a variable inductor is obtained. The inductance in this region can vary between a maximum and minimum value, until saturation is reached.

In the late 1980's, some authors named this device as a LVI, linear variable inductor or a quasi-linear controllable inductor, referring its potential in high-frequency applications, [2.12],

[2.27]. In [2.12], such a device is presented, with a similar configuration to the one presented in Fig. 2.5. It is stated that, ideally, the coupling between the ac winding and dc winding is null. As previously mentioned this implies that the ac winding will not influence the control winding. It is also stated that any impedance associated with the control winding, including its parasitic capacitance, will not influence the ac winding, which is crucial in high-frequency applications. In addition it is pointed out that this device is conceptually different from integrated magnetic components or other types of inductors or transformers designed with controllable leakage inductance [2.17], [2.31]. The same author presented posterior works with practical applications of the device, namely in dc-dc converters for telecommunications. As an example, in [2.21], the variable inductor is used to ensure continuous current conduction mode for all levels of processed power by an input-current-shaper converter, specifically a boost converter, at a switching frequency of 100 kHz.

In [2.13], a new horizon has been pointed out by suggesting the use of current-controlled variable inductors into resonant power circuits. The main objective was to develop a device capable of fulfilling the role of the typical resonant inductor in high-frequency, high-power resonant inverters. In 2003, the same authors have presented a Spice behavioural model of non-linear inductors, which was considered an initial approach for modelling the behaviour of the variable inductor [2.15].

The variable inductor, proposed by D. Medini and S. Ben Yaakov, is presented in Fig. 2.8a. The variable inductor can be implemented using a gapped E core set, as the one presented in Fig. 2.8b. This gapped core helps maintaining a low effective permeability, thereby avoiding quick saturation of the core. The main winding is placed in the middle leg of the core and the control windings are placed in the left and right legs. These windings are serially connected in opposite polarity, in order to cancel the ac voltage induced on the dc control circuit, under the assumption of symmetry.

The physical operation of the device can be simply described as follows: due to the small air gap in the middle leg, the ac flux will flow through the middle leg and then divide between the left and right legs according to the reluctance of each path. A rising dc control current tends to increase the flux density of the dc path, increasing the effective global reluctance of the core. Only a small amount of dc current will be necessary to alter the effective permeability perceived by the main winding placed in the middle leg, thus altering its inductance value, L_{ac}. A variable inductance will then allow the control of the power flow in the resonant circuit.

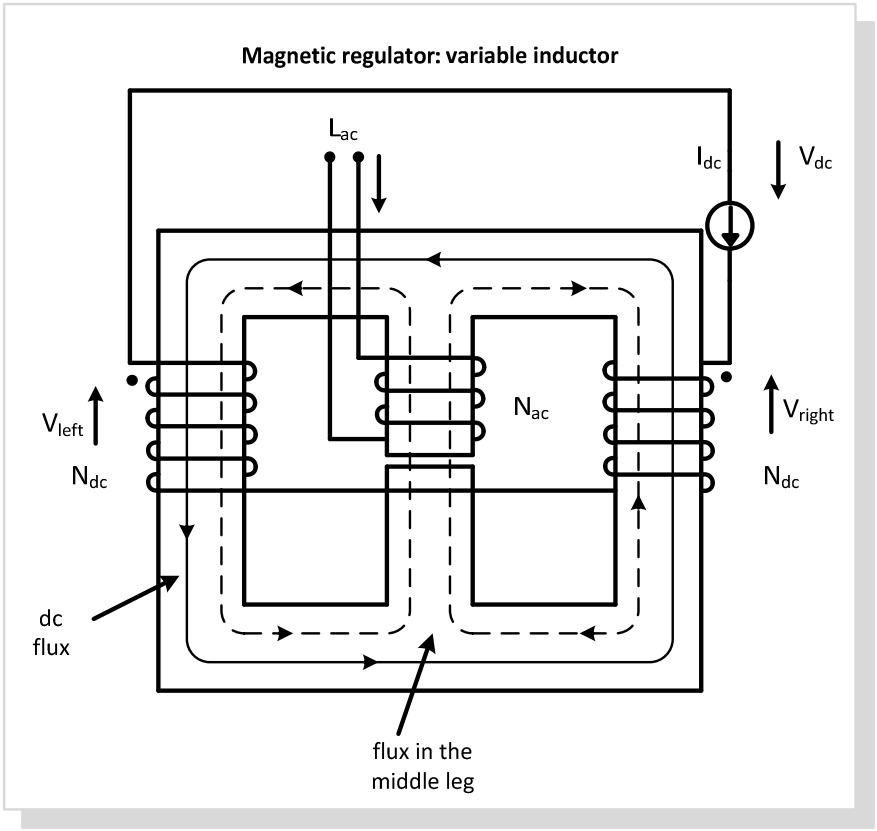

a. Current-controlled variable-inductor, [2.13], [2.16]

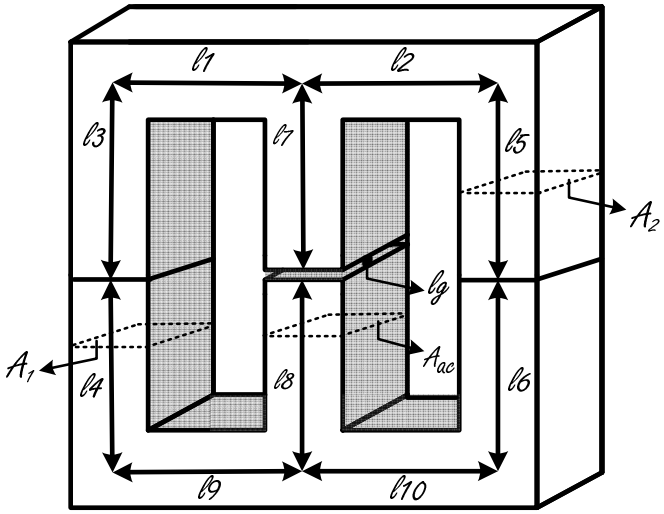

b. Gapped E core

Fig. 2.8. Magnetic regulator: variable inductor.

The magnetic-circuit analysis contributes to the understanding and prediction of the behaviour of the variable inductor, by giving an estimation of how the inductance L_{ac} evolves. The theoretical analysis of the magnetic device is a non-trivial task. An equivalent circuit model, based upon its actual physical structure, represents a practical approach. The classic theory on magnetic modelling of multi-winding devices begins by establishing a more or less complicated

reluctance model of the structure. Fig. 2.8b. shows the definition used for the magnetic paths which together make up the device. Each magnetic path is related to a specific reluctance $\mathcal{R}_i$, defined by:

$$\mathcal{R}_i = {}^{l_i}/_{\mu A_i}\,;\ \text{i=1..10} \tag{2.14}$$

where l_i is the magnetic path length, A_i the correspondent cross sectional area, μ the permeability. The estimation of these several reluctances, superposed on the core geometry, is necessary for modelling the device behaviour.

Fig. 2.9 shows the typical measurement setup. Sense windings with integrators circuits are used for flux density measurements and the voltage V_s across resistor R_s is proportional to the magnetic field in the middle leg [2.16].

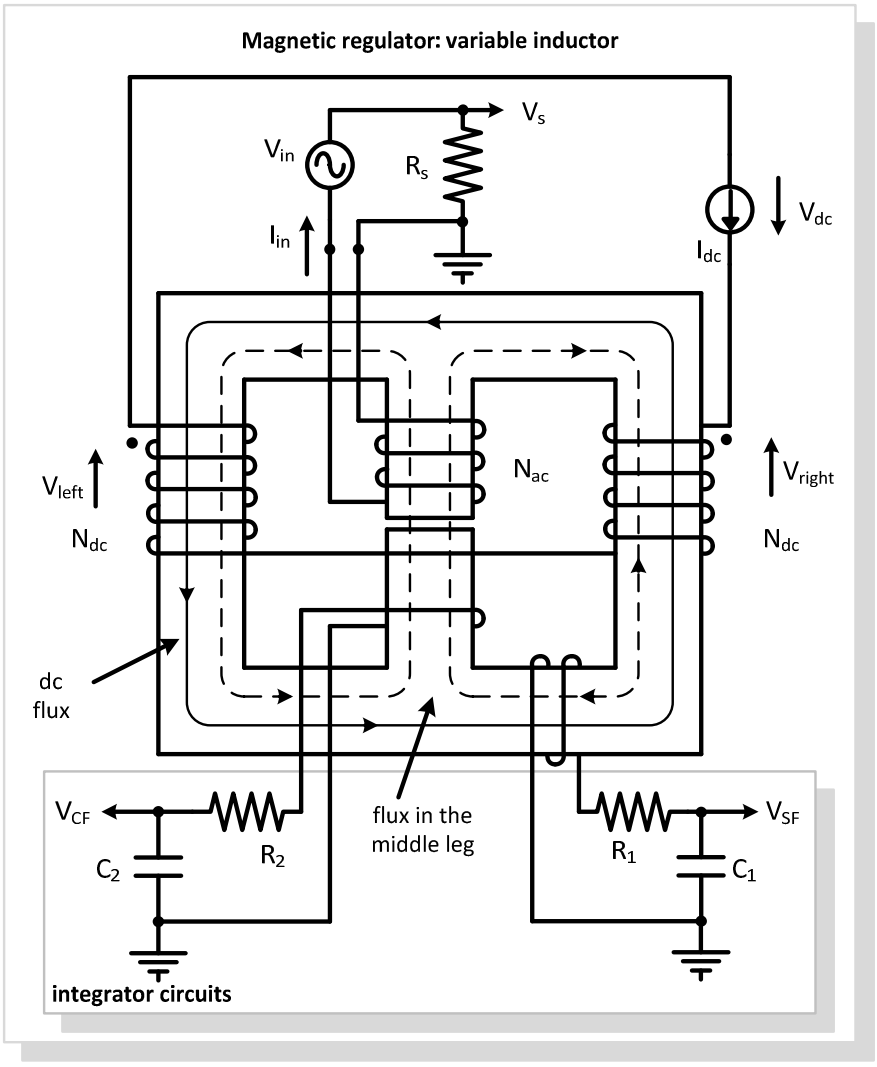

Fig. 2.9. Magnetic regulator: variable inductor [2.13], [2.16].

Throughout this work several variable inductors were design and built following the methodology exposed in [2.44], [2.45] and [2.46]. Fig. 2.10 presents the small-signal $L_{ac}(I_{dc})$ characteristic of one of these regulators. This characteristic is quite representative of the normal behaviour of a variable inductor. For a zero dc control current the inductance associated to the main winding is at its maximum value, L_{max}. If the control current increases, this value progressively decreases until a minimum value is obtained, L_{min}. If the core is completely saturated there will be a limit low value for this inductance. In these circumstances, further increasing the control current will have almost no effect on the inductance value. This characteristic may easily be obtained using an impedance analyzer or an LCR meter, by simply varying the control current in the dc windings.

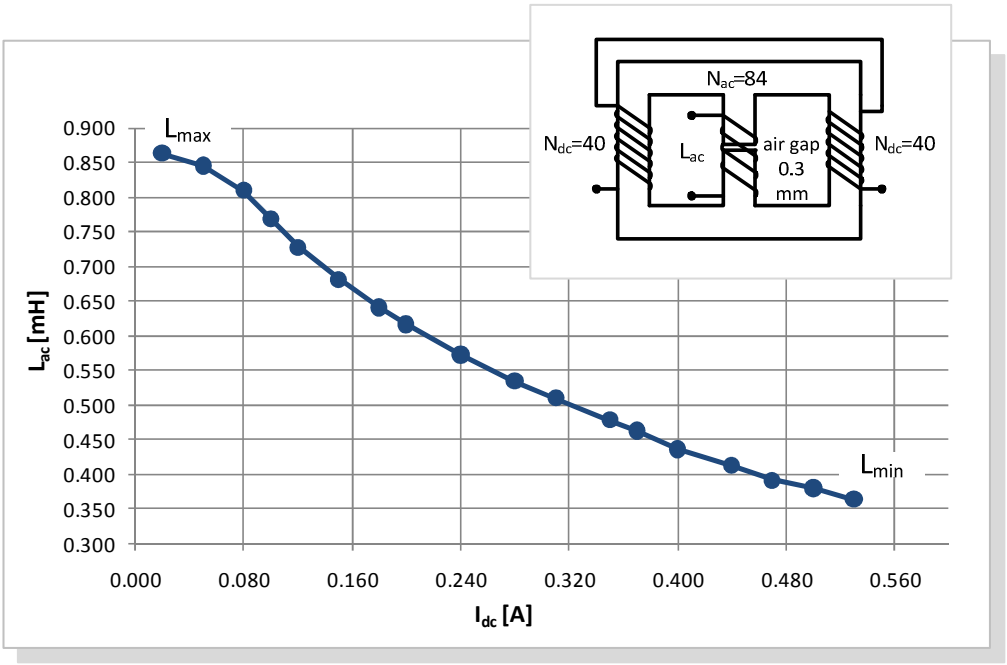

Fig. 2.10. Typical variable inductor small-signal characteristic

2.2.1.3 VARIABLE INDUCTOR STRUCTURES

The magnetic regulator in the form of a variable inductor has been the object of several patents. They all refer the device, or in this case the invention, as useful or industrially applicable. Some present one or more claims regarding the construction of the variable inductor device, comparing it with prior art, and others present claims regarding specific applications for the regulator. Fig. 2.11 illustrates a small group of magnetic regulator structures and topologies which are claimed in distinctive US Patents.

As example, a first patent, from 1971, Fig. 2.11a., claims to present a variable inductance device which requires only a low amount of dc current to obtain the desired variable range of inductance, for use in radio receivers or other electronic instruments, [2.9]. It refers some prior patented structures, basically toroidal shaped-cores. It refers that this prior art devices have a low Q value due to the coupling between the high-frequency coil and the dc coil. The quality factor Q is a measure of the relative losses in an inductor as is typically defined as the ratio between the inductive reactance to the effective resistance. In order to increase the quality factor, a large inductance was typically connected in series with the dc coil to increase its impedance. This would, however, require a large dc current to obtain the desired range of variable inductance. An important aspect clearly stated is that variable inductances for high-frequency applications normally require a magnetic core of ferrite material. The high electrical resistivity of ferrite materials assures a high Q value. The ferrite core is also required to have a widely variable range of permeability because a large value of dc current is used. This implies that the ferrite material must have a high initial permeability and low-magnetic losses in high-frequency ranges. The use of an adequate material may guarantee a lower maximum value for the dc control current.

The purpose of the proposed structure however is to avoid the large dc current required to obtain the desired variable inductance range, while maintaining a high quality factor, for high-frequency applications between 1500kHz and 500kHz. Presented in Fig. 2.11a. are several options for this variable inductor, in terms of core structures, and a perspective view of one of them (E-shaped and I-shaped, with an insertion material in the middle presenting a higher magnetic permeability). The dc current flows through the winding placed in the middle leg, inducing fluxes ϕ and ϕ', respectively in the left and right legs. The winding in the left is wound clockwise to the direction of flux ϕ and the winding on the right is wound counter-clockwise to the direction of flux ϕ'. The patent claims that these windings and the dc winding placed in the middle leg are not electrically coupled when $N\phi = N\phi'$. Under this condition, when a high-frequency voltage is applied to the external windings, no voltage is induced in the dc winding. The external windings will present a higher Q regardless of the small impedance of the dc winding and no extra inductance must be added. No air gaps must be present between the core structures since this would decrease the variable inductance range or would require a larger dc current to maintain the desired range. To avoid this problem an insertion material with a higher permeability is included between the structures. The maximum value for the dc current will dictate the lower value for the inductance.

Patents presented in Fig. 2.11b. and Fig. 2.11c. are more recent. The first one comprises a magnetically saturable EE core, with a complicated set of air gaps and so-called flux bridges in the external legs, also with a dc winding placed in the middle leg, a so-called signal winding in the external legs and a possible secondary winding, see [2.10]. The main claim is related to the lower core losses relative to the amount of energy stored, dictated by the presence of the air gaps and the flux bridges. If secondary windings are effectively used these regulators may be described as variable transformers.

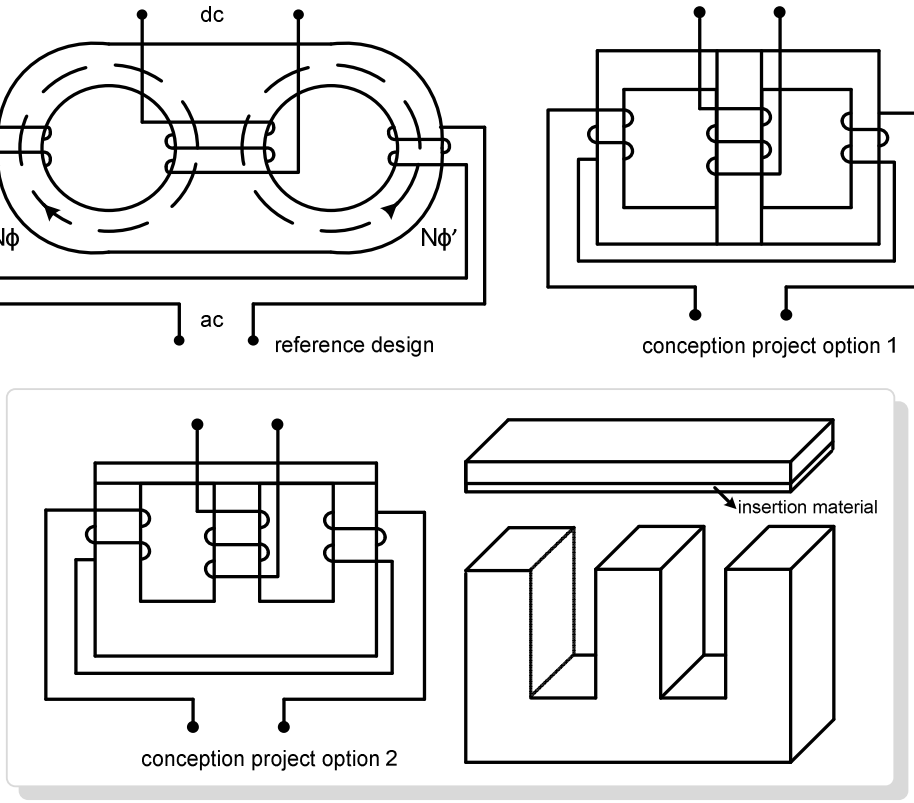

a. US Patent 3631534: Variable inductance device [2.9].

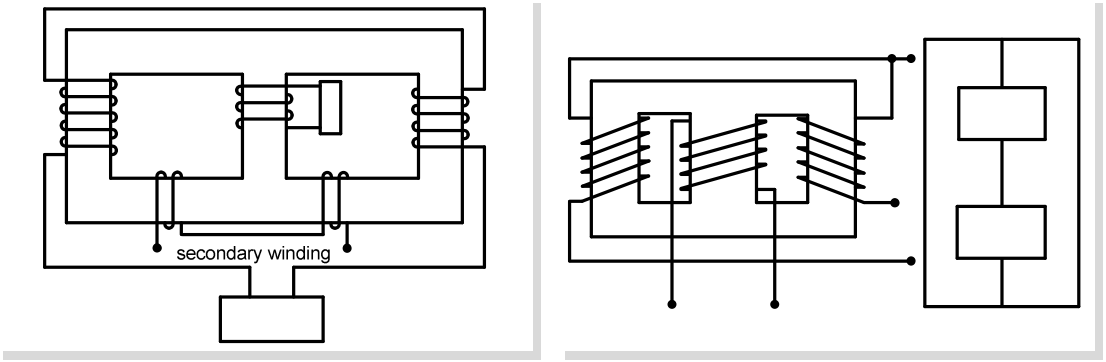

b. US Patent 5426409: Current-controlled variable inductor [2.10]

c. US Patent 6317021: Variable inductor [2.11]

Fig. 2.11. US Patents: Magnetic regulator structures and topologies.

In the second one, the structure is based on EE core as well and the dc winding is also mounted on the middle leg. The outer windings are connected in parallel and in such a way that the magnetic flux arising from currents through the windings on the outer legs is cancelled in the middle leg. So in this case, the dc control current through the middle winding is responsible for a variable inductance across the outer windings, by changing the saturation level of the outer legs, while the inductance across this dc control winding is substantially constant [2.11]. It is stated that in a preferred embodiment, the magnetic cross-section of the centre leg must be equal or somewhat larger than the sum of the magnetic cross-sections of the outer legs. It also refers prior art, where as usual, the control winding is equally divided and mounted on the external legs, serially-connected in opposite polarity, and the high-frequency winding is placed in the middle leg. It refers some of the prior art limitations, such as low variable inductance range, high dc control current range, non-symmetry and coupling between the ac and dc windings.

So, in conclusion, there are in fact several possible topologies and more or less complicated core structures for the conception of these variable inductors. These reported patents are only a small glimpse of possible solutions. Limitations and possibilities are associated with all of these options, and obviously must be considered depending on the desired application. Some of these limitations may be overcome, by selecting an appropriate core material.

As previously mentioned, a soft saturation material would be preferred. Ferrite cores saturate rather abruptly, moreover the saturation flux density is a function of temperature. For Molyperm (MPP) cores, the reduction in permeability as a function of flux is very gradual, so MPP is also a soft saturation material. Nevertheless, one of the problems with MPP cores, is that they have much higher losses than ferrites. Powdered iron cores saturate slightly harder than MPP and while a variety of permeabilities are available, they are typically lower than MPP's. This means that a powered iron regulator would be larger than a device having the same inductance and current capacity but built on a MPP core. However powdered iron cores are cheaper than MPP's. So in fact, all of this must be considered when choosing the core material. However ferrites are still the typical solution, since they are made by a wide variety of vendors, in the necessary shapes, E, I, U, EFD, E gapped cores, and workable frequency limits, which is not the case for some of the other materials [2.5].

2.2.2 VARIABLE TRANSFORMERS

The inclusion of one or more secondary windings leads to a second type of magnetic regulators: variable transformers [2.18], [2.19]. In [2.18], a US Patent from 1988, a self-regulated transformer-inductor with air gaps is presented. The transformer is designed to carry out voltage regulation by self-controlled absorption of reactive power. The inventors claimed that by disposing additional windings on the magnetic core of a specific variable inductor, one could obtain a voltage regulating apparatus both efficient and autonomous, or a transformer having the ability to supply a load from an alternating current source, for example a capacitive source, while carrying out efficiently and autonomously a regulation to compensate both the input voltage and load variations.

The physical structure of this variable transformer is illustrated in Fig. 2.12. It is a three-leg structure, with two central gaps of equal dimensions in the outer legs. An ac power source is connected to the primary winding which is placed in the middle leg. The secondary winding is also placed in the middle leg and is connected to a load, Z. There are two additional auxiliary windings, connected in series and placed in the outer legs. These windings are also supplied by the ac power source. Finally, two dc control windings, connected in series, are placed in the outer legs. These dc windings are supplied by the ac current flowing through the auxiliary windings which is then rectified by the diode bridge. An inductor of a fixed value may be connected in parallel with the auxiliary windings, so that the amplitude of the ac current generated by the power source is limited to its inductance value.

The operating principle can be described as follows: if the dc control current increases its value, the core goes further into saturation, due to the increase of the reluctance of the external magnetic path. This action results in a lower inductance value for the auxiliary and primary windings and an increase of current in these three windings. It is therefore possible, within a range of source currents, to regulate the ac voltage across them. The voltage across the secondary winding, applied to the load, is determined by the ratio of the number of turns of the primary and secondary windings.

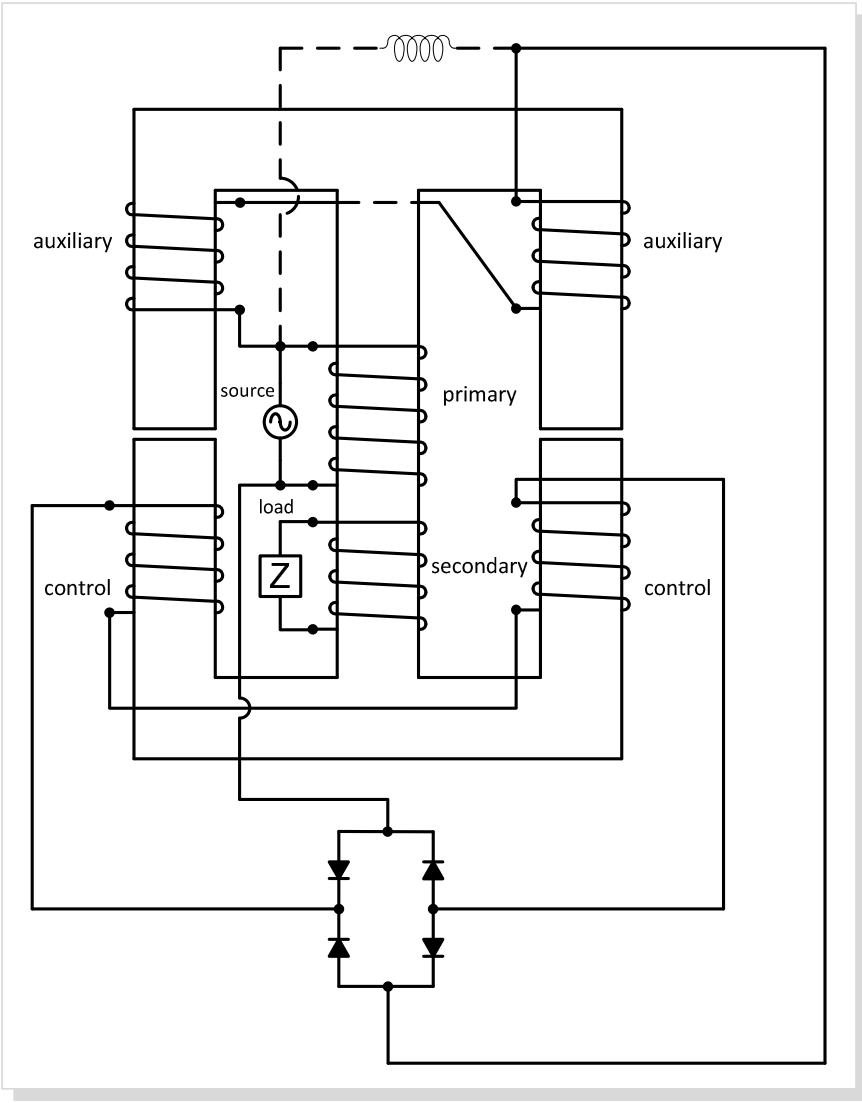

Fig. 2.12. US Patent 4766365: Self-Regulated Transformer-Inductor [2.18].

In [2.19], another US Patent from 1989, a non-saturating magnetic amplifier controller is proposed, namely for ac voltage regulation. In [2.20], the previous patent is further explored and some other alternatives regarding the regulator structure are pointed out. These structures are shown in Fig. 2.13 and will be further described.

In [2.19], it is stated that in opposition to traditional switching regulators, based on active devices, which would present some disadvantages due to the noise and additional losses generated by the switching, this magnetic amplifier would act in a similar way, switching power on and off, but without active devices and therefore without the sensitivities of active devices.

Their claim is to present a magnetic amplifier voltage regulator, without switching elements and with reduced noise and losses and which will not operate in the saturation region. The initial preferred embodiment selects a three-legged core structure, with a dc control winding, a primary

and secondary windings mounted on each one of these legs. The amplifier is operated without driving the core into saturation and the primary and secondary legs may even contain an air gap. The dc current will control the reluctance of the control leg relative to the reluctance of the secondary leg. By controlling the relative reluctance, the amount of ac magnetic flux coupled to the secondary winding may also be controlled, which in turn means controlling the output voltage provided by the secondary winding.

In the case of [2.20] it is also recalled that in high-voltage power supplies there is an obvious concern related to the switching losses, typically because some of these sources may operate at high switching frequencies. Resonant switching techniques were developed with the aim of reducing the switching losses, at these high frequencies, thereby reducing the size and weight of many of its components. However, a key problem is the fact that these resonant converters usually employ the operating frequency as a control parameter to regulate the output voltage. With a variable operating frequency it is possible to modify the characteristics of the resonant circuit and therefore control the output voltage. In some cases, the range of the operating frequency may be extremely large, which has a negative impact on the design and construction of the EMI filter which today is a basic requirement in power supplies [2.30].

In [2.20], another disadvantage is pointed out: in areas like avionics, or missile radars, there is a necessity of increasing the operating frequency, not only to reduce size and power losses, but to synchronize the operating frequency with a system clock. It is obviously impossible with a variable operating frequency. An alternative would be, obviously, the magnetic regulator, due to its variable inductance behaviour, or as pointed out by the author, a magnetic regulator exhibiting an electronically-adjustable turns ratio. The regulator in question would behave as a simple transformer, for each predetermined level of dc control current, or as a variable transformer for a variable dc current, with a variable input-to-output conversion rate.

The physical structure of this magnetic regulator is illustrated in Fig. 2.13a. It is a four-leg structure. The control windings, with the same number of turns, are wound around legs 1 and 2, serially connected in opposite polarity. The induced voltages on these windings will have opposite polarities and, under the assumption of symmetry, they should cancel each other. The primary winding, is wound around leg 3 and finally, the secondary winding is wound around leg 4, which includes two small intentional air gaps. These windings may have a different number of turns.

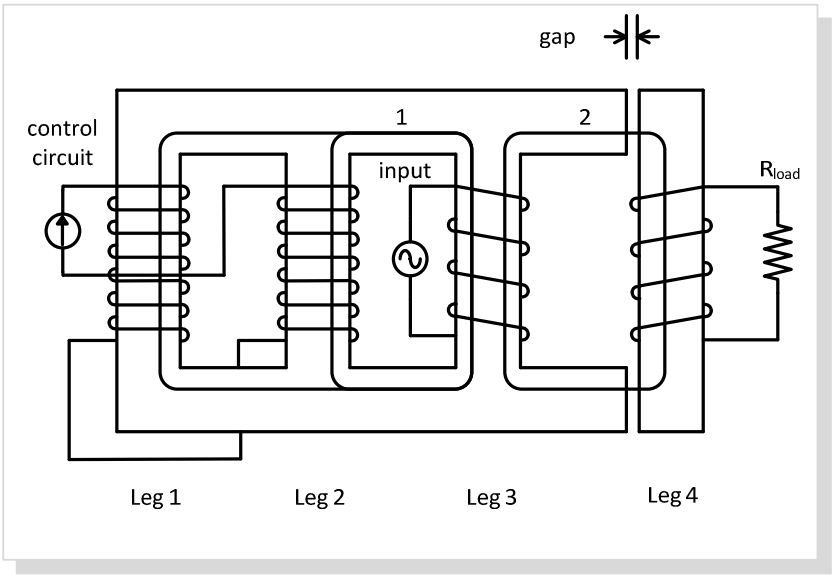

a. Physical structure of the four-leg magnetic regulator [2.20]

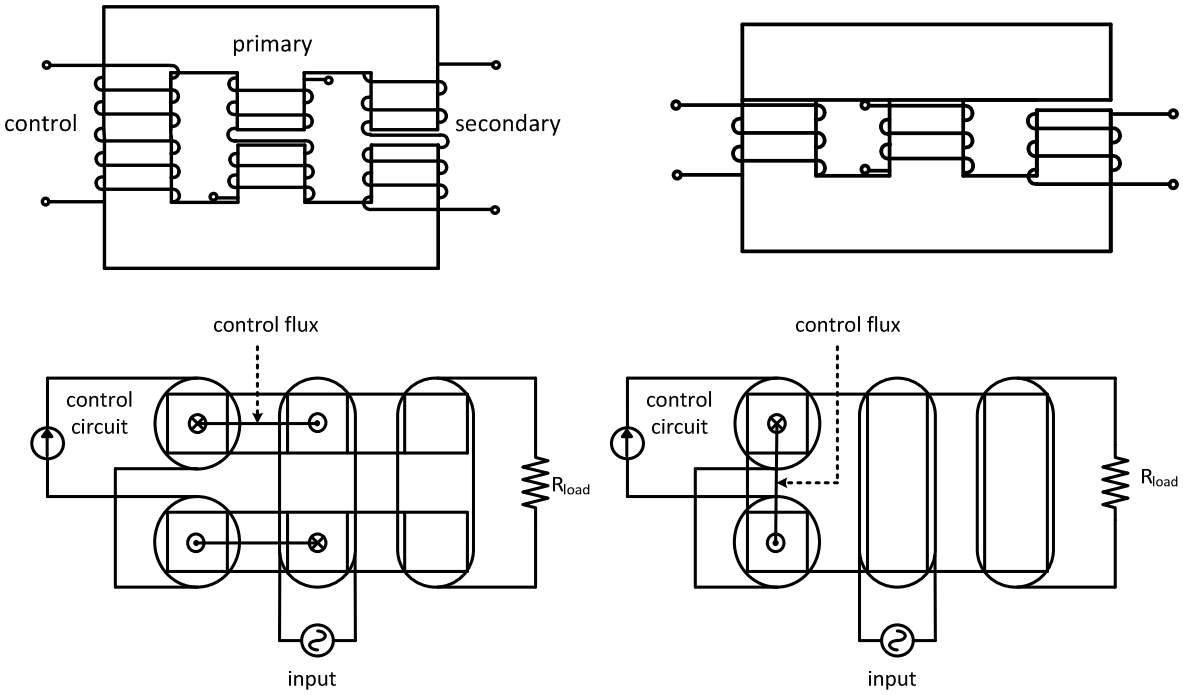

b. US Patents 4841428: Non-saturating magnetic amplifier controller [2.19]

c. Physical structure of an improved three-leg magnetic regulator [2.20]

Fig. 2.13. Magnetic regulator with additional windings: variable transformer [2.20].

By connecting an ac voltage source to the primary winding and a simple load resistance to the secondary winding, the regulator will behave as follows: the ac flux generated by the primary winding will flow through its corresponding leg and then divide between the left and right paths according to the reluctance of each path. A dc current circulating through the control windings varies the dc flux density in the left half of the structure. Considering a zero dc current, the path on the left will have a much lower reluctance due to the air gaps introduced in the right path. As a

result, the ac flux generated by the primary winding that links through the secondary will be lower, thus little ac voltage will be induced in the secondary winding. If the dc current is large enough to push the operating point towards saturation, the reluctance of the path to the left of the primary, increases relatively to the reluctance of the path to the right, making it possible to control the amount of the ac flux coupled with the secondary winding. In these conditions, the voltage induced on the secondary will be equal to the primary voltage times the turns ratio of the secondary to the primary, minus some voltage loss due to the leakage flux, which is somewhat difficult to estimate.

In [2.20], the reluctance concept together with the duality theory is used to generate, first, the magnetic equivalent circuit of the device and then, the inductances circuit model. Since the equations that describe the magnetic circuit have the same form as those for the electrical circuit, the method used to find the dual of an electrical circuit can also be applied to find the dual of a magnetic circuit. The same techniques will be applied to the variable transformer devices that were developed throughout the work, as described in future chapters.

Fig. 2.13b. shows two views of one of the possible structures suggested in [2.19]. It can be done using two EI cores or two EE cores placed side by side. The magnetic path of the control flux is also detailed. The control leg does not include an air gap as opposed to the primary leg and the secondary leg. In the following description, although referred to as single legs, all legs comprise parallel portions of the parallel core elements. The gap in the primary leg is optional, however if present, it should be smaller than the gap in the secondary leg. This will result in a higher reluctance of the secondary leg when compared to the primary and control legs. Also, the cross section of the primary leg must be sufficiently larger than the cross section of the control leg, so that, as the control leg approaches saturation, it does not significantly affect the permeance of the primary leg. In fact, to take advantage of working at the knee of the $B(H)$ curve, saturation must be approached but not reached.

As stated in [2.20], the previous structure has a clear advantage over the four-leg structure. In the four-leg structure, the magnetic paths through each control leg will have different reluctances due to the greater distance between the primary (leg 3) and control leg 1, than between the primary (leg 3) and control leg 2. This causes an ac voltage to appear across the control windings which may be shorted using a capacitor. This places the control windings in parallel, forcing an equal ac voltage in each. The fluxes through legs 1 and 2 are then forced to be equal at the expense of having some circulating current in the control windings. The dc flux is contained for the most part in the ungapped control legs whereby legs 3 and 4 are subject to insignificant dc

flux [2.19]. On the other hand, in the three-leg structure, the parallel portions of the control leg are equidistant from the primary and no circulating current will appear in the control windings. It is expected that the ac flux generated by the primary winding divides itself equally between both control portions. Nonetheless, as shown in Fig. 2.13b., the dc flux is not confined to the control leg, it also flows through the parallel portions of the primary leg. This means that the reluctance associated to the primary leg is dependent of the control current. Since the core loss in ferrite which contains a dc bias is greater than that in unbiased ferrite, the losses in the primary leg would be greater than that in the four-leg structure.

Taking into account previous considerations, Fig. 2.13c. shows two views of an improved three-leg structure as suggested in [2.20]. This structure uses a custom-made core which resembles an E-I core with a longitudinal slot cut in one of the outer legs. The windings are mounted on each leg in a similar manner to that in the previous structure. It is stated that in this case, the absence of a central gap, confines the dc flux to the parallel portions of the control leg. The core losses are expected to be lower.

2.3 APPLICATIONS OF MAGNETIC REGULATORS

Several published papers and patents show a variety of possible applications for the magnetic regulator in its various forms. The device can be used as reactive power compensator in electrical power systems, for dynamic load impedance correction in induction heaters and in other applications, involving for instance ZVS or ZCS operation in dc-dc converters. In this section some of these applications will be summarized and some starting considerations on magnetic control applied to electronic ballasts will be presented

2.3.1 GENERAL APPLICATIONS

The so-called LVI, linear variable inductor or quasi-linear controllable inductor, [2.12], was used by A. S. Kislovski, in the late 1980's and 90's, in a variety of applications mainly in the telecommunications field: in single-phase telecom rectifiers [2.21] or in dc current sensors utilized in telecom solar battery chargers [2.22]. LVI current sensors are based on the operating principle of the regulator: the inductance of the magnetic regulator is a function of the magnetic control field. If this field is created by a dc current which has to be monitored, and if an ac voltage is applied to the ac winding of the LVI, the ac current circulating in the circuit will be a

function of the said dc current. Thus, a measurement of this ac current contains information on the dc current producing the control field. The simplest way to obtain this information is to rectify the ac current and to obtain a dc voltage as shown in Fig. 2.14.

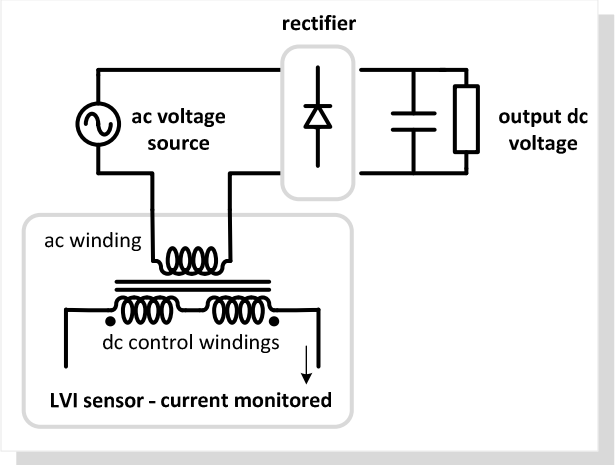

Fig. 2.14. Current sensor utilizing a LVI [2.22].

Almost at the same time, the regulator was also used in ac voltage regulation. In [2.26], a new family of LVI based ac regulators was presented. These regulators would limit the input current at the minimum value requested to sustain the output voltage for any line and load condition. Similar principles were applied by the same author to regulate high-voltage generators [2.27].

In [2.28] a "variable inductive filter" is also used to perform a "quasi-active" PFC. This solution avoids using an active filter, for instance a boost converter. The first stage, a typical full-bridge rectifier, as shown in Fig. 2.15, is followed by the classical passive PFC solution, an inductor filter, L, connected to a parallel capacitor, C_p, which may be linked to a load or a second dc-dc converter stage. It is stated that in specific conditions, this inductor filter plays no role in the output voltage ripple, however it determines the rectifier line current harmonics and the power factor. This inductive filter is then replaced by a variable inductor. Three types of variable inductors are described, whose reluctance varies according to the level of current that flows through them, I_{in}. They cannot be considered as magnetic regulators since they do not respond to an external control current. The first is a simple saturable inductor, approaching saturation when the current exceeds certain limits, thereby decreasing the inductance value. The second is a swinging inductor having a stepped air-gap. The core has two parallel reluctance paths, with two series reluctances, the core and the gap. As the current increases, the path containing the smaller gap reaches saturation first and the global reluctance increases, decreasing the inductance. Finally a sloped air-gap inductor is also presented. It is similar to the previous inductor, but instead of

having two paths with different gaps, they have one path with a graded slope gap. This implies that the variation of the inductance with the current is more gradual. Even if these variable inductors are not the typical magnetic regulators, they share however, the same basic principle: establishing a variable core reluctance in order to achieve a variable inductance winding.

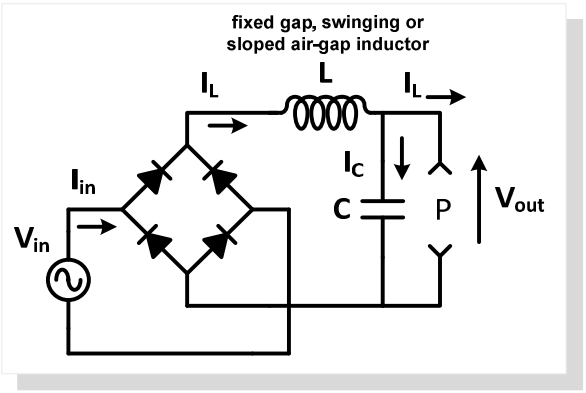

Fig. 2.15. Rectifier circuit with passive PFC with magnetic control.

In [2.34] the variable inductor is used in automated test systems for proximity sensor electronic units in the aircraft industry. Variable inductances are capable of simulating the behaviour of inductive proximity sensors. The so-called saturable core reactor solution is pointed as a better option when compared to other available variable inductors, such as the moving core inductor, where a cylindrical slug moves through a hollow cylindrical winding or the switched inductance decade boxes. These two other solutions require either a mechanical action to take place or are responsible for discontinuities in the inductance value.

In [2.35], the magnetic regulator is also used as a dynamic load for impedance correction in induction heaters. Heating ferromagnetic materials until they pass their Curie point, leads to abrupt changes on the magnetic properties of those materials. A modern induction heater typically includes an inverter, a work head (a transformer) and a work coil, both linked by a resonant circuit. Abrupt changes on the magnetic materials alter the coupling coefficient between the work head coil and the load. Since the work head is normally part of the resonant circuit, any change in the coupling coefficient, as the load heats up, causes a change in the impedance of the circuit at the resonant frequency. A variable inductor can then be used to compensate these changes.

The high increase in nonlinear loads boosts the demand for variable reactive power compensation. This is one of the most common applications which uses both variable inductors and variable transformers. Such applications, specifically for electric power systems, can be

found in [2.36], [2.37], [2.38]. In [2.37], a variable inductor is used on an active power filter strategy. Traditional solutions to control the reactive power flow would be for example the SVC, static VAR compensator, including a thyristor, a linear inductor and capacitor. The SVC can be tuned by varying the inductance in the thyristor controlled reactor. However, all of these SVC systems have a problem of harmonic currents arising and the harmonics of the output current cannot be neglected for large power applications [2.38]. To limit the harmonics, there are two approaches. One is to use an additional filter such as a passive filter or an active power filter. Another simple effective solution is to use a linear variable inductor capable of limiting the harmonics components in the output current. After introducing the conventional "shunt direct current controllable reactor", DCCR, which in fact is a variable transformer, a so-called new "shunt direct current controllable reactor", DCCR, is proposed. In [2.38], the same authors propose a variable inductor based on a ferrite orthogonal core controlled reactor as the fundamental part of a new static VAR compensator. As shown in Fig. 2.16, the so-called secondary winding, which in fact is the dc control winding, is connected to the primary ac winding through a voltage source inverter, VSI, and a switch. i_{SVC}, i_R and i_C are respectively, the current of the SVC, the current of the reactor and the current of capacitor C. At the primary side a harmonic compensating winding is added. A controller is then configured to control the current of the secondary and the current of the inverter in order to compensate the harmonic content of i_R. In this way the authors point out that it is possible to maintain a sinusoidal primary current in a wide control region.

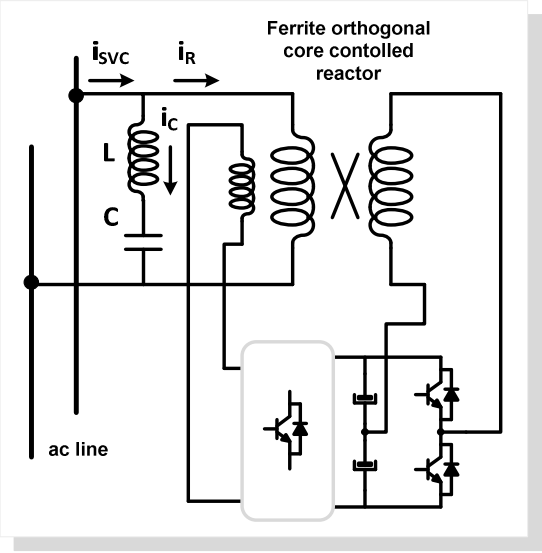

Fig. 2.16. Static Var Compensator based on a core controlled reactor [2.38].

The increasing performance of available magnetic materials, adequate for high-frequency applications, led to the inclusion of magnetic regulators into resonant power circuits. A US Patent from 1991 already mentions the use of a variable inductance into a resonant converter. The object of the invention is to disclose a parallel resonant converter which controls a variable inductor to regulate the voltage output, under ZVS conditions and CCM [2.29]. Similar to other patents, it mentions major issues: switching inductive loads at high frequencies originates high switching losses and switching stresses on the semiconductors. At megahertz frequencies, the influence of parasitic elements on the operation of converters may be significant. A parasitic element like a leakage inductance of a transformer can conveniently be used in specific circuits. However, in some cases, the adverse influence of these elements is to be expected and must be dealt with. Resonant converters are an obvious solution, since they are attractive for high-power applications; they allow high-frequency operation, low switching losses (switching at ZVS or ZCS) and reduction in size and weight, without compromising the circuit efficiency.

As mentioned in the preceding chapter, the initial goal of this work was to develop magnetic-control based techniques for luminous flux regulation. This preliminary work progressed and other lines of research were followed, such as viability and performance studies on magnetic-control based *universal* ballasts. Despite of the several possibilities to proceed in this field of research, a natural step was to explore different lines of work and continue to investigate the possibility of using magnetic regulators into other types of resonant converters, as in the previous US Patent. An attempt is being made to increase the performance of these converters and the range of possible applications, especially by the possibility to work at a constant high-frequency [2.52]. Fig. 2.17a. shows an example of a dc-dc parallel resonant converter with magnetic control. Even though this converter makes use of a series resonance between the variable inductance, L_{ac}, and the capacitance, it is usually referred to as a parallel resonant converter because in this case the load of the resonant circuit is connected in parallel with the resonant capacitor.

It seems however that the dissemination of the developed work throughout the scientific community has once again confirmed the popularity of magnetic regulators. Other lines of investigation and applications are resurging.

In [2.33], a two-phase interleaved LLC resonant converter is proposed, using a current-controlled inductor to adjust the resonance frequency of one module, for compensation of component mismatch. LLC resonant converters are currently well-accepted due to their ability to maintain ZVS down to the no-load condition, by taking advantage of the magnetizing inductance of the transformer. In low-voltage and high-current output applications, interleaved converters

stand as a solution to reduce the output current ripple and the size of the output capacitor. Since resonant converters typically use the operating frequency as the control parameter, the high gain of the resonant circuit makes the resonant current very sensitive to that control parameter. As a consequence, if two interleaved resonant converters are operated at the same frequency, any component mismatch between both modules may cause a serious current unbalance. So, as shown in Fig. 2.17b., a solution to compensate resonant component mismatch may be adopted. A variable inductance is placed in one of the converters in order to equalize the resonant frequencies of both modules. In [2.33] a comparative analysis is performed between this proposed solution and the typical operation of a balanced and unbalanced system.

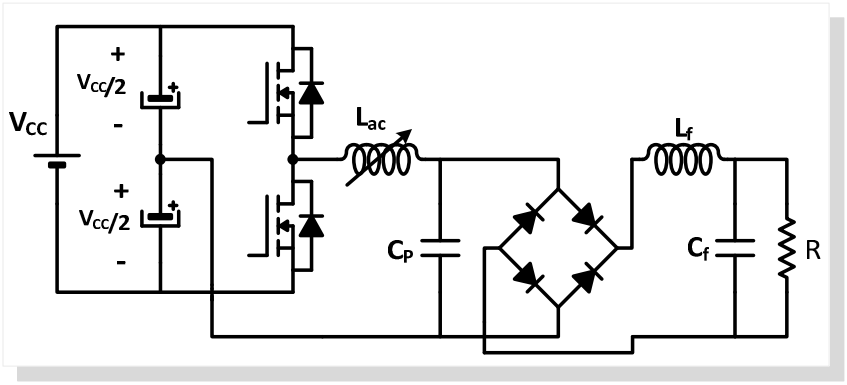

a. Dc-dc parallel resonant converter [2.29], [2.52]

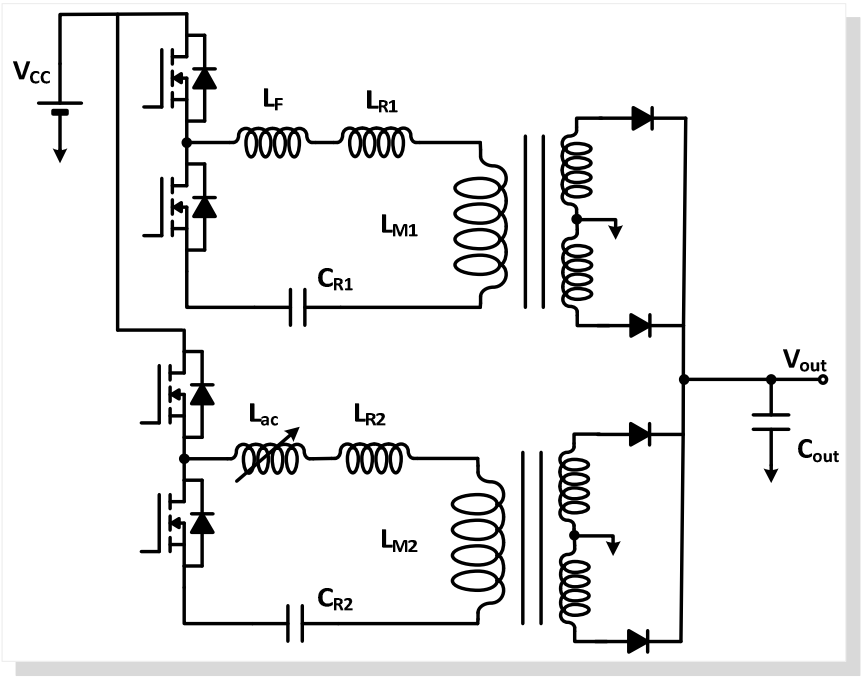

b. Two-phase interleaved LLC resonant converter [2.33]

Fig. 2.17. Examples of resonant converters with magnetic control.

In [2.32] a new phase shifted PWM full-bridge isolated dc-dc converter is also proposed. As usual the resonant inductor is replaced by the so called LVI, which in turn is controlled by the output current. With the proposed converter the authors claim an extension of the soft switching operation range and a smaller dependency of the ZVS operation on the load current.

In [2.40] and [2.41] a variable inductor is used in an Inductive Coupled Power Transfer system, IPT. Such systems are used for noncontact power transfer between a primary and secondary windings. These windings are loosely coupled meaning that the magnetic coupling between the windings is very poor. For this reason, the leakages inductances are typically much larger than the magnetizing inductance. Therefore, primary and secondary leakage inductance compensation is usually necessary to achieve the required power transfer capability [2.39]. In some cases the secondary moves relative to the primary and there is no physical contact between the both of them. Fig. 2.18a. presents the basic structure of this type of contactless power transfer system. The system is based on two electrically isolated parts. Often, the primary does not use a magnetic core in order to minimize cost. The primary part consists of a resonant power supply, with primary compensation, and an elongated conductive path which produces an ac current. The secondary part consists of the power pick-up winding with secondary compensation.

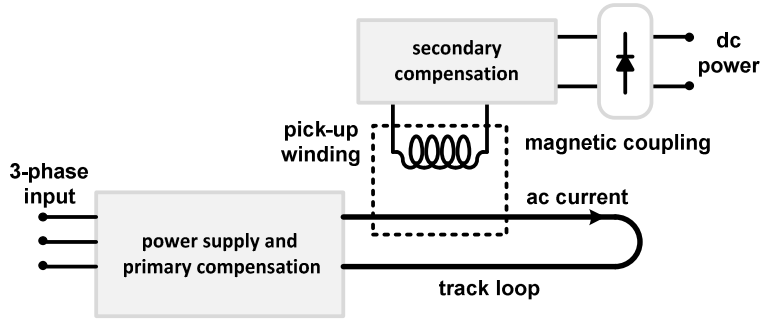

a. Basic IPT system

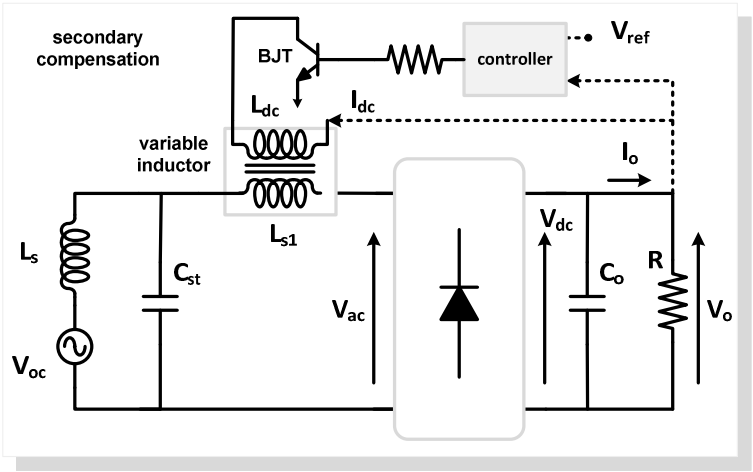

b. Proposed LCL tuning circuit for the IPT system

Fig. 2.18. IPT system with a variable inductor-based compensation circuit [2.40].

Since the system is loosely coupled, the induced voltage in the secondary is usually unsuitable for the direct use in applications. Secondary compensation or tuning is essential to provide a constant dc power to the load. Typically an LC circuit is used, however in [2.40] and [2.41], an LCL configuration is proposed. The major advantage of the proposed configuration is that one of the inductances is in fact replaced by a magnetic regulator. Its inductance value is then varied according to the output voltage feedback control signal, by means of a dynamic on-line identification control algorithm. So, in fact, the variable inductor is used to control the power flow from the secondary or pick-up winding to the load according to the desired output voltage. Since the proposed circuit, represented in Fig. 2.18b., does not involve switching due to the dynamic variation in the inductance L_{s1}, the voltage and current of the pick-up winding are kept continuous. This minimizes waveform distortion and EMI. If the output voltage, V_o, is higher than the voltage reference, V_{ref}, the controller block generates a signal to increase the inductance value, thereby detuning the circuit to lower the output voltage. On the contrary, if the output voltage is lower than the reference voltage a reverse signal is generated, capable of decreasing the inductance value, moving the circuit close to the tuned or resonance position thus increasing the output voltage.

In [2.24] and in [2.25], a variable inductor is used in a PFC circuit for a LED driver. A two-stage LED driver would normally consist of a PFC stage followed by a dc-dc converter. In this case a single-stage solution is proposed as shown in Fig. 2.19: a single-stage ac-dc PFC flyback LED driver with a variable "boost" inductance. Typically, the PFC stage operates in DCM, while the flyback converter operates at a boundary mode. The design goal is to achieve a proper PFC operation, which means that the line current has to meet the IEC 61000-3-2 Class C limits, and to limit the bulk-capacitor voltage, V_B, below 400V. This bulk capacitor, C_B, is typically used to limit the output voltage ripple of the EMI filter and rectifier stage. To reduce this capacitor voltage one terminal of the boost inductance, L_{ac}, is connected to a tap of the primary winding of the transformer, thus providing a negative feedback. The problem pointed out by the authors relates with the fact that as long as the instantaneous line voltage is lower than the voltage at the tap, no current is drawn from the input, thus reducing the power factor and increasing the line-current harmonics. This application is intended to operate with the universal line voltage (90-270Vrms). Using a variable inductance it is possible to set it at high value, at high line voltage to limit V_B, and at a low value, at low line voltage to ensure DCM operation and a low THD. If a constant boost inductance was used, at a low line voltage, the inductor would enter in CCM around the peak line voltage and this would result in an increased THD. In [2.24] and [2.25] a

detailed explanation is presented regarding the key design parameters that must be considered, particularly those affecting V_B, and the variable inductance range in order to prevent CCM.

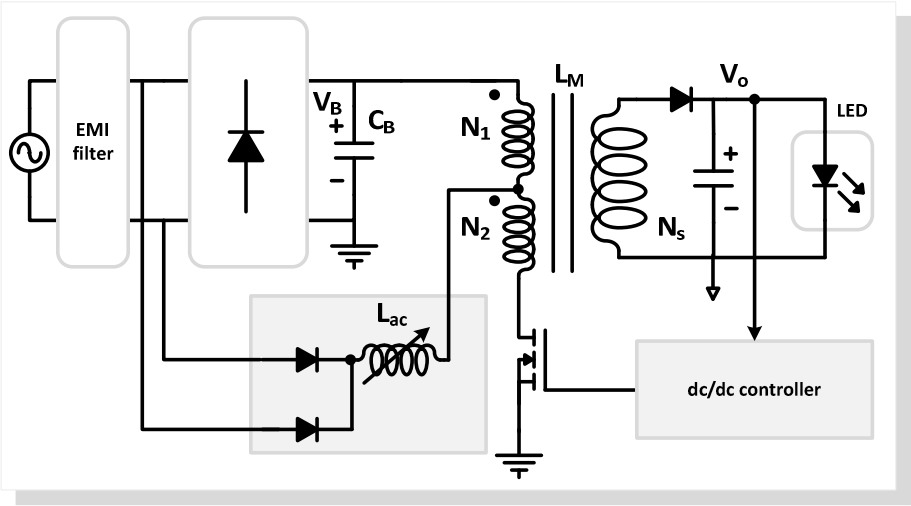

Fig. 2.19. Single-stage flyback LED driver with energy-storage capacitor at the primary side and variable "boost" inductance [2.24].

2.3.2 MAGNETIC CONTROL IN ELECTRONIC BALLASTS

In [2.42] and in [2.14] are presented two HID lamp drivers. The first one is a US Patent from 1982 and even though this type of application was already suggested, it is one of the earliest patents directly related to magnetic control applied to lamp ballasts. The magnetic regulator used is in fact an EI variable transformer, with a primary winding mounted on the first leg (connected to an ac voltage source, the example given being 120V and 60Hz) and a secondary winding mounted on the second leg (connected in series with the lamp, to serve as ballast). The control winding is mounted on the gapped third leg. A bilateral switch, a triac, is connected to the control winding and is operable to be closed once, in each half-cycle of the normal lamp operation. If the triac is in an open non-conducting state, a first value of inductance is provided in series with the lamp, limiting the lamp current. If the triac is in a closed conducting state, a second value of inductance is provided in series with the lamp. With these two predetermined values it is possible to control the average power delivered to the lamp.

In the second reference, [2.14], an electronic ballast for a HP Metal Halide lamp is proposed, based on a so called "Inductor-Controlled Current-Sourcing Push-Pull Parallel-Resonance Inverter". The circuit configuration is presented in Fig. 2.20. The push-pull inverter is operated in this case at 200kHz and the ballast includes an ignition circuitry and a dimming capability.

These are only two of many examples which suggested the application of magnetic regulators to lighting applications. A step towards the application of magnetic control to fluorescent lamps becomes natural.

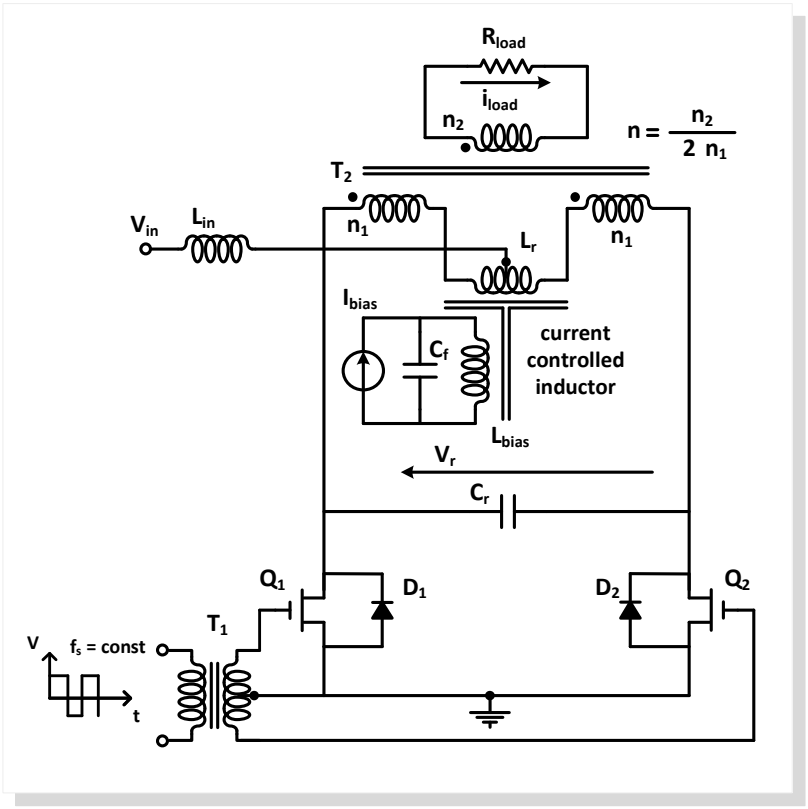

Fig. 2.20. High-Pressure Discharge Lamp Driver based on Inductor-Controlled Current-Sourcing Push-Pull Parallel-Resonance Inverter [2.14].

Magnetically-controlled electronic ballasts for fluorescent lamps are also based on the resonant half-bridge inverter. With this topology, soft starting and safe operation for the lamp can be provided [2.43]. It is also important to notice that for this application, several other possible options regarding resonant circuits configurations are available. In the next chapter a comparison among different possibilities will be carried out [2.46]. This is an important discussion since an appropriate electronic ballast design procedure, or an appropriate methodology for determining the inverter and the resonant circuit parameters, is essential for a safe, high performance operation of the system.

As shown in the simplified ballast schematics presented in Fig. 2.21, whether they refer to dimmable electronic ballasts or universal ballasts, the magnetic regulator is the key element of the resonant circuit [2.44], [2.45]. For these two applications, the selected magnetic regulator structure and core geometry may be the same. Typically, the regulator is implemented using a

double EF (EE) core as the one presented in Fig. 2.21. The ac inductance, L_{ac}, is placed in the middle leg of the core, which contains an airgap and two additional control windings are mounted in the lateral legs. The magnetic regulator is then controlled by an external dc current source which imposes the desired inductance value required by each application. For dimming applications, modifying the inductance allows providing a variable rms value for the lamp current which implies obtaining a variable luminous output. As shown in the graphical representation of $P_{lamp}(L_{ac})$ in Fig. 2.21, the minimum value is selected in order to operate the lamp at the maximum flux level and the maximum inductance value must be capable of reducing the flux level to the minimum desired value.

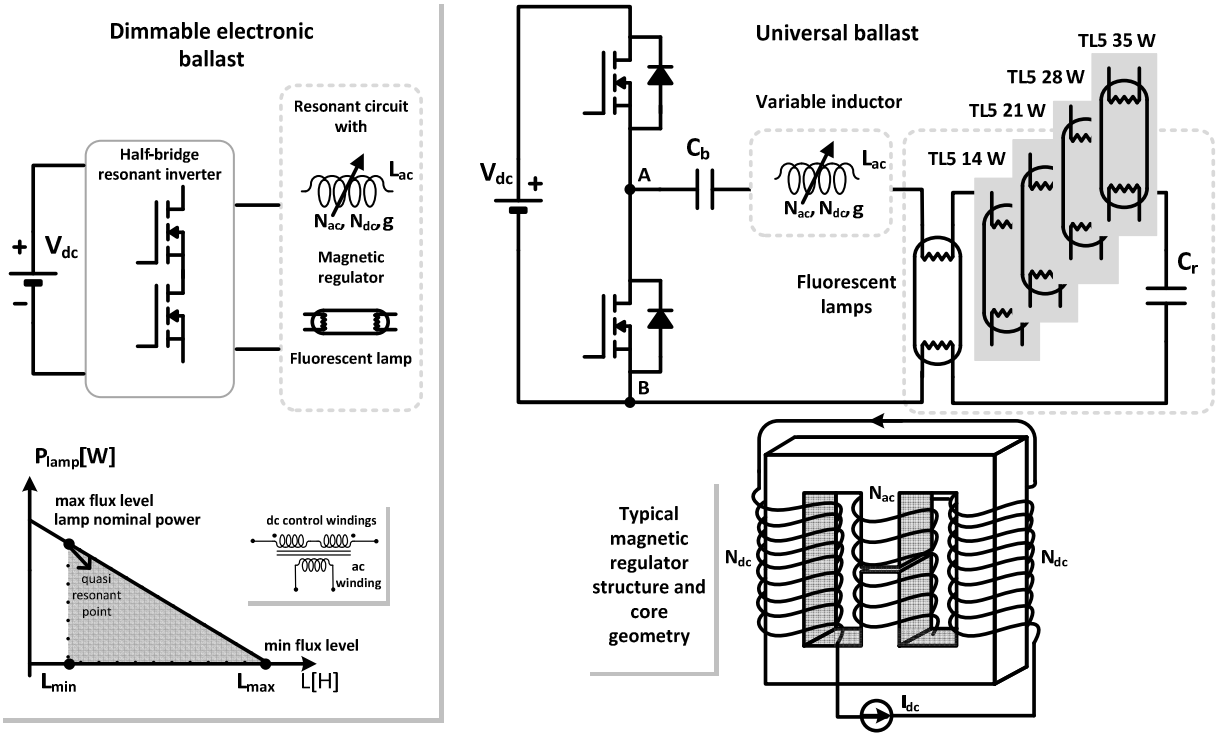

Fig. 2.21. Magnetically-controlled electronic ballasts: dimmable electronic ballast and universal ballast.

2.3.2.1 DIMMABLE ELECTRONIC BALLASTS

Preliminary work has already revealed that applying magnetic control is one way of improving the performance of dimmable electronic ballasts [2.44], [2.45]. Among the typical three dimming techniques previously described, the frequency control technique provides a wide dimming range with simple circuit configuration. This is the reason why it is popularly adopted in practical implementation. However, it is a known fact that the sensitivity of the lamp power to the switching frequency significantly increases as the luminous level decreases. The dimming control

is not linear and problems with high EMI must be taken into account during project conception [2.47]. In order to attain low dimming levels, a wide frequency range is necessary and this may imply loss of ZVS conditions for certain dimming levels. In conclusion, a major breakthrough is the ability to provide almost linear dimming curves while operating the inverter at a constant frequency.

In [2.47] a different magnetic control technique was presented. A saturable inductor was employed to improve the dimming characteristics of frequency-controlled fluorescent electronic ballasts, by stabilizing the operating point at low luminous flux levels. An unsaturated inductor, L_u, is placed in series with a saturable inductor, L_s. At high levels of lamp current L_s becomes saturated, establishing a minimum value for the series resonant inductance, and at low dimming levels, the series resonant inductance is higher, which decreases the sensitivity of the lamp power to the inverter switching frequency. Yet, the saturable inductor is controlled only by the current circulating through it and obviously, dimming is still frequency dependent. This may be translated into less flexibility in the design. As an opposite solution, magnetic regulators are controlled by an external dc current source; they allow dimming and still operate the half-bridge inverter at constant frequency. This obviously gives an additional degree of freedom to the design.

A similar technique was proposed by U. Boeke in a joint project with Philips Consumer Electronics [2.49]. A different variable inductor topology is introduced and the emphasis is given to the fact that this type of control could also be applied to CCFLs. However it is clear that if a variable transformer is used instead of the variable inductor, the lamp may be connected to the secondary side of that transformer. It is a better solution since it presents similar advantages to the ones using the variable inductor control concept, additionally yielding electrical isolation.

In [2.50] S. Boreckci gives a detailed attention and further explores the variable inductor control technique. A damaging effect which may appear at power levels below 30% of the full power is the striation phenomenon, visually translated into dark and bright bands across the tube, as represented in Fig. 2.22.

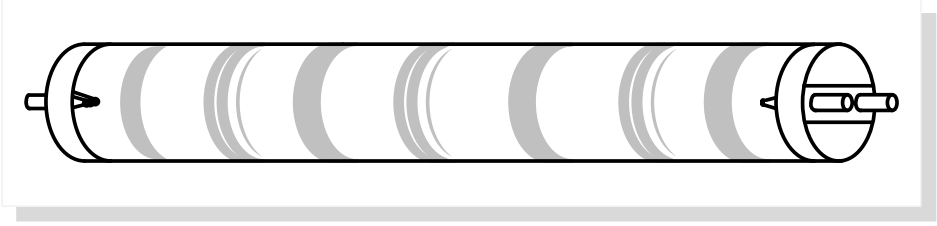

Fig. 2.22. Striation phenomenon on tubular fluorescent lamps.

This phenomenon, which occurs at low power and/or at low temperature, is a common concern in all existing dimming techniques. Striations are induced from ion oscillations; they depend on the arc current, electron density, ambient temperature and gas pressure, composition of the lamp plasma and also on the geometric scale of the tube. One way to control this phenomenon is to inject a small amount of dc current into the lamp, although it might also shorten the electrode life [2.51]. Once again, in [2.50], it is presented a new solution to prevent striations in this type of magnetic dimming techniques, called the power density modulation (PDM). It proposes to induce three different stages in each period of the arc current, by changing the level of the dc control current and consequently the inductance value. The time interval for each inductance value controls the average lamp power in each modulation period.

2.3.2.2 UNIVERSAL ELECTRONIC BALLASTS

Lighting requirements in public and commercial buildings may change enormously. Nowadays a building can be built for one particular activity and after a few years or even months have a total different purpose. Of course this translates into the need of a different lighting design installation according to the new occupation. A key answer to solve possible limitations may be, if from the start, the basic illumination system includes luminaires and electronic ballasts, which can easily adapt to a new situation or environment. In fact there is a commercial need for safe, reliable, versatile equipment which simultaneously avoids future costs and offers flexibility to the consumer. Therefore universal ballasts have recently attracted the attention of manufacturers and researchers due to the high increase in lamp types, mainly fluorescent, in terms of rated power, shapes and electrical characteristics. There is a real profit to be expected from the spread out of the use of this type of ballasts: luminaires manufacturers and retailers will benefit from lower costs and reduced complexity in development, production and storage, if such equipment is adopted. Facility managers will have more flexibility in dealing with their lighting installations.

As represented in Fig. 2.21 the main purpose is the ability to provide an electronic ballast system, typically with digital control, capable of driving any lamp within a range of nominal power ratings, while assuring safe operation. Like standard dimmable electronic ballasts, conventional universal ballasts proposed up to now also use the inverter switching frequency as the main control parameter, ensuring that each lamp is operated at nominal power. Nonetheless, each lamp has its unique characteristics, its own starting and working voltage. Using the same resonant tank with the switching frequency as the only control variable, involves a large range of operating frequencies and does not ensure optimum working conditions. To overcome these

limitations, [2.55] suggests adapting the dc voltage that supplies the resonant inverter. An additional converter with step-up and step-down characteristics is needed to perform this operation. This converter must handle the total circuit power, decreasing overall efficiency. A US Patent from 2000, [2.56], considers selectively changing simultaneously the switching frequency and duty-cycle of the inverter signal. Varying the duty ratio of the switches allows controlling the pulse width of the square waveform at the output of the inverter, which means controlling its rms value and consequently provide a variable rms current to each lamp. The main disadvantage of this control method resides in the asymmetrical lamp current waveform, which causes the premature aging of the lamp due to a mechanism called non-linear electrophoresis. An improvement was later presented in [2.57], where a boost converter is used as an input stage to supply the half bridge resonant inverter. In this case, it is proposed a strategy based on the variation of three control parameters: the dc output voltage of the boost stage, the duty-cycle and switching frequency of the inverter.

An alternative control technique would be integrating the magnetic regulator into the universal ballast. Through a dc control current it is given the ability to change and adapt the resonant circuit, due to the variable inductance, to the working parameters imposed by each lamp. The switching frequency may also be adjusted to allow the inverter to operate near the resonant frequency, ensuring that the inverter stability and efficiency are close to their optimum. Using magnetically-controlled ballasts, an additional degree of freedom in the optimization of the working conditions for each lamp is obtained, without compromising the overall efficiency of the circuit. Verifying the effectiveness of this control technique is one of the objectives of the presented work.

Lamp detection techniques are also important in this type of ballasts. Any mismatch of ballast and lamp power rating may damage the lamp or the ballast. However, after an accurate process of lamp power recognition, the ballast control parameters may be selected properly. In [2.53] one of these methods is proposed. It can differentiate the lamp power of T8 and T12, in the range of 18-70W, by measuring the lamp voltage after the lamp ignition. With this method the electronic ballast supplies the lamp at a fixed frequency during the detection period. Afterwards, this voltage is stepped down and modified as a control signal to determine the switching frequency of the inverter. In order to select and vary the switching frequency, a voltage controlled oscillator together with some mapping functions, are used [2.54]. These methods can also be used in magnetically-controlled ballasts.

REFERENCES

[2.1] Alexanderson, E.F.W.; Nixdorff, S.P.; "A Magnetic Amplifier for Radio Telephony," Proceedings of the Institute of Radio Engineers, vol.4, no.2, pp. 101- 120, April 1916.

[2.2] AVCM Keith E. Glading, "Navy Electricity and Electronics Training Series, Module 8 – Introduction to Amplifiers," NAVEDTRA 14180, Naval Education and Training Professional Development and Technology Center, 1998.

[2.3] Lufcy, C.W.; "A Survey of Magnetic Amplifiers," Proceedings of the IRE , vol.43, no.4, pp.404-413, April 1955.

[2.4] Bob Mammano, "Magnetic Amplifier Control for Simple, Low-Cost, Secondary Regulation", Unitrode Corporation, 1986.

[2.5] Ruben Lee, Leo Wilson and Charles E. Carter, Electronic Transformers and Circuits, 3rd ed. PSMA Publication. John Wiley & Sons, 1988.

[2.6] Alex Van den Bossche, Vencislav Cekov Valchev, Inductors and transformers for Power Electronics, Taylor & Francis Group, 2005.

[2.7] Paul Mali, Magnetic Amplifiers, Principles and Applications, John F. Rider Publisher, Inc., New York, 1960.

[2.8] Harada, K.; Ishihara, Y.; Todaka, T.; "A novel high power factor converter using a magnetic amplifier," Magnetics, IEEE Transactions on, vol.32, no.5, pp. 5013-5015, Sep 1996.

[2.9] Elichi Hirota, Yutaka Neichi, Minoru Sugimura, "Variable Inductance Device," U.S. Patent 3 631 534, Dec. 28, 1971.

[2.10] Leopold J. Johnson, "Current Controlled Variable Inductor," U.S. Patent 5 426 409, Jun. 20, 1995.

[2.11] Arian M. Jansen, "Variable Inductor," U.S. Patent 6 317 021 B1, Nov. 13, 2001.

[2.12] Kislovski, A.S.; "Quasi-linear controllable inductor," Proceedings of the IEEE, vol.75, no.2, pp. 267- 269, Feb. 1987.

[2.13] Medini, D.; Ben-Yaakov, S.; "A current-controlled variable-inductor for high frequency resonant power circuits," Applied Power Electronics Conference and Exposition, 1994. APEC '94. Conference Proceedings 1994, Ninth Annual, vol., no., pp.219-225 vol.1, 13-17 Feb 1994.

[2.14] Gulko, M.; Medini, D.; Ben-Yaakov, S.; "Inductor-controlled current-sourcing resonant inverter and its application as a high pressure discharge lamp driver," Applied Power Electronics Conference and Exposition, 1994. APEC '94. Conference Proceedings 1994, Ninth Annual, vol., no., pp.434-440 vol.1, 13-17 Feb 1994.

[2.15] Ben-Yaakov, S. and Peretz, M. M., "Simulation Bits: A SPICE Behavioral Model of Non-Linear Inductors," IEEE Power Electronics Society Newsletter, Fourth Quarter, pp.9-10 2003.

[2.16] Evgeny Rozanov and Sam Ben-Yaakov, "Analysis of current-controlled inductors by new SPICE behavioral model", HAIT Journal of Science and Engineering B, Volume 2, Issues 3-4, pp. 558-570, Holon Academic Institute of Technology, 2005.

[2.17] Lu, Y.; Cheng, K.W.E.; Ho, S.L.; Pan, J.F.; Kwok, K.F.; Xue, X.D.; "A Transformer with Adjustable Leakage Inductance," Electromagnetic Field Computation, 2006 12th Biennial IEEE Conference on, vol., no., pp.78.

[2.18] Bolduc Léonard, Parc Grégoire, "Self-regulated Transformer-inductor with Air gaps," U.S. Patent 4 766 365, Aug. 23, 1988.

[2.19] Robert D. Washburn and Robert F. McClanahan, “Non-saturating Magnetic Amplifier Controller,” U.S. Patent 4 841 428, Jun. 20, 1989.

[2.20] Vollin, J.; Tan, F.D.; Cuk, S.M.; "Magnetic regulator modeling," Applied Power Electronics Conference and Exposition, 1993. APEC '93. Conference Proceedings 1993, Eighth Annual , vol., no., pp.604-611, 7-11 Mar 1993.

[2.21] Kislovski, A.S.; "Linear variable inductor (LVI) in single-phase telecom rectifiers," Telecommunications Energy Conference, 1995. INTELEC '95, 17th International, vol., no., pp.93-98, 29 Oct-1 Nov 1995.

[2.22] Kislovski, A.S.; "Linear variable inductor in DC current sensors utilized in telecom solar battery chargers," Telecommunications Energy Conference, 1989. INTELEC '89. Conference Proceedings, Eleventh International, vol., no., pp.23.2/1-23.2/3 vol.2, 15-18 Oct 1989.

[2.23] Rozanov, E.; Ben-Yaakov, S.; "A SPICE behavioral model for current-controlled magnetic inductors," Electrical and Electronics Engineers in Israel, 2004. Proceedings. 2004 23rd IEEE Convention of, vol., no., pp. 338- 341, 6-7 Sept. 2004.

[2.24] Yuequan Hu; Huber, L.; Jovanovic, M.M.; "Universal-input single-stage PFC flyback with variable boost inductance for high-brightness LED applications," Applied Power Electronics Conference and Exposition (APEC), 2010 Twenty-Fifth Annual IEEE , vol., no., pp.203-209, 21-25 Feb. 2010.

[2.25] Hu, Y.; Huber, L.; Jovanovic, M.; "Single-Stage, Universal-Input AC/DC LED Driver with Current-Controlled Variable PFC Boost Inductor," Power Electronics, IEEE Transactions on, vol. PP, no.99, pp.1-1, Oct. 2010. (Early access)

[2.26] Bonanni, I.; "AC regulator controlled by LVI," Power Electronics and Applications, 1993, Fifth European Conference on, vol., no., pp.101-105 vol.7, 13-16 Sep 1993.

[2.27] Bonanni, I.; Mandelli, E.; "High performances high voltage generator regulated by LVI," Applied Power Electronics Conference and Exposition, 1990. APEC '90, Conference Proceedings 1990, Fifth Annual, vol., no., pp.323-329, 11-16 Mar 1990.

[2.28] Wolfle, W.H.; Hurley, W.G.; "Quasi-active power factor correction with a variable inductive filter: theory, design and practice," Power Electronics, IEEE Transactions on , vol.18, no.1, pp. 248- 255, Jan 2003.

[2.29] Chu-Quon Lee, Kasemsan Siri, Anand K. Upadhyay, “Parallel Resonant Converter with Zero Voltage Switching,” U.S. Patent 4 992 919, Feb. 12, 1991.

[2.30] Fischer, W.; Doebbelin, R.; Lindemann, A.; "Conducted EMI analysis of hard and soft switching arc welding power supplies," Power Electronics and Applications, 2009. EPE '09. 13th European Conference on, vol., no., pp.1-10, 8-10 Sept. 2009.

[2.31] Pernia, A.M.; Lopera, J.M.; Prieto, M.J.; Nuno, F.; "Analysis and design of a new constant frequency control for QRC and MRC based on magnetic elements modification," Power Electronics, IEEE Transactions on, vol.13, no.2, pp.244-251, Mar 1998.

[2.32] Bakan, A.F.; "A new LVI assisted PSPWM DC-DC converter," Electrical and Electronics Engineering, 2009. ELECO 2009. International Conference on, vol., no., pp.I-230-I-233, 5-8 Nov. 2009.

[2.33] Orietti, E.; Mattavelli, P.; Spiazzi, G.; Adragna, C.; Gattavari, G.; "Two-phase interleaved LLC resonant converter with current-controlled inductor," Power Electronics Conference, 2009. COBEP '09. Brazilian, vol., no., pp.298-304, Sept. 27 2009-Oct. 1 2009.

[2.34] Hooper, Rich; Guy, Bill; Perrault, Rick; "A current-controlled variable inductor," AUTOTESTCON, 2010 IEEE, vol., no., pp.1-4, 13-16 Sept. 2010.

[2.35] Sewell, H.I.; Stone, D.A.; Howe, D.; "Dynamic load impedance correction for induction heaters," Power Electronics and Drive Systems, 1999. PEDS '99. Proceedings of the IEEE 1999 International Conference on, vol.1, no., pp.110-115 vol.1, 1999.

[2.36] Huzayyin, A.A.; "Utilizing the nonlinearity of a magnetic core inductor as a source of variable reactive power compensation in electric power systems," Student Paper, 2008 Annual IEEE Conference, vol., no., pp.1-4, 15-26 Feb. 2008.

[2.37] Mu Xianmin; Wang Jianze; Ji Yanchao; Wei Xiaoxia; Fu Xiangyun; "Novel Harmonic Free Single Phase Variable Inductor Based on Active Power Filter Strategy," Power Electronics and Motion Control Conference, 2006. IPEMC 2006. CES/IEEE 5th International, vol.3, no., pp.1-4, 14-16 Aug. 2006.

[2.38] Mu Xianmin; Zhang Suli; Wang Jianze; Ji Yanchao; Novel Static Var Compensator Based on Ferrite Orthogonal Core Controlled Reactor," Industrial Technology, 2006. ICIT 2006. IEEE International Conference on, vol., no., pp.1903-1907, 15-17 Dec. 2006.

[2.39] Stielau, O.H.; Covic, G.A.; "Design of loosely coupled inductive power transfer systems," Power System Technology, 2000. Proceedings. PowerCon 2000. International Conference on, vol.1, no., pp.85-90 vol.1, 2000.

[2.40] Hsu, J.-U.W.; Hu, A.P.; Swain, A.; Xin Dai; Yue Sun; "A new contactless power pick-up with continuous variable inductor control using magnetic amplifier," Power System Technology, 2006. PowerCon 2006. International Conference on, vol., no., pp.1-8, 22-26 Oct. 2006.

[2.41] Hsu, J.-U.W.; Hu, A.P.; "Determining the variable inductance range for an LCL wireless power pick-up," Electron Devices and Solid-State Circuits, 2007. EDSSC 2007. IEEE Conference on, vol., no., pp.489-492, 20-22 Dec. 2007.

[2.42] Robert J. Spreadbury, “Discharge Device Ballast Component Which Provides Both Voltage Transformation and Variable Inductance Reactance,” U.S. Patent, 4 350 934, Sep. 21, 1982.

[2.43] Alonso, J. M., Rashid, Muhammad H., “Power Electronics Handbook, Chapter 22 Electronic Ballasts”, Academic Press, Inc., 2001, ISBN: 978-0-12-581650-2.

[2.44] Alonso, J.M.; Dalla-Costa, M.A.; Cardesin, J.; Garcia, J.; "Magnetic dimming of electronic ballasts," Electronics Letters, vol.41, no.12, pp. 718- 719, 9 June 2005.

[2.45] Alonso, J.M.; Dalla Costa, M.A.; Rico-Secades, M.; Cardesin, J.; Garcia, J.; "Investigation of a New Control Strategy for Electronic Ballasts Based on Variable Inductor," Industrial Electronics, IEEE Transactions on , vol.55, no.1, pp.3-10, Jan. 2008.

[2.46] Perdigão, M.S.; Alonso, J.M.; Dalla Costa, M.A.; Saraiva, E.S.; "Comparative Analysis and Experiments of Resonant Tanks for Magnetically Controlled Electronic Ballasts," Industrial Electronics, IEEE Transactions on, vol.55, no.9, pp.3201-3211, Sept. 2008.

[2.47] Lee, S.T.S.; Chung, H.S.-H.; Hui, S.Y.; "Use of saturable inductor to improve the dimming characteristics of frequency-controlled dimmable electronic ballasts," Power Electronics, IEEE Transactions on, vol.19, no.6, pp. 1653- 1660, Nov. 2004.

[2.48] Perdigão, M.S.; Alonso, J.M.; Costa, M.A.D.; Saraiva, E.S.; "Using Magnetic Regulators for the Optimization of Universal Ballasts," Power Electronics, IEEE Transactions on, vol.23, no.6, pp.3126-3134, Nov. 2008.

[2.49] Boeke, U.; "Scalable fluorescent lamp driver using magnetic amplifiers," Power Electronics and Applications, 2005 European Conference on, Sep. 2005.

[2.50] Borekci, S.; "Dimming Electronic Ballasts Without Striations," Industrial Electronics, IEEE Transactions on , vol.56, no.7, pp.2464-2468, July 2009.

[2.51] Tsai-Fu Wu; Yung-Chun Wu; Zing-Ying Su; , "Design considerations for single-stage electronic ballast with dimming feature," Industry Applications, IEEE Transactions on, vol.37, no.5, pp.1537-1543, Sep/Oct 2001.

[2.52] Alonso, J.M.; Perdigão, M.S.; Gacio, D.; Campa, L.; Saraiva, E.S.; , "Magnetic control of DC-DC resonant converters provides constant frequency operation," Electronics Letters , vol.46, no.6, pp.440-442, March 18 2010.

[2.53] L. M. Lee, S. Y. R. Hui, H. S. H. Chung, "An automatic lamp detection technique for electronic ballasts," Twentieth Annual IEEE Applied Power Electronics Conference and Exposition, 2005. APEC 2005, vol. 1, pp. 575-581, Mar. 2005.

[2.54] S. Y. R. Hui and L. M. Lee, "Universal electronic ballast", U.S. Patent 6 414 449, 2002.

[2.55] Busse, O.; Mayer, S.; Schemmel, B.; Storm, A.; "SEPIC converter to perform power factor correction in a ballast for fluorescent lamps," Industry Applications Conference, 2005. Fortieth IAS Annual Meeting. Conference Record of the 2005, vol.4, no., pp. 2770- 2774 Vol. 4, 2-6 Oct. 2005.

[2.56] Alexei Bogdan, "Programmable Universal Lighting System", U.S. Patent 6 040 661, March 21, 2000.

[2.57] A. Bogdan; "Universal Ballast Control Circuit," U.S. Patent 6 137 240, Oct. 2000.

BIBLIOGRAPHY

[B2.1] Ruben Lee, Leo Wilson and Charles E. Carter, "Electronic Transformers and Circuits", 3rd ed. PSMA Publication. John Wiley & Sons, 1988.

[B2.2] Alex Van den Bossche, Vencislav Cekov Valchev, "Inductors and transformers for Power Electronics", Taylor & Francis Group, 2005.

[B2.3] Paul Mali, "Magnetic Amplifiers, Principles and Applications", John F. Rider Publisher, Inc., New York, 1960.

[B2.4] John D. Kraus, "Electromagnetics", 4th Edition, McGraw-Hill International Editions, 1991.

[B2.5] Marian K. Kazimierczuk, Dariusz Czarkowski, "Resonant Power Converters", John Wiley & Sons, Inc., 1995.

3 APPLICATION OF THE VARIABLE INDUCTOR TO THE CONTROL OF ELECTRONIC BALLASTS

The present chapter reveals the main applications of the variable inductor. The chapter starts by describing the variable inductor modelling and design. It continues with the description of the proposed dimming technique. In magnetically-controlled electronic ballasts besides the classical high-frequency half-bridge inverter, two additional elements are present: the magnetic regulator, which replaces the typical resonant inductor, and the dc current source, to control this regulator. The device acts as a variable inductance dependent on the dc control current. So, if the inductance value of the resonant inductor is gradually increased, so will the impedance of the resonant circuit and thereby the luminous flux may be controlled. A comparative analysis between resonant circuits, different regulators structures, topologies and their effects on lamp operation are studied. Finally, the chapter describes the other proposed technique: magnetically-controlled universal ballasts. The technique is explained and two different prototype versions are presented, the last one with constant-frequency operation. Critical issues related to electrodes operation with these control techniques are also addressed in this chapter.

3.1 MODELLING AND DESIGN OF VARIABLE INDUCTORS

3.1.1 MODELLING ISSUES AND THEORECTICAL ANALYSIS

The theoretical and experimental study of the magnetic behaviour of variable inductors constitutes an interesting scientific challenge, not only from the electronic ballast development point of view, but also for other potential applications in power converters. Modelling is essential for a correct understanding of the behaviour of these magnetic devices and represents a useful tool for prototype design and development. The magnetic circuit analysis contributes to the

understanding and prediction of the variable inductor behaviour, by giving an estimation on how the inductance L_{ac} evolves. However, its theoretical analysis is a non-trivial task.

The variable inductor, proposed by D. Medini and S. Ben Yaakov, presented in Fig. 3.1a. is typically implemented using a gapped E core set. The main winding is placed in the middle leg of the core and the control windings are placed in the left and right legs. The control windings are serially connected in opposite polarity in order to cancel any induced ac voltage, under the assumption of symmetry. However this is not what effectively happens. A more precise analysis, as the one presented in [2.16], reveals the presence of a parasitic, non-linear coupling between the ac voltage and the dc voltage. This fact is described by means of Fig. 3.1b.

The presence of this coupling is justified by the non-linearity of the magnetic material. A constant dc control current will produce a constant *mmf* $N_{dc}I_{dc}$ in the left and right legs which will bring these sections into the non-linear region of the magnetization curve. The *mmf* in the left and right legs will be in opposite direction with respect to the *mmf* associated with the main winding, $N_{ac}i_{ac}$. This necessarily means that, at any given instance, the *mmf* generated by the ac winding will increase the permeance of one leg and decrease the permeance of the other leg, also meaning that $d\phi_{left}(t)/dt$ will differ from $d\phi_{right}(t)/dt$ [2.16]. The induced instantaneous voltages V_{left} and V_{right} will also differ and the difference, $V_{dc} = V_{right} - V_{left}$, of the serially connected control windings will be non-zero. Therefore, the maximum value of V_{dc} will depend on the amplitude of V_{in} and I_{dc}, the non-linearity of the magnetic material and the number of turns N_{ac} and N_{dc}. The analytical estimation of these non-linear phenomena is quite difficult and from the experimental point of view, this voltage V_{dc} is typically neglected. This is just one of the reasons why computer simulation models are typically used to model the variable inductor.

Existing literature commonly refers three different options for modelling complex magnetic devices such as multi-winding devices or integrated magnetics. The first one is based on finite-element-analysis, which will provide the best possible accuracy but will require an enormous effort and time dedicated to computation analysis. These models are also difficult to be applied in transient system simulation and from the practical point of view this would increase the complexity of the approach. The second one is based on the gyrator-capacitor model [3.12], [3.13]. This technique suggests employing a capacitor for the simulation of the magnetic energy storage element. In the gyrator-capacitor approach, the *mmf*, $\mathcal{F}$, is analogous to voltage, but the current corresponds to the rate-of-change of magnetic flux, $d\phi(t)/dt$.

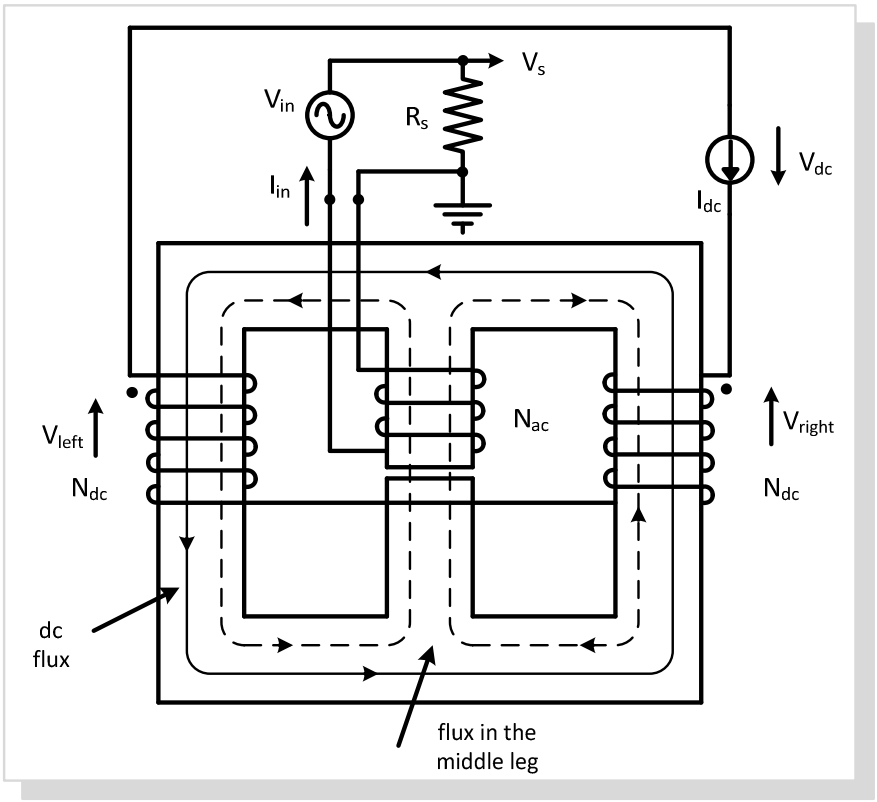

a. Current-controlled variable-inductor

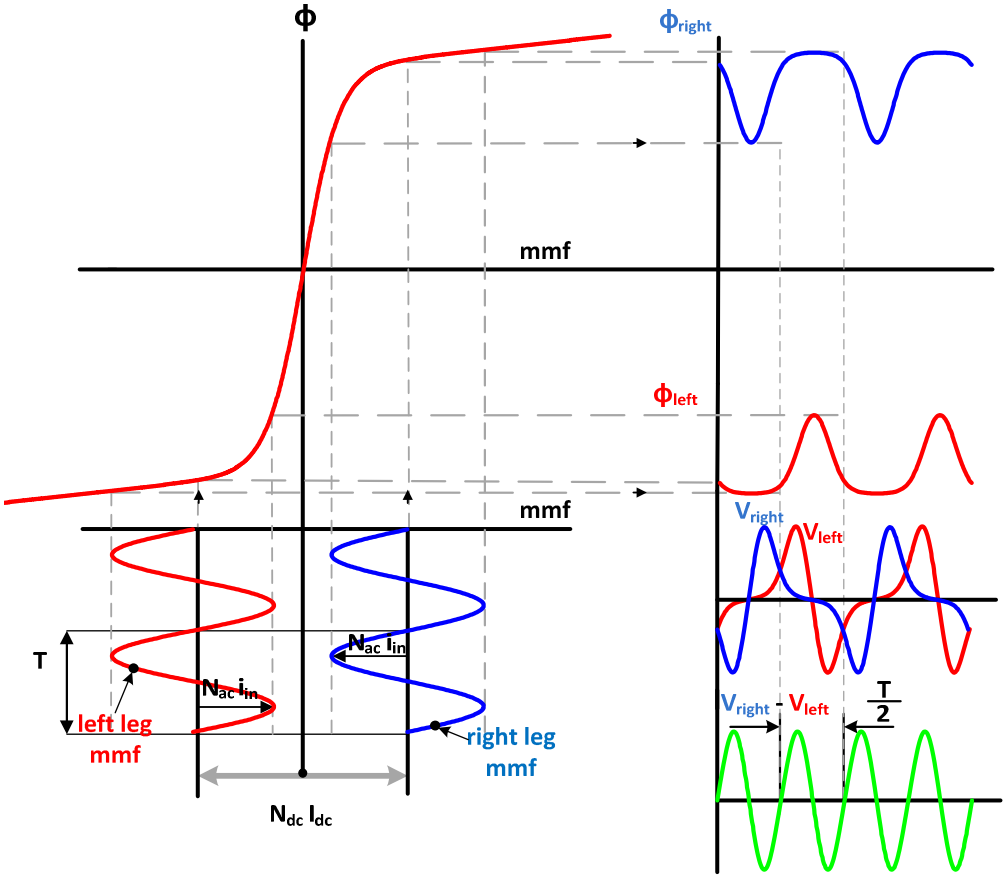

b. Non-linear coupling in the current-controlled variable-inductor

Fig. 3.1. Variable inductor, [2.16].

The gyrator-capacitor approach is considered as one of the most effective; however it is seldom used. Thus, the typical approach is the magnetic reluctance model. In this approach, the *mmf*, $\mathcal{F}$, is also analogous to voltage, but in this case the magnetic flux is considered analogous to current, instead of the rate-of-change of the magnetic flux. Since the flux produced by a *mmf* in a material depends on the material's resistance to the flux, more specifically, it depends on its reluctance, this reluctance may be simply represented by a resistor. By doing this analogy any electrical theorems or rules apply similarly. The easiest way to determine a reluctance model for a coupled inductor is to impose zero current in all of the windings except one, and then imagine the various paths that the magnetic flux could take to complete a closed loop back to the only winding responsible for the *mmf*. Finally, the application of the principle of the duality to the reluctance circuit, originates a permeance circuit which can then be transformed into an electrical equivalent circuit containing inductances [3.14]. This inductances model will result into a more or less complicated electric circuit, which may be integrated into more complex electric circuits and then be used in computer simulation programs.

3.1.1.1 RELUCTANCE MODEL

The classic theory on magnetic modelling of multi-winding devices begins by establishing a more or less complicated reluctance model of the structure. Fig. 3.2a. shows the definition used for the magnetic paths which together make up the device. Each magnetic path is related to a specific reluctance $\mathcal{R}_i$, defined by:

$$\mathcal{R}_i = {}^{l_i}/_{\mu A_i};\ \text{i=1..10} \tag{3.1}$$

where l_i is the magnetic path length, A_i the correspondent cross sectional area and μ the permeability. Fig. 3.2b. shows the equivalent circuit reluctance model. The ac winding will appear as a *mmf* source and in order to straightforward the structure, no dc *mmf* source is included in the model. The effect of the control windings is in fact, already introduced in the model since the dc control current affects the permeance and thereby the reluctance of the relevant path. Particularly, the following quantities are defined:

- $N_{ac}i_{iac}$ is the *mmf* source associated with the ac winding;
- $\mathcal{R}_1, \mathcal{R}_2, \mathcal{R}_3, \mathcal{R}_4, \mathcal{R}_5, \mathcal{R}_6, \mathcal{R}_7, \mathcal{R}_8, \mathcal{R}_9, \mathcal{R}_{10}$ are the reluctances of the magnetic paths associated to the ac flux;

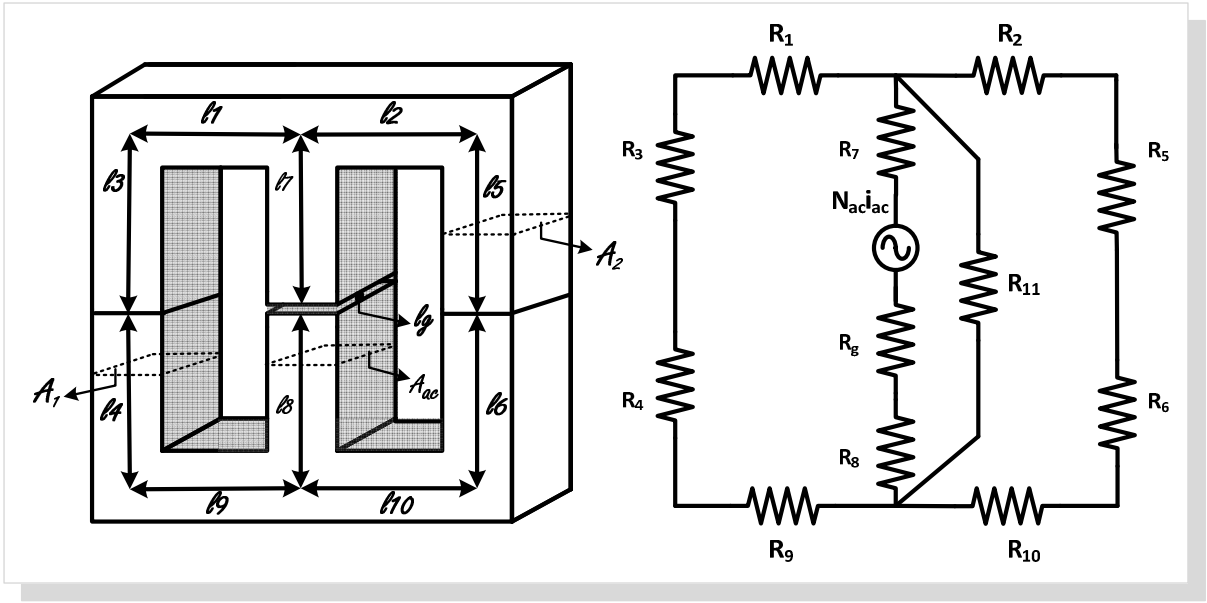

a. Gapped E core b. Reluctance model

Fig. 3.2. Variable inductor modelling.

- $\mathcal{R}_{11}$ is the reluctance of the magnetic path associated with the leakage flux (flux lines that close in the air), and $\mathcal{R}_g$ is the reluctance associated with the air gap.

The steps towards the final simplified model version presented in Fig. 3.3b. consider the following simplifications:

$$\mathcal{R}_{12} = \mathcal{R}_1 + \mathcal{R}_3 + \mathcal{R}_4 + \mathcal{R}_9 \tag{3.2}$$

$$\mathcal{R}_{13} = \mathcal{R}_2 + \mathcal{R}_5 + \mathcal{R}_6 + \mathcal{R}_{10} \tag{3.3}$$

$$\mathcal{R}_{14} = \mathcal{R}_7 + \mathcal{R}_8 \tag{3.4}$$

$$\mathcal{R}_{leak} = \mathcal{R}_{11}; \quad \mathcal{R}_c = \mathcal{R}_{14} \tag{3.5}$$

$$\mathcal{R}_x = \mathcal{R}_{12} // \mathcal{R}_{13} \tag{3.6}$$

- $\mathcal{R}_c$ is the reluctance of the magnetic path which will carry the common flux;
- $\mathcal{R}_x$ is the total sum of reluctances associated to the ac flux, which will depend on the permeability of the control legs, and thus increase with decreasing control current.

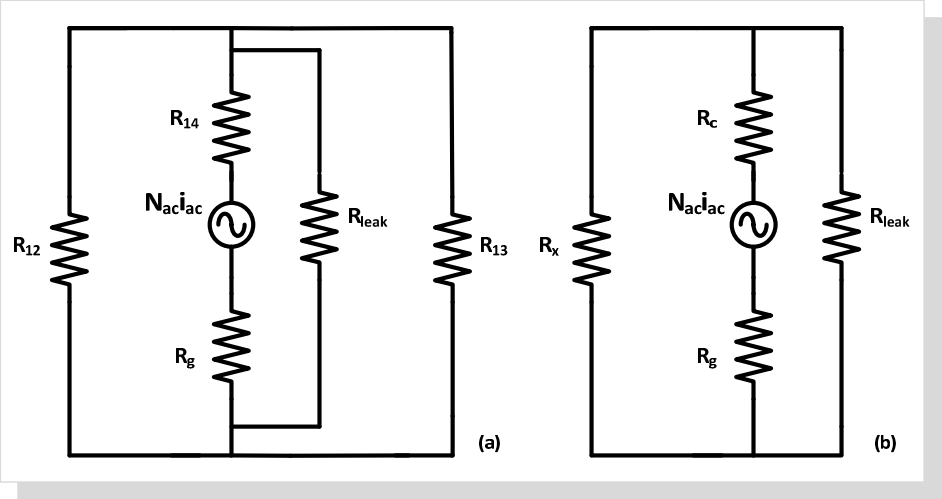

Fig. 3.3. Simplified reluctance model.

Using the basic equation of an inductor, the analytical expression for the ac inductance can be determined as:

$$L_{ac} = \frac{N^2}{\mathcal{R}} = \frac{N_{ac}^2}{\mathcal{R}_c + \mathcal{R}_g + (\mathcal{R}_x // \mathcal{R}_{leak})} \tag{3.7}$$

At this point, the main issue is of course the difficulty to estimate the reluctance associated to the leakage flux, $\mathcal{R}_{\text{leak}}$, and $\mathcal{R}_{\text{x}}$. $\mathcal{R}_{\text{x}}$ will be a function of the permeability of the core which will be a function of the magnetic field intensity H_{dc}, which in turn will be a function of I_{dc}. Since this analysis includes non-linear magnetic materials this is a quite difficult subject [2.13]. One of the main reasons is related to the necessity of using approximate relations to the $B(H)$ curves. Typically the analysis relies on curve-fitting techniques in order to carry out digital computer calculations of the device performance. Other issues like inductance definition or even the relation between prototype small and large-signal characterization are also defying. Some of these issues will be further developed throughout the chapter.

3.1.1.2 MAGNETIC CIRCUIT ANALYSIS

For the variable inductor presented in Fig. 3.4, the magnetic circuit analysis considers the following simplifications:

$$\begin{aligned} l_{dc1} &= l_1 + l_3 + l_4 + l_9 \\ l_{dc2} &= l_2 + l_5 + l_6 + l_{10} \\ l_{ac} &= l_7 + l_8 \end{aligned} \tag{3.8}$$

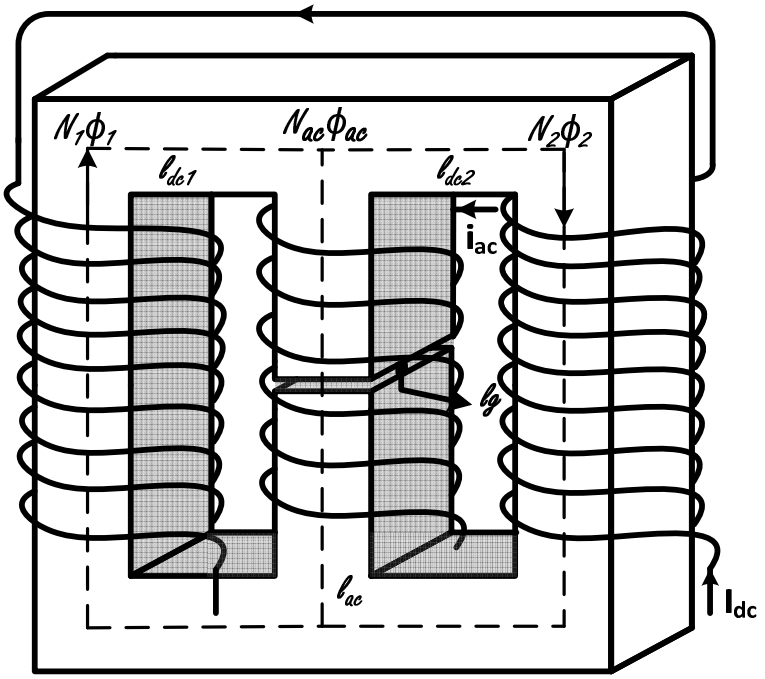

Fig. 3.4. Variable inductor magnetic structure: core geometry and magnetic behaviour.

where $l_{dc1}, l_{dc2}, l_{ac}, l_g$ are the magnetic path lengths of the left and right legs, the centre leg and of the air gap, respectively. The dc control current will have a different effect in each of the external legs. So, except for $I_{dc} = 0$, there are three levels of flux in the core. Therefore, considering the defined magnetic paths, the following equations can be established:

$$H_1 l_{dc1} - H_{ac} l_{ac} - H_g l_g = N_1 i_1 - N_{ac} i_{ac} \tag{3.9}$$

$$H_{ac} l_{ac} + H_2 l_{dc2} + H_g l_g = N_{ac} i_{ac} + N_2 i_2 \tag{3.10}$$

$$\phi_2 = \phi_1 + \phi_{ac} \tag{3.11}$$

Since $\phi = \mu H A$ and $\mathcal{R} = l/(\mu A)$ then (3.9) and (3.10) can be written as follows:

$$\phi_1 \mathcal{R}_1 - \phi_{ac} \mathcal{R}_{ac} - \phi_{ac} \mathcal{R}_g = N_1 i_1 - N_{ac} i_{ac} \tag{3.12}$$

$$\phi_{ac} \mathcal{R}_{ac} + \phi_2 \mathcal{R}_2 + \phi_{ac} \mathcal{R}_g = N_{ac} i_{ac} + N_2 i_2 \tag{3.13}$$

where:

- H_1, H_2, H_{ac}, H_g are the magnetic field intensities in the left, right, and centre legs and in the air gap respectively [A/m];

- i_1, i_2, i_{ac} are the currents in the left, right, and centre windings [A];
- N_1, N_2, N_{ac} are the numbers of turns in the left, right and centre legs, respectively;
- $\phi_1, \phi_2, \phi_{ac}$ are the magnetic fluxes in the left, right and centre legs, respectively [Wb];
- $\mathcal{R}_1, \mathcal{R}_2, \mathcal{R}_{ac}$ are the reluctances of the left, right and centre legs, respectively;
- A_1, A_2, A_{ac} are the cross-section areas of the left, right and centre legs respectively [m^2].

From (3.11), (3.12), and (3.13), ϕ_{ac} can be determined as:

$$\phi_{ac} = \frac{\mathcal{R}_1 (N_{ac} i_{ac} + N_2 i_2) - \mathcal{R}_2 N_1 i_1 + \mathcal{R}_2 N_{ac} i_{ac}}{\mathcal{R}_2(\mathcal{R}_1 + \mathcal{R}_{ac} + \mathcal{R}_g) + \mathcal{R}_1(\mathcal{R}_{ac} + \mathcal{R}_g)} \tag{3.14}$$

Assuming symmetry, $N_1 = N_2 = N_{dc}$, $A_1 = A_2 = A$, $l_{dc1} = l_{dc2} = l_{dc}$, and $i_1 = i_2 = I_{dc}$, (3.14) results in:

$$\begin{aligned} \phi_{ac} &= \frac{\mathcal{R}_1 (N_{ac} i_{ac} + N_{dc} I_{dc}) - \mathcal{R}_2 N_{dc} I_{dc} + \mathcal{R}_2 N_{ac} i_{ac}}{\mathcal{R}_2(\mathcal{R}_1 + \mathcal{R}_{ac} + \mathcal{R}_g) + \mathcal{R}_1(\mathcal{R}_{ac} + \mathcal{R}_g)} \\ &= \frac{(\mathcal{R}_1 - \mathcal{R}_2) N_{dc} I_{dc} + (\mathcal{R}_1 + \mathcal{R}_2) N_{ac} i_{ac}}{\mathcal{R}_2(\mathcal{R}_1 + \mathcal{R}_{ac} + \mathcal{R}_g) + \mathcal{R}_1(\mathcal{R}_{ac} + \mathcal{R}_g)} \end{aligned} \tag{3.15}$$

Physically, only when the ac current i_{ac} presents a zero value, may the reluctances of the left and right legs be the same, $\mathcal{R}_1 = \mathcal{R}_2$. Considering a positive and constant dc control current, a non-zero positive ac current will result in a lower *mmf* for the left mesh, (3.9), when compared with the *mmf* for the right mesh, (3.10). This issue was already referred to at the beginning of this chapter. This behaviour will imply different levels for the magnetic field intensities, H_1 and H_2, which in turn will lead to different values for the reluctances $\mathcal{R}_1$ and $\mathcal{R}_2$. Nevertheless, if the ac *mmf* is less than 10% of the dc *mmf*, it would be possible to assume that the ac inductance would depend essentially on the dc current level. The ratio $N_{ac} i_{acmax} / N_{dc} I_{dc}$ depends on the chosen design parameters for the magnetic regulator.

From (3.9) and (3.10) the following relations may be observed:

$$H_1 + H_2 = \frac{2 N_{dc} I_{dc}}{l_{dc}} \tag{3.16}$$

$$(H_1 - H_2) l_{dc} - 2 H_{ac} l_{ac} - 2 H_g l_g = -2 N_{ac} i_{ac} \tag{3.17}$$

Which implies that $(H_1 - H_2)$ will depend on the ac current i_{ac}. For a variable inductor built with two EF25 based cores, $A_{ac} = 2A_1 = 2A_2 = 2A$, and since $\phi = BA$, (3.11) can be rewritten:

$$B_1 + 2B_{ac} = B_2 \tag{3.18}$$

Another important aspect to be considered is related to the practical implementation of the variable inductor prototype. It is mandatory to use gapped E cores in order to have a proper variable inductor behaviour. Yet, the prototype assembly may lead to the presence of undesirable small lateral air gaps, l_{g1} and l_{g2}. Therefore, (3.16), (3.17) and (3.18) are rewritten as follows:

$$(H_1 + H_2)l_{dc} + \frac{B_1}{\mu_0} l_{g1} + \frac{B_2}{\mu_0} l_{g2} = 2NI_{dc} \tag{3.19}$$

$$(H_1 - H_2)l_{dc} - 2H_{ac}l_{ac} - 2H_g l'_g + \frac{B_1}{\mu_0} l_{g1} - \frac{B_2}{\mu_0} l_{g2} = -2N_{ac}i_{ac} \tag{3.20}$$

$$B_1 + 2B_{ac} = B_2 \tag{3.21}$$

where:

$$l'_g = l_g + \min(l_{g1}, l_{g2}) + \frac{|l_{g1} - l_{g2}|}{2} \tag{3.22}$$

At this point, in order to solve the system of equations formed by (3.16), (3.17) and (3.18) or by (3.19), (3.20) and (3.21), the following functions must be known:

$$B_1 = f(H_1);\ B_2 = f(H_2);\ B_{ac} = f(H_{ac}) \tag{3.23}$$

So, in fact, the magnetization curve (3.24) for the selected core material must be known

$$B(H) = \mu_0 \int_0^H \mu_{dif}(H) dH \tag{3.24}$$

where μ_{dif} is the differential or incremental permeability, defined as dB/dH at each operating point.

3.1.1.3 MAGNETIZATION AND PERMEABILITY CURVES

The practical implementation of the variable inductor depends on the specifications of the selected magnetic material. A soft saturation material is preferred since these regulators must be operated at the knee of the $B(H)$ curve. In addition, the modelling and analysis of magnetic devices including non-linear magnetic materials requires the use of approximate relations for the $B(H)$ curves. This implies using analytical approximations to represent the dependence of the relative differential permeability of the material on the magnetic field intensity [3.16], [3.17].

Existing literature suggests several approximations which are typically based on curve-fitting techniques, applied to experimental data made available by manufacturers. One of these curve-fitting functions is proposed in [3.18] and is presented in (3.25).

$$\mu_{dif}(H) = \mu_{ini} \frac{\left[1 + \left(\frac{H - h_g}{h_3}\right)^2\right]^{\sigma}}{\left[\left[1 - \left(\frac{H - h_g}{h_2}\right)^2\right]^2 + \left(\frac{H - h_g}{h_1}\right)^2\right]^{\rho}} \tag{3.25}$$

The following analysis was done considering a soft ferrite material, the 3C85 from Phillips [3.16]. From [3.18], for the 3C85 material from Philips, the analytical approximation parameters are: $h_1 = 76, \mathrm{h}_2 = 500, h_3 = 200, h_g = 0, \sigma = 1, \rho = 1.55$ and $\mu_{ini} = 2000$.

Using Mathcad software and taking into consideration the experimental data given by the manufacturer, it was possible to obtain the $\mu_{dif}(H)$ curve, through (3.25). This curve is presented in Fig. 3.5a. It can be noticed that the analytical approximation agrees quite well with the experimental data. The magnetization curve, $B(H)$, can then be determined using (3.24). The result for the magnetization curve is presented in Fig. 3.5b. This magnetization curve describes the functions defined in (3.23).

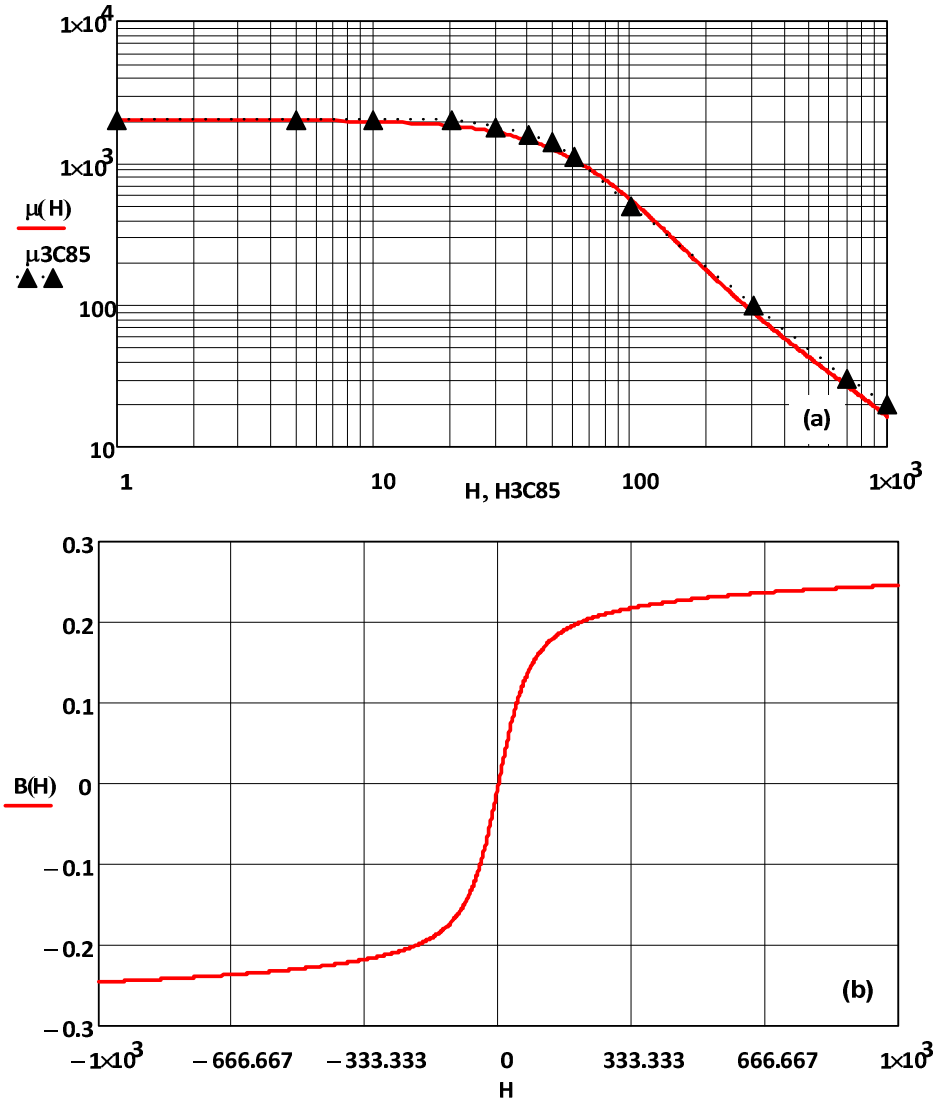

a. Dependence of the relative incremental permeability μ_{dif} on the magnetic field H

b. Calculated plot of the magnetic flux density B as function of the magnetic field H

Fig. 3.5. Permeability and magnetization curves: material 3C85 from Philips.

3.1.1.4 NON-LINEAR INDUCTANCE BEHAVIOUR

The usual inductance definition states that the constant L represents the slope of the line formed by the total flux linkage and the current through the winding. Whereas linear inductors exhibit a constant inductance value during each period of the operating frequency, which implies a straight line through the origin of the flux-current plane, nonlinear inductors are characterized by a different curve, impossible to describe by a single number [3.19]. Magnetic regulators are a specific type of nonlinear inductors. Fig. 3.6 shows the typical characteristic curve of the device, totalized flux vs. ac instantaneous current, not considering hysteresis. The eventual hysteresis loop depends on the type of material used for the core. A small linear region can be observed, but

this behaviour is not maintained for the whole excitation range, meaning that the curve corresponds effectively to a nonlinear inductor. These considerations are very important to define an accurate value for the ac variable inductance, L_{ac}.

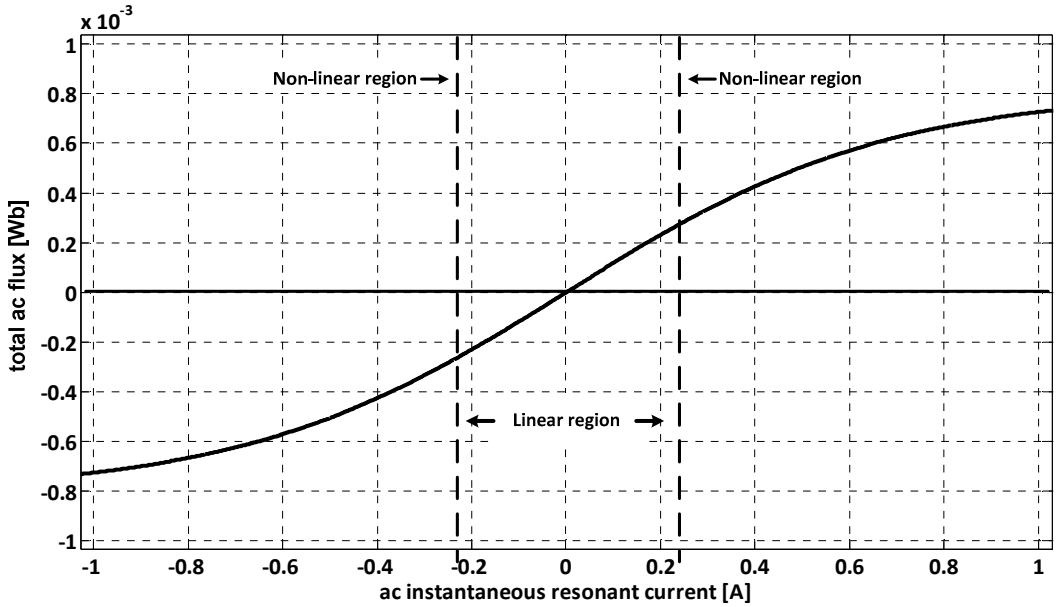

Fig. 3.6. Non-linear region of the variable inductor.

A simple analogy can be made: the voltage across a current-controlled variable inductor can be expressed in the following form:

$$v(t) = \frac{d\Psi(t)}{dt} = \frac{d\Psi(i)}{di}\frac{di(t)}{dt} = L\big(i(t)\big)\frac{di(t)}{dt} \tag{3.26}$$

Where:

$$L(i) = \frac{d\Psi(i)}{di} \tag{3.27}$$

is called the differential inductance:

$$L_{dif} = \frac{d\Psi(t)}{di(t)} \tag{3.28}$$

Taking (3.27) into account it is noticed that the regulator inductance is dependent both on the amplitude of the ac current, i_{ac}, which flows through its ac winding and on the amplitude of the dc control current, I_{dc}. In fact the total ac flux linkage, $\Psi(t)$, can be defined as:

$$\Psi_{ac} = f(I_{dc}, i_{ac}) \tag{3.29}$$

Therefore,

$$d\Psi_{ac}(i) = \frac{\partial \Psi_{ac}}{\partial I_{dc}} dI_{dc} + \frac{\partial \Psi_{ac}}{\partial i_{ac}} di_{ac} \tag{3.30}$$

Considering a constant dc current level imposed on the variable inductor, equation (3.30) can be simplified:

$$d\Psi_{ac}(i) = \frac{\partial \Psi_{ac}}{\partial i_{ac}} di_{ac} \tag{3.31}$$

Using the basic inductance equation, $L = {N^2}/{\mathcal{R}}$, and considering the differential inductance definition for non-linear inductors shown in (3.27), as well as equation (3.31), a first simplified definition for the device ac differential inductance would be:

$$L_{ac} = \frac{\partial \Psi_{ac}}{\partial i_{ac}} = \frac{\partial \phi_{ac} N_{ac}}{\partial i_{ac}} = \frac{N_{ac}^2 \mu_{dif} A_{ac}}{\left(l_{dc} + l_{ac} + l_g\right)} \tag{3.32}$$

where $l_{dc} + l_{ac} + l_g$ is the average path length of the magnetic field lines and μ_{dif} should be the effective differential permeability for the variable inductor core and gaps. This μ_{dif} should correspond to the corrected behaviour of the permeability curve given by the manufacturer, processed, taking into account the three different levels of the flux density, $B_1 = f(H_1)$; $B_2 = f(H_2)$; $B_{ac} = f(H_{ac})$, at each instant, in addition to the core dimensions and air gap dimensions.

The differential permeability curve, μ_{dif}, should be similar to the one given by the manufacturer, if an homogeneous material, non-gapped core was considered, in addition to a zero dc control current. However, this is not the case. The main goal is to take advantage of the nature of the regulator and thereby impose different control current levels on the device.

In order to obtain the differential inductance and simultaneously avoid the use of the corrected permeability curve, requires the calculation of the total ac flux derivative, $\partial \Psi_{ac}$ by means of imposing a small variation, Δi_{ac}, in the instantaneous value of the ac resonant current: $i_{ac} + \Delta i_{ac}$ and $i_{ac} - \Delta i_{ac}$,. Hence, (3.32) results in:

$$L_{ac}(i_{ac}, I_{dc}) = \frac{\Delta B(H_{ac}, I_{dc}) A_{ac} N_{ac}}{2\Delta i_{ac}} \tag{3.33}$$

In conclusion, for a specific dc control current level and for a whole period of the ac inductor current, the differential inductance L_{ac} varies according to the instantaneous value of the ac resonant current and the value for the density of the magnetic field $B(H_{ac})$.

A Mathcad program was developed to find the differential inductance of a typical variable inductor, using (3.33). The program follows the same specifications which were then used to built a prototype: two gapped EF25 cores with 3C85 material from Phillips, $N_{dc} = 2 \times 35$, $N_{ac} = 68$ and $l_g = 0.3\text{mm}$. This prototype will be used as reference in further analysis. The program solves the system of equations formed by (3.16), (3.17) and (3.18) or by (3.19), (3.20) and (3.21), and gives a solution for $B(H_{ac})$ for several levels of the dc control current, until 0.6 A. For each level of I_{dc}, it calculates the different curves of L_{ac}, as defined in (3.33). In order to solve the system of equations, the limit values for the ac instantaneous current were set at -0.7$\sqrt{2}$A and 0.7$\sqrt{2}$A.

Fig. 3.7 and Fig. 3.8 present the calculated results for the differential inductance, considering the presence or not of lateral air gaps l_{g1} and l_{g2}. Fig. 3.7a. illustrates the optimum solution, without lateral air gaps. Fig. 3.7b. and Fig. 3.7c. show the inductance values for $l_{g1} = l_{g2} = l_g/15$, and $l_{g1} = l_{g2} = l_g/5$, respectively. Finally, Fig. 3.8a. and Fig. 3.8b. both show the inductance values considering $l_{g1} \neq l_{g2}$.

From the analysis of Fig. 3.7 and Fig. 3.8 it is clear that for $I_{dc} \approx 0$, the differential inductance value does not show a significant variation for ac current values between -0.5A and 0.5A. However, if the control current level is increased the curves show a different behaviour. It is also noticed that by increasing the values of the lateral gaps, the differential inductance value decreases. This is an expected effect since the increase of the gap will affect the global reluctance of the core, increasing it, and thereby decreasing the differential inductance value. As final remark, it is also noticed that for zero ac current values, in all cases, the inductance value decreases with the increase of the control current. Nonetheless this effect is less significant for increasing lateral gap values.

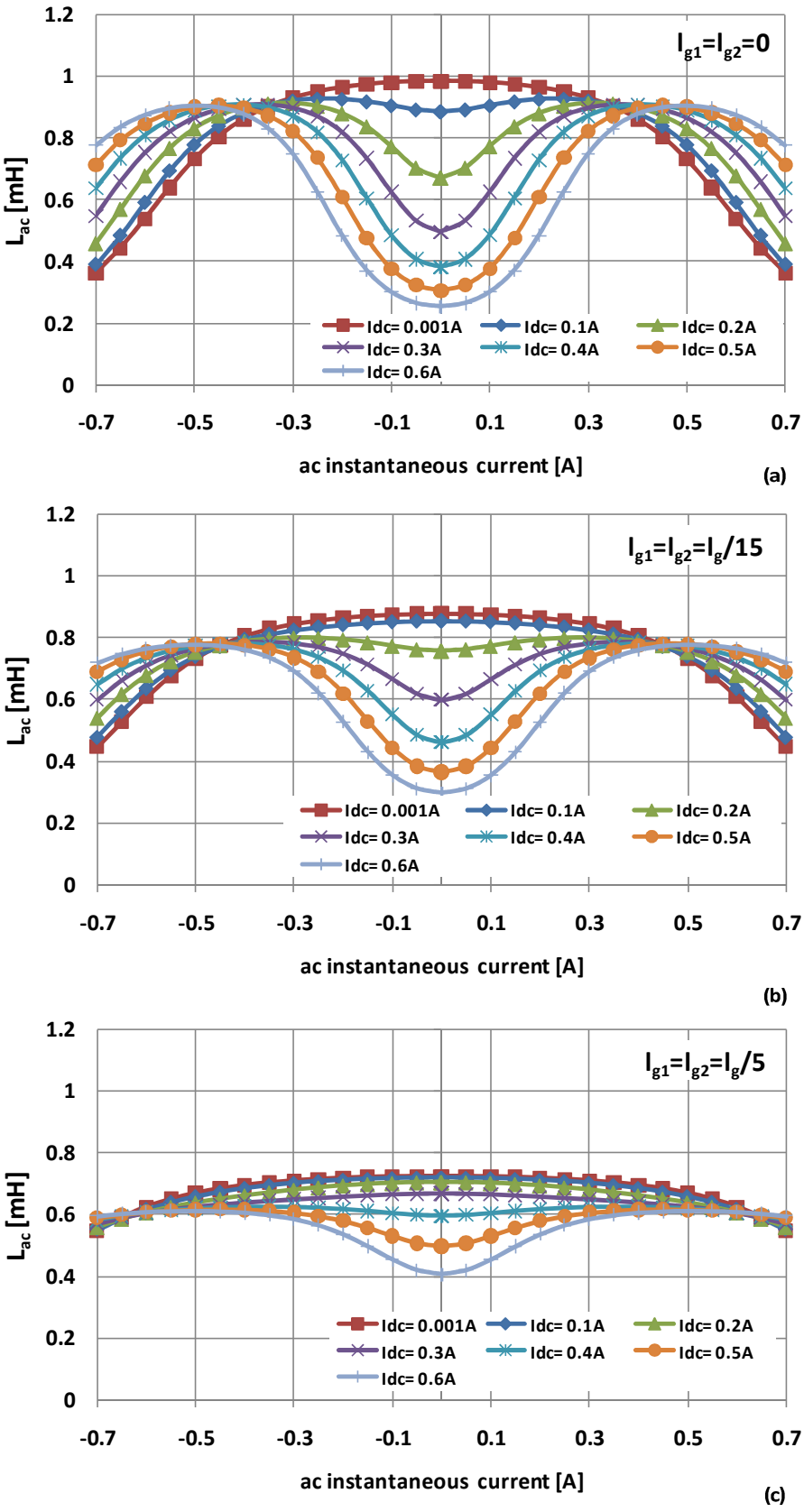

a. Not considering l_{g1} and l_{g2} b. Considering $l_{g1} = l_{g2} = l_g/15$ c. Considering $l_{g1} = l_{g2} = l_g/5$

Fig. 3.7. Differential inductance value for different levels of the dc control current with symmetric gap lengths.

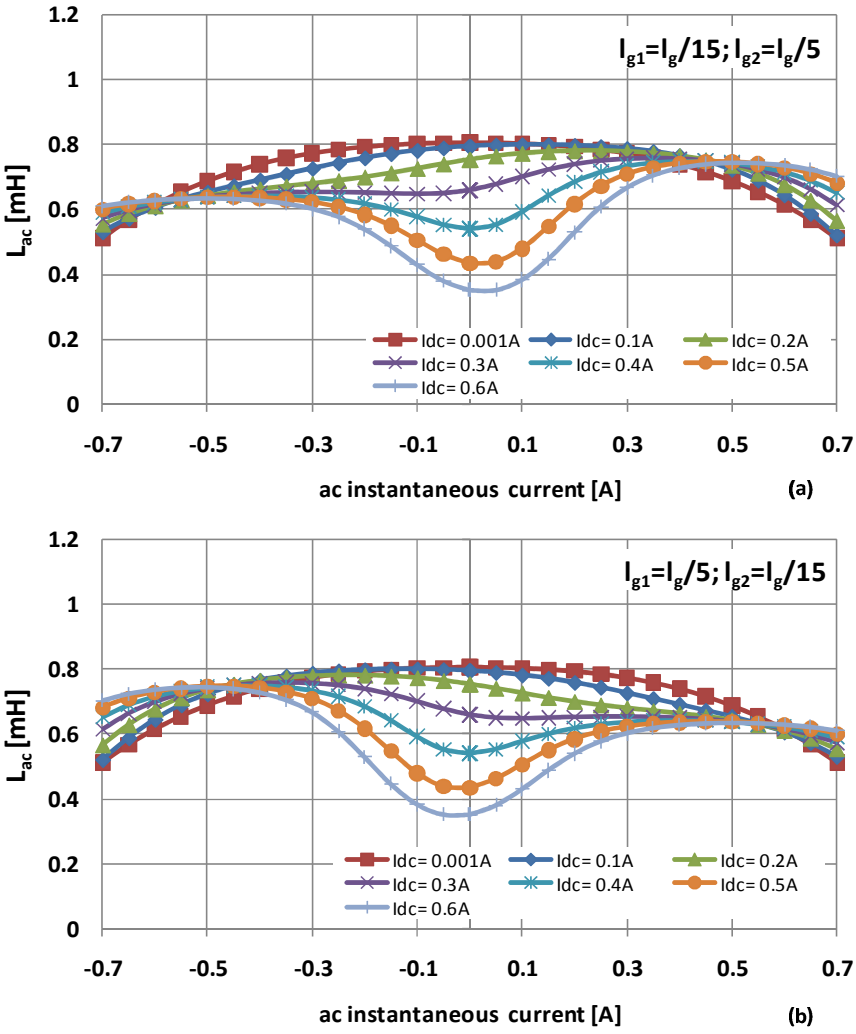

a. Considering $l_{g1} = l_g/15;\ l_{g2} = l_g/5$ b. Considering $l_{g1} = l_g/5;\ l_{g2} = l_g/15$

Fig. 3.8. Differential inductance value for different levels of the dc control current with asymmetric gap lengths.

The same program performs a comparison between the small-signal characteristic of the prototype, obtained with an impedance analyzer, and the correspondent theoretical results. In this case the inductance values are calculated for a specific level of ac current theoretically circulating in the ac winding. At this point, this value was considered to be constant for all dc current levels.

Fig. 3.9 shows the small-signal characteristic of the variable inductor prototype measured with an impedance analyzer. Fig. 3.10 shows the differential inductance value for the different levels of the dc control current. Fig. 3.10a. considers an ac current, $I_{ac} = 0.001\sqrt{2}$A, and Fig. 3.10b. considers an ac current, $I_{ac} = 0.2\sqrt{2}$A. It is clear from these curves that the ac current will affect the inductance value. In Fig. 3.10b., for the case where no lateral air gaps are considered, the theoretical curve follows the behaviour shown by the small-signal characteristic.

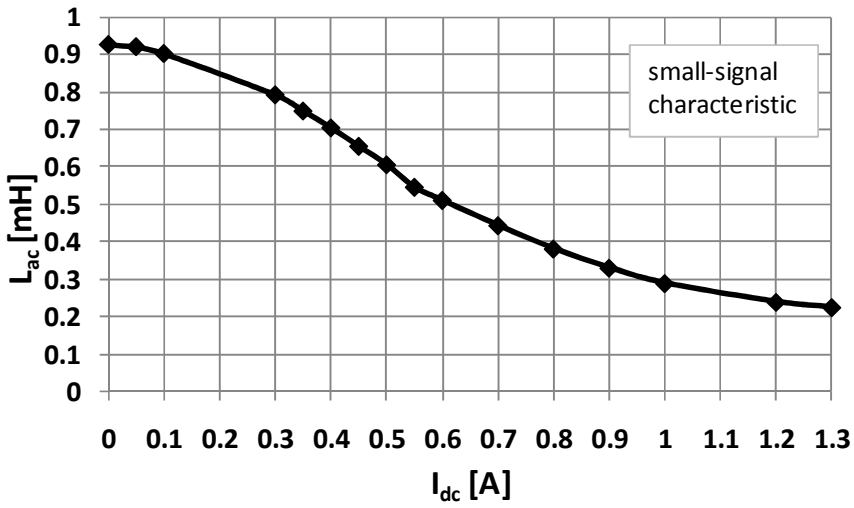

Fig. 3.9. Prototype small-signal characteristic: two gapped EF25 cores with 3C85 material from Phillips, $N_{dc} = 35$, $N_{ac} = 68$ and $l_g = 0.3$mm

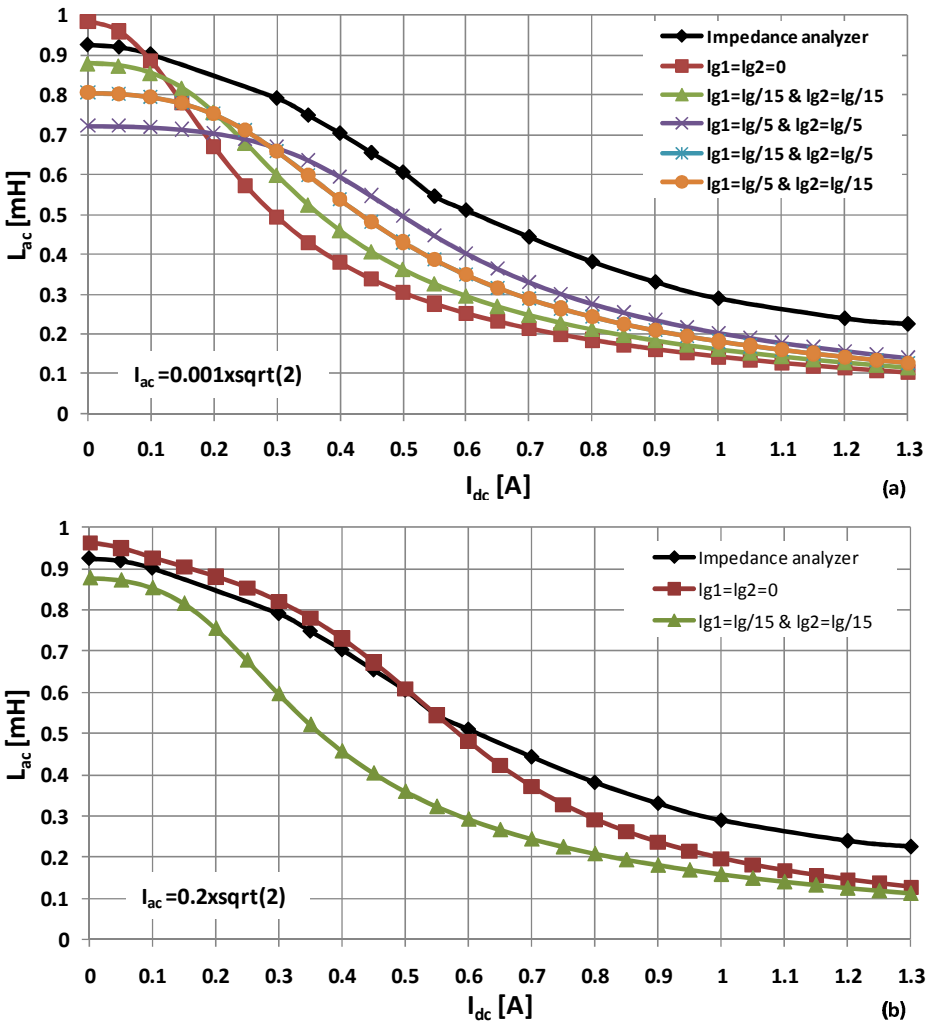

a. Considering $I_{ac} = 0.001\sqrt{2}$A

b. Considering $I_{ac} = 0.2\sqrt{2}$A

Fig. 3.10. Differential inductance value for different levels of the dc control current.

3.1.2 VARIABLE INDUCTOR SIMPLIFIED DESIGN PROCEDURE

3.1.2.1 DESIGN PROCEDURE

The variable inductor design procedure begins by selecting the core type and dimensions and the desirable variable inductance range. As initial conditions it is established that a maximum inductance value should be obtained for a zero dc control current, $L_{ac\_max} \rightarrow I_{dc} = 0$, and thereby, the minimum inductance value should be obtained for a maximum value of dc control current, $L_{ac\_min} \rightarrow I_{dc\_max}$. The basic inductor equation may be used to obtain a simplified approach to the maximum ac inductance value. This L_{ac_max} can be defined as in (3.34):

$$L_{ac\_max} = \frac{N_{ac}^2}{\mathcal{R}} = \frac{N_{ac}^2}{\frac{l_e}{\mu_r \, \mu_0 \, A_e} + \frac{g}{\mu_0 \, A_e}} \tag{3.34}$$

where N_{ac} is the number of turns in the centre leg, $\mathcal{R}$, is the global reluctance of the magnetic circuit as seen from the ac winding; A_e is the effective magnetic cross section in [m^2], l_e is the effective magnetic path length in [m], g is the air gap in [m] and μ_0 is the permeability of the vacuum. In (3.34) μ_r is the relative permeability of the core material, which in this case will be equal to the initial permeability, μ_{ini}, of the material found in the core datasheet. Typically E-type cores are used and therefore the manufacturer will also give the corresponding approximation for the values of A_e and l_e.

The design of the variable inductor should also obey to a maximum constraint which is related to the peak value of the ac current flowing through the main winding, I_{ac_max}. For I_{ac_max}, it is desirable to operate the core at a peak value of the ac magnetic flux density, B_{max}, which must be smaller than the saturation value B_{sat}, which corresponds to the maximum attainable flux density. A value between $0.1B_{sat} - 0.3B_{sat}$ may be applied, and therefore:

$$B_{max} \approx 0.1B_{sat} - 0.3B_{sat} \tag{3.35}$$

The simplified design procedure by which the number of turns of each winding, N_{ac} and N_{dc} are selected may be described as follows.

Firstly and after the selection of the core and identification of the parameters A_e and l_e, the next step is to set the required maximum inductance value. For a zero value of the dc control

current, $I_{dc} = 0$, the peak value of the ac magnetic flux density can be calculated, using the peak value of the ac current, I_{ac_max}, as follows:

$$B_{max} = \frac{N_{ac}}{\mathcal{R}A_e} I_{ac\_max} \tag{3.36}$$

This implies that by using the condition established in (3.35) and the value previously set for L_{ac_max}, (3.36) may be re-written as:

$$N_{ac} = \frac{L_{ac\_max} I_{ac\_max}}{B_{max} A_e} \tag{3.37}$$

This will immediately give the number of turns for the main ac winding. The air gap may then be calculated as:

$$g = \frac{\mu_0 N_{ac}^2 A_e}{L_{ac\_max}} - \frac{l_e}{\mu_r} \tag{3.38}$$

The diameter, d_{ac}, of the wire for the main winding may be selected using (3.39)

$$d_{ac} = \sqrt{\frac{4I_{ac\_max}}{\pi\delta}} \tag{3.39}$$

where δ is the selected current density in [A/m^2]. The diameter, d_{dc}, of the wire for the control winding may be selected using (3.40)

$$d_{dc} = \sqrt{\frac{4I_{dc}}{\pi\delta}} \tag{3.40}$$

The total winding occupation area will be given by the ac and dc winding occupation, A_w, and may be determined as follows:

$$A_w = N_{ac}\pi\left(\frac{d_{ac}}{2}\right)^2 + N_{dc}\pi\left(\frac{d_{dc}}{2}\right)^2 \tag{3.41}$$

The area available for the winding conductors may be defined as $K_u W_A$, where W_A is the core window area and K_u is the window utilization factor or fill factor. For variable inductors based on

double-E cores, W_A is considered as the area on one of the sides. In order to fit the windings into the core window the following constraint must be obeyed:

$$K_u W_A \geq A_w \tag{3.42}$$

A typical value for the fill factor is $K_u = 0.2 - 0.3$ [3.21].

Finally, the number of turns of each control winding, N_{dc} must be estimated. This estimation is done considering that the external path of the EF25 core must reach saturation, for a stipulated maximum value of the dc control current. Taking this into consideration leads to:

$$\phi_{dc}\mathcal{R}_{ext} = 2N_{dc}I_{dc\_max} \tag{3.43}$$

where $\mathcal{R}_{ext}$ is the reluctance of the external path of the core, which means the core without the centre leg. I_{dc_max} is the maximum value of the dc control current, for which the minimum inductance value is obtained. Equation (3.43) may be re-written as follows:

$$N_{dc} = \frac{1}{2}\frac{kB_{sat}l_{ext}}{\mu_{kB_{sat}}\mu_0 I_{dc\_max}} \tag{3.44}$$

where l_{ext} is the length of the external path of the core, kB_{sat} is the flux density in the external path due to I_{dc_max}, for a zero ac current, and $\mu_{kB_{sat}}$ is the permeability of the core material in the above mentioned conditions. For I_{dc_max} the core is expected to be near saturation, therefore the permeability value should be in fact the permeability of the core at that point. The value of k from experimental observation at the laboratory should be around 80%.

The preceding equations represent a brief summary of the magnetic regulator design method. This is in fact a simplified and approximate method. It is clear that the eventual core losses were not considered during this design procedure. These losses will also depend on the level of the dc control current.

3.1.2.2 DESIGN EXAMPLE

In this section the design procedure exposed previously will be illustrated by designing a variable inductor prototype with a EF25 core. The core characteristics and dimensions are presented in Fig. 3.11. The required values are available in the selected core datasheet.

The variable inductor design begins by establishing the maximum inductance value, for instance, $L_{ac\_max} = 1\text{mH}$. A maximum ac current level must also be defined: $I_{ac\_max} = 0.6\text{A}$. This is considered an acceptable value considering the future applications of the prototype. The maximum value for the control current is set at $I_{dc} = 1\text{A}$ and the maximum attainable flux density at $B_{sat} = 0.5\text{T}$. Considering $B_{max} = 0.2B_{sat}$, which is within the limits defined in (3.35), $A_e = 52 \cdot 10^{-6}\text{m}^2$, and using (3.37) it is possible to determine the number of ac turns, which gives $N_{ac} \approx 115$ turns.

E25/13/7
EF25

CORE SETS

Effective core parameters

SYMBOL	PARAMETER	VALUE	UNIT
Σ(l/A)	core factor (C1)	1.11	mm^{-1}
V_e	effective volume	2990	mm^3
l_e	effective length	58.0	mm
A_e	effective area	52.0	mm^2
A_{min}	minimum area	52.0	mm^2
m	mass of core half	≈ 8	g

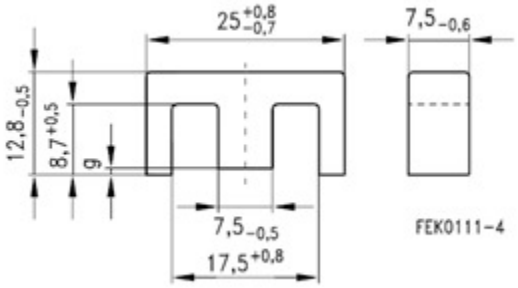

Fig. 3.11. EF25 core: dimensions and main characteristics.

The number of turns in each dc control winding is determined using (3.44). For $0.8B_{sat}$, $\mu_{kB_{sat}}$ is lower than the initial permeability of the core. For the selected core material $\mu_{0.8B_{sat}}$=1800 approximately and $\mu_0 = 4\pi \cdot 10^{-7}$. With $l_{ext} = 100\text{mm}$ and $I_{dc} = 1\text{A}$, this gives $N_{dc} \approx 35$ turns.

After knowing the number of turns of the control and ac windings it is necessary to determine the appropriate wire diameter and the window area occupation A_w. With $\delta = 4\text{A/m}^2$, d_{ac} and d_{dc} can be determined using (3.39) and (3.40) respectively. The window area occupation can then be calculated through (3.41). Knowing that for this double E core, $A_w = 87\text{mm}^2$, the fill factor can be determined trough the condition defined in (3.42), giving $K_u \approx 0.3$.

The next step is the calculation of the air gap through (3.38), where $l_e = 58\text{mm}$, which gives $g \approx 0.9\text{mm}$. An overview of several core datasheets showed that this value was typically too high for the available commercial cores. Thus, it was decided to use a more acceptable value, and the airgap was set at $g = 0.3\text{mm}$. It was then necessary to recalculate the number of turns in the ac winding, again through (3.38), which resulted in $N_{ac} \approx 68$ turns. With this new number of turns the maximum magnetic flux density in the core was estimated to be within acceptable limits. The fill factor was recalculated as $K_u \approx 0.22$ which was also considered as a more acceptable value.

With the calculated values the maximum inductance value was determined using (3.34), giving $L_{ac\_max} \approx 0.94\text{mH}$, which is close to the initially set value.

A prototype was finally built with the following set of parameters, $N_{ac} = 68$, $N_{dc} = 35$ and $g = 0.3\text{mm}$. The variable inductor small-signal characteristic and the variable inductor prototype are both shown in Fig. 3.12. The characteristic shows that this variable inductor has an acceptable variable inductance range, with more than 2:1 variable range. For control current values higher than 1.2A, the variable inductor reaches saturation.

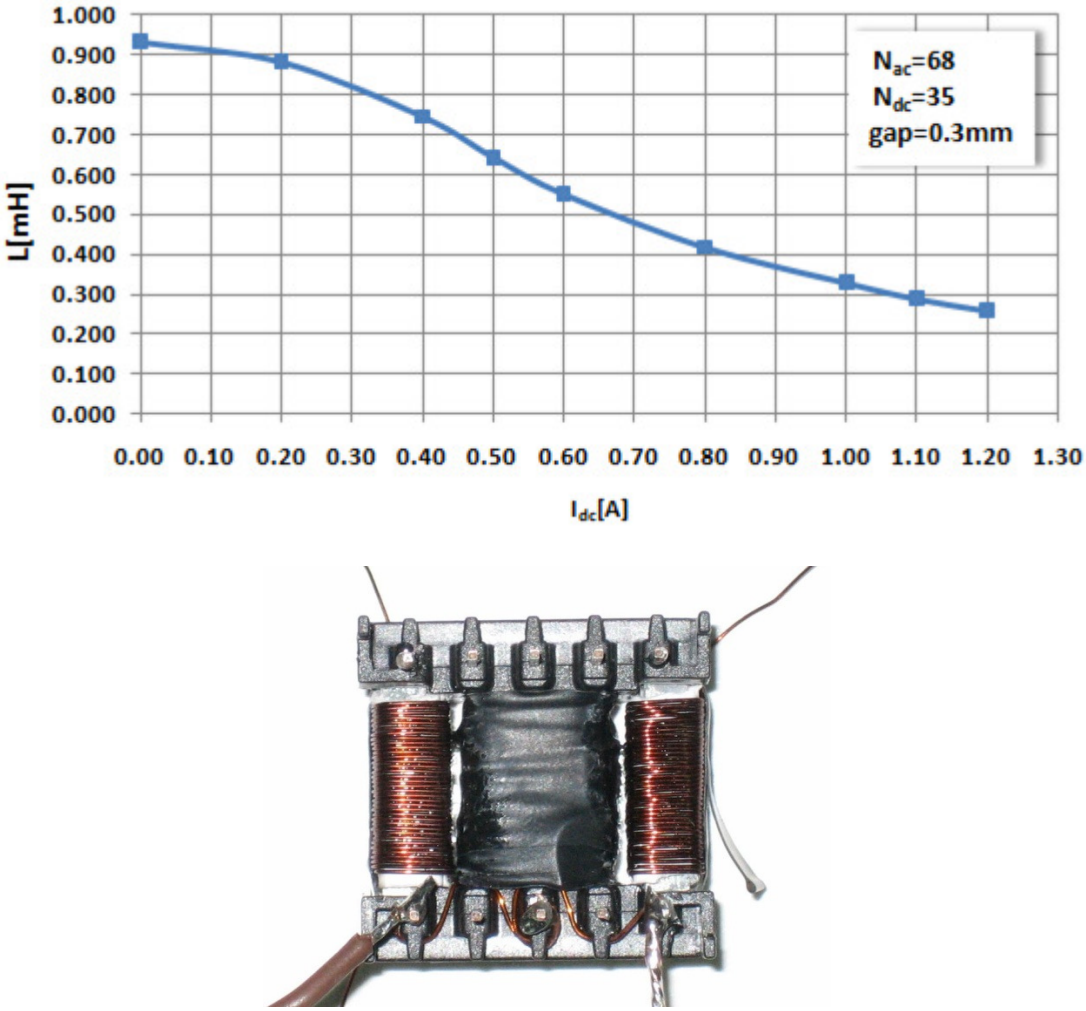

Fig. 3.12. Variable-inductor small-signal characteristic and correspondent parameters.

3.2 VARIABLE INDUCTORS APPLIED TO DIMMABLE ELECTRONIC BALLASTS

3.2.1 INTRODUCTION TO THE PROPOSED MAGNETIC CONTROL TECHNIQUE

3.2.1.1 HALF-BRIDGE RESONANT BALLAST

The voltage-source half-bridge inverter connected to a parallel-loaded resonant circuit is the most common topology used as high-frequency inverter for electronic ballasts. This topology, presented in Fig. 3.13a. guarantees proper ignition and safe lamp operation [3.1].

The operation of this type of ballast circuit may be described as follows: two bi-directional switches and a dc voltage source, V_{dc}, provide a square-wave voltage source that drives the resonant circuit formed by L, C_p and the fluorescent lamp. The load or the fluorescent lamp is connected in parallel with the resonant capacitor, C_p. Typically, the circuit is operated above resonance. In this case, the bi-directional switches can simply be replaced by *pn* junction MOSFETs, M_1 and M_2, as shown in Fig. 3.13a., which already have intrinsic anti-parallel diodes, D_1 and D_2. M_1 and M_2 are driven by rectangular-wave voltages, v_{GM1} and v_{GM2} and are alternately turned ON and OFF at the inverter switching frequency, f_s. The duty-cycle, D, should be slightly less than 50% to avoid cross conduction through the switches, due to the turn-off delay. In Fig. 3.13a., C_b is a dc-blocking capacitor which prevents the dc current flow through the lamp. The average voltage across C_b is equal to $V_{dc}/2$. This capacitor can be connected either in series with L, or in series with the lamp. It is also possible to include a transformer (or as it will be further proposed, a variable transformer) in parallel with the lamp and C_p. In this case the dc-blocking capacitor must be placed in series with the resonant inductor, L. The resonant capacitor may be located either on the primary or the secondary of the transformer. If placed on the secondary the leakage inductance of the transformer is absorbed by the resonant inductance. These aspects will be further discussed.

Typically, if the load or the lamp high-frequency equivalent resistance is much higher than the reactance of the resonant capacitor, the current through the resonant inductor, L, and the switches, M_1 and M_2, is almost independent of the load. If the load resistance increases, the voltage across the resonant capacitor and the load also increases, causing the output power to increase. Fig. 3.13b. shows the typical operating waveforms for a constant load resistance, R, considering an

operating frequency $f_s > f_r$, where $f_r = 1/(2\pi\sqrt{LC_s})$ is the resonant frequency of the $L - C_s - R_s$ equivalent series circuit, shown in Fig. 3.13e. which results from the previous parallel circuit formed by the resonant inductor L, C_p and R.

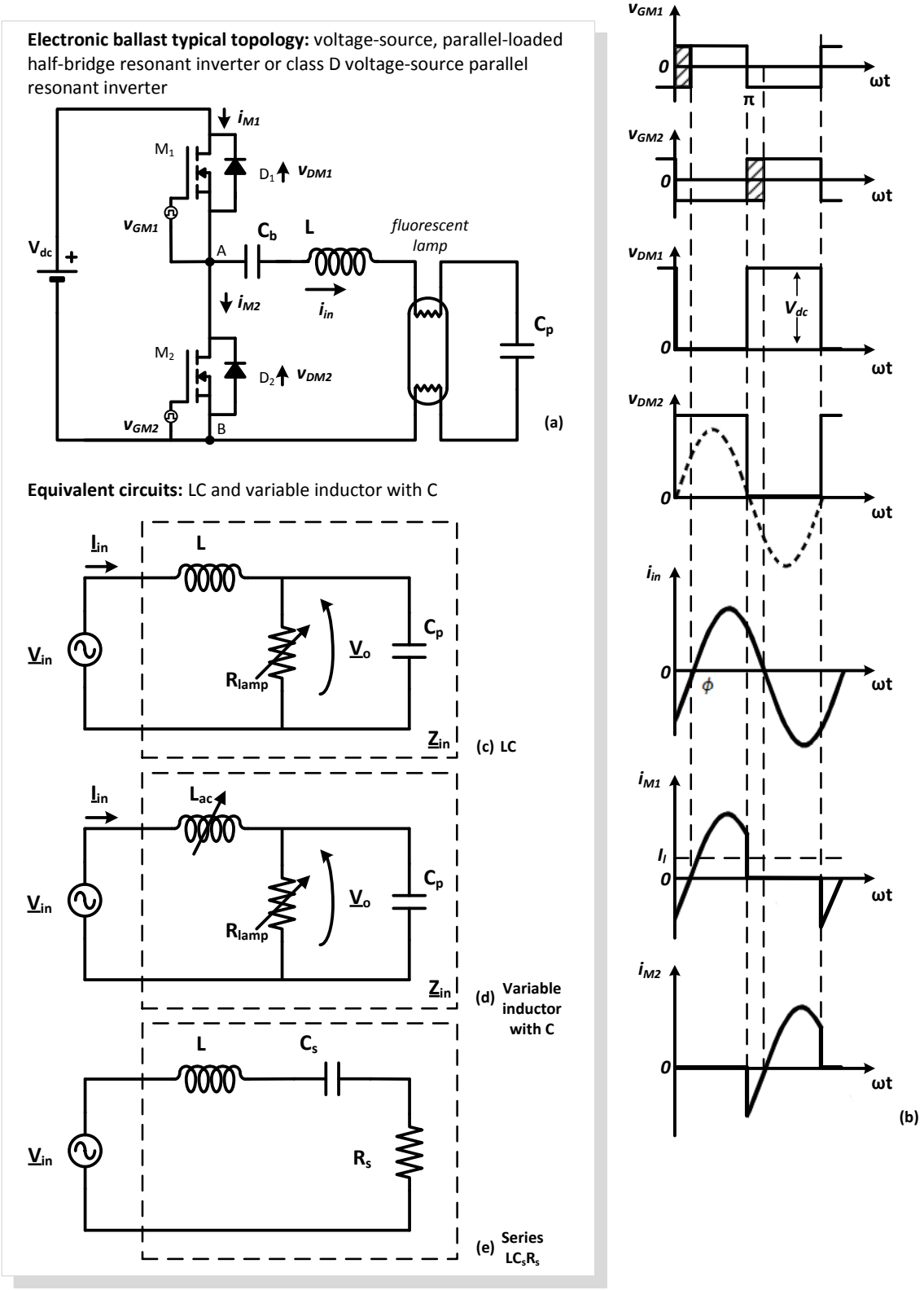

Fig. 3.13. Half-bridge resonant ballast: operating waveforms $f_s > f_r$ [3.2].

The voltages across diodes D_1 and D_2, v_{DM1} and v_{DM2} and the currents through the switches M_1 and M_2, i_{M1} and i_{M2} are presented in Fig. 3.13b.

The input voltage of the resonant circuit, v_{in}, after the dc-blocking capacitor, is also a square-wave, similar to v_{DM2}, but with a zero dc average. Using the Fourier series this voltage can be defined as follows:

$$v_{in}(t) = \sum_{n=1,3,\dots}^{\infty} \sqrt{2} V_{in,n} \sin(n\omega t) = \sum_{n=1,3,\dots}^{\infty} \frac{4\, {V_{dc}}/{2}}{n\pi} \sin(n\omega t) \tag{3.45}$$

where $V_{in,n}$ corresponds to the rms value of each harmonic.

For a constant dc input voltage, V_{dc}, as long as the quality factor of the resonant circuit, Q, is sufficiently high (typically $Q > 2.5$), the current through the resonant circuit, i_{in}, also represented in Fig. 3.13b. will be nearly sinusoidal. This implies that the fundamental component of v_{in} will be dominant in the circuit. So, in the following circuit analysis only its fundamental component, V_{in}, with $n = 1$, will be considered:

$$\left|\underline{V_{in}}\right| = V_{in,1} = V_{in} = 4 \frac{{V_{dc}}/{2}}{\pi} \frac{1}{\sqrt{2}} = \frac{\sqrt{2}}{\pi} V_{dc} \tag{3.46}$$

Considering the fundamental approximation, Fig. 3.13c. presents the equivalent half-bridge inverter circuit, considering the power-dependant lamp resistance in series with L. Finally, Fig. 3.13d. presents the equivalent circuit considering the proposed magnetic control technique, where the resonant inductance is replaced by the variable inductor. The presence of the variable inductor results in the variable behaviour of the resonant circuit with an obvious impact on the power delivered to the lamp.

The final remark is related to the turn-on and turn-off transitions of the switches and the range of dead-time indicated by the shadow areas in Fig. 3.13b. The resonant current i_{in} is conducted alternately by M_1 and M_2. In Fig. 3.13b. ϕ represents the phase angle of the resonant current relative to v_{in}, and the resonant frequency, f_r, is defined as the frequency at which the phase shift is zero.

If the inverter is operated at an operating frequency $f_s > f_r$, the phase angle of the resonant current would be $\phi < 0$. In this case the resonant circuit represents an inductive load and the

current i_{in} lags the fundamental component of the voltage v_{in}. Each MOSFET is switched OFF when its current is positive but most importantly it is switched ON when its current is negative and flows through its anti-parallel diode. In these conditions the switch begins to conduct at near zero voltage, due to the conducting diode, which guarantees ZVS and negligible losses during the turn-on transitions. On the contrary, if the inverter is eventually operated at an operating frequency $f_s < f_r$, the phase angle of the resonant current would be $\phi > 0$, in this case the resonant circuit would behave as a capacitive load and the resonant current would lead the fundamental component of the voltage v_{in}. Operation below resonance is not recommended since the anti-parallel diodes turn OFF at high $^{di}/_{dt}$, causing high current spikes in the switches which reduces efficiency and reliability [3.2].

3.2.1.2 HALF-BRIDGE RESONANT BALLAST ANALYSIS

In order to proceed with the theoretical analysis of the proposed dimming method, it is relevant to describe the basic parameters and equations which characterize the general behaviour of the parallel-loaded half-bridge inverter. Therefore, considering the equivalent circuit in Fig. 3.13c. the following parameters and equations are established.

The natural frequency, ω_o:

$$\omega_o = \frac{1}{\sqrt{LC_p}} \tag{3.47}$$

The base impedance or characteristic impedance, Z_b:

$$Z_b = \sqrt{\frac{L}{C_p}} \tag{3.48}$$

The load quality factor at the natural frequency, Q_L:

$$Q_L = \frac{R_{lamp}}{Z_b} \tag{3.49}$$

The resonant frequency that forms the boundary between capacitive and inductive loads, ω_r

$$\omega_r = \frac{1}{\sqrt{LC_s}} \tag{3.50}$$

The load quality factor at the resonant frequency, Q_r:

$$Q_r = \frac{\omega_r L}{R_s} \tag{3.51}$$

Once again, L, C_s and R_s represent the equivalent series circuit which results from the parallel circuit formed by the resonant inductor L, C_p and R.

The input impedance of the resonant circuit is

$$\underline{Z}_{in} = j\omega L + \frac{R_{lamp}\frac{1}{j\omega C_P}}{R_{lamp} + \frac{1}{j\omega C_P}} \tag{3.52}$$

If both real and imaginary parts are isolated, (3.52) can be rewritten:

$$\underline{Z}_{in} = \frac{R_{lamp}}{\left(R_{lamp}\omega C_P\right)^2 + 1} + j\left(\omega L - \frac{R_{lamp}^2 \omega C_P}{\left(R_{lamp}\omega C_P\right)^2 + 1}\right) \tag{3.53}$$

Finally, the phase angle of the resonant current can be defined as:

$$\phi_{in} = arg\left(\frac{1}{\underline{Z}_{in}}\right) \cdot \frac{180}{\pi} \tag{3.54}$$

As referred, the resonant frequency, f_r, is defined as the frequency at which the phase shift is zero. Hence the ratio of the resonant frequency, f_r, to the natural frequency, f_o is:

$$\frac{f_r}{f_o} = \sqrt{1 - \frac{1}{Q_L^2}} \qquad for \qquad Q_L \geq 1 \tag{3.55}$$

From (3.55) the following conclusions are drawn:

- For $Q_L \leq 1$, the resonant frequency does not exist and the resonant circuit represents an inductive load at any switching frequency
- For $Q_L > 1$, the ratio f_r/f_o increases with Q_L. If the switching frequency $f_s > f_r$ the resonant circuit behaves as an inductive load and the resonant current lags the inverter output voltage. This is obviously the desirable operating condition since ZVS is guaranteed. If $f_s < f_r$ the circuit behaves as a capacitive load and ZVS is lost.

Q_L and Q_r are related by the following equation, [3.2]:

$$Q_r = Q_L\left(\frac{\omega_r}{\omega_o}\right) = \sqrt{Q_L^2 - 1} \qquad for \qquad Q_L \geq 1 \tag{3.56}$$

This implies that if $Q_L^2 \gg 1$ then $Q_r \approx Q_L$.

The voltage gain of the circuit or the voltage transfer function can be defined, applying the voltage divider rule, as:

$$\underline{G}(j\omega) = \frac{\underline{V_o}}{\underline{V_{in}}} = \frac{\dfrac{R_{lamp}\dfrac{1}{j\omega C_P}}{R_{lamp} + \dfrac{1}{j\omega C_P}}}{j\omega L + \dfrac{R_{lamp}\dfrac{1}{j\omega C_P}}{R_{lamp} + \dfrac{1}{j\omega C_P}}} = \frac{1}{(1 - \omega^2 LC_P) + j\dfrac{\omega L}{R_{lamp}}} \tag{3.57}$$

(3.57) can be re-written:

$$\underline{G}(j\omega) = \frac{1}{\left(1 - \left(\frac{\omega}{\omega_o}\right)^2\right) + j\frac{1}{Q_L}\left(\frac{\omega}{\omega_o}\right)} \tag{3.58}$$

The absolute value of the voltage gain can be defined as:

$$\left|\underline{G}(j\omega)\right| = \frac{1}{\sqrt{(1 - \omega^2 LC_P)^2 + \left(\frac{\omega L}{R_{lamp}}\right)^2}} = \frac{1}{\sqrt{\left(1 - \left(\frac{\omega}{\omega_o}\right)^2\right)^2 + \left(\frac{1}{Q_L}\left(\frac{\omega}{\omega_o}\right)\right)^2}} \tag{3.59}$$

From (3.59) it can be observed that $\left|\underline{G}(j\omega)\right| = Q_L$ when ${}^{f_s}/_{f_o} = 1$ and that

$$\left|\underline{G}(j\omega)\right| \to \frac{1}{1 - \left(\frac{\omega}{\omega_o}\right)^2} \qquad as \qquad Q_L \to \infty \tag{3.60}$$

This implies that with an open circuit at the output, $\left|\underline{G}(j\omega)\right|$ increases from 1 to ∞ as ${}^{f_s}/_{f_o}$ or ${}^{\omega_s}/_{\omega_o}$ is increased from 0 to 1, and $\left|\underline{G}(j\omega)\right|$ decreases from ∞ to 0 as ${}^{\omega_s}/_{\omega_o}$ increases from 1 to ∞.

The rms value of the output voltage can be obtained by:

$$V_o = V_{in} \frac{1}{\sqrt{(1-\omega^2 L C_P)^2 + \left(\frac{\omega L}{R_{lamp}}\right)^2}} \tag{3.61}$$

And the rms value of the output current by:

$$I_o = \frac{V_o}{R_{lamp}} \tag{3.62}$$

This implies that if the circuit is operated at $f_s/f_o = 1$, (3.62) can be re-written:

$$I_o = \frac{V_o}{R_{lamp}} = \frac{V_{in} Q_L}{R_{lamp}} = \frac{V_{in}}{Z_b} \tag{3.63}$$

And the circuit will behave as a current source, and its value depends exclusively of the input voltage and Z_b.

Finally, the output power can be easily obtained by:

$$P_o = \frac{{V_o}^2}{R_{lamp}} \tag{3.64}$$

Some of the previous conclusions and observations are the reason why this specific circuit is typically adopted in electronic ballasts. Fig. 3.14 shows the frequency-response characteristic of the resonant circuit as well as the commonly used soft-start technique. The frequency response clearly shows that, around the natural frequency, a high voltage gain is obtained for a load high-resistive value. If the load resistance value decreases, the voltage gain also decreases [2.43], [3.3].

The electrodes pre-heating process is guaranteed by means of a frequency-controlled soft-start technique. As a first step, the operating frequency is adjusted to a value higher than the natural frequency of the circuit. Prior to ignition, the lamp will exhibit an almost infinite impedance, which can be translated into a high Q_L, and the resonant current will flow through C_p, heating the electrodes. After a short period of time, the operating frequency is slightly reduced and the resonant circuit will be able to generate the necessary high voltage spike for the lamp ignition. As the lamp is ignited, the value of Q_L drops, since the load reaches the nominal lamp resistance value and the circuit is then capable of limiting the lamp current without any further change on the operating frequency. This technique can be followed through points A, B and C, as represented in Fig. 3.14.

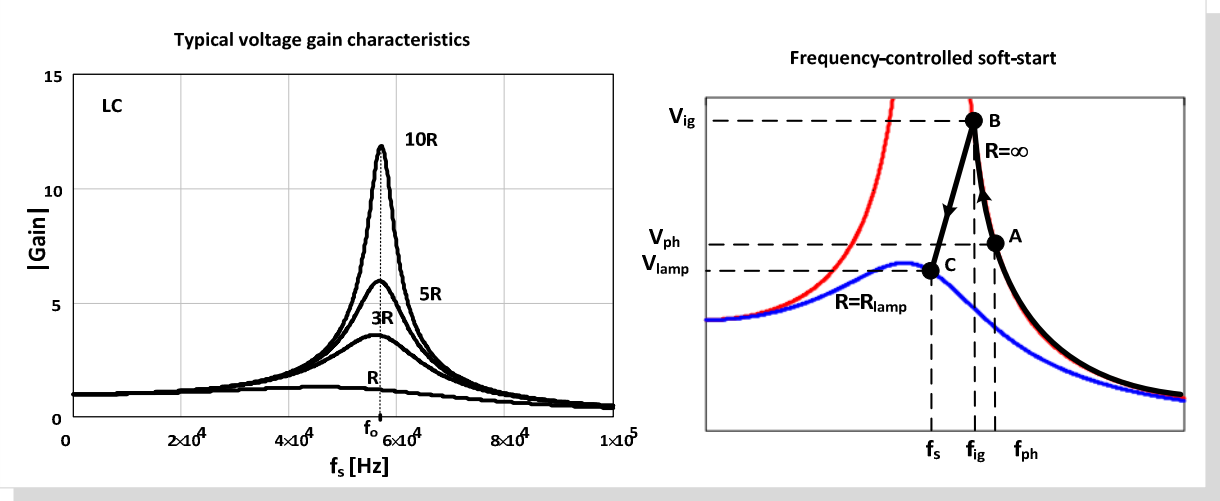

Fig. 3.14. Frequency-response characteristic of the resonant circuit and soft-start technique.

Another characteristic of this circuit is the low THD of the output voltage around the natural frequency. For low values of Q_L the THD of the output voltage tends to a value of 12%, which corresponds to the THD of a triangular wave [2.43]. For this reason, the half-bridge parallel-loaded resonant ballast will present lamp voltage and arc current waveforms almost similar to sine-waves.

3.2.1.3 DIMMING CURVES, ZVS AND SOFT-STARTING

After describing the basics of the resonant inverter circuit, the next step is to include the variable inductor in this analysis, and study the ballast dimming characteristics and some other general aspects related to the implementation of the proposed technique.

The proposed magnetic control technique requires, as an initial step, determining the dimming curves for the selected fluorescent lamp, which means obtaining the inverter output power as a function of the control variable. For a constant operating frequency, the dimming curves provide the fluorescent lamp power as a function the resonant inductance value L_{ac}. Therefore, it is necessary to determine the roots of the equation relating the average lamp power with the variable inductance for the selected range:

$$f\left(P_{lamp}, L_{ac}\right) = 0 \tag{3.65}$$

Using (3.61), (3.64) may be re-written

$$P_{lamp} = \frac{{V_o}^2}{R_{lamp}} = {V_{in}}^2 \frac{R_{lamp}}{R_{lamp}^2(1-\omega^2 L_{ac} C_P) + (\omega L_{ac})^2} \tag{3.66}$$

The roots of (3.66) can be obtained by:

$$P_{lamp}\left[R_{lamp}^2(1-\omega^2 L_{ac} C_P)^2 + \omega^2 L_{ac}^2\right] - V_{in}^2 R_{lamp} = 0 \tag{3.67}$$

Another important aspect in this power control technique is the study of the phase angle of the input current of the resonant tank, the so-called resonant current. The resonant circuit must behave as an inductive load in order to achieve ZVS in the bridge transistors. This implies evaluating the phase angle, ϕ_{in}, through (3.54), according to the selected variable inductance range and its implications on the definition of $\underline{Z}_{in}$.

The validation of the proposed dimming method depends directly on the selection of the resonant circuit parameters, which obviously includes the variable inductance range. These parameters will dictate the behaviour of the whole circuit and will have a direct impact on the dimming curve and on the phase angle of the resonant current. In addition, the real behaviour of the selected fluorescent lamp must also be considered in the calculation of the dimming characteristic. This implies that, for this purpose, the lamp resistance versus average lamp power characteristic, $R_{lamp}\left(P_{lamp}\right)$ must be included in (3.66):

$$P_{lamp}\left[R_{lamp}^2\left(P_{lamp}\right)(1-\omega^2 L_{ac} C_P)^2 + \omega^2 L_{ac}^2\right] - V_{in}^2 R_{lamp}\left(P_{lamp}\right) = 0 \tag{3.68}$$

The design of the magnetic regulator will be carried out after the selection of the resonant parameters and the lamp resistance characterization. An approximate example of a dimming curve is represented in Fig. 3.15. The design of the regulator will normally consider a variable inductance range of, at least, 2 to 1. The minimum value should be calculated considering that the lamp is operating at the maximum flux level, for a natural frequency equal to the selected inverter operating frequency, and the maximum inductance value must be capable of reducing the flux level to the minimum desired value. In these conditions ZVS must also be verified and guaranteed.

Another important aspect is the lamp soft-starting. With this technique, it is also possible to use the variable ac inductance as additional control parameter to achieve soft-starting in a narrower frequency range. This process may be observed in Fig. 3.15. Firstly, the inverter frequency must be set at the selected value. Secondly, the dc control current should be adjusted in order to get the maximum inductance value, L_{ph}. During this operation the electrodes are heated

due to the current that flows through the parallel capacitor, prior to the ignition of the fluorescent lamp. Afterwards, the value of the inductance should be lowered, L_{ig}, which means increasing the dc control current, until the fluorescent lamp is ignited. At this point the inductance should be set at the appropriate value, L_{ac}, according to the desired luminous flux level for the selected fluorescent lamp.

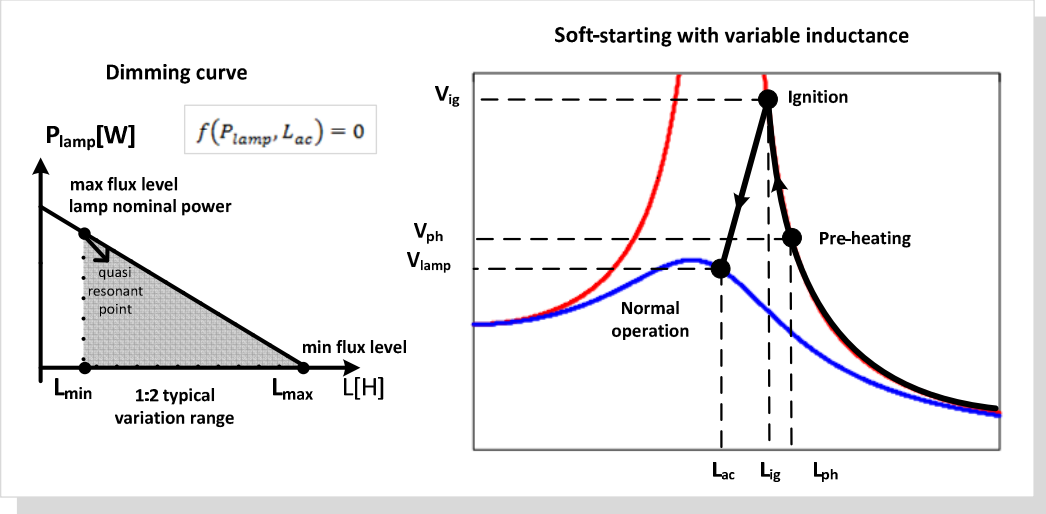

Fig. 3.15. Soft-starting process using the inductance as control parameter and dimming curve [3.5].

3.2.1.4 FLUORESCENT LAMP MODELLING FOR THE ANALYSIS OF THE PROPOSED TECHNIQUE

As referred in Chapter 1, some authors may use a constant resistance model to simulate the fluorescent-lamp behaviour at high frequency. This is one of the simplest ways to model the lamp, but it can only be used at specific conditions, for instance at nominal power. If the purpose is to investigate the impact of the variable inductor in the resonant inverter circuit and to study the lamp-ballast system response to a variable inductance it is clear that such models are not useful.

In this case a specific model which varies the lamp resistance with the average lamp power is in fact one suitable solution, $R_{lamp}(P_{lamp})$. These models, besides simulating the behaviour of the lamp arc, through the definition of an arc resistance, R_{arc}, may also simulate the behaviour of each lamp electrode, trough R_{electr}. Typically, these resistances are represented as shown in Fig. 3.16 where the electrodes resistance are evenly divided in the circuit representation. Usually the electrodes resistances are much lower than the arc resistance, and in most cases they may be

neglected. Throughout this analysis, their influence will be neglected which implies considering $R_{lamp} \approx R_{arc}$, in the following presentation, and therefore $P_{lamp} \approx P_{arc}$.

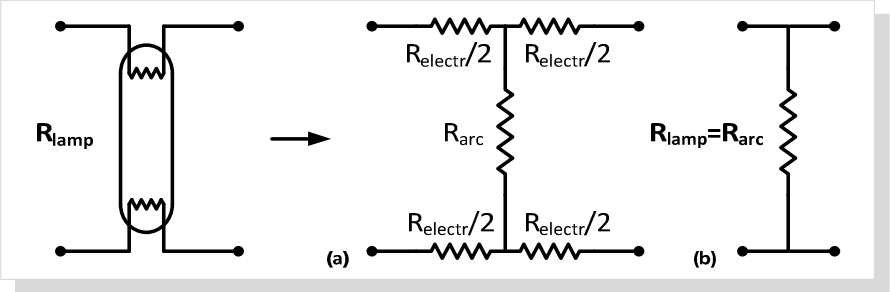

a. Complete model including electrodes effect b. Simplified model

Fig. 3.16. Lamp resistance models

As in classical approaches, the basic idea is to experimentally test the selected fluorescent lamps and obtain their power-dependent model, in order to evaluate the possibilities of this control method. The experimental work was carried out using several frequency-controlled commercial ballasts. Several lamps were selected and tested, standard T8 fluorescent lamps as well as the more efficient T5 fluorescent lamps. Initial theoretical and experimental analyses were performed considering T8 lamps. However, more recently, additional tests and verifications were done considering T5 lamps. A more detailed description of the collected data for these T5 lamps can be observed in Appendix A.

As an example, some of the collected data will be presented. Typically for each lamp type, the data are quite similar and independent of the elected manufacturer. Initially a T8 fluorescent lamp was chosen, the TLD 36W from Philips. The lamp was tested at high frequency, using a standard frequency-controlled electronic ballast, 1-10V DC dimming interface. As previously mentioned, for this type of ballast different operating frequencies will correspond to different levels of average lamp power. For each level, the rms values of the lamp voltage and arc or discharge current were measured. Instead of measuring the lamp power, the average arc power was only measured. This average arc power is easily measured multiplying the instantaneous lamp voltage by the instantaneous discharge current and then applying a dc average function. The measured data were then processed and analyzed in Mathcad as shown in Fig. 3.17.

Fig. 3.17a. presents the $V_{lamp}(I_{arc})$ rms characteristics of the lamp. Fig. 3.17b and Fig. 3.17c. present the rms values of the lamp voltage and discharge current for different values of the average arc power and corresponding curve fitting. Neglecting the electrodes, the arc equivalent resistance, R_{arc}, or the power dependent lamp resistance, $R_{lamp}(P_{arc})$, may be computed,

dividing, for each operating point, the average arc power by the square of the rms value of the arc current. Fig. 3.17d. presents the calculated values for R_{lamp}, and its corresponding curve-fitting. As expected, at low power the lamp resistance presents a high value, which decreases with increasing current. The resulting function, $R_{lamp}(P_{arc})$, will be used later on, in order to obtain the dimming characteristics of the proposed method. This function will be commonly referred to as $R_{lamp}(P_{lamp})$. For the sake of simplicity the curve-fitting was done using a linear interpolation function. It is obvious however that other curve-fitting options are available. A power-dependent exponential fluorescent-lamp-model may also be used without significant impact on the results.

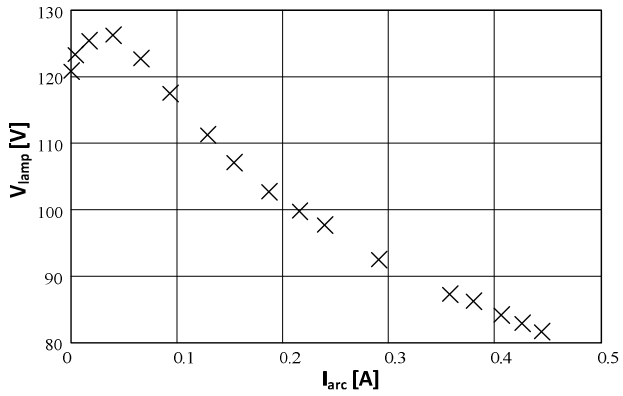

a. $V_{lamp}(I_{arc})$ rms characteristics

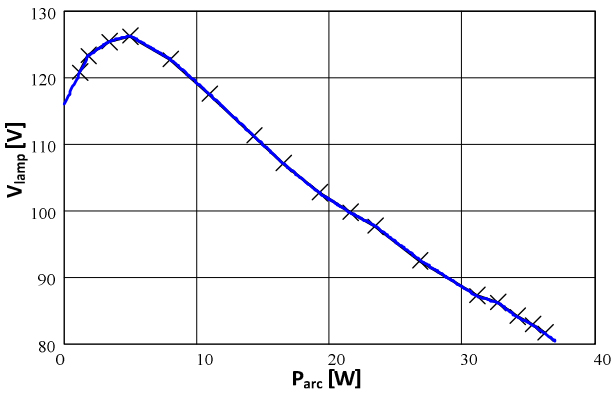

b. Curve fitting to the $V_{lamp}(P_{arc})$ characteristics: linear interpolation

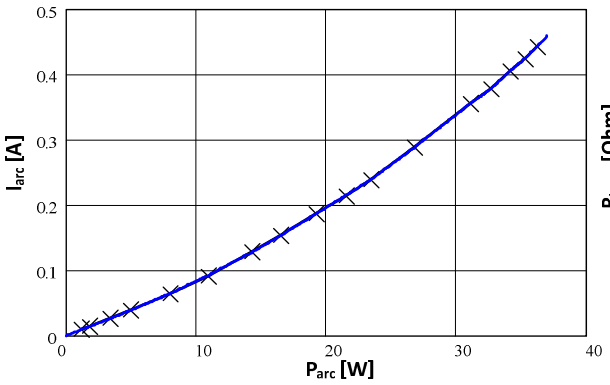

c. Curve fitting to the $I_{arc}(P_{arc})$: linear interpolation

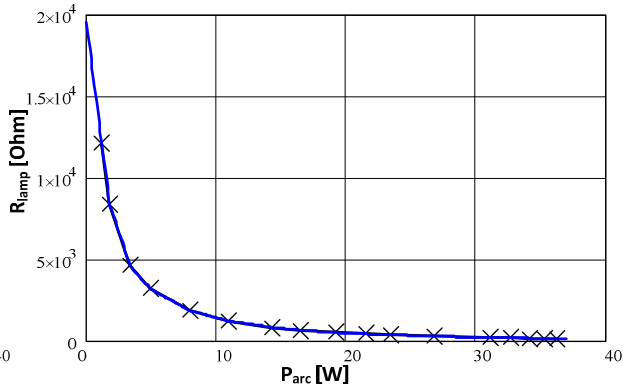

d. Curve fitting to the $R_{lamp}(P_{arc})$: linear interpolation

Fig. 3.17. TLD 36 W Philips – fluorescent-lamp electric characteristics: linear interpolation of the lamp resistance.

Fig. 3.18 shows similar characteristics for the selected T5 fluorescent lamps. A similar procedure was used. Fig. 3.18a. and Fig. 3.18c. present the $V_{lamp}(I_{arc})$ rms characteristics for the T5 HE 35W and for the T5 HO 39W. Fig. 3.18b. and Fig. 3.18d. present the rms values of the lamp voltage for different values of the average arc power and corresponding curve fitting for both lamps. Fig. 3.18e., Fig. 3.18f. and Fig. 3.18g. present the calculated values for R_{lamp}, and corresponding curve-fittings for the T5 HE 21W, for the T5 HO 39W and for the T5 HE 35W.

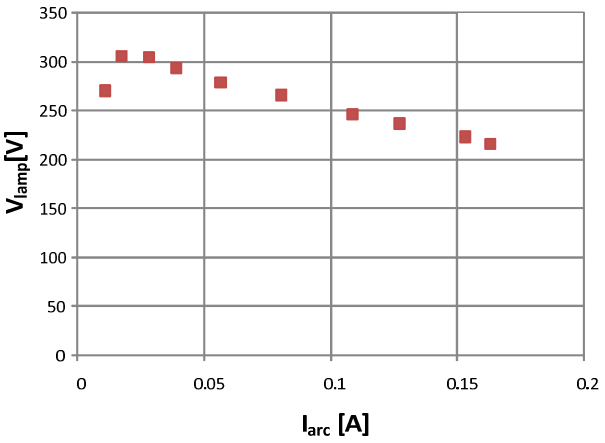

a. $V_{lamp}(I_{arc})$ rms characteristics: T5 HE 35W

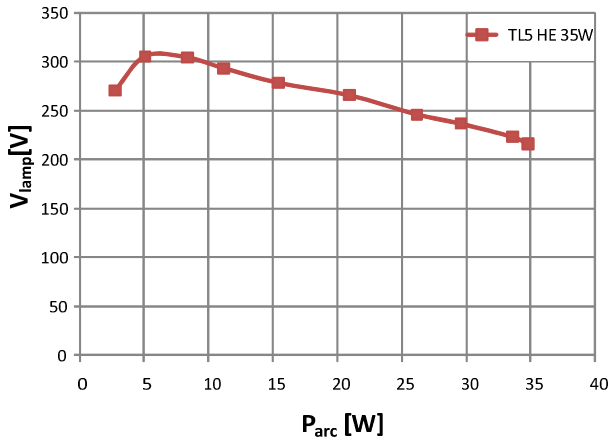

b. Curve fitting to the $V_{lamp}(P_{arc})$ characteristics: linear interpolation: T5 HE 35W

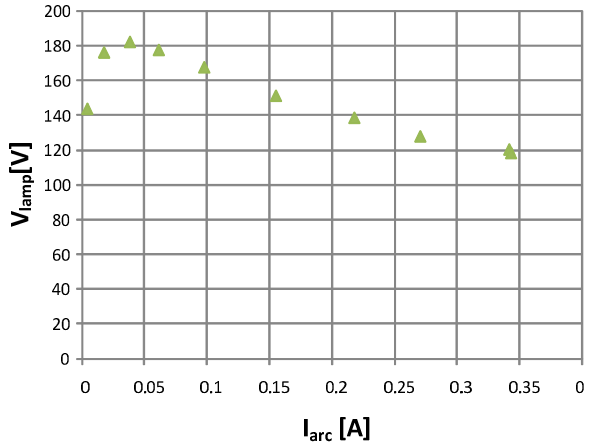

c. $V_{lamp}(I_{arc})$ rms characteristics: T5 HO 39W

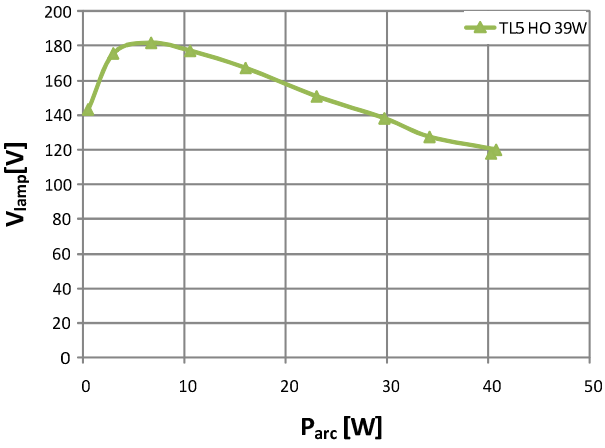

d. Curve fitting to the $V_{lamp}(P_{arc})$ characteristics: linear interpolation: T5 HO 39W

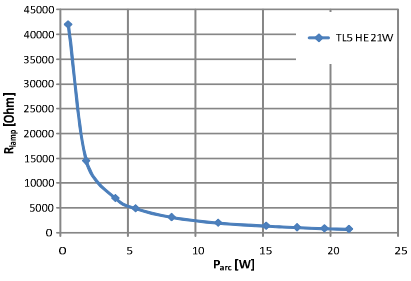

e. $R_{lamp}(P_{arc})$: T5 HE 21W

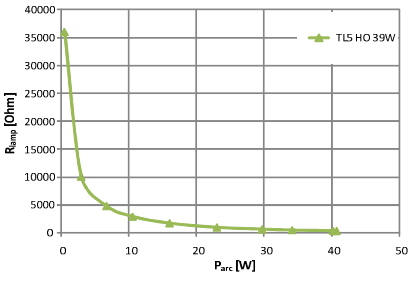

f. $R_{lamp}(P_{arc})$: T5 HO 39W

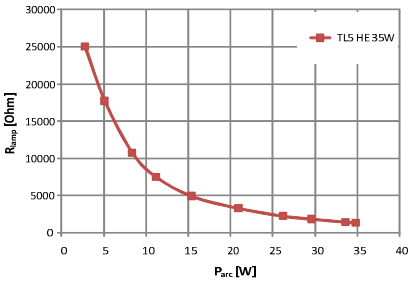

g. $R_{lamp}(P_{arc})$: T5 HE 35W

Fig. 3.18. T5 HE and HO Philips - fluorescent lamp electric characteristics.

Data observation shows that T5 lamps present a higher resistance value when compared to T8 lamps. Some T5 lamps are also specially characterized by a higher lamp voltage. In some particular cases these lamps will also exhibit a lower current. These are the main reasons why these lamps are conventionally manufactured for high-frequency operation (HF), typically above 20 kHz. T5 lamps are also characterized by higher lamp resistance values.

3.2.2 COMPARATIVE ANALYSIS OF RESONANT CIRCUITS WITH MAGNETIC CONTROL

3.2.2.1 THEORETICAL ANALYSIS

The half-bridge parallel-loaded resonant ballast might not be the only adequate choice for this type of application. A comparative analysis between several options regarding resonant circuit configurations, using the proposed dimming method, is considered to be very useful [3.6], [3.7]. Therefore, the purpose of this analysis is to clearly identify and compare the behaviour of different topologies and the achieved dimming range.

Fig. 3.19 presents all the resonant circuits which were considered for this comparative analysis: Fig. 3.19a. the LC topology, Fig. 3.19b. the LCC topology [3.8], Fig. 3.19c. the LCC-Capacitive Impedance Inverter (CII) topology and finally Fig. 3.19d. the CLL topology. The LCC configuration is expected to present a similar behaviour to the LC topology. If operated close to the natural frequency, the circuit will also behave as a current source to the load [2.43], [3.2], [3.3]. This current source behaviour is obviously the best option to supply discharge lamps since it ensures good discharge stability and keeps the lamp from being easily extinguished, particularly if transitory power fluctuations occur. The LCC topology incorporates the series capacitance into the resonant circuit. This allows limiting the ignition voltage by means of factor α, thus avoiding the sputtering damage of lamp electrodes. The LCC-CII resonant circuit was previously used in class-E based ballast applications due to its good features of high ignition voltage and lower voltage ratio at steady state [3.9]. The CLL topology, though less used in electronic ballast applications, was also proposed for resonant converters [3.10] and therefore considered in this analysis. It must be noticed that in Fig. 3.19a. and in Fig. 3.19c. the dc-blocking capacitance is high enough so that its ac voltage ripple is negligible. It avoids any dc current flow through the lamp.

Similarly to the parallel-loaded half-bridge inverter represented in Fig. 3.19a., the following assumption is made: assuming a constant dc input voltage in each circuit, as long as the quality factor of the load is sufficiently high, the current through each resonant circuit is supposed to be sinusoidal and the voltages across the switches are square waves. So, in the following comparative analysis, the fundamental approximation will be extended to the other selected circuit configurations. Fig. 3.20 collects the equivalent half-bridge resonant circuits.

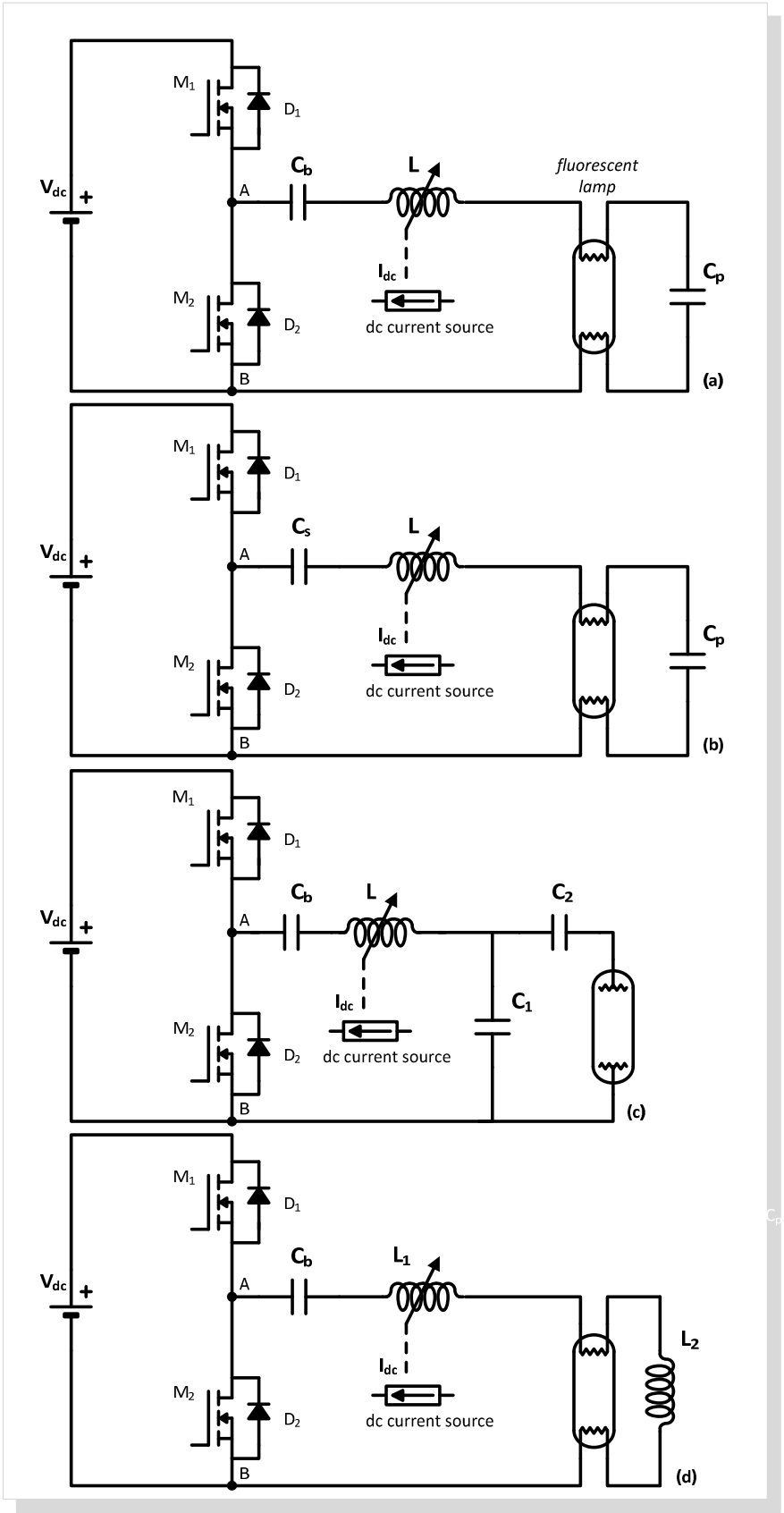

a. LC resonant circuit b. LCC resonant circuit c. LCC-CII resonant circuit d. CLL resonant circuit

Fig. 3.19. Half-bridge resonant inverter.

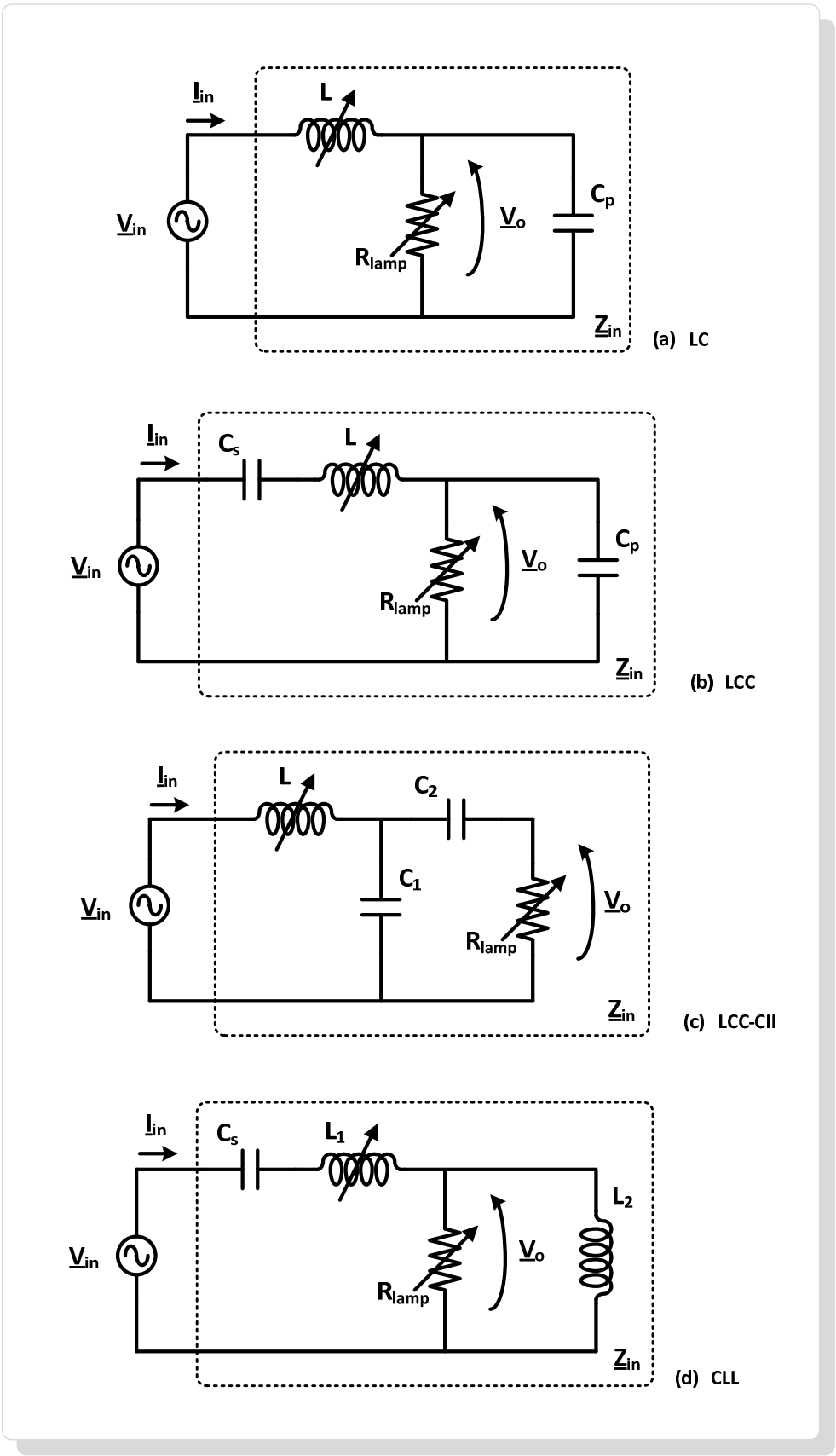

a. LC resonant circuit b. LCC resonant circuit c. LCC-CII resonant circuit d. CLL resonant circuit

Fig. 3.20. Half-bridge resonant inverter: equivalent circuits.

The proper design of the electronic ballast depends on the methodology employed for determining the resonant circuit parameters. For instance, considering the LC topology, from (3.59), the maximum voltage gain can be approximated by Q_L at the natural frequency: $\left|\underline{G}(j\omega)\right| = Q_L$ when ${f_s}/{f_o} = 1$. This implies that:

$$Q_L = \frac{R_{lamp}}{Z_b} = \frac{V_{lamp}}{V_{in}} \qquad when \qquad {f_s}/{f_o} = 1 \tag{3.69}$$

and (3.69) may be used in order to calculate the base impedance or characteristic impedance, Z_b. Subsequently, if the desired operating frequency for the lamp is considered to be equal to the natural frequency the values for the LC resonant circuit parameters may be calculated, using:

$$L = \frac{Z_b}{2\pi f_s} \qquad and\ C = \frac{1}{2\pi Z_b f_s} \qquad with \qquad {f_s}/{f_o} = 1 \tag{3.70}$$

A similar procedure will be adopted for all topologies, taking into account each topology voltage gain at the natural frequency.

- *LCC resonant circuit configuration:*

Assuming the parameter definition in the equivalent circuit of the LCC resonant circuit configuration, shown in Fig. 3.20b., the following relations and equations are established:

$$A = \frac{C_p}{C_s} \tag{3.71}$$

$$C = \frac{C_s C_p}{C_s + C_p} \tag{3.72}$$

$$\alpha = \frac{C}{C_p} \tag{3.73}$$

The natural frequency, ω_o is:

$$\omega_o = \frac{1}{\sqrt{LC}} \tag{3.74}$$

The base impedance or characteristic impedance, Z_b is:

$$Z_b = \sqrt{\frac{L}{C}} \tag{3.75}$$

The load quality factor at the natural frequency, Q_L is:

$$Q_L = \frac{R_{lamp}}{Z_b} \tag{3.76}$$

The input impedance of the resonant circuit is:

$$\underline{Z}_{in} = \frac{1}{j\omega C_S} + j\omega L + \frac{R_{lamp}\frac{1}{j\omega C_P}}{R_{lamp} + \frac{1}{j\omega C_P}} \tag{3.77}$$

If both real and imaginary parts are isolated, (3.77) can be rewritten:

$$\underline{Z}_{in} = \frac{R_{lamp}}{\left(R_{lamp}\omega C_P\right)^2 + 1} + j\left(\omega L - \frac{1}{\omega C_S} - \frac{R_{lamp}^2 \omega C_P}{\left(R_{lamp}\omega C_P\right)^2 + 1}\right) \tag{3.78}$$

Similarly to the LC circuit, the phase angle of the resonant current can also be defined as:

$$\phi_{in} = arg\left(\frac{1}{\underline{Z}_{in}}\right) \cdot \frac{180}{\pi} \tag{3.79}$$

As previously referred, the resonant frequency, f_r, is defined as the frequency at which the phase shift is zero. This resonance frequency depends on Q_L and A [3.2]. Similar to the LC configuration, if the switching frequency $f_s > f_r$ the resonant circuit behaves as an inductive load and the resonant current lags the inverter output voltage. This is obviously the desirable operating condition since ZVS is guaranteed. If $f_s < f_r$ the circuit behaves as capacitive load and ZVS is lost.

The voltage gain of the circuit or the voltage transfer function can be defined, applying the voltage divider rule, as:

$$\underline{G}(j\omega) = \frac{\underline{V_o}}{\underline{V_{in}}} = \frac{\frac{R_{lamp}}{\left(R_{lamp}\omega C_P\right)^2 + 1} - j\frac{R_{lamp}^2 \omega C_P}{\left(R_{lamp}\omega C_P\right)^2 + 1}}{\frac{R_{lamp}}{\left(R_{lamp}\omega C_P\right)^2 + 1} + j\left(\omega L - \frac{1}{\omega C_S} - \frac{R_{lamp}^2 \omega C_P}{\left(R_{lamp}\omega C_P\right)^2 + 1}\right)} \tag{3.80}$$

(3.80) can be simplified:

$$\underline{G}(j\omega) = \frac{1}{\left(1 - \omega^2 C_P L + \frac{C_P}{C_S}\right) + j\frac{1}{R_{lamp}}\left(\omega L - \frac{1}{\omega C_S}\right)} \tag{3.81}$$

(3.81) can be re-written [3.2]:

$$\underline{G}(j\omega) = \frac{1}{(1+A)\left(1 - \left(\frac{\omega}{\omega_o}\right)^2\right) + j\frac{1}{Q_L}\left(\frac{\omega}{\omega_o} - \frac{\omega_o}{\omega}\frac{A}{A+1}\right)} \tag{3.82}$$

The absolute value of the voltage gain can be defined as:

$$\begin{aligned}\left|\underline{G}(j\omega)\right| &= \frac{1}{\sqrt{(1 - \omega^2 C_P L + A)^2 + \frac{1}{R_{lamp}^2}\left(\omega L - \frac{1}{\omega C_S}\right)^2}} = \\ &= \frac{1}{\sqrt{(1+A)^2\left(1 - \left(\frac{\omega}{\omega_o}\right)^2\right)^2 + \frac{1}{Q_L^2}\left(\frac{\omega}{\omega_o} - \frac{\omega_o}{\omega}\frac{A}{A+1}\right)^2}}\end{aligned} \tag{3.83}$$

The rms value of the output voltage can be obtained by:

$$V_o = V_{in}\frac{1}{\sqrt{(1 - \omega^2 C_P L + A)^2 + \frac{1}{R_{lamp}^2}\left(\omega L - \frac{1}{\omega C_S}\right)^2}} \tag{3.84}$$

Using (3.71), (3.72) and (3.73), the voltage gain at $f_s/f_o = 1$ can be defined as:

$$\left|\underline{G}(j\omega)\right| = \frac{1}{\sqrt{\frac{1}{Q_L^2}\left(\frac{1}{A+1}\right)^2}} = \frac{Q_L}{\alpha} \tag{3.85}$$

This implies that if the circuit is operated at $f_s/f_o = 1$, the output current can be defined as:

$$I_o = \frac{V_o}{R_{lamp}} = \frac{\left|\underline{G}(j\omega)\right|V_{in}}{R_{lamp}} = \frac{Q_L V_{in}}{R_{lamp}\alpha} = \frac{V_{in}}{\sqrt{\frac{L}{C}}\alpha} \tag{3.86}$$

And finally, the lamp power can be easily obtained by:

$$P_{lamp} = \frac{{V_o}^2}{R_{lamp}} = {V_{in}}^2 \frac{R_{lamp}}{R_{lamp}^2(1 - \omega^2 LC_P + A)^2 + \left(\omega L - \frac{1}{\omega C_S}\right)^2} \tag{3.87}$$

- *LCC-CII resonant circuit configuration:*

Assuming the parameter definition in the equivalent circuit of the LCC-CII resonant circuit configuration, shown in Fig. 3.21, the following relations and equations are established:

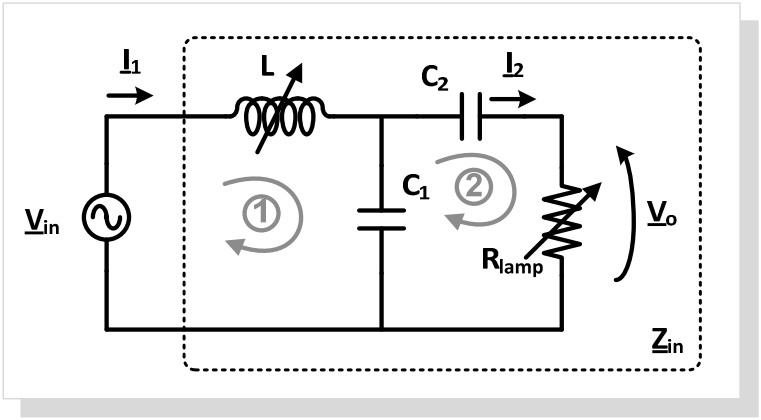

Fig. 3.21. LCC-CII resonant equivalent circuit: mesh definition

$$A = \frac{C_1}{C_2} \tag{3.88}$$

The natural frequency, ω_o:

$$\omega_o = \frac{1}{\sqrt{LC_1}} \tag{3.89}$$

The base impedance or characteristic impedance, Z_b:

$$Z_b = \sqrt{\frac{L}{C_1}} \tag{3.90}$$

The loaded quality factor at the natural frequency, Q_L:

$$Q_L = \frac{R_{lamp}}{Z_b} \tag{3.91}$$

The input impedance of the resonant circuit is:

$$\underline{Z_{in}} = j\omega L + \frac{\frac{1}{j\omega C_1}\left(R_{lamp} + \frac{1}{j\omega C_2}\right)}{R_{lamp} + \frac{1}{j\omega C_1} + \frac{1}{j\omega C_2}} \tag{3.92}$$

If both real and imaginary parts are isolated, (3.92) can be rewritten:

$$\underline{Z_{in}} = \frac{R_{lamp}C_2^2}{\left(\left(R_{lamp}\omega C_1 C_2\right)^2 + (C_1 + C_2)^2\right)} + j\left(\omega L - \frac{\frac{C_1 + C_2}{\omega} + {R_{lamp}}^2 \omega C_1 C_2^2}{\left(\left(R_{lamp}\omega C_1 C_2\right)^2 + (C_1 + C_2)^2\right)}\right) \tag{3.93}$$

Similarly to the LC circuit, the phase angle of the resonant current can also be defined as:

$$\phi_{in} = arg\left(\frac{1}{\underline{Z_{in}}}\right) \cdot \frac{180}{\pi} \tag{3.94}$$

Using Kirchhoff's laws for mesh 1:

$$\underline{V_{in}} = j\omega L\underline{I_1} + \frac{1}{j\omega C_1}\left(\underline{I_1} - \underline{I_2}\right) = \underline{I_1}\left(j\omega L - \frac{1}{j\omega C_1}\right) - \underline{I_2}\frac{1}{j\omega C_1} \tag{3.95}$$

And mesh 2:

$$0 = \underline{I_2}\left(R_{lamp} + \frac{1}{j\omega C_2}\right) + \frac{1}{j\omega C_1}\left(\underline{I_2} - \underline{I_1}\right) = \underline{I_2}\left(R_{lamp} + \frac{1}{j\omega C_2} + \frac{1}{j\omega C_1}\right) - \frac{1}{j\omega C_1}\underline{I_1} \tag{3.96}$$

The output voltage can be obtained by:

$$\underline{V_o} = \underline{I_2}R_{lamp} \tag{3.97}$$

From (3.96):

$$\frac{\underline{I_1}}{\underline{I_2}} = j\omega C_1\left(R_{lamp} + \frac{1}{j\omega C_1} + \frac{1}{j\omega C_2}\right) = \frac{C_1}{C_2} + 1 + j\omega R_{lamp}C_1 \tag{3.98}$$

Using (3.98) in (3.95):

$$\begin{aligned}\underline{V_{in}} &= \underline{I_1}\left(j\omega L - \frac{1}{j\omega C_1}\right) - \underline{I_2}\frac{1}{j\omega C_1} = \\ &= \underline{I_2}\left(\frac{C_1}{C_2} + 1 + j\omega R_{lamp} C_1\right)\left(j\omega L - \frac{1}{j\omega C_1}\right) - \underline{I_2}\frac{1}{j\omega C_1} = \\ &= \underline{I_2}\left[\left(\frac{C_1}{C_2} + 1 + j\omega R_{lamp} C_1\right)\frac{1}{j\omega C_1} - \frac{1}{j\omega C_1}\right. \\ &\left. + j\omega L\left(\frac{C_1}{C_2} + 1 + j\omega R_{lamp} C_1\right)\right] \\ &= \underline{I_2}\left[\left(\frac{C_1}{C_2} + j\omega R_{lamp} C_1\right)\left(\frac{1}{j\omega C_1} + j\omega L\right) + j\omega L\right]\end{aligned} \tag{3.99}$$

If both real and imaginary parts are isolated, (3.99) can be rewritten:

$$\frac{\underline{V_{in}}}{\underline{I_2}} = \left[R_{lamp}(1 - \omega^2 L C_1)\right] + j\left[\omega L\left(\frac{C_1}{C_2} + 1\right) - \frac{1}{\omega C_2}\right] \tag{3.100}$$

Using (3.100), (3.97) can be rewritten:

$$\underline{V_o} = \underline{I_2} R_{lamp} = \frac{R_{lamp}}{\left[R_{lamp}(1 - \omega^2 L C_1)\right] + j\left[\omega L\left(\frac{C_1}{C_2} + 1\right) - \frac{1}{\omega C_2}\right]}\underline{V_{in}} \tag{3.101}$$

The voltage gain of the circuit or the voltage transfer function can then be defined

$$\begin{aligned}\underline{G}(j\omega) = \frac{\underline{V_o}}{\underline{V_{in}}} &= \frac{R_{lamp}}{\left[R_{lamp}(1 - \omega^2 L C_1)\right] + j\left[\omega L\left(\frac{C_1}{C_2} + 1\right) - \frac{1}{\omega C_2}\right]} = \\ &= \frac{1}{(1 - \omega^2 L C_1) + j\frac{1}{R_{lamp}}\left[\omega L\left(\frac{C_1}{C_2} + 1\right) - \frac{1}{\omega C_2}\right]}\end{aligned} \tag{3.102}$$

The absolute value of the voltage gain can be defined as:

$$\left|\underline{G}(j\omega)\right| = \frac{1}{\sqrt{(1 - \omega^2 L C_1)^2 + \left(\frac{1}{R_{lamp}}\left[\omega L(A + 1) - \frac{1}{\omega C_2}\right]\right)^2}} \tag{3.103}$$

Using (3.88), (3.89) and (3.90), the voltage gain at $f_s/f_o = 1$ can be defined as:

$$\left|\underline{G}(j\omega)\right| = \\ = \frac{1}{\sqrt{\left(1-\left(\frac{1}{\sqrt{LC_1}}\right)^2 LC_1\right)^2 + \left(\frac{1}{R_{lamp}}\left[\frac{1}{\sqrt{LC_1}}L(A+1) - \frac{1}{\frac{1}{\sqrt{LC_1}}\frac{C_1}{A}}\right]\right)^2}} \\ = \frac{R_{lamp}}{\sqrt{\frac{L}{C_1}}} = \frac{R_{lamp}}{Z_b} \tag{3.104}$$

This implies that if the circuit is operated at $f_s/f_o = 1$, the output current can be defined as:

$$I_o = \frac{V_o}{R_{lamp}} = \frac{\left|\underline{G}(j\omega)\right|V_{in}}{R_{lamp}} = \frac{V_{in}}{\sqrt{\frac{L}{C_1}}} \tag{3.105}$$

And finally, the lamp power can be easily obtained by:

$$P_{lamp} = \frac{{V_o}^2}{R_{lamp}} = \left|\underline{G}(j\omega)\right|^2 \frac{\left|\underline{V_{in}}\right|^2}{R_{lamp}} = \\ = \frac{{V_{in}}^2}{R_{lamp}} \frac{1}{(1-\omega^2 LC_1)^2 + \left(\frac{1}{R_{lamp}}\left[\omega L(A+1) - \frac{1}{\omega C_2}\right]\right)^2} \tag{3.106}$$

- *CLL resonant circuit configuration:*

Assuming the parameter definition in the equivalent circuit of the LCC-CII resonant circuit configuration, shown in Fig. 3.22, the following relations and equations are established:

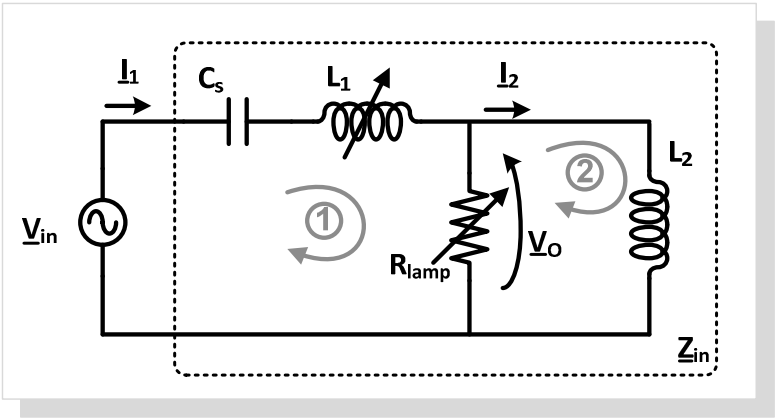

Fig. 3.22. CLL resonant equivalent circuit: mesh definition

$$A = \frac{L_2}{L_1} \tag{3.107}$$

$$L = L_1 + L_2 \tag{3.108}$$

The natural frequency, ω_o:

$$\omega_o = \frac{1}{\sqrt{LC_s}} \tag{3.109}$$

The base impedance or characteristic impedance, Z_b:

$$Z_b = \sqrt{\frac{L}{C_s}} \tag{3.110}$$

The loaded quality factor at the natural frequency, Q_L:

$$Q_L = \frac{R_{lamp}}{Z_b} \tag{3.111}$$

The input impedance of the resonant circuit is

$$\underline{Z}_{in} = \frac{1}{j\omega C_S} + j\omega L_1 + \frac{j\omega L_2 R_{lamp}}{R_{lamp} + j\omega L_2} \tag{3.112}$$

If both real and imaginary parts are isolated, (3.112) can be rewritten:

$$\underline{Z}_{in} = \frac{R_{lamp}(\omega L_2)^2}{R_{lamp}^2 + (\omega L_2)^2} + j\left(\omega L_1 - \frac{1}{\omega C_S} + \frac{\omega R_{lamp}^2 L_2}{R_{lamp}^2 + (\omega L_2)^2}\right) \tag{3.113}$$

Similarly to the previous circuits, the phase angle of the resonant current can also be defined as:

$$\phi_{in} = arg\left(\frac{1}{\underline{Z}_{in}}\right) \cdot \frac{180}{\pi} \tag{3.114}$$

Using Kirchhoff's laws for mesh 1:

$$\begin{aligned} \underline{V}_{in} &= \underline{I}_1\left(j\omega L_1 + \frac{1}{j\omega C_S}\right) + j\omega L_2(\underline{I}_1 - \underline{I}_2) \\ &= \underline{I}_1\left(j\omega(L_1 + L_2) + \frac{1}{j\omega C_S}\right) - j\underline{I}_2\omega L_2 \end{aligned} \tag{3.115}$$

And mesh 2:

$$0 = \underline{I_2} R_{lamp} + j\omega L_2 \left(\underline{I_2} - \underline{I_1}\right) \tag{3.116}$$

The output voltage can be obtained by:

$$\underline{V_o} = \underline{I_2} R_{lamp} \tag{3.117}$$

From (3.116):

$$\frac{\underline{I_1}}{\underline{I_2}} = \frac{R_{lamp} + j\omega L_2}{j\omega L_2} = 1 - j\frac{R_{lamp}}{\omega L_2} \tag{3.118}$$

Using (3.118) in (3.115)

$$\underline{V_{in}} = \underline{I_2}\left[\left(1 - j\frac{R_{lamp}}{\omega L_2}\right)\left(j\omega(L_1 + L_2) - j\frac{1}{\omega C_S}\right) - j\omega L_2\right] \tag{3.119}$$

(3.119) can be rewritten:

$$\frac{\underline{V_{in}}}{\underline{I_2}} = \left[\frac{R_{lamp}}{\omega L_2}\left(\omega(L_1 + L_2) - \frac{1}{\omega C_S}\right)\right] + j\left[\omega(L_1 + L_2) - \omega L_2 - \frac{1}{\omega C_S}\right] \tag{3.120}$$

If current $\underline{I_2}$ is isolated then (3.120) can be rewritten:

$$\underline{I_2} = \underline{V_{in}} \frac{1}{\left[\frac{R_{lamp}}{L_2}\left(L_1 + L_2 - \frac{1}{\omega^2 C_S}\right)\right] + j\left[\omega L_1 - \frac{1}{\omega C_S}\right]} \tag{3.121}$$

Using (3.121), (3.117) can be rewritten:

$$\underline{V_o} = \underline{I_2} R_{lamp} = \underline{V_{in}} \frac{R_{lamp}}{\left[\frac{R_{lamp}}{L_2}\left(L_1 + L_2 - \frac{1}{\omega^2 C_S}\right)\right] + j\left[\omega L_1 - \frac{1}{\omega C_S}\right]} \tag{3.122}$$

The voltage gain of the circuit or the voltage transfer function can then be defined

$$\underline{G}(j\omega) = \frac{\underline{V_o}}{\underline{V_{in}}} = \frac{R_{lamp}}{\left[R_{lamp}\left(1 + \frac{L_1}{L_2} - \frac{1}{\omega^2 L_2 C_S}\right)\right] + j\left[\omega L_1 - \frac{1}{\omega C_S}\right]} \tag{3.123}$$

The absolute value of the voltage gain can be defined as:

$$\left|\underline{G}(j\omega)\right| = \frac{1}{\sqrt{\left(1+\frac{L_1}{L_2}-\frac{1}{\omega^2 L_2 C_S}\right)^2+\frac{1}{R_{lamp}^2}\left[\omega L_1-\frac{1}{\omega C_S}\right]^2}} \tag{3.124}$$

Using (3.107), (3.108), (3.109) and (3.110), the voltage gain at $^{f_s}/_{f_o} = 1$ can be defined as:

$$\begin{aligned}\left|\underline{G}(j\omega)\right| = & \frac{1}{\sqrt{\left(1+A-\frac{1}{\left(\frac{1}{\sqrt{LC_s}}\right)^2 L_2 C_S}\right)^2+\frac{1}{R_{lamp}^2}\left[\frac{L_1}{\sqrt{LC_s}}-\frac{1}{\frac{1}{\sqrt{LC_s}}C_S}\right]^2}} \\ = & \frac{R_{lamp}\sqrt{LC_S}}{L_2} = \frac{(1+A)R_{lamp}C_S Z_b}{L}\end{aligned} \tag{3.125}$$

This implies that if the circuit is operated at $^{f_s}/_{f_o} = 1$, the output current can be defined as:

$$I_o = \frac{V_o}{R_{lamp}} = \frac{\left|\underline{G}(j\omega)\right|V_{in}}{R_{lamp}} = \frac{(1+A)C_S\sqrt{\frac{L}{C_s}}V_{in}}{L} \tag{3.126}$$

And finally, the lamp power can be easily obtained by:

$$\begin{aligned}P_{lamp} = & \frac{{V_o}^2}{R_{lamp}} = \left|\underline{G}(j\omega)\right|^2\frac{\left|\underline{V_{in}}\right|^2}{R_{lamp}} = \\ = & \frac{{V_{in}}^2}{R_{lamp}}\frac{1}{\left(1+\frac{L_1}{L_2}-\frac{1}{\omega^2 L_2 C_S}\right)^2+\frac{1}{R_{lamp}^2}\left[\omega L_1-\frac{1}{\omega C_S}\right]^2}\end{aligned} \tag{3.127}$$

Table 3.1 summarizes some of the key equations regarding each circuit configuration. The numerical results that follow were obtained considering an input dc voltage, $V_{dc} = 150$ V.

Table 3.1 Half-bridge resonant inverter analysis, [3.7].

RESONANT CIRCUIT	$V_{dc} = 150$ V	$V_{in} = \frac{4\left(\frac{V_{dc}}{2}\right)}{\pi\sqrt{2}}$	$\phi = arg\left(\frac{1}{Z_{in}}\right) \cdot \frac{180}{\pi}$
LC	$P_{lamp} = \frac{V_{in}^2 . R_{lamp}(P_{lamp})}{R_{lamp}(P_{lamp})^2 . (1 - \omega^2 L C_p)^2 + \omega^2 L^2}; Z_{in} = j\omega L + \frac{1}{j\omega C_p + \frac{1}{R_{lamp}(P_{lamp})}}$		
LCC	$A = \frac{C_p}{C_s}$	$C = \frac{C_s C_p}{C_s + C_p}$	$\alpha = \frac{C}{C_p}$
	$P_{lamp} = {V_{in}}^2 \frac{R_{lamp}}{R_{lamp}^2 (1 - \omega^2 L C_P + A)^2 + \left(\omega L - \frac{1}{\omega C_S}\right)^2};$		
	$Z_{in} = \frac{1}{j\omega C_s} + j\omega L + \frac{R_{lamp}(P_{lamp})}{j\omega C_p R_{lamp}(P_{lamp}) + 1}$		
LCC-CII Capacitive Impedance Inverter	$A = \frac{C_1}{C_2}$		
	$P_{lamp} = \frac{{V_{in}}^2}{R_{lamp}} \frac{1}{(1 - \omega^2 L C_1)^2 + \left(\frac{1}{R_{lamp}}\left[\omega L(A+1) - \frac{1}{\omega C_2}\right]\right)^2};$		
	$Z_{in} = j\omega L + \frac{\frac{1}{j\omega C_1}\left(R_{lamp} + \frac{1}{j\omega C_2}\right)}{R_{lamp} + \frac{1}{j\omega C_1} + \frac{1}{j\omega C_2}}$		
CLL	$A = \frac{L_2}{L_1}$		
	$P_{lamp} = \frac{V_{in}^2}{R_{lamp}(P_{lamp})} \cdot \frac{1}{\left(1 + \frac{L_1}{L_2} - \frac{1}{\omega^2 L_2 C_s}\right)^2 + \frac{1}{R_{lamp}(P_{lamp})^2}\left(\omega L_1 - \frac{1}{\omega C_s}\right)^2}$		
	$Z_{in} = \frac{1}{j\omega C_s} + j\omega L_1 + \frac{j\omega L_2 R_{lamp}(P_{lamp})}{R_{lamp}(P_{lamp}) + j\omega L_2}$		

Table 3.2 presents the estimated resonant tank parameters, considering that each circuit is operated at $f_s/f_o = 1$. For each topology, the selected operating frequency was 50 kHz.

Using the key equations presented Table 3.1, and the estimated resonant parameters in Table 3.2, it is possible to determine the roots of the equation relating the average lamp power, for each particular circuit configuration, with the variable inductance, for the selected variable range and verify if in these conditions the phase shift between the resonant current and the inverter square-wave voltaje is negative:

$$f\left(P_{lamp_{LC,LCC,LCC-CII,CLL}}, L_{ac}\right) = 0 \tag{3.128}$$

$$\phi = arg\left(\frac{1}{\underline{Z}_{in_{LC,LCC,LCC-CII,CLL}}}\right) \cdot \frac{180}{\pi} \qquad must\ be < 0\ to\ ensure\ ZVS \tag{3.129}$$

For each equation the real behaviour of the selected fluorescent lamp is considered in the deduction of the dimming characteristic. This is the reason why in Table 3.1 all the equations are represented using a power dependent lamp resistance model, $R_{lamp}\left(P_{lamp}\right)$.

All resonant circuits topologies were evaluated considering a TLD 36 W fluorescent lamp from Philips as load, using the characteristic presented in Fig. 3.17d.

Table 3.2 Half-bridge resonant inverter parameters.

RESONANT CIRCUIT AND OPERATING FREQUENCY	PARAMETERS		
$f_s = 50$ kHz	L [mH]	C [nF]	A
LC	0.5	18	N/A
LCC	0.977	20	1
LCC-CII	0.488	20	1
CLL	0.488	10	1

The theoretical and comparative analysis was first performed in Mathcad using numerical methods. The resulting dimming curves and the phase angle of the input resonant current, as a function of the control parameter, for the LC, LCC, LCC capacitive impedance inverter (CII) and CLL inverter resonant circuits, considering the obtained dimming range, are illustrated in Fig. 3.23.

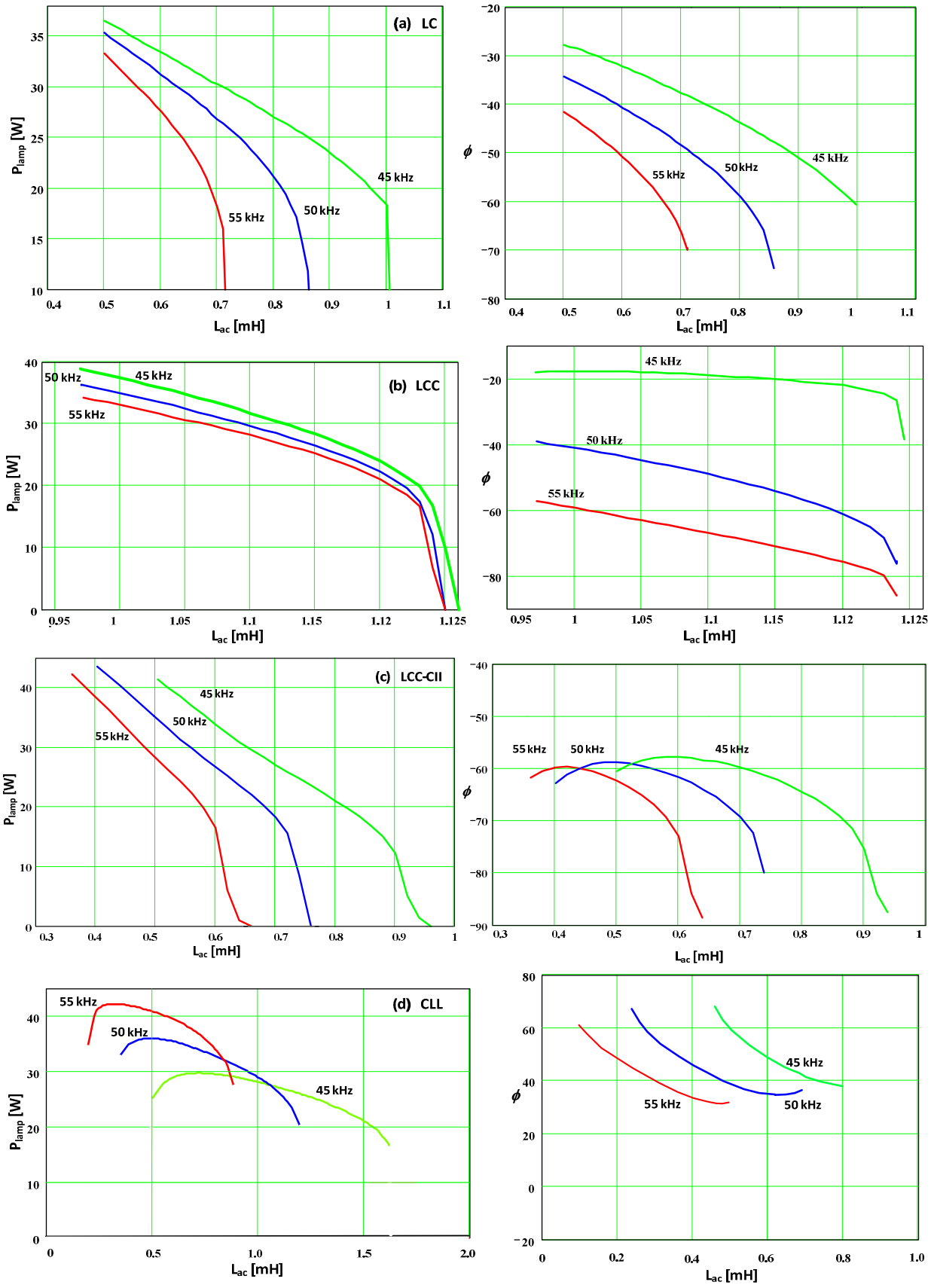

a. LC resonant circuit b. LCC resonant circuit c. LCC-CII resonant circuit d. CLL resonant circuit

Fig. 3.23. Comparative analysis: theoretical dimming curves and phase angle of the input filter current, as a function of the variable inductance, at 45 kHz, 50 kHz and 55 kHz.

For the first three resonant circuits, the obtained dimming curves showed that almost linear regulation can be obtained with this dimming method. Nevertheless, for higher values of the switching frequency, and low dimming levels, there is a region with high $\left|dP_{Lamp}/dL_{ac}\right|$. Therefore, operation in this region is not recommended and can even produce arc instabilities. If a small ripple in the dc control current exists, the lamp power may oscillate between a maximum and a minimum level. The small ripple may also appear due to the fact that the non-linearity of the magnetic material leads to a non-linear coupling between the ac voltage and the control winding voltage [2.16].

With respect to the phase angle of the resonant current, as can be seen from Fig. 3.23a., Fig. 3.23b. and Fig. 3.23c., the phase angle is negative within the whole dimming range, thus ensuring the required ZVS operation. Regarding the CLL resonant circuit topology, this theoretical analysis shows that, even if almost linear regulation is possible, ZVS is not ensured. This can be clearly identified from the phase angle presented in Fig. 3.23d., which is always positive, for $A = 1$. For very restricted values of the A constant, different from 1, which in turn corresponds to a very small variation of the magnetic regulator, ZVS is restricted to a very small operating region. The same analysis was performed considering the possibility of exchange places between the inductance L_2 and the magnetic regulator, but the results were similar. For this reason this resonant circuit topology will not be further considered.

3.2.2.2 SIMULATION AND EXPERIMENTAL RESULTS

- *MATLAB-Simulink implementation:*

  In spite of the importance of performance comparison, the purpose of this analysis was to clearly identify the dimming range achieved by each topology, and then confirm these results by practical implementation of a prototype. However, prior to the experimental testing a simulation analysis was also made using MATLAB-Simulink tools.

  In MATLAB-Simulink, models are hierarchical, so they can be built using both top-down and bottom-up approaches. The system can be viewed at a high level and then, by double-clicking the blocks, one can go down to see increasing levels of model detail. After defining a model, it can be simulated using a menu of integration methods, either from the Simulink menus or by entering commands in the MATLAB Command Window. Scope and other display blocks allow seeing the simulation results while the simulation is

running. The simulation results can also be put in the MATLAB workspace for post processing and visualization.

The schematic of the electronic ballast circuit, for the LCC-CII topology, is presented in Fig. 3.24. In Fig. 3.24a. the Scope block displays its inputs with respect to simulation time. It displays the lamp voltage and the lamp arc current, the filtered lamp arc power and the inverter voltage waveforms. The rms values of the lamp voltage, lamp arc current and finally the lamp arc average power are also calculated and displayed. Once more the electrodes effect is neglected in this simulation.

The fluorescent-lamp model is presented in Fig. 3.24b. The electronic ballast parameters and the fluorescent-lamp model parameters are shown in Table 3.3. Fig. 3.25 presents simulation results considering two different values for the magnetic regulator at the same switching frequency. These results are similar to the theoretical Mathcad predictions, with a lower average lamp power for a higher value of tank inductance. A comparative analysis between the theoretical results obtained with Mathcad and the simulation results obtained with MATLAB-Simulink is presented in Fig. 3.26. The simulated results correspond to the operating points marked with a cross.

The measured lamp electric characteristics were introduced by means of a Lookup Table. This lookup table approximates a one-dimensional function using the specified lookup method. The Interpolation-Extrapolation was the chosen method; it performs linear interpolation and extrapolation of the inputs. Arc current and lamp voltage are sensed and multiplied. The resulting instantaneous power is then filtered in order to estimate the low-pass filtered lamp arc power. The time constant of the filter is related to the ionization constant of the arc discharge. With this filtered lamp arc power a value for the lamp arc resistance is obtained. Lamp arc current is then generated by a controlled current source, controlled by the multiplication of lamp voltage and lamp conductance.

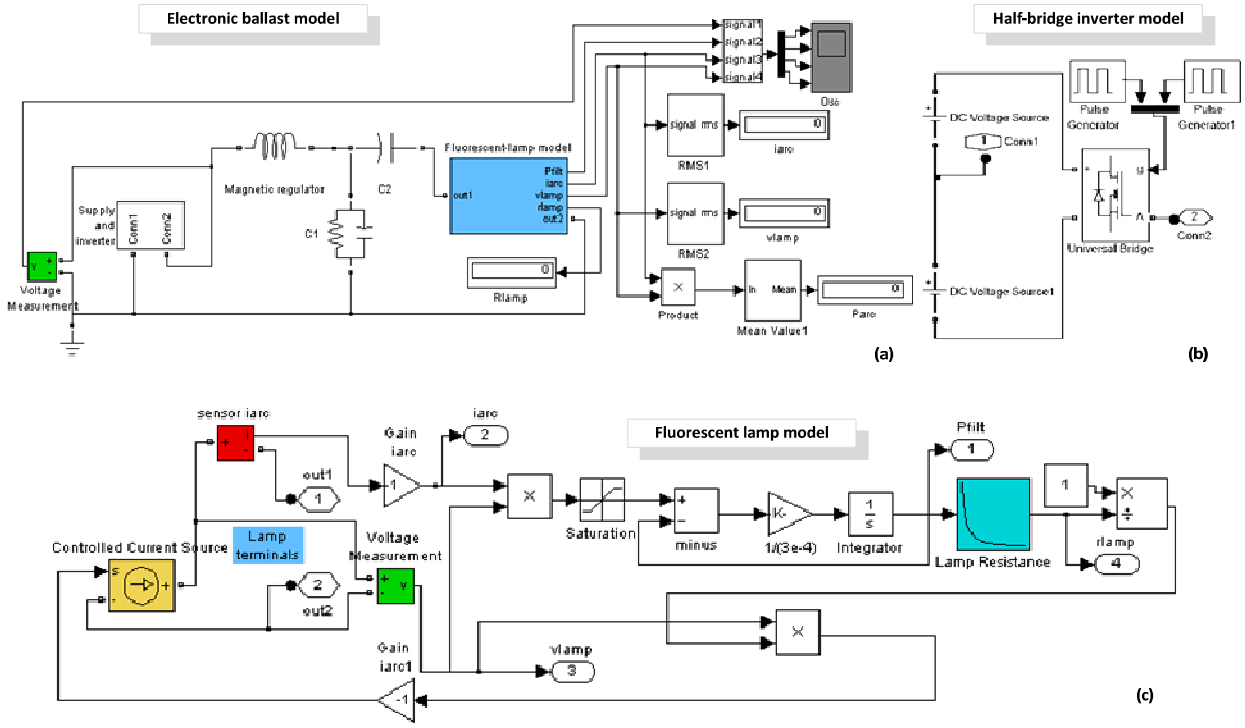

a. Half-bridge resonant ballast model b. Half-bridge inverter model c. Fluorescent-lamp model

Fig. 3.24. Electronic ballast MATLAB-Simulink implementation: LCC-CII resonant circuit.

Table 3.3 Simulation parameters.

PARAMETERS	RESONANT CIRCUIT		
	L [mH]	C [nF]	A
LCC-CII	0.488	20	1
Capacitive Impedance Inverter	0.6	20	C_1/C_2
Switching frequency	$f_s = 50$ kHz		
Time constant	$\tau = 3 \times 10^{-4}$ s		
Dc voltage source	$V_{dc} = 150$ V		

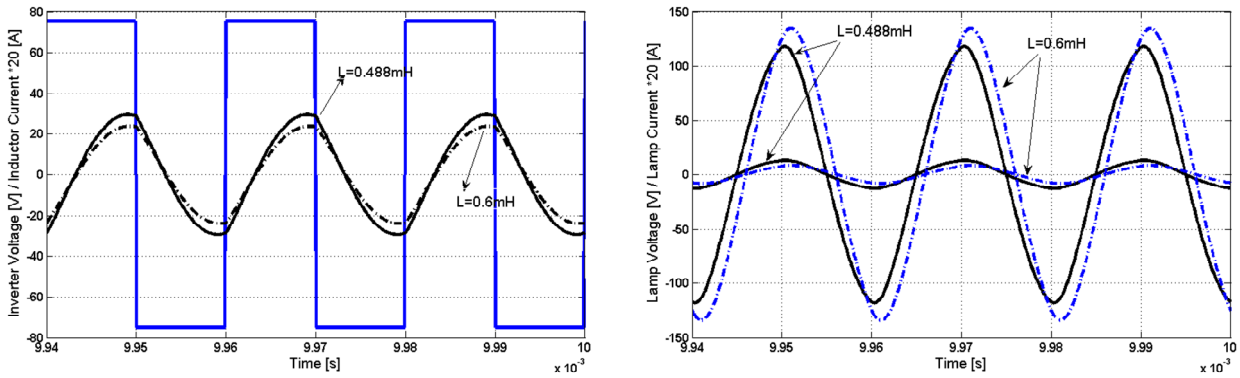

a. Ensured ZVS for two different values for the magnetic regulator

b. Lamp voltage and arc current waveforms

Fig. 3.25. Simulation results for the electronic ballast MATLAB-Simulink implementation: LCC-CII resonant circuit.

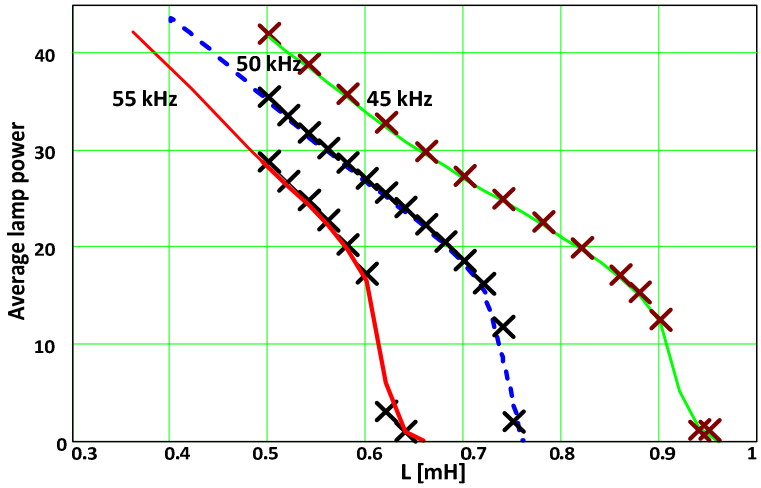

Fig. 3.26. Comparison between simulation results and theoretical results using MatCad: LCC-CII resonant circuit.

- *Variable inductor small-signal characterization and experimental results:*

The small-signal characterization of a magnetic regulator can be done using a variable dc source and an impedance analyzer, as represented in Fig. 3.27. Each level of dc voltage corresponds to a different level of dc current in the control winding, which dictates a specific inductance value indicated by the analyzer. Two different magnetic regulators were built following the methodology previously exposed, using EF25 cores with material 3C85 from Phillips.

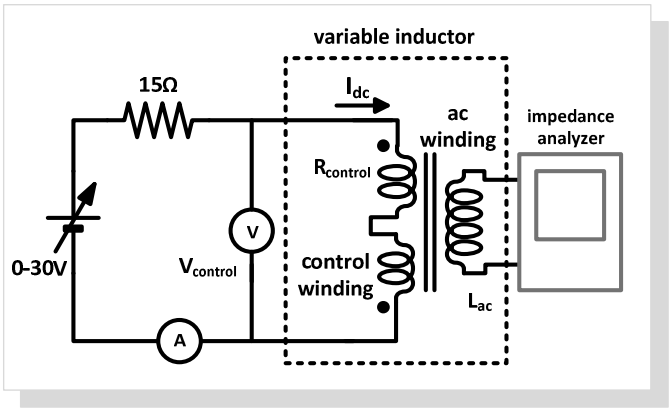

Fig. 3.27. Small-signal characterization of the variable inductor.

Fig. 3.28 presents the measured characteristic and the schematic of the magnetic regulator used in the LC and LCC-CII resonant circuit configurations. The main inductor coil was built with 84 turns and each control winding with 40 turns. Two 0.15mm gapped cores were used. As required, this magnetic regulator presented a nominal value close to 1mH. Its characteristic was obtained under small signal conditions, using the procedure shown in Fig. 3.27. A similar process was followed for the second magnetic regulator. In this case a nominal value close to 1.6mH was considered. The main inductor coil was built with 150 turns, each control winding with 40 turns. For this second magnetic regulator the selected core presented an air gap of 0.5mm.

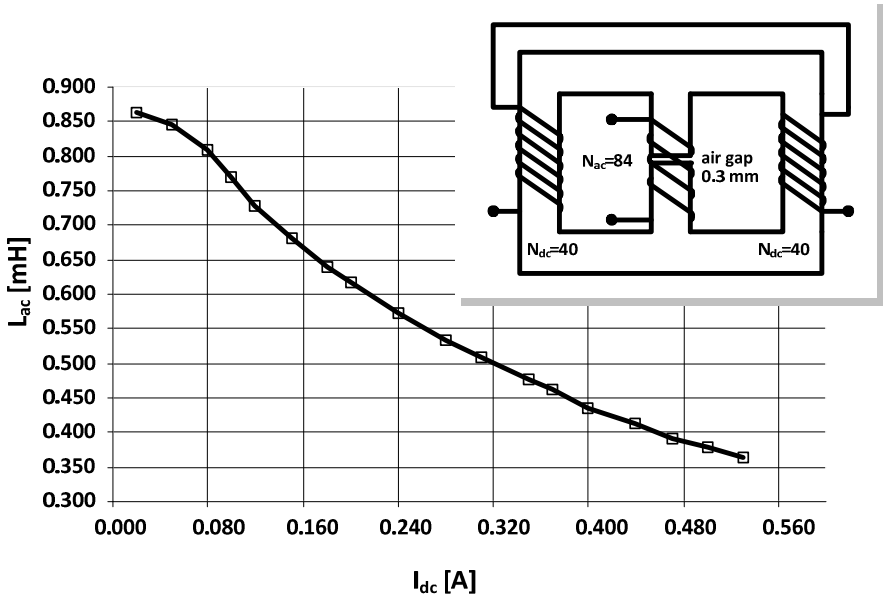

Fig. 3.28. Experimental value of the magnetic regulator as a function of the dc current for the LC and LCC-CII circuit configurations.

According to the previously presented theoretical analysis only the first three resonant circuit topologies will be discussed in terms of experimental results.

Fig. 3.29a. and Fig. 3.29b. present the obtained experimental results for the LC and the LCC laboratory prototypes. Further sections will give more details regarding the experimental implementation of the ballast prototype. Again, the selected fluorescent lamp was a TLD 36W fluorescent lamp from Philips, using the characteristic presented in Fig. 3.17d.

In this particular case, the measurements performed were the average power in the arc, and in the lamp, which means arc power plus electrode power. The electrode power is obtained by subtracting the arc power from the total lamp power. The phase angle of the resonant current was also verified and for the tested configurations ZVS was achieved.

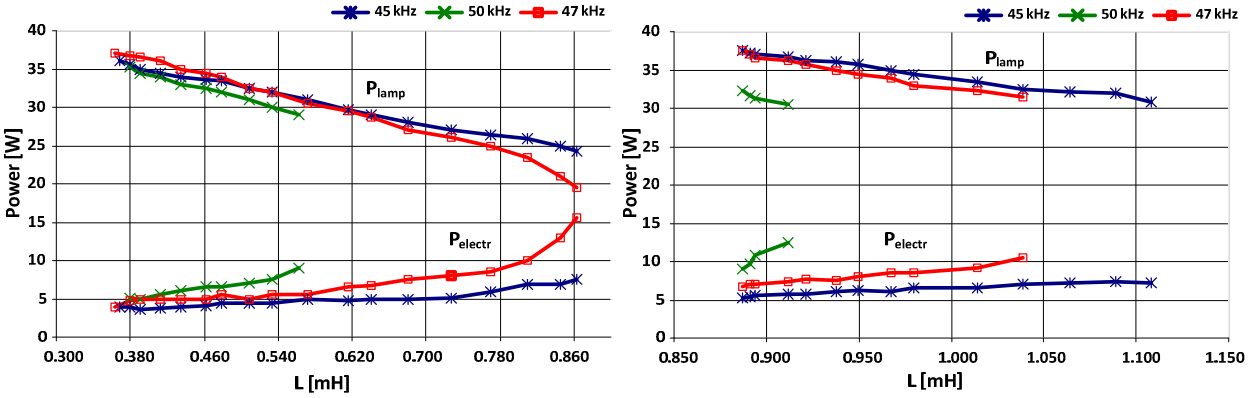

a. LC resonant circuit

b. LCC resonant circuit

Fig. 3.29. Experimental results for the average lamp power and electrode power for the LC and LCC-CII circuit configurations.

From the analysis of both figures it is concluded that a better response is obtained with the LC tank. For instance, at 47kHz, the dimming curve is quite linear and smooth, showing also a large dimming range. The last measurement point, 19W of average lamp power, corresponds to a very low light output, because the arc power is only about 5W, since the remaining power is dissipated in the lamp electrodes. With the LCC tank, the obtained dimming range is limited to a narrower range. For each presented value of switching frequency, instability regions appear beyond the last measurement point, which are translated into lamp power oscillations between a maximum and a minimum level. In both configurations, decreasing the switching frequency leads to a larger dimming range, particularly for the LC resonant tank configuration, nonetheless, even with this

configuration, instabilities can still occur if the operating frequency is not chosen adequately. A similar behaviour was observed in the case of the LCC-CII resonant ballast.

In conclusion, analysis and experiments showed that oscillations may appear when the lamp power is decreased below a minimum value. This effectively limits the dimming range of the ballast, particularly for two of the studied configurations. However, if the switching frequency and dimming range are adequately chosen and if the resonant tank is selected and designed properly, this dimming method is able to provide a linear and smooth lamp output control. This control method can be extended to higher load power levels, or other fluorescent-lamp types, simply following the theory exposed. Further experimental results will reveal that T5 lamps will behave in a similar way. For higher load power levels, higher efficiency is predictable since the power losses in the regulator are expected to be the same.

3.2.2.3 DESIGN CONSIDERATIONS REGARDING INSTABILITY REGIONS

The previous studies revealed the existence of instability regions which originate lamp power oscillations. An example of the observed oscillations is presented in Fig. 3.30. As can be seen, these oscillations do not affect the inverter output voltage. Still, this behaviour leads to an unstable lamp operation and undesirable luminous flux fluctuations.

The previous design method implies that the design of the magnetic regulator is done considering that it should present an inductance variation of 2:1 and its minimum value is estimated considering that the lamp is working at nominal power, for a resonant frequency equal to the switching frequency. The same assumption is made to estimate the value for the remaining parameters, according to the selected filter configuration.

A more adequate project for the magnetic regulator can be achieved if instead of considering the nominal lamp power for determining the resonant circuit parameters, a lower power value is chosen as a reference, at the desired switching frequency. This methodology will avoid this instability region [3.22].

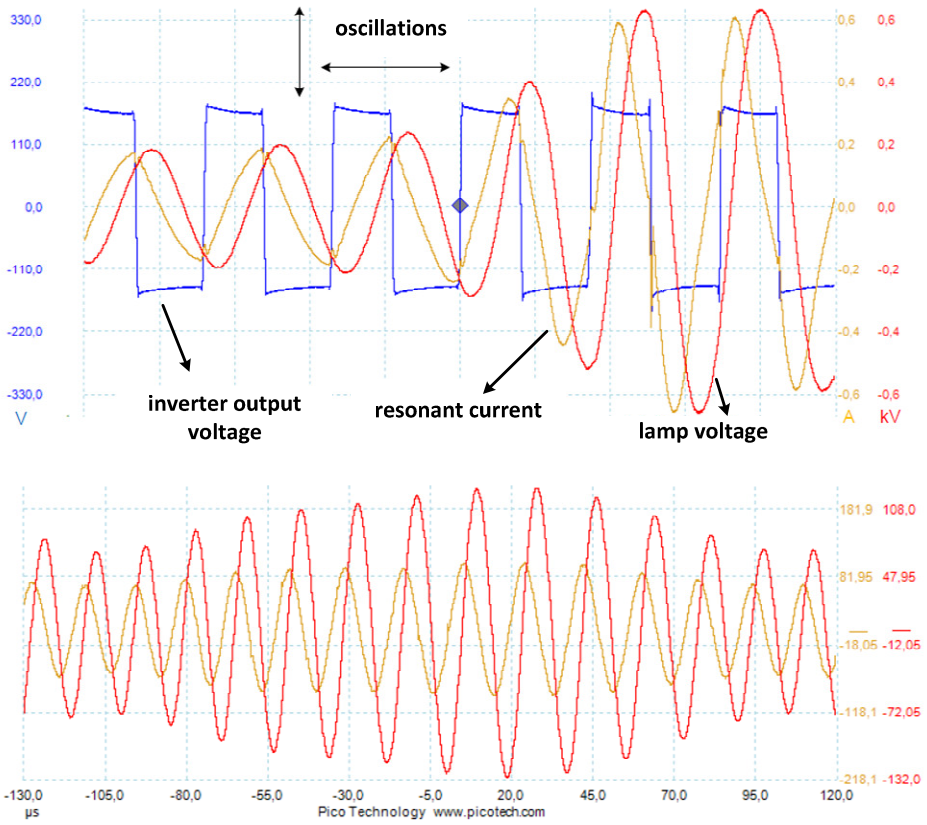

Fig. 3.30. Oscillations in the experimental waveforms.

In order to confirm this methodology and compare to the previous presented results, the same fluorescent lamp was used: the TLD 36W from Philips.

Therefore, with this method, instead of considering the nominal lamp power for determining the resonant circuit parameters, a middle value of 29W was chosen as a reference, at the desired switching frequency, 50kHz. This value corresponds to 80% of the nominal lamp power. The working range for the magnetic regulator was then determined. Table 3.4 presents the new design parameters for the two selected topologies, LC and LCC. The capacitors values were calculated in order to use the same regulator for both topologies. The magnetic regulator was built, considering the classical design method, and following the methodology previously exposed, using an EF25 core with material 3C85 from Phillips. Fig. 3.31 presents the theoretical dimming curves for both methods, obtained through (3.128). It is clear that the proposed method leads to a smaller instability region, avoiding oscillations in the defined dimming range.

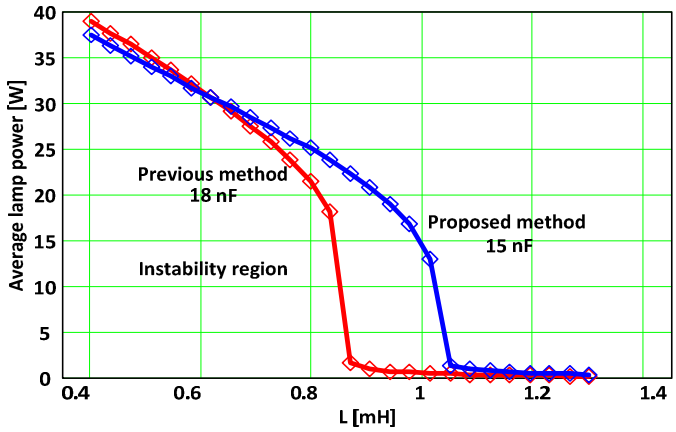

Fig. 3.31. Theoretical comparison between the previous and the proposed method: LC resonant circuit configuration.

Table 3.4 New design parameters.

RESONANT CIRCUITS	LC	LCC	
C [nF]	$C_p = 15$	$C_s = 47;\ C_p = 12$	
f_s	50 kHz	60 kHz	
POWER LEVEL	MAXIMUM	MEDIUM	MINIMUM
P_{lamp} [W]	36 W = 100 %	29 W ≅ 80%	19 W ≅ 50%
R_{lamp} [Ω]	187	299	449
L [mH]	0.47	0.67	0.96

- *Variable-inductor small-signal characterization, large-signal characterization and experimental results:*

  The small-signal characterization of the magnetic regulator was done using a variable dc source and an impedance analyzer, HP4284A, as represented in Fig. 3.27. The large signal characterization of the regulator was done using the circuit presented in Fig. 3.32a. The fluorescent lamp was replaced by its equivalent resistance under nominal conditions. The power in the resistance is measured for several levels of the dc current in the control winding. The measured data were processed and analyzed using a linear interpolation which relates the power in the resistance with the dc current in the control winding, $P_R(I_{dc})$. Finally, the value of the inductance for each measurement point, L_{ac}, was determined rearranging the lamp power equation for the LC resonant circuit configuration, (3.66) as follows:

$$L_{ac}^2[P_R(I_{dc})R^2\omega^4C^2 + P_R(I_{dc})\omega^2] - L_{ac}[P_R(I_{dc})R^2 2\omega^2 C] + P_R(I_{dc})R^2 - V_{in}^2 R = 0 \quad (3.130)$$

This mathematical analysis was performed in Mathcad using numerical methods. The measured small-signal and large signal characteristics of the magnetic regulator are presented in Fig. 3.32b. It can be seen that there is a significant difference between the two characteristics.

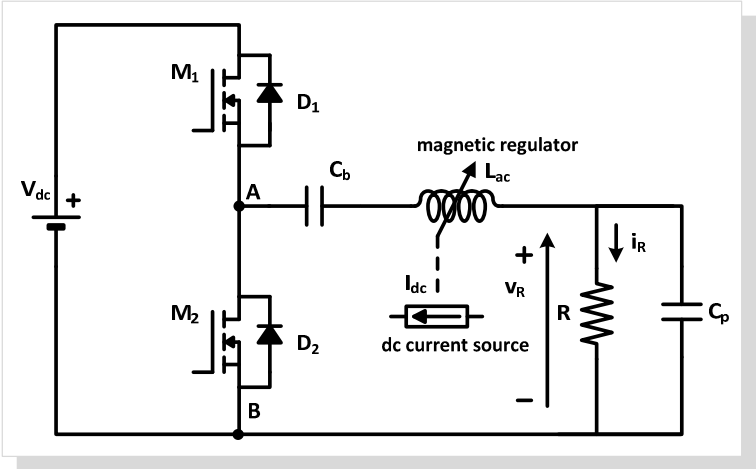

a. Circuit schematic for large-signal characterization

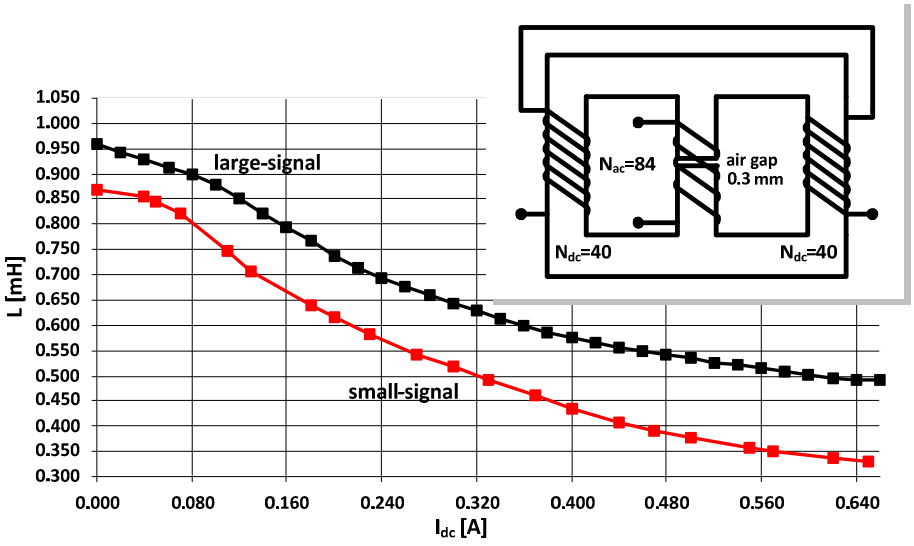

b. Small-signal and large-signal characteristics

Fig. 3.32. Characterization of the magnetic regulator.

Fig. 3.33, Fig. 3.34, Fig. 3.35 and Fig. 3.36, present the obtained experimental results for the two laboratory prototypes. The measurements performed were the average power in the arc, in the lamp, in the electrodes, and at the input of the ballast. The efficiency of the converter was also calculated as the ratio between the average lamp power and the input

power. At this point, the regulator was controlled by an external current source. The input power measurement does not include this current source. The luminous flux was measured using an integrating sphere. For both topologies, the phase angle of the input resonant tank current was also verified.

Fig. 3.33 shows that both experimental dimming curves are quite linear and smooth, showing also a large dimming range. Compared to the previous method, lower lamp power levels were achieved. It was also possible to operate the ballast using a LCC configuration, at a higher switching frequency, without oscillations.

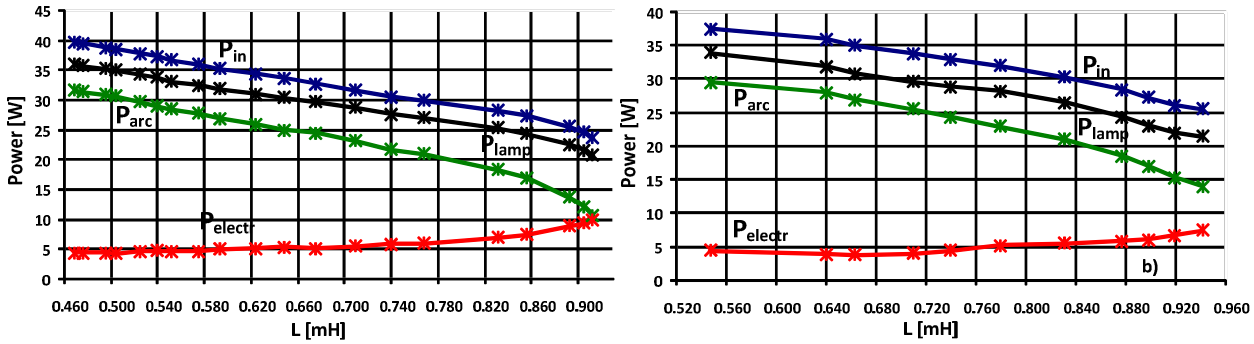

a. LC resonant circuit b. LCC resonant circuit

Fig. 3.33. Experimental results for the average input power, lamp power, arc power and electrode power for the new design.

Fig. 3.34 shows the measured luminous flux. In this figure it is possible to compare the lamp power level with the luminous flux level. For instance, regarding the LC topology, the last measurement point presents a luminous flux of approximately 750 lux which in turn corresponds to about 30 % of the maximum obtained luminous flux.

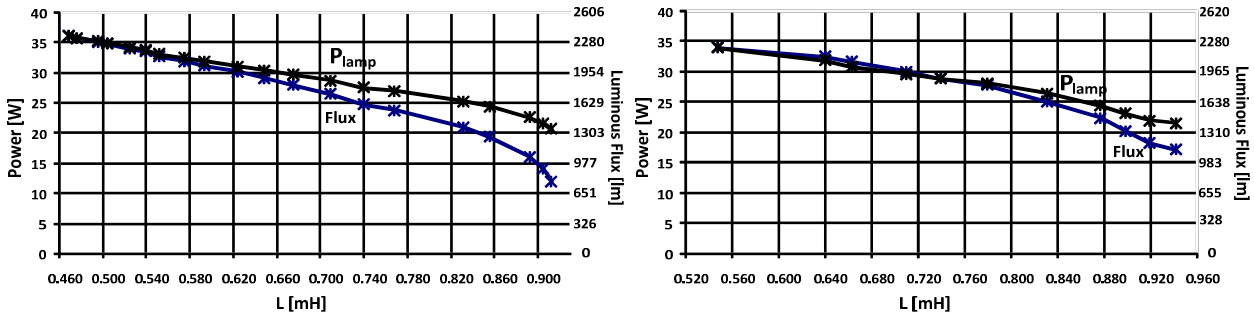

a. LC resonant circuit b. LCC resonant circuit

Fig. 3.34. Experimental results for the average lamp power and luminous flux for the new design.

Fig. 3.35 shows the converter efficiency for both resonant tanks. Even if the control of the regulator was not included in this efficiency estimation, the ballast prototype presented

some promising results, with efficiency values higher than 84%. This is the lowest attained value in the whole dimming range and only for the LCC circuit configuration. It should also be noticed that low efficiency is only attained for very low power levels. For the LC circuit configuration, the efficiency is quite stable, over 90%, for almost all the dimming range.

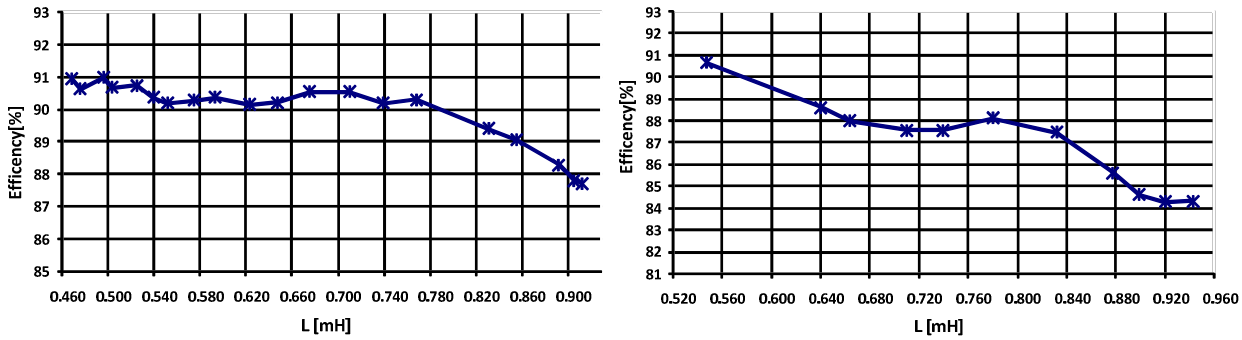

a. LC resonant circuit b. LCC resonant circuit

Fig. 3.35. Experimental results for the converter efficiency for the new design.

Fig. 3.36 presents the waveforms of the output inverter voltage and the input resonant current, at maximum and minimum average lamp power.

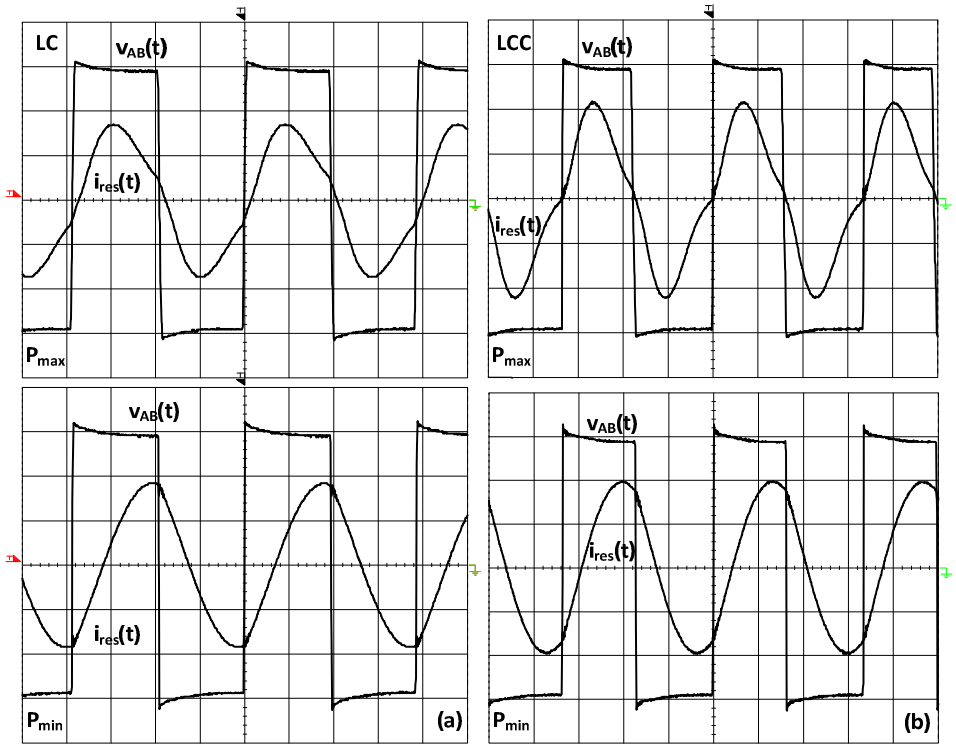

a. LC resonant circuit b. LCC resonant circuit

Fig. 3.36. Waveforms of the inverter output voltage and resonant current at maximum and minimum average lamp power (25V/div; 0.4A/div; and 5 μs/div).

It can be observed that for both operating points, the current is delayed when compared to the voltage, ensuring ZVS operation. In fact, the phase angle is larger at maximum dimming level, which corresponds to minimum average lamp power, and smaller at minimum dimming level. This in turn means that less reactive energy is handled by the circuit during operation at nominal power thereby ensuring low conduction losses. On the other hand, switching losses are also low, especially at high output power since the resonant current is near to zero at the switching instant. This is the reason why high efficiency is attained at nominal lamp power.

3.2.3 COMPARATIVE ANALYSIS OF MAGNETIC REGULATOR TOPOLOGIES

This section explores the proposed dimming method, considering a specific type of fluorescent lamps, T5 lamps, and other magnetic regulator structures, with different cores and topologies. It also presents a simple experimental method to estimate an average value for the ac inductance during dimming operation [3.27].

3.2.3.1 T5 FLUORESCENT LAMP SELECTION

In terms of tubular fluorescent lamp technology, the T5 lamp represents the state of the art. Over recent years, luminaire manufacturers and lighting designers have promoted and created innovative long-lasting T5-based lighting systems to be implemented in modern and high-tech buildings.

T5 fluorescent lamps are available for standard output, high efficiency, (HE) and high output, (HO). HO lamps deliver more light than standard T5 lamps and are available in higher wattages.

The light output per unit length of standard T5 lamps is almost identical to the standard T8 lamps. According to manufacturers, the T5 lamp provides a peak light output at 35°C air temperature, whereas the T8 and the T12 lamp provide peak light output at a 25°C ambient air temperature. Consequently, in luminaires where there is little or no air circulation, the T5 lamp can have a higher lumens/W than a T8 lamp of about the same wattage. Therefore, for an adequate selection, several factors affecting the light output, and therefore efficacy, should be considered: lamp life, lumen maintenance, ambient temperature, etc. So, the choice between T5 or T8 depends on the specific application.

Another important aspect is that compared to the larger T8 or T12 lamps, T5 lamps use less material. Even if the efficacy of T5 lamps is considered to be equivalent to that of T8 lamps, their compactness reduces the amount of materials used in their manufacturing, the potential for toxic substance contamination, and packaging materials needed for shipment and sale. As a result, T5 lamps are considered to have less impact on the global environment than T8 lamps. In addition to their smaller dimensions, T5 lamps have an improved phosphor coating that prevents mercury from being absorbed into the phosphor and the bulb glass. This technology allows for reduced mercury content in the lamp [3.26].

T5 lamps are specially characterized by a high lamp voltage, and in some particular cases, low current. This is the reason why they are conventionally manufactured for high-frequency operation, typically above 20kHz. Since maximum efficiency is only attained with this HF operation, 50/60Hz operation is typically not recommended. This information makes the use of electronic ballasts almost mandatory. Nevertheless, some authors have recently investigated the use of low-frequency low-loss magnetic ballasts [3.24], [3.25].

The main argument is the fact that there will be an obvious health consequence due to electronic waste accumulation in the environment, with other adverse impacts such as soil and water pollution. Another argument which is also common, especially in LED-lighting based systems is the fact that electronic ballasts are limited by the short life of the electrolytic capacitors. So, of course the issue here is to point out more sustainable lighting technology. These authors suggest the control of T5 28W lamps, which are the common replacement of T8 36W lamps, with ultra-low-losses LC magnetic ballasts. Evidences show the possibility to ignite and operate the 28W lamp at low frequency, with very small consequences in the lamp efficacy. The fact is that there is an obvious advantage which is inherent to the low-current feature of this lamp, which enables a significant reduction in both conduction and core losses in the magnetic ballast. Nonetheless, the advantages of T5 with their small and compact luminaires, may turn the use of heavy and bulky ballasts an impracticable solution. It is possible, however, that in special circumstances, magnetic ballasts may stand as a correct choice but, their application will also limit the possibility to control the lamp operation in terms of flux regulation and distant control.

Considering all future and possible features offered by electronic ballasts it was important to verify the applicability of the proposed dimming technique to this type of lamps. The experimental data retrieved from the application of this type of magnetic control to standard T5 lamps is hereby presented. Taking into account the above issues and due to the rising use of these lamps, it was considered relevant to verify their response under this dimming technique [3.27].

3.2.3.2 BALLAST CONFIGURATION AND RESONANT PARAMETERS

The previous theoretical and experimental results lead to the conclusion that a better response could be obtained using the LC circuit configuration. Therefore, the LC filter was preferred for this study. The selected lamps were the Master TL5 HE 14W and 21W from Philips. Table 3.5 presents some nominal characteristics of the lamps, retrieved from the manufacturer information.

Table 3.5 MASTER TL5 High Efficiency.

FLUORESCENT LAMP	V_{lamp} [V]	I_{lamp} [mA]	R_{lamp} [Ω]
TL5 HE 14W Philips	83	170	489
TL5 HE 21W Philips	125	170	735

Electrical specifications defined at an ambient temperature of 25 °C in free burning position on reference ballast

Following the design procedure, for a specific V_{in}, determined according to the selected ballast dc voltage, and knowing the values for R_{lamp} and V_{lamp} for nominal operating conditions, Z_b is determined using (3.69). Then, after setting the ballast operating frequency, using (3.70), the nominal values for the inductance and the resonant capacitance for each lamp are calculated. This is finally followed by the evaluation of the dimming curves for both lamps. The dimming characteristics of each lamp were determined using (3.68), considering a 2:1 inductance variation.

Consequently, for an input dc voltage, $V_{dc} = 310\text{V}$ and for an operating frequency, $f_s = 80\text{kHz}$, Z_b was calculated using the values presented in Table 3.5. The nominal values for C_p and L_{ac} were then determined using (3.70). As an example, for the TL5 HE 21W lamp, it was determined that the lamp would operate at nominal power using approximately $C_p = 2.2\text{nF}$ and $L_{ac} = 1.65\text{mH}$.

Fig. 3.37 shows the theoretical dimming curves for that lamp, considering two operating frequencies, $f_s = 80\text{kHz}$ and 85kHz. The T5 21W characteristics of the lamp resistance versus average arc power, $R_{lamp}(P_{arc})$ used in this calculation, are also presented in Fig. 3.37. The analysis of these dimming curves shows that with a higher switching frequency the dimming range is expected to be larger. Fig. 3.37 also shows the phase angle of the resonant filter input current (the square-wave inverter voltage is taken as reference for the phase). In both situations, the phase angle is negative, which means that ZVS is guaranteed. The theoretical value of the phase angle was obtained using (3.53) and (3.54).

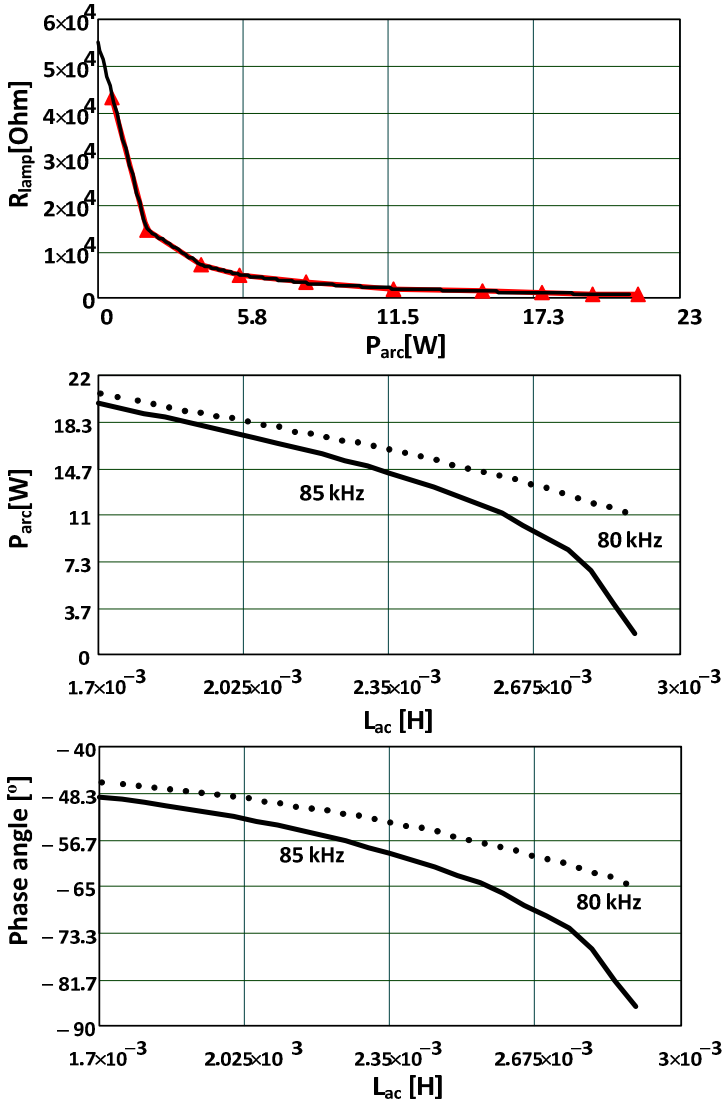

Fig. 3.37. Master TL5 21W Philips: curve fitting to the $R_{lamp}\ (P_{arc})$ - linear interpolation; theoretical dimming curves and phase angle of the resonant current for the LC circuit configuration.

3.2.3.3 REGULATOR TOPOLOGIES AND CORE STRUCTURES

Typically the variable inductor would be implemented using a gapped E core set, specifically, EF25 cores. This study proposes the use of two other different core structures. Each core structure leads to a different regulator topology. Firstly, an attempt was made to reduce the variable inductor size, from the previous EF25 to a smaller core, a gapped EFD20. For this regulator, the wiring is similar to the classical wiring and is presented in Fig. 3.38: the main winding is placed in the middle leg of the core and the control windings are placed on the left and right legs, and are serially connected in opposite polarity.

The second regulator is similar to the topology suggested in [3.28]. In this case, two sets of U15 cores are used and the wiring is differently implemented. Fig. 3.39 shows the magnetic structure of the U15 variable inductor. In this topology, the main winding is divided in two smaller windings which are connected in series and placed on the outer legs. Consequently, their magnetic loops are almost uncoupled if no polarization is present. This regulator has only one control winding which is placed in the middle leg. For a zero dc control current, no ac voltage will be induced in the control winding because the two ac windings are connected in opposite polarity. As can be seen from Fig. 3.39, a small air gap is introduced between each core set. This regulator behaviour is similar to the first topology: increasing the dc control current pushes some core regions towards saturation, decreasing the ac inductance.

Two variable inductor prototypes were built considering these two structures. Both prototypes are shown in Fig. 3.40. The cores dimensions for the EFD20 and the U15 are also presented. The EFD20 prototype was designed with a relatively large variable inductance range. For the U15 regulator, a larger number of turns were used in the control windings.

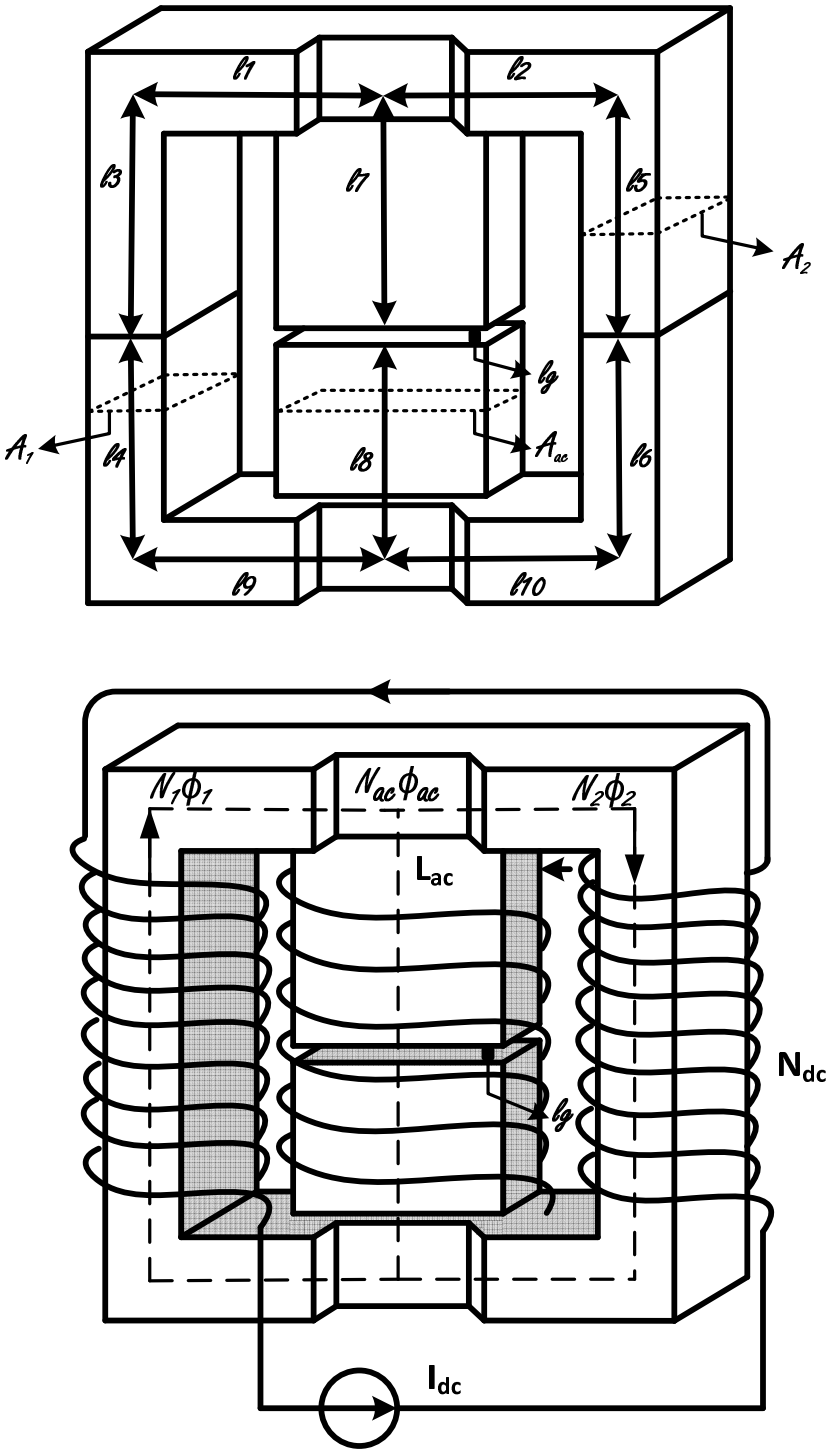

Fig. 3.38. Magnetic regulator: variable inductor based on EFD core.

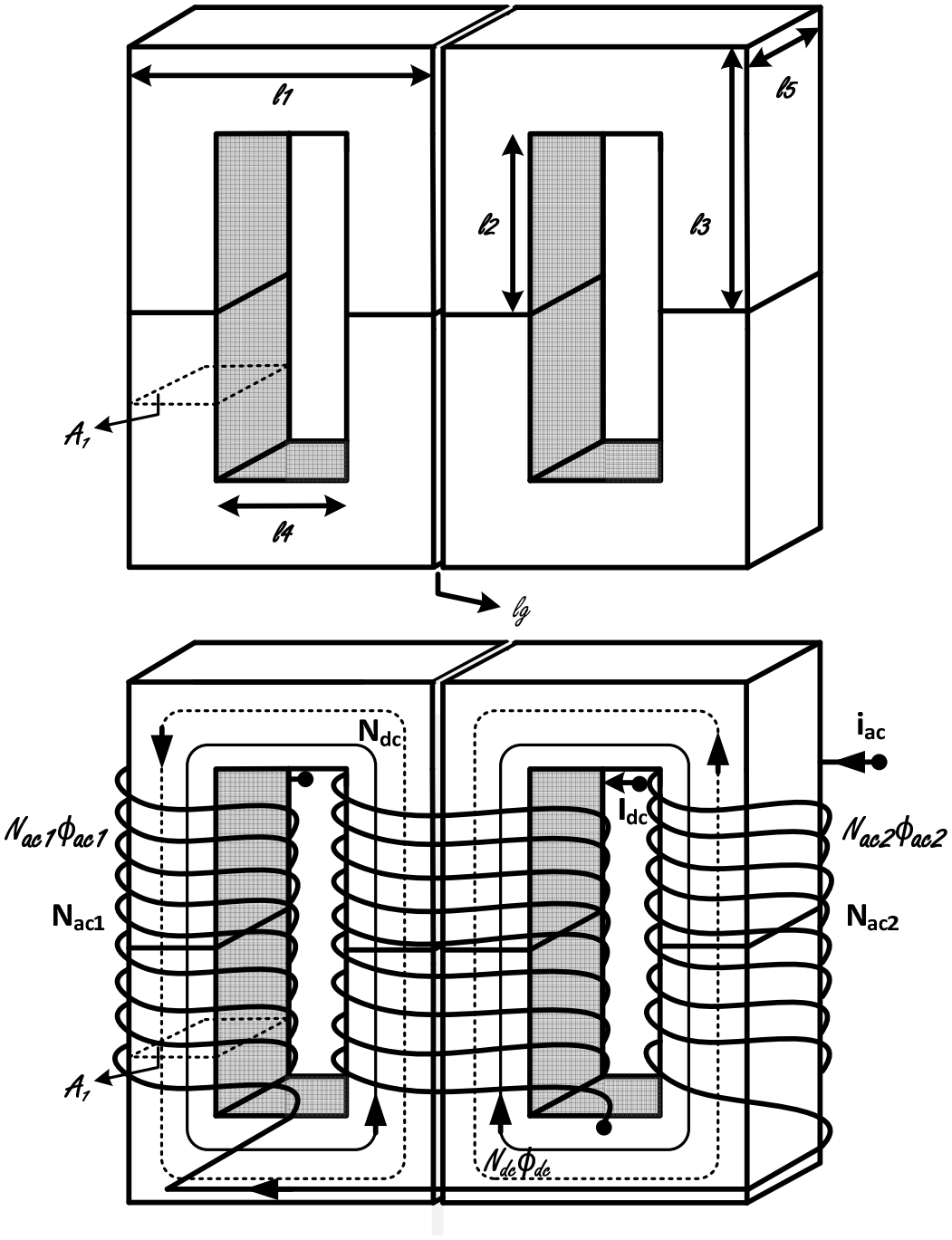

Fig. 3.39. Magnetic regulator: variable inductor based on U core.

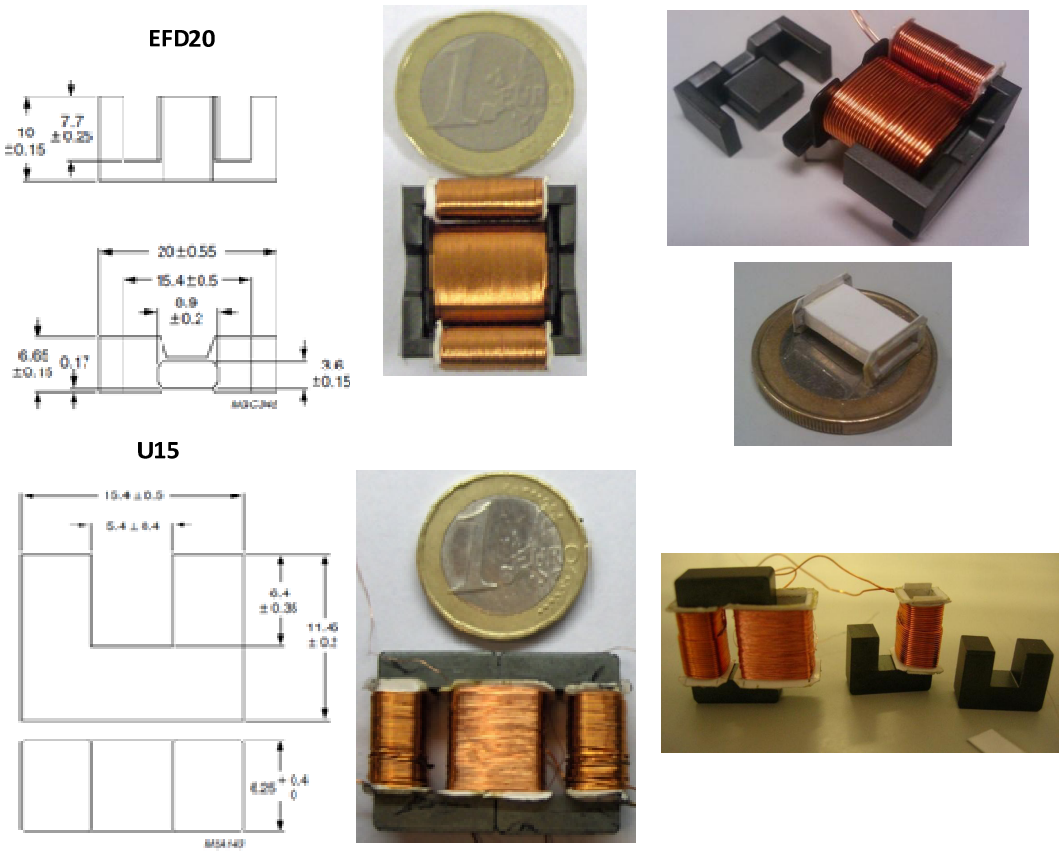

Fig. 3.40. Core structures, dimensions and experimental prototypes: EFD20 and U15.

3.2.3.4 REGULATORS CHARACTERIZATION, MEASUREMENT SETUP AND EXPERIMENTAL RESULTS

The final purpose was to verify the effectiveness of using this control technique with different topologies of regulators, applied to the T5 fluorescent lamp. The first step was to measure the small-signal characteristic of the variable inductors. Secondly, some experimental tests using a commercial electronic ballast were also carried out. Finally, a simple experimental ballast prototype was implemented and the selected lamps behaviour were analysed.

- *Variable inductors small-signal characterization:*

  For these regulators, the small-signal characterization of the prototypes was done using a LCR meter, BK Precision 889A, LCR/ESR meter, at 100 kHz and 1V rms. Two EFD20 regulators were built with a different combination of turns in the control windings, one having a higher number of turns than the other. Both small-signal characteristics are presented in Fig. 3.41a. These characteristics show that for a higher number of turns, the

same variable inductance range is covered by a smaller dc control current. The U15 small-signal characteristic is shown in Fig. 3.41b. The U15 regulator had 600 turns in the control winding. Compared to the previous EF25 regulators, the EFD and U regulators were controlled with smaller dc current values. From the practical point of view, a smaller control current leads to lower losses in the control windings, even though the associated resistance may be slightly higher.

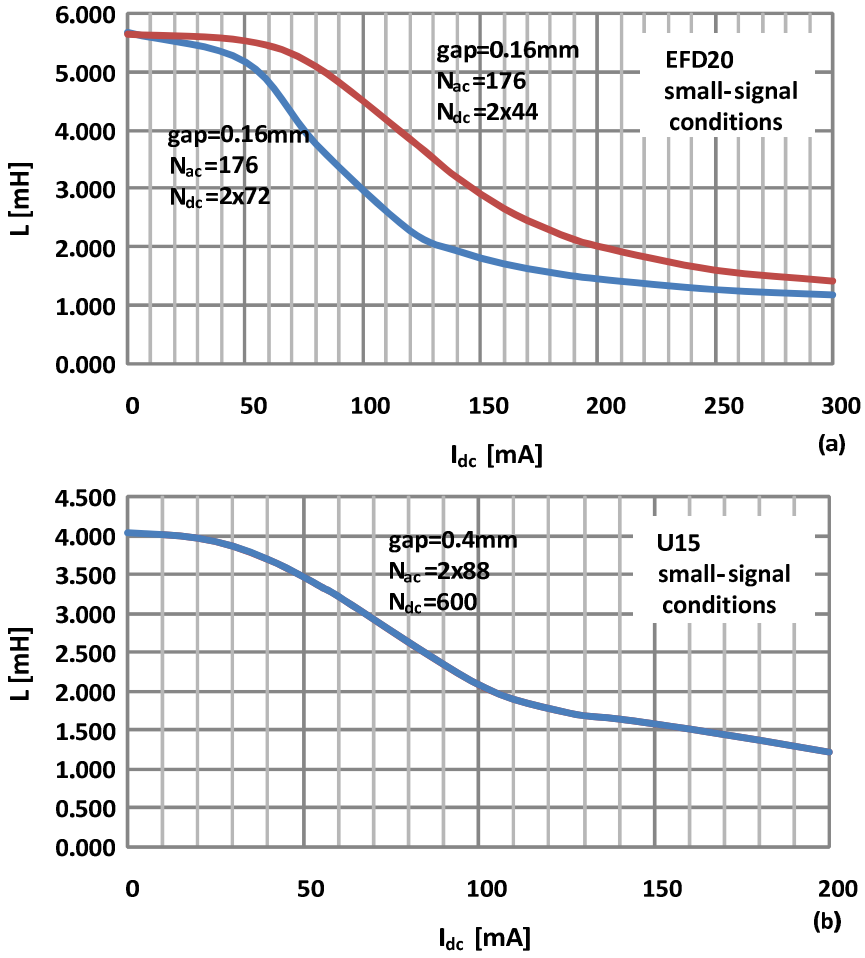

a. EFD20 b. U15

Fig. 3.41. Small-signal characterization of the variable inductors.

- *Measurement setup for large-signal characterization and experimental results:*

The experimental electronic ballast prototype was implemented as shown in Fig. 3.42. The large-characterization of the regulators was done during dimming operation and for simplicity the dc control current was generated by a programmable power source. All of the necessary data were collected through a Picoscope, as represented in Fig. 3.42.

The problem with small-signal characterization is the fact that the measurements are not made under the operating conditions of the device. If the objective is to characterize nonlinear inductances, for instance coils with cores operating in the saturation or near the saturation region, it is necessary to test them under operating or near-operating conditions [3.20]. This is the case of variable inductors. In these regulators the total ac flux is not a linear function of the resonant current. An approximation is therefore necessary in order to get an average inductance value for each operating point.

The variable inductor was estimated by a simplified approach using a peak-to-peak-based inductance model. This allowed a basic estimation of the inductance value for each operating point. It implies defining the inductance value as represented in (3.131), using the peak-to-peak values of the resonant current and total ac flux:

$$L_{ac} = \frac{\Psi(t)}{i(t)} \rightarrow L_{ac} = \frac{N_{ac}\phi_{ac,pp}}{i_{ac,pp}} = \frac{\Psi_{ac,pp}}{i_{ac,pp}} \tag{3.131}$$

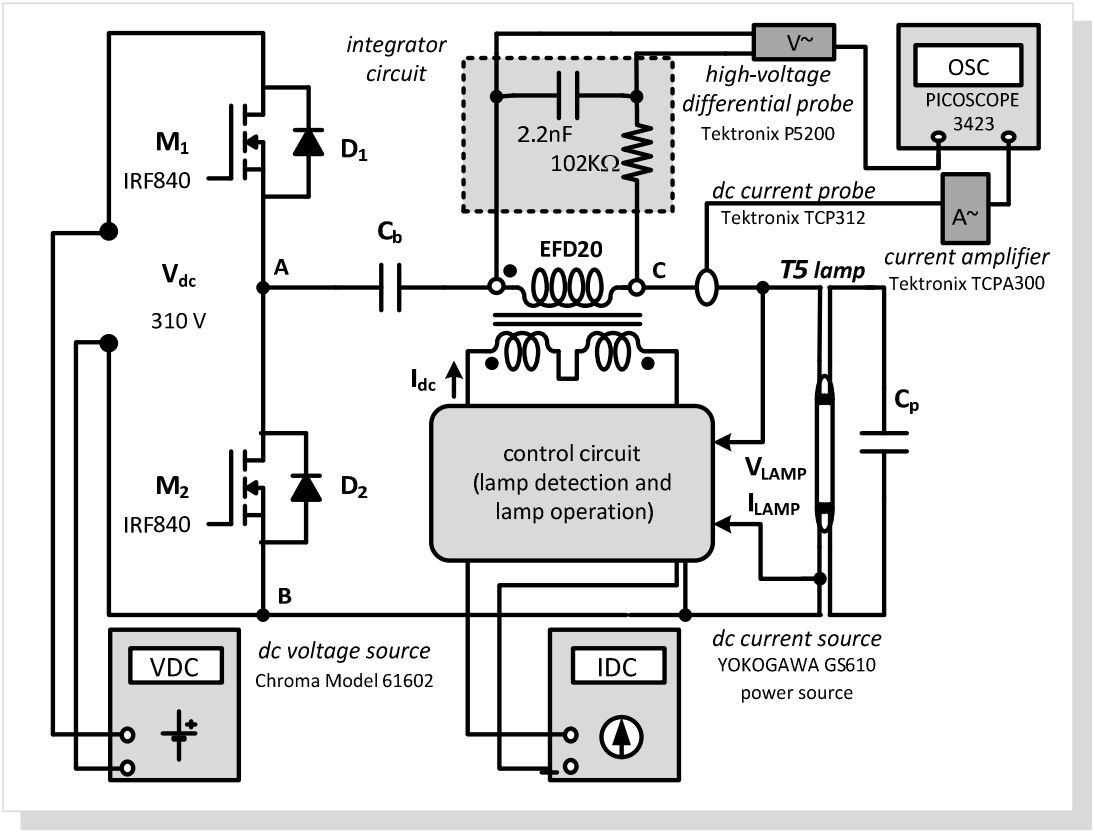

Fig. 3.42. Electronic ballast prototype: experimental setup for large-signal characterization.

The totalized flux can be easily measured using an RC integrator circuit as shown in Fig. 3.42. Considering v_C as the capacitor voltage and $v_{L_{ac}}$ as the variable inductor voltage:

$$v_{L_{ac}} = L_{ac}\frac{di}{dt} = \frac{d\Psi_{ac}}{dt} \tag{3.132}$$

$$v_C \cong \frac{1}{RC}\int v_{L_{ac}} \qquad if \qquad R \gg X_C \tag{3.133}$$

This means that:

$$\Psi_{ac} = N_{ac}\phi_{ac} = RC \times v_C \tag{3.134}$$

And therefore, using (3.134), the peak-to-peak average inductance can be calculated. So, the large-signal characteristics of the EFD20 and U15 variable inductors, were done measuring the output voltage of an RC integrator circuit, with $R = 102\text{k}\Omega$ and $C = 2.2\text{nF}$, identifying the peak-to-peak values of this voltage, measuring the resonant current, identifying the peak-to-peak values of this current and finally applying (3.131).

A commercial electronic ballast PHILIPS HF-R 14-35 TL5 220-240, was also tested in order to get some reference results. The commercial electronic ballasts were supplied by a Chroma 61602 power source which provided a 230V/50Hz voltage, simulating the standard power supply. All the selected ballasts had an analogue 1-10V DC dimming interface. The interface dictates the desired luminous flux level, through the dc level imposed on the control circuit. This voltage was provided by a Yokogawa GS610 power source. The measurement unit consisted of a PC oscilloscope, the Picoscope 3423, two voltage probes (Tektronix P5200), and two current probes (Tektronix TCP312 30A, amplifier Tektronix TCPA300).

With this equipment and with additional functions provided by the Chroma 61602 power source, it was possible to acquire several parameters: the lamp voltage, the electrode voltages, the discharge or arc current and the electrodes currents. With these measurements it was possible to obtain the average lamp power, the average arc power and the average electrode power at each power level. It is assumed that the lamp power is equal to the sum of the arc power and the electrode power. It was also possible to estimate the power consumption and efficiency of the system and the power factor seen by the utility line. Table 3.6 presents the results for the TL5 HE 21W. These results are also shown in Appendix A, together with similar data retrieved from other T5 lamps.

Table 3.6 TL5 HE 21W Philips operated with PHILIPS HF-R 14-35 TL5 220-240.

MEASUREMENTS						CALCULATED VALUES				
V_{DC} [V]	f_s [kHz]	V_{lamp} [V]	I_D [mA]	*Line Power Factor*	P_{in} [W]	*Efficiency* [%]	P_{lamp} [W]	P_{arc} [W]	P_{electr} [W]	R_{lamp} [Ω]
1	82.4	158.11	4	0.660	5.3	49	2.60	0.58	2.02	41969
2	81.0	168.10	12	0.760	6.6	59	3.88	1.91	1.97	14489
3	80.0	170.34	25	0.832	8.5	71	6.07	4.08	1.99	6948
4	79.8	166.61	34	0.850	9.9	76	7.55	5.57	1.98	4891
5	78.4	161.98	52	0.911	12.1	83	10.04	8.23	1.80	3118
6	74.8	153.47	78	0.936	15.2	87	13.24	11.67	1.57	1977
7	68.5	145.62	106	0.945	18.1	91	16.56	15.22	1.34	1370
8	60.7	137.82	129	0.965	20.6	90	18.50	17.51	0.99	1065
9	53.0	129.34	154	0.964	22.7	89	20.24	19.53	0.71	840
10	46.7	124.89	174	0.970	24.5	90	22.04	21.34	0.70	719

From Table 3.6 it is identified that this ballast uses a variable-frequency technique to achieve dimming and that a good power factor cannot be maintained for all operating points. The efficiency of the ballast, computed as the ratio between the lamp power, P_{lamp}, and the input ballast power, P_{in}, is around 90% for high power values, decreasing rapidly for lower dimming levels. In conclusion, this dimmable electronic ballast is only optimized for nominal lamp power operation.

Fig. 3.43 and Fig. 3.44 both show the dimming curves for the T5 21W lamp, obtained with the two ballasts: the commercial electronic ballast and the magnetically-controlled electronic ballast prototype. Fig. 3.43 shows P_{lamp}, P_{arc} and P_{electr} as function of V_{DC} and Fig. 3.44 shows P_{lamp}, P_{arc} and P_{electr}, as function of the large-signal inductance value and the dc control current.

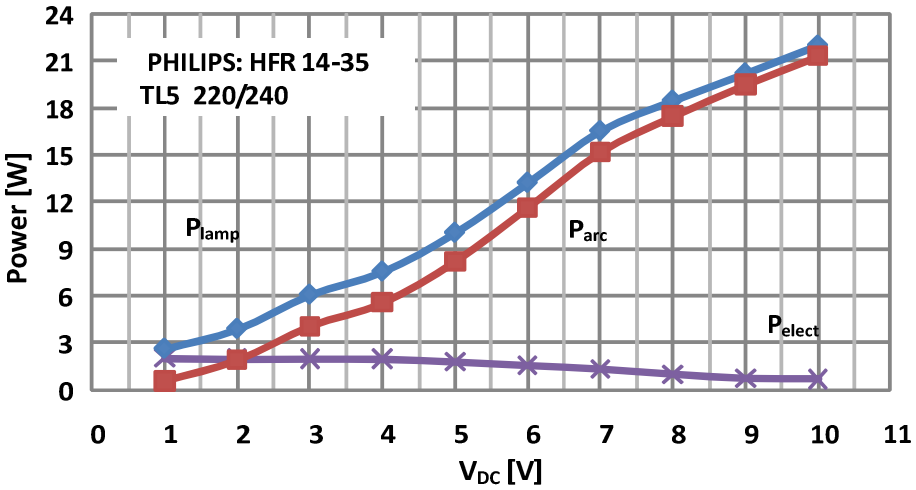

Fig. 3.43. Experimental results for the TL5 HE 21W with commercial ballast: average lamp power, arc power and electrode power, as function of the control voltage.

The prototype data were obtained using the EFD20 regulator, using the following parameters: $V_{dc} = 310\text{V}$, $C_p = 2.2\text{nF}$ and $f_s = 85\text{kHz}$. Fig. 3.44 also shows the prototype efficiency for all dimming levels. The observation of both figures clearly reveals that the proposed magnetically-controlled prototype was also capable of dimming the lamp from the rated power to a near zero power level. This control required an inductance range between 1.9 and 3.1mH, which was guaranteed by a small control current variation, approximately 140mA. Similar to the commercial ballast, a low electrode power was also maintained during the whole operating range. This power, however, was not as low as to damage the electrodes, due to low heating temperatures.

Another relevant issue is the efficiency of the ballast. Compared to the commercial ballast the results were not disappointing, since these results were obtained with an early prototype version. The ballast, at rated power, showed an efficiency value around 90%, which is quite acceptable. Those values were maintained for higher power levels. However, for low power levels, the efficiency of the ballast decreased. This can be better observed in Fig. 3.45.

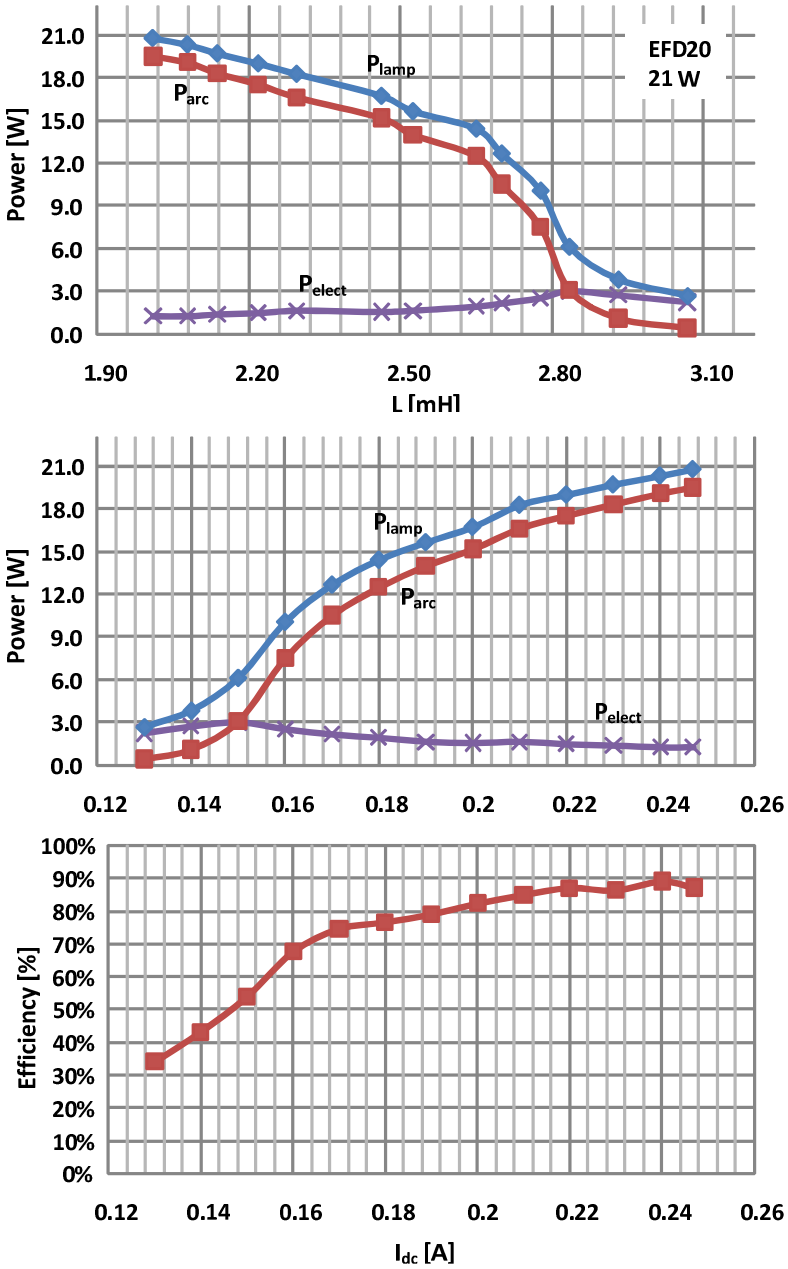

Fig. 3.44. Experimental results for the TL5 HE 21W with electronic ballast prototype – EFD20: average lamp power, arc power and electrode power, as functions of the control parameters, and ballast efficiency as a function of the dc control current.

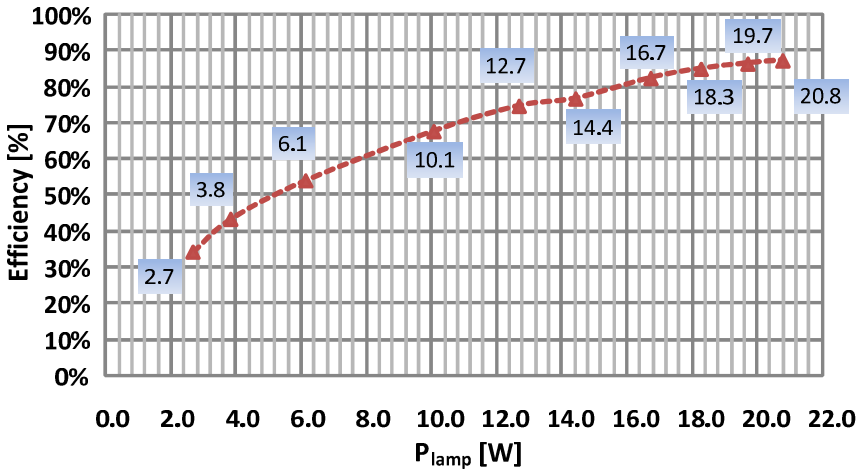

Fig. 3.45. Experimental results for the TL5 HE 21W with electronic ballast prototype – EFD20: ballast efficiency as a function of lamp power.

Fig. 3.46 presents a comparison between the theoretical predictions and the experimental results which also confirmed the theoretical approach previously exposed.

Fig. 3.47 shows similar experimental results for the T5 14W lamp. The following parameters were kept constant: $V_{dc} = 310\text{V}$, $C_p = 2.2\text{nF}$ and $f_s = 85\text{kHz}$. In this particular case the dimming curves showed a more linear behaviour. Low electrode power was also maintained through the whole dimming range. The efficiency of the ballast was slightly lower than in the previous case.

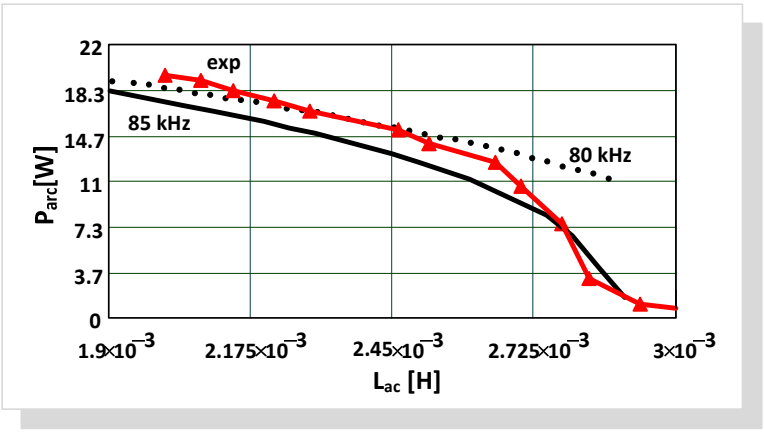

Fig. 3.46. Comparison between dimming curves: theoretical and experimental results for the TL5 HE 21W with electronic ballast prototype: $V_{dc} = 310\text{V}$; $C_p = 2.2\text{nF}$; $f_s = 85\text{kHz}$.

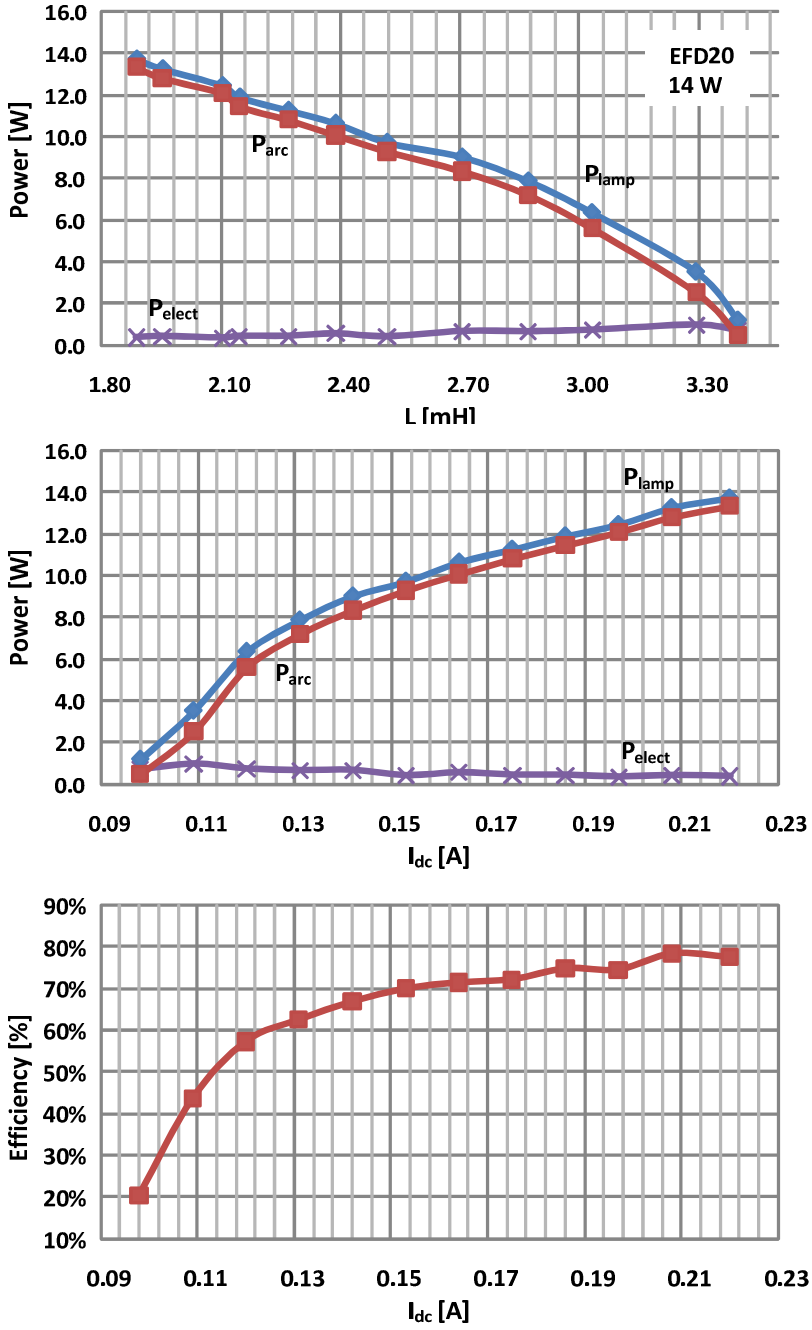

Fig. 3.47. Experimental results for the TL5 HE 14W with electronic ballast prototype – EFD20: average lamp power, arc power and electrode power, as functions of the control parameters, and ballast efficiency as a function of the dc control current.

Fig. 3.48 shows the experimental waveforms obtained for the T5 21W lamp at three lamp power levels: nominal, medium and minimum levels. Stable operation can be recognized in all of the reported operating points. The lamp voltage and arc current are quite sinusoidal and the resonant current lags the output inverter voltage, ensuring ZVS in the bridge MOSFETs. A similar behaviour was observed in the case of the T5 14 W lamp.

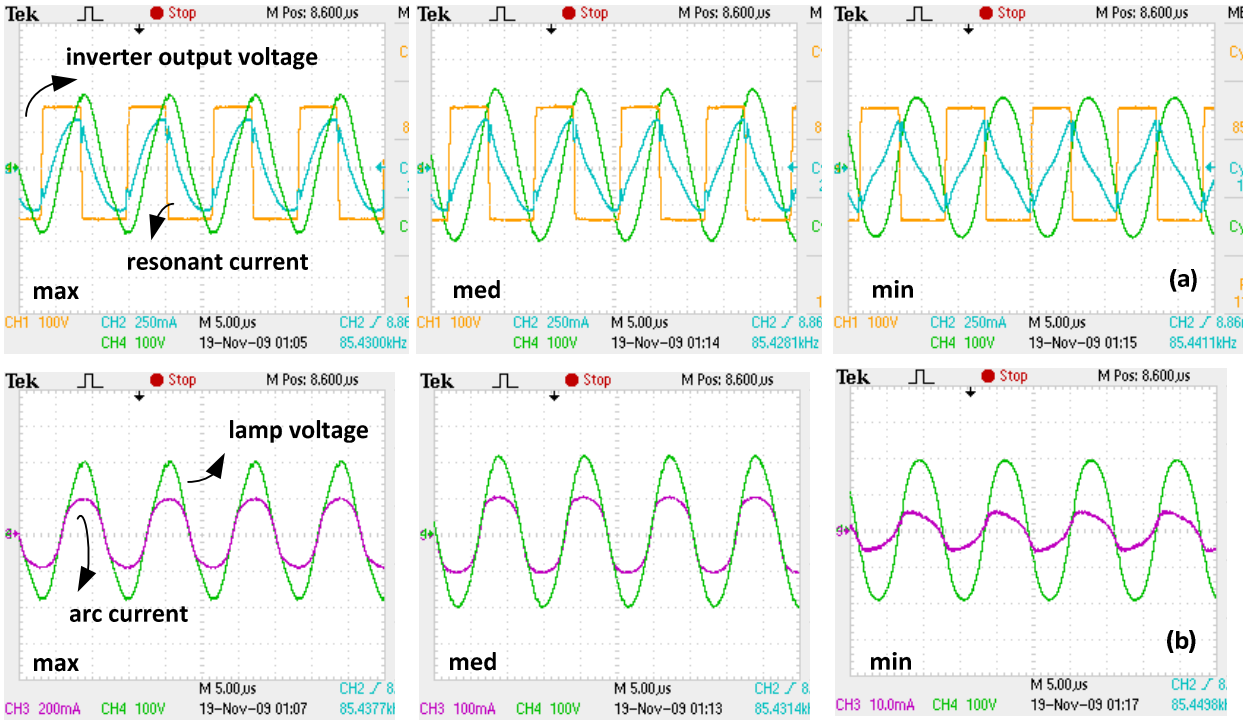

a. Inverter output voltage, resonant current, lamp voltage

b. Lamp voltage and arc current

Fig. 3.48. Experimental waveforms for the TL5 HE 21W-EFD20 at nominal power, medium and at minimum power level, 85 KHz.

The EFD20 non-linear behaviour can be verified in Fig. 3.49, which shows the curve-fitting to the experimental results of the totalized ac flux versus the resonant current for two operating levels of the T5 14W lamp: maximum lamp power and minimum lamp power.

The peak-to-peak slope of each curve corresponds to the average inductance value, established by the regulator, for that specific operating point. For both lamps, a complete dimming range was achieved without completely saturating the regulator. In conclusion it was verified the effectiveness of this smaller regulator structure in the control of T5 lamps. Since all available T5 HE lamps present the same nominal current, the regulator is expected to work properly in all cases. Their increasing lamp voltage, for increasing rated power, may be easily handled by changing the resonant capacitor value.

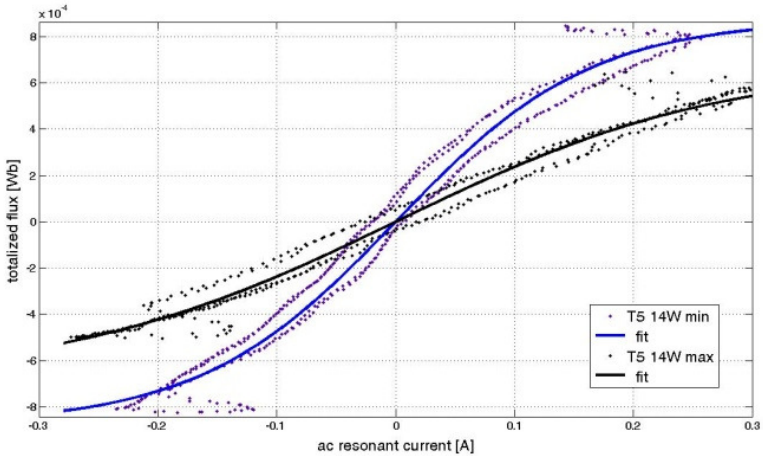

Fig. 3.49. Experimental results for the TL5 HE 14W with electronic ballast prototype – EFD20: totalized ac flux versus resonant current.

The experimental results obtained with the U15 regulator were not as satisfying as the previous ones, even though large dimming ranges were also guaranteed for both lamps. Fig. 3.50 presents the dimming curves for the T5 21W lamp considering the following parameters $V_{dc} = 310\text{V}$, $C_p = 3.3\text{nF}$ and $f_s = 80\text{kHz}$. It shows P_{lamp}, P_{arc} and P_{electr}, as a function of the large-signal inductance value and the dc control current. The region with high $\left|dP_{Lamp}/dL_{ac}\right|$ could have been avoided using a smaller capacitor. However this required a larger inductance variation for the same dimming range. A smaller capacitor also meant lower electrode power, which could jeopardize the life of the electrodes. Fig. 3.50 also shows the estimated ballast efficiency. Operating the ballast in the region with high $\left|dP_{Lamp}/dL_{ac}\right|$, leads to lower efficiency values. Higher power levels of operation correspond to higher efficiency values. This observation is coherent with the results obtained with the EFD20 regulator.

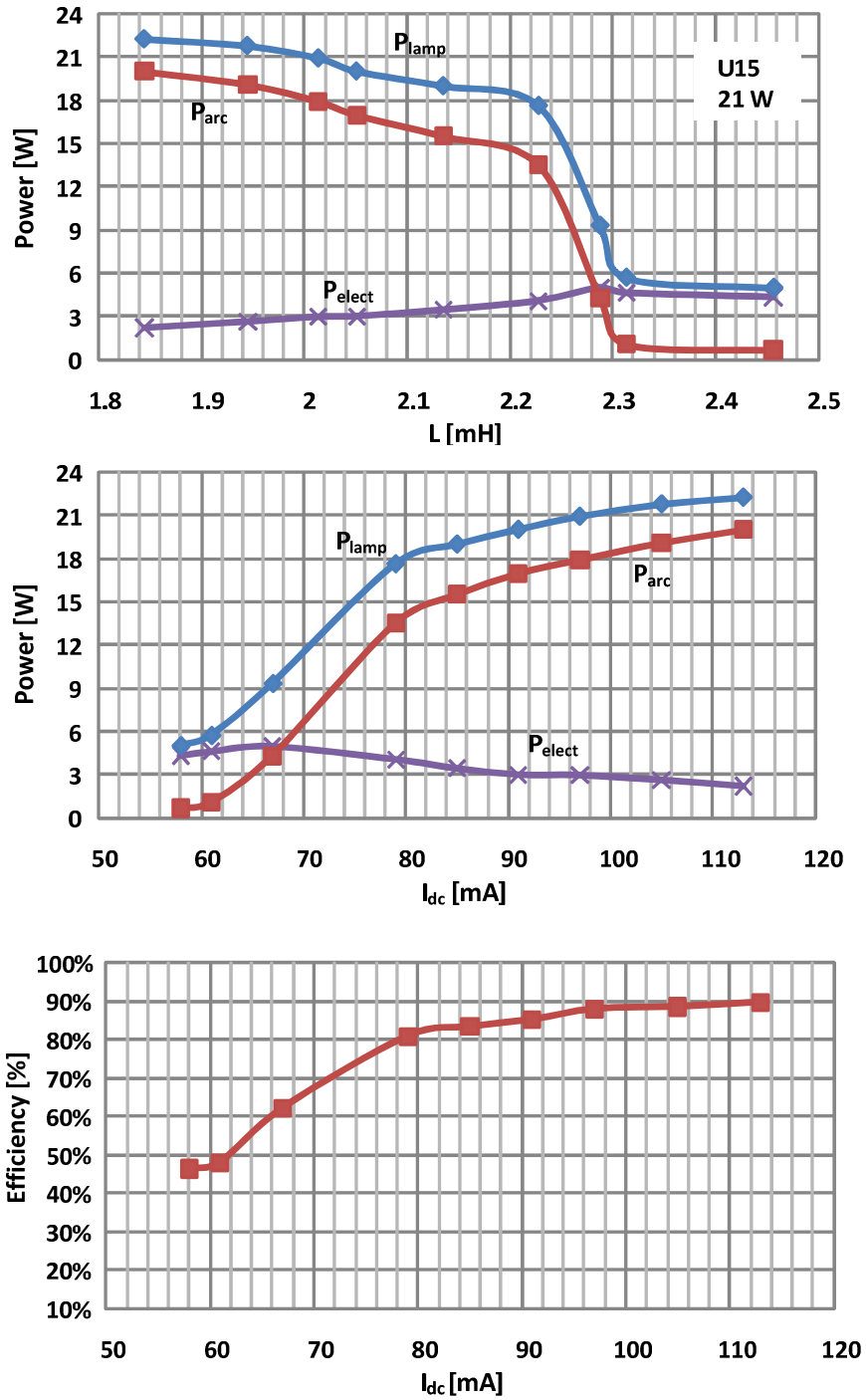

Fig. 3.50. Experimental results for the TL5 HE 21W with electronic ballast prototype – U15: average lamp power, arc power and electrode power, as functions of the control parameters, and ballast efficiency as a function of the dc control current.

A former version of the U15 prototype was used with the T5 14W lamp. This regulator had the same number of turns in the control winding, 600, but a lower number of turns in the two ac windings, $N_{ac} = 2 \times 58$ and a smaller air gap= 0.1mm. A test was done using the following parameters, $C_p = 1.6\text{nF}$ and $f_s = 53\text{kHz}$. Due to insufficient air gap, the

lamp experimental waveforms revealed that the regulator was near saturation at maximum power level. This can be observed in Fig. 3.51a. The resonant current, the lamp voltage and the arc current are significantly distorted. At a lower power level, the resonant current flowing through the regulator is obviously smaller and this distortion effect was not observed.

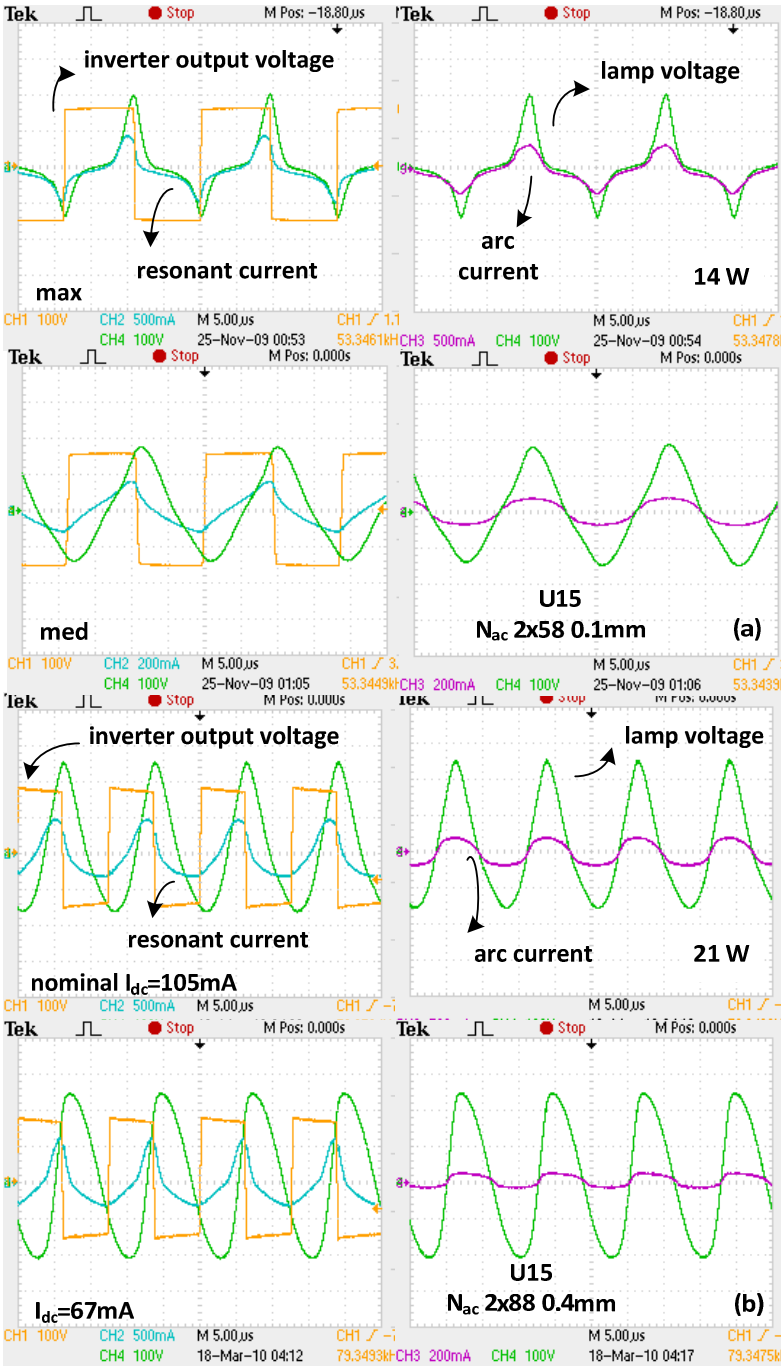

a. Inverter output voltage, resonant current, lamp voltage, arc current with U15, N_{ac}=2x58 gap=0.1mm

b. Inverter output voltage, resonant current, lamp voltage, arc current with U15, N_{ac}=2x88 gap=0.4mm

Fig. 3.51. Experimental waveforms for the TL5 HE 14/21W - U15 regulators

The waveforms presented in Fig. 3.51b, were obtained using the final version of the U15 regulator. They correspond to two operating points of the experimental results presented in Fig. 3.50. More specifically, to the maximum power level of the 21W lamp and also to a lower level. It was verified that a small asymmetry in the regulator, in terms of number of ac turns had a great influence in the resonant current and lamp waveforms. This effect was particularly observed at high power levels. Connecting the regulator in opposite polarity showed that the small peak in the resonant current would appear in the other half cycle, which would prove this asymmetry. The small offset in the waveforms, easily observed in the lamp voltage at nominal power was also related to asymmetry issues.

Some of the disadvantages presented by the U15 regulator were due to the fact that this variable inductor topology is built using four different U parts, which increases the complexity of prototype assemblage and may easily lead to asymmetries. In addition, the air gap is more difficult to control when compared to the EFD20 which are already available in gapped versions.

The purpose of this study was to confirm if the proposed magnetic regulator topologies and core structures were adequate for this dimming technique, applied to T5 lamps. With the data collected from the two tested lamps, it was concluded that the smaller size EFD20 regulator behaved as expected and no odd effects appeared in the experimental waveforms. The U15 regulator was clearly a solution harder to implement, for which small prototype faults showed a negative influence in the lamp behaviour. Even though stable lamp operation was observed in both circumstances the EFD20 showed more promising results.

3.3 VARIABLE-INDUCTOR MODELLING FOR DIMMING APPLICATIONS

3.3.1 BALLAST PROTOTYPE AND EXPERIMENTAL RESULTS

In the following section, a dynamic-inductance model for magnetically-controlled electronic ballasts simulations is proposed. The ballast model represents a useful tool for prototype design and development. The variable-inductor model itself is based on the theoretical magnetic analysis of the proposed variable inductor prototype and simulation results will be confronted with experimental results retrieved from a magnetically-controlled dimmable ballast.

The ballast prototype is identical to the one previously presented in Fig. 3.42, which is now re-called in Fig. 3.52. The ballast controlled the luminous flux of a T8 36W fluorescent lamp using an EF25 variable inductor, built with $N_{ac} = 68$ and $N_{dc} = 35$. The ballast was operated at 80kHz and the selected resonant capacitor value was $C_p = 6{,}8$nF. This EF25 regulator was the same prototype which was used as reference for the theoretical analysis presented in Section 3.1.

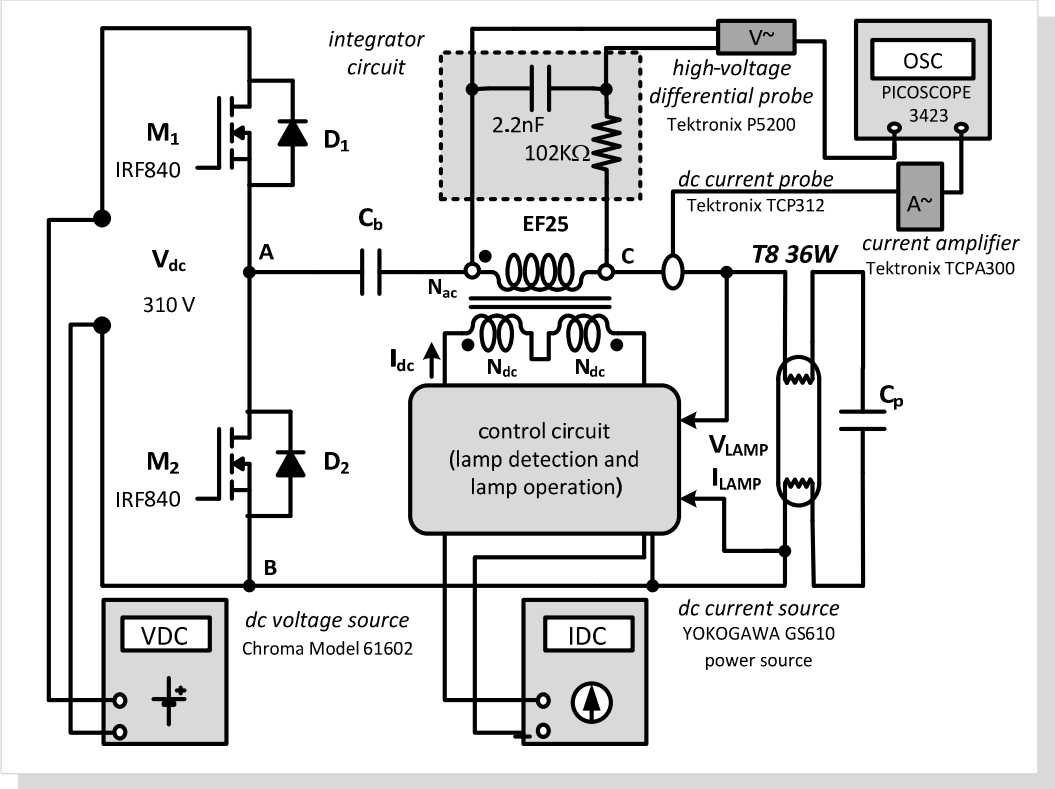

Fig. 3.52. Electronic ballast prototype: experimental setup for large-signal characterization.

The collected experimental results from dimming operation are presented in Table 3.7. For several levels of I_{dc}, the rms value of the lamp voltage, V_{lamp}, lamp current, I_{lamp} and arc current, I_D were measured. The average values of the lamp power, P_{lamp}, arc power, P_{arc}, and electrode power, P_{electr}, were also obtained as well as the peak-to-peak values of the lamp current and the integrator circuit capacitor voltage, V_{c_pp}. It was also possible to obtain the average inductance value for all dimming levels using the peak-to-peak values of the resonant current and totalized flux as shown in (3.131). These experimental results, showed in Table 3.7 are also presented in Fig. 3.53a., where it is also possible to compare this average inductance value with the regulator small-signal characteristic. The large-signal characteristic shows higher L_{ac} values when compared to the small-signal results. It is noticed once again that contrary to the small-signal measurement, in large-signal operating conditions, the ac resonant current flowing through the regulator will vary, which will also affect the inductance value.

Table 3.7 Experimental results obtained with the EF25 prototype.

I_{dc} [A]	V_{lamp} [V]	I_D [A]	I_{lamp} [A]		V_{c_pp} [V]	P_{lamp} [W]	P_{arc} [W]	P_{electr} [W]	L_{ac} [mH]
			rms	*pp*					
0	111.260	0.214	0.456	1.396	7.165	26.308	23.452	2.856	1.149
0.05	111.040	0.218	0.454	1.382	7.148	26.487	23.816	2.672	1.158
0.10	110.168	0.228	0.458	1.389	6.944	27.503	24.724	2.779	1.120
0.15	108.317	0.241	0.461	1.396	6.882	28.313	25.816	2.497	1.104
0.20	106.323	0.258	0.468	1.423	6.597	29.899	27.160	2.739	1.038
0.25	103.668	0.284	0.475	1.506	6.416	31.584	29.114	2.470	0.954
0.30	100.309	0.313	0.489	1.617	6.170	33.419	31.106	2.313	0.855
0.35	97.669	0.341	0.507	1.682	5.968	35.594	32.929	2.665	0.795
0.40	94.877	0.371	0.522	1.782	5.993	37.015	34.886	2.129	0.753
0.45	93.261	0.398	0.542	1.845	5.691	39.112	36.753	2.359	0.691

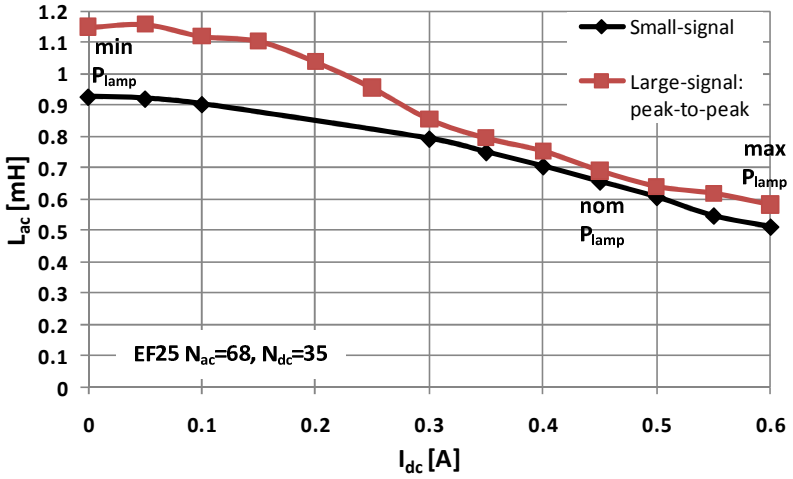

Fig. 3.53. Comparison between the small-signal and large-signal characteristics of the prototypes based on the peak-to-peak average inductance value.

The observation of Fig. 3.54, which plots the total ac flux vs. the instantaneous resonant current, for several dimming levels, reveals the non-linear behaviour of the EF25 regulator. If the variable inductor handled even larger currents, the magnetic material would most likely reach saturation.

Typically, if the control current increases and the average inductance value decreases, the power in the lamp is higher as well as the value of the resonant current. In these conditions the

total ac flux through the regulator will not increase as rapidly as the current and the slope of the curve $\Psi_{ac}(i_{ac})$ tends to decrease.

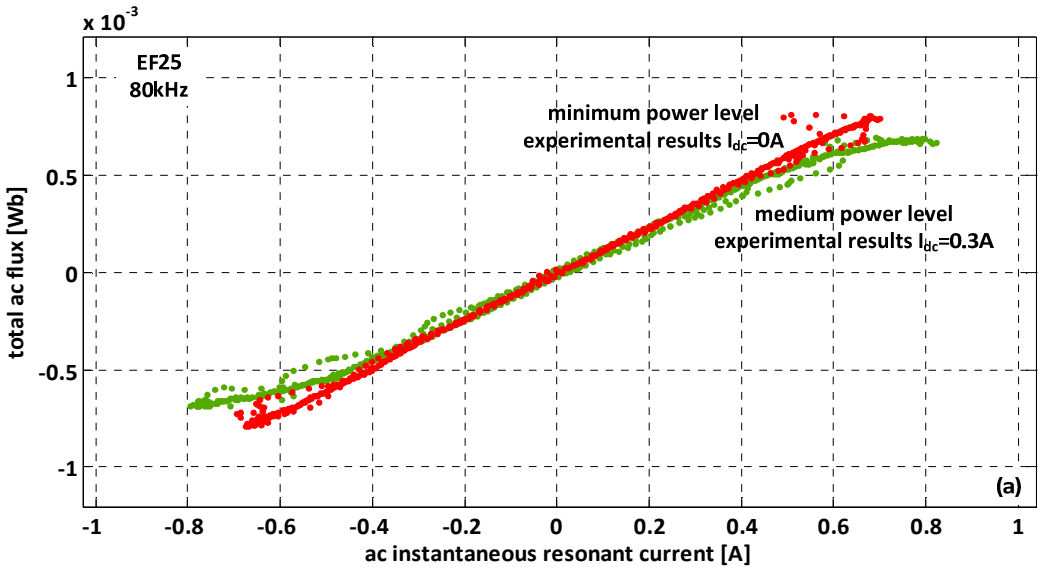

Fig. 3.54. Non-linear behaviour of the regulator prototype at $I_{dc} = 0$A and 0.3A.

3.3.2 MATLAB-SIMULINK MODEL

3.3.2.1 DYNAMIC-INDUCTANCE MODEL

The electronic ballast model, the half-bridge inverter model and the fluorescent lamp model are similar to the ones presented in Section 3.2, considering a *LC* resonant circuit. The ballast and the fluorescent lamp model can both be observed in Fig. 3.55. In this case, the lamp electrodes were included in the fluorescent-lamp model. The inclusion of the electrodes resistance can be identified in Fig. 3.55b. The integrator circuit was also included in the model in order to obtain the simulated value of the peak-to-peak average inductance.

The proposed variable-inductor model is presented in Fig. 3.55c. In the previous Matlab-Simulink model developed in Section 3.2, the variable inductor was simply simulated by an inductor. Its inductance value was selected according to the dc current level, using the small-signal characteristic of the prototype. In this model, a lookup-table was used to simulate the dynamic-inductance behaviour of the variable inductor.

In Section 3.1, the theoretical values of the differential inductance as a function of the instantaneous value of ac current were already determined for this particular variable inductor. A different curve was obtained for each value of the dc control current. This may be recalled by

referring to Fig. 3.7. The differential inductance curves were introduced in the variable inductor model by means of a lookup table as shown in the schematic of Fig. 3.55c. For this simulation analysis, the presence of lateral air gaps was not considered in the model.

The model itself is quite simple. The inductor voltage is measured through a voltage sensor and then the equation that relates the voltage across an inductor with the current that passes through it is implemented, as in (3.135). In this equation, $L_{ac}(i_{res}, I_{dc})$ is the differential inductance value determined by the lookup table. In the proposed model, the resonant ac current, i_{res} is defined to flow from the positive terminal to the negative terminal of the variable inductor.

$$i_{L_{ac}} = \frac{1}{L_{ac}(i_{res}, I_{dc})} \cdot \frac{v_{L_{ac}}}{s} \tag{3.135}$$

As a first approach, the dc control current value was simply introduced using a constant block. This dc current value, together with the ac resonant current value at that instant, dictates the value for the inductance that is calculated by the Lookup Table block. Between data points, the Lookup Table block uses the method specified by the Lookup Method parameter to determine the differential inductance value. It is recalled that the resulting model does not include core losses or temperature effects.

The electronic ballast model was used to simulate the prototype behaviour in the previously presented dimming conditions. The operating parameters such as the dc bus voltage, the operating frequency, the resonant capacitor voltage, the lamp $V(I)$ characteristic and finally the theoretical differential inductance values were included in the model. Each operating point was simulated by inserting in the model the dc control current value for each specific power level. Thus, for a dc control current from 0 to 0.45A, each dimming level was simulated. The obtained simulating results are presented in the next section.

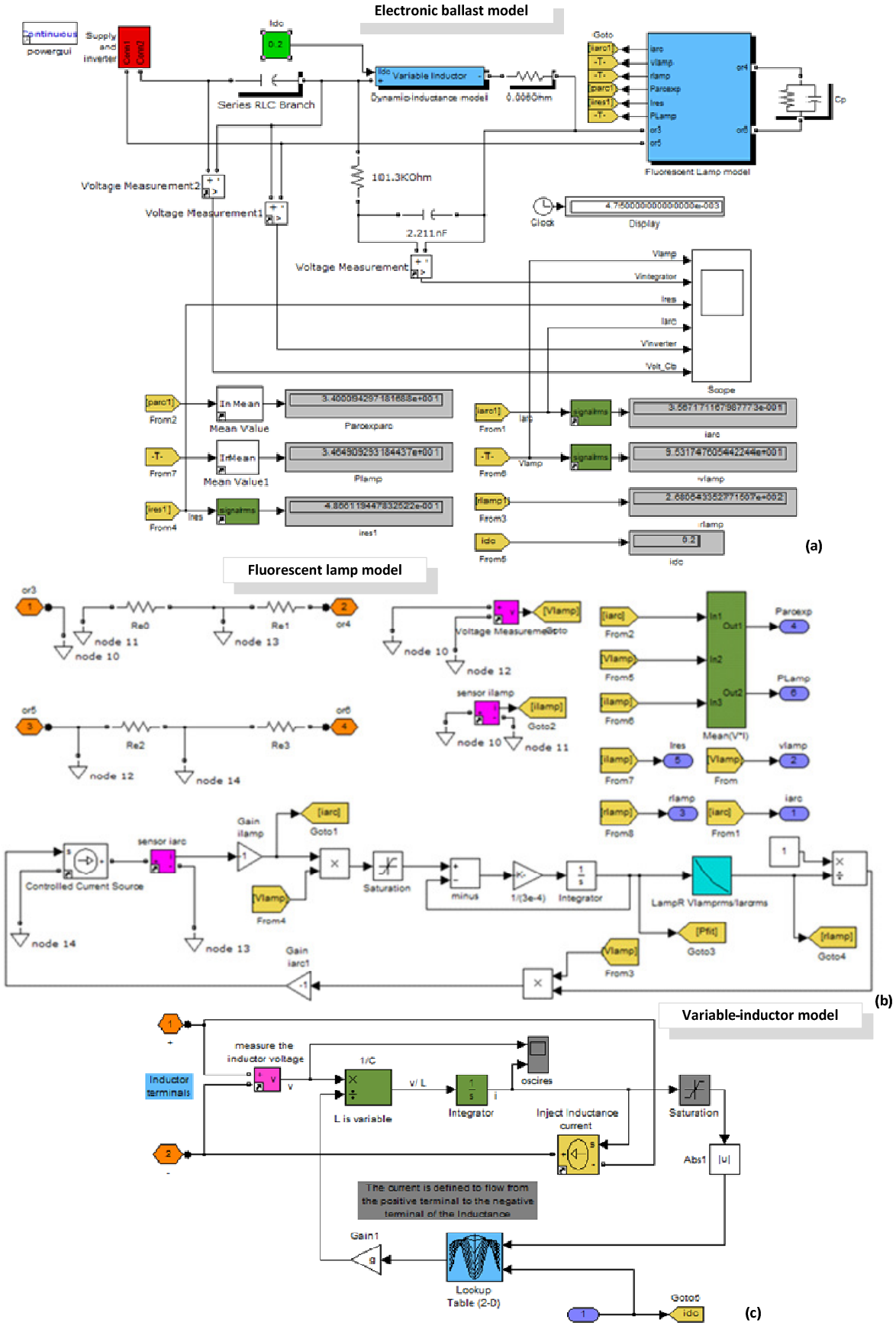

a. Half-bridge resonant ballast model b. Fluorescent-lamp model c. Variable-inductor model

Fig. 3.55. Electronic ballast MATLAB-Simulink implementation: dynamic-inductance model.

3.3.2.2 COMPARISON BETWEEN EXPERIMENTAL AND THEORETICAL RESULTS

In Fig. 3.56 it is possible to compare the simulation results for several dc control current levels with the experimental ones. In Fig. 3.56a. it is presented the simulated peak-to-peak inductance value together with the equivalent experimental result. Fig. 3.56b., Fig. 3.56c. and Fig. 3.56d. present the simulation and experimental results of the arc power, lamp voltage and arc current respectively.

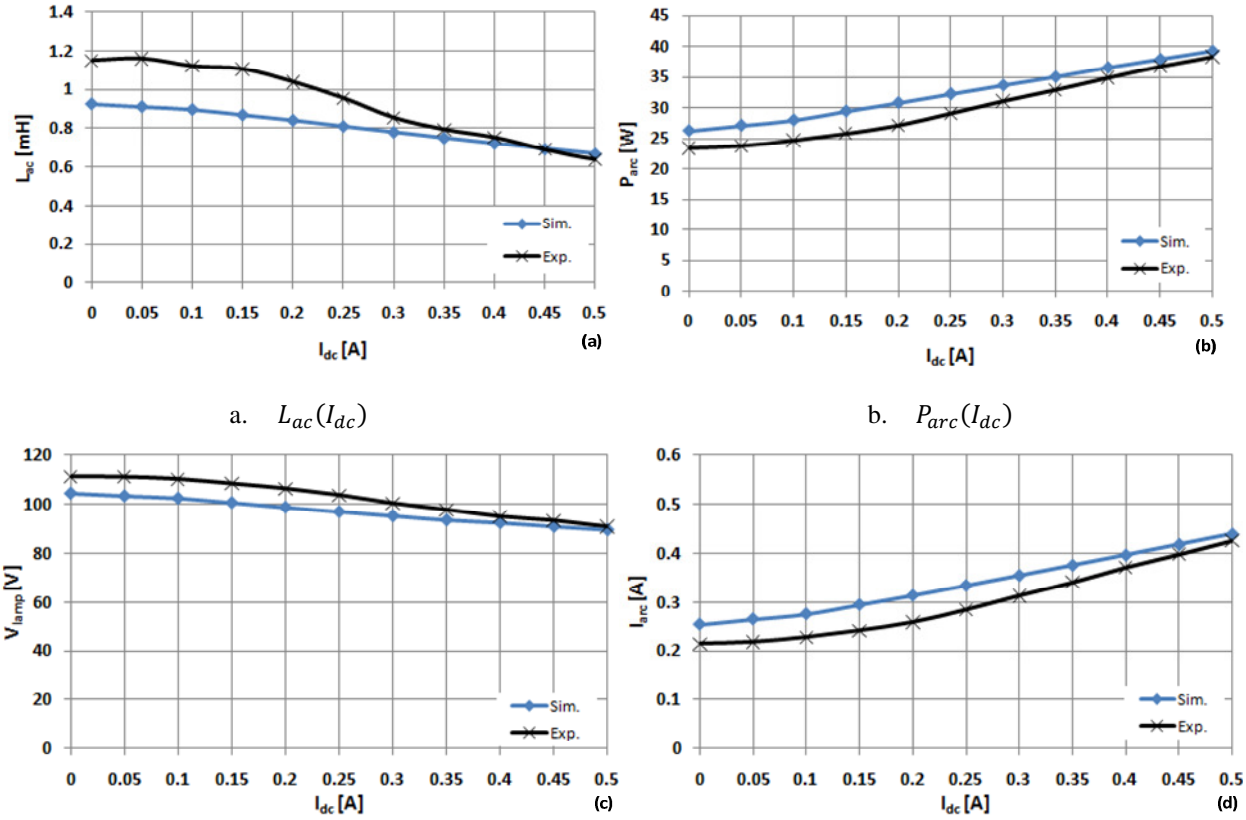

a. $L_{ac}(I_{dc})$ b. $P_{arc}(I_{dc})$

c. $V_{lamp}(I_{dc})$ d. $I_{arc}(I_{dc})$

Fig. 3.56. Comparison between experimental and simulation results.

As expected, all simulated results follow the experimental behaviour. The small difference between experimental and simulation results is due to the fact that the inductor model is based on the theoretical analysis of the variable inductor prototype. However the proposed ballast model is sufficiently accurate to simulate the proposed dimming techniques. As a future step, in order to improve the variable inductor model, the differential inductance values could be obtained by applying the first derivative to the curve fit of the experimental total ac flux linkage vs. resonant current curve, for each dc current level.

3.4 ELECTRODE OPERATION IN DIMMABLE ELECTRONIC BALLASTS WITH MAGNETIC CONTROL

Tubular fluorescent lamps present restrictions that must be taken into account in the design of any electronic ballast [3.30]. Presently, there are several regulations regarding ballast and luminaire design. Issues regarding installation, environment, performance, operation conditions, ignition and electrodes pre-heating are referred to in several IEC standards [3.31]-[3.34]. A key issue when developing electronic ballasts for fluorescent lamps is to evaluate the physical conditions of the fluorescent lamp electrodes during the lamp operation since, as stated in [3.29], the lifetime of a fluorescent lamp is determined by the electrode operation. In order to ensure sufficient electrode lifetime, its temperature should be kept within certain limits. Above a certain temperature the electrodes will be too hot, leading to enhanced evaporation of the emissive material and severe end-blackening. Below a certain temperature the electrodes will be too cold and sputtering of the emitter will occur. Both situations may lead to an extremely short lamp life. The purpose of the following study was to evaluate the electrodes operation under the proposed control technique.

3.4.1 PERFORMANCE ISSUES

3.4.1.1 PRE-HEATING AND HEATING CURRENTS DURING DIMMING OPERATION

The ignition process is a decisive factor in terms of electrode preservation, with an immediate effect on the lamp life. Avoiding the sputtering effect requires pre-heating the electrodes, which will in turn increase the power losses. In addition, in order to avoid evaporation of the emissive material, it is extremely important to maintain the electrodes temperatures at an appropriate level during normal fluorescent-lamp operation. Thus, soft-starting, electrodes preheating, and safe electrodes operation are critical aspects to be considered while developing new highly efficient electronic ballasts [3.38].

A common way to guarantee adequate electrodes heating is through external heating sources (North America practice) as represented in the simplified circuit shown in Fig. 3.57a. This is quite customary in rapid-start circuits or warm-start circuits [3.33], and is currently the common practice is most commercial ballasts. Depending on the internal impedance of these sources, the arc current I_D will divide between the electrode wires. The higher lead wire current, I_{LH}, will

carry I_H and a percentage a of I_D, aI_D. The lower lead wire current, I_{LL}, will carry I_H and the rest of I_D, $(a-1)I_D$ [3.36]. These two currents can be measured directly and the arc or discharge current can be measured by taking the two wires together in a current probe. Their nomenclature is represented in Fig. 3.57b.

As previously referred, in magnetically-controlled ballasts, the current through the parallel resonant capacitor may also be used to heat the electrodes prior to the lamp ignition, as shown in Fig. 3.57a., and it is possible to use the variable ac inductance as an additional control parameter to achieve soft-starting in a narrower frequency range. This action may be easily accomplished by a microcontroller and must be done respecting the pre-heating times, defined for each fluorescent lamp.

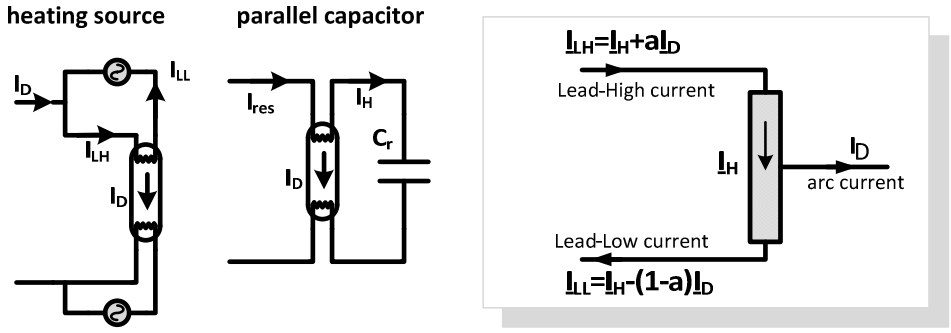

a. Pre-heating techniques b. Nomenclature of electrode currents

Fig. 3.57. Preheating techniques

There is however another concern which is related to the behaviour of the electrodes during nominal power operation or during dimming operation. Current standards clearly indicate, particularly for T5 lamps, a simple tool to evaluate and limit the electrodes operating currents, the so-called SoS limits.

3.4.1.2 THE SoS LIMITS

One way to evaluate the conditions for proper and safe operation of the electrodes is based on the sum of squares of the lead-in wire rms currents known as, SoS:

$$SoS = I_{LH}^2 + I_{LL}^2; \qquad I_{LH} > I_{LL} \tag{3.136}$$

These limits are based in the maximum permissible currents that may pass through the electrodes. In 2006 these limits were still under discussion at the European Lamp Manufacturers Association for the Preparing of Standards, but, in due time, it was expected that they would

result in new data in the relevant IEC standards [3.29]. These limits are now referred to in the IEC 60081 international standard (recent edition 2010) [3.35].

The definition takes into account both electrodes currents, as defined in Fig. 3.57b. For each rated lamp power, maximum limit values are defined for each of these currents, for nominal power operation or dimming operation. In dimming operation, instead of having one SoS value for each lamp, maximum, minimum and target SoS curves are defined for the whole dimming range. Lighting engineers involved in standards preparation consider this definition as the simplest and most unambiguous way to describe the requirements for the electrode conditions during the dimming of fluorescent lamps [3.29], [3.35], [3.36].

The electrodes are designed in such a way that the lamp current can be varied around its rated value within certain limits. The normal operation is therefore bounded by the minimum and maximum discharge current, I_{Dmin} and I_{Dmax} values. Within these limits of the lamp current, additional heating is not strictly required. If the lamp current is to be dimmed over a broader range, it may be necessary to supply additional heating to the electrodes to maintain its optimum temperature. This additional heating is only necessary to keep the cathode at a sufficiently high temperature for thermionic emission. The amount of this additional heating power is determined by the dissipation of the additional heating current through the electrodes. So, if the ballast does include external heating sources, the currents in the lead-in wires I_{LH} and I_{LL} should also be kept below the maximum values, I_{LHmax} and I_{LLmax}, given in [3.29], [3.34], [3.35].

The value of the required additional heating current is a function of the arc current, but it is also dependent on the ballast circuit layout. Using a parallel-loaded resonant circuit, as shown in Fig. 3.57a. there is an obvious phase-shift between these currents. However, the work which led to this so-called SoS approach showed a linear dependency between the sum of the squared rms lead currents to the electrode and the discharge current, where neither the phase shift between I_D and I_H, nor the distribution of the discharge current trough the leads, has an influence [3.36]. This linear dependence establishes current boundary limits related to the SoS value. In some other ballast circuits where the additional heating current is delivered by separate heating sources, it is not clear through which lead-in wire will flow part of the lamp current. Nevertheless, whatever the configuration, all these effects can be taken into account by measuring the currents through the two lead-in wires to the electrode and calculating the sum of the rms squares of these two currents as a function of the discharge current. If this definition is applied to magnetically-controlled electronic ballasts, it becomes clear that $I_{res} = I_{LH}$ and $I_H = I_{LL}$.

The minimum sum of squares, SoS_{min}, needed to keep the electrode just at a sufficient temperature to prevent cathode sputtering in dimming operation, is defined by:

$$SoS_{min} = I_{LH}^2 + I_{LL}^2 > X_1 - Y_1 \times I_D \tag{3.137}$$

where X_1 and Y_1 are lamp parameters given by the manufacturer and depend on the discharge current.

The overheating of the electrode is prevented in a similar way as for low temperatures by giving values for a maximum SoS line:

$$SoS_{max} = I_{LH}^2 + I_{LL}^2 < X_2 - Y_2 \times I_D \tag{3.138}$$

where X_2 and Y_2 are also given by the manufacturer. However, in order to protect the electrodes from overheating, three different regions of the cathodes must be protected: the hot spot region, which is protected by the SoS_{max} description, the bare tungsten part, which is protected by a maximum value of I_{LH}, I_{LHmax} and finally, the coated part, which is also protected by a maximum value of I_{LL}, I_{LLmax}.

As in some applications both SoS boundaries can still be critical for the lamp performance, a safe setting of the SoS values is given by the target SoS line:

$$SoS_{target} = I_{LH}^2 + I_{LL}^2 \cong X_1 - z \times Y_1 \times I_D \tag{3.139}$$

The deviating slope of this target line is described by the factor z. However this line has no physical background and can be understood as merely indicative. The purpose of this target line is to show how far above the critical minimal SoS line a ballast design should be positioned without violating any maximum electrode heating criteria [3.36]. This maximum heating criteria corresponds to the heating current that results in sufficient electrode heating without causing accelerated end-blackening. In deep dimming mode the discharge current contribution is typically neglected and the safe setting is based only on the considered maximum heating criteria.

3.4.2 STUDY OF THE PROPOSED DIMMING TECHNIQUE UNDER THE *SoS* LIMITS

3.4.2.1 LAMP SELECTION, VARIABLE INDUCTOR PROTOTYPE AND CHARACTERIZATION

The operating conditions of the electrodes under the proposed dimming technique were analysed for two different T5 lamps: TL5 HE 21W and TL5 HO 39W. The SoS evaluation technique, currently adopted in IEC standards, was also applied to T5 commercial ballasts driving the same lamps, in order to validate the reference results. Similar SoS lines were then obtained for the HE 21W and HO 39W, using the proposed ballast prototype.

The implementation of the prototype immediately requires the calculation of the ballast working parameters. Thus, by following the typical design procedure, it was possible to determine the resonant circuit parameters to operate the selected lamps at nominal power, at the desired operating frequency. Afterwards, it was necessary to define the limits for the inductance in order to cover all the dimming range. Normally, a 2:1 variation is found to be sufficient to guarantee 90% of power variation. The dimming curves were then obtained using the equation relating the average lamp power with the control variable, L_{ac}, defined in (3.68). The influence of the electrodes resistances is neglected when using the necessary design equations, $R_{lamp} \approx R_{arc}$. This is only an approximation, since heated electrodes can have resistances up to four times higher than their normal cold resistances. For instance, TL5 HE lamps have a cold electrode resistance around 9Ω, and a heated electrode resistance around 40Ω [3.29], [3.49]. Fig. 3.58 presents the TL5 HO 39W characteristic of the lamp resistance versus average arc power, $R_{lamp}(P_{arc})$ plus two dimming curves, for a ballast dc voltage V_{dc} =310V, for different operating frequencies, using a specific resonant capacitance. It also presents different dimming curves for the TL5 HE 21W lamp.

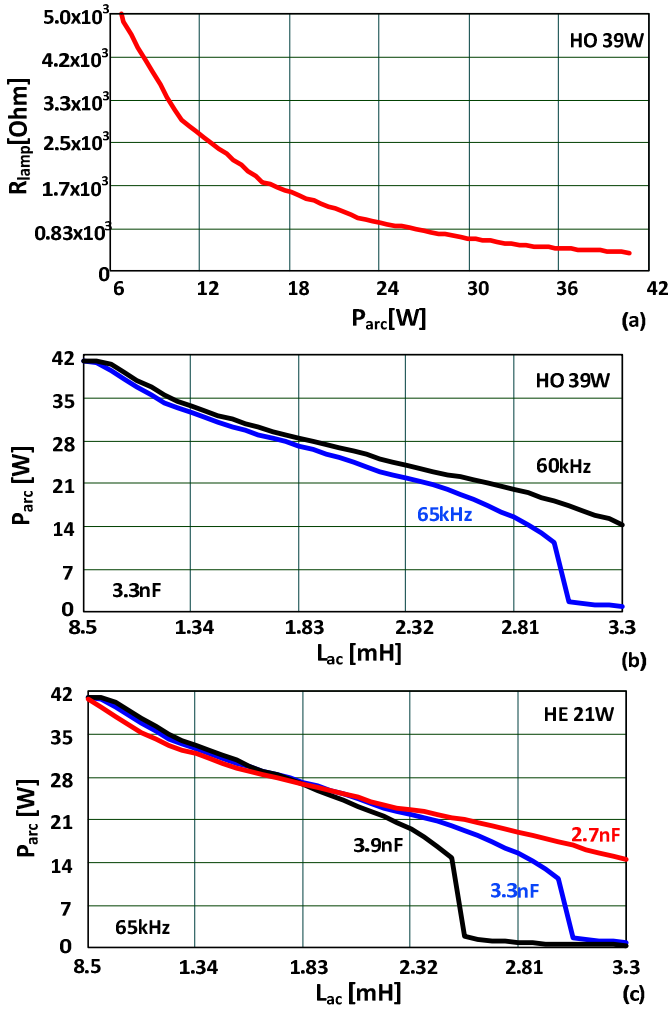

a. Curve fitting to the $R_{lamp}(P_{arc})$ linear interpolation b. Dimming curves at 60kHz and 65kHz c. Dimming curves at 65kHz with different resonant capacitors

Fig. 3.58. TL5 HO 39W Philips and TL5 HE 21W Philips theoretical analysis.

The analysis of these curves shows that theoretically, there are several dimming options. Some of these options were experimentally tested in order to verify their performance in terms of lamp stability and electrode working conditions.

The magnetic regulator was designed and built using an EFD20 core set, according to the topology presented in Fig. 3.38. The schematic and the experimental prototype are shown in Fig. 3.59a. and Fig. 3.59b. Fig. 3.59a. shows that this variable inductor presented multiple options in terms of number of turns. With this arrangement it was possible to provide a flexible variable inductor, with different configuration in terms of inductance range (A-D). This was considered to be useful for testing the lamps in different dimming conditions, eventually using other working parameters (f_s and C_p). The regulator small-signal characteristics, for some of these different combinations were measured with the previously referred LCR meter, and are presented in Fig. 3.59c.

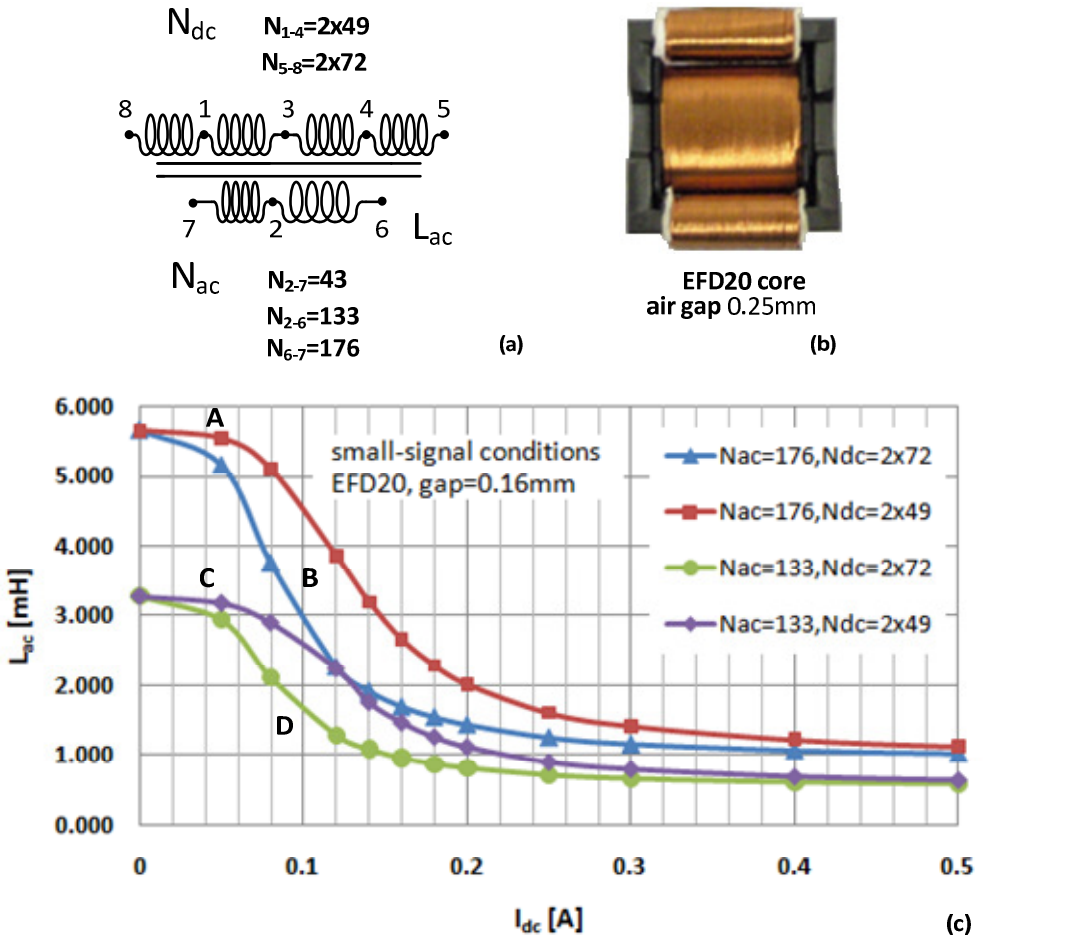

a. Schematic b. Experimental prototype c. Small signal characteristics

Fig. 3.59. Variable inductor

3.4.2.2 COMMERCIAL BALLASTS TESTS AND PROTOTYPE RESULTS UNDER THE *SoS* LIMITS

Two commercial electronic ballasts, PHILIPS HF-R 14-35 TL5 220-240 and HF-R 139 TL5 220-2240, were used in order to obtain reference results related to the lamp operation and to compare them to the IEC standard. For the TL5 HE 21W lamp, all the measurements performed were already detailed in Table 3.6. It is noticed that this ballast is also capable of driving other T5 lamps, with different power ratings. The TL5 HO 39W lamp was tested in a similar way. The obtained results are presented in Table 3.8. For both lamps, each electrode power was calculated, multiplying the voltage across the electrode by the lead-in current. It was then assumed that the corresponding lamp power would be equal to the sum of the arc power and twice the electrode power. The analysis of Table 3.8 also shows that this ballast uses a variable-frequency technique to achieve dimming and that a good power factor cannot be maintained for all operating points.

The efficiency of the ballast is around 90% for high power values, decreasing rapidly for dimming levels below 50%.

Table 3.8 TL5 HO 39W Philips operated with PHILIPS HF-R 139 TL5 220-240.

MEASUREMENTS						CALCULATED VALUES				
V_{DC} [V]	f_s [kHz]	V_{lamp} [V]	I_D [mA]	*Line Power Factor*	P_{in} [W]	*Efficiency* [%]	P_{lamp} [W]	P_{arc} [W]	P_{electr} [W]	R_{lamp} [Ω]
1	87.8	143.61	4	0.640	6.1	41	2.51	0.54	1.97	35991
2	84.2	176.02	17	0.780	8.6	57	4.86	3.02	1.85	10074
3	83.0	182.10	38	0.860	12.1	70	8.47	6.76	1.70	4784
4	83.0	177.44	61	0.890	15.1	81	12.21	10.60	1.61	2901
5	81.8	167.48	98	0.930	20.3	86	17.46	16.07	1.39	1717
6	77.8	151.09	155	0.960	27.1	89	24.05	23.06	0.99	975
7	69.4	138.44	218	0.970	33.3	92	30.69	29.74	0.95	636
8	59.7	127.72	271	0.974	38.1	92	35.02	34.18	0.84	472
9	47.4	120.22	342	0.989	44.5	93	41.36	40.75	0.61	352
10	46.1	118.17	343	0.981	44.9	91	40.85	40.25	0.60	344

The next step was to obtain the actual or the real SoS lines for both lamps, in dimming operation, and compare them to the maximum, minimum and target lines as defined by the manufacturer. The required SoS line parameters are indicated in Table 3.9 and the graphical representation of these lines is presented in Fig. 3.60. As expected, both real SoS lines are almost coincidental with the target lines. It is recalled that these ballasts use external heating sources which control the electrodes operation.

Table 3.9 *SoS* line parameters.

FLUORESCENT LAMP	X_1	X_2	Y_1	Y_2	z
TL5 HE 21W Philips	$0.05A^2$	$0.058A^2$	0.33A	-0.075A	0.1
TL5 HO 39W Philips	$0.21A^2$	$0.270A^2$	0.63A	-0.170A	0.3

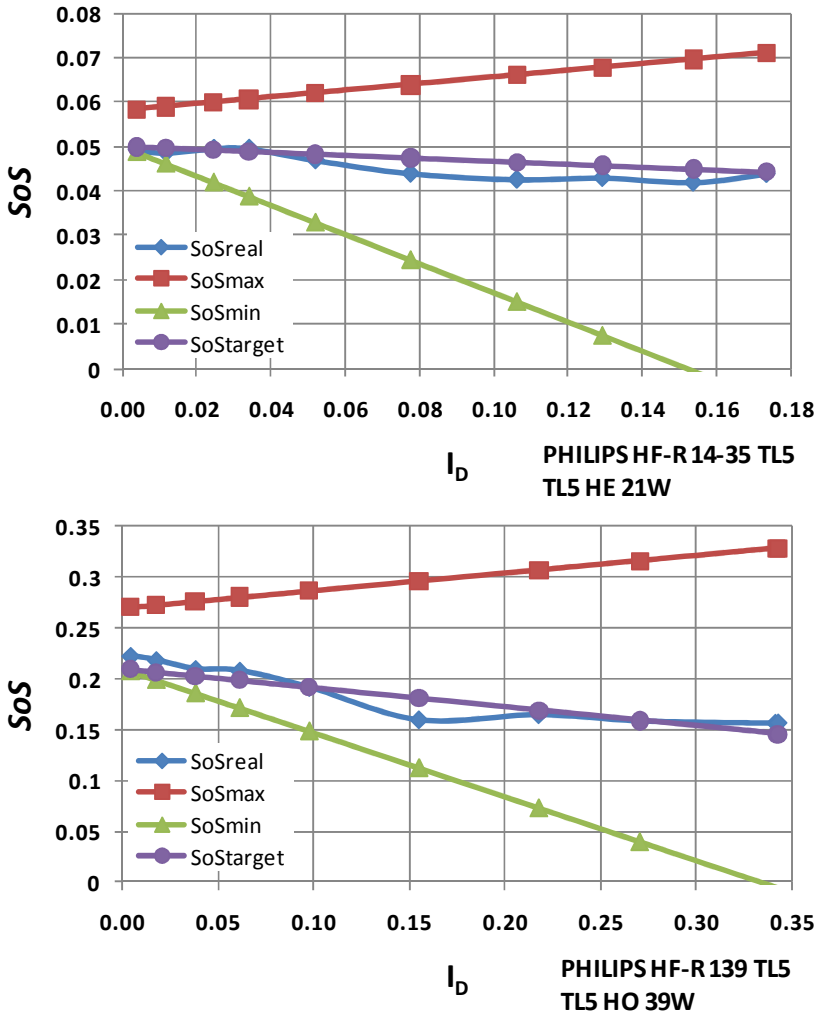

Fig. 3.60. Graphical representation of the *SoS* lines for the TL5 HO 39W and the TL5 HE 21W with commercial ballasts.

The study of the electrodes behaviour and compliance with the *SoS* limits was done using the ballast prototype already presented in Fig. 3.42. For each lamp, the selected ballast parameters are presented in Table 3.10. It is also referred the selected variable-inductor terminals. Using these terminals it was expected an inductance variation of 3.2mH to 0.5mH.

Table 3.10 Operating frequency and resonant circuit parameters for each lamp

FLUORESCENT LAMP	V_{dc} [V]	f_s [kHz]	Regulator terminals	Configuration	C_p [nF]
TL5 HE 21W Philips	310	85	AC:2-6 – DC:1-4	C	2.2
TL5 HO 39W Philips	310	65	AC:2-6 – DC:1-4	C	3.3

Similar to previous laboratory testing, several measurements were taken: P_{lamp}, P_{arc} and P_{electr}. The large-signal inductance value for each dimming level was also estimated. The main objective was however the evaluation of the electrodes operation. The real SoS value for each operating point was determined, using the following approximations:

$$I_{res}^2 = I_{LH}^2 \qquad and \qquad I_{LL}^2 = I_{res}^2 - I_D^2 \tag{3.140}$$

This implies that the electrode impedance was considered small enough when compared to the lamp resistance and was thereby neglected. Fig. 3.61 and Fig. 3.62 present the real SoS lines obtained with the experimental prototype, for both lamps, respectively TL5 HO 39W and TL5 HE 21W. Fig. 3.61 and Fig. 3.62 also show the maximum, minimum and target lines as defined by the manufacturer. These curves were determined using the measured discharge current, I_D and the parameters collected in Table 3.9.

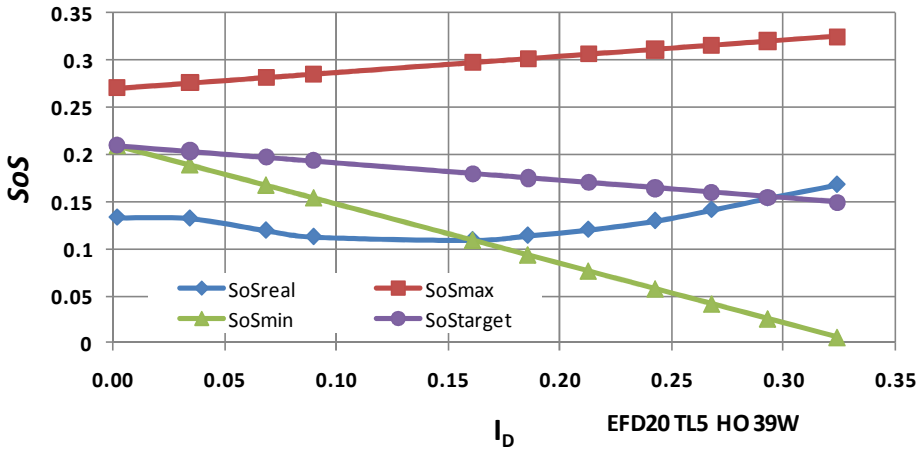

Fig. 3.61. Graphical representation of the SoS lines for the TL5 HO 39W with ballast prototype.

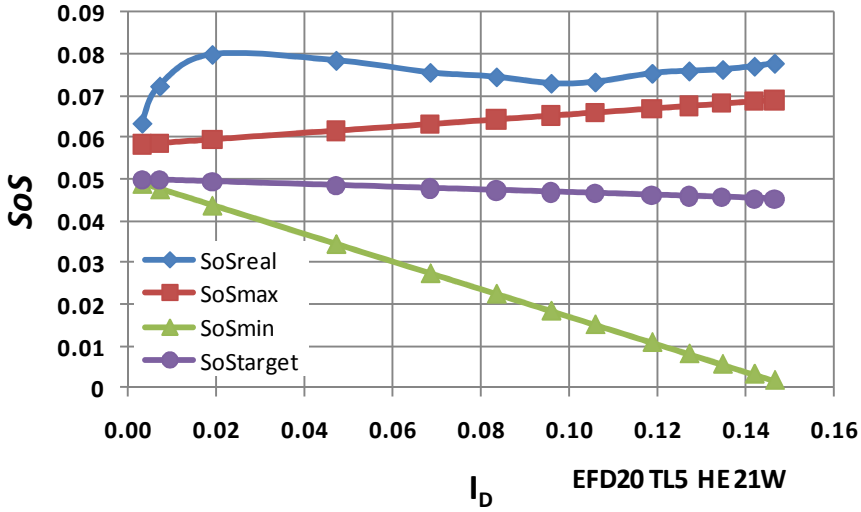

Fig. 3.62. Graphical representation of the SoS lines for the TL5 HE 21W with ballast prototype

From the analysis of these two graphical representations the following is observed: for the TL5 39W lamp, at lower dimming levels, the real SoS line is below the minimum SoS line. In the first case, the obtained results suggest that an external heating source should be implemented to maintain the SoS value within the proper range. This could easily solve the problem. It should be noted however, that the rules determining the required extra heating at dimming levels higher than 10% cannot be extrapolated to the so-called lower deep dimming levels [3.29]. For the TL5 21W lamp, the real SoS line is about 10% higher than the maximum SoS line. This may occur due to an excessive value of the resonant capacitance. This capacitance is directly related to the heating current.

In order to solve the excessive electrode current in the case of the 21W lamp, an alternative was to use the solution presented in Fig. 3.63a. It is also possible to control the electrodes currents using other circuits as presented in Fig. 3.63b. and Fig. 3.63c. The circuit shown in Fig. 3.63a. is very often used in self-oscillating ballasts, where the switches are driven from the resonant current using a current transformer [3.39]. In this circuit the PTC is initially cold and capacitor C_1 is practically short-circuited by the PTC. The resonant circuit under these conditions is formed by the ac inductance and C_2 . This circuit can be designed to heat the lamp electrodes with a heating voltage low enough to avoid lamp cold ignition. Since the PTC is also heated by the circulating current, after a certain period of time it reaches the threshold temperature and trips. At this moment, the new resonant circuit is formed by the regulator and the series equivalent of C_1 and C_2. This circuit was implemented and the results considering the series combination of capacitors C_1 and C_2 correspond to the SoS_{real} line presented in Fig. 3.61, with C_1 and C_2 being respectively 3.3nF and 2.2nF.

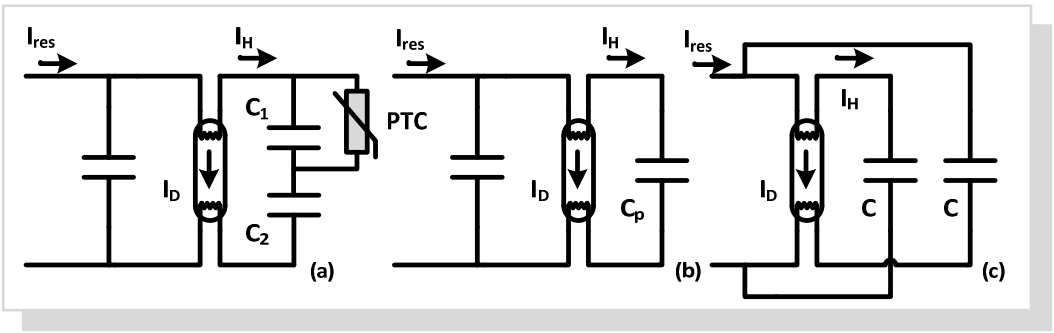

Fig. 3.63. Changing the level of the SoS lines

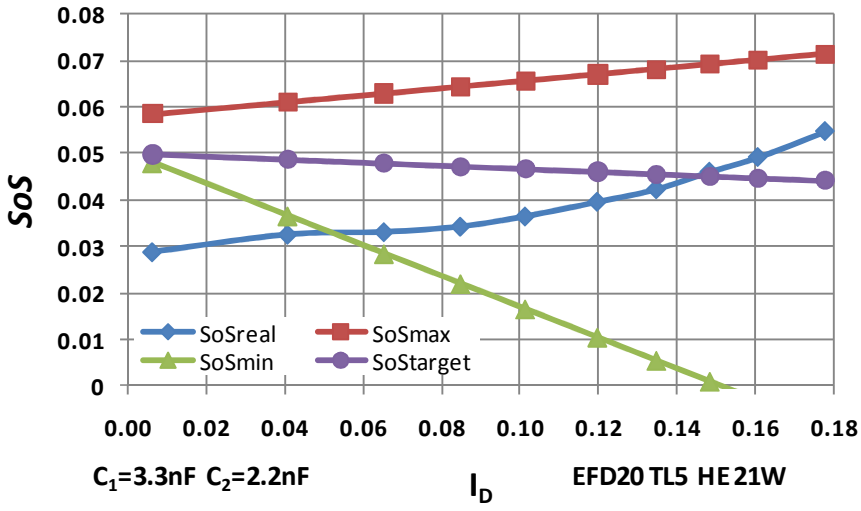

Fig. 3.64. Graphical representation of the SoS lines for the TL5 HE 21W with ballast prototype

These results show that the real SoS line is maintained within limits, except for the lowest power levels. Again this can be avoided with an external heating source, acting on deep dimming levels, or by a more adequate choice of capacitors. It is noticed that, the so-called target line, assumes a small variation of $I_{LH}^2 + I_{LL}^2$ for the whole dimming range. This is quite difficult to achieve without a separate control of these currents. However, this implies an additional cost for the ballast. It is however possible to maintain the electrodes operating between maximum and minimum limits without the requirement of an extra heating source, except for low power levels. These results also suggest that using an adequate choice of resonant circuit it is possible to control the operation of the electrodes. This is a relevant aspect in the control of these variable-inductor based ballasts.

As expected, normal behaviour was verified for both lamps. The operating waveforms of the TL5 39W lamp may be observed in Fig. 3.65. Stable operation can be recognized in all of the reported operating points. The lamp voltage and arc current show a low THD, and the resonant current lags the output inverter voltage, ensuring ZVS in the bridge transistors, which is also an important aspect. Fig. 3.66 shows both the average arc power as a function of the average inductance value, which was estimated using the peak-to-peak values of the resonant current and the total ac flux as shown in (3.131). Fig. 3.66 also reports the value of the dc control current for the three reported operating points shown in Fig. 3.65.

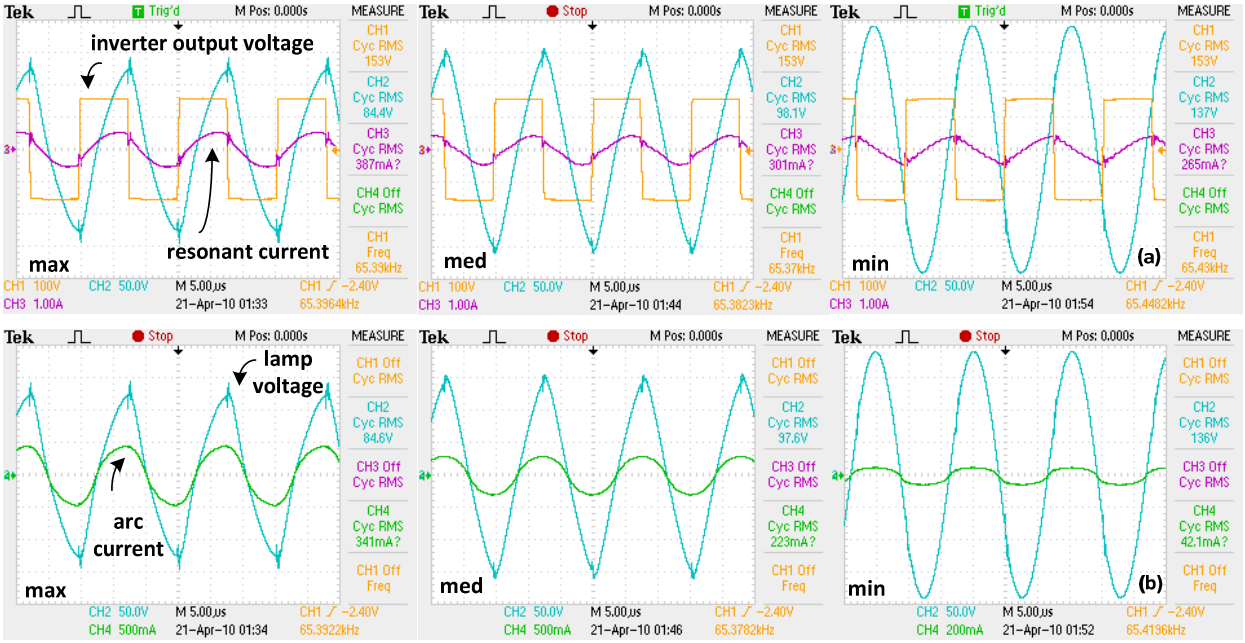

a. Inverter output voltage, resonant current, lamp voltage

b. lamp voltage and arc current

Fig. 3.65. Experimental waveforms for the TL5 HO 39W-EFD20 at nominal power, medium and at minimum power level, 65 kHz.

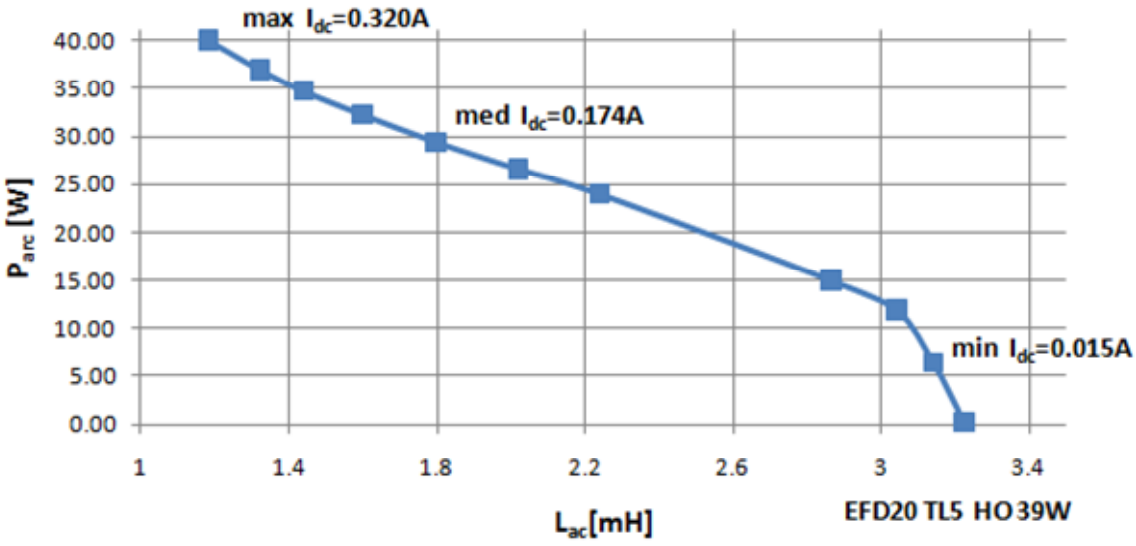

Fig. 3.66. Experimental results for the TL5 HO 39W-EFD20 at nominal power, medium and at minimum power level, 65 kHz.

3.5 VARIABLE INDUCTORS APPLIED TO UNIVERSAL BALLASTS

3.5.1 INTRODUCTION TO THE PROPOSED MAGNETIC CONTROL TECHNIQUE

The main purpose of universal ballasts is the ability to drive different lamps within a range of nominal power ratings without requiring any physical change in the hardware. These ballasts must incorporate the necessary intelligence to measure the electrical characteristics of the lamps wired to their output, and must be able to adjust their internal operation in order to correctly ignite and supply these lamps, simultaneously guaranteeing proper lamp operation and flexibility of the installed lighting system. Universal ballasts proposed up to now, also use the inverter switching frequency, f_s, as the main control parameter, thereby ensuring that each lamp is operated at nominal power. The major disadvantage is the fact that using the same resonant circuit for each lamp requires a large range of operating frequencies. This eventually leads to high switching losses and EMI stresses. Moreover, the design methodology of the resonant inverter can be very different depending on the lamp type and characteristics, inverter topology and design goals, and this also has an impact on this type of operation. Consequently and as described in the preceding chapter, additional control parameters are necessary to provide this type of multi-watt operation.

The proposed magnetically-controlled universal ballast gives the ability to change and adapt the resonant circuit to the working parameters imposed by each lamp. With this new technique, it is possible to provide lamp soft-starting, and to operate each lamp near resonance, which guarantees a stable and optimum operating point. By simply controlling the magnetic device with a dc control current, a variable resonant inductor is obtained, and consequently an adaptable and flexible resonant circuit is provided. Together with the operating frequency, two different control parameters are now available. Hence, a simple and effective control method is proposed which avoids the necessity to adapt the dc bus voltage, V_{dc}, or to change simultaneously both the switching frequency and the duty-ratio of the inverter signal, with their respective disadvantages. The magnetically-controlled universal ballast general topology can be observed in Fig. 3.67. With this technique it will be demonstrated the control of T8 and T5 HE and HO lamps [3.40]-[3.45].

The primary goal was to verify the feasibility of the proposed technique. The first implemented prototype was quite simple. There were initially no concerns regarding the optimization of the ballast itself. The proposed technique is hereby detailed and the design procedure of the resonant parameters is described.

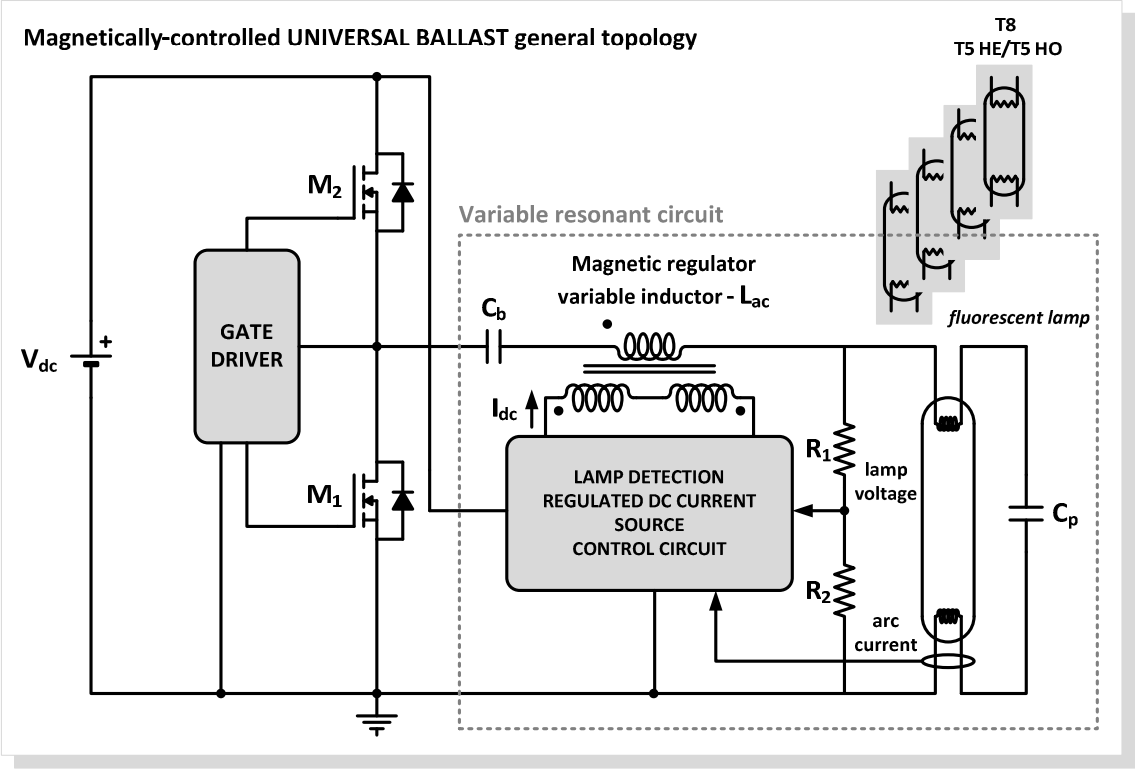

Fig. 3.67. Magnetically-controlled universal ballast: circuit schematic

3.5.2 DESIGN PROCEDURE

The objective is to operate a group of TLD lamps, with different power ratings, at nominal power, using two different control parameters, the switching frequency, f_s and the inductance value of the resonant circuit, while maintaining the same resonant circuit capacitance. The selected lamps nominal characteristics, for high-frequency operation, are presented in Table 3.11. The selected power ratings are between 15W and 58W.

Table 3.11 Lamp nominal characteristics at high-frequency.

FLUORESCENT LAMP	V_{lamp} [V]	I_D [mA]	R_{lamp} [Ω]
TLD 18W Philips	51	0.37	136.4
TLD 36W Philips	80	0.48	166.7
TLD 58W Philips	100	0.60	166.7

The design procedure begins by obtaining each lamp electrical parameters at nominal power as collected in Table 3.11. Afterward; one of these lamps is selected as the reference lamp. The next steps are associated to the calculation of resonant parameters and the selection of the operating frequency. The flowchart of this design procedure is presented in Fig. 3.68.

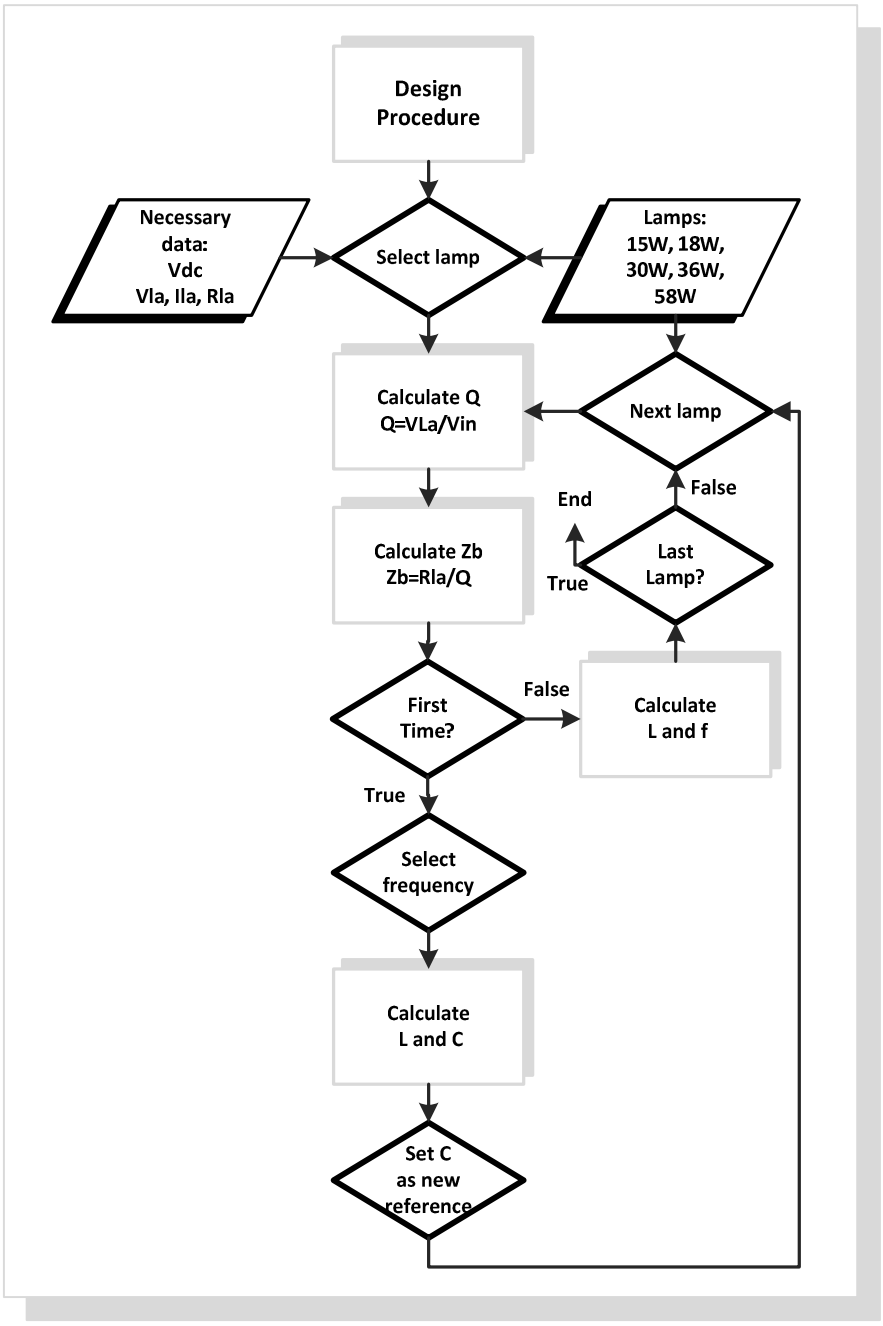

Fig. 3.68. Flowchart of the design procedure for obtaining the suitable working parameters.

Therefore, it is necessary to calculate the capacitance and the inductance values required by each lamp. For the half-bridge inverter connected to a parallel-loaded resonant circuit, from

(3.59) it can be observed that $\left|\underline{G}(j\omega)\right| = Q_L$ when ${f_s}/{f_o} = 1$. In other words, the maximum voltage gain can be approximated by Q at the natural frequency, f_o, Q being the normalized load, as represented in (3.141). This equation can be used to calculate the base impedance of each resonant circuit, Z_b, for each lamp, using the nominal values for the lamp voltage, V_{lamp}, and the lamp resistance, R_{lamp}. So, as a first step, the estimation of the resonant filter parameters, L_{ac} and C_p, is done considering that $f_s = f_o$, and $\omega_o = {1}/{\sqrt{LC}}$, using (3.141), (3.142), (3.143) and (3.144).

$$Q = \frac{V_{lamp}}{V_{in}} = \frac{R_{lamp}}{Z_b}; \quad for\ f_s = f_o \tag{3.141}$$

$$Z_b = \sqrt{\frac{L}{C}}; \quad for\ f_s = f_o \tag{3.142}$$

$$L_{ac} = \frac{Z_b}{2\pi f_o} \tag{3.143}$$

$$C = \frac{1}{2\pi Z_b f_o} \tag{3.144}$$

So, more precisely, the rms value of the lamp discharge or arc current, I_D, can be defined as:

$$I_D = \frac{V_{lamp}}{R_{lamp}} \tag{3.145}$$

It implies that if the circuit is operated at $f_s = f_o$, (3.145) can be re-written as follows:

$$I_D = \frac{V_{lamp}}{R_{lamp}} = \frac{V_{in}Q}{R_{lamp}} = \frac{V_{in}}{Z_b} \tag{3.146}$$

Therefore, the circuit will behave as a current source, and its value depends exclusively on the input voltage and Z_b. After this first-time operation the desired operating frequency, f_s, is selected for this first lamp. Then, taking into account the preceding considerations, the capacitance and inductance values for the selected lamp may be calculated by rewriting (3.143) and (3.144), respectively:

$$L_{ac} = \frac{V_{in}}{2 \cdot \pi \cdot f_s \cdot I_D} \tag{3.147}$$

$$C_p = \frac{I_D}{2 \cdot \pi \cdot f_s \cdot V_{in}} \tag{3.148}$$

For each of the other lamps, the inductance value is a control parameter that can be modified, but the resonant capacitance must remain the same. With the capacitance value obtained in the first iteration, and using an iterative process, the new values for the inductance and operating frequencies, f_s, for the other lamps are also calculated. This procedure is carried out until all the lamps are analysed. During the design procedure it must be ensured that the obtained frequencies are in an acceptable working range, normally between 45kHz and 100kHz. If not, the procedure should be repeated.

For example, choosing the 58W lamp as the reference lamp, the normalized load and the base impedance are calculated using the nominal lamp characteristics presented in Table 3.11. If this is the first iteration, the operating frequency must be selected, for instance at 100kHz. The values for, L_{ac} and C_p are then calculated, resulting in 0.37mH and 6.4nF respectively. The closest available commercial value for this capacitor is 6.8nF. Maintaining this value for the next iterations with the remaining lamps, the process is repeated. The normalized load and base impedance are calculated and finally the resonance frequency and the inductance value for each lamp are also determined. For this design procedure the ballast input dc voltage was set at V_{dc}=310V and the calculated values for each lamp are shown in Table 3.12.

In conclusion, the range of operating frequencies is established between 62kHz and 100kHz and C_p is set at 6.8nF. In order to implement the prototype it is also necessary to design and implement a magnetic regulator with a variable inductance range between 1mH and at least 0.3mH.

Table 3.12 Operating frequency and resonant circuit parameters for each lamp

FLUORESCENT LAMP	L_{ac} [mH]	f_s [kHz]	C_p [nF]
TLD 15W Philips	0.96	62	6.8
TLD 18W Philips	0.96	62	6.8
TLD 30W Philips	0.96	62	6.8
TLD 36W Philips	0.58	80	6.8
TLD 58W Philips	0.37	100	6.8

3.5.3 PROTOTYPE IMPLEMENTATION

3.5.3.1 VARIABLE INDUCTOR CHARACTERIZATION AND CONTROL

For this first universal ballast prototype, the variable inductor was implemented using a double E gapped core as shown in Fig. 3.69a. As usual, two dc control windings, with the same number of turns N_{dc}, were mounted in the lateral legs of the core. The main winding, with N_{ac} turns, corresponding to the ac resonant inductor, L_{ac}, was calculated in order to have the required variable inductance range. The regulator project was done considering that it should have an inductance variation between 1mH and 0.25mH. The prototype was built using an EF25 core with 3C85 material from Phillips. According to the design procedure, the calculated parameters were $N_{dc} = 35$ and $N_{ac} = 68$. An airgap of 0.3mm was used. Fig. 3.69b. shows two photographs of the implemented prototype.

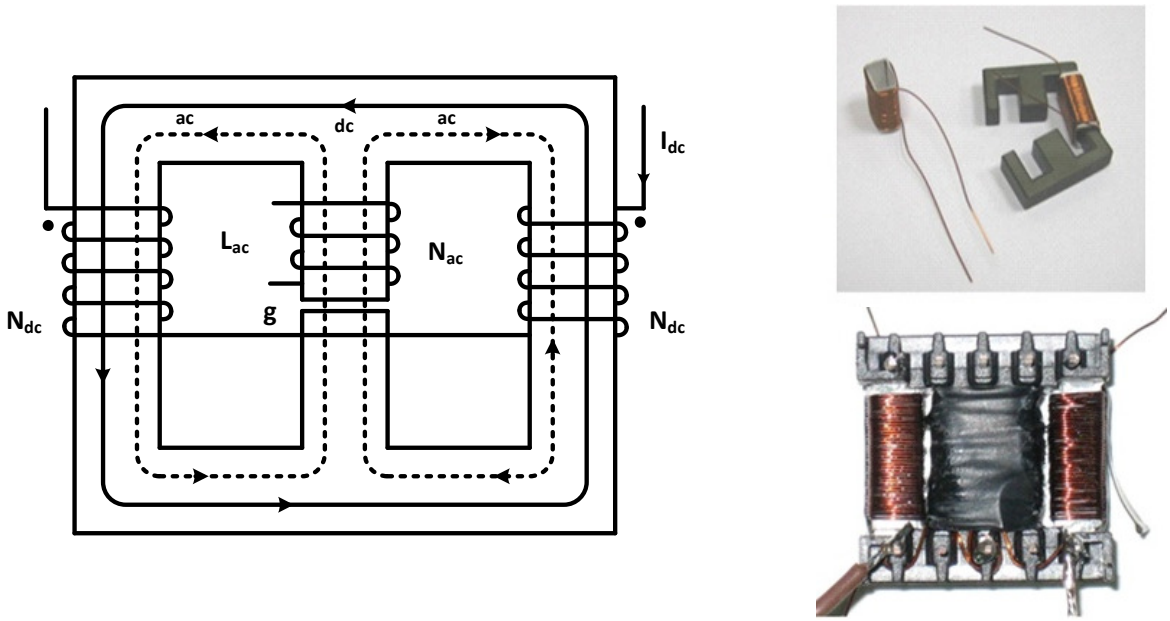

a. Schematic

b. Gapped core, control windings and final prototype

Fig. 3.69. Variable inductor.

The characterization of the magnetic regulator was done using a variable dc source and an impedance analyzer, HP4284A, as previously represented in Fig. 3.27. Each level of dc voltage corresponds to a different level of dc current in the control winding, which gives a specific inductance value. Table 3.13 presents the obtained values for the dc control current and inductance, considering a current variation of 0 to 1.2 A. In order to evaluate the power handled

by the control windings at each dc current level, the measurement of its voltage, $V_{control}$, and resistance, $R_{control}$, was also done. The collected values are also presented in Table 3.13.

It must be noted that the measurements shown in Table 3.9 were taken under small-signal conditions for the ac winding. However, in normal operation, as a part of the electronic ballast resonant circuit, the variable inductor will be operating with larger current values, that will lead to changes in the inductance value [3.22].

Table 3.13 Variable inductor characteristics.

I_{dc} [A]	$V_{control}$ [V]	$R_{control}$ [Ω]	$P_{control}$ [W]	L_{ac} [mH]
0.00	0.00	-	0	0.932
0.20	0.10	0.50	0.02	0.882
0.40	0.20	0.50	0.08	0.745
0.50	0.25	0.50	0.125	0.643
0.60	0.31	0.52	0.186	0.551
0.80	0.42	0.53	0.336	0.418
1.00	0.54	0.54	0.54	0.329
1.10	0.59	0.54	0.649	0.289
1.20	0.66	0.55	0.792	0.259

The small-signal characteristic of the variable inductor is presented in Fig. 3.70a. As expected the inductance variation is within the defined limits. The maximum inductance value is obtained for a zero level of dc current, and the minimum value for 1.2A. Fig. 3.70b. presents the power handled by the control windings as a function of the dc control current. Maximum power losses were attained at 1.2A, but these losses were below 1W.

In these universal ballasts, the variable inductor must be controlled by a separate converter. The challenge was at first, what option to consider for the small dc-dc converter needed for providing the dc current. In this first prototype, the control windings are supplied by an isolated dc-dc converter, a forward converter, directly supplied by the ballast dc voltage. It should be noted that this converter will only handle the control windings power, and that ideally the associated power losses should be null. In fact, from the analysis of Table 3.13, it is observed that very low power levels are managed by the control windings. As recalled, these power losses do

not exceed 1W. Consequently, it is expected that they will not have a significant impact on the efficiency of the entire ballast circuit.

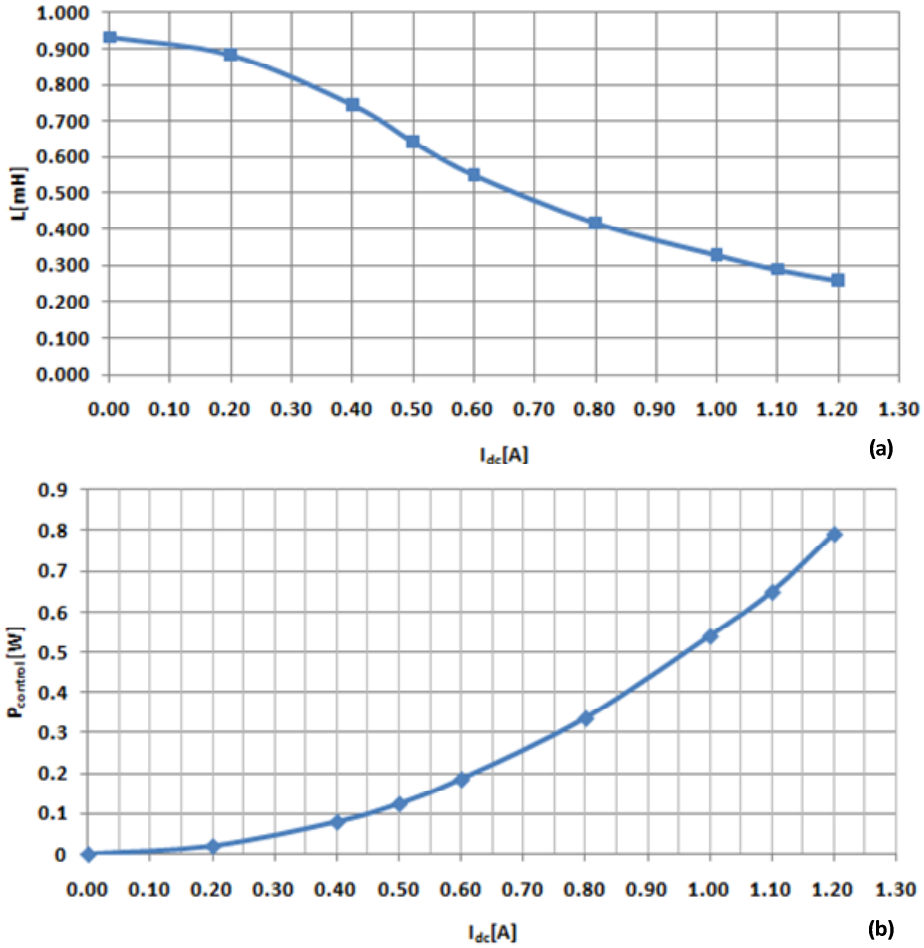

a. Experimental value of the inductance as a function of the dc control current

b. Power handled by the control winding as a function of the dc control current

Fig. 3.70. Variable inductor characterization.

As shown in Fig. 3.71, a forward converter was selected for supplying the dc control current. The forward converter will be operated in continuous current mode, [3.51]. The turns ratio N_d/N_p limits the peak voltage seen by the switch M_3. With an equal number of turns for the primary and the demagnetizing windings, $N_p = N_d$, the maximum duty-ratio is limited to 0.5. Under this condition the switch must block $2V_{dc}$ during turn-off. After taking into account switching delays, this duty-ratio falls to 0.45. The design of the forward converter was done considering that it should have the following specifications: $V_{dc} = 310\text{V}$, $D = 0.3$, $I_{dc} = 1.5\text{A}$. The relation between the windings, N_d/N_p, was calculated to be approximately 0.017.

The LC filter is typically calculated in order to ensure a very low ripple in the output current. This may be achieved using high values for both the inductor and the capacitor, and by operating the forward converter in closed loop, trough the regulation of the dc output current. In this prototype an inductance of 200μH and a capacitor of 220μF have been used and a current ripple lower than 20mA was attained. The design parameters are presented in Table 3.14.

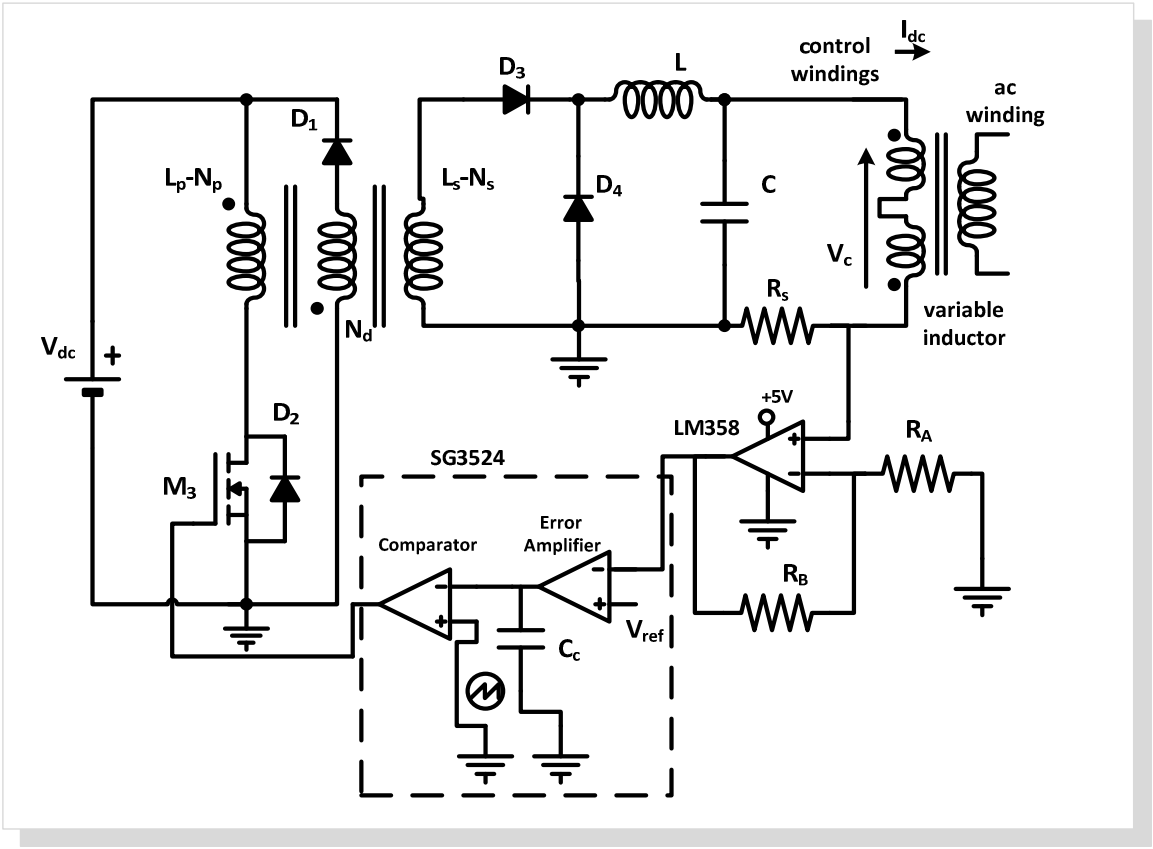

Fig. 3.71. Forward converter used for supplying the dc control current to the variable inductor.

Table 3.14 Design parameters of the forward converter.

$N_p;\ N_d$	N_s	L	C	$D_1;\ D_4$	D_3
160	3	200μH	220μF	MUR180	11DQ10
R_s	M_3	R_A	R_B	C_c	IC
0.5Ω	IRF840	10kΩ	10kΩ	820nF	LM358 SG3524

The output of the forward converter is regulated by means of a feedback control, which employs a PWM controller, the SG3524. This type of control, allows adjusting the output current, giving an adequate value for the control of the variable inductor, according to the working

parameters imposed by each lamp. Fig. 3.71 shows that the output dc current of the converter is sensed, through $R_{S,}$ and then amplified, using the LM358 operational amplifier. This output signal is fed to the transconductance error amplifier of the SG3524. Theoretically, a transconductance amplifier is an equivalent voltage-controlled current source. It multiplies the difference of the input voltages by a certain gain and generates a current into the output node. So, this error amplifier produces an error feedback signal which is proportional to the difference between the reference input voltage and the output voltage of the LM358 operational amplifier. Its compensation network was chosen to be a shunt capacitor, acting as an integrator, since there is no need of a fast response. Finally, the sawtooth waveform is compared with the error amplifier output in an internal comparator at the selected switching frequency, to determine the duty-cycle of the switch M_3.

3.5.3.2 GENERAL OPERATING ISSUES

Previous to the description of the implemented prototype, it is relevant to discuss some of the general operating issues. As mentioned, all the following requirements must be fulfilled: the lamp must be ignited properly; the lamp operation must be stable at steady state; the lamp must be operated as close to its rated power as possible, and the ballast efficiency with each lamp should be as high as possible. The design procedure guarantees, from the start, that each lamp is properly ignited and operated at rated power. Soft-starting concerns can be overcome by using the common technique for electrodes pre-heating: the pre-heating process may be guaranteed by means of a frequency-controlled soft-start technique or, as already described, a soft-starting process using the variable inductance itself, may be used.

Another important issue is related to the power control of the electronic ballast: At first, it implies the study of the phase angle of the input current of the resonant circuit for each case. If a delayed current is enforced, it is possible to achieve ZVS in the bridge MOSFETs. Therefore, this analysis must also be done. In addition, this phase analysis is important to ensure near-resonance conditions.

Other concerns are related to the lamp identification. After ignition, the lamp voltage typically falls to a lower operating voltage. If the lamp is not dimmed, this lamp voltage will remain more or less constant under steady state conditions. In [2.53], a comparison of lamp characteristics of major brand names is presented. It is stated that for all popular standard T8 fluorescent lamps, with the same rated power, the lamp voltage as well as lamp currents, are almost identical. Yet,

for Philips' lamps of 18W and 30W, the lamp current is the same, so they cannot be differentiated by means of current sensors. Similar current values also occur for 58W and 70W lamps from GEC and Thorn, which leads to the same conclusion. The same does not happen to the lamp voltage. It is demonstrated that for T8 lamps, the largest voltage variance among different manufacturers is below 3.5%, which represents a theoretical acceptable tolerance. Similar observations apply to tubular lamps of equal diameter. So, different power or types of fluorescent lamps are distinguished by the detection of the lamp voltage through a voltage sensor.

Table 3.15 shows the electrical characteristics for the selected fluorescent lamps from two main manufacturers, Philips and Osram. From Table 3.15, it is clear that the lamp voltage increases with the lamp power. Therefore the lamp voltage can be used to identify the rated power of the lamp connected to the ballast. In order to achieve this recognition, different voltage regions have been defined for each lamp, as illustrated by the dashed lines depicted in Fig. 3.72. For example, if the lamp voltage is measured to be between 77.0V and 99.5V, it will be assumed that the lamp connected to the ballast is the 30W lamp. In a future arrangement, a microcontroller is used to detect the lamp voltage and command the ballast to supply each lamp according to its rated power.

Table 3.15 T8 Lamp voltage and current for two main manufacturers

LAMP POWER T8	PHILIPS (TLD)		OSRAM	
	V_{lamp} [V]	I_{lamp} [mA]	V_{lamp} [V]	I_{lamp} [mA]
15W	51	0.34	55	0.33
18W	59	0.34	57	0.37
30W	96	0.37	96	0.36
36W	103	0.44	103	0.43
58W	111	0.68	110	0.67

Electrical specifications defined for operation at 50/60 Hz

For T8 fluorescent lamps this method is considered to be quite simple and of easy implementation. However, for other lamp types, some lamp voltages are similar, and the method may lead to a wrong recognition of the lamp. In order to overcome this drawback, another method that enables the ballast to determine the power rating of the connected lamp and drive the lamp with proper operating frequency was proposed [3.47]. This method avoids the mismatch due to lamp voltage overlapping [3.47]. It presents an automatic lamp detection using lamp power

regulation and frequency detection. To ensure that the lamp is recognized correctly, a possibility weight distribution is used. An algorithm is then applied to regulate the power and define the appropriate switching frequency. However, the values of frequency versus lamp power are highly dependent on the resonant components and their deviations. This makes the controller regulate the lamp output power through the operating frequency, which may also result in wrong lamp recognition. In [3.48], the operating frequency and phase shift compensation are used in order to overcome the eventual deviation of the resonant filter components.

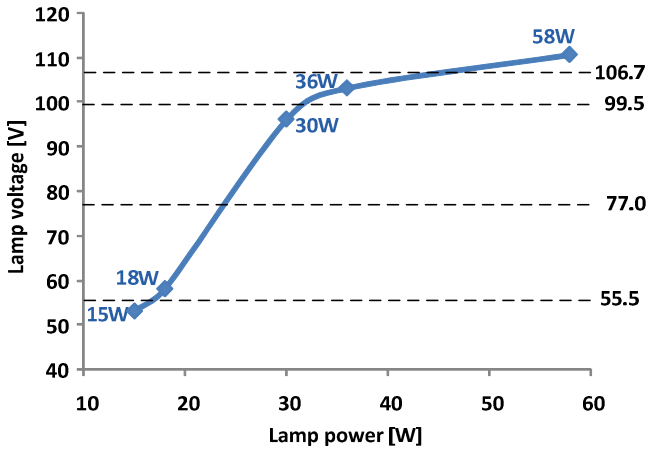

Fig. 3.72. Lamp voltage versus lamp power for lamp detection purpose.

In [3.49], another algorithm for lamp detection and operation for T5, T8 and T12 fluorescent lamps is proposed. A fuzzy logic controller analyses the heated lamp electrodes, the lamp voltage and the lamp current. Then, a classification system is generated that maps the lamp characteristics into distinct groups in order to automatically detect each lamp. At the present time this method seems to be the best alternative for the identification of different lamp ratings jointly with different lamp types. Nonetheless, the main purpose of this work is not the implementation of a lamp recognition method. The key concern was to guarantee proper lamp ignition and operation for all considered lamps. Lamp detection is however a subject which must be addressed in a posterior phase of the ballast optimization.

3.5.3.3 EXPERIMENTAL RESULTS

The electronic ballast prototype was implemented as shown in Fig. 3.73. The adopted starting procedure may be easily described as follows. Initially, the operating frequency of the inverter is set at a predetermined value in order to ignite all lamps without causing electrode damage, and to allow lamp recognition. Then, the dc control current is adjusted in order to get the maximum inductance value. Afterwards, the value of the inductance is lowered, by increasing the dc control

current, until the lamp is ignited. After the lamp identification, the frequency is finally adjusted in order to get near-resonance working conditions and stable operation. This implies setting the ballast parameters according to the design procedure. The implementation of the lamp detection and control circuit implies that after the lamp recognition, the inverter frequency and inductance values are delivered as outputs. For instance, as represented in Fig. 3.73, the detection algorithm must give the adequate value for the reference voltage in order to supply the correct dc control current, to obtain the right inductance value for the resonant circuit.

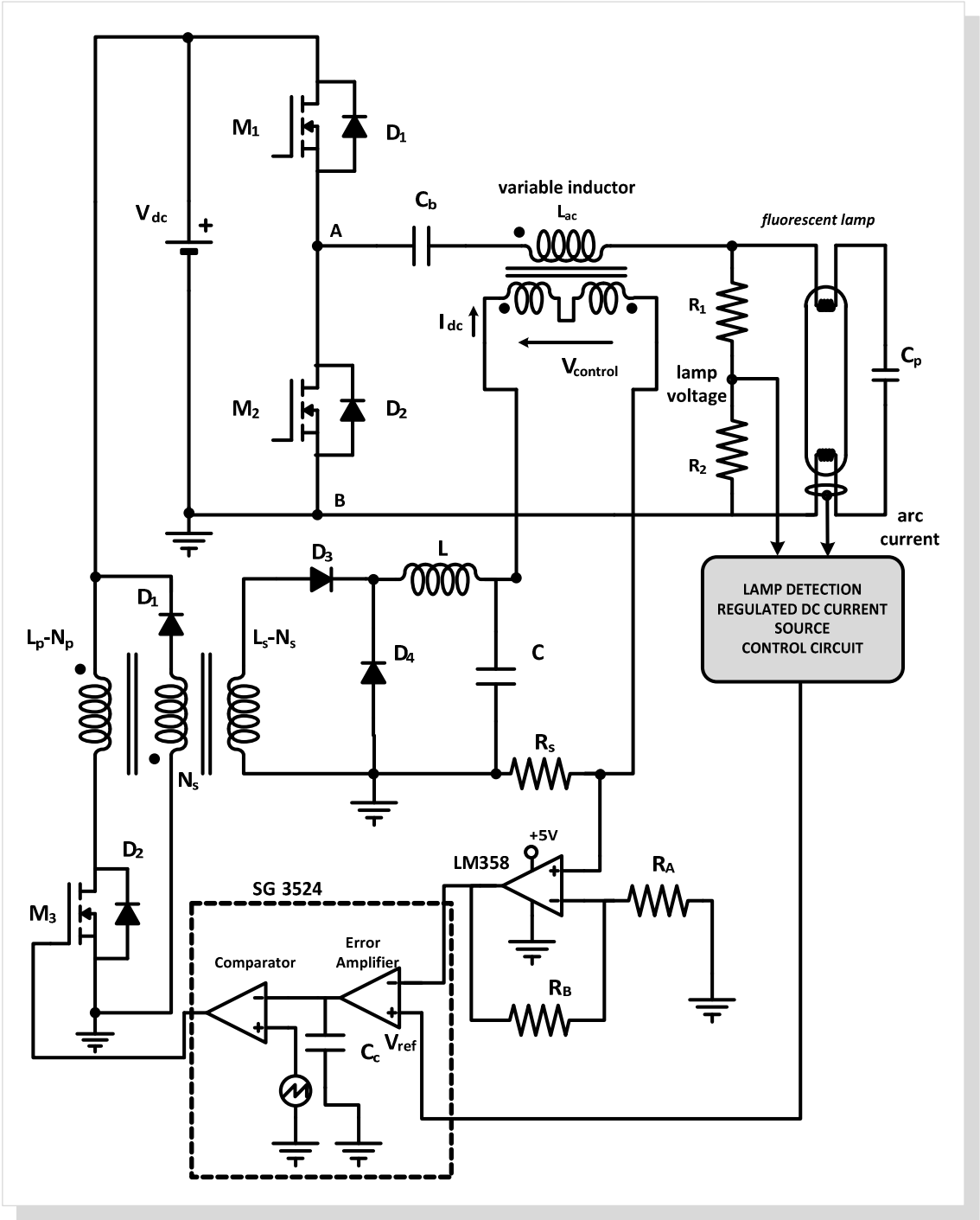

Fig. 3.73. Universal ballast prototype.

Fig. 3.74, Fig. 3.75 and Fig. 3.76 show the obtained experimental results for the laboratory prototype, for three different fluorescent lamps, respectively, 18W, 36W and 58W. Fig. 3.74a., Fig. 3.75a. and Fig. 3.76a., present the resonant current and lamp voltage waveforms for each lamp. Fig. 3.74b., Fig. 3.75b. and Fig. 3.76b., present the waveforms of the inverter output voltage and the input resonant current for each lamp. This resonant current is also defined as lamp current.

As an initial analysis, stable operation for each lamp can be recognized from Fig. 3.74a., Fig. 3.75a. and Fig. 3.76a. This was the main purpose for this ballast prototype. For the 18W lamp the forward converter was off, since the necessary inductance value should be at its maximum. For the 58W lamp some distortion can be observed in the resonant current, nevertheless, this did not result in any working instability. The upper traces in Fig. 3.74a., Fig. 3.75a. and Fig. 3.76a. correspond to the product of the lamp voltage waveform and the resonant current waveform; in fact these upper traces represent the instantaneous lamp power. Similarly for Fig. 3.74b., In Fig. 3.75b. and Fig. 3.76b., the upper traces correspond to the instantaneous power delivered by the inverter.

Similarly to the previous dimmable ballast prototypes, there are several important issues which deal with the power control of the electronic ballast. This implies the study of the phase angle of the input current of the resonant tank for each case. Therefore, the phase angle of the input resonant tank current must be verified. Besides, this phase analysis is important to ensure near-resonance conditions. This first prototype works in open loop, which means that after the detection of the lamp power and setting of the lamp working parameters, the phase angle of the input resonant tank current is not verified by the system. Therefore only experimental verification was performed. From the analysis of Fig. 3.74b., In Fig. 3.75b. and Fig. 3.76b., which present the waveforms of the inverter output voltage and the input resonant tank current for all three lamps, it can be observed that the current lags the voltage, thus ensuring ZVS in the bridge transistors. Once the inductance was adjusted for each lamp, there was no control loop to assure near-resonance operation. This mode of operation is similar to the one found in typical commercial ballasts where usually there is no phase detection to adjust the operation point. The inclusion of phase detection in this prototype is also possible but it would increase the cost and complicate the system. Experimental work has shown that there is no excessive variation of inductance in the variable inductor provided that the dc current is regulated.

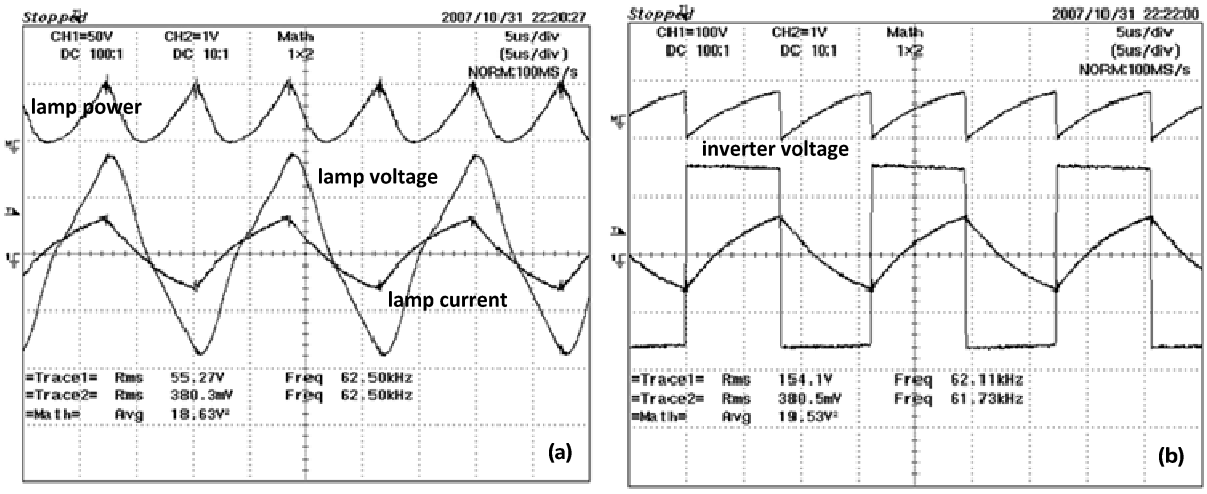

a. Waveforms of the lamp voltage and resonant current (50V/div, 1A/div, 5μs/div)

b. Waveforms of the inverter output voltage and resonant current (100V/div, 1A/div, 5μs/div)

Fig. 3.74. Experimental results for the TLD 18W.

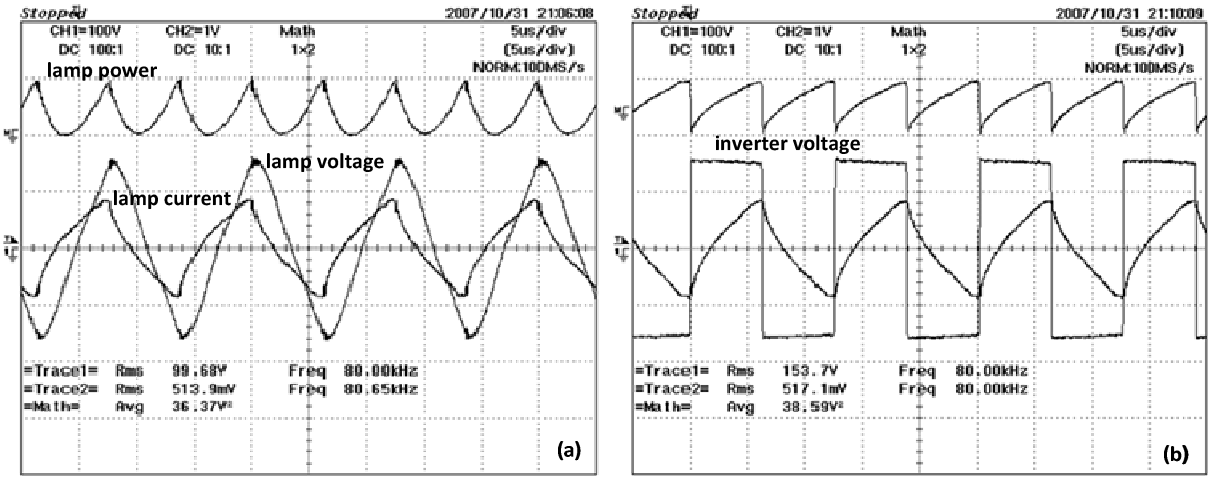

a. Waveforms of the lamp voltage and resonant current (100V/div, 1A/div, 5μs/div)

b. Waveforms of the inverter output voltage and resonant current (100V/div, 1A/div, 5μs/div)

Fig. 3.75. Experimental results for the TLD 36W.

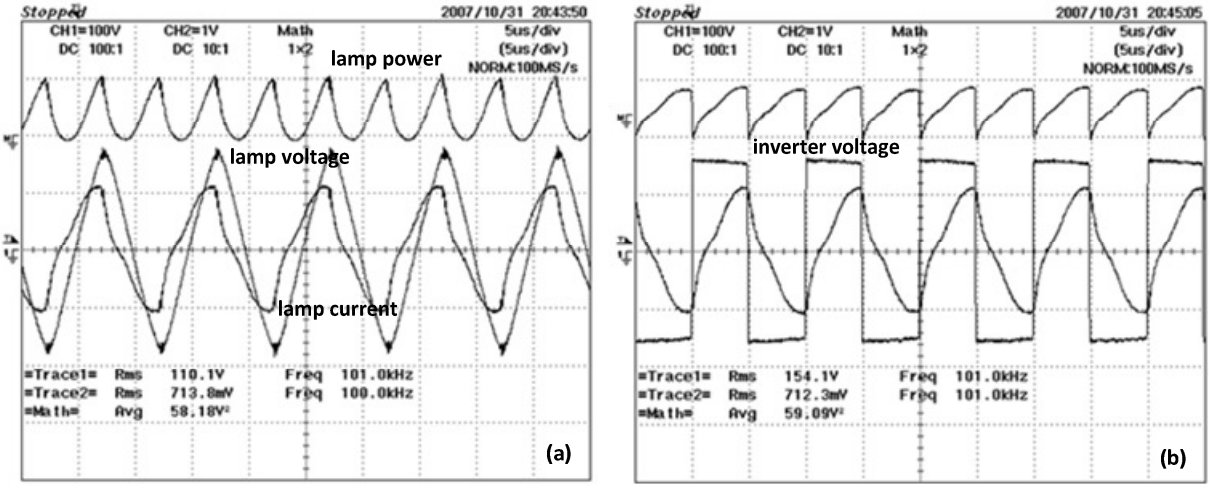

a. Waveforms of the lamp voltage and resonant current (50V/div, 1A/div, 5μs/div)

b. Waveforms of the inverter output voltage and resonant current (100V/div, 1A/div, 5μs/div)

Fig. 3.76. Experimental results for the TLD 58W.

Another issue is the analysis of the overall efficiency. The measurements performed were the lamp power, which means arc power plus electrode power; the ballast input power and the dc value of the control current. These measurements are presented in Fig. 3.77a. A graphical view of the experimental results, is also presented in Fig. 3.77a. The joint table shows the dc current level in the control winding for each lamp. The obtained current levels comply with the estimated working parameters in terms of inductance value, guaranteeing near resonance working conditions for each lamp. The obtained operating frequencies agreed with the calculated values.

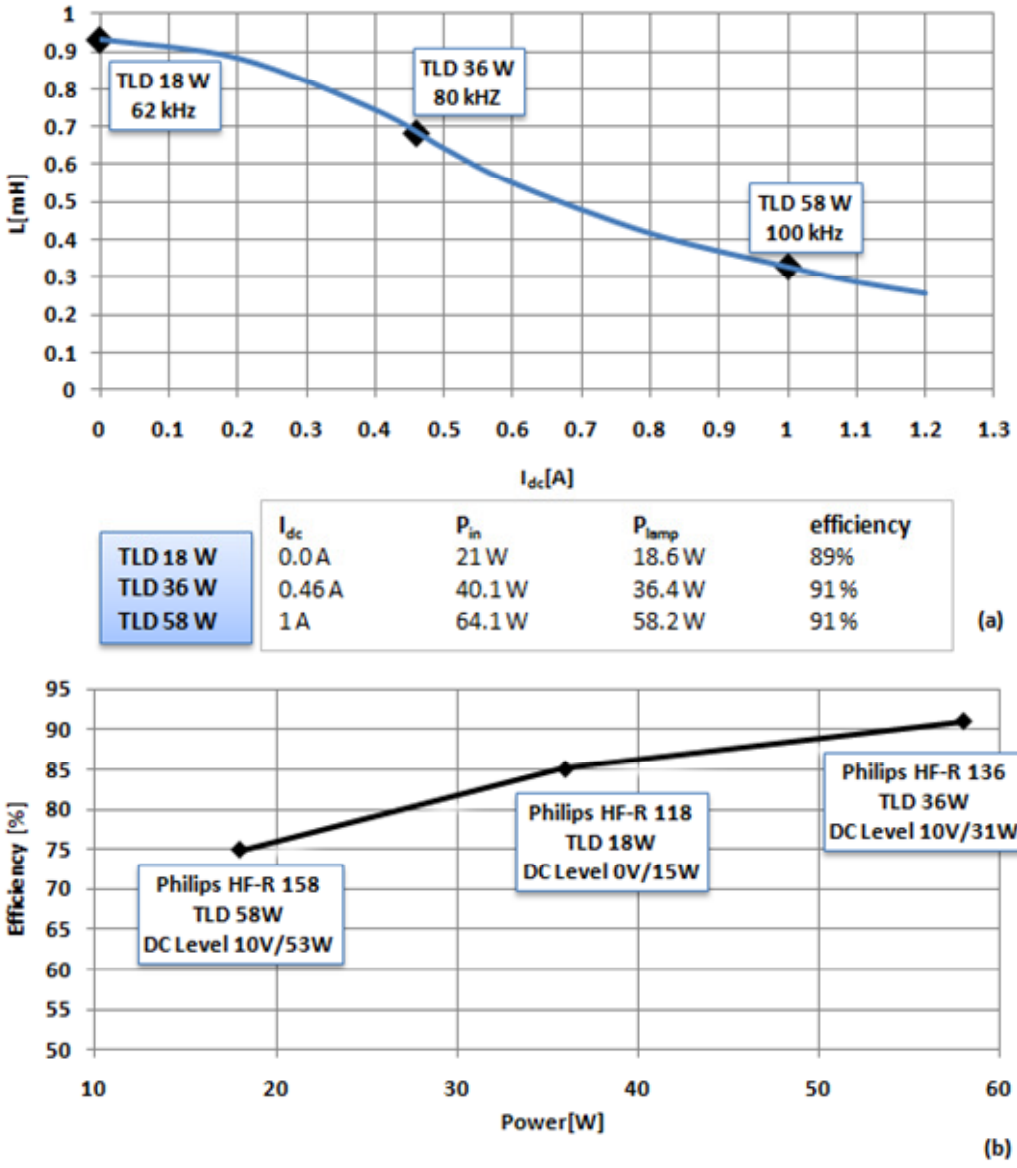

a. Universal ballast: nominal operating points for three lamps, in terms of inductance value, control current, lamp power, ballast input power and overall efficiency

b. Philips HF-R 118/136/158 commercial ballasts: efficiency and lamp power

Fig. 3.77. Experimental results for the universal ballast vs. commercial ballasts.

The ballast efficiency, calculated as the ratio between the lamp power and the input power is also shown in Fig. 3.77a. It is noted that this measured input power includes also the power absorbed by the forward converter. From the analysis of the obtained values, it can be concluded that high efficiency is guaranteed with this technique. However it is considered pertinent to perform a comparison between the prototype results and the ones collected from three commercial electronic ballasts from Philips. The efficiency of the commercial ballasts is presented in Fig. 3.77b. A known technique in commercial ballasts is to operate the lamp at a lower level than its rated power, since at high-frequencies a 10% higher luminous flux level is expected. Nevertheless, for the 18W lamp the efficiency is below 80%. Comparing all the collected data, it can be observed that the efficiency of the proposed magnetic control solution is close to 90% for all fluorescent lamps. Nevertheless, it must be taken into account that the commercial ballast includes the PFC stage, which contributes to the lowering of the efficiency.

As a conclusion, the proposed magnetically-controlled universal ballast can successfully supply T8 fluorescent lamps ranging from 18W to 58W close to their nominal power maintaining very good efficiency. However, in future work, the PFC stage should be included in the topology in order to evaluate its impact in the global efficiency of the ballast.

3.5.4 PROTOTYPE IMPLEMENTATION WITH DIGITAL CONTROL

Digital control based on low-cost microcontrollers can be used in this type of ballasts without an excessive cost penalty, and that will provide robust, flexible and reliable universal ballasts. In fact, nowadays, it is almost mandatory the use of digital control to perform all the tasks requested by this type of electronic ballasts. In this particular application, this includes the control of both the half-bridge inverter used to supply the lamps and the forward converter which drives the magnetic regulator. The main control parameters remain the same: the switching frequency and the variable inductance. In the following description the emphasis will be put on the control of the half-bridge inverter and on the universal ballast lamp control.

3.5.4.1 GENERAL DESCRIPTION

Fig. 3.78 shows the proposed schematic of the magnetically-controlled universal ballast with digital control. In order to provide the necessary control capability a PSoC CY8C29466 digital control circuit from Cypress was used. This circuit incorporates both analog and digital modules along with a microprocessor and therefore most of additional peripheral units, such as operational

and instrument amplifiers, filters, timers, digital logic circuits, analog-to-digital (A/D) and digital-to-analog (D/A) converters that would be necessary when using traditional microcontrollers can be eventually avoided. As a general rule, implementation of extra peripherals brings in additional difficulties, for instance in terms of space or increased power consumption. All of these factors can significantly affect the ballast project.

As illustrated in Fig. 3.78, the μC will drive both the half-bridge inverter and the forward converter via the pulse width modulation signals, PWM1 and PWM2. In this case, the forward converter will be operated under closed-loop control, so that the dc current at its output can be maintained constant independently of the dc voltage source changes. This closed loop operation of the forward converter is incorporated in the μC, using an A/D converter and a digital regulator which are implemented in the microprocessor circuit.

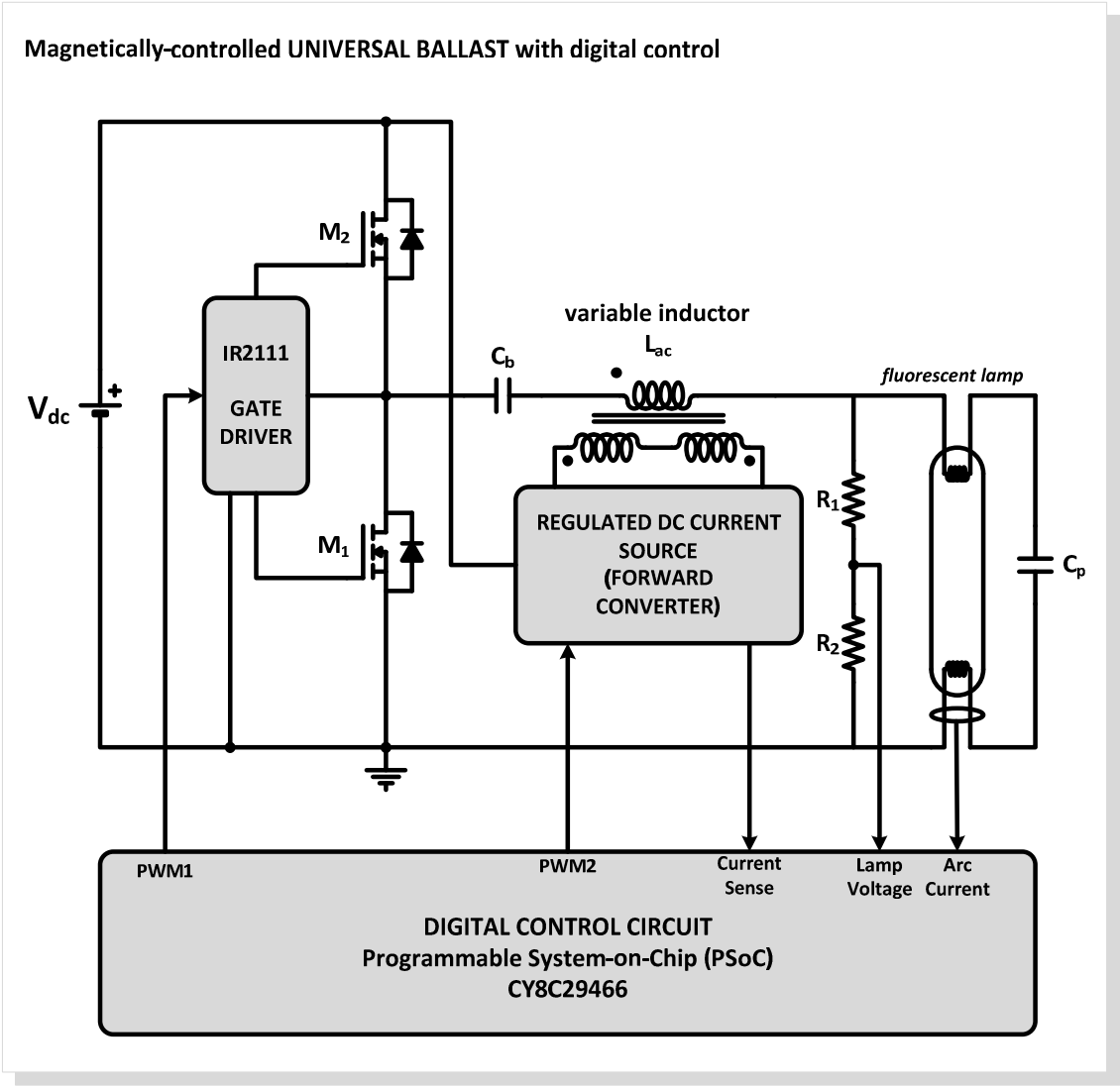

Fig. 3.78. Magnetically-controlled universal ballast with digital control: circuit schematic.

So, the basic idea proposed in this universal ballast is that the lamp power rating will be detected by measuring some of the lamp electrical parameters, voltage, current or power. Specifically, in order to detect the lamp type and to provide lamp power regulation, lamp voltage and current are measured by using two A/D converters provided by the μC. Then, both switching frequency and inductance will be changed so that the operation is adjusted close to the $L_{ac}C_p$ circuit resonant frequency.

It is recalled that the reactive energy handled by the inverter will be lower if the operation is close to the resonant frequency. Therefore, the rms value of the resonant current for a given output power will also be lower, thus providing higher efficiency. On the other hand, in order to attain a stable operation, it is important to have an open-circuit voltage at the operating point sufficiently high to adapt to the lamp voltage and its possible perturbations. If the lamp voltage becomes higher than the resonant circuit output voltage, the arc will extinguish. The maximum open-circuit voltage of the resonant circuit is obtained by operating the inverter at the natural resonant frequency. Thus, it is concluded that the operation close to the natural resonant frequency will provide a better compromise between efficiency and stability.

3.5.4.2 ELECTRONIC BALLAST EXPERIMENTAL PROTOTYPE

Fig. 3.79a. illustrates the schematic diagram of the inverter stage, including the control circuitry implemented by means of the CY8C29466.

A dual 8-bit A/D converter was used for the lamp voltage and current measurements. The lamp voltage and arc current were used in the CPU program in order to perform the lamp ignition, lamp detection and lamp current regulation. The dual A/D converter operates with an internal clock (VC2) at 375kHz and the sampling time was adjusted to 3ms, which gives a sampling frequency of 333Hz. Fig. 3.79b. shows the loop gain diagram of the inverter stage.

The VCO was implemented using a digital PWM module inside the CY8C29466, which operates with an internal clock (VC1) running at 6MHz. The switching period is obtained from an 8-bit digital value, X, as $T = X/6\mu s$. The average resolution to control the switching frequency with this VCO is about 1kHz per bit.

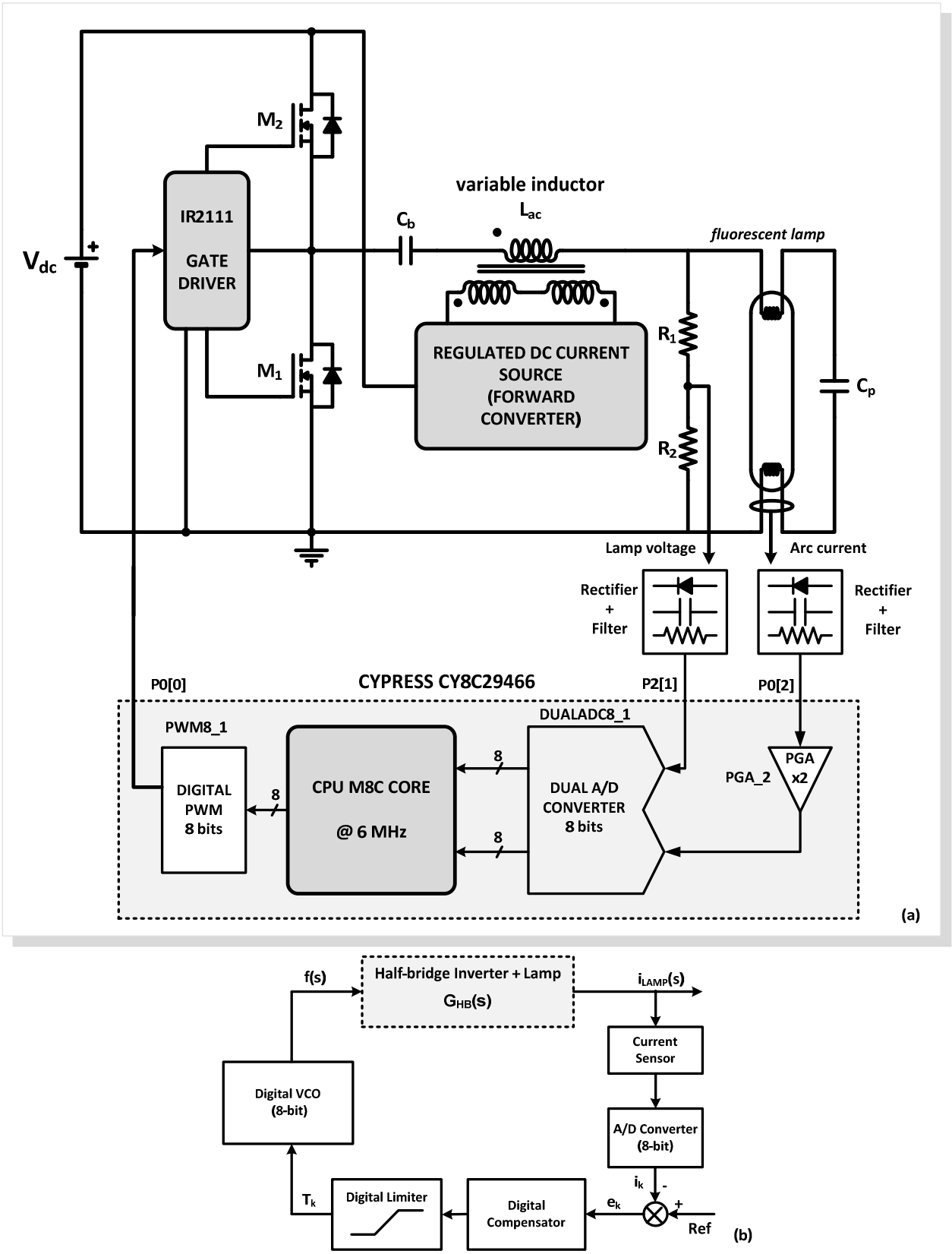

a. Circuit schematic b. Loop gain diagram

Fig. 3.79. Magnetically-controlled universal ballast with digital control: circuit schematic.

In some dc-supplied applications, such as indoor lighting in transportation (trains, undergrounds, buses, etc.), electronic ballasts are supplied from a non-regulated dc input voltage, with $\pm 20\%$ voltage excursions. Therefore, it was considered important to implement a lamp power regulation strategy that could also assure the maximum lamp life. In other cases, when the ballast is supplied from an ac line, the lamp power regulation can be used to simplify the input power factor correction (PFC) stage by relaxing the output voltage constrains for this stage.

Closed loop operation of the ballast is also essential to compensate changes in other parameters such as lamp impedance, clock frequency, resonant elements, etc. Therefore, in order to control the lamp current in closed-loop operation for the different lamps, a non-linear compensator was employed. The digital compensator implements the following algorithm:

$$T_k = T_{k-1} + sign(e_{k-1}) \tag{3.149}$$

where T_k represents the period of the inverter switching frequency in each iteration.

The operating frequency was always maintained above the resonant frequency of the resonant circuit, thus ensuring ZVS operation. In this way, and due to the behaviour of the resonant circuit, a decrease of the switching period will provide a decrease of the lamp current, and conversely, an increase of the switching period will generate an increase of the lamp current. Therefore, as can be inferred from (3.149), if for any reason the lamp current tends to decrease below the reference level, the calculated error will be positive and the switching period is increased continuously, one bit in each iteration, so that the lamp current will tend to increase due to the behaviour of the resonant tank. The opposite action is taken when the lamp increases above the reference level; then, the error is negative and the switching period is continuously decreased to reduce the lamp current.

The switching frequency range was limited digitally to ± 20% around the nominal point, so that the operation above resonant frequency was guaranteed. Laboratory tests showed that this frequency range was sufficient to compensate bus voltage variations from 250 to 350 V, which is sufficiently wide for this type of applications. The proposed compensator was tested with the same lamps ranging from 15W to 58W, and has always obtained good static and dynamic results, which will be proved through experimental data.

3.5.4.3 FORWARD CONVERTER

The schematic diagram of the forward converter including the control circuitry located inside the μC is shown in Fig. 3.80. In order to perform an accurate control of the dc current supplied to the variable inductor control windings, the forward converter is operated in closed loop. It is noticed the low external component count which is due to the use of this type of microcontrollers. The dc output current is measured by means of a series resistor, then amplified using a programmable gain amplifier (PGA), and finally quantified by using an 8-bit delta-sigma analog-to-digital (A/D) converter. A regulator is implemented by programming the CPU of the μC, which finally generates the 8-bit input to the digital PWM (DPWM) generator. The output of the DPWM generator is then used to command the power switch through a simple gate driver in order to regulate the output current. As previously referred, in order to minimize volume and cost, the selected switching frequency was 100 kHz. The inductance and capacitance have been selected to be high enough to assure a very low ripple on the dc output current. Otherwise, the current ripple superposed to the dc level would introduce a modulation in the inductance value and, as a consequence, in the lamp current and power [3.44], [3.45].

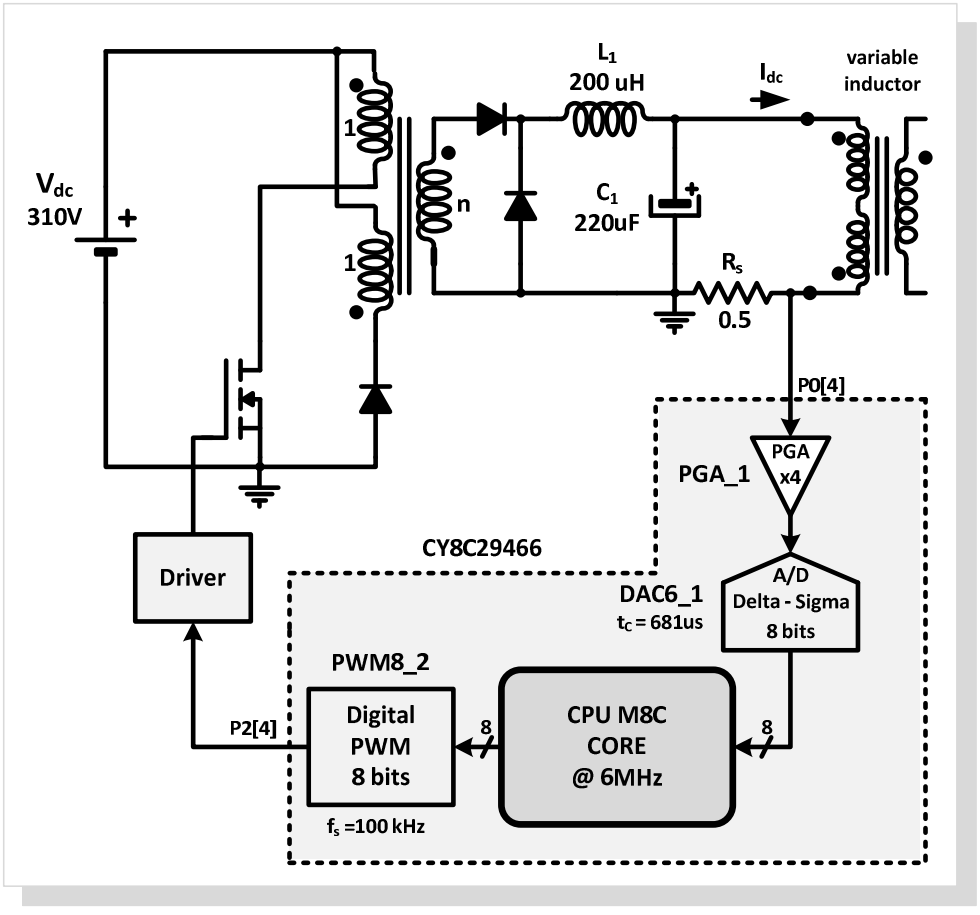

Fig. 3.80. Forward converter: circuit schematic.

3.5.4.4 CONTROL ALGORITHM

Fig. 3.81 illustrates the basic flowchart of the proposed control algorithm. This algorithm may be described as follows: once the system has been initialized, the inductance is set to its maximum value. This value is used to ignite all the lamps connected to the ballast. The operating frequency is initially set at a known value, around 62.5kHz. Specifically, in order to provide lamp electrode heating and soft-start, a decreasing frequency ramp is carried out, starting from 100kHz down to 62.5kHz, at which the lamp should be started. The lamp current is then measured to ensure that the lamp has been ignited properly. Afterwards, a waiting period of 30 seconds is initiated in order to give the lamp time to reach the voltage and current steady-state values. This 30 seconds time interval is long enough to provide a correct warming-up phase for all the TLD lamps. For other lamp types the waiting period should be determined experimentally or set according to data provided by manufacturers. Once the lamp is stabilized, its voltage is measured and the lamp power rating is detected, as shown in previous sections. A look-up table is used to select the correct circuit parameters, resonant inductance and switching frequency for the detected lamp. Then, both the switching frequency and inductance are adjusted. Finally, the algorithm for the closed-loop operation is initiated to compensate the arc current variations.

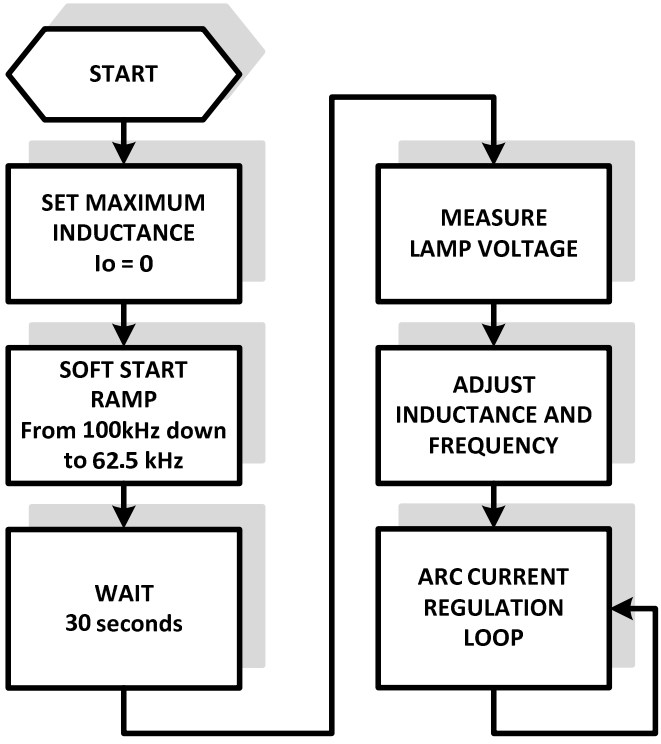

Fig. 3.81. Flowchart of the proposed control algorithm.

3.5.4.5 EXPERIMENTAL RESULTS

Several experiments were carried out in the laboratory in order to evaluate the behaviour of the proposed ballast. In regard to the lamp operation, Fig. 3.82a., Fig. 3.83a. and Fig. 3.84a. show the lamp arc current, lamp voltage and lamp power waveforms for three lamps, 18 W, 36 W and 58 W. Each lamp was operated with its corresponding switching frequency and inductance value. It is also possible to observe that the nominal lamp power was achieved by each lamp. Fig. 3.82b., Fig. 3.83b. and Fig. 3.84b. show the output inverter voltage, after the dc-blocking capacitor and resonant current waveforms. As can be seen, stable waveforms were obtained and ZVS operation was present in all cases.

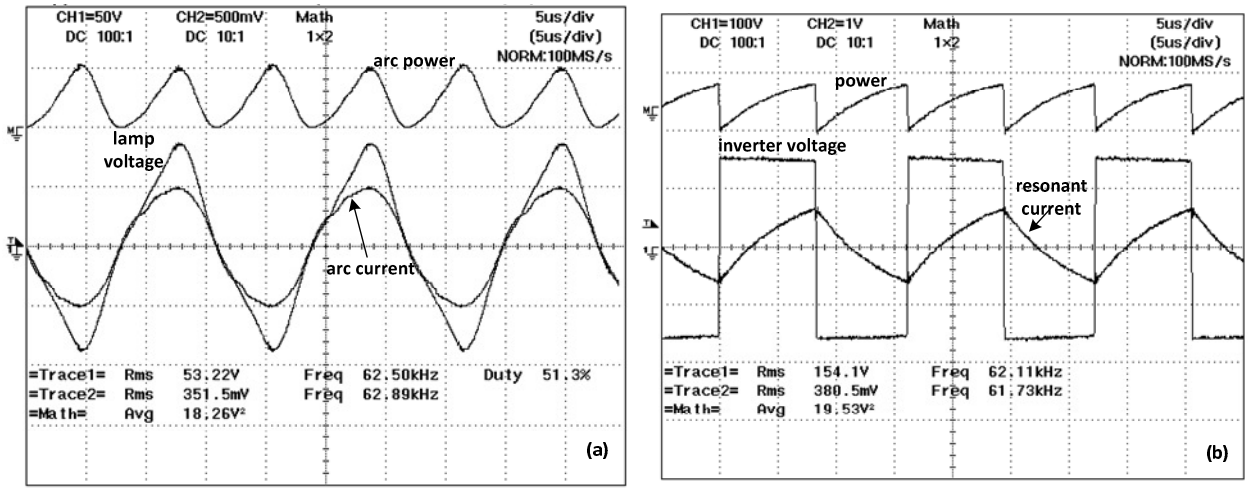

a. Waveforms of the lamp voltage and arc current at rated power (50V/div, 0.5A/div, 5µs/div)

b. Waveforms of the inverter output voltage and resonant current (100V/div, 1A/div, 5µs/div)

Fig. 3.82. Experimental results for the TLD 18W.

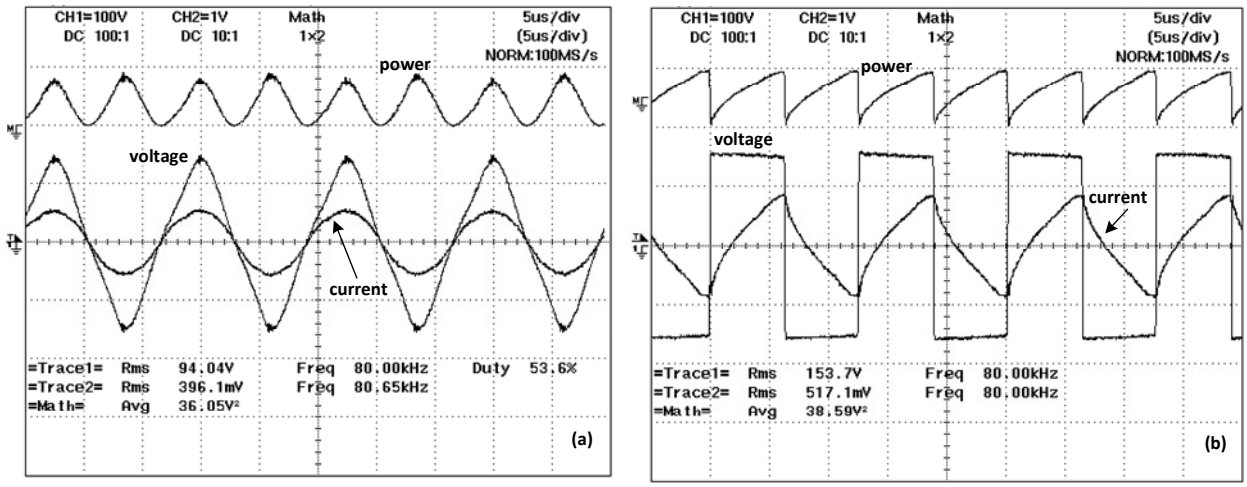

a. Waveforms of the lamp voltage and arc current (100V/div, 1A/div, 5µs/div)

b. Waveforms of the inverter output voltage and resonant current (100V/div, 1A/div, 5µs/div)

Fig. 3.83. Experimental results for the TLD 36W.

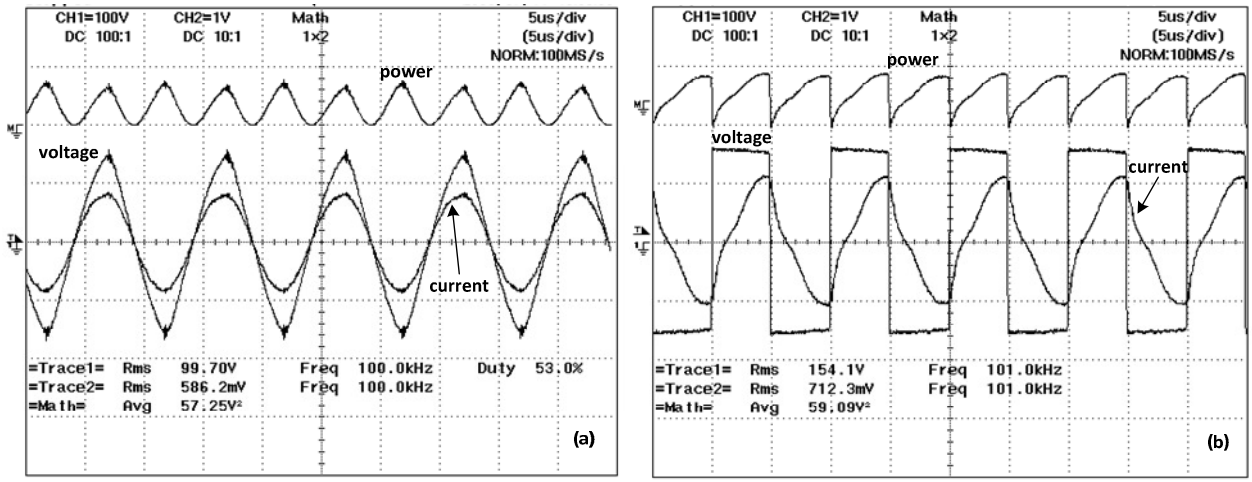

a. Waveforms of the lamp voltage and arc current (50V/div, 1A/div, 5µs/div)

b. Waveforms of the inverter output voltage and resonant current (100V/div, 1A/div, 5µs/div)

Fig. 3.84. Experimental results for the TLD 58W.

Table 3.16 shows the power distribution and efficiency for the proposed ballast. It also shows the required dc control current value for the selected lamps. As can be seen, a high efficiency range was achieved, between 89% and 91%. Other measurements were carried out, which proved that when two lamps with a 50% difference in power rating are supplied by the same resonant circuit, by changing only the switching frequency, the efficiency reduction can be as high as 20 points.

Table 3.16 Power distribution and efficiency for the proposed converter

FLUORESCENT LAMP	TLD 18W	TLD 36W	TLD 58W
I_{dc} [A]	0.0	0.46	1.0
Forward converter input power [W]	0.0	1.15	2.50
Resonant inverter input power [W]	21.0	40.1	64.1
P_{in} [W]	21.0	41.3	66.6
P_{arc} [W]	18.6	36.4	58.2
η [%]	88.6	88.2	90.8

The behaviour of the lamp current compensator is shown in Fig. 3.85 and in Fig. 3.86. Fig. 3.85 shows the lamp power and the inverter switching frequency for a 250 to 350V dc bus voltage variation, for three different lamps. In these experiments, the lamp power was adjusted for a nominal power equal to 90% of the rated power. The reason why this value was adopted is

related to the fact that typically, the lamp efficiency at high frequency is at least 10% higher than that at line frequency. This allows the ballast to handle lower lamp power and therefore save energy. This is a usual practice when designing electronic ballast for high-frequency operation. As can be seen in Fig. 3.85, even though the lamp current is the parameter used for closed-loop regulation, the lamp power is also well regulated. It can also be seen how the switching frequency is increased as the bus voltage rises so that the lamp current and power can be maintained nearly constant.

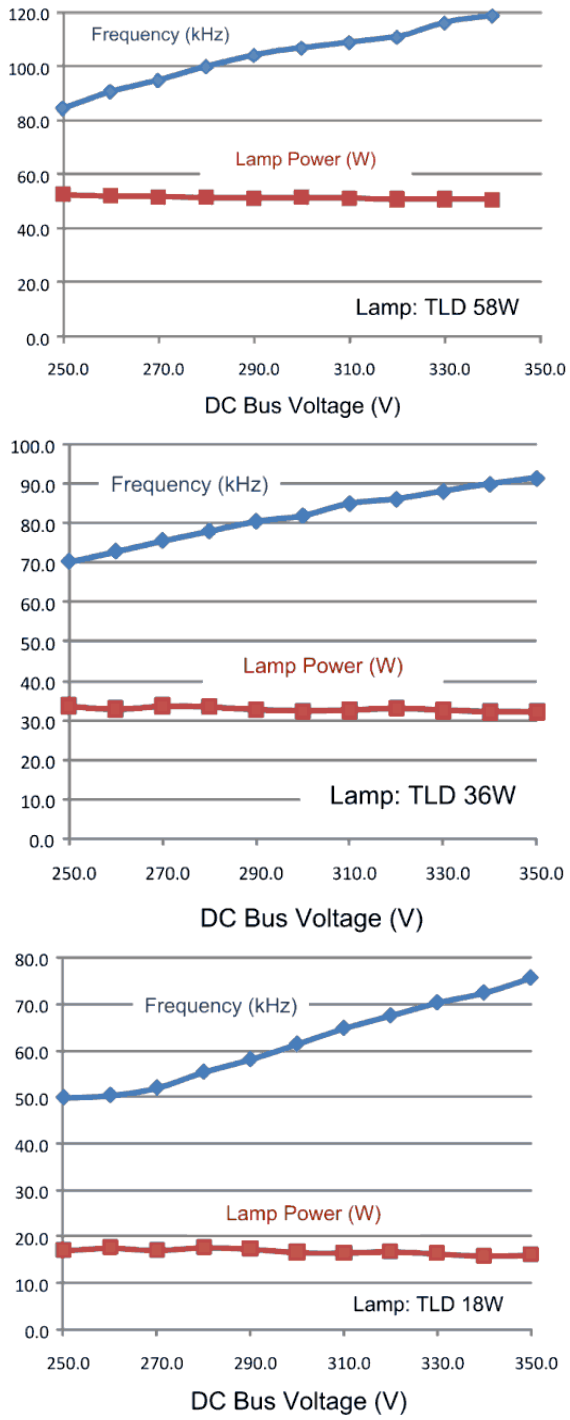

Fig. 3.85. Closed loop operation of the resonant inverter: average lamp power and switching frequency range for an

input voltage variation from 250V to 350V.

Finally, Fig. 3.86 shows the dynamic response of the resonant inverter for a 280 to 320V dc input voltage step. As can be seen, the lamp current is compensated in less than 100ms.

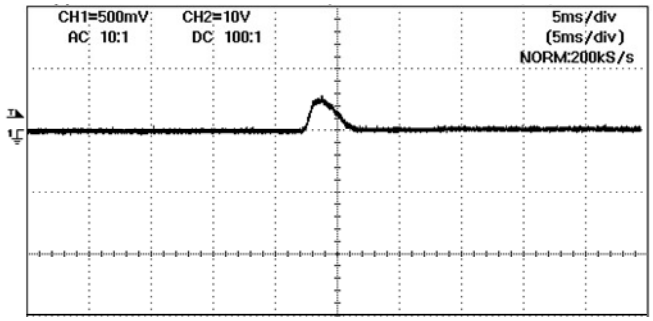

Fig. 3.86. Dynamic response of the resonant inverter for an input voltage step from 280 to 320 V - lamp under test: TLD 36W. The waveform corresponds to the output voltage of the lamp current sensor, which has a gain of 0.375mA$_{rms}$/mV (vertical scale: 500 mV/div, horiz. scale: 100 ms/div).

In conclusion, a digital control circuit was developed to control both the resonant inverter used to supply the lamp and the forward converter employed to drive the control winding of the magnetic regulator. Experimental results obtained from a laboratory prototype confirmed that the proposed converter can successfully detect and supply fluorescent lamps ranging from 15 W to 58 W close to their nominal power while assuring a very good efficiency [3.44], [3.45].

It must be noted that the presented ballast was designed to supply lamps of a similar type, in this case T8 linear lamps. The development of universal ballasts for any kind of tubular fluorescent lamps is complicated due to their different characteristics in terms of warm-up period, time constants and equivalent impedances.

In the next section another magnetically-controlled universal ballast will be proposed, which will be able to control a large group of T5 lamps. In this new ballast the forward converter will be replaced by a simple buck converter. The major concern in this new proposal was autonomous operation, and SoS compliance.

3.5.5 CONSTANT-FREQUENCY OPERATION IN UNIVERSAL BALLASTS WITH *SoS* COMPLIANCE

Another magnetically-controlled universal ballast prototype is hereby presented. This digitally-controlled universal ballast was especially developed for T5 lamps in order to evaluate the possibilities of this new control strategy. The ballast is capable of supplying tubular fluorescent lamps in the range of 14W to 49W, HE series and HO series. It uses the same control technique, yet, in this particular case, the ballast prototype will exhibit a constant-frequency operation. Besides operating at constant frequency, this prototype guarantees safe-electrode operation for all the lamps, which will result in a higher lamp-life. This was accomplished by a strict control of the design procedure under the SoS limits.

Since this ballast is supplied by a dc-bus voltage and due to the relatively high complexity of the proposed prototype, a digital control circuit was also developed to control the half-bridge resonant inverter and the buck converter. This buck converter has the same function as the preceding forward converter; it supplies the control windings of the magnetic regulator.

Finally, another objective was to move towards a completely autonomous ballast. An additional converter was therefore used to supply the inverter gate drives and the buck converter. This converter is connected to the dc bus voltage which also supplies the inverter.

3.5.5.1 ELECTRONIC BALLAST SCHEMATIC AND PROPOSED CONTROL TECHNIQUE

Each T5 lamp was supplied by a voltage-fed resonant inverter connected to a parallel-loaded resonant circuit, as shown in Fig. 3.87. The ballast requires two additional dc-dc converters and a microcontroller unit, μC and functions similarly to the preceding prototypes. The two bi-directional switches and the dc voltage source, V_{dc}, provide a square-wave voltage source that drives the resonant circuit formed by the magnetic regulator, with the variable inductance L_{ac}, the resonant capacitor C_p and the fluorescent lamp. The output lamp power is defined as in (3.150).

$$P_{lamp} = \frac{{V_{lamp}}^2}{R_{lamp}} = \frac{{V_{in}}^2 R_{lamp}}{R_{lamp}^2(1-\omega^2 L_{ac} C_P) + (\omega L_{ac})^2} \tag{3.150}$$

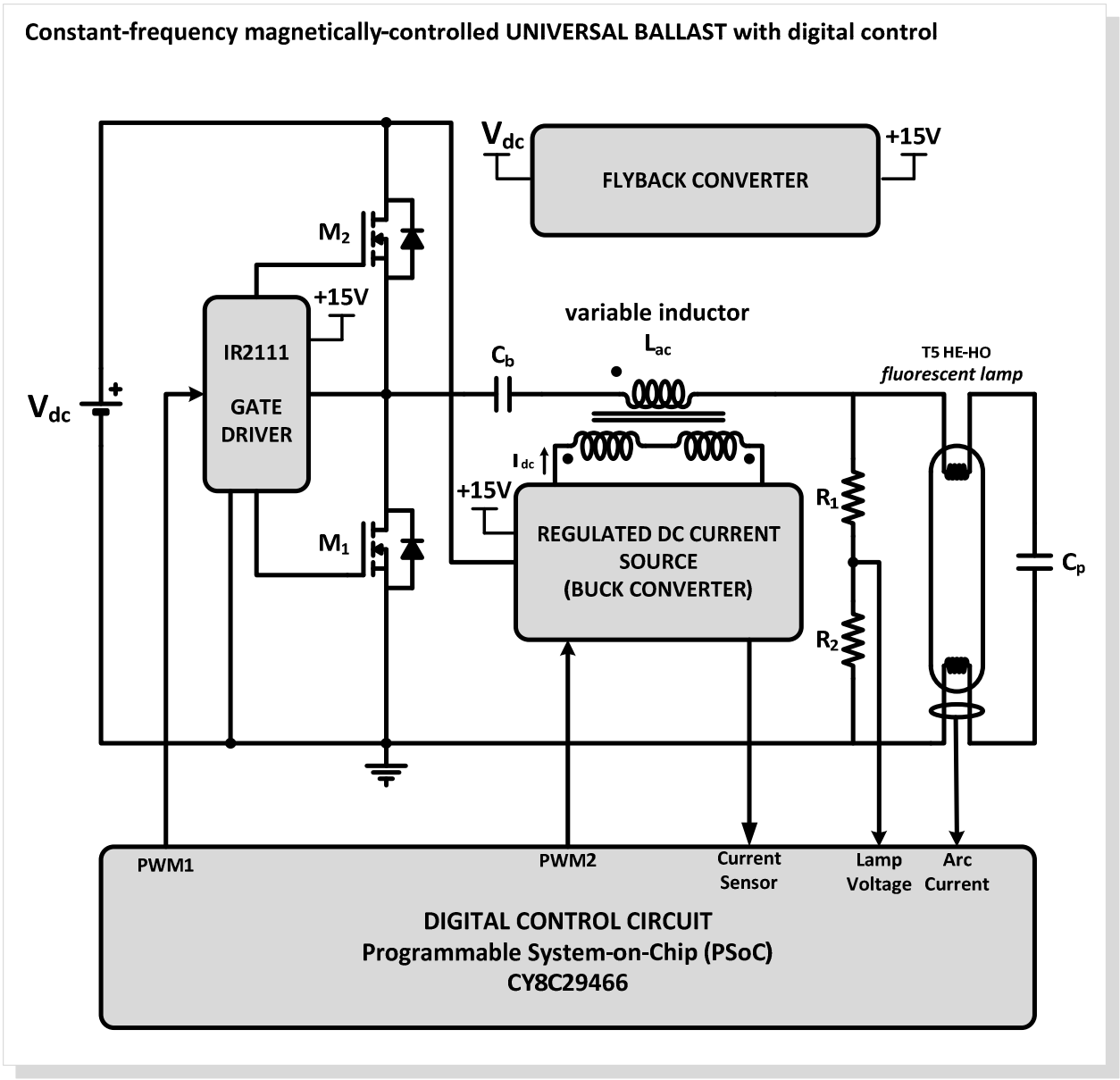

Fig. 3.87. Constant-frequency magnetically-controlled universal ballast with digital control: circuit schematic.

The analysis of the lamp power equation shows that if the inverter is operated at a constant switching frequency, and if the capacitor value remains constant, it is possible to control the delivered power by simply adjusting the inductance value, L_{ac}. As previously mentioned, the ability to supply different lamps is typically based on controlling each lamp current by doing a shift in the operating frequency. However, using the same resonant circuit involves a large range of operating frequencies, which may not be feasible, due to the high switching losses and EMI stresses [3.53]. This is one of the main reasons why the magnetic regulator control technique was suggested as an efficient alternative. However in the first presented approach, two different parameters were used, the variable inductance and the switching frequency. Using both

parameters led to an acceptable operating frequency range. Therefore and contrary to previous proposed ballast, where the delivered power was controlled by two different parameters, the switching frequency and the variable inductance, this new prototype is capable of controlling several lamps using only one control parameter.

The ballast operating procedure will be as usual: after the lamp recognition, a dc control current, I_{dc}, is delivered to the magnetic regulator which will then change its inductance according to the estimated value for the attached lamp. The current I_{dc} is supplied by a regulated dc-current source, a dc-dc buck converter operating in continuous conduction mode. So, in fact, the inductance variation is imposed by the output dc current of the converter, which is directly connected to the control windings of the magnetic regulator. The μC has also the ability to measure this dc current. The control of I_{dc} itself, is done by adjusting the duty-cycle of a PWM signal generated by the μC, and applied to the buck converter, according to a voltage reference, V_{ref}. This voltage reference may be imposed manually, or by the μC according to the implemented lamp detection method. As a suggestion this voltage reference could be defined according to the methodology and the results obtained from the application of the fuzzy logic algorithm proposed in [3.49].

As illustrated in Fig. 3.87, the voltage required for the gate driver and the buck converter, 15V, is generated by a dc-dc flyback converter, powered by the ballast dc bus voltage, V_{dc}. As in previous cases, this ballast prototype is supplied at $V_{dc} = 310\text{V}$. The flyback converter will ensure electrical isolation between the power stage and the control stage of the ballast. This isolation is also guaranteed by two additional optocouplers, one used in the dc-dc buck converter and the other in the gate driver. At last, the gate driver, responsible for setting the inverter switching frequency, f_s, is also managed by the μC, during the preheating mode and at steady-state conditions. As usual, the generated PWM signal will have a duty-cycle of approximately 50%, for an even aging of the lamp electrodes.

3.5.5.2 RESONANT CIRCUIT DESIGN

3.5.5.2.1 Standard design procedure

The primary goal is to operate all different TL5 lamps at nominal power while maintaining the same switching frequency, f_s and the same resonant circuit capacitance. So, it is necessary to calculate this capacitance and the inductance values required by each lamp. The circuit is

characterized as a low-pass resonant filter and the design procedure is similar to the one described for the first universal ballast prototype. The values for L_{ac} and C_p may be easily determined using (3.147) and (3.148). In this case the operating frequency was set at 55kHz. The estimated parameters for each lamp are presented in Table 3.17. The dc blocking capacitor value was maintained at 1μF as in the previous ballasts prototypes.

Table 3.17 Operating frequency and resonant circuit parameters for each lamp: theoretical values

FLUORESCENT LAMP	L_{ac} [mH]	C_p [nF]	f_s [kHz]
TL5 HE series (14/21/28/35)	2.35	3.48	55
TL5 HO 24W	1.33	6.15	55
TL5 HO 39W	1.17	6.94	55
TL5 HO 49W	1.53	5.33	55

As expected and according to Table 3.17, the resonant capacitor is different for each attached lamp. However, the nature of the desired universal operation requires a slightly different design procedure. In this particular case, it is necessary to determine just one parallel capacitor C_p for all T5 Lamps and their respective inductances. Since the value of capacitor C_p will be different from the defined values represented in Table 3.17 it is practically impossible to expect proper operation of the electronic ballast without further investigation. As initial approach and through the analysis of Table 3.17, it was necessary to specify an intermediate C_p value. A reasonable option was to set C_p around 4.7nF, since it is the nearest commercial value for all the selected T5 lamps. It was also possible to verify that a change in the value of the parallel capacitor will not have a significant effect in the fluorescent lamp power for the same inductance value.

Since the new set of parameters may not guarantee proper electrode operation, a more detailed analysis must be done, considering the SoS limits, ZVS operation and overall ballast efficiency. In the next sections a step-by-step methodology will be presented to verify the adequacy of the parameters determined in this section.

3.5.5.2.2 Capacitance selection based on the SoS limits

The important issue is to comply with the established SoS limits, while identifying a maximum limit value for C_p, and simultaneously guarantee that with this value the ignition of the

fluorescent lamp will not be compromised. Once the manufacturer defines the limits for the currents I_{LL} and I_{LH}, the first step is to check if the value of C_p previously defined maintains the electrodes operating in a safe mode.

Fig. 3.88a. shows the typical fluorescent model which considers the electrodes resistance, R_{electr}, evenly distributed. In fluorescent-lamp electronic ballasts, the impedance of the parallel capacitor C_p is normally very high compared to the value of R_{electr}, so, the maximum C_p can be evaluated considering $R_{electr} = 0$.

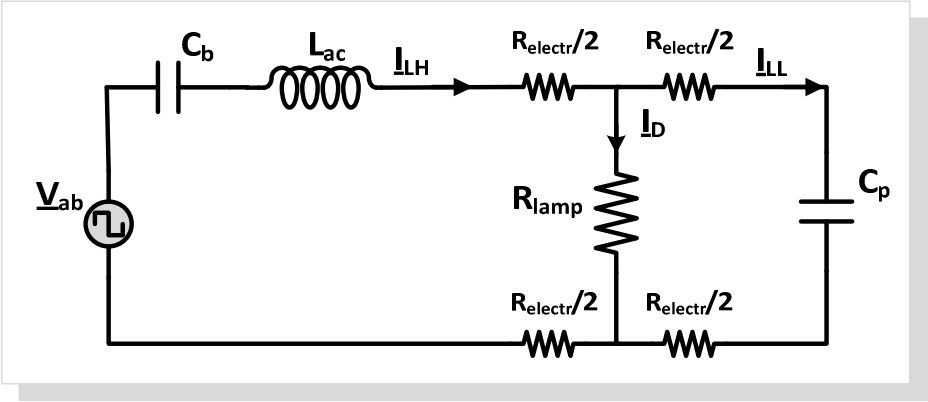

Fig. 3.88. Conventional equivalent circuit schematic.

In this case, the capacitor voltage, V_{C_p}, can be considered equal to the fluorescent lamp voltage. The lamp voltage can be defined as:

$$\left|\underline{V}_{lamp}\right| = \left|\underline{I}_{LL}\right| \cdot \left|\frac{1}{j\omega_s C_p} + R_{electr}\right| \tag{3.151}$$

Taking into consideration that $1/\omega_s C_p \gg R_{electr}$, the maximum capacitance value for each TL5 can be determined by (3.152), using a specific I_{LL} and V_{lamp} modulus for each lamp and according to the data of the manufacturer [3.29], [3.35].

$$C_p = \frac{\left|\underline{I}_{LL}\right|}{\left|\underline{V}_{lamp}\right| \cdot 2\pi f_s} \tag{3.152}$$

Table 3.18 shows the maximum defined values for I_{LL}, and I_{LH} for each T5 lamp, and the lowest maximum allowed C_p value in the filter circuit, obtained from (3.152). From Table 3.18, the lowest maximum admissible value of C_p is determined by the lamp T5 HE 35W, since this is the lamp with the highest lamp voltage, V_{lamp} and the lowest discharge current, I_D. It is now clear

that, capacitance values higher than 2.37nF may damage or reduce the lifetime of this lamp, since the electrodes will be submitted to excessive heating. However, on the other hand, the T5 HO 24W could admit capacitance values higher than 12nF without electrodes deterioration.

It is recalled once again that this control technique requires the use of a single capacitor and that the optimal value of C_p should be around 4.7nF, as previously defined. However, the I_{LL} current limit imposes a lower C_p value to operate in a safe condition, 2.37nF. It is therefore necessary to develop an alternative method to meet the necessary conditions, which means guaranteeing the lamp ignition and not exceeding the maximum permissible value for I_{LL} for all lamps.

Table 3.18 Nominal and Safe Operation conditions for TL5 Philips lamps at 25ºC: lamp voltage, discharge current, electrode resistance, *SoS* limits and maximum parallel capacitor

FLUORESCENT LAMP	V_{lamp} [V]	I_D [mA]	R_{electr} [Ω]	I_{LHmax} [mA]	I_{LLmax} [mA]	C_{pmax} [nF]
TL5 HE 14W	83±10	170±40	40	240	170	5.82
TL5 HE 21W	125±10	170±40	40	240	170	4.00
TL5 HE 28W	1667±17	170±40	40	240	170	2.96
TL5 HE 35W	208±20	170±40	40	240	170	2.37
TL5 HO 24W	80±8	300±30	12	475	370	13.38
TL5 HO 39W	119±10	340±70	12	475	370	9.13
TL5 HO 49W	195±20	260±50	16.5	370	275	4.07

3.5.5.2.3 Dual-parallel capacitor configuration

The limit value for C_p was identified as 2.3nF and the nearest commercial value is 2.2nF. However, it is possible that such a low value does not guarantee a proper ignition for the remaining lamps, nor that each lamp is even capable of delivering the rated power. A possible solution which simultaneously limits the current I_{LL} and ensures proper lamp operation is to use two parallel resonant capacitors instead of using a single C_p, as shown in Fig. 3.88. The capacitor C_p is therefore replaced by the capacitors C_{p1} and C_{p2} connected as shown in Fig. 3.89a. During ignition, these two capacitors will act as an equivalent resonant capacitor circuit, $C_{peq} = C_{p1} + C_{p2}$, thereby guaranteeing a higher ignition voltage spike. Thus, with this configuration it is

possible to reduce I_{LL} to an acceptable value by imposing a limit value for C_{p2} given by (3.152), and according to Table 3.18, set at 2.2nF. Nonetheless, C_{p1}, must be evaluated in order to verify the I_{LH} current limits.

A simple method to perform this analysis is to simplify the circuit shown in Fig. 3.89a. employing the Thévenin theorem between points a and b. Fig. 3.89b. shows the simplified circuit.

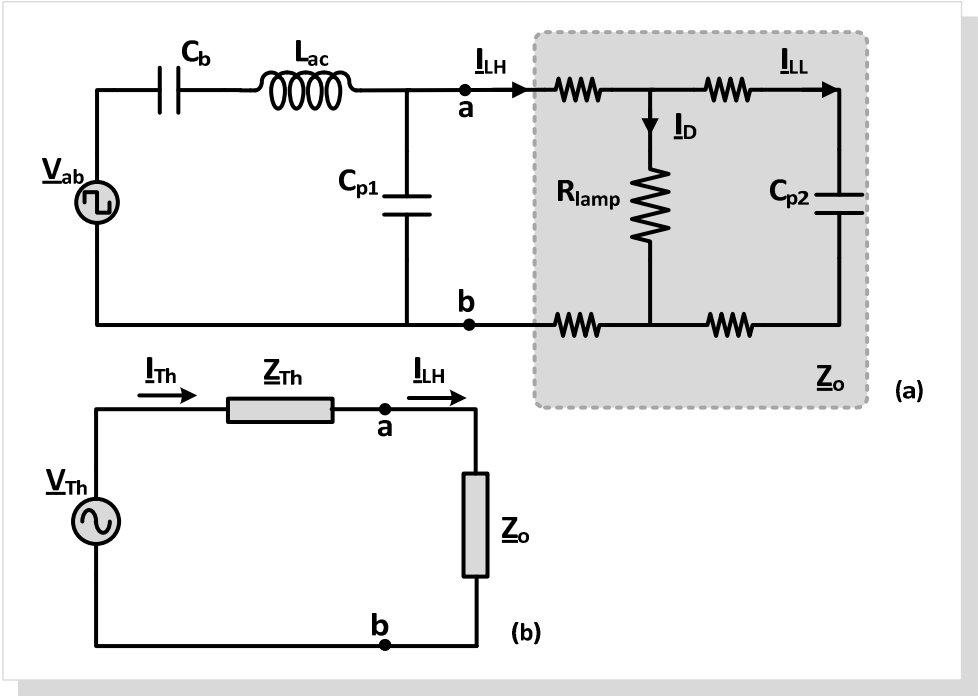

a. Modified b. Thévenin equivalent circuit

Fig. 3.89. Equivalent circuit schematic.

It can easily be observed that $\underline{I}_{LH} = \underline{I}_{Th}$, and therefore the modulus of $\underline{I}_{LH}$ and $\underline{I}_{LL}$ can be determined as a function of C_{p1} using (3.153) and (3.154), respectively:

$$\left|\underline{I}_{LH}(C_{p1})\right| = \left|\underline{I}_{Th}(C_{p1})\right| = \frac{\left|\underline{V}_{Th}(C_{p1})\right|}{\left|\underline{Z}_{Th}(C_{p1}) + \underline{Z}_{O}\right|} \tag{3.153}$$

$$\left|\underline{I}_{LL}(C_{p1})\right| = \left|\underline{I}_{LH}(C_{p1}) \cdot \frac{R_{lamp}}{R_{lamp} + R_{electr} + \underline{Z}_{C_{p2}}}\right| \tag{3.154}$$

where $\underline{Z}_O$ is the load impedance, obtained by the combination of the lamp resistance, electrode resistance and C_{p2}; $\underline{V}_{Th}$, and $\underline{Z}_{Th}$ are the Thévenin equivalent voltage and impedance. These quantities can be defined as follows:

$$\underline{Z}_O = \frac{\left(\underline{Z}_{C_{p2}} + R_{electr}\right) \cdot R_{lamp}}{\underline{Z}_{C_{p2}} + R_{electr} + R_{lamp}} + R_{electr} \tag{3.155}$$

$$\underline{V}_{Th}(C_{p1}) = \frac{\underline{Z}_{C_{p1}}}{\underline{Z}_{L_{ac}} + \underline{Z}_{C_b} + \underline{Z}_{C_{p1}}} \cdot \underline{V}_{in} \tag{3.156}$$

$$\underline{Z}_{Th}(C_{p1}) = \frac{\left(\underline{Z}_L + \underline{Z}_{C_b}\right)}{\underline{Z}_{L_{ac}} + \underline{Z}_{C_b} + \underline{Z}_{C_{p1}}} \cdot \underline{Z}_{C_{p1}} \tag{3.157}$$

and where $\underline{Z}_{L_{ac}} = j\omega L_{ac}$; $\underline{Z}_{C_b} = {}^{1}/_{j\omega C_b}$; $\underline{Z}_{C_{p1}} = {}^{1}/_{j\omega C_{p1}}$; and finally $\underline{Z}_{C_{p2}} = {}^{1}/_{j\omega C_{p2}}$.

Fig. 3.90a. shows the plots of I_{LL} and I_{LH} rms values as a function of C_{p1} and the current limits imposed by the manufacturer. The minimum values for I_{LL} and I_{LH} are set by the T5 HE series. The T5 HE 35W presents the highest lamp voltage and lowest discharge current. As a result, this lamp presents the worst limiting conditions from the set of the selected T5 lamps.

Fig. 3.90b shows the plot of the resonant current phase as a function of C_{p1}. It is noted that the resonant current phase is equal to the phase of the input admittance, $1/\underline{Z}_{in}$. These plots assume C_{p2} at the previously determined value, 2.2nF, R_{lamp} at the rated values of voltage and current for the T5 HE 35W lamp, L_{ac} as calculated in (3.147) and C_b at 1μF. From Fig. 3.90b it is noticed that ZVS operation will not be put at risk for any possible value of C_{p1}, since the resonant current phase will always be negative. Moreover, according to Fig. 3.90a. any value of C_{p1} may be employed without exceeding the limits of I_{LL} and I_{LH} defined by the dotted lines. Thus, an ideal value of C_{p1} may be selected, around 2.2nF, in order to obtain an equivalent capacitance, $C_{peq} = C_{p1} + C_{p2}$, near 4.7nF, which corresponds to the ideal capacitance defined in the traditional design methodology.

Experimental tests were performed with all T5 lamps which presented I_{LL} and I_{LH} values according to the limits defined by the manufacturers. However, lamp voltage oscillations were observed for the T5 HE 35W lamp using this set of C_{p1} and C_{p2}.

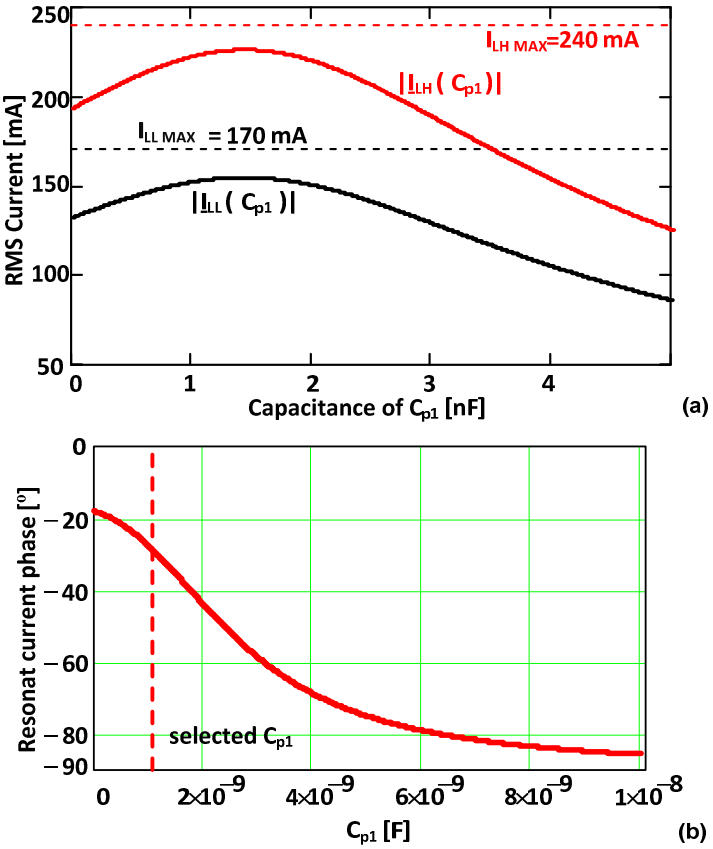

a. Selection of C_{p1} according to I_{LH} and I_{LL} limits b. Resonant current phase as function of C_{P1}

Fig. 3.90. Selection of C_{p1}.

In order to overcome this problem, the next step was the analysis of the quality factor, Q, of the circuit, considering each T5 lamp. It is recalled that for the parallel-loaded half-bridge inverter, if the quality factor of the load, Q_L, defined in (3.158), is smaller than 1, the resonant frequency does not exist and the circuit is only characterized as an inductive circuit at any switching frequency.

$$Q = \frac{V_{lamp}}{V_{in}} = \frac{R_{lamp}}{Z_b} \tag{3.158}$$

On the contrary, if Q_L is equal or greater than 1, and if the switching frequency, $f_s > f_r$, the circuit is defined as a resonant circuit and will also behave as an inductive load. It is recalled that in these conditions, the resonant frequency, f_r, is defined as in (3.159):

$$f_r = f_o \sqrt{1 - \frac{1}{Q_L^2}} \qquad for \qquad Q_L \geq 1 \tag{3.159}$$

Table 3.19 shows the value of Q and the damping factor ζ, both obtained using (3.158) and (3.160), as well as the resonant frequency and the phase, φ, of the circuit impedance, $\underline{Z}_{in}$.

$$\zeta = \frac{1}{2Q} \tag{3.160}$$

Table 3.19 Quality and damping factors for C_{peq}=4.4nF

FLUORESCENT LAMP	Q	ζ	f_r [kHz]	φ [º]
TL5 HE 14W	0.66	0.76	-	60.9
TL5 HE 21W	0.99	0.51	-	54.6
TL5 HE 28W	1.36	0.37	33.60	51.1
TL5 HE 35W	1.71	0.29	40.10	49.7
TL5 HO 24W	0.43	1.17	-	59.1
TL5 HO 39W	0.62	0.80	-	45.7
TL5 HO 49W	1.26	0.40	37.50	29.9

For all T5 lamps and corresponding inductance values the phase φ of the circuit impedance is always positive. According to Table 3.19, the lowest ζ and the highest Q values for the T5 HE 35W lamp were considered as the cause of the lamp voltage oscillations. In order to avoid these oscillations, ζ should be increased, which can be done by selecting a lower value of C_{p1}.

New tests were performed using $C_{p1} = 1.1\text{nF}$. The experimental results showed proper lamp operation and the critical lamp revealed no voltage oscillations. The new values of Q and ζ are shown in Table 3.20. The natural frequency, the resonant frequency and the phase, φ, of the circuit impedance, $\underline{Z}_{in}$ are also shown in Table 3.20. In conclusion, assuming the new value of C_{p1}, the equivalent capacitance C_{peq} is now equal to 3.3nF, and for all T5 lamps the phase φ is also always positive. Fig. 3.91 presents a final comparison between the standard design procedure using a single capacitor of 4.7nF and the dual capacitor configuration. It clearly shows how the single capacitor configuration imposes excessive current to the electrodes, especially for the HE series. This would be translated into their quicker degradation over time. On the other hand, the dual capacitor configuration significantly counteracts the results obtained with the initial configuration. All the currents considered are now below their permissible limit.

Table 3.20 Quality and damping factors for C_{peq}=3.3nF

FLUORESCENT LAMP	Q	ζ	f_r [kHz]	φ [º]
TL5 HE 14W	0.57	0.88	-	66.1
TL5 HE 21W	0.85	0.59	-	56.7
TL5 HE 28W	1.18	0.42	30.40	48.0
TL5 HE 35W	1.48	0.34	42.10	41.1
TL5 HO 24W	0.37	1.35	-	63.9
TL5 HO 39W	0.54	0.93	-	51.6
TL5 HO 49W	1.09	0.46	28.70	32.3

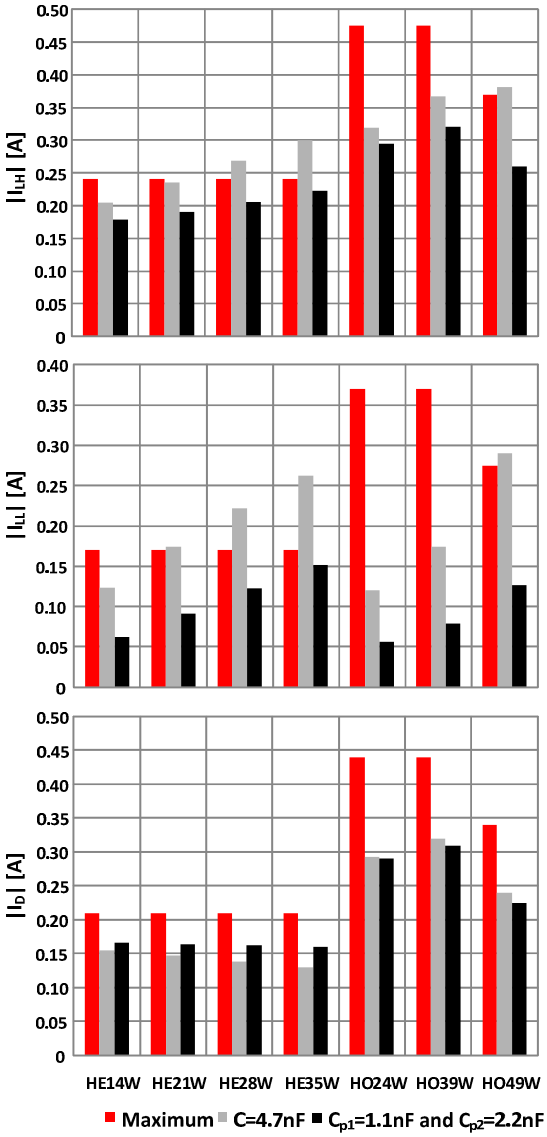

Fig. 3.91. I_{LH}, I_{LL}, I_D currents considering both capacitors configurations: comparison with maximum limits.

3.5.5.2.4 ZVS operation

In order to guarantee ZVS operation, the traditional design procedure considers as a sufficient condition to operate the half-bridge inverter at a frequency f_s above the resonant frequency of the circuit. However, if $Q_L < 1$, the filter will not behave as a resonant circuit, but simply as an inductive circuit, and this principle cannot be applied. Despite of this behaviour, the inverter circuit will keep ZVS operation, since the input circuit current also lags the inverter output voltage, for an inductive load. In conclusion, the resonant frequency concept cannot be applied in such cases and there will be no corresponding resonant frequency to be shown in Table 3.19 and in Table 3.20 when $Q_L < 1$.

Therefore, with the traditional method which uses the fundamental approximation, a quality factor $Q_L \geq 1$ is enough to evaluate ZVS operation just for the T5 HE 28W, 35W and T5 HO 49W lamps. Although for some set of components this concept is not applicable, it is clear from Table 3.20 that for all T5 lamps the phase φ is also always positive, which implies a resonant current with a negative phase, ϕ_{in}. However, for the T5 HE 14W, 21W, and T5 HO 24W and 39W the circuit behaves as an inductive load and this also justifies the ZVS operation. However, in these cases, it is expected a less sinusoidal resonant current waveform.

3.5.5.3 ELECTRONIC BALLAST EXPERIMENTAL PROTOTYPE

Fig. 3.92 shows the ballast experimental prototype. The main driver, IR2111, also used in the previous ballast, is responsible for the command of the half-bridge inverter. Since the supply voltage of the IR2111 driver is 15V, the amplitude of the PWM signal generated by the μC had to be adapted for the driver to work properly. This was accomplished using a HCLP3120 driver, which grants electrical isolation from the power stage. A digital 16 bit PWM, PWM1, as previously shown in Fig. 3.87, was applied to the gate driver in order to set the inverter switching frequency, f_s, at 55kHz according to the selected value. This PWM signal was generated by the same μC, used in the previous section, PSoC CY8C29446. In order to block the dc component of the input voltage of the filter, capacitor C_b was chosen to be 1μF and according to the previous design procedure $C_{p2} = 2.2$nF and $C_{p1} = 1.1$nF. An integrator RC circuit was also used to estimate the large-signal inductance value for each lamp.

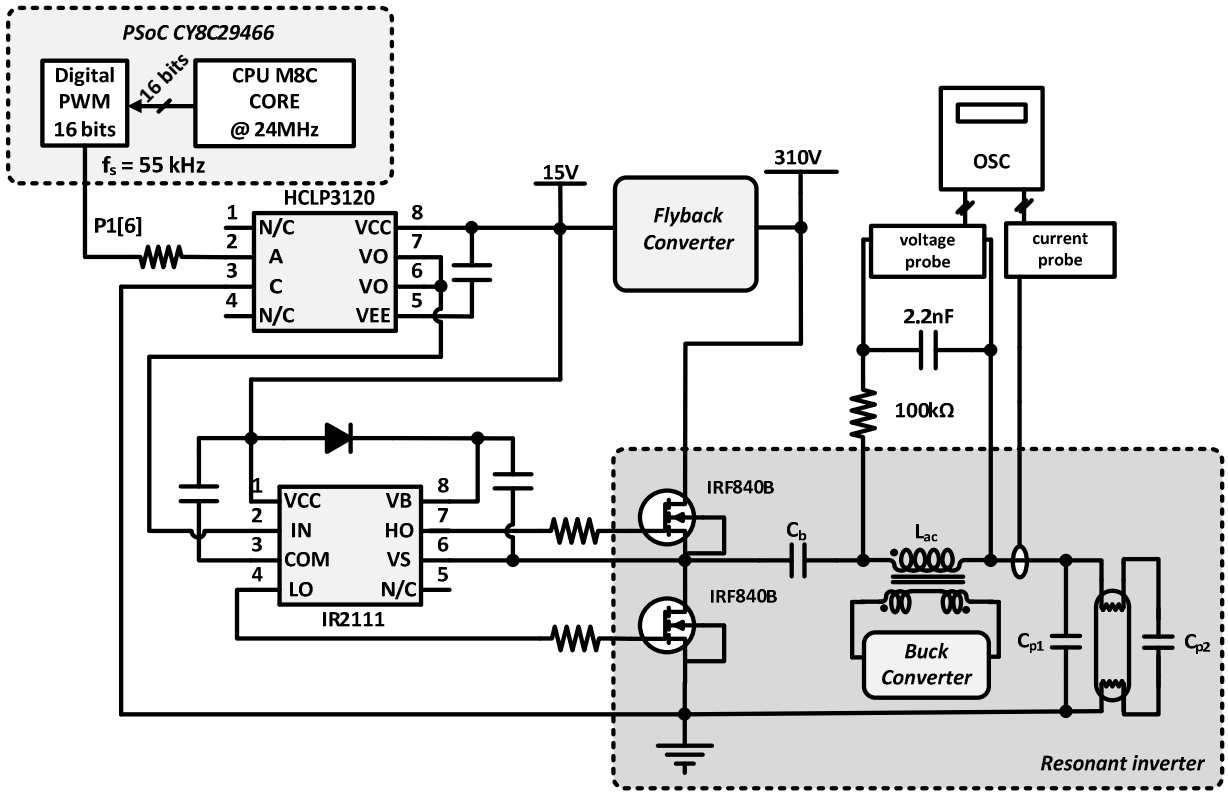

Fig. 3.92. Constant-frequency magnetically-controlled universal ballast with digital control: experimental prototype.

The design of the magnetic regulator was done considering that it should have a quite broad range, in order to cover all estimated inductances. According to the values presented in Table 3.17, the magnetic regulator should have as a minimum, an inductance variation between 1mH and 2.5mH, approximately. An experimental prototype was built using two EFD20/10/7 cores, with N87 type core material. The built prototype and the small-signal characteristic of the magnetic regulator, for a dc control current of 0 to 1A, are both presented in Fig. 3.93. The main winding, N_{ac} is composed of 150 turns while the control windings, N_{dc} is equal to 55 turns. The gap in the main winding is 0.25mm. The small-signal characteristic was obtained using a LCR meter, BK Precision 899A.

Fig. 3.94 shows the schematic of the implemented dc-dc buck converter. Its output was adjusted to supply a maximum of 1A of current in CCM. The PWM signal, referred in Fig. 3.87 as PWM2, was set at 100kHz and the control of the duty-cycle was imposed by the voltage reference, V_{ref}, which varies between 0 and 5V. In this prototype, this voltage reference was externally controlled. In an optimized ballast version, this V_{ref} should be dependent of the implemented lamp detection routine. At this stage, the μC was also configured and programmed to measure the dc current that passes through the control windings of the magnetic regulator,

through an incremental ADC of 10 bit resolution. The HCPL3120 optocoupler was used to provide electrical isolation between the control stage and the power stage and finally, diode D_2 was used to block any induced ac voltage from the magnetic regulator, due to asymmetries in the construction of the magnetic regulator, and due to the magnetic nonlinear coupling.

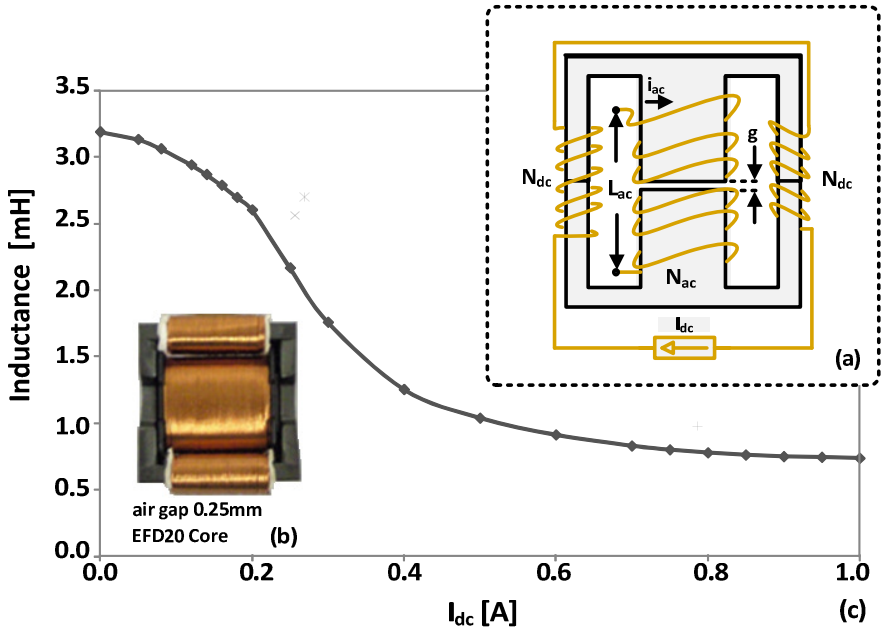

a. Schematic b. Experimental prototype c. Small-signal characteristic

Fig. 3.93. Variable inductor.

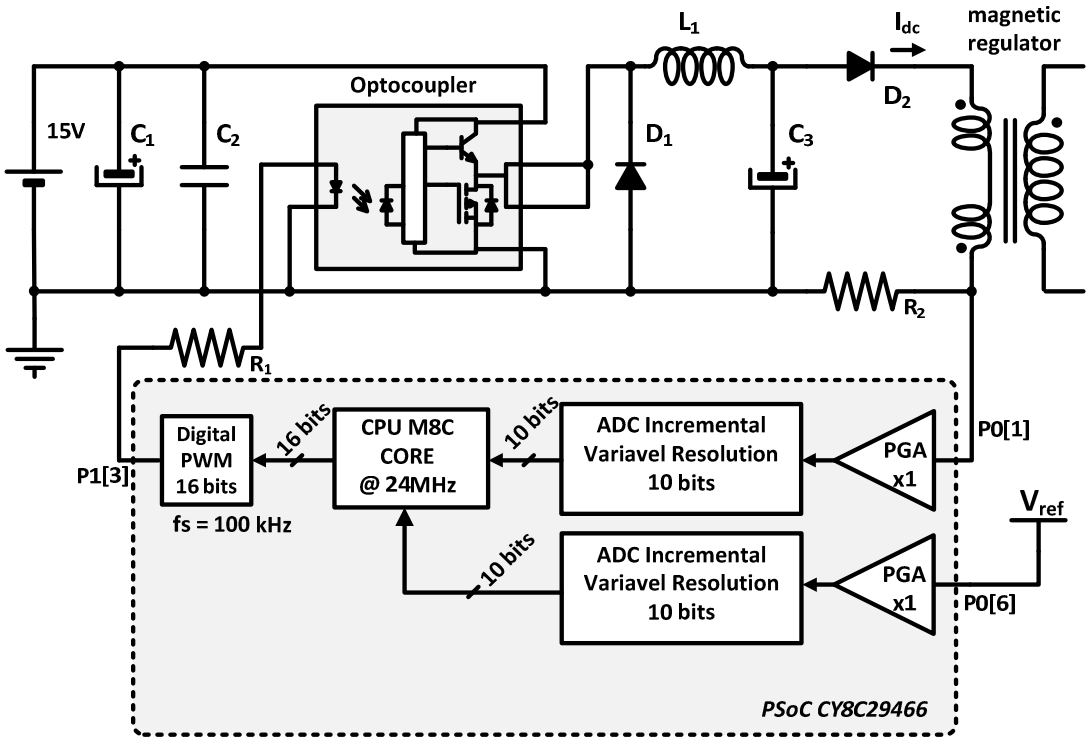

Fig. 3.94. Schematic of the dc-dc converter.

In order to simplify the design, the flyback converter was based on the IC VIPer 50A. This IC combines in the same chip a PWM circuit with a Vertical Power MOSFET (700V/1.5A/5.7Ohm) working in discontinuous conduction mode. The design of this converter was based on the software tool provided by the manufacturer, ST Microelectronics, [3.54]. Fig. 3.83 shows the implemented flyback converter. An additional output of 5V was considered in order to supply the necessary voltage to power the microcontroller.

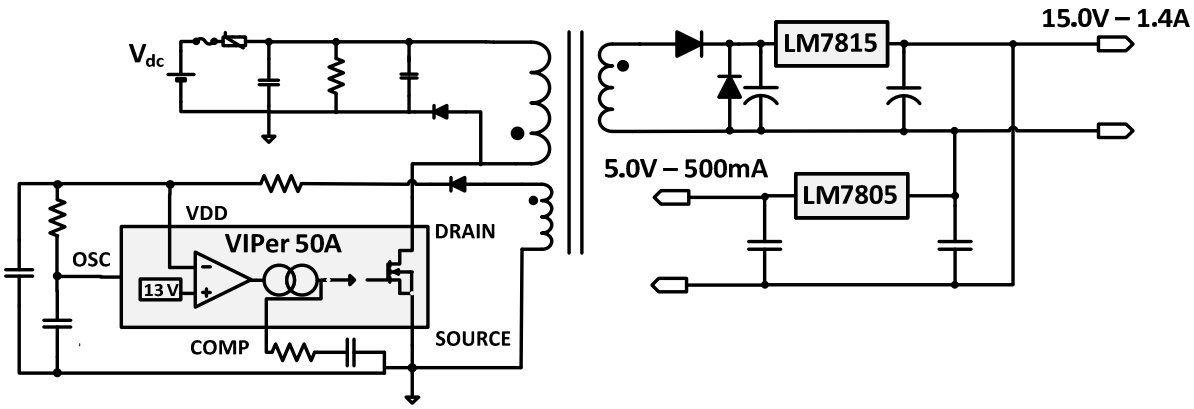

Fig. 3.95. Schematic of the flyback converter.

3.5.5.4 EXPERIMENTAL RESULTS

The data collected during prototype testing were obtained with a Picoscope. The magnetic regulator inductance was adjusted until both rms values of lamp voltage and arc current were coherent with the values imposed by the manufacturer [3.29].

Table 3.21 shows the obtained values for all lamps in terms of V_{lamp}, I_D, heating currents, I_{LH}, and I_{LL}. It also shows the measured electrode voltage, V_{electr}, and the average lamp power, P_{lamp}. The lamp power is given by the dc average value of the product between the lamp voltage and I_{LH}, which is the resonant current. Except for the T5 HO 49W all the lamps are operated at rated lamp power. The T5 HO 49W is however operated at a value higher than the lower limit recommended by the manufacturer. It presents a discharge current value 7.6% lower than the recommended value. Heating currents I_{LH} and I_{LL} show satisfactory results when compared to the maximum limits, previously presented in Table 3.18.

Fig. 3.96 shows a graphic view of I_{LH} and I_{LL} for all T5 lamps. It is possible then to compare the measured experimental values with the maximum limits for each lamp series. It can be seen that for almost all selected lamps, the rms values of I_{LH} and I_{LL} are below or within the maximum

admissible limits. There is only one limit case: the T5 HE 35W lamp presented an I_{LL} 6% higher than the permitted value. However, this percentage is acceptable considering the features of the proposed universal electronic ballast that limit the design to attend almost all of T5 fluorescent lamps.

Table 3.21 Experimental results for all T5 lamps

LAMP	V_{lamp} [V]	I_D [mA]	V_{electr} [V]	I_{LH} [mA]	I_{LL} [mA]	P_{lamp} [W]
TL5 HE 14W	88.0	161	2.46	168	77	14.0
TL5 HE 21W	129.2	166	3.50	202	108	21.4
TL5 HE 28W	175.6	162	5.26	221	141	28.8
TL5 HE 35W	219.5	160	6.29	238	181	36.0
TL5 HO 24W	79.6	306	0.86	326	72	24.1
TL5 HO 39W	122.9	319	0.95	349	105	38.7
TL5 HO 49W	223.7	195	1.17	274	175	44.0

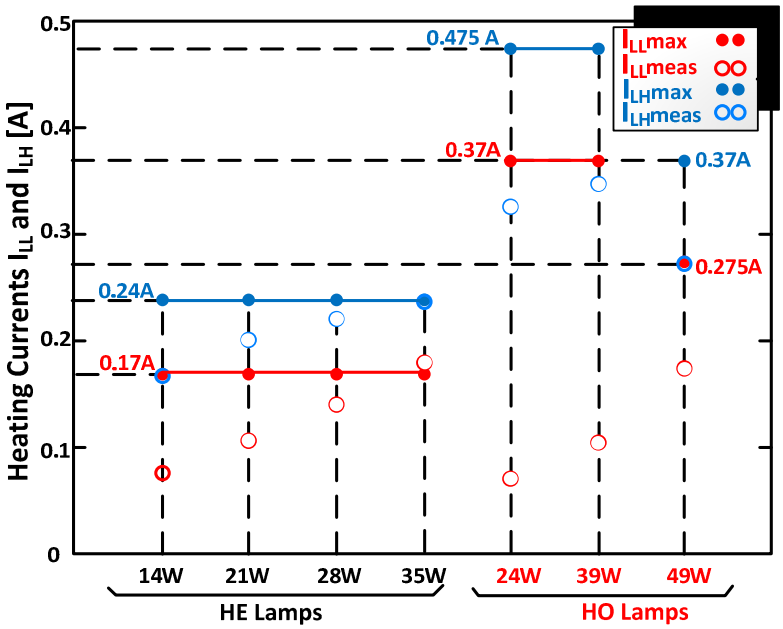

Fig. 3.96. Experimental results of the heating currents for all tested T5 fluorescent lamps.

In order to verify if the lamps present a normal operating condition at steady-state, the typical lamp voltage and arc current waveforms were also analysed. Fig. 3.97 shows the lamp voltage, arc current and arc power waveforms for the TL5 HE 14W and TL5 HE 35W which represent the

limits of the TL5 HE series. The discharge current and the lamp voltage waveforms are in phase and stable lamp operation can be recognized.

Fig. 3.98 shows the voltage, current and power waveforms at the input of the resonant tank for the same lamps. By analyzing both waveforms, it can be observed the resonant or inductive behaviour for each case through the shape of the currents. In Fig. 3.98a., the resonant current waveform lags the inverter output voltage, so the circuit behaves as an inductive load, as expected ($Q < 1$), whereas Fig. 3.98b. presents a resonant current with a near sinusoidal waveform, meaning that the circuit is near its resonance point, ($Q > 1$). In all conditions the resonant current lags the inverter output voltage, and ZVS operation is achieved in all of them.

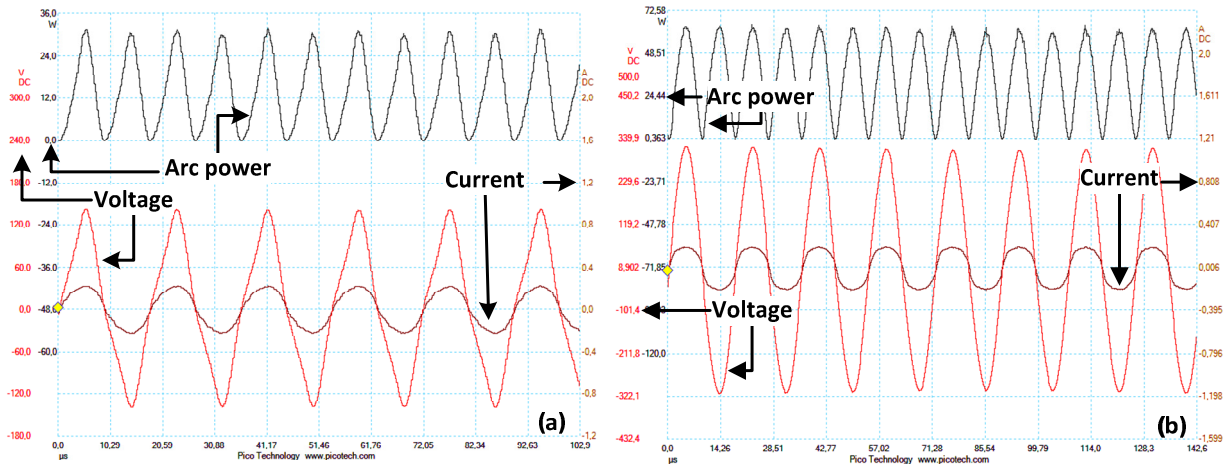

a. HE 14W (12W/div, 60V/div, 0.4A/div, 10.29μs/div)

b. HE 35W (24.08W/div, 110.3V/div, 0.4A/div, 14.26μs/div)

Fig. 3.97. Lamp voltage and arc current waveforms at rated power

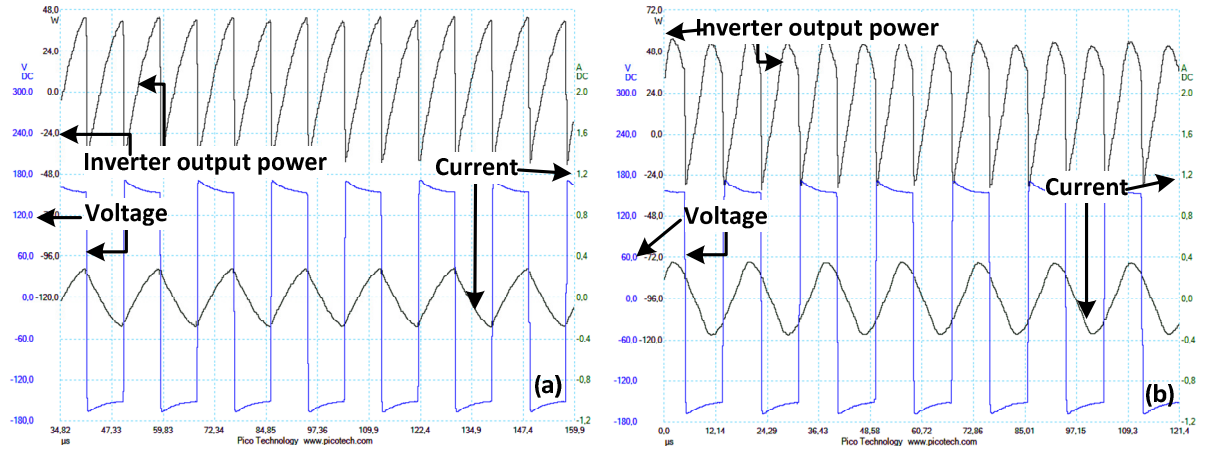

a. HE 14W (24W/div, 60V/div, 0.4A/div, 12.54 μs/div)

b. HE 35W (24W/div, 60V/div, 0.4A/div, 12.14 μs/div)

Fig. 3.98. Voltage and current at the input of the resonant circuit

Fig. 3.99 and Fig. 3.100 present similar waveforms for the TL5 HO 24W and TL5 HO 49W. The same characteristics are present. For the HO 24W the resonant circuit behaves as an inductive load, since its Q factor is less than one, whereas for the HO 49W, the circuit has a Q factor greater than one, and the resonant inverter output waveforms exhibit the expected behaviour.

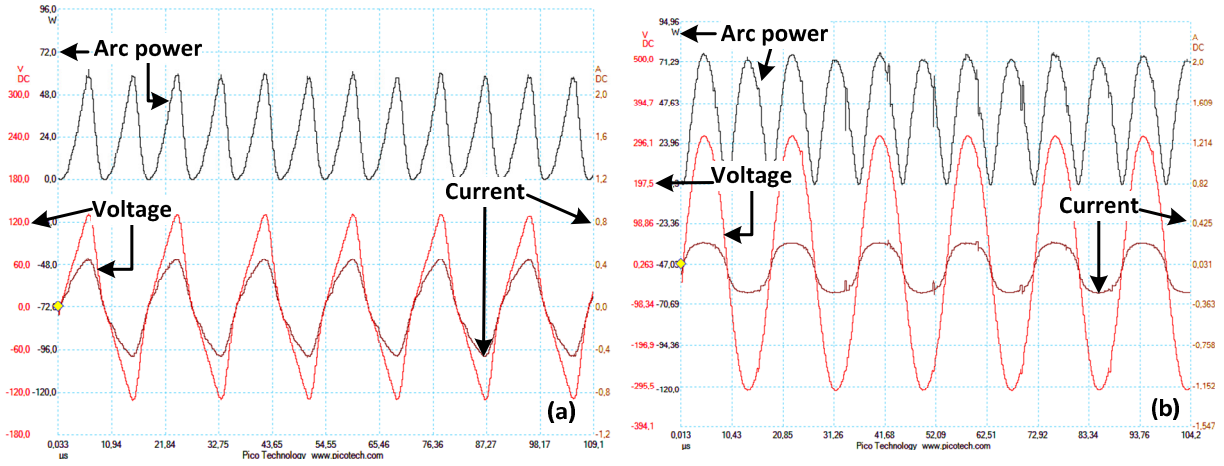

a. HO24W (24W/div, 60V/div, 0.4A/div, 10.91μs/div)

b. HO49W (20.96W/div, 98.6V/div, 0.394A/div, 10.42μs/div)

Fig. 3.99. Lamp voltage, arc current and lamp power waveforms at nominal power

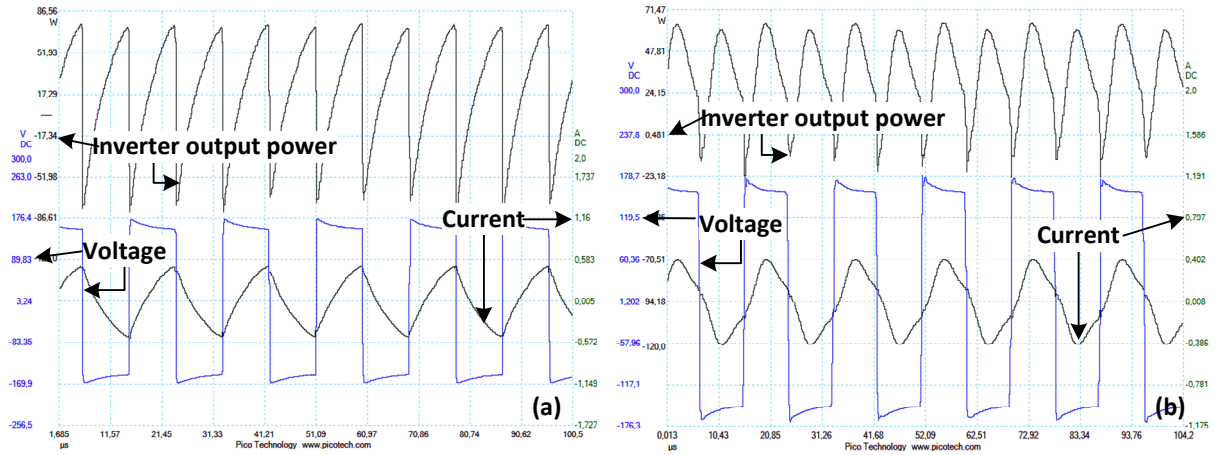

a. HO24W (17.29W/div, 86.59V/div, 0.57A/div, 9.885μs/div)

b. HO49W (23.67W/div, 59.16V/div, 0.394A/div, 10.42μs/div)

Fig. 3.100. Power, voltage and current waveforms at the input of the resonant circuit

Fig. 3.101 shows the waveforms of the electrodes voltage v_{electr}, the lead currents i_{LL}, and i_{LH}, and the resulting discharge current i_D that is composed by both currents, for all fluorescent lamps, HE series and HO series.

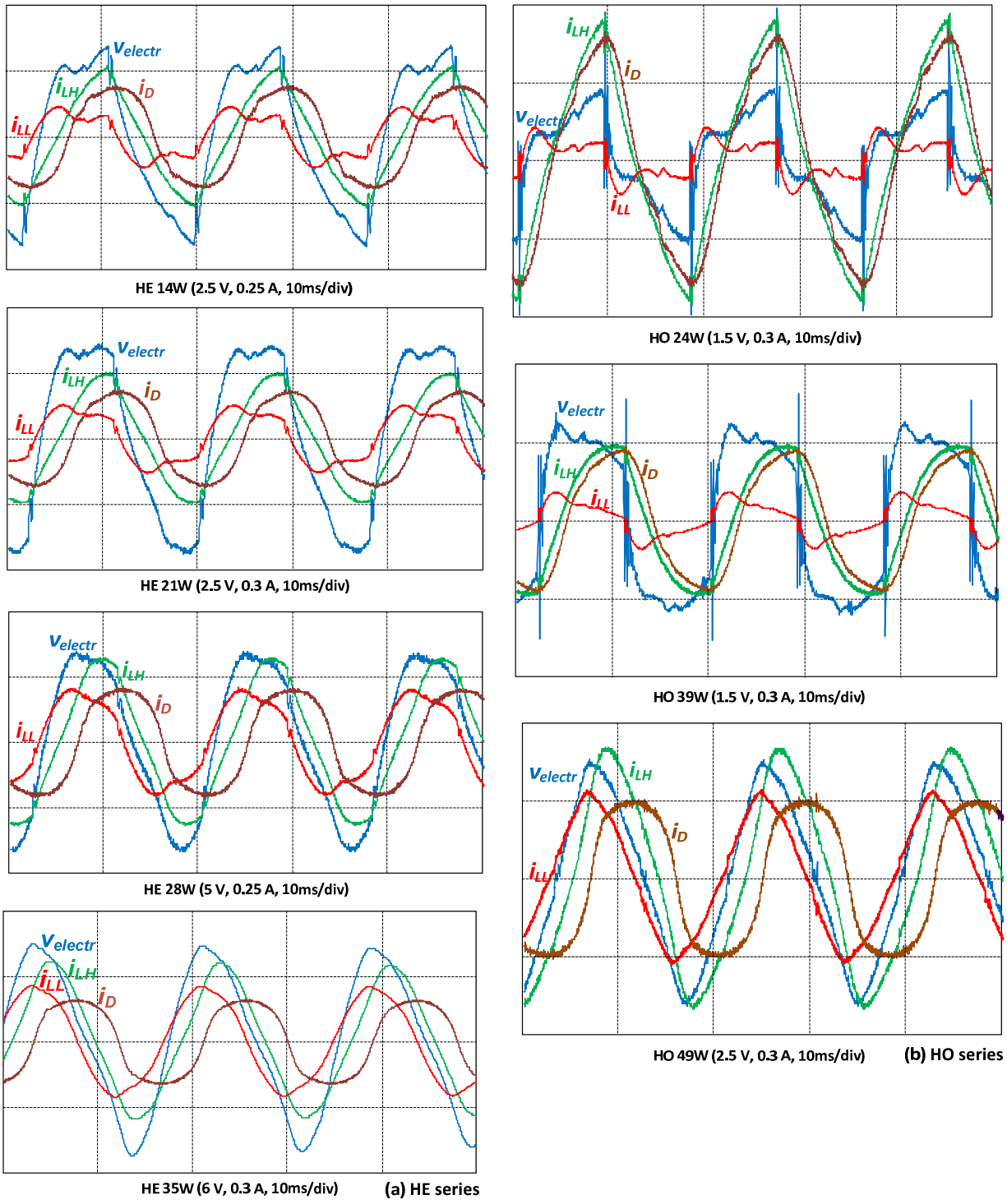

Fig. 3.101. Experimental waveforms for the T5 HE lamp series and the T5 HO lamp series: electrodes voltage, v_{electr}, heating currents, i_{LH}, i_{LL}, and discharge current, i_D.

The waveforms show the typical heating currents based on limited rms lead currents values, as defined by the manufacturers. It is clear that not all waveforms present similar shapes, mainly for i_{LL} and v_{electr}. Nevertheless all current waveforms present rms values within current standards. Thus, the electrodes temperature is kept within the limit which is enough to guarantee the lifetime

of the electrodes. As a result, the proposed design procedure and the ballast operation, both guarantee a standard lifetime for the all selected T5 fluorescent lamps.

Table 3.22 presents the power ratings achieved by each tested lamp with the ballast prototype. The values presented were considered as follows: P_{lamp} is the lamp power; P_{arc} is the discharge power or arc power, given by the dc average value of the product between the lamp voltage and the discharge current, I_D; P_{electr} is the total power loss in the lamp electrodes, given by the average value of the product of the lamp electrode voltage by i_{LH}; P_{in} is the dc input power of the ballast, supplied by an external dc power source. The overall efficiency of the magnetically-controlled ballast is given by the ratio between P_{lamp} and P_{in}. The efficiency of the prototype with each lamp rounds about 89%, which is fairly acceptable for this universal electronic ballast. It is once again recognized that the T5 HO 49W does not reach its nominal lamp power, however it still operates at a value higher than the minimum recommended power. With the implemented prototype, a fine adjustment to the inductance of the magnetic regulator could be done but this would take V_{lamp} over the maximum recommended voltage. Table 3.22 also presents the dc control current value dictated by the operation of the buck converter and the experimental large-signal inductance values for each attached lamp.

Table 3.22 Power rating of the ballast and tested lamps, experimental values of L_{ac} and I_{dc}

LAMP	P_{in} [W]	P_{lamp} [W]	P_{arc} [W]	P_{electr} [W]	η [%]	L_{ac} [mH]	I_{dc} [A]
TL5 HE 14W	17.3	14.0	13.9	0.72	81	2.63	0.2283
TL5 HE 21W	23.6	21.4	21.1	1.22	91	2.35	0.2595
TL5 HE 28W	31.0	28.8	28.0	2.09	93	2.54	0.2565
TL5 HE 35W	38.3	36.0	34.7	2.74	94	2.68	0.2692
TL5 HO 24W	28.3	24.1	24.21	0.45	85	1.10	0.6548
TL5 HO 39W	44.4	38.7	38.95	0.44	87	9.64	0.7863
TL5 HO 49W	48.1	44.0	43.2	1.17	92	1.89	0.5234

Fig. 3.102 presents the integrator voltage, v_C, the resonant current, i_{res} and the dc control current waveforms at rated power for the T5 HO 49W, which has a small ripple component. In these conditions the magnetic regulator was supplying the lamp with higher power rating. It is recalled that the integrator circuit is used to measure the total ac flux in order to estimate the inductance value for each operating point.

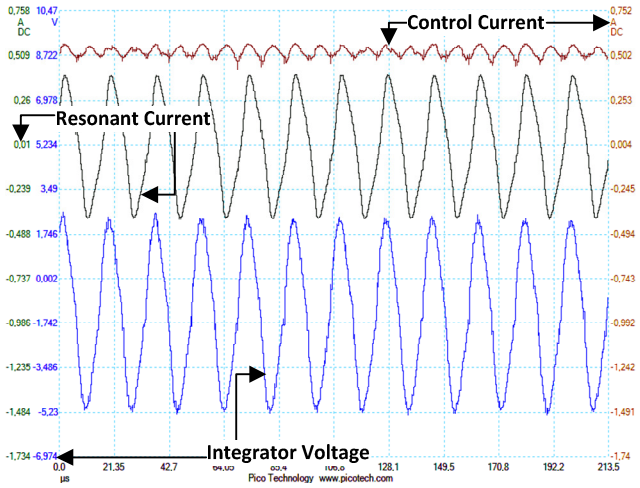

Fig. 3.102. T5 HO 49W: integrator voltage, resonant current and control current waveforms at rated power: (1.744V/div, 0.25A/div, 0.249A/div, 21.35ms/div).

Fig. 3.103a. shows the magnetic regulator small-signal characteristic and the experimental large-signal inductance values, L_{ac} for each tested lamp. These values are distributed according to the dc current value flowing through the control windings of the magnetic regulator, measured by the μC. All values are approximately distributed along the presented characteristic. It should be noticed that only the T5 HO 49W lamp shows a significant difference. This can be explained by the fact that this lamp is not working exactly at rated power. It is also noticed that the large-signal inductance values tend to be higher for the same dc control current value.

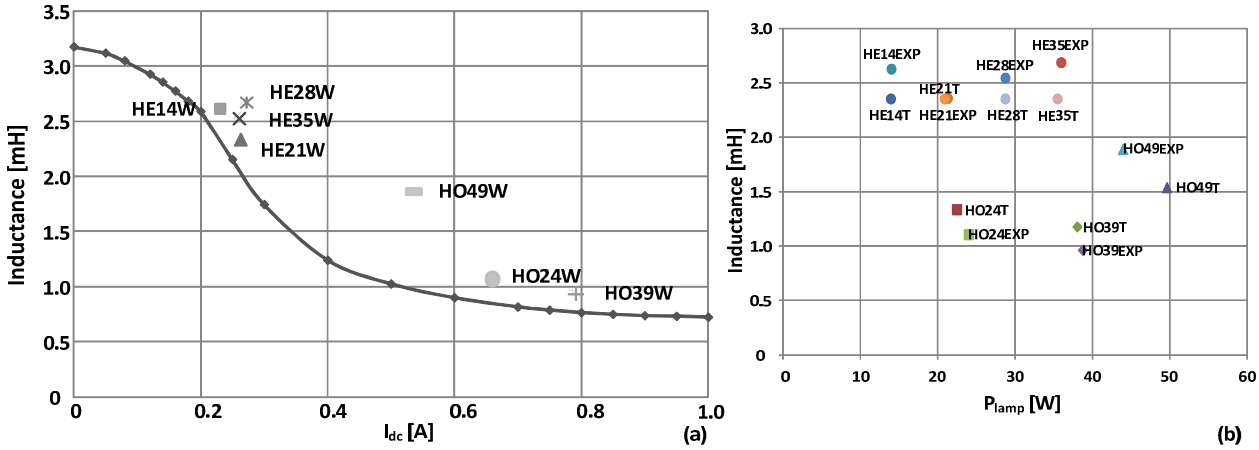

a. Small-signal and large-signal inductance as a function of the control current

b. Comparison between theoretical and experimental inductance values for each lamp

Fig. 3.103. Considerations on inductance values.

Fig. 3.103b. shows the difference between theoretical and experimental results for the estimated inductance values. This slightly different behaviour was expected. The method that was used for determining the resonant circuit parameters is based on the fundamental approximation

and the equations are defined assuming that the circuit is operating near resonance. However some of the sets of fluorescent lamp plus LC circuit are not in resonant mode and in those circumstances the resonant current will not assume an almost perfect sinusoidal waveform. This implies that the real inductance value required to operate each lamp at its rated power is expected to be slightly different.

In conclusion, the results showed that it was possible to achieve the nominal power for near all the selected T5 lamps using only one control parameter: the resonant circuit inductance. All the lamps were operated at a constant frequency, avoiding concerns related to EMI and switching losses. Safe electrode operation was verified and ensured through the application of the SoS technique. Each SoS limit was respected using a dual parallel capacitor configuration and a good performance was obtained for the entire prototype. ZVS operation was verified for all tested lamps as shown in the presented experimental results.

If a discrete set of operating frequencies together with the variable inductance were used as control parameters, the next obvious step would be to include dimming as a new feature in this magnetically-controlled universal ballast. In such case, the concern would be designing an EMI filter capable of dealing with this set of frequencies. However, even in these conditions, for each lamp and using a similar magnetic control technique, the role of reducing the luminous flux level would only be dictated by the variable inductance. The prototype would actually work for each of these lamps at a constant operating frequency, thereby limiting the known problems dictated by frequency control.

REFERENCES

[3.1] Alonso, J. M., Rashid, Muhammad H., "Power Electronics Handbook, Chapter 22 Electronic Ballasts", Academic Press, Inc., 2001, ISBN: 978-0-12-581650-2.

[3.2] Marian K. Kazimierczuk, Dariusz Czarkowski, "Resonant Power Converters", John Wiley & Sons, Inc., 1995.

[3.3] M. S. Perdigão, "Estudos sobre balastros electrónicos", Master Thesis, DEEC-FCTUC, October 2004.

[3.4] Alonso, J.M.; Dalla-Costa, M.A.; Cardesin, J.; Garcia, J.; "Magnetic dimming of electronic ballasts," Electronics Letters, vol.41, no.12, pp. 718- 719, 9 June 2005.

[3.5] Alonso, J.M.; Dalla Costa, M.A.; Rico-Secades, M.; Cardesin, J.; Garcia, J.; "Investigation of a New Control Strategy for Electronic Ballasts Based on Variable Inductor," Industrial Electronics, IEEE Transactions on , vol.55, no.1, pp.3-10, Jan. 2008.

[3.6] Perdigão, M.S.; Saraiva, E.S.; Alonso, J.M.; Dalla Costa, M.A.; "Comparative Analysis and Experiments of Resonant Tanks for Magnetically-Controlled Electronic Ballasts," Industrial Electronics, 2007. ISIE 2007. IEEE International Symposium on, vol., no., pp.3041-3046, 4-7 June 2007.

[3.7] Perdigão, M.S.; Alonso, J.M.; Dalla Costa, M.A.; Saraiva, E.S.; "Comparative Analysis and Experiments of Resonant Tanks for Magnetically Controlled Electronic Ballasts," Industrial Electronics, IEEE Transactions on, vol.55, no.9, pp.3201-3211, Sept. 2008.

[3.8] Ponce, M.; Vazquez, R.; Arau, J.; "High power factor electronic ballast for compact fluorescent lamps based in a class E amplifier with LCC resonant tank," Power Electronics Congress, 1998. CIEP 98. VI IEEE International, vol., no., pp.22-28, 12-15 Oct 1998.

[3.9] Ponce, M.; Arau, J.; Alonso, J.M.; "Analysis of the class E amplifier with two current sources used as a high-power-factor electronic ballast for fluorescent lamps," Applied Power Electronics Conference and Exposition, 2000. APEC 2000. Fifteenth Annual IEEE, vol.1, no., pp.591-596 vol.1, 2000.

[3.10] Czarkowski, D.; Kazimierczuk, M.K.; "Phase-controlled CLL resonant converter," Applied Power Electronics Conference and Exposition, 1993. APEC '93. Conference Proceedings 1993, Eighth Annual, vol., no., pp.432-438, 7-11 Mar 1993.

[3.11] Evgeny Rozanov and Sam Ben-Yaakov, "Analysis of current-controlled inductors by new SPICE behavioral model", HAIT Journal of Science and Engineering B, Volume 2, Issues 3-4, pp. 558-570, Holon Academic Institute of Technology, 2005.

[3.12] Hamill, D.C.; "Gyrator-capacitor modeling: a better way of understanding magnetic components," Applied Power Electronics Conference and Exposition, 1994. APEC '94. Conference Proceedings 1994. Ninth Annual, vol., no., pp.326-332 vol.1, 13-17 Feb 1994.

[3.13] Qianhong Chen; Ligang Xu; Xinbo Ruan; Siu Chung Wong; Tse, C.K.; "Gyrator-Capacitor Simulation Model of Nonlinear Magnetic Core," Applied Power Electronics Conference and Exposition, 2009. APEC 2009. Twenty-Fourth Annual IEEE, vol., no., pp.1740-1746, 15-19 Feb. 2009.

[3.14] Ludwig, G.W.; El-Hamamsy, S.-A.; "Coupled inductance and reluctance models of magnetic components," Power Electronics, IEEE Transactions on, vol.6, no.2, pp.240-250, Apr 1991.

[3.15] Medini, D.; Ben-Yaakov, S.; "A current-controlled variable-inductor for high frequency resonant power circuits," Applied Power Electronics Conference and Exposition, 1994. APEC '94. Conference Proceedings 1994. Ninth Annual, vol., no., pp.219-225 vol.1, 13-17 Feb 1994.

[3.16] Phillips, "3C85, Material grade specification", Data sheet.

[3.17] J. Rivas, J. M. Zamarro, E. Martín and C. Pereira; "Simple Approximation for Magnetization Curves and Hysteresis Loops", IEEE Trans. Magnetics, vol. 17,Issue 4, pp. 1498-1502, July 1981.

[3.18] A. S. Kislovski, "Relative Incremental Permeability of Soft Ferrites as a Function of the Magnetic Field H: An Analytic Approximation" Power Electronics Specialists Conference, PESC '96, 27th Annual IEEE, pp 1469-1475, June 1996.

[3.19] Leon O. Chua, "Linear and Non-linear Circuits", McGraw-Hill Inc., US, 1987.

[3.20] Il'in, O. G. and Shenderovich, A. M., "Measurement of nonlinear inductances", Journal on Measurement Techniques, Springer New York, pp.775-776, vol. 8, Issue 8, 1965.

[3.21] Robert W. Erikson and Dragan Maksimovic, "Fundamentals of Power Electronics", 2nd Edition, Springer, January 2001.

[3.22] M. S. Perdigão, J. M. Alonso, Marco Dalla Costa, E. S. Saraiva, "Design Considerations for the Optimization of Magnetically Dimmed Electronic Ballasts", X Portuguese-Spanish Congress on Electrical Engineering, XCLEE, 2007.

[3.23] M. S. Perdigão, E. S. Saraiva, J. M. Alonso, M. A. Dalla Costa, "Iluminação fluorescente: a garantia de eficiência energética mediante novas técnicas de controlo para balastros electrónicos com dimming", CLME 2008, Congresso Luso Moçambicano de Engenharia, Maputo, September 2008.

[3.24] Ng, W.; Lin, D.; Hui, R.; "Design of a Single Ultra-Low-Loss Magnetic Ballast for a Wide Range of T5 High-Efficiency Fluorescent Lamps," Industrial Electronics, IEEE Transactions, early access, March 2011.

[3.25] Hui, S.Y.; Lin, D.Y.; Ng, W.M.; Wei Yan; "A "Class-A2" Ultra-Low-Loss Magnetic Ballast for T5 Fluorescent Lamps—A New Trend for Sustainable Lighting Technology," Power Electronics, IEEE Transactions on , vol.26, no.2, pp.622-629, Feb. 2011.

[3.26] T5 Fluorescent Systems, Lighting Research Center, Access in: April 2011, http://www.lrc.rpi.edu/.

[3.27] Perdigão, M.S.; Baptista, B.; Alonso, J.M.; Saraiva, E.S.; "Magnetic regulator topologies for dimmable electronic ballasts," Industrial Electronics (ISIE), 2010 IEEE International Symposium on , vol., no., pp.921-926, 4-7 July 2010.

[3.28] Boeke, U.; "Scalable fluorescent lamp driver using magnetic amplifiers," Power Electronics and Applications, 2005 European Conference on, Sep. 2005.

[3.29] Philips MASTER TL5 lamps, Philips 2006, Access in: Jan. 2011, http://www.lighting.philips.com.

[3.30] Gules, R.; Santos, W.; Romaneli, E.; Andrea, C.; Annunziato, R.; "An Auxiliary Self-Oscillating Preheating System for Self-Oscillating Fluorescent Lamp Electronic Ballast," Industrial Electronics, IEEE Transactions on, March 2011. (Early access)

[3.31] Branas, C.; Azcondo, F.; Zane, R.; "Power-mode control of multiphase resonant electronic ballast," Industrial Electronics, IEEE Transactions on, Febr. 2011. (Early access)

[3.32] International Electrotechnical Commission. Ballasts for tubular fluorescent lamps - Performance requirements, IEC 60921, 2006.

[3.33] International Electrotechnical Commission. AC supplied electronic ballasts for tubular fluorescent lamps - Performance requirements, IEC 60929, 2006.

[3.34] IEC60081. Double-capped fluorescent lamps. Performance specifications. 2010.

[3.35] GE Lighting, T5 Long Last, linear fluorescent lamps, Datasheet, April 2009.

[3.36] Goud, L.H.; Dorleijn, J.W.F.; "Standardized data for dimming of fluorescent lamps," Industry Applications Conference, 2002. 37th IAS Annual Meeting. Conference Record of the, vol.1, no., pp. 673- 679 vol.1, 2002.

[3.37] Dorleijn, J.W.F.; Goud, L.H.; "Standardisation of the static resistances of fluorescent lamp cathodes and new data for preheating," Industry Applications Conference, 2002. 37th IAS Annual Meeting. Conference Record of the , vol.1, no., pp. 665- 672 vol.1, 2002

[3.38] Robert Nachtrieb, Farheen Khan and John F. Waymouth, "Cathode fall measurements in fluorescent lamps", J. Phys. D: Appl. Phys, 38, pp 3226-3236, August 2005.

[3.39] Application Report: Electronic Ballasts for Fluorescent Lamps using BUL770/791 Transistors", Texas Instruments, 1992

[3.40] Perdigão, M.S.; Alonso, J.M.; Dalla Costa, M.A.; Saraiva, E.S.; "Optimization of universal ballasts through magnetic regulators," Applied Power Electronics Conference and Exposition, 2008. APEC 2008. Twenty-Third Annual IEEE, vol., no., pp.1214-1220, 24-28 Feb. 2008.

[3.41] Perdigão, M.S.; Alonso, J.M.; Costa, M.A.D.; Saraiva, E.S.; "Using Magnetic Regulators for the Optimization of Universal Ballasts," Power Electronics, IEEE Transactions on, vol.23, no.6, pp.3126-3134, Nov. 2008.

[3.42] Perdigão, M.S.; E. S. Saraiva, J. M. Alonso, M. A. Dalla Costa; "Balastros Electrónicos Universais: Nova Técnica de Controlo Baseada em Reguladores Magnéticos," CBA 2008, Conferência Brasileira de Automática September 2008.

[3.43] M. S. Perdigão, J. M. Alonso, J. Ribas, D. Gacio, E. S. Saraiva; "Universal Ballast: A flexible solution based on magnetic regulator control concept," Seminario Anual de Automática, Eletrónica Industrial e Instrumentación, SAAEI'09, July 2009.

[3.44] Alonso, J.M.; Perdigão, M.S.; Ribas, J.; Gacio, D.; Saraiva, E.S.; "A digitally-controlled universal ballast based on magnetic regulator and PSoC device," Industrial Electronics, 2009. ISIE 2009. IEEE International Symposium on, vol., no., pp.2010-2015, 5-8 July 2009.

[3.45] Alonso, J. M.; Perdigao, M. S.; Ribas, J.; Gacio Vaquero, D.; Saraiva, E. S., "Optimizing Universal Ballasts using Magnetic Regulators and Digital Control," Industrial Electronics, IEEE Transactions on , vol. PP, no.99, pp.1, 0. (Early access)

[3.46] L. M. Lee, S. Y. R. Hui, H. S. H. Chung, "An automatic lamp detection technique for electronic ballasts," Twentieth Annual IEEE Applied Power Electronics Conference and Exposition, 2005. APEC 2005, vol. 1, pp. 575-581, Mar. 2005.

[3.47] P. N. N. Ayudhya, S. Naetiladdanon, A. Sangswang, "Automatic Fluorescent Lamp Detection Technique for Electronic Ballasts," IEEE International Conference on Robotics and Biomimetics, 2008. ROBIO 2008., 2009, vol. 1, pp. 1047-1052, Feb. 2009.

[3.48] P. N. N. Ayudhya, S. Naetiladdanon, A. Sangswang, "Automatic Fluorescent Lamp Detection for Electronic Ballasts Based on Operating Frequency and Phase Shift Compensation," IEEE International Symposium on Industrial Electronics, 2009. ISIE 2009, vol. 1, pp. 53-58, July 2009.

[3.49] L-M. Lee, S. Y. Hui, "Automatic Lamp Detection and Operation for Warm-Start Tubular Fluorescent Lamps," Power Electronics, IEEE Transactions on, vol. 24, no.12, pp. 2933 – 2941, Dec. 2009.

[3.50] Perdigão, M. S.; Baptista, B.; Marques, H.; Saraiva, E. S.; Alonso, J. M.; "On the use of magnetic regulators in electronic ballasts," Universities Power Engineering Conference (UPEC), 2010 45th International , vol., no., pp.1-6, Aug. 31 2010-Sept. 3 2010.

[3.51] M. Brown, "The one-transistor forward converter", Application Note AND8039/D, Semiconductor Components Industries, LLC, Phoenix, AZ, Application Note AND8039/D, 2005.

[3.52] M. Qiao, P. Parto and R. Amirani, "Stabilize the Buck Converter with Transconductance Amplifier", Application Note AN1043, International Rectifier.

[3.53] Lam, J.C.W.; Jain, P.K.; "A Novel High-Power-Factor Single-Switch Electronic Ballast," Industry Applications, IEEE Transactions on , vol.46, no.6, pp.2202-2211, Nov.-Dec. 2010

[3.54] ST Microelectronics, "VIPer Flyback Converter Design", available in: www.st.com. Access in Sep. 2010, 2005.

BIBLIOGRAPHY

[B3.1] Marian K. Kazimierczuk, Dariusz Czarkowski, “Resonant Power Converters”, John Wiley & Sons, Inc., 1995.

4 APPLICATION OF THE VARIABLE TRANSFORMER TO THE CONTROL OF ELECTRONIC BALLASTS

In the present chapter the variable transformer solution is presented as a step forward in magnetically-controlled electronic ballasts. The proposed technique takes advantage of the magnetic behaviour of the device to provide a new flexible way for luminous flux regulation. By integrating the magnetic component necessary to control the lamp current into a variable transformer, output electrical isolation and constant-frequency operation are both guaranteed by the proposed technique. Two different variable transformer topologies are suggested, five-leg and three-leg, and a comprehensive description of their behaviour, modelling and characterization, using a simple methodology is also presented. The modelling of the transformer is implemented using duality transformations and partition of matrices techniques. Model parameters are obtained from a combination of open-circuit and short-circuit tests. The large-signal characterization of the three-leg variable transformer is also presented. Different fluorescent lamps were selected to validate this new technique and experimental results clearly show its adequate behaviour.

4.1 INTRODUCTION TO THE PROPOSED MAGNETIC CONTROL TECHNIQUE

A step forward in this type of magnetic control led to the incorporation of variable transformers into the classical electronic ballast topology. This is a quite different approach to magnetically-controlled electronic ballasts since these magnetic regulators will be granting output electrical isolation in addition to the control of the lamp operation [4.1]-[4.3].

4.1.1 ISOLATED HALF-BRIDGE RESONANT BALLAST

As previously stated, the adopted topology will be the half-bridge parallel-loaded resonant ballast shown in Fig. 4.1. This circuit reveals the absence of the typical resonant inductance. As in the case of the variable inductor, the variable transformer will act upon the characteristic of the resonant circuit. It will integrate the magnetic element responsible for limiting the lamp current due to its negative impedance characteristic. The variable transformer will function as a simple transformer for a zero dc polarizing current and since the attached lamp is connected to its secondary side it is thereby isolated from the mains voltage. This is one of the main advantages of the proposed magnetic control. In essence, adapting the behaviour of the resonant circuit formed by the variable transformer equivalent circuit model and the resonant capacitor allows controlling the lamp operation. Therefore, this solution may provide, simultaneously dimming capability and electrical isolation, which seems to be a perfect combination for CCFLs in LCD backlighting applications. For safety purposes, these applications are always dependent on the inclusion of an isolation transformer between the inverter and the circuit which directly supplies the lamp.

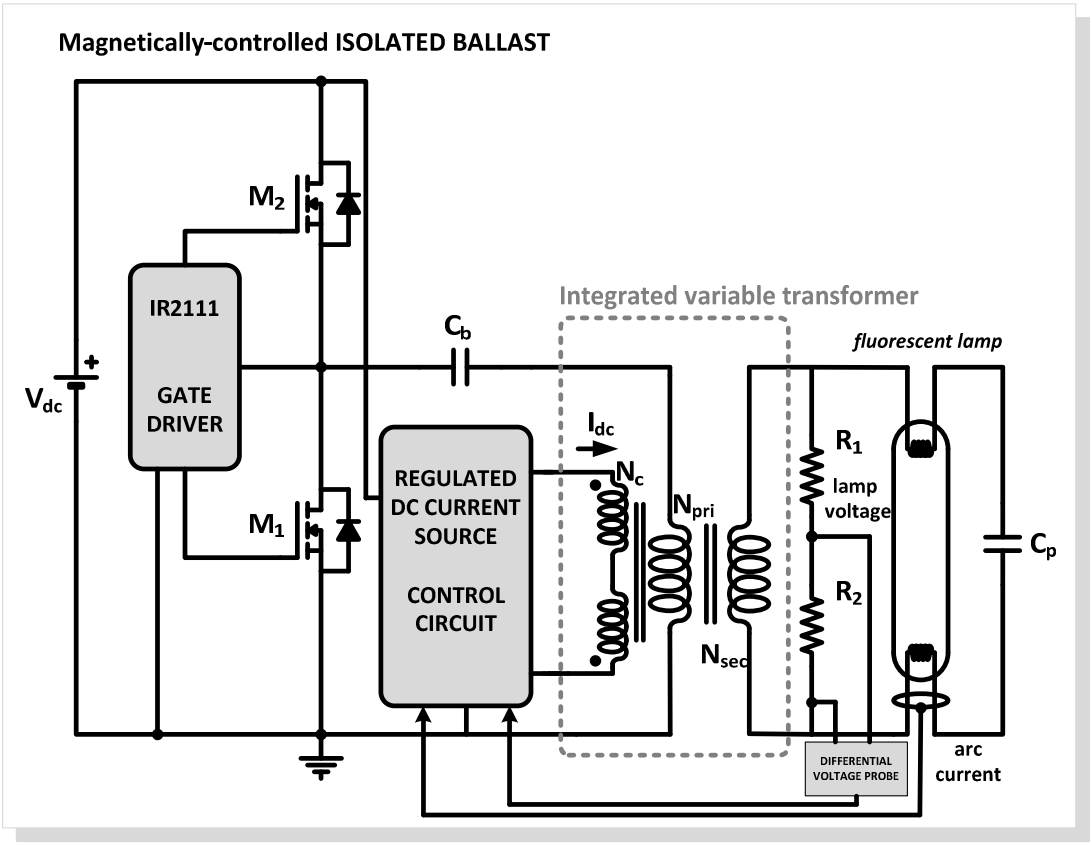

Fig. 4.1. Isolated half-bridge resonant ballast with an integrated variable transformer.

4.2 MODELLING AND CHARACTERIZATION OF VARIABLE TRANSFORMERS

The main purpose of this work is to demonstrate the possibility of using an integrated variable transformer to ignite and control the operation of a fluorescent lamp. By changing the level of the dc control current, the magnetic elements that constitute the transformer equivalent circuit can be altered, meaning that, modelling the device is essential to understand and control its inductive behaviour.

4.2.1 VARIABLE TRANSFORMER STRUCUTURES, TOPOLOGIES AND OPERATING PRINCIPLE

Two different variable transformer structures and topologies will be presented [4.1]-[4.4]. Both transformers are built using four gapped E cores, with the same materials used in variable inductors.

The first topology is presented in Fig. 4.2 and this regulator is designated as the five-leg variable transformer. This so-called five-leg topology consists of two double E cores placed in a row as represented in Fig. 4.2a. The variable transformer connections are represented in Fig. 4.2b. The primary winding is wound around the centre leg. Its terminals are represented by $pri(1)$ and $pri(2)$. The control winding is evenly distributed in the outer legs, C_A and C_B, and connected in opposite polarity The control winding terminals are represented by $con(1)$ and $con(2)$. The purpose of this connection is to reduce or substantially cancel the ac voltage on the control winding itself [4.6]. Finally the secondary winding is evenly distributed around the inner legs S_A and S_B, which include a small air gap. Its terminals are represented by $sec(1)$ and $sec(2)$. This new structure is somewhat inspired in the behaviour of previous magnetic regulator topologies, such as the four-leg magnetic regulator, or the two E-I cores, placed side-by-side, suggested in [4.5] and [4.6], but represents an attempt to avoid some undesirable influences of the prior solutions. Compared to the four-leg variable transformer, the control legs C_A and C_B are equidistant from the primary, which contributes to a more symmetric magnetic behaviour.

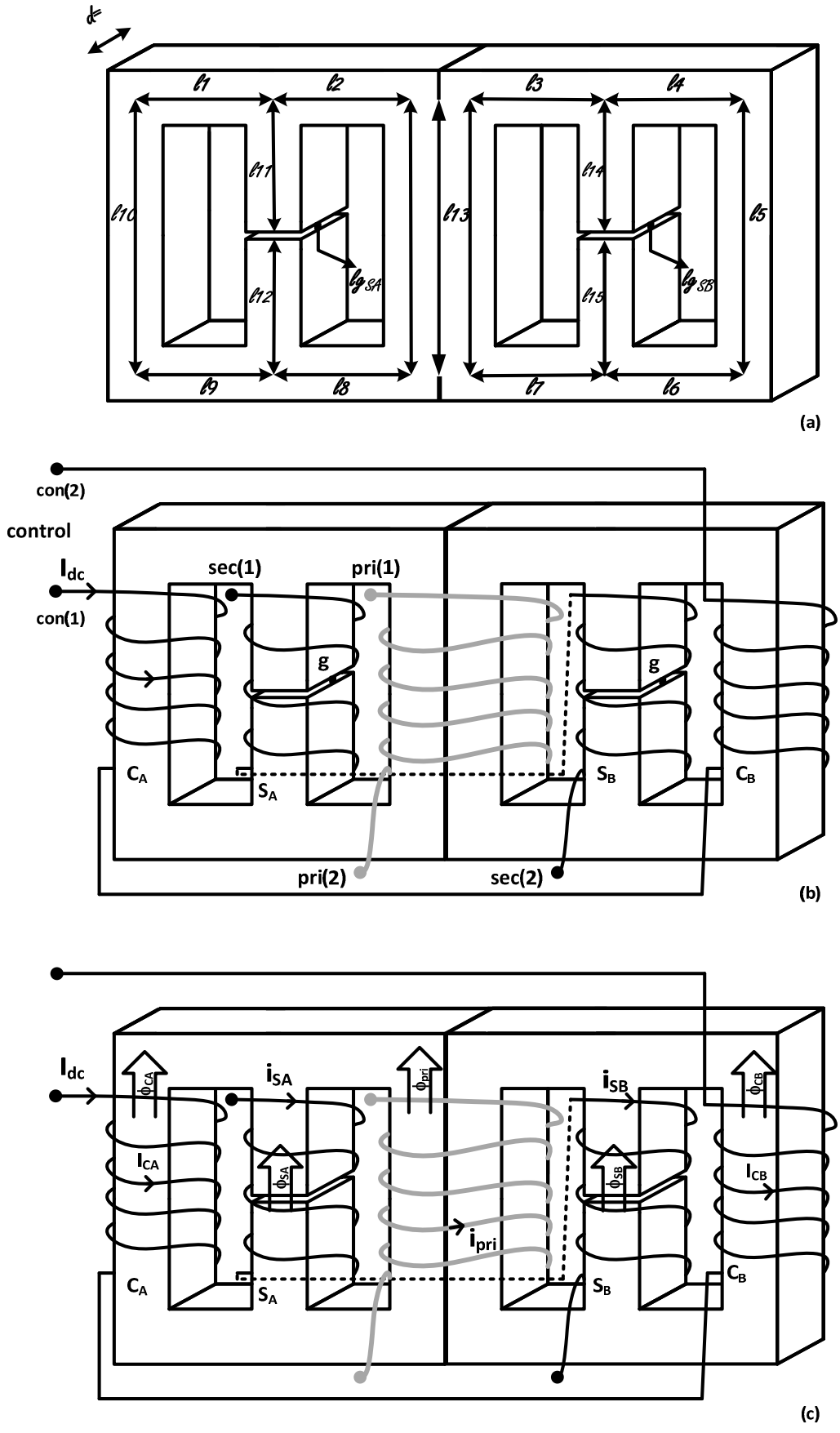

Fig. 4.2. Variable transformer: five-leg structure and topology.

Connecting the output inverter voltage to the primary terminals of the transformer, the ac flux generated by the primary winding will flow through its corresponding leg and then divide between the right and left paths. For a zero dc control current, and due to the presence of the small air gap in legs S_A and S_B, this flux tends to be coupled to the control winding, in the outer legs, with obviously lower reluctance. On the contrary, if the dc polarizing current has an increasing non-zero value, the reluctances of these paths change and therefore the amount of primary flux coupled to the secondary winding tends to increase, meaning that more voltage will be developed across this winding. In conclusion, the basic principle of this magnetic regulator is to provide the ability to control the leakages associated to the main magnetic circuit, increasing the effective global reluctance of the outer legs of the transformer core. Therefore, this device may be used for ballast purposes, since it enables the control of the power delivered to the lamp, also providing another advantage besides electric isolation: it works at a constant switching frequency.

The second topology is presented in Fig. 4.3 and this regulator is designated as the parallel three-leg variable transformer. This so-called three-leg topology consists of two double E cores placed in parallel and is inspired in the analysis presented in [4.5] and [4.11]. Fig. 4.3a. and Fig. 4.3b. present the left and right view of this variable transformer.

The control windings are wound around one of the outer legs of each core separately; serially connected in opposite polarity and then placed side-by-side. The control winding terminals are represented in Fig. 4.3 by C_1 and C_2. The induced voltages on these windings have opposite polarities and, under the assumption of symmetry should cancel each other. As explained in [4.19], there will be a parasitic, non-linear coupling between the input voltage and the control windings voltage, due to the non-linearity of the magnetic material. As a result, the control windings only exhibit a negligible voltage with a frequency equal to twice the operating frequency. The primary winding is wound around the centre legs of both cores. Its terminals are represented by P_1 and P_2. Finally, the secondary winding is wound around the remaining outer legs of both cores, which include a small air gap. The secondary winding terminal are also represented in Fig. 4.3 by S_1 and S_2.

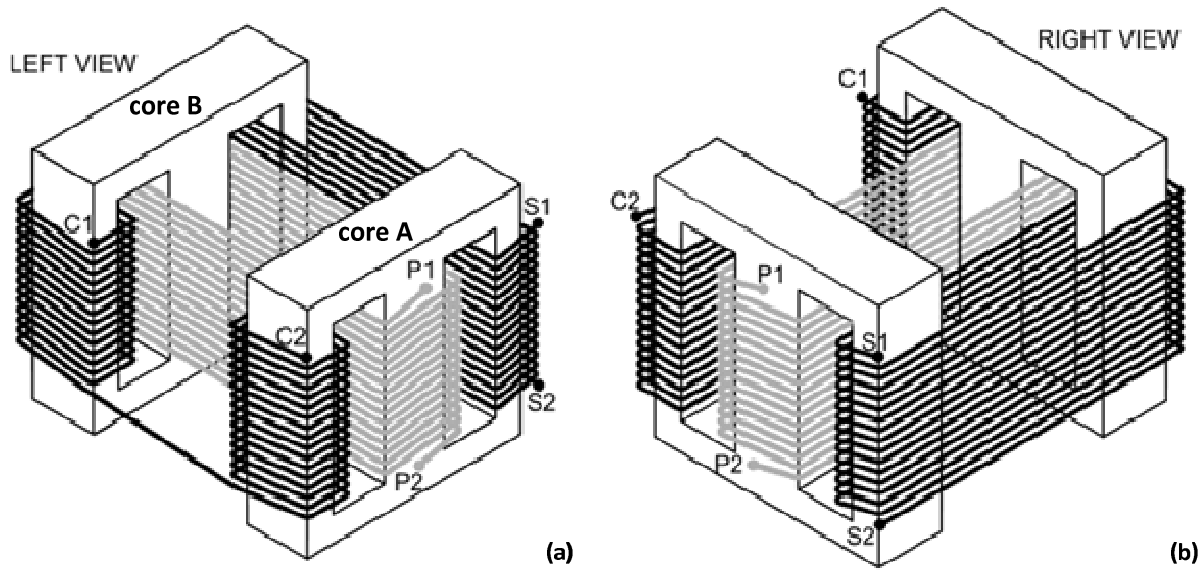

Fig. 4.3. Variable transformer: parallel three-leg structure and topology.

Connecting the inverter output voltage to the primary terminals of the transformer, the ac flux generated by the primary winding will flow through its corresponding leg and then divide between the left and right paths according to the reluctance of each path. This behaviour is similar to the first topology. A dc current circulating through the control windings varies the dc flux density in the left half of the structure. Considering a zero dc current, the path on the left will have a much lower reluctance due to the air gap introduced in the right path. As a result, the ac flux generated by the primary winding that links through the secondary will be lower, thus little ac voltage will be induced in the secondary winding. If the dc current is large enough to push the operating point towards saturation, the reluctance of the path to the left of the primary, increases relatively to the reluctance of the path to the right, thereby controlling the amount of ac flux coupled with the secondary winding.

As stated in [4.5], the cross section of the primary legs must be sufficiently larger than the cross section of the control legs, so that, as the control legs approach saturation, it does not affect the permeance of the primary legs. In fact, to take advantage of working at the knee of the $B(H)$ curve, saturation must be approached but not fully reached. As in the first transformer, the basic principle is to provide the ability to control the leakages associated to the main magnetic circuit, increasing the effective global reluctance of the left side of the transformer cores, without completely saturating the core. For a better understanding of the operating principle of this transformer, the magnetic flux generated by the primary winding, in the cores, may be defined in (4.1).

$$\phi_P = \phi_c + \phi_{lc} \tag{4.1}$$

where ϕ_c is the magnetic flux generated by the primary winding that links through the secondary winding in Wb, and ϕ_{lc} is the magnetic flux generated by the primary winding that does not link through the secondary winding, meaning the primary leakage flux, also in Wb.

4.2.2 VARIABLE TRANSFORMER MODELLING

The theoretical analysis of the magnetic device is a non-trivial task, so in order to have prior notion of its behaviour, an equivalent circuit model, based upon its actual physical structure, represents a practical approach. The classic theory on magnetic modelling of multi-winding devices begins by establishing a more or less complicated reluctance model of the structure. In [4.11], the reluctance concept together with the duality theory is used to generate, first, the magnetic equivalent circuit and then, the inductances circuit model. This inductances model will result into a more or less complicated electric circuit, which may be combined with other electric circuits, such as the half-bridge resonant inverter.

According to [4.11], since the equations that describe the magnetic circuit have the same form as those for the electrical circuit, the method used to find the dual of an electrical circuit can be also applied to find the dual of a magnetic circuit. In traditional equivalent-circuit models, magnetomotive force is analogous to voltage, and magnetic flux is analogous to current. Consequently the reluctance can be represented by a resistor.

4.2.2.1 FIVE-LEG VARIABLE TRANSFORMER MODELLING

Fig. 4.2a. represents the definition used for the magnetic paths which together make up the device [4.12]. Each magnetic path relates to a specific reluctance, $\mathcal{R}_\mathrm{i}$, defined by:

$$\mathcal{R}_i = {}^{l_i}/_{\mu A_i} \tag{4.2}$$

where l_i is the magnetic path length, A_i the correspondent cross sectional area and μ the permeability. In fact, these several reluctances represent part of the magnetic behaviour of the device, by superposition on the core geometry. Fig. 4.4 shows firstly a more complex reluctance model of the five-leg variable transformer structure, directly related with the core geometry. The

primary, secondary and control windings will appear as *mmf* sources. Particularly, the following quantities are defined:

- $N_p i_p, N_{SA} i_{SA}, N_{SB} i_{SB}$ are the *mmf* sources associated with the primary and secondary winding, leg S_A and leg S_B respectively;
- $N_{CA} I_{dc}, -N_{CB} I_{dc}$ are the *mmf* sources associated with the control winding, leg C_A and leg C_B, respectively;
- $\mathcal{R}_{18}, \mathcal{R}_{16}, \mathcal{R}_{17}$ are the reluctances of the magnetic paths associated to the primary and secondary leakage fluxes.

In order to straightforward the structure, no dc *mmf* source is included in the second version of the reluctance model, also shown in Fig. 4.4. The effect of the control winding is in fact, already introduced in the model since the dc control current affects the permeance and thereby the reluctance of the relevant path. The following simplifications are made:

$$\mathcal{R}_{19} = \mathcal{R}_{16} // (\mathcal{R}_1 + \mathcal{R}_9 + \mathcal{R}_{10});\ \ \mathcal{R}_{20} = \mathcal{R}_{17} // (\mathcal{R}_4 + \mathcal{R}_5 + \mathcal{R}_6) \tag{4.3}$$

$$\mathcal{R}_{21} = \mathcal{R}_{11} + \mathcal{R}_{\mathrm{g}} + \mathcal{R}_{12};\ \ \mathcal{R}_{22} = \mathcal{R}_{14} + \mathcal{R}_{\mathrm{g}} + \mathcal{R}_{15} \tag{4.4}$$

$$\mathcal{R}_{23} = \mathcal{R}_2 + \mathcal{R}_8;\ \ \mathcal{R}_{24} = \mathcal{R}_3 + \mathcal{R}_7 \tag{4.5}$$

The procedure to find the structure of the dual circuit is based on the fact that the inductances values can be calculated using the typical equation which relates the number of turns with the permeance or the reluctance of the magnetic path [4.13]:

$$L_i = N_p^2 P_i = {N_p^2}/{\mathcal{R}_i} \tag{4.6}$$

Each *mmf* source should be replaced by an ideal transformer in order to match the input and output voltages and currents of the model, with those of the original circuit. The dual circuit can be scaled by any number; nonetheless, by choosing the appropriate physical turns ratio, $N = N_p$, where N_p represents the number of turns on the primary winding, an 1:1 ideal transformer can be inserted at the primary terminals. Moreover, two networks are dual if the loop equations for one network are in the same form as the node equations for the other [4.13]. This analysis is essential to obtain the direction of the new branches.

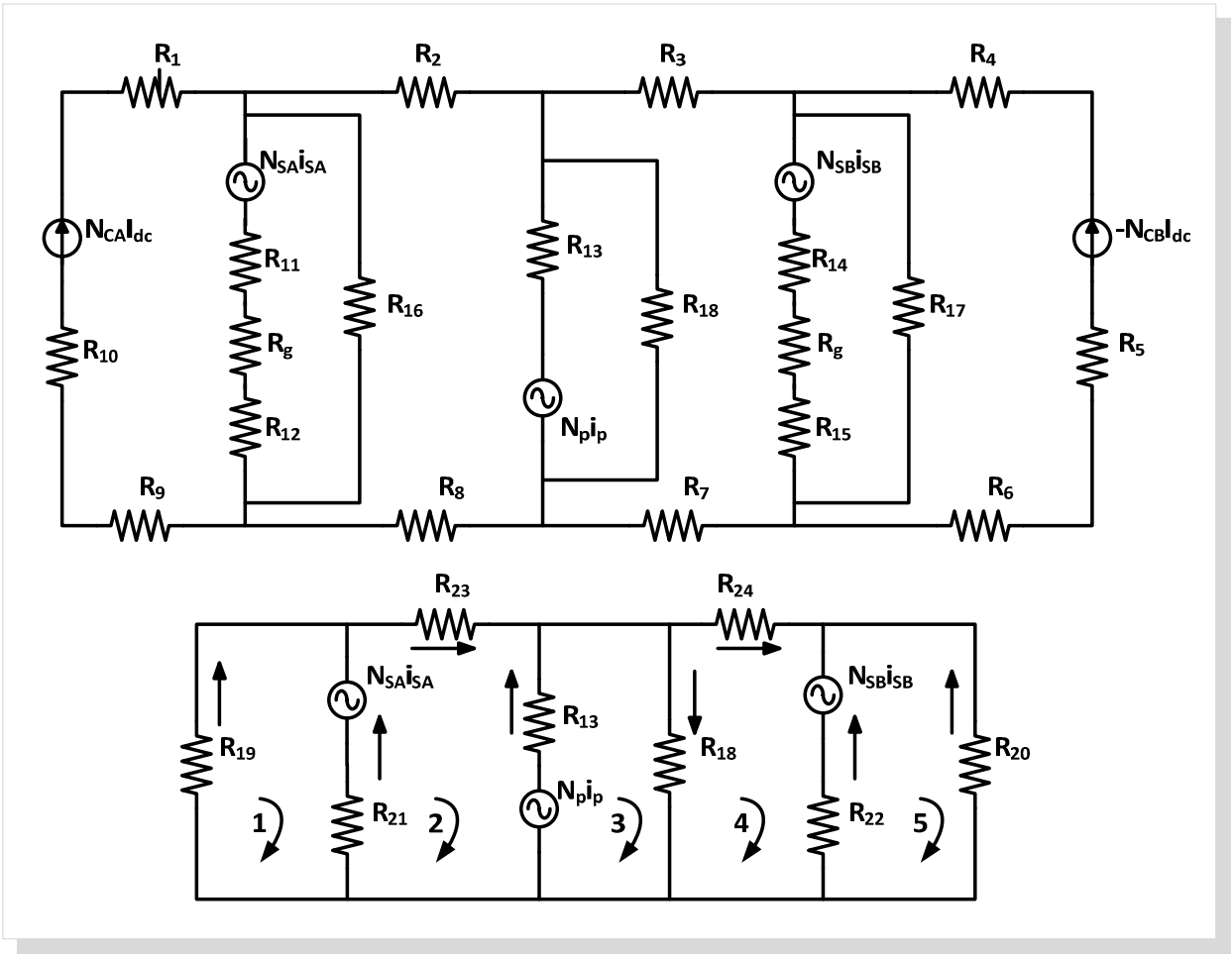

Fig. 4.4. Variable transformer: five-leg structure and topology.

Fig. 4.5 and Table 3.8 present the necessary steps to obtain the electric circuit model. Each dot in the original reluctance model corresponds to a node of the dual network. The permeances circuit model will be scaled using $N = N_p$.

Obviously, in the final electric circuit model, only the ideal transformer inserted at the primary terminals may be neglected. Since the secondary winding is evenly distributed around the inner legs S_A and S_B, two ideal transformers with an appropriate physical turns ratio are inserted at their terminals.

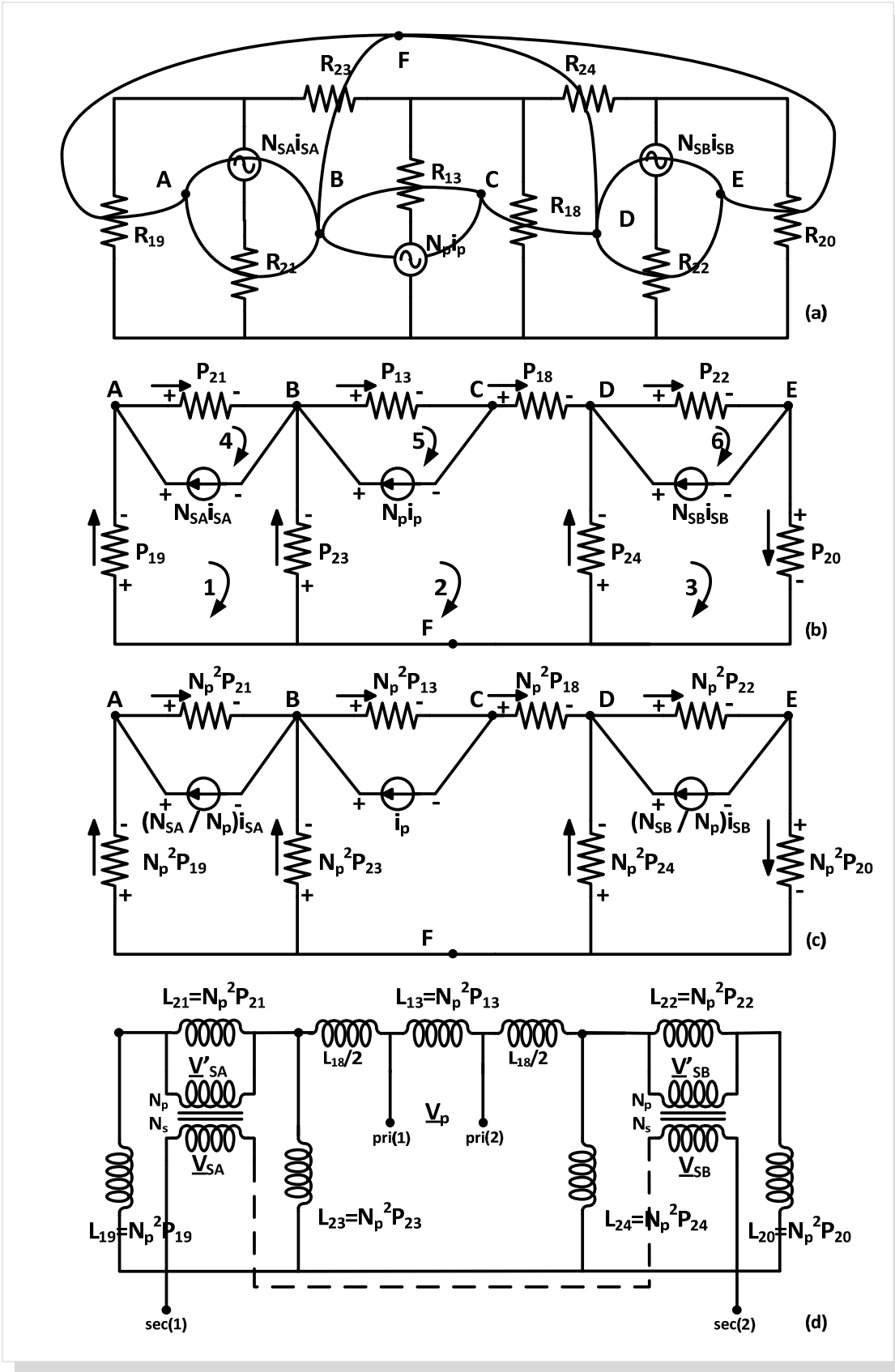

a. Finding the structure of the dual circuit b. The dual circuit c. Scaling the permeances by N_p d. The electric circuit model

Fig. 4.5. Duality theory.

Table 4.1 Applying the duality theory.

MAGNETIC CIRCUIT: LOOP AND NODAL ANALYSIS	ELECTRIC EQUIVALENT CIRCUIT
LOOP 1-5	NODE 1-5
$\mathcal{R}_{19}.\phi_{19} - N_{SA}.i_{SA} - \mathcal{R}_{21}.\phi_{21} = 0$	$P_{19}.F_{19} - N_{SA}.V_{SA} - P_{21}.F_{21} = 0$
$N_{SA}.i_{SA} - N_p.i_p = \mathcal{R}_{23}.\phi_{23} + \mathcal{R}_{21}.\phi_{21} - \mathcal{R}_{13}.\phi_{13}$	$N_{SA}.V_{SA} - N_{p_{th}}.V_{p_{th}} = P_{23}.F_{23} + P_{21}.F_{21} - P_{13}.F_{13}$
$N_p.i_p = \mathcal{R}_{13}.\phi_{13} + \mathcal{R}_{18}.\phi_{18}$	$N_p.V_p = P_{13}.F_{13} + P_{18}.F_{18}$
$-N_{SB}.i_{SB} = \mathcal{R}_{24}.\phi_{24} - \mathcal{R}_{22}.\phi_{22} - \mathcal{R}_{18}.\phi_{18}$	$-N_{SB}.V_{SB} = P_{24}.F_{24} - P_{22}.F_{22} + P_{18}.F_{18}$
$N_{SB}.i_{SB} = -\mathcal{R}_{20}.\phi_{20} + \mathcal{R}_{22}.\phi_{22}$	$N_{SB}.V_{SB} = -P_{20}.F_{20} + P_{22}.F_{22}$
NODE 1-6	LOOP 1-6
$\phi_{19} + \phi_{SA} = \phi_{23}$	$F_{19} + F_{SA} = F_{23}$
$\phi_{23} + \phi_{13} = \phi_{18} + \phi_{24}$	$F_{23} + F_{13} = F_{18} + F_{24}$
$\phi_{SB} + \phi_{24} + \phi_{20} = 0$	$F_{SB} + F_{24} + F_{20} = 0$
$\phi_{21} = \phi_{SA};\ \phi_p = \phi_{13}; \phi_{SB} = \phi_{22}$	$F_{21} = F_{SA};\ F_p = F_{13};\ F_{SB} = F_{22}$

In order to proceed with the modelling and characterization of the variable transformer, the next step will be obtaining the 2x2 matrix that relates the external voltages and currents. The electric circuit model presented in Fig. 4.5d. includes only the inductive effects of the variable transformer: the secondary and primary voltages do not include the resistive drops. The following explanation uses the subscript i to enhance this fact.

The matrix equation is obtained writing firstly the loop equations of the six independent meshes of the electric circuit model. Secondly, using the partition of matrices technique, the internal currents can be eliminated [4.17]. Considering:

$$\underline{V_p} = R_p\underline{I_p} + \underline{V_{pi}};\ \ \underline{V_S} = R_S\underline{I_S} + \underline{V_{Si}};\ \ \underline{V'_{Si}} = \underline{V'_{SA}} + \underline{V'_{SB}} \tag{4.7}$$

and maintaining the initial mesh notation:

$$\underline{I_{m4}} = \underline{I'_{SA}} = \underline{I'_{SB}} = \underline{I_{m6}} = \underline{I'_S};\ \ \underline{I_{m5}} = \underline{I_p} \tag{4.8}$$

the matrix equation can be written as follows:

$$\begin{bmatrix} \underline{V}'_{ext} \\ \underline{V}'_{int} \end{bmatrix} = j\omega . \begin{bmatrix} A & B \\ C & D \end{bmatrix} . \begin{bmatrix} \underline{I}'_{ext} \\ \underline{I}'_{int} \end{bmatrix} \tag{4.9}$$

where

$$\underline{V}'_{ext} = \begin{bmatrix} \underline{V}_{pi} \\ \underline{V}'_{Si} \end{bmatrix};\ \underline{V}'_{int} = \begin{bmatrix} 0 \\ 0 \\ 0 \end{bmatrix};\ \underline{I}'_{ext} = \begin{bmatrix} \underline{I}_{p} \\ \underline{I}'_{S} \end{bmatrix};\ \underline{I}'_{int} = \begin{bmatrix} \underline{I}_{m1} \\ \underline{I}_{m2} \\ \underline{I}_{m3} \end{bmatrix} \tag{4.10}$$

and

$$A = \begin{bmatrix} L_{13} & 0 \\ 0 & L_{13} + L_{13} \end{bmatrix};$$

$$B = \begin{bmatrix} 0 & L_{13} & 0 \\ L_{21} & 0 & L_{22} \end{bmatrix};$$

$$C = \begin{bmatrix} 0 & L_{21} \\ L_{13} & 0 \\ 0 & L_{22} \end{bmatrix};$$

$$D = \begin{bmatrix} L_{19} + L_{21} + L_{23} & -L_{23} & 0 \\ -L_{23} & L_{23} + L_{18} + L_{13} + L_{24} & -L_{24} \\ 0 & -L_{24} & L_{22} + L_{20} + L_{24} \end{bmatrix} \tag{4.11}$$

Finally, in order to obtain the inductances matrix $[L_{ext}]$ that characterizes the variable transformer, the internal voltages and current should be eliminated:

$$[0] = j\omega\left([C]\left[\underline{I}'_{ext}\right] + [D]\left[\underline{I}'_{int}\right]\right) \Leftrightarrow -([D]^{-1}[C]\left[\underline{I}'_{ext}\right] = [D]^{-1}[D]\left[\underline{I}'_{int}\right]) \tag{4.12}$$

$$\begin{aligned} \left[\underline{V}'_{ext}\right] &= j\omega\left([A]\left[\underline{I}'_{ext}\right] + [B]\left[\underline{I}'_{int}\right]\right) = j\omega\left([A]\left[\underline{I}'_{ext}\right] + [B](-[D]^{-1}[C])\left[\underline{I}'_{ext}\right]\right) \\ &= j\omega([A] - [B][D]^{-1}[C])\left[\underline{I}'_{ext}\right] \end{aligned} \tag{4.13}$$

where:

$$[L'_{ext}] = [A] - [B][D]^{-1}[C] \tag{4.14}$$

$[L'_{ext}]$ is still referred to the primary side of the transformer. Applying the following relation, $[L_{ext}]$ is finally obtained:

$$\begin{bmatrix} \underline{I}_p \\ \underline{I}'_S \end{bmatrix} = \begin{bmatrix} 1 & 0 \\ 0 & \frac{N_S}{N_p} \end{bmatrix} \cdot \begin{bmatrix} \underline{I}_p \\ \underline{I}_S \end{bmatrix} = [T] . \begin{bmatrix} \underline{I}_p \\ \underline{I}_S \end{bmatrix} \tag{4.15}$$

$$[L_{ext}] = [T]^T . [L'_{ext}] . [T] \tag{4.16}$$

So in conclusion, the variable transformer can be characterized by a 2x2 inductance matrix:

$$[L_{ext}] = \begin{bmatrix} L_{11} & L_{12} \\ L_{21} & L_{22} \end{bmatrix} \tag{4.17}$$

This means that the five-leg variable transformer can be represented by a typical T inductance model as presented in Fig. 4.6, [4.16], [4.17]. The T model parameters $L_X; L_Y; L_Z$ are directly related with the inductance matrix as shown in (4.18). There are however some issues related to this T inductance model which will be further discussed in the modelling of the three-leg variable transformer.

$$L_X = L_{11} - L_{12}\ ;\ \ L_Y = L_{22} - L_{12};\ \ L_Z = L_{12} = L_{21} \tag{4.18}$$

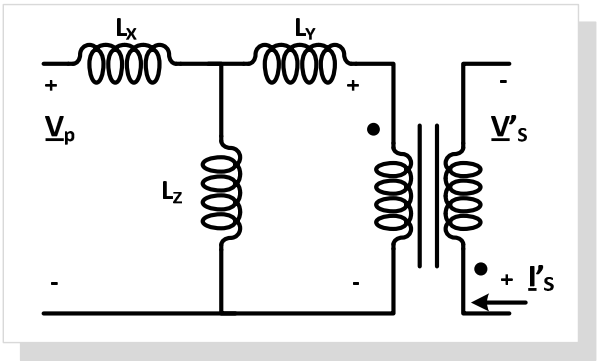

Fig. 4.6. Proposed T inductance model.

4.2.2.2 PARALLEL THREE-LEG VARIABLE TRANSFORMER MODELLING

Fig. 4.7a. shows the reluctance model of the variable transformer structure. The several reluctances characterize part of the magnetic behaviour of the device, by superposition on the core geometry. In this case, each magnetic path *i* relates to a specific core reluctance, $\mathcal{R}_i^j$, as defined in (4.19):

$$\mathcal{R}_i^j = {}^{l_i}/_{\mu A_i} \tag{4.19}$$

where l_i is the magnetic path length, A_i the correspondent cross sectional area, μ the permeability and j the core A or B. Since the permeance is a function of the control current, so will be the reluctance.

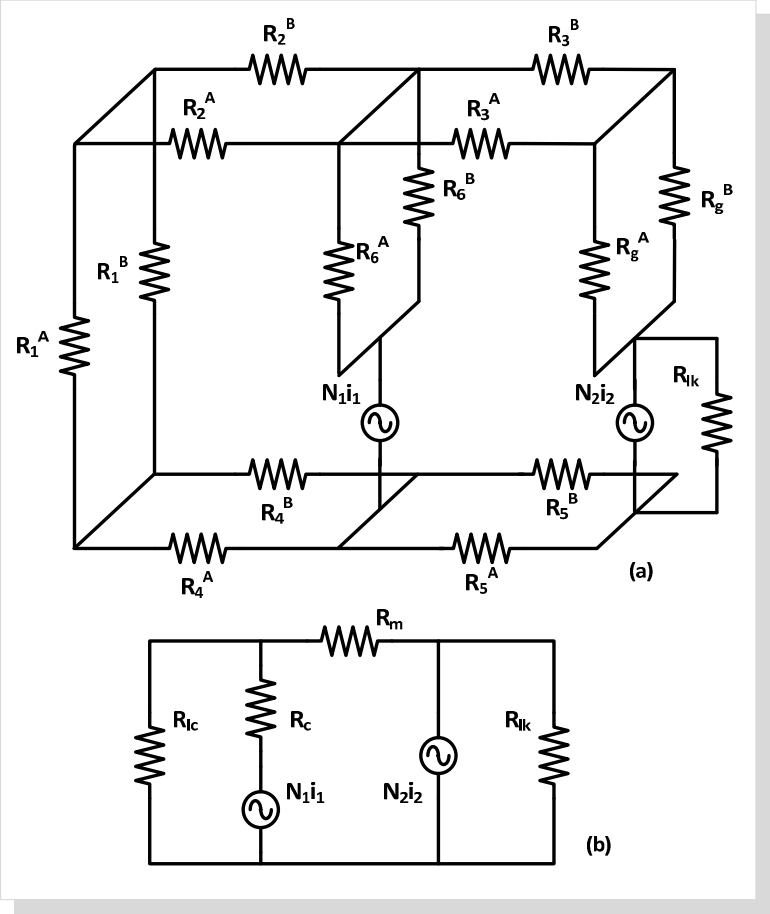

a. Model of the variable transformer circuit b. Model of the simplified circuit

Fig. 4.7. Reluctance models.

In order to simplify the model, no dc *mmf* source is included in the first version of the reluctance model, shown in Fig. 4.7a. The effect of the control winding is in fact, already introduced in the model since the dc control current affects the permeability and thereby the reluctance of the relevant path. The primary and secondary windings will appear as *mmf* sources. It should be noted that the reluctance of the right leg, which is very small in comparison to the reluctance of the existent air gap, is included in $\mathcal{R}_3^A$. At this point, no reluctance associated to the primary leakage flux was introduced since it could be later represented by a series inductance in the final inductance model. However, due to the presence of the air gap in the right leg, the secondary leakage flux is expected to be higher, which in turn led to the definition of reluctance $\mathcal{R}_{lk}$.

The final reluctance model shown in Fig. 4.7b. corresponds to a simplified version of the first model, taking into account the quantities of Fig. 4.7a. and trough the definition of the following reluctances:

$$\mathcal{R}_{lc}^{A} = \mathcal{R}_{1}^{A} + \mathcal{R}_{2}^{A} + \mathcal{R}_{4}^{A};\ \ \mathcal{R}_{lc}^{B} = \mathcal{R}_{1}^{B} + \mathcal{R}_{2}^{B} + \mathcal{R}_{4}^{B} \tag{4.20}$$

$$\mathcal{R}_{c}^{A} = \mathcal{R}_{6}^{A};\ \ \mathcal{R}_{c}^{B} = \mathcal{R}_{6}^{B} \tag{4.21}$$

$$\mathcal{R}_{m}^{A} = \mathcal{R}_{3}^{A} + \mathcal{R}_{5}^{A} + \mathcal{R}_{g}^{A};\ \ \mathcal{R}_{m}^{B} = \mathcal{R}_{3}^{B} + \mathcal{R}_{5}^{B} + \mathcal{R}_{g}^{B} \tag{4.22}$$

where:

- $\mathcal{R}_{lc} = \mathcal{R}_{lc}^{A} // \mathcal{R}_{lc}^{B}$; being $\mathcal{R}_{lc}^{A}$ and $\mathcal{R}_{lc}^{B}$ the total sum of the reluctances of the magnetic paths associated to the ac flux not linked to the secondary, meaning the total primary leakage flux for each core;
- $\mathcal{R}_{m} = \mathcal{R}_{m}^{A} // \mathcal{R}_{m}^{B}$; being $\mathcal{R}_{m}^{A}$ and $\mathcal{R}_{m}^{B}$ the reluctances of the magnetic paths associated with the coupled ac flux for each core;
- $\mathcal{R}_{c} = \mathcal{R}_{c}^{A} // \mathcal{R}_{c}^{B}$; being $\mathcal{R}_{c}^{A}$ and $\mathcal{R}_{c}^{B}$ the reluctances of the magnetic paths which carry the common flux, both the coupled and leakage fluxes for each core;

and:

- $N_1 i_1, N_2 i_2$ are the *mmf* sources associated with the primary and secondary windings respectively;
- $\mathcal{R}_{lk}$ are the reluctance of the magnetic path associated to the secondary leakage flux;

Once again the procedure to find the structure of the dual circuit, presented in Fig. 4.8, is based on the fact that the inductances values can be calculated using the typical equation which relates the number of turns with the reluctance of the magnetic path as already defined in (4.6). Also in this case, by choosing the appropriate physical turns ratio, $N = N_1$, a 1:1 transformer is inserted at the primary terminals and then neglected. All the model inductances are fixed except for L_{lc} and L_c, which depend on the permeability of the control legs and thus will decrease with increasing control current.

In the four-leg structure presented in [4.11] it is stated that $\mathcal{R}_c$ is relatively small when compared to the other reluctance values and therefore it can be neglected. Nevertheless, for this particular structure, $\mathcal{R}_c$ is influenced by the presence of the dc control flux; thereby it must be

included in the model. The simplification of the dual circuit into the model shown in Fig. 4.9 considers this fact. The most common equivalent circuit of a transformer is the T model, where typically the parameters assume physical meaning. Due to the specific nature of this variable transformer, the inductances are rearranged in order to include L_c in the T model.

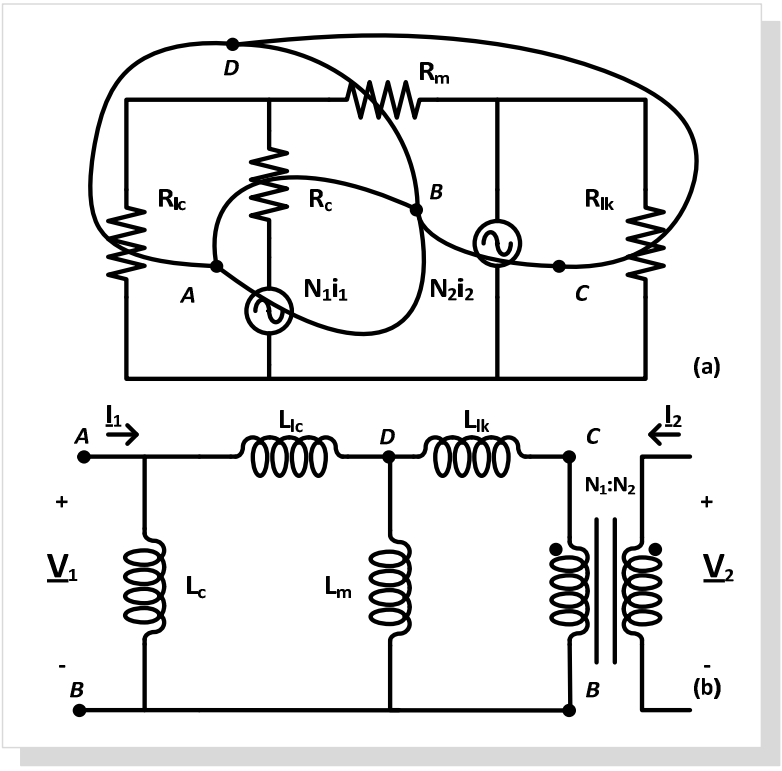

a. Finding the structure of the dual circuit b. The dual circuit

Fig. 4.8. Duality theory.

In the dual circuit shown in Fig. 4.8b., five different parameters can be identified: four different inductances and the relation between the input and output of the ideal transformer. If the variable transformer is understood as a quadripole, the following equations can be established:

$$\begin{bmatrix} \underline{V}_1 \\ \underline{V}_2 \end{bmatrix} = \begin{bmatrix} Z_{11} & Z_{12} \\ Z_{21} & Z_{22} \end{bmatrix} \cdot \begin{bmatrix} \underline{I}_1 \\ \underline{I}_2 \end{bmatrix} \tag{4.23}$$

where $Z_{12} = Z_{21}$. If the resistive effect is neglected, the variable transformer behaviour can be represented by a 2x2 inductances matrix, as in the case of the five-leg variable transformer:

$$[L_{\text{model}}] = \begin{bmatrix} L_{11} & L_{12} \\ L_{21} & L_{22} \end{bmatrix} \tag{4.24}$$

where $L_{12} = L_{21}$. Since there are only three independent elements it is implicit that only three different parameters can be determined. This means that the model presented in Fig. 4.8b. must

be simplified. So, the variable transformer is from then on represented by one of the T inductance models, as presented in Fig. 4.9 [4.17]. Therefore:

$$L_{lc} = L_{11} - L_{12}\ ;\ \ L_{lk} = L_{22} - L_{12};\ \ L_m = L_{12} = L_{21} \tag{4.25}$$

The inductances L_{lc}, L_{lk} and L_m have now different values, because they must also include the effect of L_c which does not exist in this new model. *TR'* represents the transformation ratio of the ideal transformer. If *TR'* equals the turns ratio of the real transformer, $N_1 : N_2$, the inductive elements of the T model are often interpreted magnetically, as so-called magnetizing inductance and leakage inductances [4.16]. However, for this particular case, due to the non-linear behaviour of the transformer and the imposed operation near saturation, the leakage inductances are not constant, and *TR'* must be interpreted as a voltage transformation ratio.

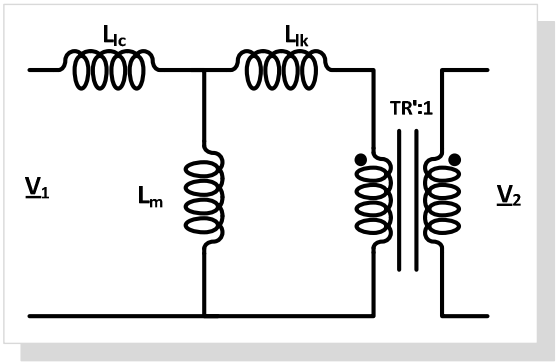

Fig. 4.9. Proposed T inductance model.

In conclusion, for both variable transformers a T inductance model was obtained. This can be observed comparing Fig. 4.9 to Fig. 4.6. The next step involves the characterization of the corresponding prototypes.

4.2.3 VARIABLE TRANSFORMER CHARACTERIZATION

The characterization methodology of magnetic multi-winding devices, for modelling purposes, is always a defying task [4.15]. Naturally, knowledge of the internal structure of the device and of the used magnetic materials should be included in the initial model. But, simple and easily-developed models would be preferred for the final use. In this way, the model parameters can easily be determined by measurements at the terminals of the device. In this particular case, the non-linear behaviour of the regulator raises some issues and adds some difficulties to the modelling and the characterization of the transformer.

The experimental prototype presented in Fig. 4.10a., the five-leg variable transformer, was built using two EF25 ferrite cores, with $N_p = 100$ turns, $N_{SA} = N_{SB} = 50$, and for each control winding, $N_{CA} = N_{CB} = 80$ turns. The experimental prototype presented in Fig. 4.10b., the parallel three-leg variable transformer, was also built using two EF25 cores, with $N_1 = N_2 = 100$ turns, and for each control winding $N_c = 80$ turns.

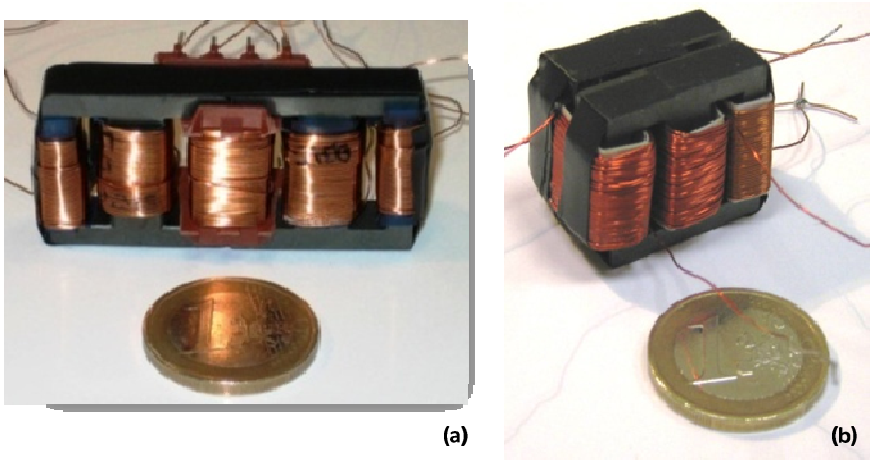

a. Five-leg b. Parallel three-leg

Fig. 4.10. Variable transformers prototypes.

To perform the experimental small-signal characterization of the magnetic devices several measurements were taken by means of open-circuit and short-circuit tests. For both transformers, the open-circuit test was done measuring firstly the primary open-circuit inductance, L_{11oc}, with the secondary open and vice-versa, measuring the secondary open-circuit inductance, L_{22oc} with the primary open. Similarly, for the same range of the dc control current, the short-circuit test was done measuring firstly the primary short-circuit inductance, L_{1cc}, with the secondary short-circuited and vice-versa, measuring the secondary short-circuit inductance, L_{2cc} with the primary short circuited. These inductances were measured by an LCR meter (test conditions: 1Vrms, 1kHz), for a dc control current range between 0 and 0.6A in the case of the five-leg transformer and for a dc control current range between 0 and 1 A, in the case of the three-leg transformer. For the parallel three-leg transformer the secondary voltage in open-circuit was also measured. The collected data is presented in Table 4.2 and in Table 4.3.

With the data collected Table 4.2 in and in Table 4.3, the T model inductances could be determined using (4.26), (4.27), (4.28) and (4.29), for the five-leg prototype, and using (4.30); (4.31); (4.32) and (4.33) for the three-leg prototype.

$$L_{11oc} = L_X + L_Z \tag{4.26}$$

$$L_{1cc} = L_X + \frac{L_Y L_Z}{L_Y + L_Z} \tag{4.27}$$

$$L_{2cc} = \frac{1}{TR'^2} L_Y + \frac{1}{TR'^2} \frac{L_X L_Z}{L_X + L_Z} \tag{4.28}$$

$$L_{22oc} = \frac{1}{TR'^2} (L_Y + L_Z) \tag{4.29}$$

$$L_{11oc} = L_{lc} + L_m \tag{4.30}$$

$$L_{1cc} = L_{lc} + \frac{L_{lk} L_m}{L_{lk} + L_m} \tag{4.31}$$

$$L_{2cc} = \frac{1}{TR'^2} L_{lk} + \frac{1}{TR'^2} \frac{L_{lc} L_m}{L_{lc} + L_m} \tag{4.32}$$

$$L_{22oc} = \frac{1}{TR'^2} (L_{lk} + L_m) \tag{4.33}$$

Table 4.2 Open-circuit and short-circuit tests: inductance measurements for the five-leg transformer.

CONTROL CURRENT	OPEN-CIRCUIT INDUCTANCE [mH]		SHORT-CIRCUIT INDUCTANCE [mH]	
I_{dc} [A]	PRIMARY SIDE L_{11oc}	SECONDARY SIDE L_{22oc}	PRIMARY SIDE L_{1cc}	SECONDARY SIDE L_{2cc}
0	15.52	1.174	14.63	1.088
0.04	14.69	1.170	13.37	1.071
0.08	10.21	1.115	9.22	0.944
0.12	7.24	1.042	4.77	0.716
0.16	5.74	0.988	3.31	0.574
0.20	5.08	0.950	2.54	0.480
0.24	4.68	0.919	2.08	0.412
0.28	4.40	0.895	1.80	0.361
0.32	4.21	0.876	1.60	0.325
0.36	4.09	0.863	1.47	0.300
0.40	4.02	0.853	1.38	0.284
0.44	3.93	0.844	1.31	0.271
0.48	3.91	0.839	1.27	0.262
0.52	3.87	0.834	1.24	0.255
0.56	3.85	0.830	1.22	0.251
0.60	3.83	0.827	1.19	0.246

Table 4.3 Open-circuit and short-circuit tests: inductance measurements for the three-leg transformer.

CONTROL CURRENT	OPEN-CIRCUIT TESTS			SHORT-CIRCUIT INDUCTANCE [mH]	
I_{dc} [A]	PRIMARY SIDE L_{11oc} [mH]	SECONDARY SIDE L_{22oc} [mH]	SECONDARY VOLTAGE [Vrms]	PRIMARY SIDE L_{1cc}	SECONDARY SIDE L_{2cc}
0	14.14	6.80	0.126	13.23	6.59
0.1	13.42	6.77	0.138	12.34	6.42
0.2	12.10	6.70	0.167	10.56	6.00
0.3	9.53	6.55	0.217	7.62	4.92
0.4	7.74	6.43	0.257	4.56	3.76
0.5	6.78	6.37	0.279	3.07	2.89
0.6	6.20	6.33	0.290	2.19	2.24
0.7	5.91	6.31	0.298	1.73	1.85
0.8	5.74	6.31	0.302	1.46	1.61
0.9	5.65	6.30	0.304	1.31	1.47
1	5.59	6.30	0.304	1.22	1.38

However, it is clear that in each set of four equations, (4.26)-(4.29); (4.30)-(4.33), one of the equations is redundant because the T model presents only three independent parameters. In the 2x2 inductances matrixes there are only three independent elements, so it is implicit that only three different parameters can be determined. The relation between the input and output voltage of the ideal transformer remains unknown.

Solving this non-linear system of equations, with typical mathematical programs leads to a miscalculation of the model inductances, highly dependent on initial conditions. This was confirmed using Matlab and MathCad software. One way to solve this problem is to assume one of the parameters, for instance *TR'*, constant. Other way is to use estimation methods. However, from the electrical analysis point of view, each T model can be simplified even further through its Thévenin equivalent, as presented in Fig. 4.11a. and Fig. 4.11b.

In both cases, T_{Th} represents the ideal transformer which transforms the input voltage, $\underline{V_p}$ or $\underline{V_1}$ into its Thevenin equivalent, $\underline{V_{Th}}$, as in (4.34)or (4.37). The Thévenin inductance, L_{Th}, can be determined using (4.35) or (4.38). The inductance L_p, defined in (4.36) or in (4.39), represents the current through the primary of each variable transformer when the load current is zero.

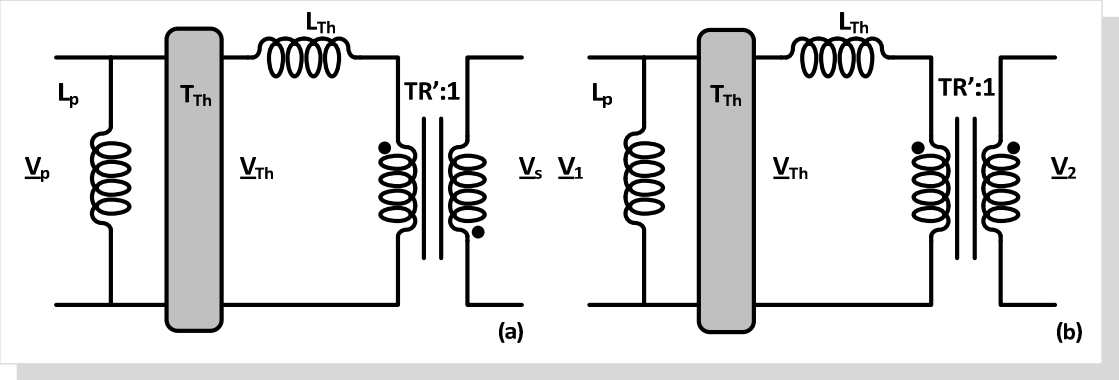

a. Five-leg b. Parallel three-leg

Fig. 4.11. Thévenin equivalent of the proposed T inductance model.

$$\underline{V}_{Th} = \underline{V}_p \frac{L_Y}{L_X + L_Z} \tag{4.34}$$

$$L_{Th} = L_Y + \frac{L_X L_Z}{L_X + L_Z} \tag{4.35}$$

$$L_p = L_X + L_Z \tag{4.36}$$

$$\underline{V}_{Th} = \underline{V}_1 \frac{L_{lk}}{L_{lc} + L_m} \tag{4.37}$$

$$L_{Th} = L_{lk} + \frac{L_{lc} L_m}{L_{lc} + L_m} \tag{4.38}$$

$$L_p = L_{lc} + L_m \tag{4.39}$$

Combining the variable transformer with the ideal transformer into a single one, leads to the final model version presented in Fig. 4.12, where the series inductance L_s, is defined as in (4.40), in the case of the five-leg transformer, or (4.41) in the case of the three-leg transformer. Indeed, the final transformer ratio, *TR*, cannot be constant, and is dependent on the core saturation level.

$$L_s = L_{Th} \left(\frac{\underline{V}_p}{\underline{V}_{Th}} \right)^2 = L_{Th} \left(\frac{L_X + L_Z}{L_Y} \right)^2 \tag{4.40}$$

$$L_s = L_{Th} \left(\frac{\underline{V}_1}{\underline{V}_{Th}} \right)^2 = L_{Th} \left(\frac{L_{lc} + L_m}{L_{lk}} \right)^2 \tag{4.41}$$

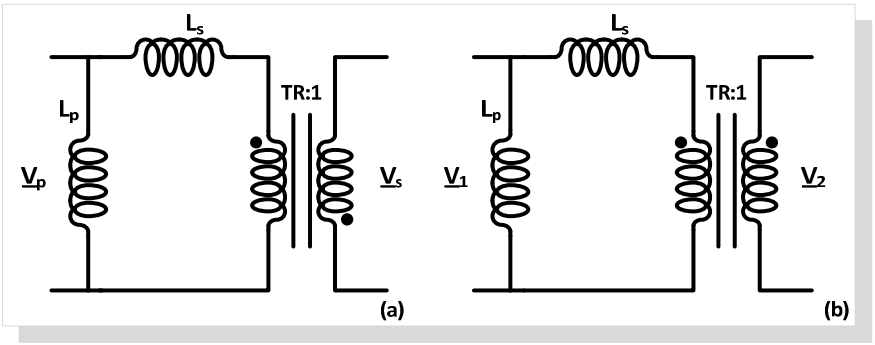

Fig. 4.12. Simplified variable transformer model.

At this point, with the data collected in Table 4.2 and Table 4.3, the final model parameters can be determined:

$$L_{11oc} = L_p \tag{4.42}$$

$$L_{1cc} = \frac{L_p\, L_s}{L_p + L_s} \tag{4.43}$$

$$L_{2cc} = \frac{L_s}{TR^2} \tag{4.44}$$

$$L_{22oc} = \frac{1}{TR^2}\left(L_s + L_p\right) \tag{4.45}$$

Once again, one of the previous equations is redundant. The selected equations for the calculation are (4.43), (4.44) and (4.45). The calculated values are presented in Table 4.4 and in Table 4.5, for the five-leg variable transformer and the three-leg variable transformer respectively. The comparison of both Table 4.4 and Table 4.5, shows that in the case of the five-leg variable transformer there is no dc control range where the transformer voltage ratio behaves as 1:1. However, in the case of the three-leg variable transformer, between 0.7 and 1A the transformer voltage ratio is approximately 1:1.

In the case of the three-leg variable transformer, a large-signal characterization was also done. It was done using a resonant inverter, supplying a power resistance, $\mathrm{R} = 165\Omega$, employing a resonant circuit formed by an external inductor, $L_{ext} = 0.8\mathrm{mH}$ and a capacitor $C = 6.8\mathrm{nF}$, $V_{dc} = 150\mathrm{V}, f = 80\mathrm{kHz}$, as shown in Fig. 4.13a. For a dc control current range between 0 and 1 A, several measurements were taken: the rms value of the primary and secondary voltages, V_1 and V_2, the rms value of the primary current, I_1, and the phase angle between the primary voltage and current, ϕ.

Table 4.4 Model parameters for the five-leg transformer.

CONTROL CURRENT I_{dc} [A]	L_S [mH]	L_P [mH]	TR
0	15.520	255.121	15.313
0.04	14.690	148.792	11.787
0.08	10.210	95.087	10.036
0.12	7.240	13.982	4.419
0.16	5.740	7.819	3.691
0.20	5.080	5.080	3.253
0.24	4.680	3.744	3.015
0.28	4.400	3.046	2.905
0.32	4.210	2.581	2.818
0.36	4.090	2.295	2.766
0.40	4.020	2.101	2.720
0.44	3.930	1.965	2.693
0.48	3.910	1.881	2.679
0.52	3.870	1.825	2.675
0.56	3.850	1.786	2.667
0.60	3.830	1.726	2.649

Table 4.5 Model parameters for the three-leg transformer.

CONTROL CURRENT I_{dc} [A]	L_S [mH]	L_P [mH]	TR
0	206	14.14	5.585
0.1	153	13.42	4.887
0.2	83	12.10	3.719
0.3	38	9.53	2.780
0.4	11	7.74	1.718
0.5	5.610	6.78	1.393
0.6	3.386	6.20	1.229
0.7	2.446	5.91	1.150
0.8	1.958	5.74	1.103
0.9	1.705	5.65	1.077
1	1.561	5.59	1.063

Experimental observation showed that the voltage on the secondary lagged the voltage on the primary, which was not the case for the primary and secondary currents, which remained in phase. Using the primary impedance, $\underline{Z_1} = \underline{V_1}/\underline{I_1}$, together with the phase angle, the reactance, X_1, and its corresponding inductance, L_1, can be calculated. The variable transformer plus load arrangement is implicitly seen as an equivalent series impedance $\underline{Z_1} = R_1 + jX_1$. The voltage ratio, $\left|\underline{V_2}/\underline{V_1}\right|$, was also calculated.

These large-signal experimental results are then compared to the small-signal results, considering that the variable transformer is replaced by the model presented in Fig. 4.12, supplying the same type of resistive load at the same operating frequency, using the parameters presented in Table 4.5. For this, the following relations were used:

$$\underline{Z_s} = j\omega L_s;\ \ \underline{Z_p} = j\omega L_p;\ \ \ \underline{Z_{load}} = R \cdot TR^2 \tag{4.46}$$

$$\underline{Z_1}_{smallsignal} = \frac{\underline{Z_p}\left(\underline{Z_s} + \underline{Z_{load}}\right)}{\underline{Z_p} + \underline{Z_s} + \underline{Z_{load}}} \tag{4.47}$$

With (4.47), the small-signal inductance can be determined using:

$$L_{1_{smallsignal}} = \frac{Im\left(\underline{Z_1}_{smallsignal}\right)}{2\pi f} \tag{4.48}$$

Finally, the ratio between the transformer output and input voltage can also be determined:

$$\left|\frac{\underline{V_2}}{\underline{V_1}}\right| = \frac{\left|\dfrac{\underline{Z_{load}}}{\underline{Z_s} + \underline{Z_{load}}}\right|}{TR} \tag{4.49}$$

Fig. 4.13b. presents the small-signal and large-signal experimental results as a function of the dc control current. A comparison between the small-signal and large-signal inductances shows that these values agree quite well. The same observation can be made by comparing the output to input voltage ratio.

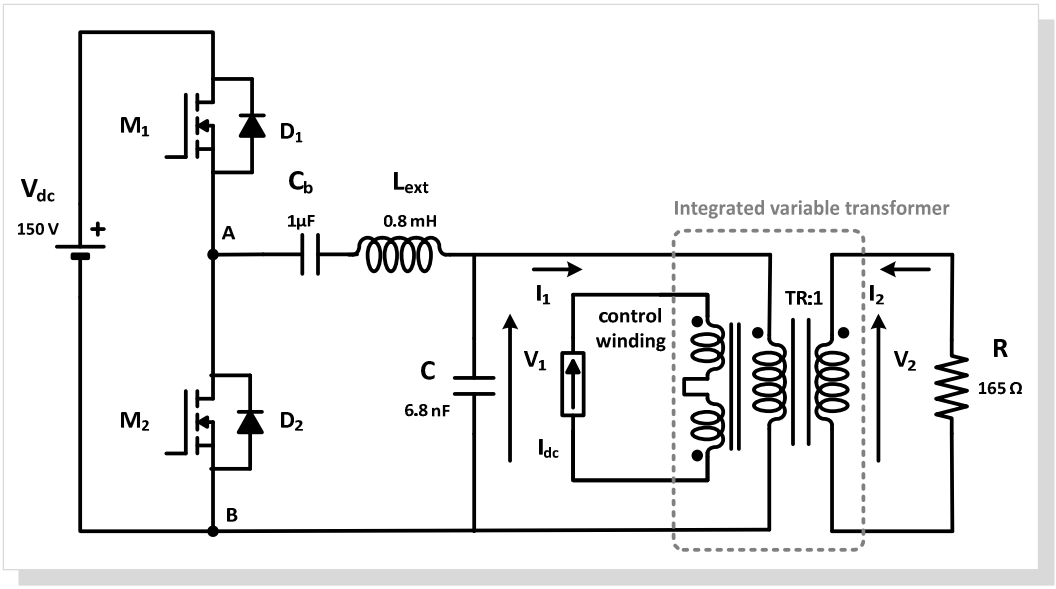

a. Circuit schematic for large-signal characterization

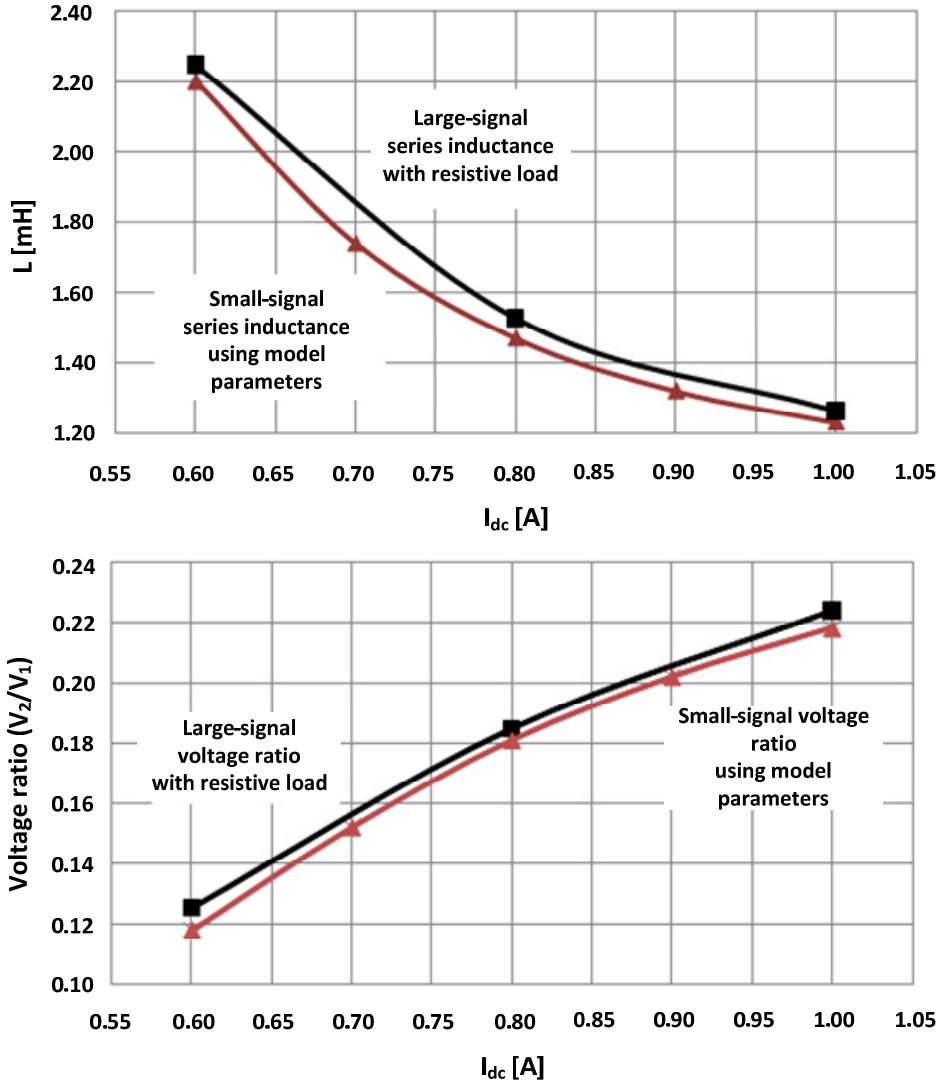

b. Comparison between small-signal and large-signal experimental values as a function of the dc control current

Fig. 4.13. Characterization of the three-leg variable transformer.

4.3 LAMP OPERATION WITH A VARIABLE TRANSFORMER

4.3.1 ANALYSIS OF THE EQUIVALENT CIRCUIT WITH VARIABLE TRANSFORMER

The analysis of the equivalent ballast circuit with the variable transformer follows the same methodology defined in the previous chapter. However, in the general case, the magnetic device will not be represented by a single equivalent inductance. In the LC equivalent circuit, the variable inductor is now replaced by the simplified transformer model, presented in Fig. 4.12. The new schematic is shown in Fig. 4.14a. The simplified model of the transformer has three variable parameters, L_S, L_p and the transformer voltage ratio, TR, all depending on the dc current level. The schematic shown in Fig. 4.14a. may then be simplified as represented in Fig. 4.14b., where R'_{lamp} is the lamp resistance referred to the primary side and C'_p is the resonant capacitor also referred to the primary side of the transformer.

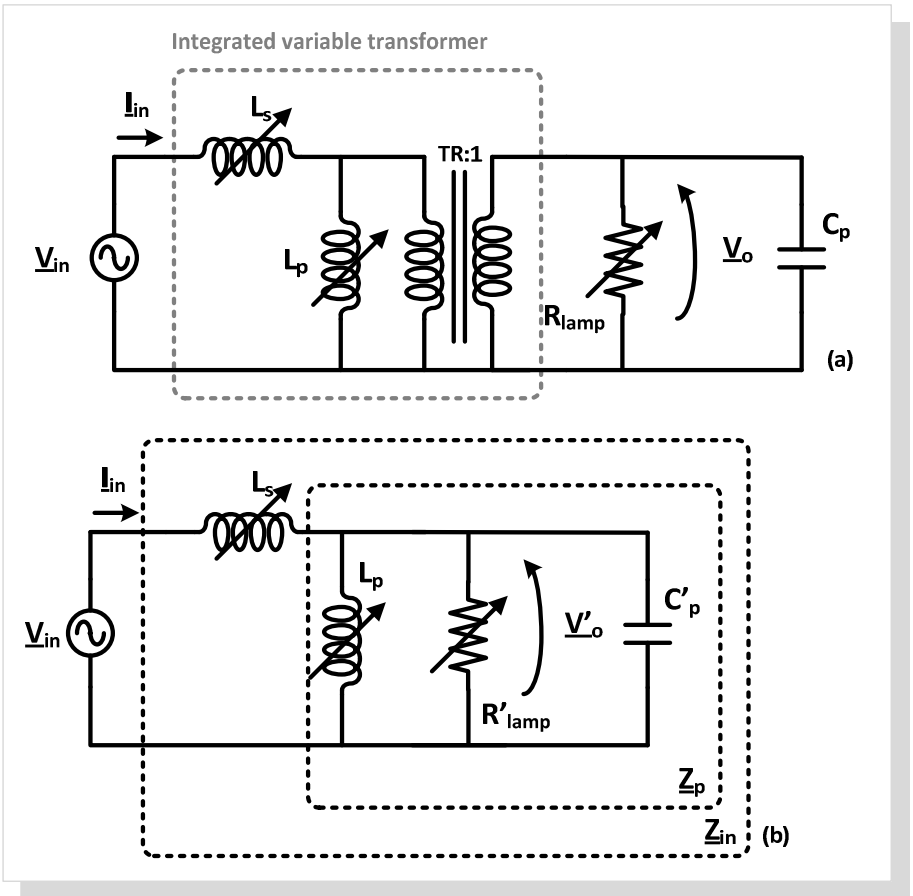

a. Equivalent circuit b. Equivalent circuit referred to the primary side

Fig. 4.14. Half-bridge resonant inverter with variable transformer: equivalent circuit

R'_{lamp} and C'_p are defined as:

$$R'_{lamp} = R_{lamp} TR^2 \quad and \quad C'_p = \frac{C_p}{TR^2} \tag{4.50}$$

The parallel admittance $\underline{Y_p}$ may be defined as:

$$\underline{Y_p} = \frac{1}{\underline{Z_p}} = \frac{1}{j\omega L_p} + \frac{1}{R'_{lamp}} + j\omega C'_p \tag{4.51}$$

Therefore, the input impedance is defined as:

$$\underline{Z_{in}} = j\omega L_s + \underline{Z_p} \tag{4.52}$$

$$\underline{Z_{in}} = \frac{(\omega L_p)^2 R'_{lamp} + j\omega L_p {R'_{lamp}}^2 (1 - \omega^2 L_p C'_p)}{{R'_{lamp}}^2 (1 - \omega^2 L_p C'_p)^2 + (\omega L_p)^2} + j\omega L_s \tag{4.53}$$

If both real and imaginary parts are isolated, (4.53) can be rewritten:

$$Re(\underline{Z_{in}}) = \frac{(\omega L_p)^2 R'_{lamp}}{{R'_{lamp}}^2 (1 - \omega^2 L_p C'_p)^2 + (\omega L_p)^2} \tag{4.54}$$

$$Im(\underline{Z_{in}}) = \frac{\omega {R'_{lamp}}^2 (1 - \omega^2 L_p C'_p)(L_p + L_s) + \omega^3 {L_p}^2 L_s}{{R'_{lamp}}^2 (1 - \omega^2 L_p C'_p)^2 + (\omega L_p)^2} \tag{4.55}$$

Similarly to the LC circuit, the phase angle of the resonant current can also be defined as:

$$\phi_{in} = arg\left(\frac{1}{\underline{Z_{in}}}\right) \cdot \frac{180}{\pi} \tag{4.56}$$

The input current can be defined as:

$$\underline{I_{in}} = \frac{\underline{V_{in}}}{\underline{Z_{in}}} = \frac{\frac{\underline{V_{in}}}{\underline{Z_p}}}{1 + \frac{j\omega L_s}{\underline{Z_p}}} = \underline{V_{in}} \frac{\frac{1}{R'_{lamp}} + j\left(\omega C'_p - \frac{1}{\omega L_p}\right)}{\left(1 + \frac{L_s}{L_p} - \omega^2 L_s C'_p\right) + j\left(\frac{\omega L_s}{R'_{lamp}}\right)} \tag{4.57}$$

The voltage gain of the circuit or the voltage transfer function referred to the primary can be defined, applying the voltage divider rule, as:

$$\underline{G'}(j\omega) = \frac{\underline{V_o'}}{\underline{V_{in}}} = \frac{\underline{Z_p}}{\underline{Z_{in}}} = \frac{\underline{Z_p}}{j\omega L_s + \underline{Z_p}} = \frac{1}{1 + \frac{j\omega L_s}{\underline{Z_p}}}$$

$$= \frac{1}{1 + j\omega L_s \left(\frac{-j}{\omega L_p} + \frac{1}{R'_{lamp}} + j\omega C'_p \right)} \tag{4.58}$$

Equation (4.58) can be simplified:

$$\underline{G'}(j\omega) = \frac{1}{\left(1 + \frac{L_s}{L_p} - \omega^2 L_s C'_p\right) + j\left(\frac{\omega L_s}{R'_{lamp}}\right)} \tag{4.59}$$

The absolute value of the voltage gain can be defined as:

$$\left|\underline{G'}(j\omega)\right| = \frac{1}{\sqrt{\left(1 + \frac{L_s}{L_p} - \omega^2 L_s C'_p\right)^2 + \left(\frac{\omega L_s}{R'_{lamp}}\right)^2}} = \tag{4.60}$$

Therefore, the output voltage referred to the primary can be calculated as:

$$\underline{V_o'} = \frac{\underline{V_{in}}}{\left(1 + \frac{L_s}{L_p} - \omega^2 L_s C'_p\right) + j\left(\frac{\omega L_s}{R'_{lamp}}\right)} \tag{4.61}$$

And finally, the value of the output voltage can be obtained by:

$$V_o = \frac{V_{in}}{TR} \frac{1}{\sqrt{\left(1 + \frac{L_s}{L_p} - \omega^2 L_s C'_p\right)^2 + \left(\frac{\omega L_s}{R'_{lamp}}\right)^2}} \tag{4.62}$$

In terms of ballast design procedure, the following step would be determining the resonant capacitor value in order to operate a specific fluorescent lamp at nominal power. Therefore, using the lamp high-frequency characteristics, at the selected operating frequency, the resonant capacitor value can be calculated from (4.62) as follows:

$$C_p = C'_p TR^2 = \left(\frac{1}{\omega^2 L_s} \left[1 - \sqrt{\left(\frac{V_{in}}{V_o TR}\right)^2 - \left(\frac{\omega L_s}{R'_{lamp}}\right)^2} \right] + \frac{1}{\omega^2 L_p} \right) TR^2 \tag{4.63}$$

It is noticed that in (4.63), the values for L_S, L_p and the transformer voltage ratio, TR should be defined according to the variable transformer dc current level, as shown in Table 4.4.

4.3.2 EXPERIMENTAL RESULTS USING THE FIVE-LEG VARIABLE TRANSFORMER

In order to verify the capability of igniting and driving a fluorescent lamp with this type of magnetic device, a T8 fluorescent lamp was selected. The lamp high-frequency characteristics are presented in Table 4.6.

Table 4.6 Lamp nominal characteristics at high-frequency and experimental measurements.

FLUORESCENT LAMP	V_{lamp} [V]	I_D [mA]	R_{lamp} [Ω]
L 18W/840Lumilux OSRAM	55	280	196

In terms of equivalent model, the five-leg and the three-leg variable transformers show a different behaviour. In the case of the three-leg transformer, a 1:1 voltage ratio region is identified. In that same region L_p is higher than L_S. This implies that if the transformer is operated in this region, it would roughly behave as a simple variable inductor. In the case of the five-leg variable transformer this behaviour is not observed.

Following the design procedure has led to some inconclusive results. Using (4.63) together with the transformer and lamp parameters shown in Table 4.4 and in Table 4.6, resulted into a set of capacitor values and operating frequencies which were not considered acceptable. However, the laboratory prototype was still implemented as shown in Fig. 4.15, and no external resonant inductor was added to the topology. For an input dc voltage of $V_{dc} = 250\text{V}$, an operating frequency of 78 kHz and for a dc control current level of 0.51A it was possible to ignite and operate the lamp in a stable way.

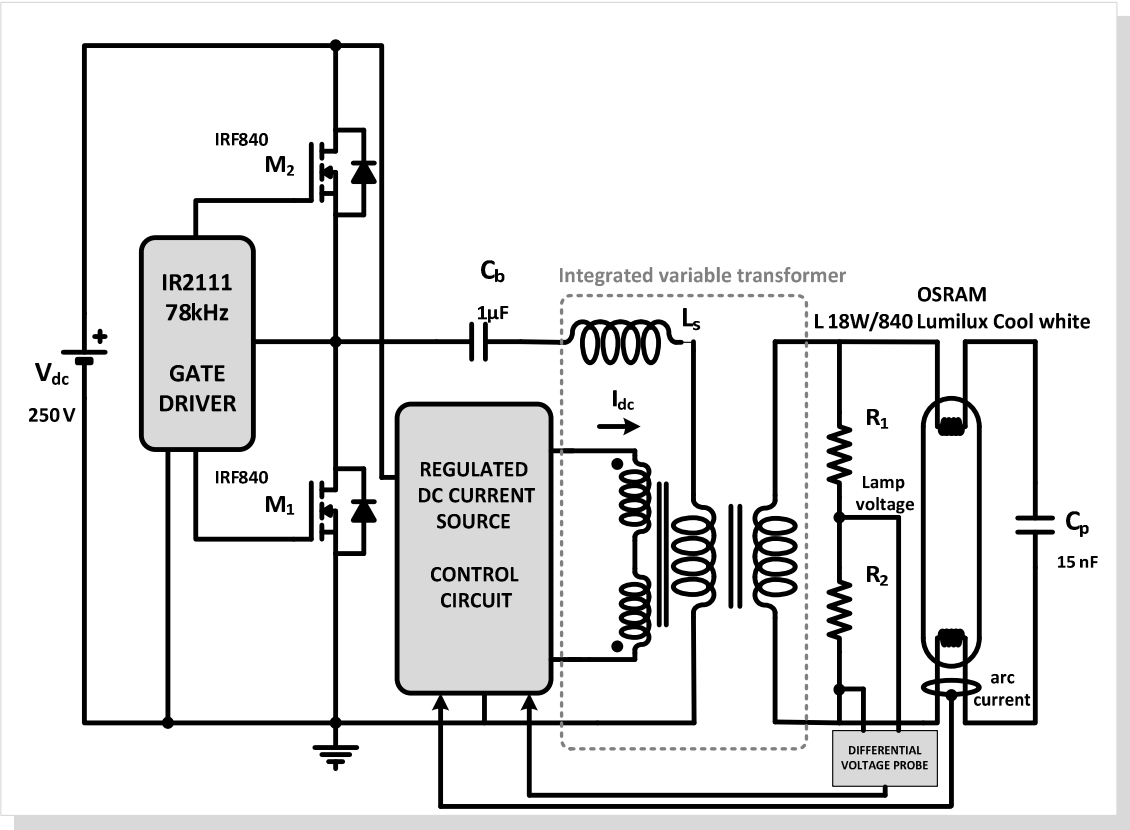

Fig. 4.15. Electronic ballast prototype

Fig. 4.16 shows the experimental waveforms retrieved from the prototype at nominal power. Fig. 4.16a. shows the inverter output voltage, the resonant current, which in this case corresponds to the current in the primary side. From the analysis of Fig. 4.16a. it is clearly seen that the phase angle of the primary current of the resonant tank is delayed when compared to the inverter output voltage. This is mandatory to achieve zero voltage switching in the bridge transistors. Fig. 4.16b. shows the lamp voltage and the current in the secondary and finally Fig. 4.16c. shows the lamp voltage and the arc current. The top waveforms shown in Fig. 4.16b. and Fig. 4.16c. correspond to the instantaneous lamp and arc power respectively. The lamp voltage and arc current are in phase and both lamp and arc current are similar to sinusoids. The lamp voltage, the lamp and arc current waveforms are all stable, which is mandatory for a safe-lamp-operation.

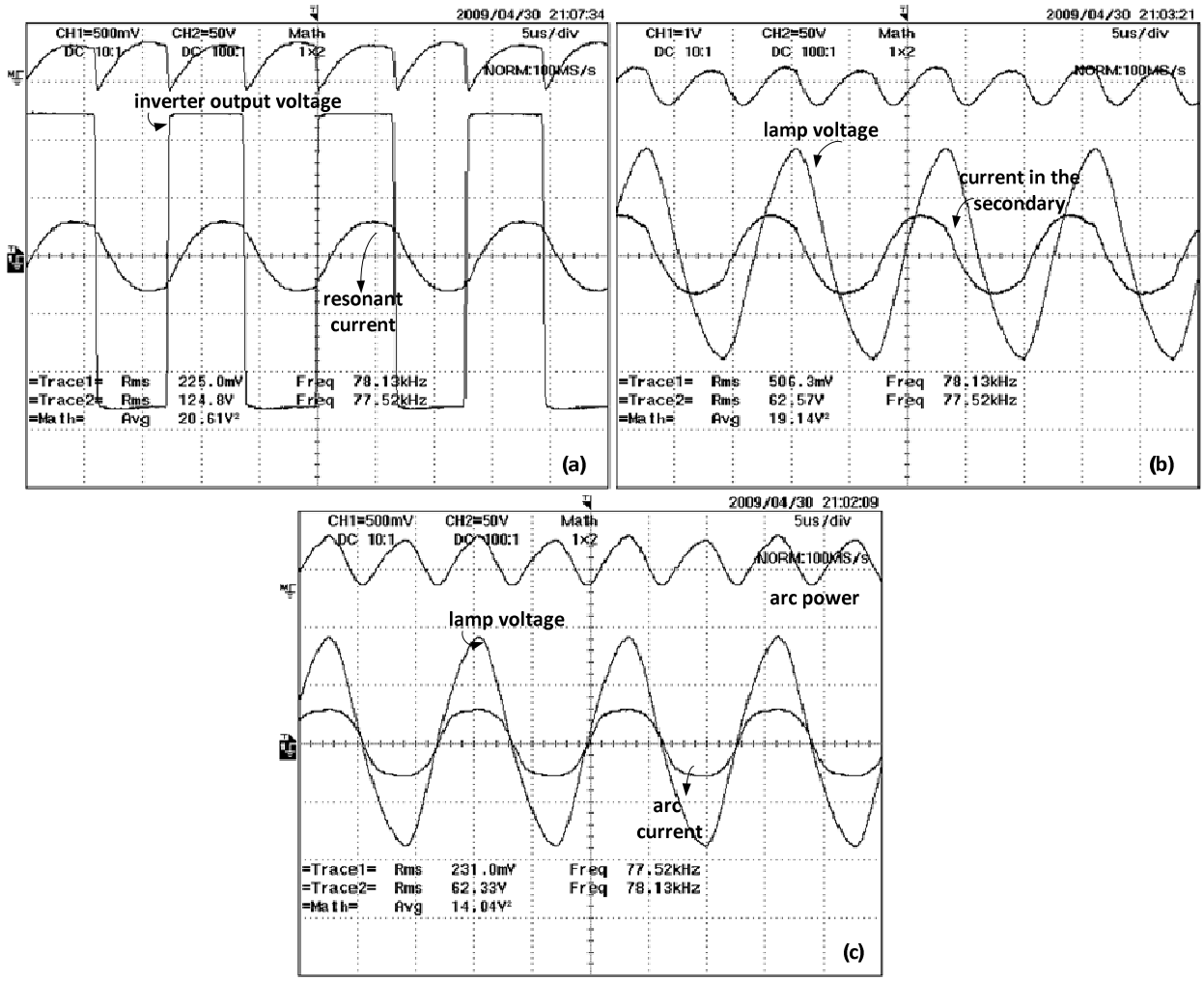

a. Inverter output voltage and current in the primary side (50V/div, 0.5A/div, 5µs/div)

b. Lamp voltage and current in the secondary side (50V/div, 1A/div, 5µs/div)

c. Lamp voltage and arc current (50V/div, 0.5A/div, 5µs/div)

Fig. 4.16. Experimental waveforms at nominal power for the L18W/840 from Osram

Table 4.7 shows the experimental measurements related to the power delivered to the electronic ballast circuit and to the lamp. The electrode power was obtained by subtracting the arc power from the total lamp power. The efficiency was calculated as the ratio between the average lamp power and the input average power, giving for this case a high value, about 90%. The power delivered to the dc current source was not considered in this analysis. However, it should have a small effect in the overall ballast efficiency.

Table 4.7 Experimental measurements.

I_{dc} [A]	P_{in} [W]	P_{lamp} [W]	P_{arc} [W]	P_{electr} [W]
0.51	21	19.3	14	5.3

The obtained experimental results have clearly shown the possibility of using this type of magnetic device to operate fluorescent lamps at nominal power. A stable operating point was achieved; however the design procedure was not confirmed. It is possible that in this case, the large-signal behaviour of the variable transformer differs from the small-signal behaviour, which then introduces miscalculations into the design procedure. At this point, the five-leg transformer was disregarded. The attention was then focused on the three-leg variable transformer. The final objective was not only to operate the fluorescent lamp at nominal power but also to take advantage of the integrated variable transformer to control the luminous flux level of the lamp. The following work, involving isolated dimmable ballasts, has shown some promising results.

4.4 VARIABLE TRANSFORMER APPLIED TO DIMMABLE ELECTRONIC BALLASTS

CCFL backlights are the most common backlight technology and are used in several types of displays. High-brightness LEDs are also an effective alternative for backlight sources. While CCFL backlights typically provide white light, LED backlights may supply either white light or a mixture of red, green, and blue. However, LEDs may have very distinct electrical characteristics depending on the technology (very different threshold voltages from 1.7 to 3.6V). In addition, all LEDs have a small reverse breakdown voltage, around 5V. In addition, due to the manufacturing process, LEDs are not identical. The small variation of electrical characteristics from one LED to another may involve significant changes in the power circuit, especially in terms of maintaining the power set in high levels of performance. Besides, high-efficiency LEDs are very sensitive to voltage and operating current. Deviations from the operating point leads to a drastic reduction of component life and output light quality (apparent colour change). For these reasons, CCFLs are still the main stream in large size LCD backlighting systems [4.8]-[4.10]. For safety purposes, these applications are always dependent on the inclusion of an isolation transformer between the inverter and the circuit which directly supplies the lamp. The most common dimming method is called burst dimming, where the CCFL is driven between no current and rated current, thereby causing surge currents and hence reducing the lamp life [4.7]. Other methods are similar to the most common ones; duty-ratio control, frequency and voltage control. This application can be useful in this field of research since it presents similar advantages to the ones using the variable inductor control concept, additionally yielding electrical isolation. It will be demonstrated that the

proposed technique takes advantage of the device equivalent series inductance to provide a new flexible way for lamp luminous flux regulation.

4.4.1 DESIGN PROCEDURE

The design procedure is similar to the procedure described in the previous chapter. It defines the necessary limits for the inductance value in order to cover all the dimming range for the selected lamp. These limits are then compared with the results obtained from the small-signal and large-signal characterization of the transformer, verifying the applicability of the device. Therefore, the first step is to determine the resonant-circuit parameters in order to operate the lamp at nominal power and then obtain the corresponding dimming curve, using the equation which relates the average lamp power with the control variable, for the LC resonant circuit configuration:

$$P_{lamp}\left[R_{lamp}^2\left(P_{lamp}\right)\left(1-\omega^2 L_{ac}C_P\right)^2+\omega^2 L_{ac}^2\right]-V_{in}^2 R_{lamp}\left(P_{lamp}\right)=0 \tag{4.64}$$

For analysis, two T5 14W lamps were selected. Their electrical characteristics at nominal power, retrieved from manufacturers' data, are presented in Table 4.8 and can be considered quite similar.

Table 4.8 Lamp nominal characteristics at high-frequency.

FLUORESCENT LAMP	V_{lamp} [V]	I_D [mA]
FH 14W/840 OSRAM	86	165
TL5 HE 14W PHILIPS	83	170

Fig. 4.17 illustrates the measured T5 14W characteristics of the lamp resistance versus average arc power, $R_{lamp}(P_{arc})$. For an input voltage $V_{dc} = 310\text{V}$ and operating frequency $f_s = 85\text{kHz}$, the resonant tank parameters were calculated to be approximately $C_p = 2.4\text{nF}$ and $L = 1.46\text{mH}$ in order to operate the lamp at nominal power. Fig. 4.17 also presents two theoretical dimming curves for the same values of input voltage, and operating frequency, but for two different and commercial values of resonant capacitors, $C_p = 2.7\text{nF}$ or 3.3nF. From the analysis of these dimming curves and comparing them with the equivalent small-signal or large-signal inductances shown in Fig. 4.13b., it is concluded that by choosing a higher capacitor value, the necessary

inductance variation can fall within the variable transformer series inductance range. For this, the desired operating region must be defined to be within 0.7A and 1A for the dc control current. Furthermore, a low capacitor value may not be enough to maintain an accurate electrode heating current. By recalling Fig. 4.12 and the model parameters defined in Table 4.5, it is noticed that in that region, L_p is relatively high when compared to L_s and will almost have no effect on the lamp operation. This also confirms that the addition of an external resonant inductor for this application is unnecessary. This is one of the expected advantages of this magnetic control technique.

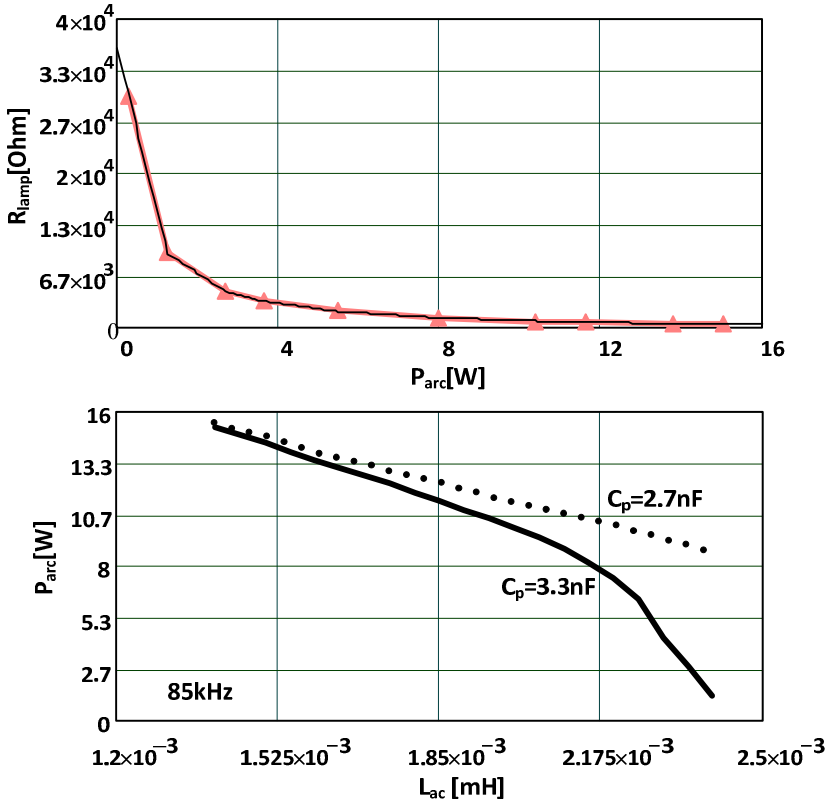

Fig. 4.17. 14W fluorescent lamp: curve fitting to the $R_{lamp}\,(P_{arc})$ - linear interpolation; theoretical dimming curves.

This technique was applied to a T5 14W lamp but it may also control the flux level of higher-power lamps. The only requirement is to guarantee that the system is able to ignite the lamp. It is recalled that one of the main characteristics of T5 HE lamps is the similar nominal current. For lamps ranging between 14W and 35W, the nominal current is the same: 0.170mA. So, if the variable transformer and the resonant capacitor are designed in order to adequately ignite any of those lamps, or particularly if the capacitor remains the same, there is no reason why it is not possible to extend this operation to lamps of higher power ratings. In that case, the proposed forward converter would not present a higher power consumption. The required dc control

current should stay in exactly the same boundaries, since the several operating points of the regulator would be similar. Theoretical and experimental observations have shown that, typically, a 2:1 inductance variation is enough to cover the necessary dimming range for tubular fluorescent lamps. This was valid for the variable inductor but it may also be applied to the variable transformer. For higher-power lamps, additional turns could be included in the control windings in order to obtain a smoother change in the series equivalent inductance.

A proper design must consider from the start the tolerances of the magnetic device and capacitors. One of the advantages of using variable inductors and transformers in electronic ballast applications is that with these regulators it is somewhat possible to minimize or counterbalance the effect of the tolerances of the components, without compromising the whole design project. The dc control current may be used to fine tune the inductance value if necessary. Tolerances for inductances used in electronic ballasts can be as high as 20% for mass production. This can give different lamp powers for each unit. When operating at closed loop with a variable magnetic element, the inductance can be self-adjusted to the correct value, assuring a correct lamp power for each operating point. The repeatability of the proposed solution is assured as long as the variable component can be built with a range of variation wide enough to adapt each design.

4.4.2 EXPERIMENTAL RESULTS USING THE THREE-LEG VARIABLE TRANSFORMER

The final purpose of this work was to verify the effectiveness of using the variable transformer in the development of this new dimming technique. The selected lamp was the FH 14W/840 from Osram. The laboratory prototype, shown in Fig. 4.18, driven at an operating frequency, $f_s = 85\,\text{kHz}$, was able to start and drive the lamp in a stable way, showing also quite linear and smooth experimental dimming curves. Except for the presence of the variable transformer, the prototype is similar to commercial solutions. For simplicity reasons, regarding the analysis of the proposed technique, the typical blocks corresponding to the EMI filter and PFC stage were not considered. It is clearly seen from Fig. 4.18 that no external resonant inductor was added to the prototype. For the selected operating control range the variable transformer behaves like a variable inductor, and similarly, increasing the control current decreases the value of L_s.

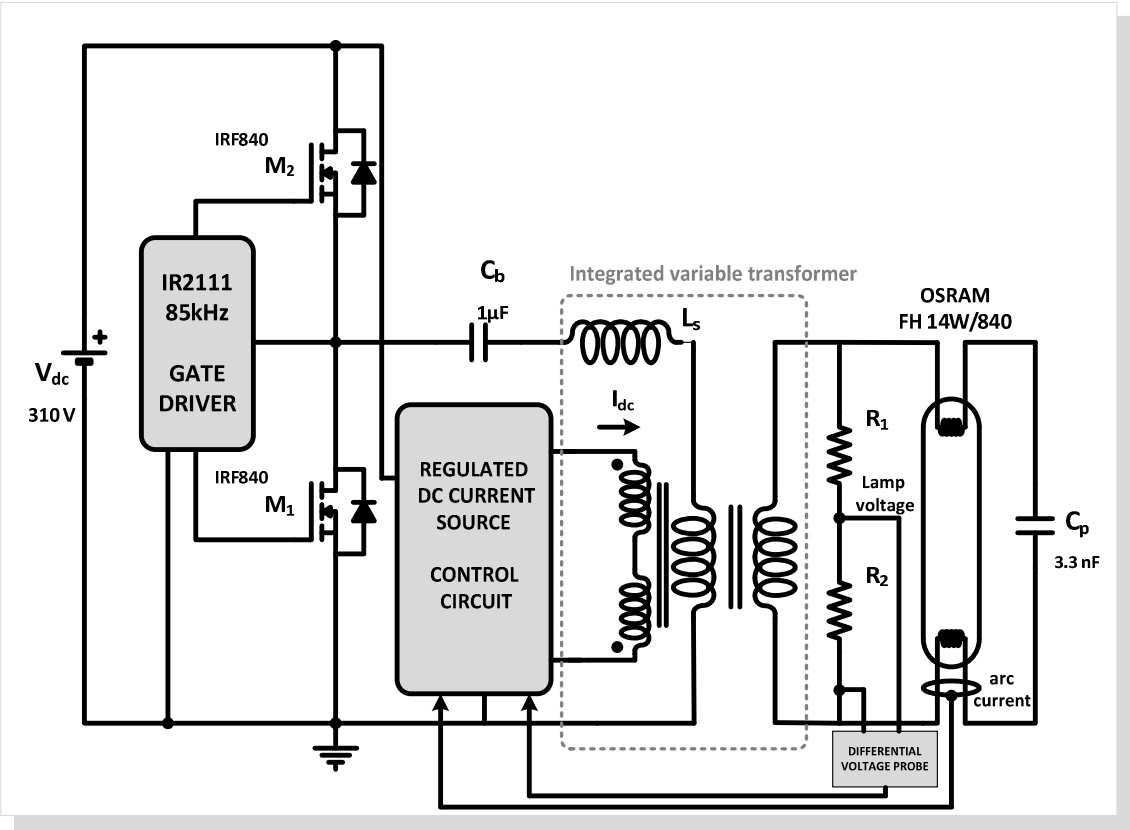

Fig. 4.18. Electronic ballast prototype.

As previously explained, the best method for soft starting the lamp is to control the resonant inverter switching frequency. Initially, the frequency is set to a value higher than the natural resonant frequency of the circuit; the electrodes heating current is thereby adjusted to the necessary value, maintaining a lamp voltage much lower than the starting voltage. After a short period, the frequency is reduced until the starting voltage is obtained, igniting the lamp. With this new technique a similar approach was used, but now, with the inductance L_s as the control parameter. So firstly, the inverter frequency was set to the selected value. Secondly, the dc current was adjusted in order to get the maximum equivalent inductance value. Afterwards, the value of the inductance was lowered, by increasing the dc control current, until the lamp was ignited. Finally, the frequency was slightly adjusted in order to get near resonance conditions and stable operation at nominal power. The ignition process is comparable to the one presented in the previous chapter, adopted for the variable inductor.

In order to perform a thorough analysis of the application, the following measurements were taken: the average power in the arc, in the lamp and at the input of the ballast. As usual, the electrode power was obtained by subtracting the average arc power from the average total lamp power. The efficiency was calculated as the ratio between the average lamp power and the

average input power. The main objective was to correlate the power delivered to the inverter to the average lamp power consumption, and in doing so, the losses in the variable transformer itself were considered. Of course if a commercial ballast prototype was developed, other stages (mains filter, rectifier, PFC stage) should be considered. This is also valid for the converter used as dc drive. The selected converter for the dc current source could be the same forward converter, as in the previously proposed universal ballast, but other solutions could be implemented and optimized to reduce the losses to a minimum level.

The above mentioned measurements are presented in Fig. 4.19. Almost constant electrode power was guaranteed. The lowest efficiency operating point was, as expected, at a low power level. For the remainder operating points, high efficiency is demonstrated. As referred in the previous chapter, for a dc current output in the range of 0.4 and 1A, the power absorbed by the forward converter stands between 1 and 2.5W. A closer analysis reveals that for the selected diming range, only a small variation of 0.3A of the dc control current, was required. Increasing the number of turns in the control windings of the variable transformer should enhance this effect. The forward converter shows the maximum power consumption at 1A which means that at nominal power the efficiency could drop to 6-8%. For lower lamp power levels, the effect would be less significant since in order to obtain a higher inductance value it would be required a lower value of dc current. However, at this point there was no immediate concern to optimize this dc drive, as the main purpose was to verify the effectiveness of this new control technique.

A further issue regarding the power control of the electronic ballast is related to the inverter switches operation, more specifically, zero voltage switching (ZVS) in the bridge MOSFETs. So it is important to verify the phase angle of the primary current in relation to the output inverter voltage. Fig. 4.20 presents the obtained experimental waveforms of the inverter output voltage, current in the primary of the transformer, lamp voltage, also considered as the arc voltage, and current in the secondary of the transformer, at nominal power and at the lowest power level.

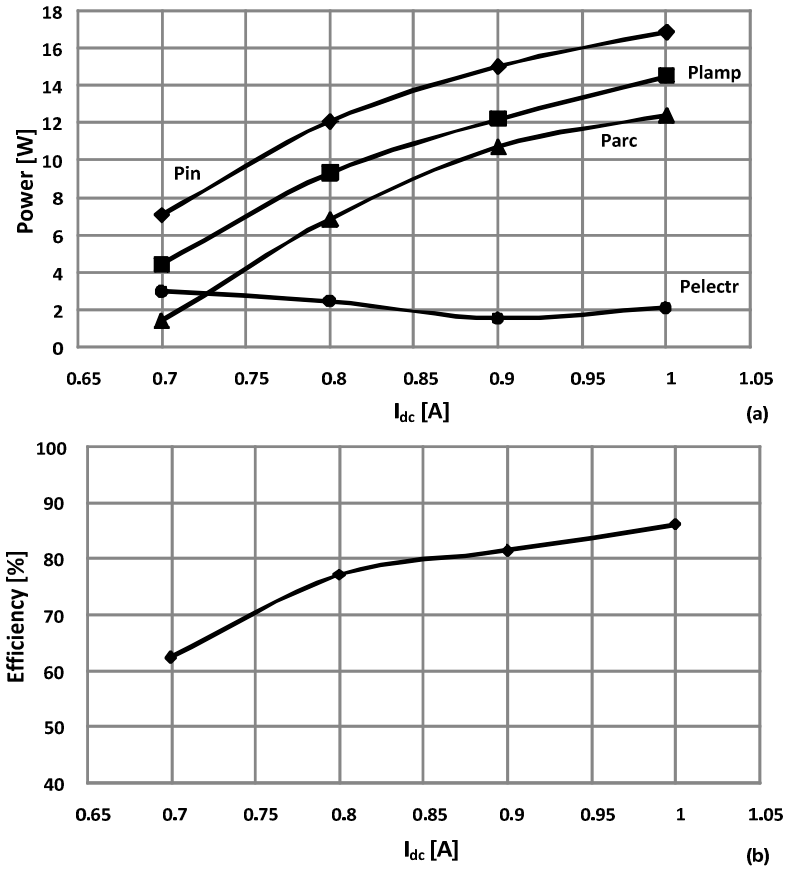

Fig. 4.19. Experimental results for the FH 14W/840 from Osram with electronic ballast prototype: ballast input power, average lamp power, arc power and electrode power, and ballast efficiency as a function of the dc control current.

It is noticed that the secondary current is the current through the lamp plus resonant capacitor arrangement, which includes the lamp arc and electrode currents. As expected, the secondary current and lamp voltage are not in phase for both dimming levels and the current exhibits the typical waveform. Only the arc current and lamp voltage should be in phase.

During the whole dimming range ZVS was ensured, since the primary current is delayed to the inverter output voltage. Besides, the lamp voltage is stable. At low power level, a slight distortion can be observed in the primary and secondary currents, due to the small amount of power delivered to the lamp. For all remaining operating points, stable lamp operation was guaranteed.

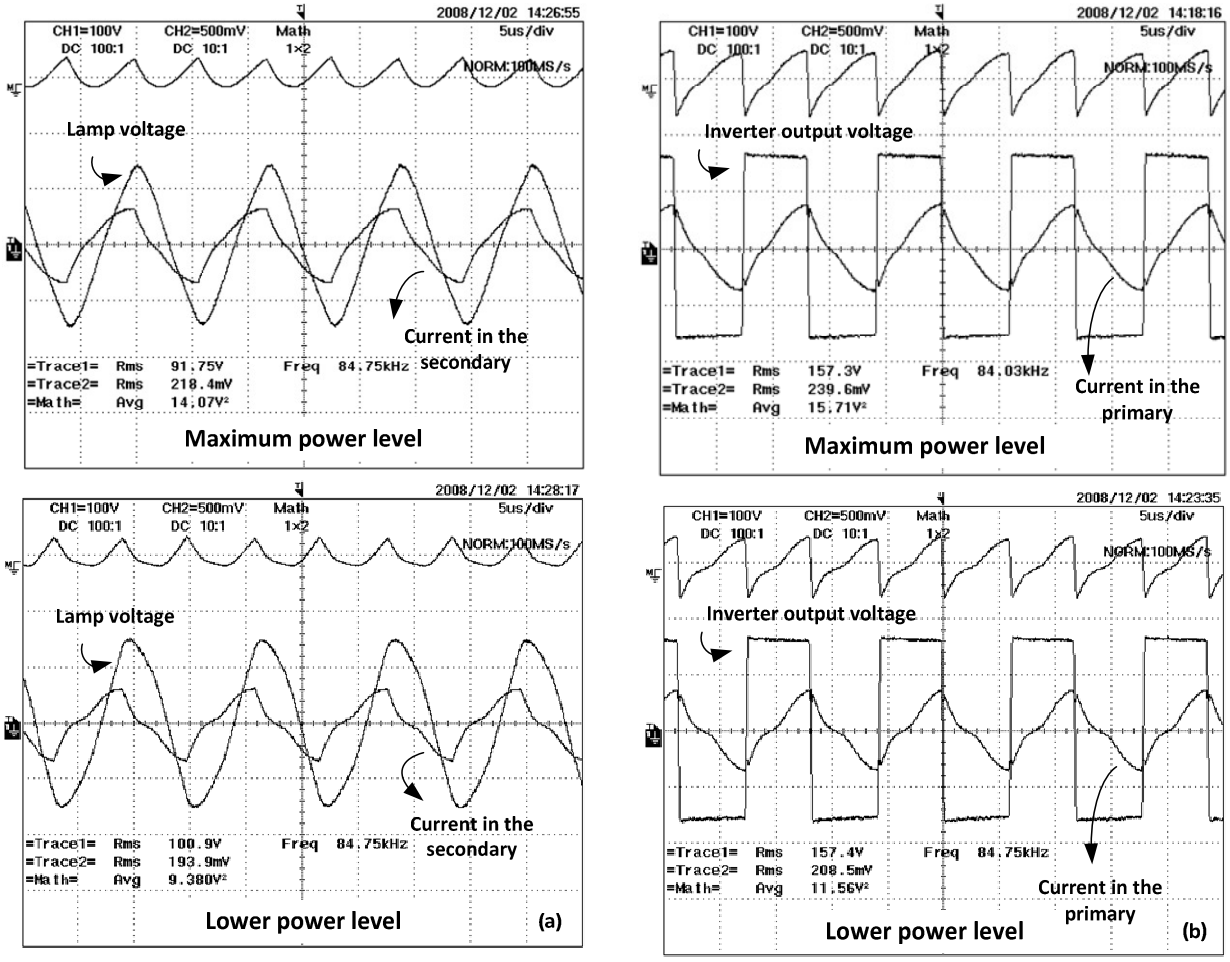

a. Waveforms of the lamp voltage and current in the secondary side (100V/div, 0.5A/div, 5µs/div)

b. Waveforms of the inverter output voltage and current in the primary side (100V/div, 1A/div, 5µs/div)

Fig. 4.20. Experimental results for the FH 14W/840 from Osram at nominal power and at the lowest power level.

Fig. 4.21 shows the lamp voltage and arc current, considering three dimming levels. As expected these operating waveforms are always in phase. These waveforms present a low harmonic distortion value as well as a low crest factor. No oscillations of the lamp voltage or the arc current were observed during the whole dimming range. The top waveforms shown in Fig. 4.21a., Fig. 4.21b. and Fig. 4.21c. correspond to the instantaneous arc power for each dimming level.

Fig. 4.22a. and Fig. 4.22b. both present the currents in the primary and secondary sides of the variable transformer. These waveforms are in phase with each other. Similar behaviour was observed for the other power levels: once again the variable transformer behaved as expected.

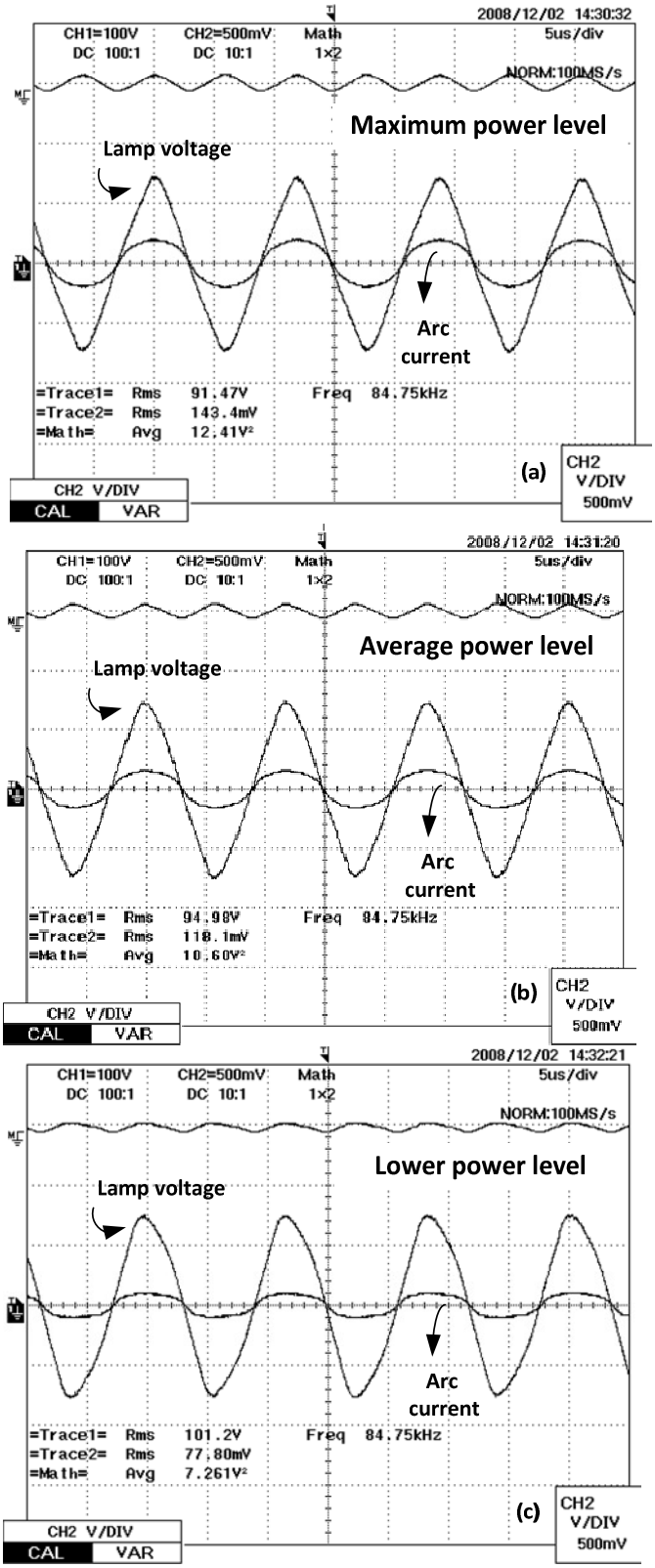

a. Maximum power level b. Average power level c. Lower power level

Fig. 4.21. Experimental results for the FH 14W/840 from Osram: waveforms of the lamp voltage and arc current (100V/div, 0.5A/div, 5μs/div).

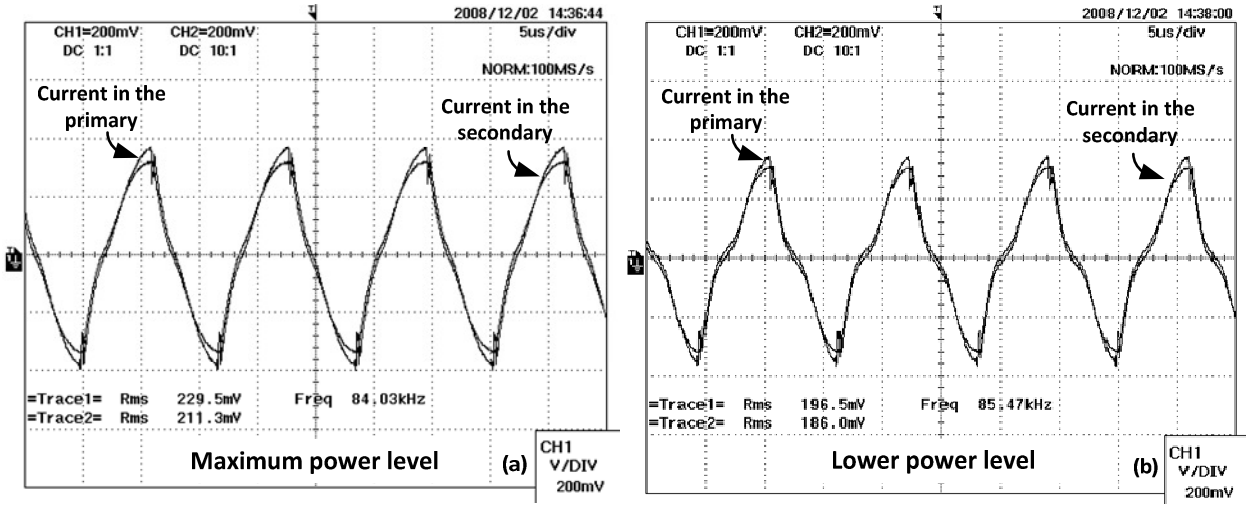

a. Maximum power level b. Lower power level

Fig. 4.22.Current in the primary side (CH1) and in the secondary side (CH2): 0.2 A/DIV, 5 μs/DIV.

It was also necessary to verify the experimental value of L_s, for several operating points or dimming levels. In order to retrieve the inductance value, the equation which relates the average lamp power with the control variable, (4.64), was used. The adopted methodology was as follows: the lamp voltage and lamp current were measured for several levels of the dc current in the control windings; then the corresponding lamp resistance was determined. Finally, the value of the inductance for each measurement point was computed rearranging the lamp power equation, using a linear interpolation which relates the average lamp power with the inductance value, $P(L_s)$ as in (4.65) [4.19].

$$L_s^2\left(P_{lamp}R_{lamp}\left(P_{lamp}\right)^2\omega^4C_p^2+P_{lamp}\omega^2\right)-L_s\left(P_{lamp}R_{lamp}\left(P_{lamp}\right)^2 2\omega^2C_p\right) + P_{lamp}R_{lamp}\left(P_{lamp}\right)^2-V_{in}^2R_{lamp}\left(P_{lamp}\right)=0 \tag{4.65}$$

It should be noted that for each operating point a different resistance value was used. It was considered unnecessary to refer the lamp resistance value to the primary side because TR is approximately one in the selected control range.

The final results are represented in Fig. 4.23. The calculated values are slightly higher than those obtained during the initial transformer characterization, but, considering that the lamp is operated at slightly higher operating frequency and the lamp resistance was not referred to the primary side, they agree quite well.

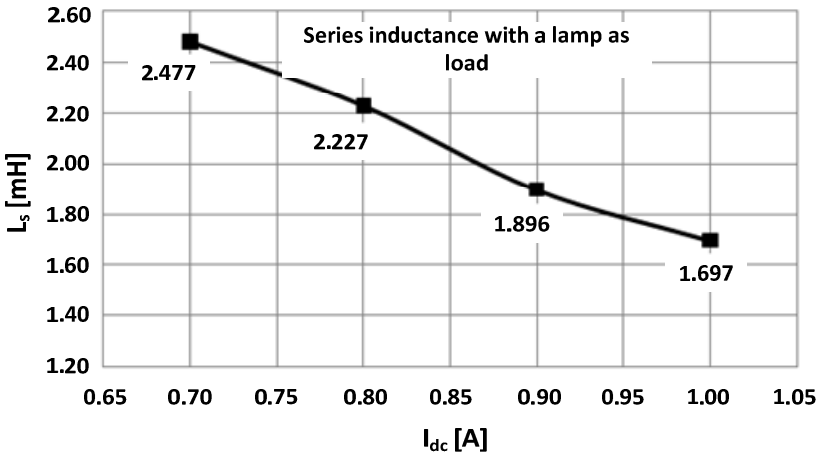

Fig. 4.23.Experimental value of the magnetic regulator as a function of the dc control current with lamp.

In brief, the application of both devices was experimentally verified for the L18W/840 Lumlux and for the FH 14W/840 lamps from Osram. The obtained results demonstrated clearly the viability of using this solution for both stable operation and dimming purposes. By taking advantage of the non-linear behaviour of the variable transformer it was possible to provide luminous flux regulation. The ballast prototype presented as main advantage the constant-frequency operation. A general comparison between traditional commercial ballasts and the presented prototype also reveals that, in terms of inverter topology, the solution is similar. Yet, the introduction of a variable transformer capable of integrating the inductive element is advantageous since it guarantees output isolation. The most popular technique in commercial dimmable ballasts is based on the control of the switching frequency of the inverter. Here, a constant-frequency operation was proposed avoiding typical problems such as: sensitivity of the lamp power to the switching frequency (it significantly increases as the luminous level decreases); non-linear dimming control and problems with high EMI. The dimming function was implemented without compromising the general aspects of the control of the fluorescent lamp. Soft-starting and stable operations were achieved at all power levels.

The next obvious step would be to verify this technique with CCFLs for which similar encouraging results should be expected.

REFERENCES

[4.1] Perdigão, M. S.; Alonso, J. M.; Saraiva, E. S.; "Magnetically-controlled dimming technique with isolated output", Electronics Letters vol. 45, Issue 14, July 2009 pp. 756-758.

[4.2] Perdigão, M.S.; Alonso, J.M.; Gacio, D.; Saraiva, E.S.; "Magnetically-controlled electronic ballasts with isolated output: The variable transformer solution," Industrial Electronics, 2009. ISIE 2009. IEEE International Symposium on , vol., no., pp.59-64, 5-8 July 2009.

[4.3] (Early access) Perdigao, M. S.; Alonso, J. M.; Gacio Vaquero, D.; Saraiva, E. S.; , "Magnetically-controlled Electronic Ballasts with Isolated Output: The Variable Transformer Solution," *Industrial Electronics, IEEE Transactions on* , vol.PP, no.99, pp.1, 0.

[4.4] Perdigão, M.S.; Alonso, J.M.; Saraiva, E.S.; "A new integrated variable transformer topology for electronic ballasts," Industrial Electronics, 2009. IECON '09. 35th Annual Conference of IEEE, vol., no., pp.3484-3489, 3-5 Nov. 2009

[4.5] R. D. Washburn and R.F. McClanahan, "Non-saturating Magnetic Amplifier Controller", U. S. Patent, #4841428 June 20, 1989.

[4.6] Asensi, R.; Prieto, R.; Cobos, J.A.; Uceda, J.; "Modeling High-Frequency Multiwinding Magnetic Components Using Finite-Element Analysis", IEEE Transactions on Magnetics , Vol.43 , issue 10, September 2007.

[4.7] Hwu, K. I. and Chen, Y. H., "A Novel Dimming Technique for Cold Cathode Fluorescent Lamp", PEDS 2007, International Conference on Power Electronics and Drive Systems, pp. 1085-1090, 2007.

[4.8] Yu-Kang Lo; Kuan-Hung Wu; Kai-Jun Pai; Huang-Jen Chiu; "Design and Implementation of RGB LED Drivers for LCD Backlight Modules," Industrial Electronics, IEEE Transactions on , vol.56, no.12, pp.4862-4871, Dec. 2009.

[4.9] Ke, Yu-Lung; Chuang, Ying-Chun; Chuang, Hung-Shiang; Wu, Yuan-Kang; Chang, Chun-Chih; "Self-excited electronic ballast for cold cathode fluorescent lamps," Industrial and Commercial Power Systems Technical Conference (I&CPS), 2010 IEEE , vol., no., pp.1-6, 9-13 May 2010.

[4.10] Hau-Chen Yen; "Analysis of Balancing Driver for Multiple Cold Cathode Fluorescent Lamps," Industrial Electronics, IEEE Transactions on , vol.57, no.4, pp.1354-1359, April 2010.

[4.11] Vollin, Jeff, F. Dong Tang, S. M. Cuk, "Magnetic Regulator Modeling", APEC 1993, IEEE Applied Power Electronics Conference, pp. 604-611.

[4.12] Mork, B.A.; "Five-legged wound-core transformer model: derivation, parameters, implementation and evaluation, "Power Delivery, IEEE Transactions on , vol.14, no.4, pp.1519-1526, Oct 1999.

[4.13] Zhe Zhang, "Coupled-Inductor Magnetics in Power Electronics", PhD Thesis, California Institute of Technology, Pasadena, California, 1987.

[4.14] Ruben Lee, Leo Wilson, Charles E. Carter, "Electronic Transformers and Circuits", Third Edition, PSMA Publication, John Wiley & Sons.

[4.15] Basso, Christophe, "How to deal with Leakage Elements in Flyback Converters", Motorola Application Note AN1679, 1999.

[4.16] Jan Deskur, "Models of magnetic circuits and their equivalent electrical diagrams", COMPEL, The International Journal for Computation and Mathematics in Electrical and Electronic Engineering, vol.18, nº4, 1999, pp.600-610.

[4.17] Charles V. Jones, "The Unified Theory of Electrical Machines", Butterworth & Co. (Publishers) Ltd., 1967.

[4.18] J. M. Alonso; POWER ELECTRONICS HANDBOOK. Chapter 21: Electronic Ballasts. Editor: Muhammad H. Rashid. Editorial: Academic Press. Canadá. 2001.

[4.19] Perdigão, M. S., J. M. Alonso, Marco Dalla Costa, E. S. Saraiva, "Design Considerations for the Optimization of Magnetically Dimmed Electronic Ballasts", X Portuguese-Spanish Congress on Electrical Engineering, XCLEEE, Madeira, Portugal, July 2007.

[4.20] Evgeny Rozanov and Sam Ben-Yaakov, "Analysis of current-controlled inductors by new SPICE behavioral model", HAIT Journal of Science and Engineering B, Volume 2, Issues 3-4, pp. 558-570.

5 CONCLUSIONS, CONTRIBUTIONS, AND FUTURE WORK

This final chapter presents the conclusions and main contributions related to the application of magnetic regulators to electronic ballasts. As conclusions, the main achieved goals will be emphasized in this chapter and a special attention will be given to future work. A list of published papers is presented at the end of the chapter.

5.1 CONCLUSIONS AND CONTRIBUTIONS

Highly-efficient fluorescent lamps are expected to be a dominant, cost-effective lighting solution in the following years. The flexibility expected from modern fluorescent lighting systems requires an intensive use of electronic ballasts, since this type of electronic control offers higher levels of adaptability, not viable with traditional magnetic ballasts. For that reason, there is a clear opportunity to invest and develop new control techniques for electronic ballasts, specially dedicated to fluorescent lamps.

This Ph. D. Thesis proposed a set of new ballast control techniques which are based on a magnetic device commonly referred as magnetic regulator. The presented work began with an extensive research on fluorescent lighting systems. The operating principle and main characteristics of fluorescent lamps and the fundamental requirements of these systems were investigated and detailed in Chapter 1. Traditional luminous flux regulation techniques were detailed and main advantages and disadvantages were pointed out. This was the starting point of the subsequent work. Of course, it was also necessary to gather knowledge on magnetic regulators. This device has been known from several decades; however, recently, modern technology was capable of finding some new interesting applications, by adapting and changing topologies, core structures and materials, and most of all, by interpreting those former

applications in a different way. This is in fact the novelty of the presented research: using this regulator into a modern and useful application such as modern fluorescent lighting control.

In Chapter 2, an extensive literature review on magnetic regulators, describing the state of the art on variable inductors and variable transformers was presented. This assessment is considered very helpful for researchers inclined to investigate this subject. A vast list of applications of these regulators was presented, and general aspects, related to the device operating principle and construction, were also discussed. Chapter 2 ended with a brief description of magnetic control applied to electronic ballasts. Basic concepts behind the proposed new control techniques were underlined.

In the remaining chapters, the presentation, development and the validation of these novel techniques were discussed. The work presented in this thesis was divided into two main areas: variable inductors and variable transformers, with their corresponding applications for the control of electronic ballasts. This supposed the development and presentation of several, new prototype versions of dimmable electronic ballasts and universal electronic ballasts.

In conclusion, the work presented in this Ph. D. Thesis may be detailed as follows. The published papers related to these contributions are shown in Section 5.3.

- Variable-inductor based electronic ballasts:

  A magnetically-controlled electronic ballast topology was proposed based on the half-bridge parallel-loaded resonant inverter where the typical resonant inductor was substituted by a variable inductor. The novelty of this proposal is the fact that this variable inductor, controlled by a dc current, is able to modify the resonant circuit in order to vary the rms values of the lamp current and thereby the luminous output. This new dimming technique allows constant-frequency inverter operation, which compared to typical commercial ballasts, based on a variable-frequency technique, is a breakthrough since it avoids well know-disadvantages [J5.1].

  Comparative analysis between resonant circuits, magnetic regulators structures and topologies, clearly showed how this new control technique is effective, and does not compromise the lamp operation. It was proved by a complete set of experimental results that safe, reliable and stable operation was achieved, along with ZVS operation, and promising efficiency levels [J5.2], [IC5.1], [IC5.2], [IC5.3], [IC5.7]. A simple study, for T5 lamps, regarding electrode operation and compliance with recent IEC standards was

also carried out in order to validate this new dimming method [IC5.16]. Different regulator structures and topologies were also tested with this dimming technique [IC5.15].

Another magnetic control technique was developed and presented for universal electronic ballasts. There is a recent commercial demand of these ballasts which are able to supply different lamps without requiring any physical change in the hardware. Similarly to the previous dimmable electronic ballast, the variable inductor was used to adapt the characteristics of the resonant circuit to each attached lamp. In these cases, the ballast must incorporate the necessary intelligence to measure the electrical characteristics of the lamps wired to their output, and must be able to adjust their internal operation in order to correctly ignite and supply these lamps. The technique was previously exposed using a forward converter to properly control the magnetic regulator [J5.3], [IC5.4], [IC5.8], [IC5.10].

Universal ballasts are of a more complex nature. One of the challenges is the identification of the lamp and the other the routine which is necessary to operate each lamp at the appropriate power level. This implies the active control of all ballast parameters. Digital control based on low-cost microcontrollers can be used in this type of ballasts without an excessive cost penalty and all the required functions can be easily implemented. It is also pointed out that the development of universal ballasts for any kind of tubular fluorescent lamps is complicated due to their different characteristics in terms of warm-up period, time constants and equivalent impedances. Using μC permits a higher level of control of the system. Two different digital prototype versions were therefore proposed. In the first one, dedicated to T8 lamps, besides the variable inductance, an additional control parameter is used: the inverter switching frequency. The effectiveness of the control technique is clearly demonstrated using a simple lamp identification method, based on the measurement of the lamp voltage. The collected experimental results showed all lamps were operated at nominal power with a stable operation [J5.7], [IC5.12].

In the second proposed prototype, especially dedicated to T5 lamps, the ballast was operated at constant-frequency and only the variable inductance was used as control parameter. It is noticed that in this particular case the ballast is able to operate a large number of T5 lamps, HE and HO. In addition, this second prototype was designed with special concern regarding the electrodes operation. A simple resonant circuit design

procedure was presented and experimental results showed that external heating sources, common in commercial ballasts, may be avoided. In this second proposal, the ballast incorporates two other converters, a buck and a flyback converter, in order to properly operate the magnetic regulator and to power the ballast using a single dc voltage source, [IC5.18], [IC5.19].

- Variable-transformer based electronic ballasts

  In this case the variable inductor was replaced by a variable transformer. It was demonstrated how the variable behaviour of the resonant circuit depends on the transformer equivalent circuit model and resonant capacitor, which is also dictated by the dc current flowing through the control windings included in the regulator structure. Two new different variable transformer structures were proposed and analysed. The innovation of this technique resides in the fact that, while simultaneously controlling the luminous flux of the lamp, the ballast is capable of guaranteeing electric isolation. This is pointed out as a useful combination for applications with CCFLs in LCD backlighting applications [J5.4], [J5.6], [IC5.10], [IC5.14].

In addition to these ballast solutions, a special attention was given, throughout the work, to the modelling, design, small-signal and large-signal characterization of variable inductors and variable-transformers. Detailed examples were given. This analysis pointed out the importance of these concepts and modelling techniques on the experimental application of these devices, whether it is referred to electronic ballast applications or potentially new and different technologies [IC5.5], [IC5.6], [IC5.13].

In conclusion, the main contributions may be detailed as follows:

- An overall review was presented on general aspects regarding lighting, lighting efficiency and fluorescent lighting systems.
- An extensive literature review was provided on magnetic regulators with a special emphasis on their known applications.
- A new dimming technique was proposed and developed based on the variable inductor.

  The technique was validated through experimental testing with a magnetically-controlled electronic prototype, based on the parallel-loaded half-bridge resonant inverter, for T8 and T5 lamps, using EF25 and EFD20 based regulators. The ballast was operated at

constant-frequency and the lamp power was controlled by changing only the regulator inductance. It was shown that with an appropriate selection of the ballasts parameters all lamps could be dimmed from nominal power to a very low power level.

A theoretical comparison between several resonant circuits and their impact on the lamp dimming operation was provided. Two ballast prototypes using an LC and LCC circuits were tested. Experimental results with a T8 36W lamp, confirmed theoretical predictions. It was demonstrated that with this new flux regulation technique, quasi linear regulation can be obtained and ZVS operation could be guaranteed over the desired dimming range.

The T5 lamp dimming behaviour was also tested using two different variable inductors prototypes with different winding connections. The two prototypes were based on two different core structures the EFD20 and the U15 core [5.3]. The EFD20 regulator showed better results, especially due to the complexity of the assemblage of the U15 regulator.

As example, the T5 HE 21W and T5 HO 39W electrodes behaviour was also tested under the proposed dimming technique in order to verify its compliance with current standards, based on the SoS limits. The obtained results were compared with the experimental values retrieved from commercial dimmable-ballasts. Promising results were obtained considering that no additional heating sources were included in the proposed ballast layout. This aspect is considered quite relevant since this type of study is recent. IEC standards referring the necessity of SoS compliance are recent (2010).

- It was developed and proposed a new control technique based on the variable inductor for universal ballasts applications.

  It was demonstrated that it was possible to control the operation of multiple lamps with different power ratings, T8 15W-58W using the variable inductance and the inverter operating frequency as control parameters. A prototype with digital control based on a PSoC CY8C29466 μC was developed. Experimental results were presented which showed the proper behaviour of the ballast. All lamps were operated at nominal power and ZVS operation was achieved in each case. The variable inductor was properly controlled by a forward converter. The proposed ballast showed a high efficiency, around 90%.

It was also demonstrated the possibility to control the operation of a vast set of T5 HE and HO lamps, ranging from 14W to 49W, with a similar digital ballast prototype, at constant frequency. In this ballast, only the variable inductance was used as control parameter. This is considered a major breakthrough. Currently, there is no commercial product capable of simultaneously controlling all of these lamps. It was also developed a design procedure which gave the ability of operating all lamps with compliance of the SoS limits. A simple solution was proposed using two parallel capacitors, which act as a single equivalent capacitance for proper lamp ignition. All T5 HE and HO lamps were operated at nominal power, or in the case of the T5 HO 49W within the limits imposed by the manufacturer, with safe electrode operation. In all circumstances ZVS was achieved in the ballast inverter.

- Two dc-dc converters were proposed for the control of the variable inductors: a forward and a buck converter.

  The forward converter was designed to be directly supplied by the dc bus voltage of the ballast. It was demonstrated the low power consumption of the variable inductor. The buck converter was integrated into the second digitally-controlled ballast, where an additional converter (flyback) was used to lower the dc bus voltage level and supply the buck-converter.

- Large-signal characterization methods based on flux measurements and short-circuit and open-circuit tests were adapted to the proposed variable inductors and variable transformer prototypes, and tested under the proposed control techniques.

  In the case of the variable inductor, it was proposed a simple definition for the calculation of the inductance, using the peak-to-peak values of the resonant current and total ac flux, measured during dimming operation. This model was tested with several variable inductor prototypes.

- A Matlab-Simulink electronic-ballast-dynamic model was developed, including the fluorescent-lamp model and the variable-inductor model

- A new control technique based on the variable transformer was proposed and developed, which has the advantage of providing output isolation.

Two variable transformers were built and tested: the five-leg and the three-leg versions. With the three-leg version it was demonstrated the possibility of dimming a T5 lamp and simultaneously guarantee isolation between the lamp and the inverter circuit. This is considered a benefit, and is essential for CCFLs control.

5.2 FUTURE WORK

The main subject of this work was to investigate new control techniques for electronic ballasts based on magnetic regulators. The key objective in terms of future work would be continuing this line of research and several options just naturally follow the work which was already presented by pursuing an optimized version of the proposed ballast prototypes. This Ph. D Thesis validates the proposed techniques but also points out some critical issues, revealed during the recollection of experimental data, which deserve a more profound study.

Therefore, regarding ballast applications, it would be relevant to proceed in the following directions:

- In magnetically-controlled dimmable-electronic ballasts, the ballast is operated at constant-frequency. The system was implemented in open loop. The technique was validated by controlling the level of dc current in the control windings to operate the lamp at the required power level. High-efficiency and ZVS operation was achieved. However, with a phase-locked-loop circuit it would be possible to impose near resonance operation for all dimming levels. This obviously could imply changing the operating frequency of the ballast but would result in ballast-optimum-operation conditions for all dimming levels. The impact of this near-resonance operation should be analysed.
- The inclusion of PFC techniques in magnetically-controlled electronic ballasts is also a possible line of research. The impact of additional converters in the system should be analysed. In addition, when PFC stages are included in the ballast, integrated topologies are occasionally used. These integrated topologies are characterized by sharing one of the switches, for instance the boost switch with one of the half-bridge inverter switches. In those circumstances, the operating frequency can no longer be used as control parameter for dimming. Using an integrated topology with the presence of a variable inductor in the system will avoid that disadvantage; however the behaviour of this new circuit should be investigated.

- It would be interesting to further investigate the cause of the eventual lamp instabilities. A study on the dynamic behaviour of the ballast using small-signal dynamic lamp models would be the direction to follow. The influence of the non-linear behaviour of the magnetic regulator on the dynamic behaviour of the circuit should also be investigated. This would determine with exactitude the limits for stable operation.
- Analysis of the impact of striations in magnetically-controlled electronic ballasts. S. Boreckci already presented a striation control technique for the proposed variable-inductor based ballast. This new solution called power density modulation (PDM) proposes to induce three different stages in each period of the arc current, by changing the level of the dc control current and consequently the inductance value. The time interval for each inductance value controls the average lamp power in each modulation period [2.50]. The impact of this technique on the lamp behaviour should be further investigated.
- Optimization of the proposed digital prototypes, especially regarding energy efficiency. Investigation of other options for the dc-dc converter used to supply the magnetic regulator dc control current. Selection of the most energy efficient converter in order to reduce the power consumption of the ballast prototype.
- Continuation of prototypes development, especially in terms of lamp recognition techniques. Even if almost all lamps can be identified by the analysis of the lamp voltage, a better solution to identify T12, T8 and T5 lamps has been proposed in [3.49]. A fuzzy logic controller analyses the heated lamp electrodes, the lamp voltage and the lamp current. Then, a classification system is generated that maps the lamp characteristics into distinct groups in order to automatically detect each lamp. Adapting this detection method to the proposed universal ballast prototypes would represent an improvement. The possibility to extend the application to the other lamps types may also be considered as other option.
- At the moment, the proposed ballasts are divided in dimming operation and universal operation. It would be relevant to investigate the possibility of combining these operations into a single prototype version. The impact on the operation of the ballast should be characterized. Eventual additional control parameters should be considered in this intent.
- It would also be relevant to study the use of variable transformers in universal ballasts applications and to perform a theoretical study and experimental analysis of the control of CCFLs with variable transformers.

Some other issues are specifically related to the variable inductor and variable transformer behaviour in order to better predict and understand their impact in the suggested application. Therefore it would be pertinent to follow the subsequent lines of research:

- Investigation of a more detailed design procedure regarding the design of the variable inductor or the variable transformer, possibly including losses.
- Modelling of variable inductors and variable transformers with finite element analysis, FEA. 3D finite element modeling may be used to model the distribution of flux density and to identify the region of saturation which is believed to result in the decrease in the inductance of the variable inductor, or in the change of the parameters of the variable transformer.

General applications for the variable inductor or the variable transformer were already suggested in Chapter 2. Some of these applications resulted from the increasing attention given to the proposed ballast applications and the new magnetic control techniques, due to the several published results. This also served as motivation to follow different lines of research: the operation of dc-dc resonant converters at constant frequency is one direction which was already followed [J5.5], [IC5.17]. This work is expected to proceed.

Then again, some other alternatives are aligning, mainly regarding the use of variable inductors in the luminous flux control of LED lamps. Another option would be to investigate the possibility of using variable inductors to actively control the saturation level of buck-boost inductors, in electric vehicles applications. Due to the large currents involved, it implies large-signal characterization of variable inductors through more advance measurement techniques.

5.3 PUBLISHED PAPERS

5.3.1 JOURNALS

[J5.1] Alonso, J. Marcos, **Perdigão M.S.**, Marco A. Dalla Costa, Eduardo S. Saraiva; *"Empleo de Reguladores Magnéticos en el Control de Balastos Electrónicos,"* Revista Mundo Electrónico. Cetisa Editores, May 2007. **ISSN-0300-3787**

[J5.2] **Perdigão, M.S.**; Alonso, J.M.; Dalla Costa, M.A.; Saraiva, E.S.; "Comparative Analysis and Experiments of Resonant Tanks for Magnetically Controlled Electronic Ballasts," Industrial Electronics, IEEE Transactions on, vol.55, no.9, pp.3201-3211, Sept. 2008. **IEEE JOURNALS, ISSN-0278-0046**

URL: http://ieeexplore.ieee.org/stamp/stamp.jsp?tp=&arnumber=4558040&isnumber=4609005

[J5.3] **Perdigão, M.S.**; Alonso, J.M.; Costa, M.A.D.; Saraiva, E.S.; "Using Magnetic Regulators for the Optimization of Universal Ballasts," Power Electronics, IEEE Transactions on, vol.23, no.6, pp.3126-3134, Nov. 2008. **IEEE JOURNALS, ISSN- 0885-8993**

URL: http://ieeexplore.ieee.org/stamp/stamp.jsp?tp=&arnumber=4712527&isnumber=4712525

[J5.4] **Perdigão, M.S.**; Alonso, J.M.; Saraiva, E.S.; "Magnetically-controlled dimming technique with isolated output," Electronics Letters, vol.45, no.14, pp.756 -758, July 2 2009. **IET JOURNALS, ISSN-0013-5194**

URL: http://ieeexplore.ieee.org/stamp/stamp.jsp?tp=&arnumber=5159729&isnumber=5159700

[J5.5] Alonso, J.M.; **Perdigão, M.S.**; Gacio, D.; Campa, L.; Saraiva, E.S.; "Magnetic control of DC-DC resonant converters provides constant frequency operation," Electronics Letters , vol.46, no.6, pp.440-442, March 18 2010. **IET JOURNALS, ISSN-0013-5194**

URL: http://ieeexplore.ieee.org/stamp/stamp.jsp?tp=&arnumber=5434635&isnumber=5434595

[J5.6] **Perdigão, M. S.**; Alonso, J. M.; Gacio Vaquero, D.; Saraiva, E. S.;"Magnetically-controlled Electronic Ballasts with Isolated Output: The Variable Transformer Solution," Industrial Electronics, IEEE Transactions on, vol., no., pp., December. 2010. IEEE JOURNALS, **ISSN-0278-0046 – Early Access**

URL: http://ieeexplore.ieee.org/stamp/stamp.jsp?tp=&arnumber=5675678&isnumber=4387790

[J5.7] J. Marcos Alonso, **Perdigão, M.S.**; Javier Ribas; David Gacio; Eduardo S. Saraiva;" Optimizing Universal Ballasts using Magnetic Regulators and Digital Control," Industrial Electronics, IEEE Transactions on, vol., no., pp., December. 2010. IEEE JOURNALS, **ISSN-0278-0046 – Early Access**

URL: http://ieeexplore.ieee.org/stamp/stamp.jsp?tp=&arnumber=5575415&isnumber=5873561

[J5.8] H. V. Marques, Á. R. Seidel, **M. S. Perdigão**, J. M. Alonso, E. S. Saraiva; "Constant-Frequency Magnetically-Controlled Universal Ballast with SoS Compliance for TL5 Fluorescent Lamps" Power Electronics, IEEE Transactions on. **IEEE JOURNALS – Accepted for publication**

[J5.9] J. Marcos Alonso, **M. S. Perdigão**, David Gacio, Antonio J. Calleja, Eduardo S. Saraiva; "Analysis, Design and Experimentation on Constant-Frequency DC-DC Resonant Converters with Magnetic Control" Power Electronics, IEEE Transactions on. **IEEE JOURNALS – Accepted for publication**

5.3.2 INTERNATIONAL CONFERENCES

[IC5.1] **Perdigão, M.S.**; Saraiva, E.S.; Alonso, J.M.; Dalla Costa, M.A.; *"Comparative Analysis and Experiments of Resonant Tanks for Magnetically-Controlled Electronic Ballasts,"* Industrial Electronics, 2007. ISIE 2007. IEEE International Symposium on, vol., no., pp.3041-3046, 4-7 June 2007.

URL: http://ieeexplore.ieee.org/stamp/stamp.jsp?tp=&arnumber=4375100&isnumber=4374555

[IC5.2] **Perdigão, M.S.**; J. M. Alonso; Marco Dalla Costa; E. S. Saraiva; "Design Considerations for the Optimization of Magnetically Dimmed Electronic Ballasts," X Portuguese-Spanish Congress on Electrical Engineering, XCLEE, 5-7 July 2007.

[IC5.3] **Perdigão M.S.**, E. S. Saraiva, J. M. Alonso, M. A. Dalla Costa, "Design Method to Prevent Instabilities in Magnetically-controlled Electronic Ballasts," CEE'07 International Conference on Electrical Engineering, 26-29 November 2007.

[IC5.4] **Perdigão, M.S.**; Alonso, J.M.; Dalla Costa, M.A.; Saraiva, E.S.; "Optimization of universal ballasts through magnetic regulators," Applied Power Electronics Conference and Exposition, 2008. APEC 2008. Twenty-Third Annual IEEE, vol., no., pp.1214-1220, 24-28 February 2008.

URL: http://ieeexplore.ieee.org/stamp/stamp.jsp?tp=&arnumber=4522877&isnumber=4522647

[IC5.5] **Perdigão, M.S.**; Alonso, J.M.; Dalla Costa, M.A.; Saraiva, E.S.; "A variable inductor MATLAB/Simulink behavioral model for application in magnetically-controlled electronic ballasts," Power Electronics, Electrical Drives, Automation and Motion, 2008. SPEEDAM 2008. International Symposium on , vol., no., pp.349-354, 11-13 June 2008.

URL: http://ieeexplore.ieee.org/stamp/stamp.jsp?tp=&arnumber=4581201&isnumber=4581062

[IC5.6] **Perdigão, M.S.**; Saraiva, E.S.; Alonso, J.M.; Cervi, M.; "The controllable non-linear reactor in electronic ballasts applications: A behavioral analysis of the inductance as a function of both ac and dc bias currents," Universities Power Engineering Conference, 2008. UPEC 2008. 43rd International, vol., no., pp.1-5, 1-4 September 2008.

URL: http://ieeexplore.ieee.org/stamp/stamp.jsp?tp=&arnumber=4651669&isnumber=4651429

[IC5.7] **Perdigão, M.S.**; E. S. Saraiva, J. M. Alonso, M. A. Dalla Costa; "Iluminação fluorescente: a garantia de eficiência energética mediante novas técnicas de controlo para balastros electrónicos com dimming," CLME 2008, Congresso Luso Moçambicano de Engenharia, Maputo, September 2008, ISBN: 978-972-8826-20-8.

[IC5.8] **Perdigão, M.S.**; E. S. Saraiva, J. M. Alonso, M. A. Dalla Costa; "Balastros Electrónicos Universais: Nova Técnica de Controlo Baseada em Reguladores Magnéticos," CBA 2008, Conferência Brasileira de Automática September 2008.

[IC5.9] **Perdigão, M.S.**; Baptista, B.; Alonso, J.M.; Saraiva, E.S.; "Reguladores Magnéticos aplicados em balastros electrónicos: a problemática da sua caracterização", II Jornada Luso-Brasileira de Ensino e Tecnologia em Engenharia – JLBE 2009, Febrruary 2009.

[IC5.10] **M. S. Perdigão**, J. M. Alonso, J. Ribas, D. Gacio, E. S. Saraiva; "Universal Ballast: A flexible solution based on magnetic regulator control concept," Seminario Anual de Automática, Eletrónica Industrial e Instrumentación, SAAEI'09, July 2009.

[IC5.11] **Perdigão, M.S.**; Alonso, J.M.; Gacio, D.; Saraiva, E.S.; "Magnetically-controlled electronic ballasts with isolated output: The variable transformer solution," Industrial Electronics, 2009. ISIE 2009. IEEE International Symposium on , vol., no., pp.59-64, 5-8 July 2009.

URL: http://ieeexplore.ieee.org/stamp/stamp.jsp?tp=&arnumber=5214261&isnumber=5213059

[IC5.12] Alonso, J.M.; **Perdigão, M.S.**; Ribas, J.; Gacio, D.; Saraiva, E.S.; "A digitally-controlled universal ballast based on magnetic regulator and PSoC device," Industrial Electronics, 2009. ISIE 2009. IEEE International Symposium on, vol., no., pp.2010-2015, 5-8 July 2009.

URL: http://ieeexplore.ieee.org/stamp/stamp.jsp?tp=&arnumber=5215663&isnumber=5213059

[IC5.13] **Perdigão, M.S.**; Baptista, B.; Saraiva, E.S.; Alonso, J.M.; "A dynamic-inductance model for magnetically controlled Electronic Ballasts," Universities Power Engineering Conference (UPEC), 2009 Proceedings of the 44th International, vol., no., pp.1-5, 1-4 September 2009.

URL: http://ieeexplore.ieee.org/stamp/stamp.jsp?tp=&arnumber=5429496&isnumber=5429361

[IC5.14] **Perdigão, M.S.**; Alonso, J.M.; Saraiva, E.S.; "A new integrated variable transformer topology for electronic ballasts," Industrial Electronics, 2009. IECON '09. 35th Annual Conference of IEEE, vol., no., pp.3484-3489, 3-5 November 2009.

URL: http://ieeexplore.ieee.org/stamp/stamp.jsp?tp=&arnumber=5415197&isnumber=5414636

[IC5.15] **Perdigão, M. S.**; Baptista, B.; Alonso, J. M.; Saraiva, E. S.; "Magnetic Regulator Topologies for Dimmable Electronic Ballasts", Industrial Electronics (ISIE), 2010 IEEE International Symposium on, Issue Date: 4-7, Page(s): 921 - 926 July 2010.

URL: http://ieeexplore.ieee.org/stamp/stamp.jsp?tp=&arnumber=5637141&isnumber=5635477

[IC5.16] **Perdigão, M. S.**; Baptista, B.; Marques, H.; Alonso, J. M.; Saraiva, E. S.; "On the use of magnetic regulators in electronic ballasts," Universities Power Engineering Conference (UPEC), 2010 45th International, Page(s): 1 – 6, 31 August to 3 September 2010.

URL: http://ieeexplore.ieee.org/stamp/stamp.jsp?tp=&arnumber=5649301&isnumber=5648789

[IC5.17] J. Marcos Alonso, **Perdigão M. S.**, David Gacio, Lidia Campa and Eduardo Saraiva, "Achieving Constant Frequency Operation in DC-DC Resonant Converters through Magnetic Control," 2010 Energy Conversion Congress and Exposition (ECCE), 2010 IEEE, Page(s): 2011 – 2018, 12-16 September 2010.

URL: http://ieeexplore.ieee.org/stamp/stamp.jsp?tp=&arnumber=5618109&isnumber=5617696

[IC5.18] Á. R. Seidel; **Perdigão M. S.**; H. V. Marques; J. M. Alonso; E. S. Saraiva; "Safe Electrode Operation In Universal Electronic Ballasts", COBEP2011, September 2011.

[IC5.19] H. V. Marques; Á. R. Seidel; **Perdigão, M. S.**, J. M. Alonso; E. S. Saraiva; "Development of a Universal Electronic Ballast for TL5 Lamps Using a Magnetic Regulator," Industry Application Conference, IAS2011, October 2011.

REFERENCES

[5.1] Borekci, S.; "Dimming Electronic Ballasts Without Striations," Industrial Electronics, IEEE Transactions on , vol.56, no.7, pp.2464-2468, July 2009.

[5.2] L-M. Lee, S. Y. Hui, “Automatic Lamp Detection and Operation for Warm-Start Tubular Fluorescent Lamps,” IEEE Transactions on Power Electronics, vol. 24, pp. 2933 – 294, Dec. 2009.

[5.3] Boeke, U.; "Scalable fluorescent lamp driver using magnetic amplifiers," Power Electronics and Applications, 2005 European Conference on, Sep. 2005.

APPENDIX A: OPERATION OF T5 FLUORESCENT LAMPS WITH COMMERCIAL BALLASTS

In this appendix, the experimental results that characterize the operation of T5 fluorescent lamps with commercial ballasts are presented.

A.1 SELECTED LAMPS

The group of tested lamps and corresponding commercial electronic ballasts are presented in Table A.1. Table A.2 presents several electrical characteristics of the tested lamps provided by the manufacturer.

Table A.1. Selected lamps and corresponding commercial ballast

SERIES	FLUORESCENT LAMP	ELECTRONIC BALLAST
High Efficiency, HE	PHILIPS MASTER TL5 HE 14W/840	PHILIPS ELECTRONIC BALLAST HF-R 114-35 TL5EII 220-240
	PHILIPS MASTER TL5 HE 21W/840	
	PHILIPS MASTER TL5 HE 28W/840	
	PHILIPS MASTER TL5 HE 35W/840	
High Output, HO	PHILIPS MASTER TL5 HO 39W/840	PHILIPS ELECTRONIC BALLAST HF-R 139 TL5EII 220-240 50/60Hz

Table A.2. Lamp voltage, discharge current, electrode resistance and SoS limits at nominal operation

FLUORESCENT LAMP	V_{lamp} [V]	I_D [mA]	r_e [Ω]	I_{LHmax} [mA]	I_{LLmax}[mA]
TL5 HE 14W	82±10	170±40	40	240	170
TL5 HE 21W	123±10	170±40	40	240	170
TL5 HE 28W	167±17	170±40	40	240	170
TL5 HE 35W	209±20	170±40	40	240	170
TL5 HO 39W	112±10	340±70	12	475	370

A.2 CONDITIONS FOR PROPER ELECTRODE OPERATION

The lifetime of a fluorescent lamp is determined by the lifetime of the electrode and in order to ensure sufficient electrode lifetime, its temperature should be kept within certain limits. Electrodes in MASTER TL5 lamps consist of a coiled construction of tungsten wire which is filled with emissive material. Above a certain temperature the electrodes will be too hot, leading to enhanced evaporation of the emissive material and severe end-blackening. Below a certain temperature the electrode is too cold and sputtering of the emitter occurs. If MASTER TL5 lamps are dimmed by reducing the lamp current, the power dissipation in the electrodes will decrease, resulting in a lower temperature of the electrode. Thus, in general, additional heating should be supplied to the electrode to maintain its proper temperature. The temperature of an electrode is primarily influenced by three currents. A simplified diagram of electrode currents is depicted in Fig. A.1.

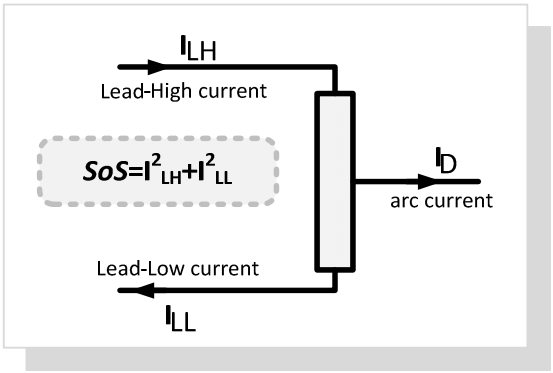

Fig. A.1. Lamp electrode current definition

One way to evaluate the conditions for proper and safe operation of the electrodes is based on the sum of squares of the lead-in wires rms currents known as, SoS:

$$SoS = I_{LH}^2 + I_{LL}^2; \qquad I_{LH} > I_{LL} \tag{A.1}$$

The definition takes into account both electrode currents, as defined in Fig. A.1. The currents I_{LH} and I_{LL} can be measured with a current probe around each lead-in wire. By definition, the higher of the two currents is called I_{LH}, and the lower of the currents is called I_{LL}. If the two lead-in wires are taken together through one current probe, it is possible to measure the arc current I_D.

For each rated lamp power, maximum and minimum limit values are defined for each of these currents, for nominal power operation or dimming operation, as presented in Table A.3. In

dimming operation, instead of having one SoS value for each lamp, maximum, minimum and target SoS curves are defined for the whole dimming range.

Table A.3. Current boundaries and SoS lines for the tested lamps [1]

LAMP	NORMAL OPERATION		DIMMING OPERATION			
HIGH EFFICIENCY TL5 HE 14W TL5 HE 21W TL5 HE 28W TL5 HE 35W	I_{Dmin} [mA]	130	I_{Dmin} [mA]	15	$SoS = I_{LH}^2 + I_{LL}^2$	
	I_{Dmax} [mA]	210	I_{Dmax} [mA]	130	X_1 [A^2]	0.050
					Y_1 [A]	0.330
					z	0.1
	I_{LHmax} [mA]	240	I_{LHmax} [mA]	170	X_2 [A^2]	0.058
	I_{LLmax} [mA]	170	I_{LLmax} [mA]	240	Y_2 [A]	-0.075
HIGH OUTPUT TL5 HO 24W TL5 HO 39W	I_{Dmin} [mA]	270	I_{Dmin} [mA]	35	$SoS = I_{LH}^2 + I_{LL}^2$	
	I_{Dmax} [mA]	440	I_{Dmax} [mA]	270	X_1 [A^2]	0.210
					Y_1 [A]	0.630
					z	0.3
	I_{LHmax} [mA]	475	I_{LHmax} [mA]	370	X_2 [A^2]	0.270
	I_{LLmax} [mA]	370	I_{LLmax} [mA]	475	Y_2 [A]	-0.170
TL5 HO 49W	I_{Dmin} [mA]	210	I_{Dmin} [mA]	25	$SoS = I_{LH}^2 + I_{LL}^2$	
	I_{Dmax} [mA]	340	I_{Dmax} [mA]	210	X_1 [A^2]	0.120
					Y_1 [A]	0.480
					z	0.3
	I_{LHmax} [mA]	370	I_{LHmax} [mA]	370	X_2 [A^2]	0.150
	I_{LLmax} [mA]	275	I_{LLmax} [mA]	275	Y_2 [A]	-0.120

A.3 EXPERIMENTAL SETUP

Each lamp high-frequency electrical characteristics was extracted with the experimental setup shown in Fig. A.2. It was also possible to verify the behaviour of each lamp during dimming and start-up conditions.

All commercial electronic ballasts were supplied by a Chroma 61602 power source which provided a 230V/50Hz voltage, simulating the standard power supply. All the selected ballasts had an analog 1-10V DC dimming interface. The interface dictates the desired luminous flux level, through the dc level imposed on the control circuit. This voltage was provided by a Yokogawa GS610 power source.

The measurement unit consisted of a PC oscilloscope, the Picoscope 3423, two voltage probes (Tektronix P5200), and two current probes (Tektronix TCP312 30A, amplifier Tektronix TCPA300). With this equipment and with additional functions provided by the Chroma 61602 power source, it was possible to acquire several parameters: the lamp voltage, the electrode voltages, the discharge or arc current and the electrodes currents. With these measurements it was possible to obtain the average lamp power, the average arc power and the average electrode power at each power level. It is assumed that the lamp power is equal to the sum of the arc power and the electrode power. It was also possible to estimate the power consumption and efficiency of the system and the power factor seen by the utility line. Finally, the actual or the real SoS lines for all lamps were also obtained, in order to compare them to the maximum, minimum and target lines as defined by the manufacturer.

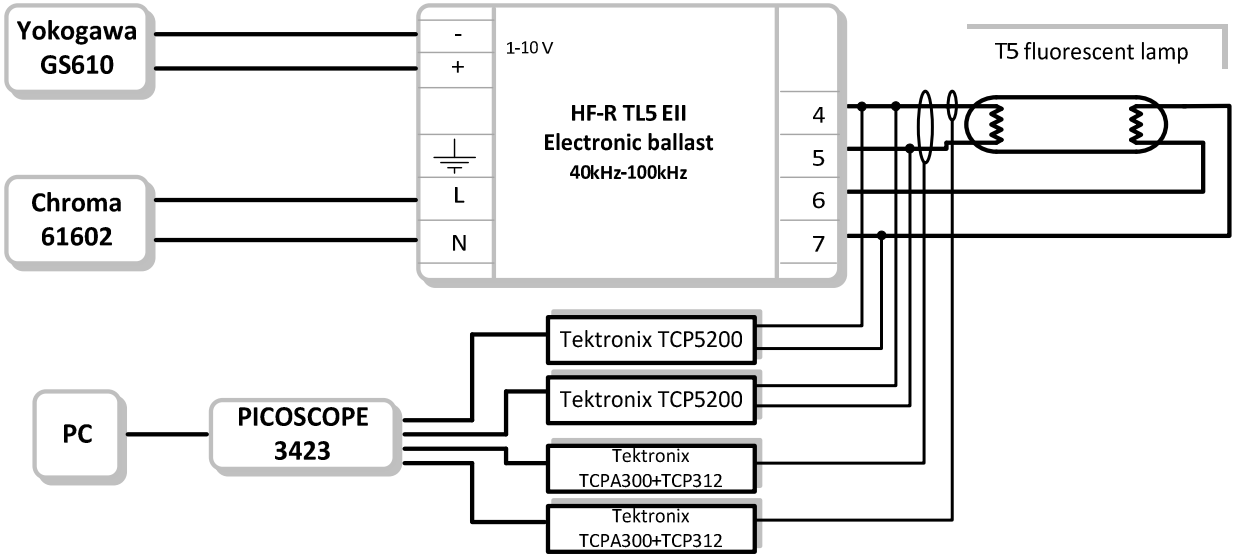

Fig. A.2. Laboratory experimental setup

A.4 EXPERIMENTAL RESULTS

In Fig. A.3, Fig. A.5, Fig. A.7, Fig. A.9, and Fig. A.11, the lamp voltage and the discharge current, are presented in a power ON/OFF situation. The voltage ignition spike is easily observed in Fig. A.9. Once the lamp is ignited, the discharge current and the lamp voltage stabilize at the nominal values.

Fig. A.4, Fig. A.6, Fig. A.8 Fig. A.10 and Fig. A.12, also show the lamp voltage and the discharge current in a dimming variation process. The lamps were kept at each dimming level for 60 seconds. The general behaviour shows that the power level of the lamp decreases with the DC

control voltage level. This fact is easily related to the decrease of the lamp current. Fig. A.12 also shows that the lamp voltage remains almost constant during the dimming operation. This is also valid for all the remaining lamps.

From the measurements and calculated values presented in Table A.4, Table A.5, Table A.6, Table A.7, and Table A.8, it is identified that all ballasts use a variable-frequency technique to achieve dimming and that a good power factor cannot be maintained for all operating points. The efficiency of the ballasts, computed as the ratio between the lamp power, P_{lamp}, and the input ballast power, P_{in}, is around 90% for high power values, decreasing rapidly for lower dimming levels. In conclusion, these dimmable electronic ballasts are only optimized for nominal lamp power operation.

Fig. A.13 presents the SoS lines determined for ech tested lamp, according with the parameters given in Table A.2. For all tested lamps, the actual or real SoS lines are typically below the SoS target line. It is recalled that typically these commercial ballasts use external heating sources which control the electrodes operation.

Fig. A.14 shows the lamp power variation as a function of the discharge current, the lamp voltage, the lamp resistance and the lamp operating frequency. Fig. A.15 shows the lamp resistance variation as a function of the lamp power, the discharge current, the lamp voltage and the lamp operating frequency.

Fig. A.16 shows the high frequency $v(i)$ characteristic for three different lamps, at different power levels.

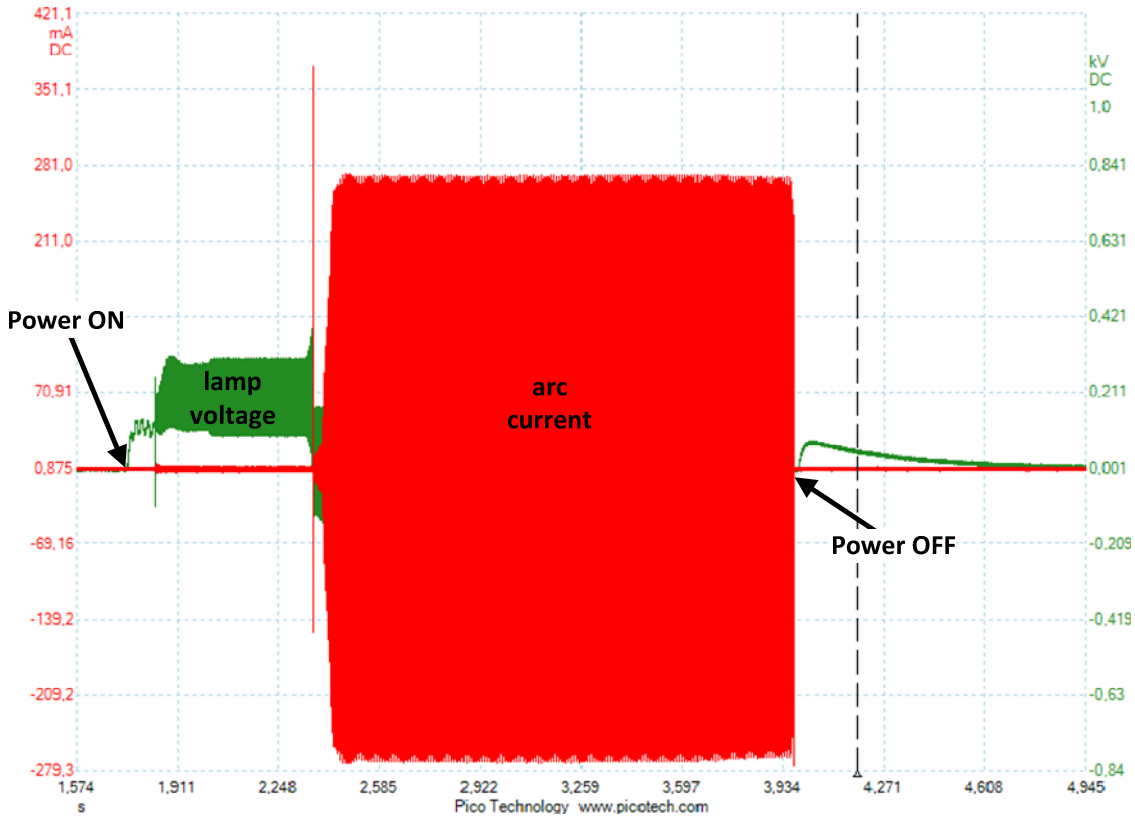

Fig. A.3. T5 HE 14W: Lamp voltage and arc current starting behaviour.

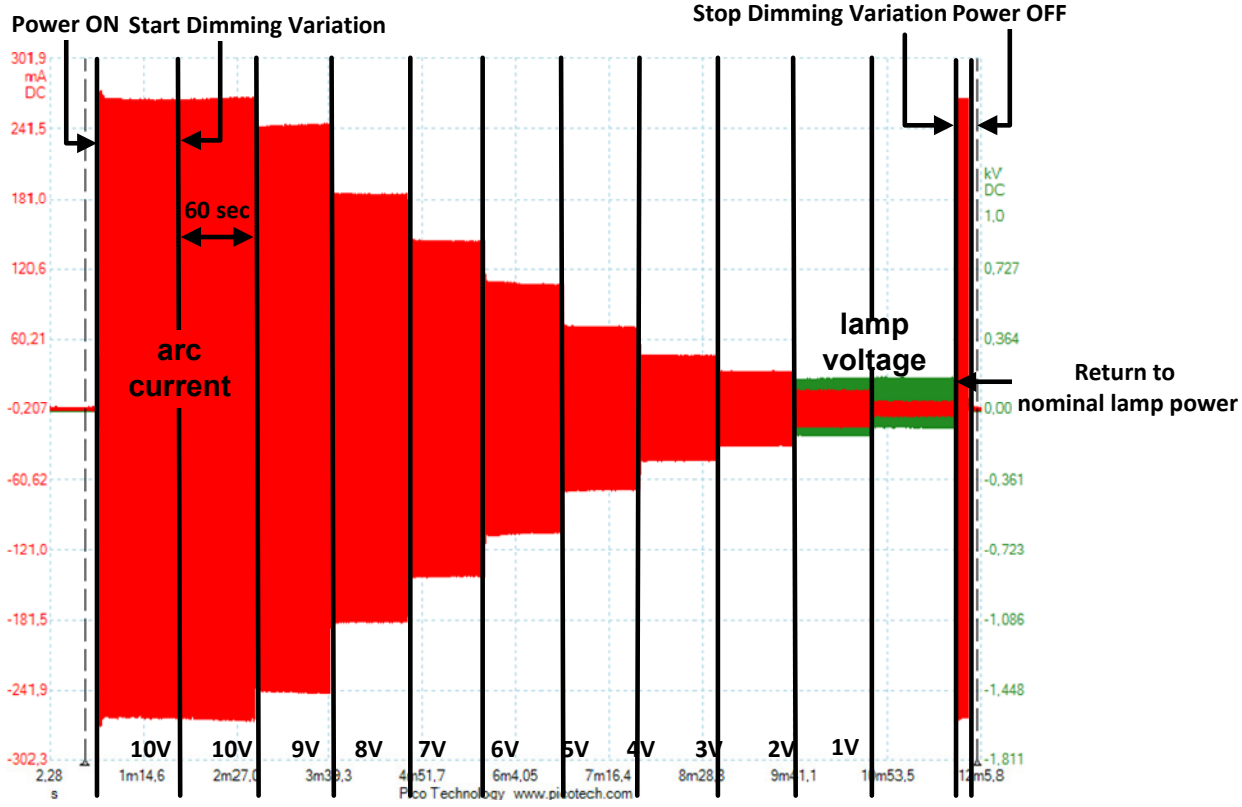

Fig. A.4. T5 HE 14W: Lamp voltage and arc current behaviour during dimming.

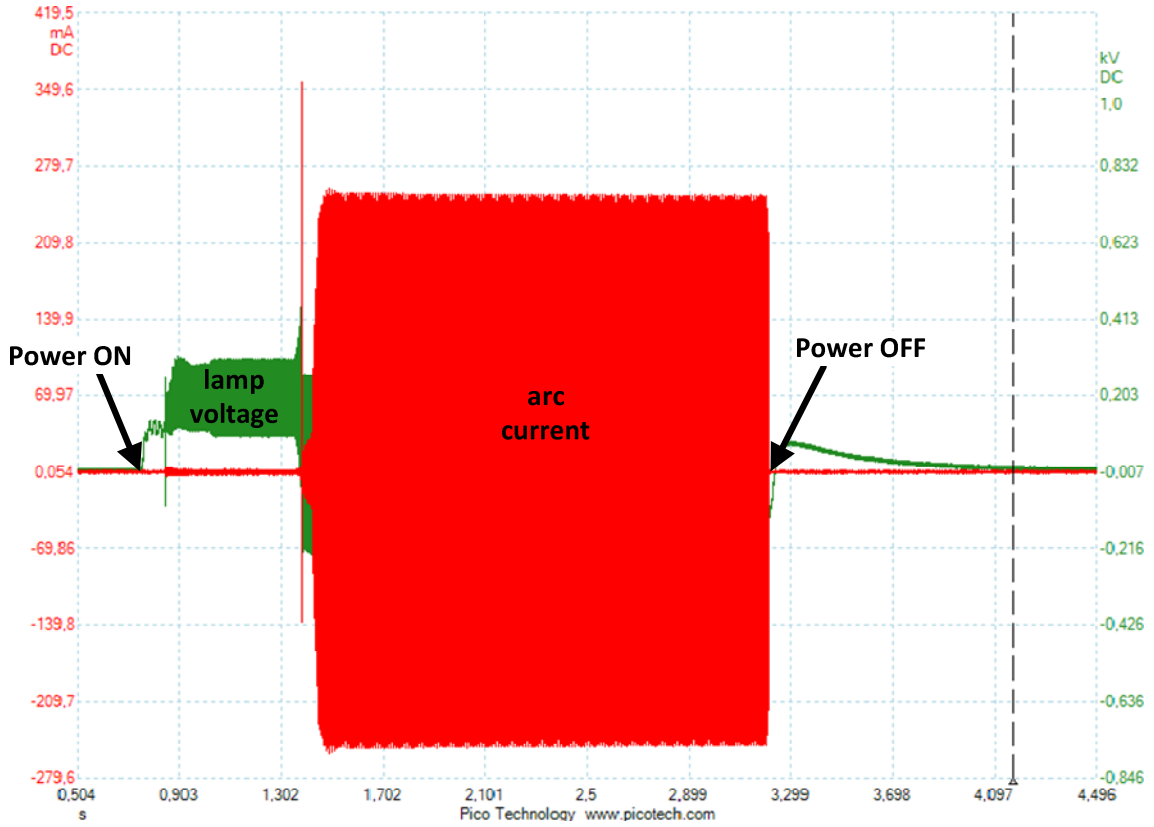

Fig. A.5. T5 HE 21W: Lamp voltage and arc current starting behaviour.

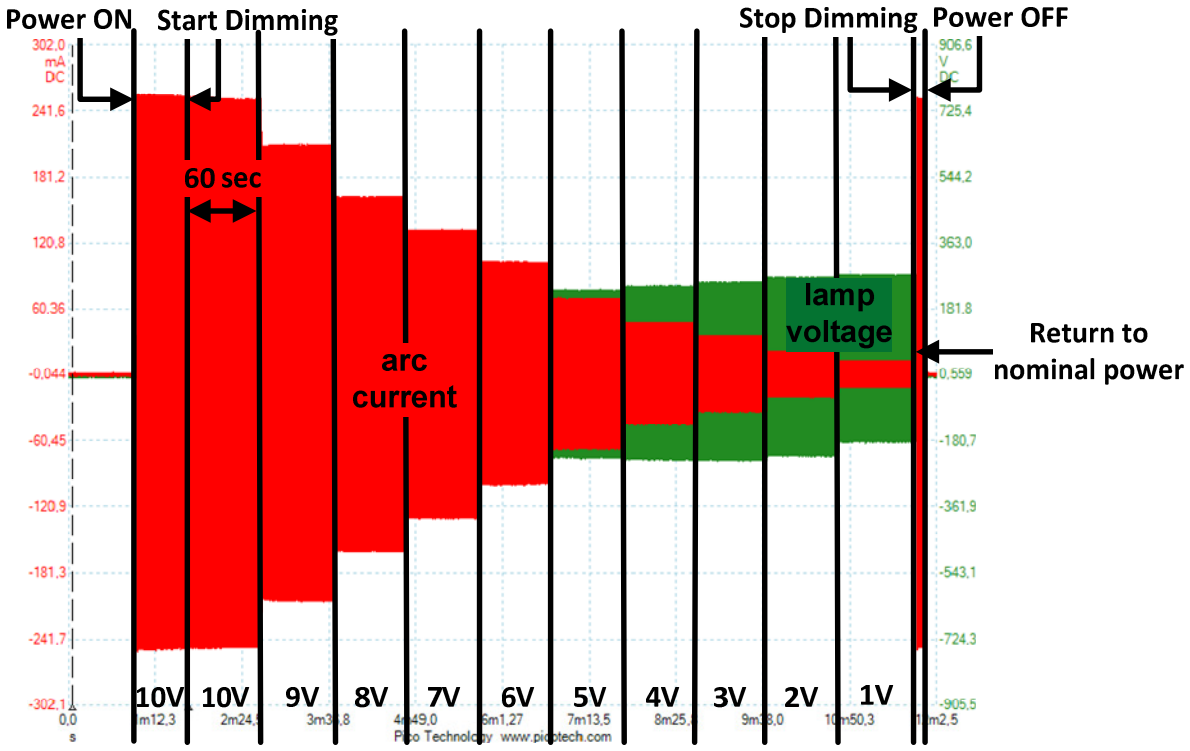

Fig. A.6. T5 HE 21W: Lamp voltage and arc current behaviour during dimming.

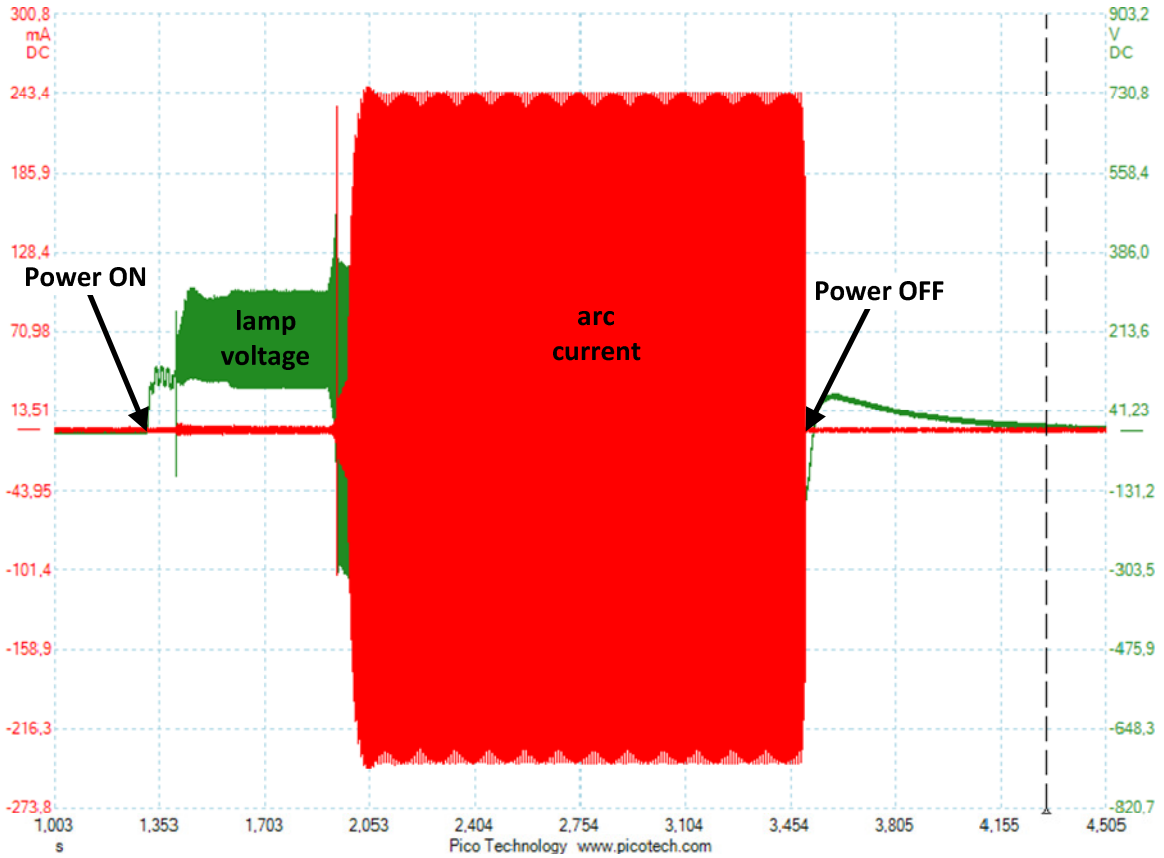

Fig. A.7. T5 HE 28W: Lamp voltage and arc current starting behaviour.

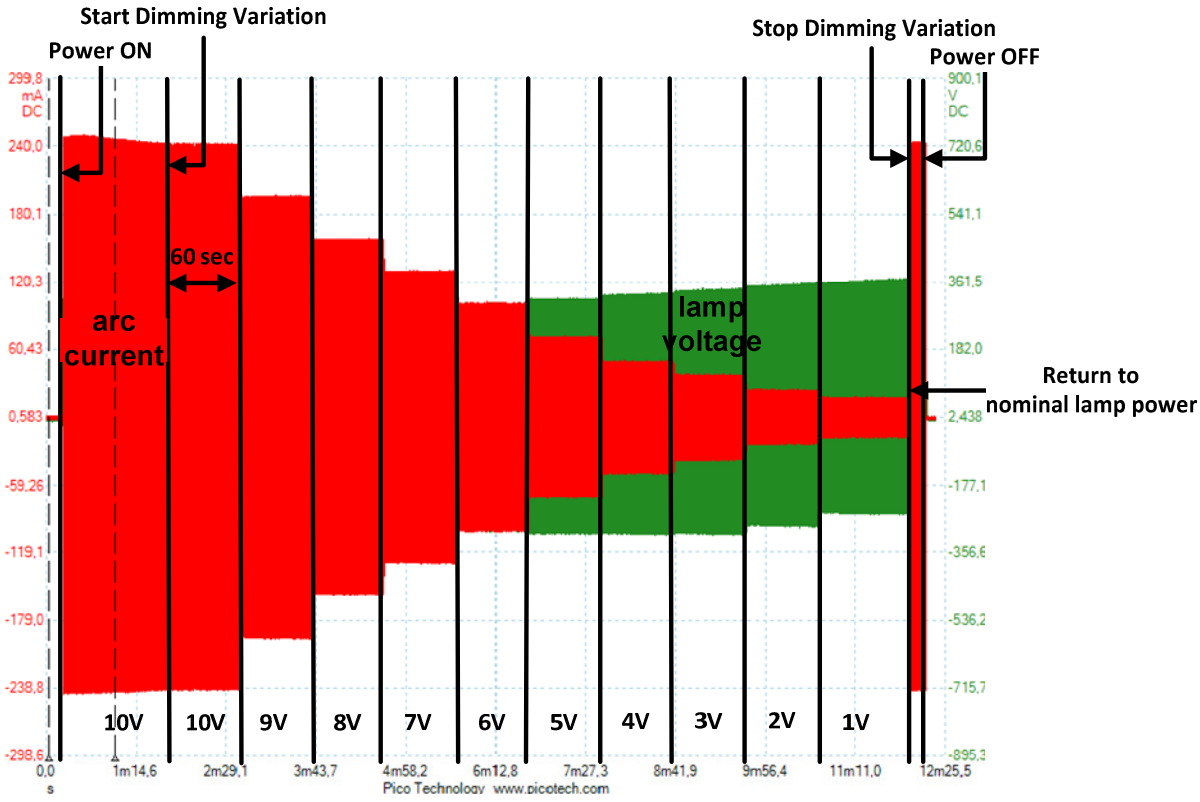

Fig. A.8. T5 HE 28W: Lamp voltage and arc current behaviour during dimming.

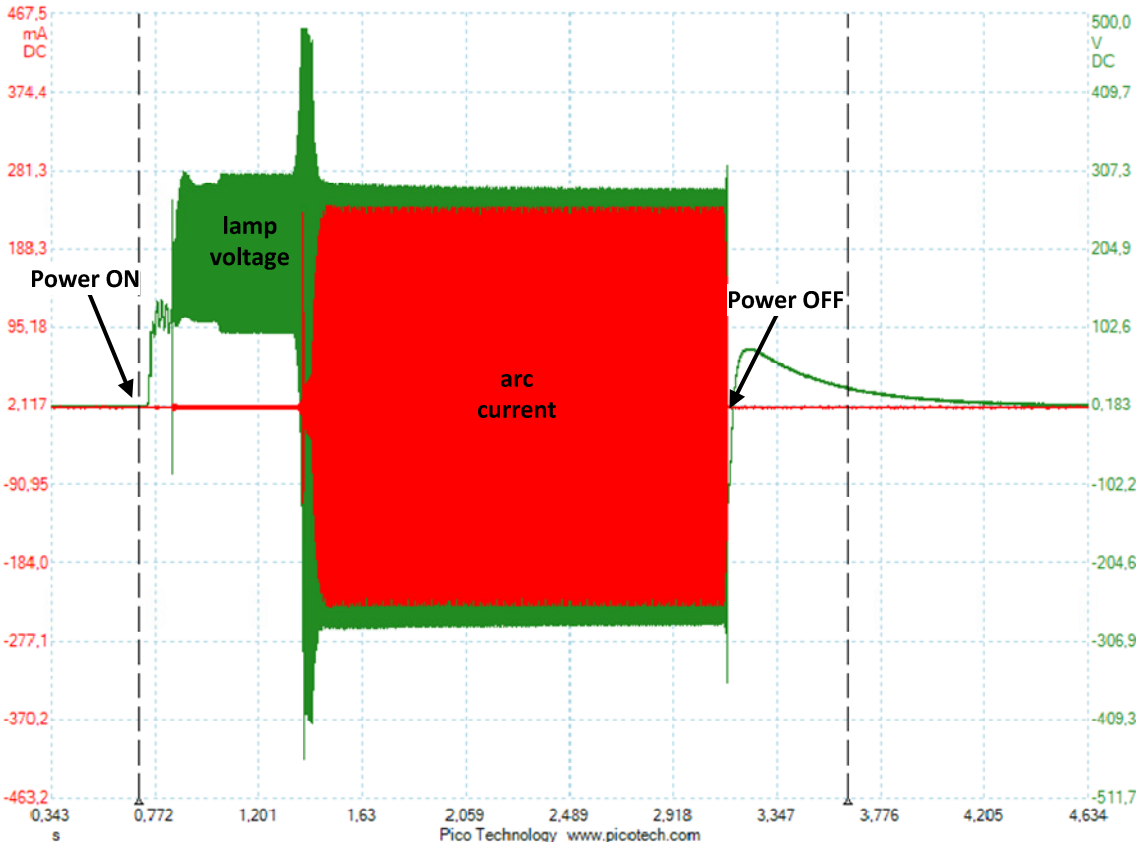

Fig. A.9. T5 HE 35W: Lamp voltage and arc current starting behaviour.

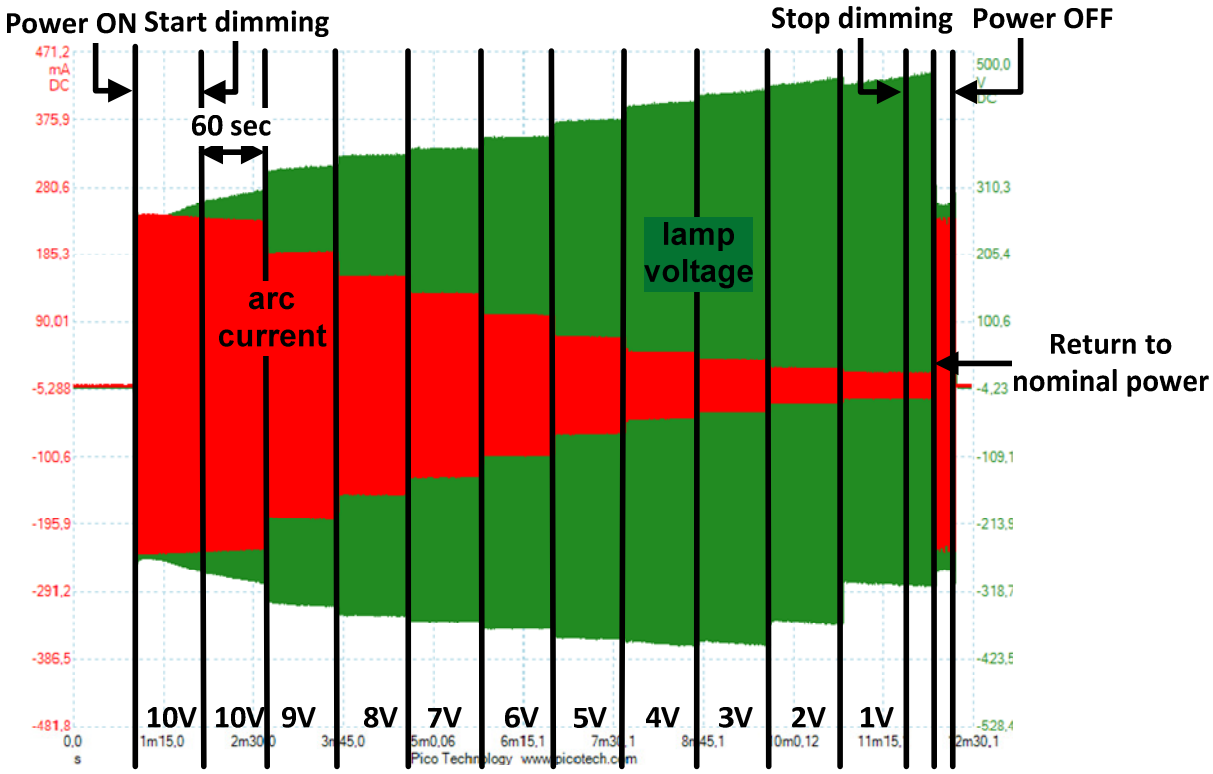

Fig. A.10. T5 HE 35W: Lamp voltage and arc current behaviour during dimming.

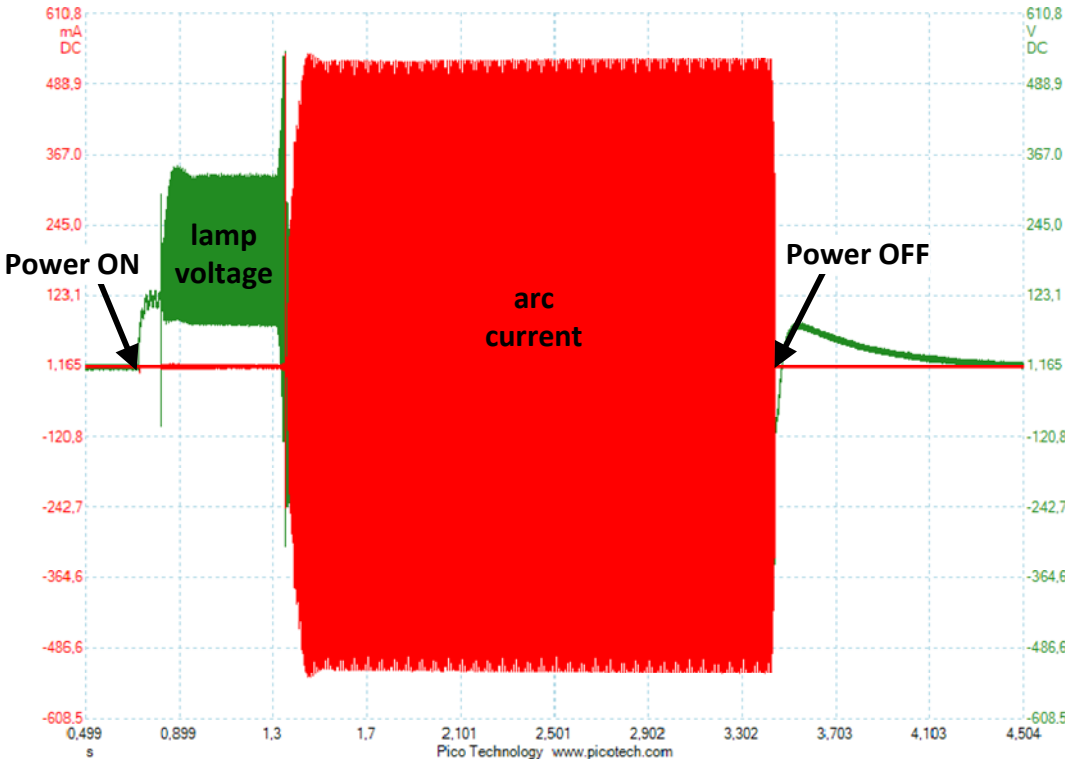

Fig. A.11. T5 HO 39W: Lamp voltage and arc current starting behaviour.

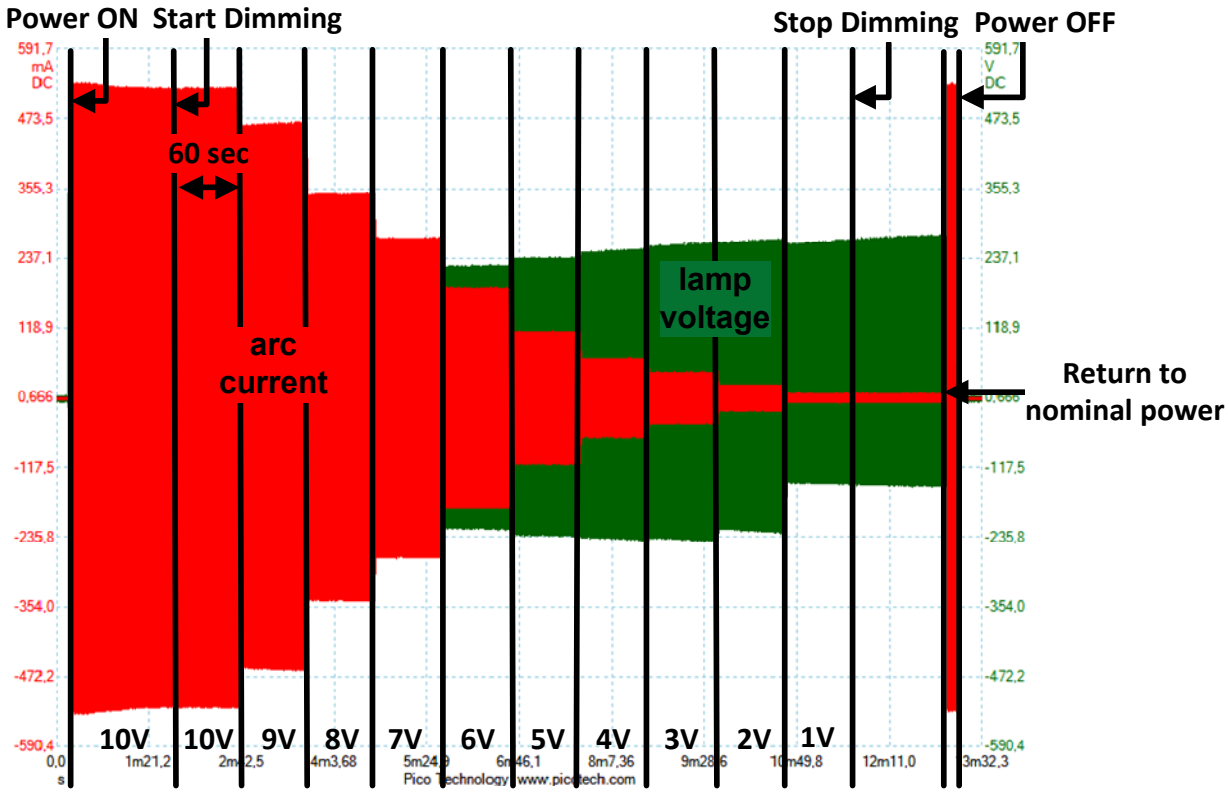

Fig. A.12. T5 HO 39W: Lamp voltage and arc current behaviour during dimming.

Table A.4. TL5 HE 14W Philips operated with PHILIPS HF-R 14-35 TL5 220-240.

MEASUREMENTS						CALCULATED VALUES				
V_{DC} [V]	f_s [kHz]	V_{lamp} [V]	I_D [mA]	*Line Power Factor*	P_{in} [W]	*Efficiency* [%]	P_{lamp} [W]	P_{arc} [W]	P_{electr} [W]	R_{lamp} [Ω]
1	97.2	94.78	3	0.650	5.1	0.51	2.58	0.30	2.27	28744
2	91.7	109.95	12	0.700	5.9	0.60	3.53	1.25	2.28	9453
3	89.8	112.15	24	0.750	7.2	0.68	4.92	2.68	2.24	4601
4	88.6	112.29	33	0.800	8.2	0.71	5.78	3.65	2.13	3380
5	86.4	107.98	52	0.840	9.7	0.76	7.36	5.47	1.89	2087
6	80.2	101.41	80	0.872	11.6	0.83	9.64	7.96	1.68	1271
7	69.7	95.28	111	0.915	13.5	0.86	11.57	10.40	1.16	862
8	62.0	91.68	129	0.925	14.6	0.85	12.44	11.64	0.80	712
9	50.6	86.22	162	0.942	16.7	0.86	14.38	13.80	0.58	532
10	46.7	83.74	181	0.950	17.5	0.89	15.55	15.02	0.53	462

Table A.5. TL5 HE 21W Philips operated with PHILIPS HF-R 14-35 TL5 220-240.

MEASUREMENTS						CALCULATED VALUES				
V_{DC} [V]	f_s [kHz]	V_{lamp} [V]	I_D [mA]	*Line Power Factor*	P_{in} [W]	*Efficiency* [%]	P_{lamp} [W]	P_{arc} [W]	P_{electr} [W]	R_{lamp} [Ω]
1	82.4	158.11	4	0.660	5.3	49	2.60	0.58	2.02	41969
2	81.0	168.10	12	0.760	6.6	59	3.88	1.91	1.97	14489
3	80.0	170.34	25	0.832	8.5	71	6.07	4.08	1.99	6948
4	79.8	166.61	34	0.850	9.9	76	7.55	5.57	1.98	4891
5	78.4	161.98	52	0.911	12.1	83	10.04	8.23	1.80	3118
6	74.8	153.47	78	0.936	15.2	87	13.24	11.67	1.57	1977
7	68.5	145.62	106	0.945	18.1	91	16.56	15.22	1.34	1370
8	60.7	137.82	129	0.965	20.6	90	18.50	17.51	0.99	1065
9	53.0	129.34	154	0.964	22.7	89	20.24	19.53	0.71	840
10	46.7	124.89	174	0.970	24.5	90	22.04	21.34	0.70	719

Table A.6. TL5 HE 28W Philips operated with PHILIPS HF-R 14-35 TL5 220-240.

MEASUREMENTS						CALCULATED VALUES				
V_{DC} [V]	f_s [kHz]	V_{lamp} [V]	I_D [mA]	*Line Power Factor*	P_{in} [W]	*Efficiency* [%]	P_{lamp} [W]	P_{arc} [W]	P_{electr} [W]	R_{lamp} [Ω]
1	79.2	183.54	4	0.674	5.4	50	2.73	0.70	2.03	47089
2	76.2	211.03	13	0.804	7.6	63	4.76	2.81	1.95	15667
3	75.2	216.17	26	0.874	10.3	73	7.47	5.59	1.88	8248
4	74.8	215.18	37	0.912	12.1	81	9.77	7.84	1.93	5812
5	73.7	210.42	54	0.936	15.2	84	12.76	11.07	1.69	3932
6	70.6	201.37	81	0.952	19.7	89	17.60	16.11	1.49	2477
7	64.8	187.79	114	0.962	24.9	90	22.48	21.06	1.42	1651
8	58.8	182.75	133	0.974	27.3	93	25.51	23.93	1.59	1374
9	51.8	174.37	156	0.968	30	94	28.18	26.79	1.39	1119
10	46.7	167.16	181	0.978	31.7	98	31.11	29.90	1.21	924

Table A.7. TL5 HE 35W Philips operated with PHILIPS HF-R 14-35 TL5 220-240.

MEASUREMENTS						CALCULATED VALUES				
V_{DC} [V]	f_s [kHz]	V_{lamp} [V]	I_D [mA]	*Line Power Factor*	P_{in} [W]	*Efficiency* [%]	P_{lamp} [W]	P_{arc} [W]	P_{electr} [W]	R_{lamp} [Ω]
1	70.5	270.46	11	0.820	9.7	46	4.46	2.76	1.69	25013
2	69.4	305.59	17	0.870	11.6	56	6.50	5.10	1.40	17703
3	69.1	304.23	28	0.910	14.6	66	9.62	8.36	1.26	10775
4	68.8	293.19	39	0.940	16.8	74	12.43	11.17	1.25	7513
5	68.5	278.37	57	0.960	20.6	80	16.50	15.42	1.08	4923
6	67	265.66	80	0.971	25.8	85	21.88	20.93	0.95	3303
7	64	246.09	109	0.982	30.4	88	26.84	26.18	0.65	2268
8	60.4	236.71	127	0.971	33.6	89	30.06	29.56	0.51	1860
9	54	223	153	0.986	37.1	92	34.14	33.61	0.53	1456
10	46.7	211.15	163	0.980	39.8	89	35.35	34.80	0.55	1326

Table A.8. TL5 HO 39W Philips operated with PHILIPS HF-R 139 TL5 220-240.

MEASUREMENTS						CALCULATED VALUES				
V_{DC} [V]	f_s [kHz]	V_{lamp} [V]	I_D [mA]	*Line Power Factor*	P_{in} [W]	*Efficiency* [%]	P_{lamp} [W]	P_{arc} [W]	P_{electr} [W]	R_{lamp} [Ω]
1	87.8	143,61	4	0.640	6.1	41	2.51	0.54	1.97	35991
2	84.2	176.02	17	0.780	8.6	57	4.86	3.02	1.85	10074
3	83.0	182.10	38	0.860	12.1	70	8.47	6.76	1.70	4784
4	83.0	177.44	61	0.890	15.1	81	12.21	10.60	1.61	2901
5	81.8	167.48	98	0.930	20.3	86	17.46	16.07	1.39	1717
6	77.8	151.09	155	0.960	27.1	89	24.05	23.06	0.99	975
7	69.4	138.44	218	0.970	33.3	92	30.69	29.74	0.95	636
8	59.7	127.72	271	0.974	38.1	92	35.02	34.18	0.84	472
9	47.4	120.22	342	0.989	44.5	93	41.36	40.75	0.61	352
10	46.1	118.17	343	0.981	44.9	91	40.85	40.25	0.60	344

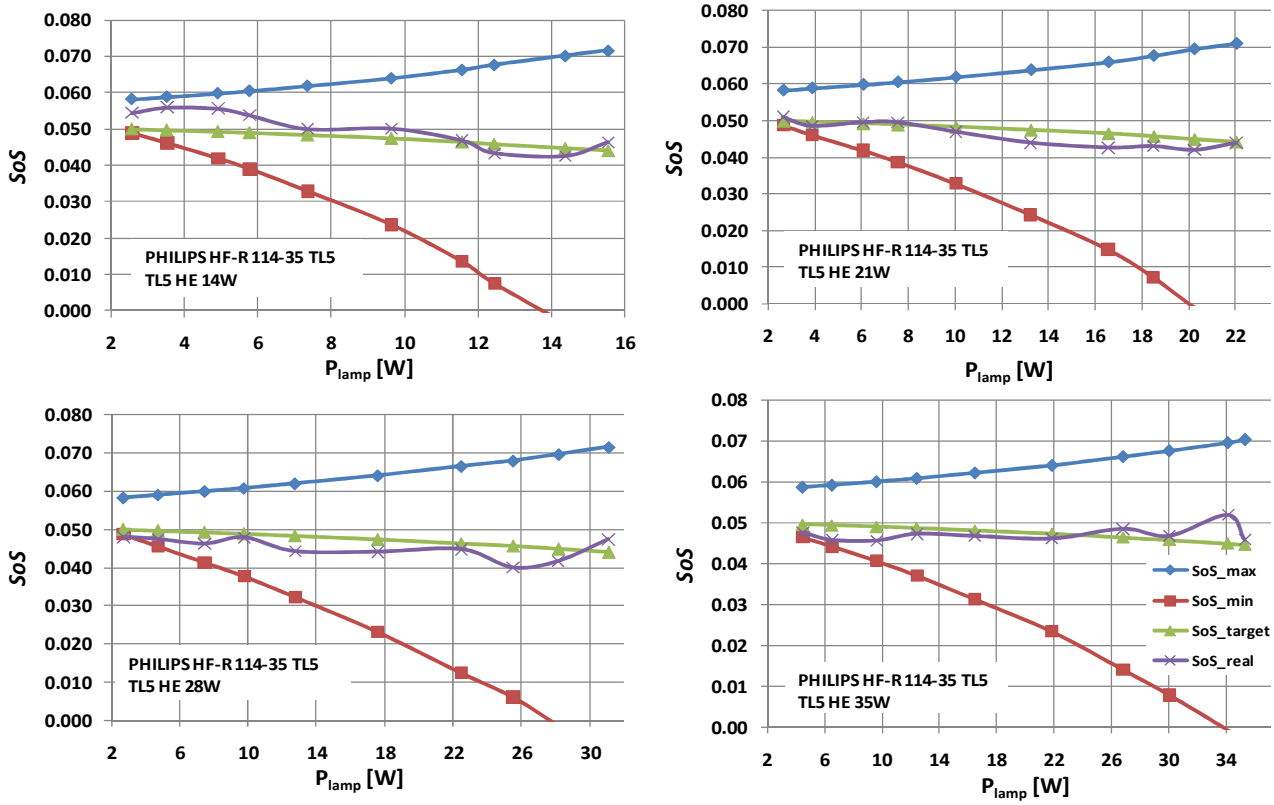

Fig. A.13. *SoS* lines: TL5 HE 14W, TL5 HE 21W, TL5HE 28W, TL5 HO 35W.

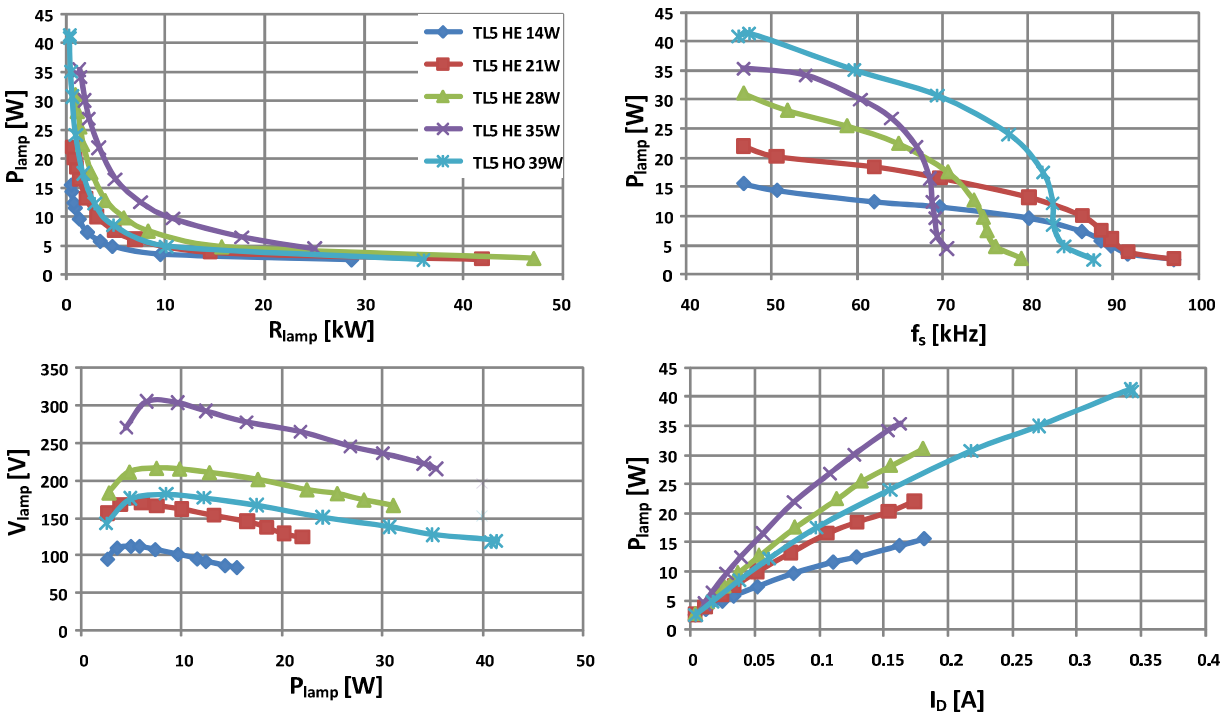

Fig. A.14. Lamp power variation as function of discharge current, lamp voltage, lamp resistance and lamp operating frequency.

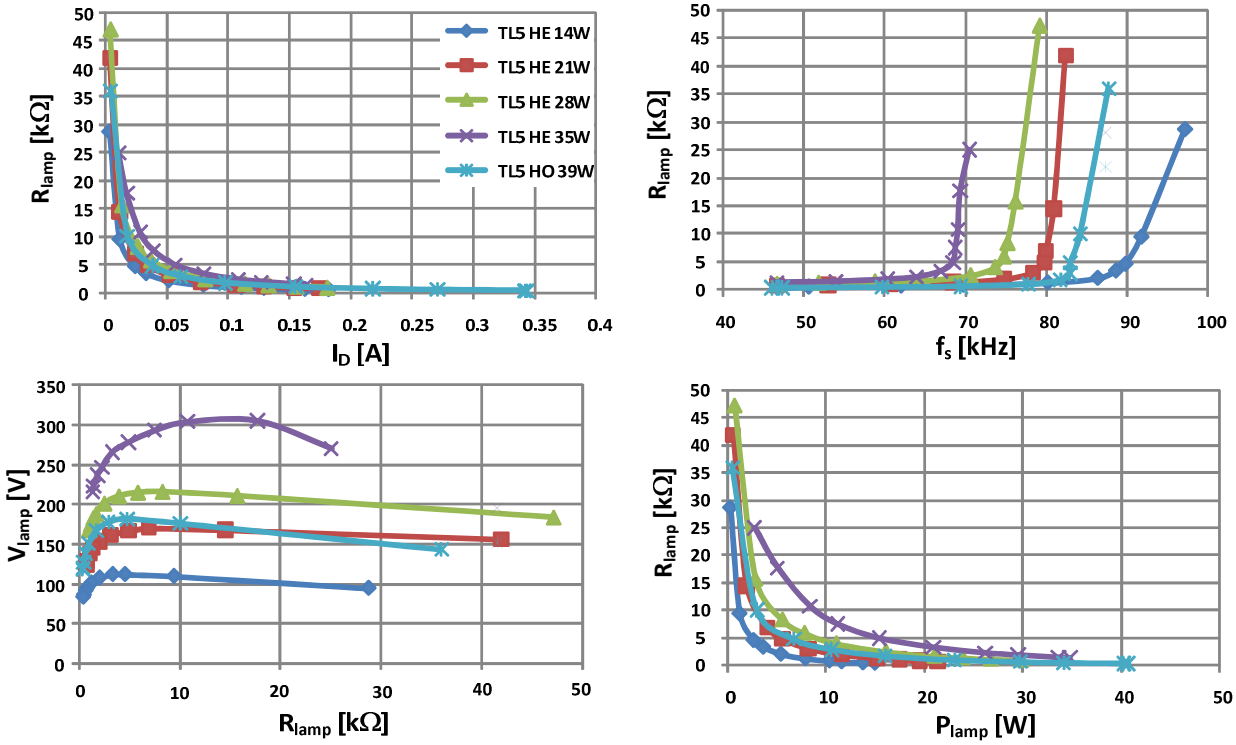

Fig. A.15. Lamp resistance variation as function of lamp power, discharge current, lamp voltage and switching frequency.

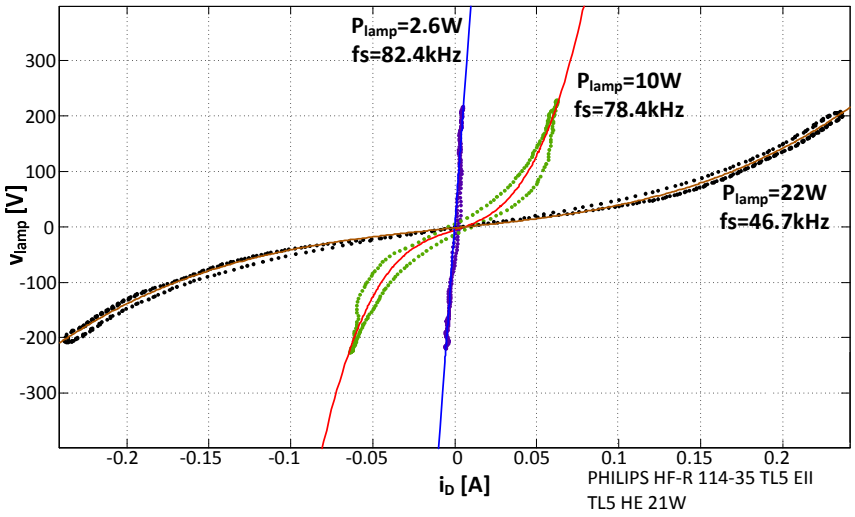

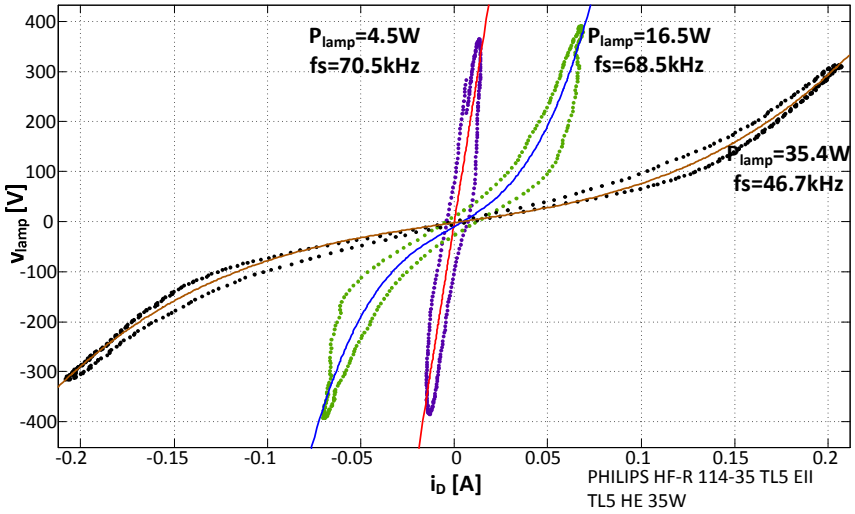

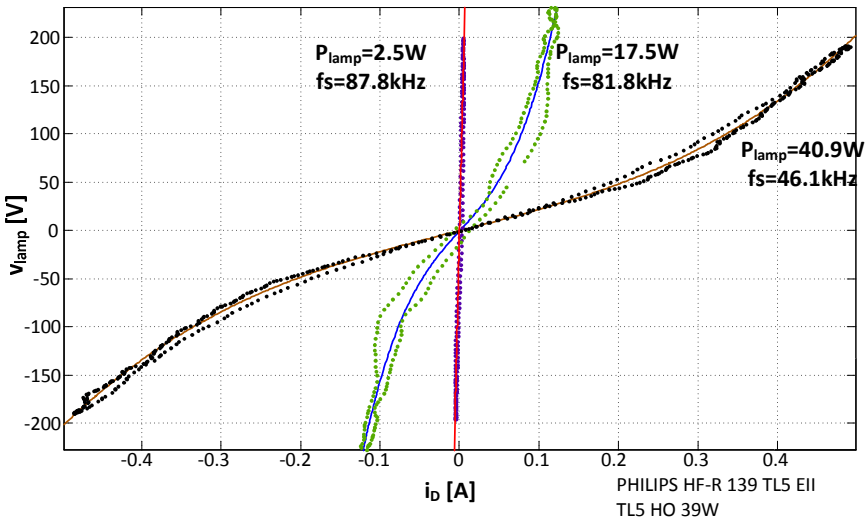

Fig. A.16. High frequency $v(i)$ characteristics of T5 fluorescent lamp at different power levels

REFERENCES AND BIBLIOGRAPHY

[1]. Philips MASTER TL5 lamps, Philips 2006, Access in: Jan. 2011, http://www.lighting.philips.com

[2]. International Electrotechnical Commission. Ballasts for tubular fluorescent lamps - Performance requirements, IEC 60921, 2006.

[3]. International Electrotechnical Commission. AC supplied electronic ballasts for tubular fluorescent lamps - Performance requirements, IEC 60929, 2006.

[4]. IEC60081. Double-capped fluorescent lamps. Performance specifications. 2010.

[5]. GE Lighting, T5 Long Last, linear fluorescent lamps, Datasheet, April 2009.

APPENDIX B: MATHCAD FILES

In this appendix, some of the developed Mathcad files are presented.

LIST OF FILES

- **B.1** DESIGN METHODOLOGY FOR DETERMINING THE VARIABLE INDUCTOR PARAMETERS;
- **B.2** CALCULATION OF THE DIFFERENTIAL INDUCTANCE L_{ac};
- **B.3** LCC RESONANT CIRCUIT ANALYSIS;
- **B.4** DESIGN METHODOLOGY FOR DETERMINING THE RESONANT TANK PARAMETERS - LC CIRCUIT;
- **B.5** CALCULATION OF THE THEORETICAL DIMMING CURVES FOR A T5 HE 21W LAMP, PHASE OF THE INPUT RESONANT CURRENT AND COMPARISON WITH EXPERIMENTAL RESULTS.

B.1 DESIGN METHODOLOGY FOR DETERMINING THE VARIABLE INDUCTOR PARAMETERS:

Type of core: EF25

- To IEC 61246
- Delivery mode: single units

Magnetic characteristics (per set)

$\Sigma l/A$ = 1.1 mm^{-1}
l_e = 57.5 mm
A_e = 52.5 mm^2
A_{min} = 51.5 mm^2
V_e = 3020 mm^3

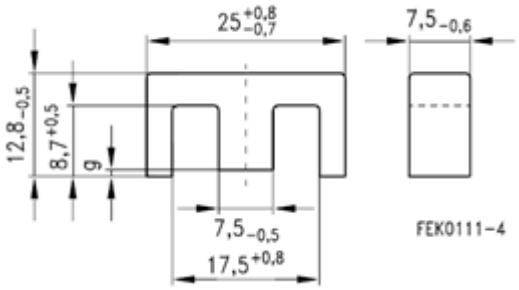

core parameters:

$Ae := 52\cdot10^{-6}$	effective magnetic cross section (m^2)	$Wa := 87$	area of window (m^2)
$g := 0.3\cdot10^{-3}$	air gap (m)	$lext := 100\cdot10^{-3}$	external path (m)
$le := 58\cdot10^{-3}$	effective magnetic path length (m)	$\mu0 := 4\cdot\pi\cdot10^{-7}$	air permeability
$Bs := 0.5$	saturation magnetization (T)	$\mu r := 3000$	relative permeability
$Idc := 1$	maximum control current (A)	$\lambda := 0.7$	decreasing permeability factor

magnetic field density and maximum ac current

$Iacmax := 0.6$ Acceptable value in terms of resonant current

$$Bmax := \frac{Bs}{5}$$

magnetic parameters:

$\delta := 4$ Current density (A/m^2)

$Lmax := 1\cdot10^{-3}$ Required maximum inductance value

number of turns of the main winding:

$$Nac := \frac{Lmax\cdot Iacmax}{Bmax\cdot Ae}$$ Number of turns of the main winding $Nac = 115.385$

$$d := \sqrt{\frac{4\cdot Iacmax}{\pi\cdot\delta}}$$ Diameter of wire of the main winding $d = 0.437$

number of turns of the control winding:

$k := 0.8$ decreasing permeability factor

$\mu kBsat := 1800$

$$Ndc := \frac{k\cdot Bs\cdot lext}{0.5\cdot\mu kBsat\cdot\mu0\cdot Idc}$$ Number of turns of the control winding $Ndc = 35.368$

$$dc := \sqrt{\frac{4 \cdot Idc}{\pi \cdot \delta}}$$ Diameter of the wire of the control winding $dc = 0.564$

ac and dc winding area ocupation:

$$Aw := Nac \cdot \frac{\pi \cdot d^2}{4} + Ndc \cdot \frac{\pi \cdot dc^2}{4}$$ Ocupied area by the main winding $Aw = 26.15$

$$Ku := \frac{Aw}{Wa}$$ $Ku = 0.301$ limit value, needs second iteration?

gap

$$gap := \frac{\left(Nac^2 \cdot \mu r \cdot Ae - le \cdot Lmax\right) \cdot \mu 0}{Lmax \cdot \mu r}$$ $gap = 8.7 \times 10^{-4}$ gap to large!

$$gap := 3 \cdot 10^{-4}$$ typical value of air gap in gapped EF25 cores

$$Nac := \sqrt{\frac{\left(gap \cdot Lmax \cdot \frac{\mu r}{\mu 0} + le \cdot Lmax\right)}{(\mu r \cdot Ae)}}$$ $Nac = 67.757$ new value of ac turns

new ac and dc winding area ocupation:

$$Aw := Nac \cdot \frac{\pi \cdot d^2}{4} + Ndc \cdot \frac{\pi \cdot dc^2}{4}$$ Ocupied area by the main winding $Aw = 19.005$

$$Ku := \frac{Aw}{Wa}$$ $Ku = 0.218$ smaller value!

Calculation of Inductance:

$$L := \frac{Nac^2}{\frac{le}{\mu r \cdot \mu 0 \cdot Ae} + \frac{gap}{\mu 0 \cdot Ae}}$$ Inductance of the main winding $L = 9.395 \times 10^{-4}$

Experimental prototype:

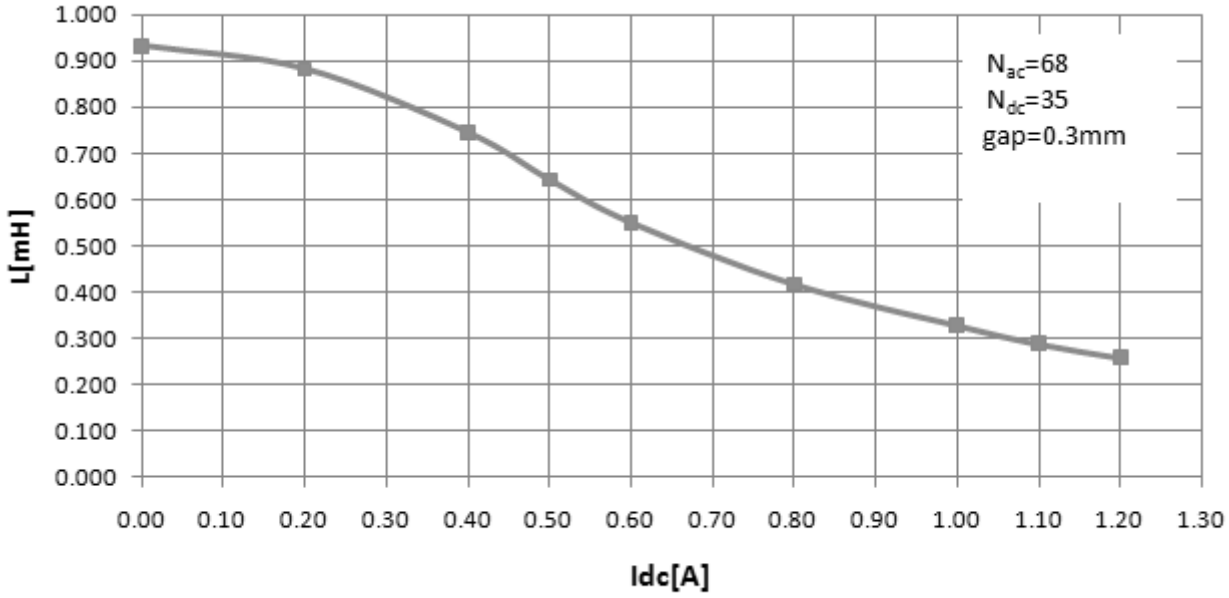

Magnetic flux density in the core:

$$B(I) := \frac{Nac \cdot Iacmax}{\frac{le}{\mu r \cdot \mu 0} + \frac{gap}{\mu 0}}$$

$$\frac{B(Iacmax)}{Bs} = 0.32 \qquad B(Iacmax) = 0.16$$

B.2 CALCULATION OF THE DIFFERENTIAL INDUCTANCE Lac

Analytical approximation to represent the dependence of the relative incremental permeability of the material on the magnetic field

The used approximation is in:
A. S. Kislovski, "Relative Incremental Permeability of Soft Ferrites as a Function of the Magnetic Field H: An Analytic Approximation" *Power Electronics Specialists Conference, PESC '96, 27th Annual IEEE*, pp 1469-1475, June 1996

permeability μ(H) core material 3C85 from Philips

$TOL := 1 \cdot 10^{-4}$

$\mu ini := 2000 \qquad \mu 0 := 4 \cdot \pi \cdot 10^{-7}$

$a1 := 76 \qquad a2 := 500 \qquad a3 := 200 \qquad ag := 0 \qquad \rho := 1.55 \qquad \sigma := 1$

$H := -2000 .. 2000$

$$\mu(H) := \mu ini \cdot \frac{\left[1 + \left(\frac{H - ag}{a3}\right)^2\right]^{\sigma}}{\left[\left[1 - \left(\frac{H - ag}{a2}\right)^2\right]^2 + \left(\frac{H - ag}{a1}\right)^2\right]^{\rho}}$$

relative incremental permeabilty

$$B(H) := \left(\int_0^H \mu(H)\, dH\right) \cdot 4\pi \cdot 10^{-7}$$

B(H) curve

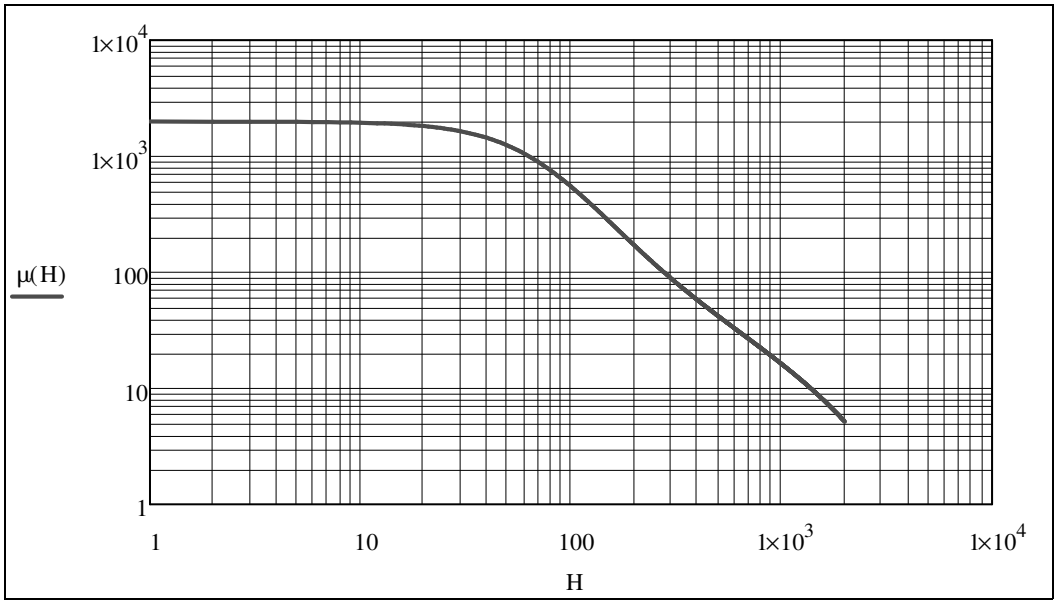

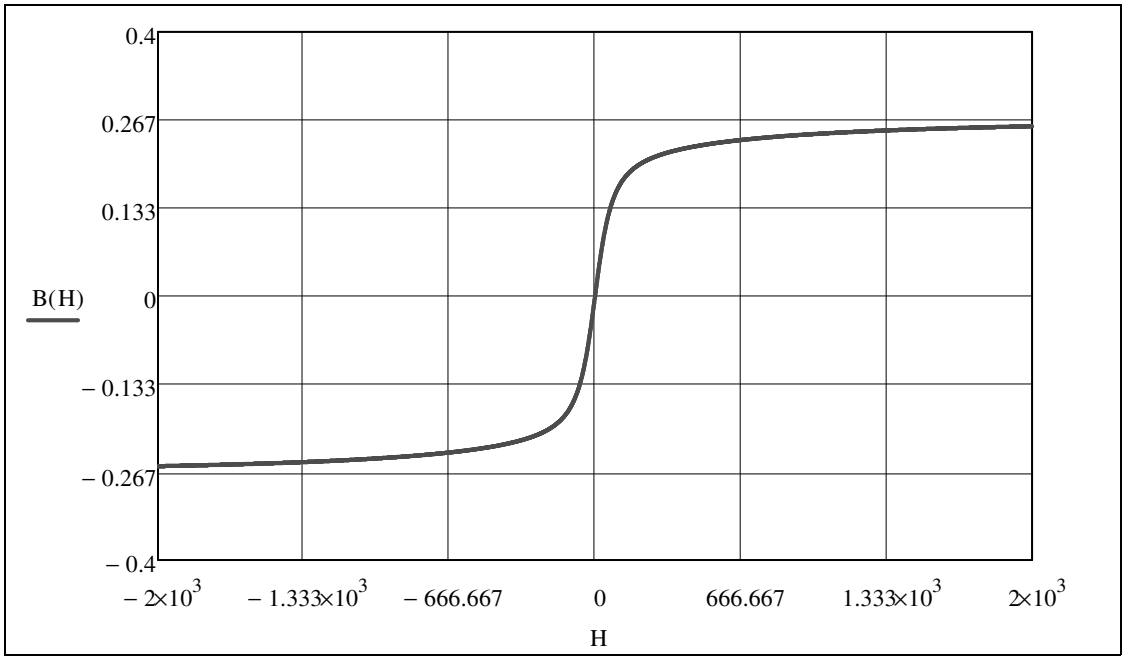

EF25 variable inductor (APEC 2008)

$lg := 0.3 \cdot 10^{-3}$ airgap length $lac := 2 \cdot 10.75 \cdot 10^{-3}$

$lg1 := 0\frac{lg}{15}$ $lg2 := 0\frac{lg}{5}$ lateral airgaps

$lgap := lg + \min(lg1, lg2) + \frac{|lg2 - lg1|}{2}$ gap is affected by the lateral gaps

$lgap = 3 \times 10^{-4}$

$ldc := 42.75 \cdot 10^{-3}$ magnetic path length of the left or right leg

$Aac := 7.5 \cdot 10^{-3} \cdot 7.5 \cdot 10^{-3}$ core parameters

$Ndc := 35$ number of turns of the control winding

$Nac := 68$ number of turns of the main winding

$k := 0 .. 30$ $j := 0 .. 27$

Objective: plot differentiall inductance vs resonant current

resonant current maximum values (operating points)

k =

0
1
2
3
4
5
6
7
8
9
10
11
12
13
14
...

$$Iac := \begin{pmatrix} -0.7 \\ -0.65 \\ -0.6 \\ -0.55 \\ -0.5 \\ -0.45 \\ -0.4 \\ -0.35 \\ -0.3 \\ -0.25 \\ -0.2 \\ -0.15 \\ -0.1 \\ -0.05 \\ -0.001 \\ 0 \\ 0.001 \\ 0.05 \\ 0.1 \\ 0.15 \\ 0.2 \\ 0.25 \\ 0.3 \\ 0.35 \\ 0.4 \\ 0.45 \\ 0.5 \\ 0.55 \\ 0.6 \\ 0.65 \\ 0.7 \end{pmatrix} \cdot \sqrt{2}$$

$Ibias := 0.7$ level of the dc control current

$\Delta iac := \frac{10}{100} \cdot Ibias$ small disturbance in the ac resonant current

$h1_k := \frac{Ndc}{ldc} \cdot Ibias$ $h2_k := h1_k$ $hac_k := 0$ initial conditions for the field H

$Iacsup_k := Iac_k + \Delta iac$

$Iacinf_k := Iac_k - \Delta iac$

maximum and minimum possible levels for the resonant current with disturbance

Given

$$B\left(h1_k\right) + 2 \cdot B\left(hac_k\right) = B\left(h2_k\right)$$

$$\left(h1_k + h2_k\right) \cdot ldc + \frac{B\left(h1_k\right)}{\mu 0} \cdot lg1 + \frac{B\left(h2_k\right)}{\mu 0} \cdot lg2 = 2 \cdot Ndc \cdot Ibias$$

$$\left(h1_k - h2_k\right)\cdot ldc - 2\cdot hac_k\cdot lac - 2\cdot\frac{B\left(hac_k\right)}{\mu 0}\cdot lgap + \frac{B\left(h1_k\right)}{\mu 0}\cdot lg1 - \frac{B\left(h2_k\right)}{\mu 0}\cdot lg2 = -2\cdot Nac\cdot Iacsup_k$$

$X(k) := Find(h1, h2, hac)$

$hacsup_k := \left(X(k)_2\right)_k$

$X(k) =$

	0
0	[3, 1]
1	[3, 1]
2	[3, 1]
3	[3, 1]
4	[3, 1]
5	[3, 1]
6	[3, 1]
7	[3, 1]
8	[3, 1]
9	[3, 1]
10	[3, 1]
11	[3, 1]
12	[3, 1]
13	[3, 1]

$X(k)_0 =$

	0
0	[14, 1]
1	[14, 1]
2	[14, 1]
3	[14, 1]
4	[14, 1]
5	[14, 1]
6	[14, 1]
7	[14, 1]
8	[14, 1]
9	[14, 1]
10	[14, 1]
11	[14, 1]
12	[14, 1]
13	[14, 1]

$$X(0) = \begin{pmatrix} \{14,1\} \\ \{14,1\} \\ \{14,1\} \end{pmatrix}$$

Interpretation of results:

- The Matrix X(k) has 14 matrices 3x1.
$X(k)_0 = h1(k)$ $X(k)_1 = h2(k)$ e $X(k)_2 = h3(k)$

For k=0, to simplify, we have a matrix 3x1, where each column is built with a vector 14x1.

TUsing only the first element, $X(0)_0$, we have a vector of 14 elements, with values

Given

$$B\left(h1_k\right) + 2\cdot B\left(hac_k\right) = B\left(h2_k\right)$$

$$\left(h1_k + h2_k\right)\cdot ldc + \frac{B\left(h1_k\right)}{\mu 0}\cdot lg1 + \frac{B\left(h2_k\right)}{\mu 0}\cdot lg2 = 2\cdot Ndc\cdot Ibias$$

$$\left(h1_k - h2_k\right)\cdot ldc - 2\cdot hac_k\cdot lac - 2\cdot\frac{B\left(hac_k\right)}{\mu 0}\cdot lgap + \frac{B\left(h1_k\right)}{\mu 0}\cdot lg1 - \frac{B\left(h2_k\right)}{\mu 0}\cdot lg2 = -2\cdot Nac\cdot Iacinf_k$$

$X(k) := Find(h1, h2, hac)$

$hacinf_k := \left(X(k)_2\right)_k$

$$Lacincr_k := \frac{\left(B\left(hacsup_k\right) - B\left(hacinf_k\right)\right)\cdot Aac\cdot Nac}{2\cdot \Delta iac}$$

differential inductance definition Lacincr

Ibias = 0.7

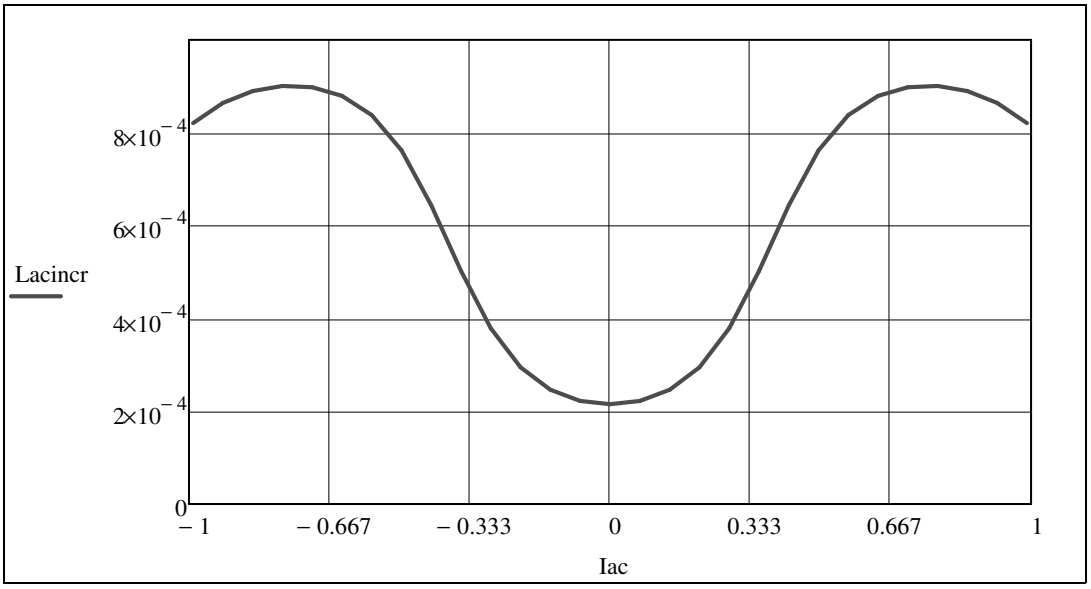

$Lacincr_k =$

$8.212 \cdot 10^{-4}$
$8.648 \cdot 10^{-4}$
$8.903 \cdot 10^{-4}$
$9.012 \cdot 10^{-4}$
$8.987 \cdot 10^{-4}$
$8.802 \cdot 10^{-4}$
$8.389 \cdot 10^{-4}$
$7.627 \cdot 10^{-4}$
$6.445 \cdot 10^{-4}$
$5.031 \cdot 10^{-4}$
$3.79 \cdot 10^{-4}$
$2.953 \cdot 10^{-4}$
$2.471 \cdot 10^{-4}$
$2.23 \cdot 10^{-4}$
$2.156 \cdot 10^{-4}$
$2.156 \cdot 10^{-4}$
$2.156 \cdot 10^{-4}$
$2.23 \cdot 10^{-4}$
$2.471 \cdot 10^{-4}$
$2.953 \cdot 10^{-4}$
$3.79 \cdot 10^{-4}$
$5.031 \cdot 10^{-4}$
$6.445 \cdot 10^{-4}$
$7.627 \cdot 10^{-4}$
$8.389 \cdot 10^{-4}$
$8.802 \cdot 10^{-4}$
$8.987 \cdot 10^{-4}$
$9.012 \cdot 10^{-4}$
$8.903 \cdot 10^{-4}$
$8.648 \cdot 10^{-4}$
$8.212 \cdot 10^{-4}$

Objective: plot incremental inductance vs dc control current (Ibias)

$j =$

0
1
2
3
4
5
6
7
8
9
10
11
12
13
14
...

dc control current operating points

Ibias goes from 0.001 to 1.35

$Ibias :=$

0.001
0.05
0.1
0.15
0.2
0.25
0.3
0.35
0.4
0.45
0.5
0.55
0.6
0.65
0.7
0.75
0.8
0.85
0.9
0.95
1
1.05
1.1
1.15
1.2
1.25
1.3
1.35

$Iac := 0.001 \cdot \sqrt{2}$ level of the ac resonant current

$\Delta iac := \frac{10}{100} Iac$ small disturbance in the ac resonant current

$h1_j := \frac{Ndc}{ldc} \cdot Ibias_j$ $h2_j := h1_j$ $hac_j := 0$ initial conditions for the field H

$Iacsup_j := Iac + \Delta iac$

$Iacinf_j := Iac - \Delta iac$

maximum and minimum possible levels
for the resonant current with disturbance

Given

$$B(h1_j) + 2 \cdot B(hac_j) = B(h2_j)$$

$$(h1_j + h2_j) \cdot ldc + \left(\frac{B(h1_j)}{\mu 0} \cdot lg1 + \frac{B(h2_j)}{\mu 0} \cdot lg2 \right) = 2 \cdot Ndc \cdot Ibias_j$$

$$(h1_j - h2_j) \cdot ldc - 2 \cdot hac_j \cdot lac - 2 \cdot \frac{B(hac_j)}{\mu 0} \cdot lgap + \left(\frac{B(h1_j)}{\mu 0} \cdot lg1 - \frac{B(h2_j)}{\mu 0} \cdot lg2 \right) = -2 \cdot Nac \cdot Iacsup_j$$

$X(j) := Find(h1, h2, hac)$

$hacsup_j := (X(j)_2)_j$

$X(k) =$

	0
0	[3, 1]
1	[3, 1]
2	[3, 1]
3	[3, 1]
4	[3, 1]
5	[3, 1]
6	[3, 1]
7	[3, 1]
8	[3, 1]
9	[3, 1]
10	[3, 1]
11	[3, 1]
12	[3, 1]
13	[3, 1]

$X(k)_0 =$

	0
0	[14, 1]
1	[14, 1]
2	[14, 1]
3	[14, 1]
4	[14, 1]
5	[14, 1]
6	[14, 1]
7	[14, 1]
8	[14, 1]
9	[14, 1]
10	[14, 1]
11	[14, 1]
12	[14, 1]
13	[14, 1]

$$X(0) = \begin{pmatrix} \{14,1\} \\ \{14,1\} \\ \{14,1\} \end{pmatrix}$$

Interpretation of results:

- The Matrix X(k) has 14 matrices 3x1.
$X(k)_0 = h1(k)$ $X(k)_1 = h2(k)$ e $X(k)_2 = h3(k)$

For k=0, to simplify, we have a matrix 3x1, where each column is built with a vector 14x1.

TUsing only the first element, $X(0)_0$, we have a vector of 14 elements, with values

Given

$$B(h1_j) + 2 \cdot B(hac_j) = B(h2_j)$$

$$(h1_j + h2_j) \cdot ldc + \left(\frac{B(h1_j)}{\mu 0} \cdot lg1 + \frac{B(h2_j)}{\mu 0} \cdot lg2 \right) = 2 \cdot Ndc \cdot Ibias_j$$

$$(h1_j - h2_j) \cdot ldc - 2 \cdot hac_j \cdot lac - 2 \cdot \frac{B(hac_j)}{\mu 0} \cdot lgap + \left(\frac{B(h1_j)}{\mu 0} \cdot lg1 - \frac{B(h2_j)}{\mu 0} \cdot lg2 \right) = -2 \cdot Nac \cdot Iacinf_j$$

$X(j) := Find(h1, h2, hac)$

$hacinf_j := (X(j)_2)_j$

$$Lacincr_j := \frac{(B(hacsup_j) - B(hacinf_j)) \cdot Aac \cdot Nac}{2 \cdot \Delta iac}$$

differential inductance definition Lacincr

$Lacincr_j =$

$9.841 \cdot 10^{-4}$

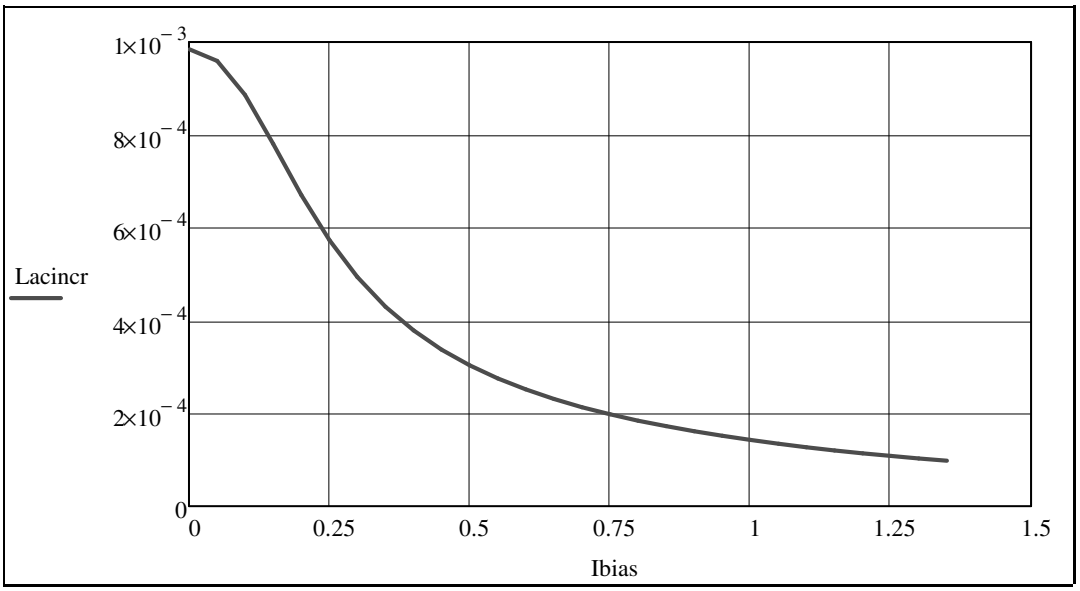

$9.593 \cdot 10^{-4}$
$8.86 \cdot 10^{-4}$
$7.807 \cdot 10^{-4}$
$6.706 \cdot 10^{-4}$
$5.733 \cdot 10^{-4}$
$4.936 \cdot 10^{-4}$
$4.298 \cdot 10^{-4}$
$3.787 \cdot 10^{-4}$
$3.374 \cdot 10^{-4}$
$3.035 \cdot 10^{-4}$
$2.753 \cdot 10^{-4}$
$2.514 \cdot 10^{-4}$
$2.31 \cdot 10^{-4}$
$2.134 \cdot 10^{-4}$
$1.979 \cdot 10^{-4}$
$1.843 \cdot 10^{-4}$
$1.722 \cdot 10^{-4}$
$1.613 \cdot 10^{-4}$
$1.515 \cdot 10^{-4}$
$1.426 \cdot 10^{-4}$
$1.345 \cdot 10^{-4}$
$1.271 \cdot 10^{-4}$
$1.203 \cdot 10^{-4}$
$1.14 \cdot 10^{-4}$
$1.082 \cdot 10^{-4}$
$1.028 \cdot 10^{-4}$
$9.779 \cdot 10^{-5}$

B.3 LCC RESONANT CIRCUIT ANALYSIS

$$pla := \begin{pmatrix} 1.2 \\ 1.8 \\ 3.40 \\ 4.95 \\ 8.0 \\ 10.9 \\ 14.3 \\ 16.5 \\ 19.2 \\ 21.5 \\ 23.4 \\ 26.8 \\ 31.1 \\ 32.7 \\ 34.1 \\ 35.3 \\ 36.2 \end{pmatrix} \qquad vla := \begin{pmatrix} 120.9 \\ 123.3 \\ 125.5 \\ 126.3 \\ 122.8 \\ 117.6 \\ 111.2 \\ 107.1 \\ 102.7 \\ 99.8 \\ 97.8 \\ 92.6 \\ 87.2 \\ 86.2 \\ 84.1 \\ 82.9 \\ 81.6 \end{pmatrix}$$

$k := 0 .. 16$

$p := 0.01, 0.1 .. 37$

$vinterp(p) := linterp(pla, vla, p)$

$ila_k := \frac{pla_k}{vla_k}$ $\qquad$ $rla_k := \frac{vla_k}{ila_k}$

$iinterp(p) := linterp(pla, ila, p)$

$rinterp(p) := linterp(pla, rla, p)$

$rla\_nom := rinterp(36)$ $\qquad$ $rinterp(36) = 186.327$

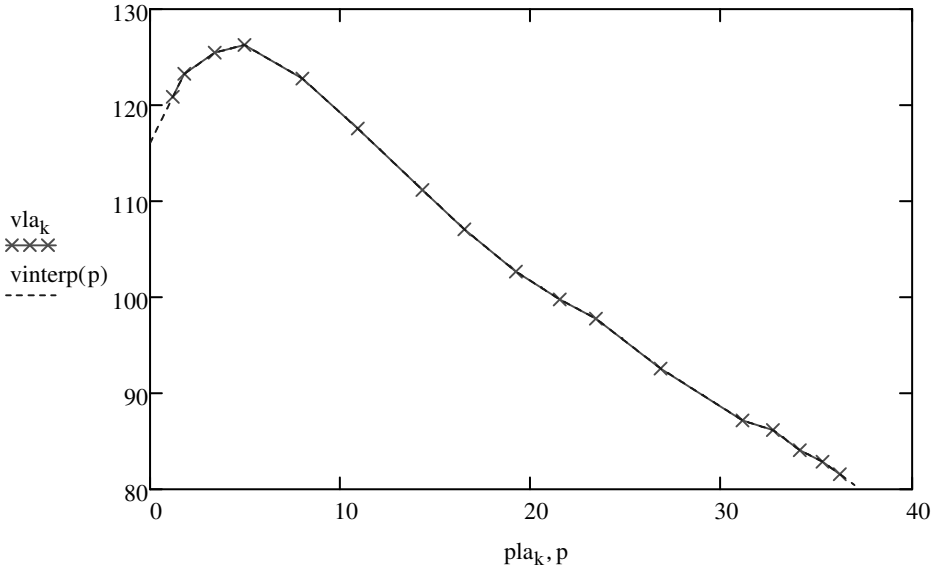

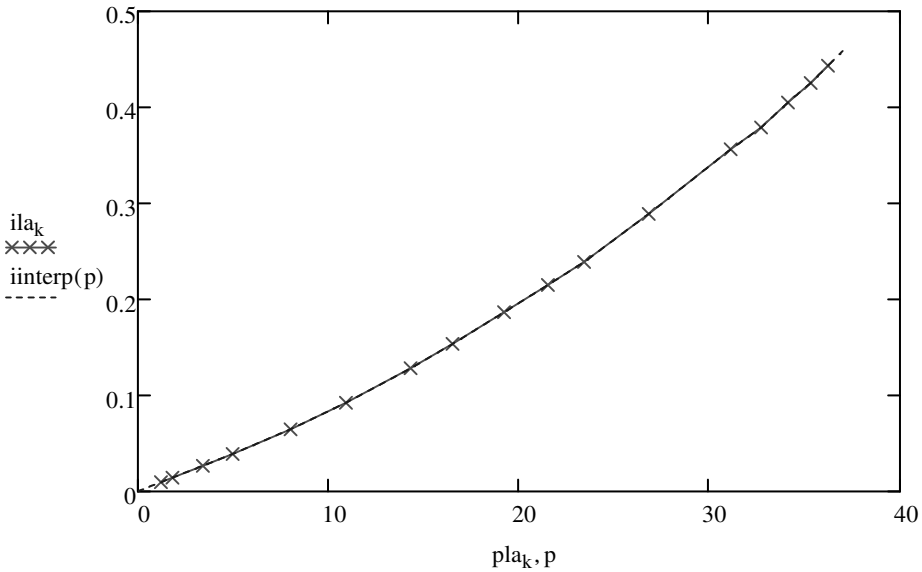

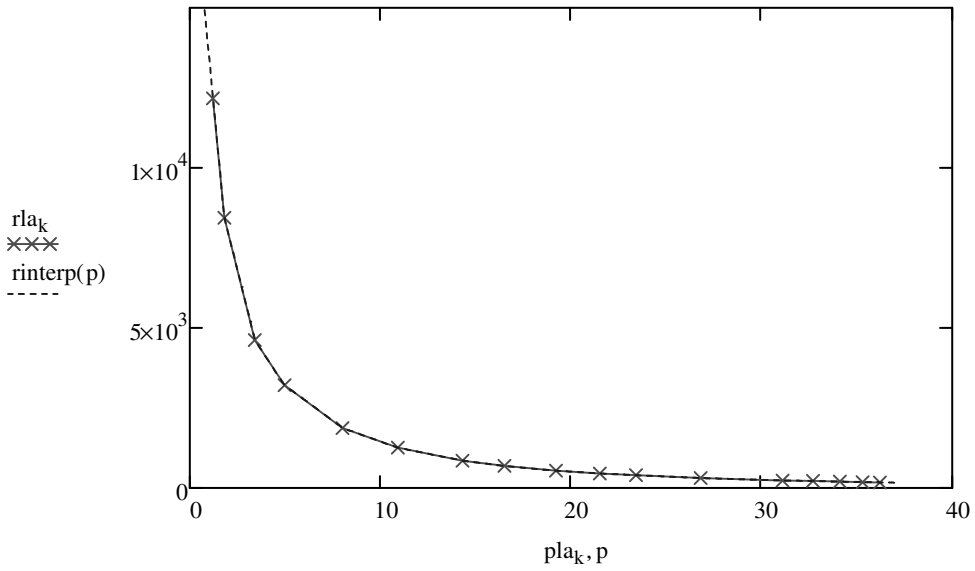

$Vdc := 150$ $f := 50 \cdot 10^3$

$$V1 := \frac{4 \cdot \left(\frac{Vdc}{2}\right)}{\pi \cdot \sqrt{2}} \quad V1 = 67.524$$

$\omega := 2 \cdot \pi \cdot f$ $\omega = 3.142 \times 10^5$

$j := 0 .. 12$

$i := 0, 0.1 .. 2.2$

$$imed := \begin{pmatrix} 0 \\ 0.2 \\ 0.4 \\ 0.5 \\ 0.7 \\ 0.9 \\ 1.0 \\ 1.2 \\ 1.4 \\ 1.6 \\ 1.8 \\ 2.0 \\ 2.2 \end{pmatrix} \quad Lmed := \begin{pmatrix} 1.130 \cdot 10^{-3} \\ 1.056 \cdot 10^{-3} \\ 0.916 \cdot 10^{-3} \\ 0.846 \cdot 10^{-3} \\ 0.744 \cdot 10^{-3} \\ 0.657 \cdot 10^{-3} \\ 0.611 \cdot 10^{-3} \\ 0.569 \cdot 10^{-3} \\ 0.511 \cdot 10^{-3} \\ 0.465 \cdot 10^{-3} \\ 0.449 \cdot 10^{-3} \\ 0.433 \cdot 10^{-3} \\ 0.412 \cdot 10^{-3} \end{pmatrix}$$

$Linterp(i) := linterp(imed, Lmed, i)$ $Linterp(0) = 1.13 \times 10^{-3}$

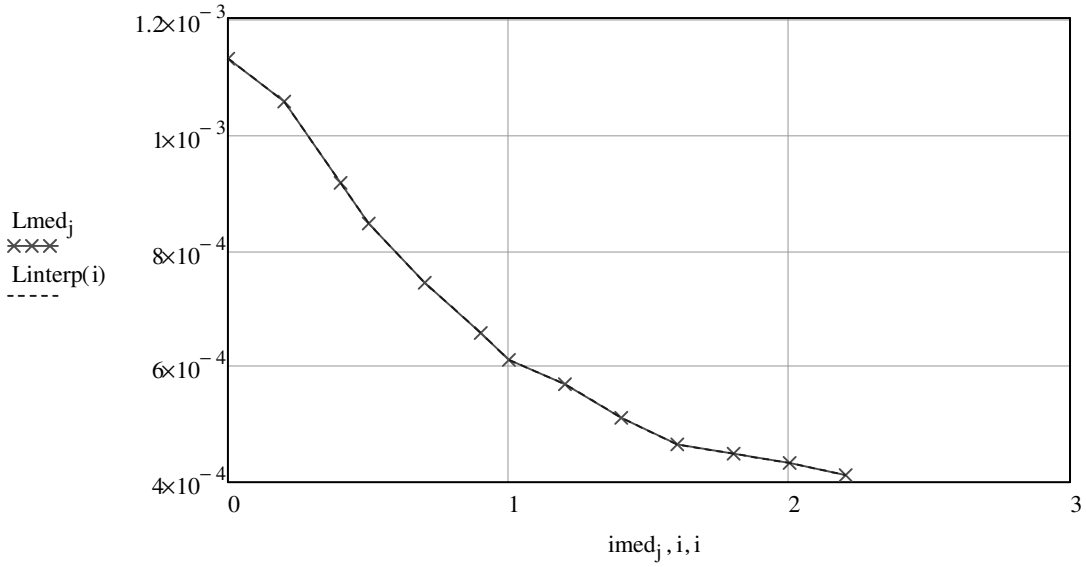

CIRCUIT PARAMETERS

$Vdc := 150$

$V1 := \dfrac{4\cdot\left(\dfrac{Vdc}{2}\right)}{\pi\cdot\sqrt{2}}$ $\quad V1 = 67.524$ $\quad Ila := 0.44$

$\alpha := 0.5$ $\quad A := \dfrac{1-\alpha}{\alpha}$ $\quad fd := 50000$

$Zd := \dfrac{V1}{\alpha\cdot Ila}$ $\quad Zd = 306.926$

$Ld := \dfrac{Zd}{2\cdot\pi\cdot fd}$ $\quad Ld = 9.77\times 10^{-4}$

$Ced := \dfrac{1}{2\cdot\pi\cdot fd\cdot Zd}$ $\quad Ced = 1.037\times 10^{-8}$

$Cpd := \dfrac{Ced}{\alpha}$ $\quad Cpd = 2.074\times 10^{-8}$

$A = 1$ $\quad Csd := \dfrac{Cpd}{A}$ $\quad Csd = 2.074\times 10^{-8}$

$\omega(f) := 2\cdot\pi(f)$

$$g(P) := P\cdot\left[\frac{\sqrt{\frac{Ld}{Ced}}}{rinterp(P)}\cdot\left(\omega(fd)\cdot\sqrt{Ld\cdot Ced}-\frac{1-\alpha}{\omega(fd)\cdot\sqrt{Ld\cdot Ced}}\right)^2+\frac{rinterp(P)}{\alpha^2\cdot\left(\sqrt{\frac{Ld}{Ced}}\right)}\cdot\left(\omega(fd)^2\cdot Ld\cdot Ced-1\right)^2\right]-\frac{V1^2}{\sqrt{\frac{Ld}{Ced}}}$$

$P := 36$ $\quad root(g(P), P) = 36.022$

$$x(P,L,C,f) := P\cdot\left[\frac{\sqrt{\frac{L}{Ced}}}{rinterp(P)}\cdot\left(\omega(fd)\cdot\sqrt{L\cdot Ced}-\frac{1-\alpha}{\omega(f)\cdot\sqrt{L\cdot Ced}}\right)^2+\frac{rinterp(P)}{\alpha^2\cdot\left(\sqrt{\frac{L}{Ced}}\right)}\cdot\left(\omega(fd)^2\cdot L\cdot Ced-1\right)^2\right]-\frac{V1^2}{\sqrt{\frac{L}{Ced}}}$$

$root(x(P,Ld,Ced,fd),P) = 36.022$

DIMMING CURVES WITH L

$L50min := 0.97\cdot10^{-3}$ $L50max := 1.242\cdot10^{-3}$ $Np := 20$

$k := 0..Np$ $L50_k := L50min + \frac{L50max - L50min}{Np}\cdot k$

$PregLCC50_k := root\left(x\left(P,L50_k,Ced,50\cdot10^3\right),P\right)$

$P50(l) := \begin{cases} 0 & \text{if } l < L50min \\ 0 & \text{if } l > L50max \\ linterp(L50,PregLCC50,l) & \text{otherwise} \end{cases}$ $rla50_k := rinterp\left(PregLCC50_k\right)$

$L45min := 0.97\cdot10^{-3}$ $L45max := 1.259\cdot10^{-3}$ $Np := 20$

$k := 0..Np$ $L45_k := L45min + \frac{L45max - L45min}{Np}\cdot k$

$PregLCC45_k := root\left(x\left(P,L45_k,Ced,45\cdot10^3\right),P\right)$

$P45(l) := \begin{cases} 0 & \text{if } l < L45min \\ 0 & \text{if } l > L45max \\ linterp(L45,PregLCC45,l) & \text{otherwise} \end{cases}$ $rla45_k := rinterp\left(PregLCC45_k\right)$

$L55min := 0.97\cdot10^{-3}$ $L55max := 1.245\cdot10^{-3}$ $Np := 20$

$k := 0..Np$ $L55_k := L55min + \frac{L55max - L55min}{Np}\cdot k$ $root\left(x\left(P,1.26\cdot10^{-3},Ced,55\cdot10^3\right),P\right) = 1.02$

$PregLCC55_k := root\left(x\left(P,L55_k,Ced,55\cdot10^3\right),P\right)$ $root\left(x\left(P,1.25\cdot10^{-3},Ced,55\cdot10^3\right),P\right) = 1.191$

$P55(l) := \begin{cases} 0 & \text{if } l < L55min \\ 0 & \text{if } l > L55max \\ linterp(L55,PregLCC55,l) & \text{otherwise} \end{cases}$ $rla55_k := rinterp\left(PregLCC55_k\right)$

$l := 0.8 \cdot 10^{-3}, 0.81 \cdot 10^{-3} .. 1.3 \cdot 10^{-3}$

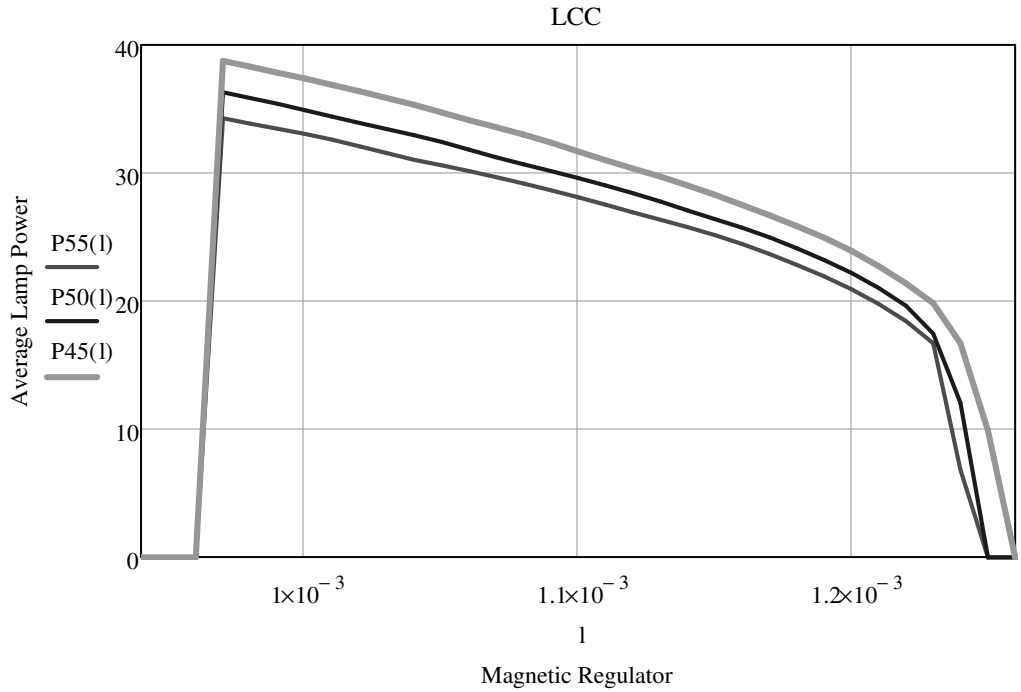

PHASE OF THE RESONANT CURRENT

$$j := \sqrt{-1}$$

$$Ze(L,C,R,f) := \frac{R \cdot \left[(1+A) \cdot \left(1 - \omega(f)^2 \cdot L \cdot C\right) + j \cdot \frac{\sqrt{\frac{L}{C}}}{R} \cdot \left(\omega(f) \cdot \sqrt{L \cdot C} - \frac{1}{\omega(f) \cdot \sqrt{L \cdot C}} \cdot \frac{A}{A+1} \right) \right] \cdot \left[1 - j \cdot \frac{R}{\sqrt{\frac{L}{C}}} \cdot \left(\omega(f) \cdot \sqrt{L \cdot C}\right) \cdot (1+A) \right]}{1 + \frac{C \cdot R^2}{L} \omega(f)^2 \cdot L \cdot C \cdot (1+A)^2}$$

$$\phi(L,C,R,f) := \arg\left(\frac{1}{Ze(L,C,R,f)} \right) \cdot \frac{180}{\pi}$$

$$\phi LCC50_k := \phi\left(L50_k, Ced, rla50_k, 50 \cdot 10^3 \right)$$

$$\phi 50(l) := \begin{cases} 0 & \text{if } l < L50min \\ 0 & \text{if } l > L50max \\ linterp(L50, \phi LCC50, l) & \text{otherwise} \end{cases}$$

$$\phi LCC45_k := \phi\left(L45_k, Ced, rla45_k, 45 \cdot 10^3 \right)$$

$$\phi 45(l) := \begin{cases} 0 & \text{if } l < L45min \\ 0 & \text{if } l > L45max \\ linterp(L45, \phi LCC45, l) & \text{otherwise} \end{cases}$$

$$\phi LCC55_k := \phi\left(L55_k, Ced, rla55_k, 55\cdot 10^3\right)$$

$$\phi 55(l) := \begin{cases} 0 & \text{if } l < L55min \\ 0 & \text{if } l > L55max \\ linterp(L55, \phi LCC55, l) & \text{otherwise} \end{cases}$$

$$Li := 0.8\cdot 10^{-3}, 0.81\cdot 10^{-3} .. 1.3\cdot 10^{-3}$$

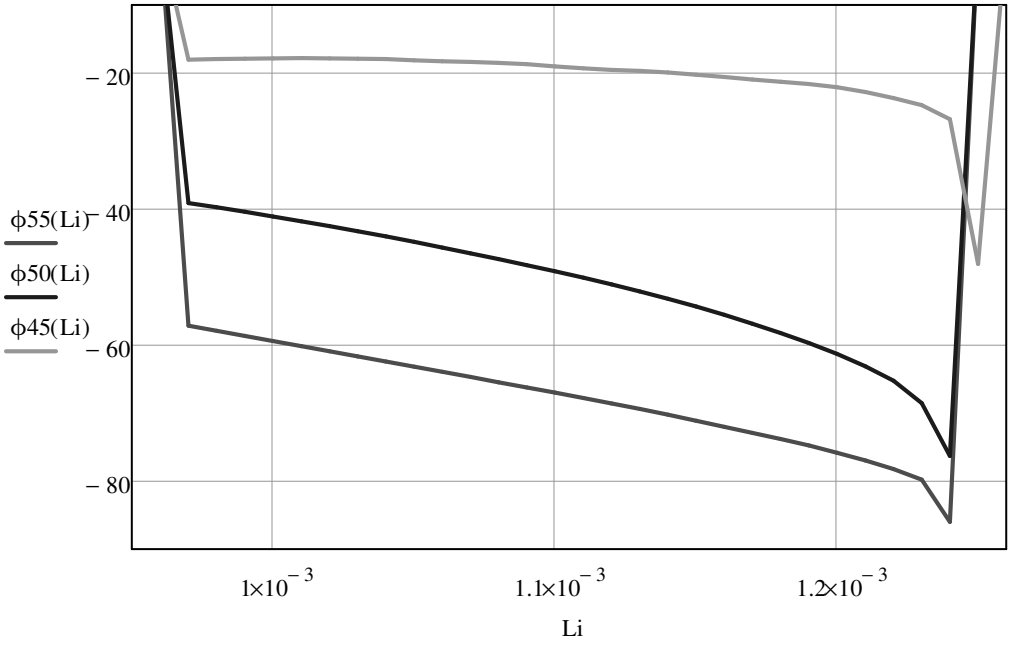

B.4 DESIGN METHODOLOGY FOR DETERMINING THE RESONANT TANK PARAMETERS FOR THE:

half-bridge inverter connected to a parallel-loaded resonant tank, using the fundamental approximation

Resonant tank	$V_{DC} = 310$ V	$V_{in} = \frac{4 \cdot \left(\frac{V_{DC}}{2}\right)}{\pi \cdot \sqrt{2}}$	$\phi = \arg\left(\frac{1}{Z_{in}}\right) \cdot \frac{180}{\pi}$	$Q = \frac{V_{lamp}}{V_{in}} = \frac{R_{lamp}}{Z_b}$
LC		$P_{LA} = \frac{V_{in}^2 \cdot R_{LA}(P_{LA})}{R_{LA}(P_{LA})^2 \cdot \left(1-\omega^2 LC\right)^2 + \omega^2 L^2}$; $Z_{in} = j\omega L + \frac{1}{j\omega C + \frac{1}{R_{LA}(P_{LA})}}$		$Z_b = \sqrt{\frac{L}{C}}$; $L = \frac{Z_b}{2\pi f_r}$, $C = \frac{1}{2\pi Z_b f_r}$

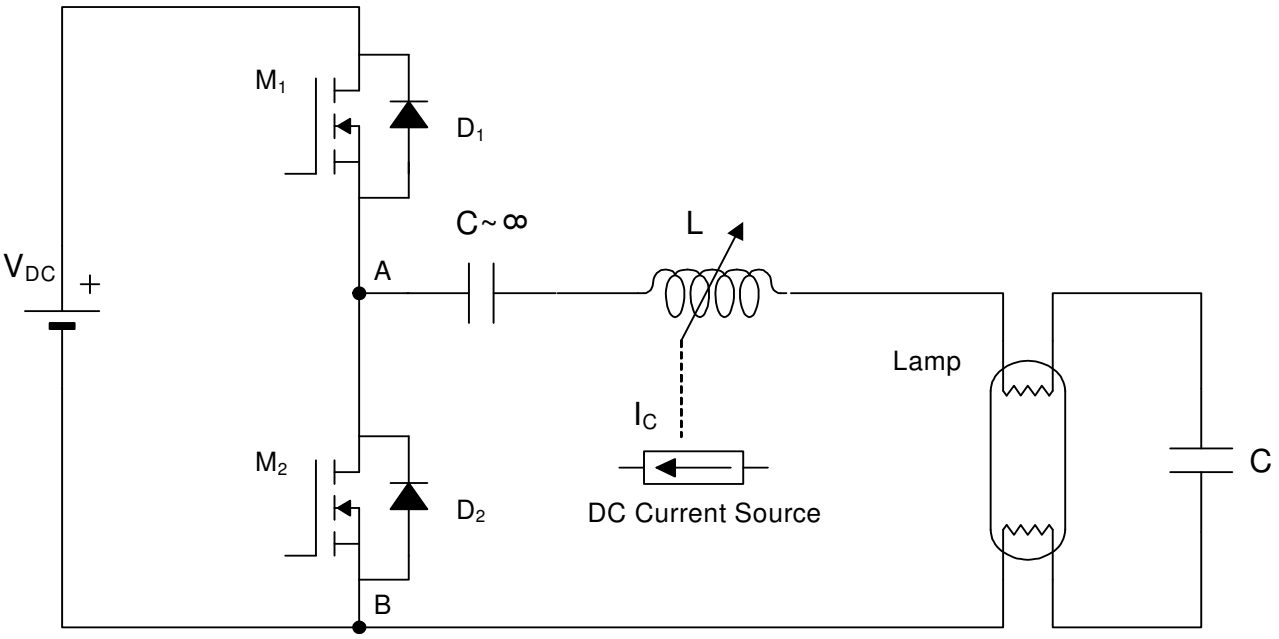

DC voltage

Vdc := 310

rms value of the fundamental component of the square wave inverter voltage

$V1 := \frac{4 \cdot 0.5 \cdot Vdc}{\pi \cdot \sqrt{2}}$ V1 = 139.549

Lamp characteristics at nominal power: (Vla, Ila, Rla):

Vla := 80 Ila := 0.48 $Rla := \frac{Vla}{Ila}$ Rla = 166.667 $Pla := \frac{Vla^2}{Rla}$ Pla = 38.4

Inverter switching frequency:

$fr := 50 \cdot 10^3$

For the half-bridge inverter witl LC resonant tank the maximum voltage gain can be approximated to the normalized load Q at the natural frequency

$Q := \frac{Vla}{V1}$ Q = 0.573 $Zb := \frac{Rla}{Q}$ Zb = 290.727

Resonant tank parameters:

If the value for C is not iniatially set

$$L := \frac{Zb}{2 \cdot \pi \cdot fr} \qquad L = 9.254 \times 10^{-4}$$

$$C := \frac{1}{2 \cdot \pi \cdot Zb \cdot fr} \qquad C = 1.095 \times 10^{-8}$$

If the value for C is iniatially set

$$C := 10 \times 10^{-9}$$

$$Zb := \frac{1}{2 \cdot \pi \cdot C \cdot fr} \qquad Zb = 318.31$$

$$L := \frac{Zb}{2 \cdot \pi \cdot fr} \qquad L = 1.013 \times 10^{-3}$$

If the value for L is iniatially set

$$L := 1 \times 10^{-3}$$

$$Zb := 2 \cdot \pi \cdot L \cdot fr \qquad Zb = 314.159$$

$$C := \frac{1}{2 \cdot \pi \cdot Zb \cdot fr} \qquad C = 1.013 \times 10^{-8}$$

B.5 CALCULATION OF THE THEORETICAL DIMMING CURVES FOR A T5 HE 21 W LAMP, PHASE OF THE INPUT RESONANT CURRENT AND COMPARISON WITH EXPERIMENTAL RESULTS

Master TL5 HE 21W from Philips
Experimental results obtained with PHILIPS HF-R 214-35 TL5 EII 220-240
Table I
MASTER TL5 HIGH EFFICIENCY

Lamp	VLA [V]	ILA [mA]	RLA [Ω]
TL5 HE 14W Philips	83	170	489
TL5 HE 21W Philips	125	170	735

Electrical specifications defined at an ambient temperature of 25 °C in free burning position on reference ballast
source: www.philips.com

TABLE II
TL5 HE 21W PHILIPS OPERATED WITH PHILIPS HF-R 214-35 TL5 EII 220-240

Measurements						Calculated values		
VDC [V]	Freq [kHz]	VLA [V]	ILA [mA]	IARC [mA]	PF	PLA [W]	PARC [W]	PElectr [W]
10	46,35	125,3	0,176	46,35	0,97	22,91	22,05	0,85
9	52,31	129,8	0,158	52,31	0,96	21,68	20,51	1,17
8	62,04	136,4	0,130	62,04	0,95	19,74	17,73	2,01
7	68,04	141,6	0,109	68,04	0,95	18,07	15,43	2,63
6	73,81	148,1	0,082	73,81	0,94	15,58	12,14	3,44
5	77,44	154,8	0,056	77,44	0,92	12,8	8,67	4,13
4	79,22	156,3	0,037	79,22	0,88	10,36	5,78	4,57
3	80,08	155,8	0,026	80,08	0,85	8,89	4,05	4,84
2	81,94	148,8	0,012	81,94	0,76	6,95	1,79	5,16
1	85,71	131,9	0,005	85,71	0,70	5,96	0,61	5,35

Half-bridge resonant inverter LC

$$pla := \begin{pmatrix} 0.61 \\ 1.79 \\ 4.05 \\ 5.78 \\ 8.67 \\ 12.14 \\ 15.43 \\ 17.73 \\ 20.51 \\ 22.05 \end{pmatrix} \qquad vla := \begin{pmatrix} 131.9 \\ 148.8 \\ 155.8 \\ 156.3 \\ 154.8 \\ 148.1 \\ 141.6 \\ 136.4 \\ 129.8 \\ 125.3 \end{pmatrix}$$

$k := 0..9$

$p := 0.01, 0.1..21$

$vinterp(p) := linterp(pla, vla, p)$

$ila_k := \frac{pla_k}{vla_k} \qquad rla_k := \frac{vla_k}{ila_k}$

$rinterp(p) := linterp(pla, rla, p)$

$iinterp(p) := linterp(pla, ila, p)$

$rla\_nom := rinterp(21)$

rinterp(21) = 786.635

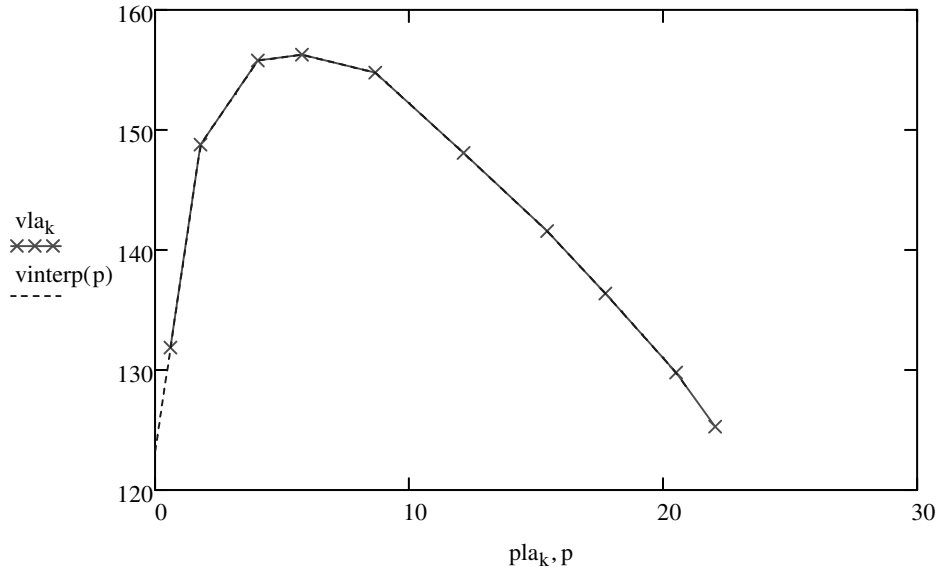

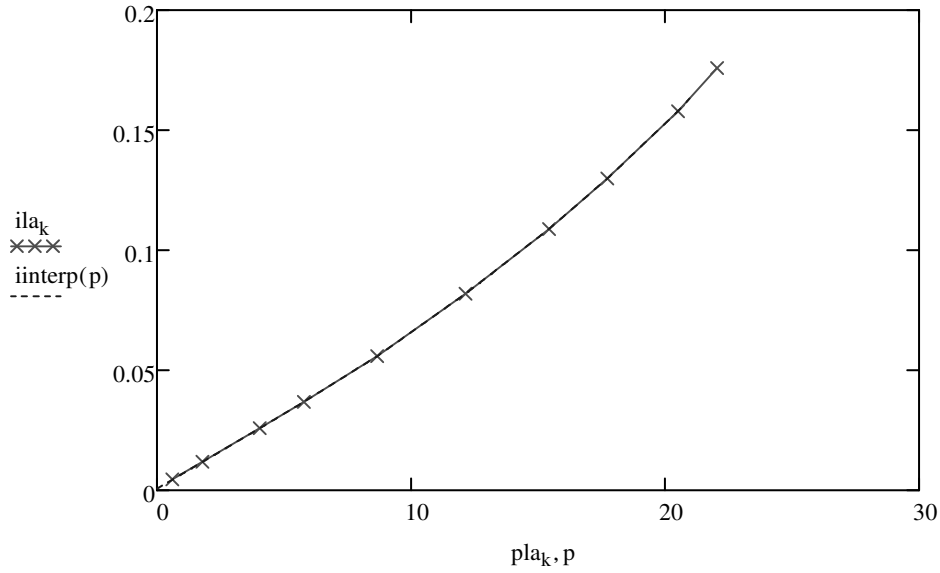

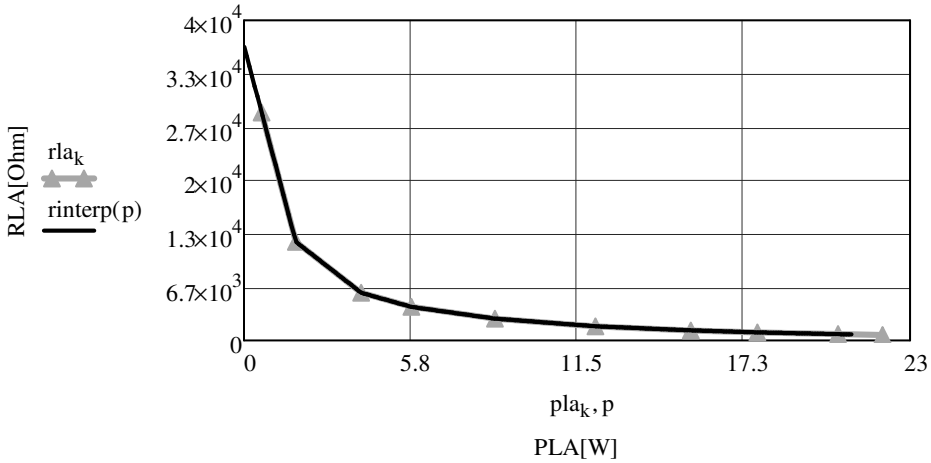

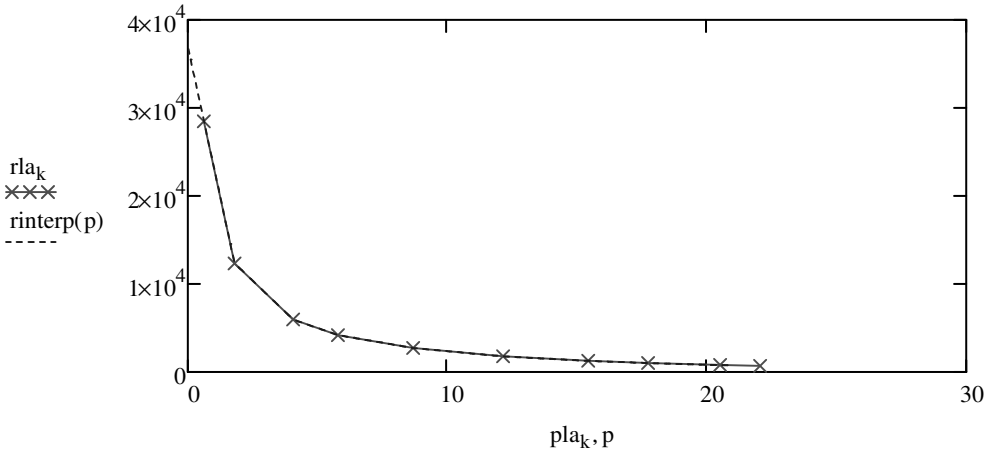

Circuit Parameters

Vdc := 310 inverter voltage

$$V1 := \frac{4\cdot\left(\frac{Vdc}{2}\right)}{\pi\cdot\sqrt{2}} \qquad V1 = 139.549$$

f := 80·10^3 operating frequency

ω := 2·π·f ω = 5.027 × 10^5

Ld := 1.9·10^−3 Cd := 2.2·10^−9 Ila := 0.170

fd := f Rd := rinterp(21)

ω(f) := 2·π·f

$$g(P) := P\cdot\left[rinterp(P)^2\cdot\left(1 - 4\cdot\pi^2\cdot fd^2\cdot Ld\cdot Cd\right)^2 + 4\cdot\pi^2\cdot fd^2\cdot Ld^2\right] - V1^2\cdot rinterp(P)$$

P := 21 root(g(P), P) = 19.409

$$x(P,L,C,f) := P\cdot\left[rinterp(P)^2\cdot\left(1 - 4\cdot\pi^2\cdot f^2\cdot L\cdot C\right)^2 + 4\cdot\pi^2\cdot f^2\cdot L^2\right] - V1^2\cdot rinterp(P)$$

root(x(P, Ld, Cd, fd), P) = 19.409

Dimming Curves with L as the control parameter

L85min := 2·10^−3 L85max := 3.07·10^−3 Np := 20

$$k := 0\,..\,Np \qquad L85_k := L85min + \frac{L85max - L85min}{Np}\cdot k$$

$$PregLC85_k := root\left(x\left(P, L85_k, Cd, 85\cdot10^3\right), P\right)$$

$$P85(l) := \begin{cases} 0 & \text{if } l < L85min \\ 0 & \text{if } l > L85max \\ linterp(L85, PregLC85, l) & \text{otherwise} \end{cases} \qquad rla85_k := rinterp\left(PregLC85_k\right)$$

$$root\left(x\left(P, 3.0\cdot10^{-3}, Cd, 85\cdot10^3\right), P\right) = 2.144$$

$$L80min := 2\cdot10^{-3} \qquad L80max := 3.4\cdot10^{-3} \qquad Np := 20$$

$$k := 0..Np \qquad L80_k := L80min + \frac{L80max - L80min}{Np}\cdot k$$

$$PregLC80_k := root\left(x\left(P, L80_k, Cd, 80\cdot10^3\right), P\right)$$

$$P80(l) := \begin{cases} 0 & \text{if } l < L80min \\ 0 & \text{if } l > L80max \\ linterp(L80, PregLC80, l) & \text{otherwise} \end{cases} \qquad rla80_k := rinterp\left(PregLC80_k\right)$$

$$l := 2\cdot10^{-3}, 2.05\cdot10^{-3}..3.079\cdot10^{-3}$$

$$i := 2\cdot10^{-3}, 2.05\cdot10^{-3}..3.4\cdot10^{-3}$$

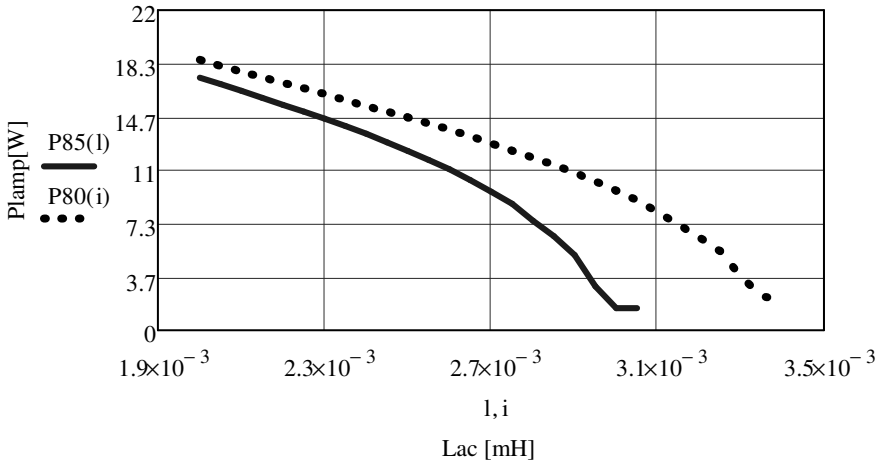

l =
$2\cdot10^{-3}$
$2.05\cdot10^{-3}$
$2.1\cdot10^{-3}$
$2.15\cdot10^{-3}$
$2.2\cdot10^{-3}$
$2.25\cdot10^{-3}$
$2.3\cdot10^{-3}$
$2.35\cdot10^{-3}$
$2.4\cdot10^{-3}$
$2.45\cdot10^{-3}$
$2.5\cdot10^{-3}$
$2.55\cdot10^{-3}$

experimental values

Power lamp [W]	Power Arc[W]	Power Elect[W]	Lac [H]	L [mH]
2.7	0.44	2.3	0.003067628	3,07
3.8	1.12	2.7	0.002930949	2,93
6.1	3.13	3.0	0.002833893	2,83
10.1	7.54	2.5	0.002777159	2,78
12.7	10.52	2.2	0.002700133	2,70
14.4	12.49	1.9	0.002650021	2,65
15.6	13.99	1.7	0.002524647	2,52
16.7	15.17	1.6	0.002462223	2,46
18.3	16.62	1.6	0.002294829	2,29
19.0	17.52	1.5	0.002218938	2,22
19.7	18.31	1.4	0.002137683	2,14
20.3	19.07	1.3	0.002078515	2,08
20.8	19.51	1.3	0.002010037	2,01

$2.6\cdot10^{-3}$
$2.65\cdot10^{-3}$
$2.7\cdot10^{-3}$
...

$$Pexp := \begin{pmatrix} 0.44 \\ 1.12 \\ 3.13 \\ 7.54 \\ 10.52 \\ 12.49 \\ 13.99 \\ 15.17 \\ 16.62 \\ 17.52 \\ 18.31 \\ 19.07 \\ 19.51 \end{pmatrix} \quad Lmed := \begin{pmatrix} 3.07\cdot10^{-3} \\ 2.93\cdot10^{-3} \\ 2.83\cdot10^{-3} \\ 2.78\cdot10^{-3} \\ 2.7\cdot10^{-3} \\ 2.65\cdot10^{-3} \\ 2.52\cdot10^{-3} \\ 2.46\cdot10^{-3} \\ 2.29\cdot10^{-3} \\ 2.22\cdot10^{-3} \\ 2.14\cdot10^{-3} \\ 2.08\cdot10^{-3} \\ 2.01\cdot10^{-3} \end{pmatrix}$$

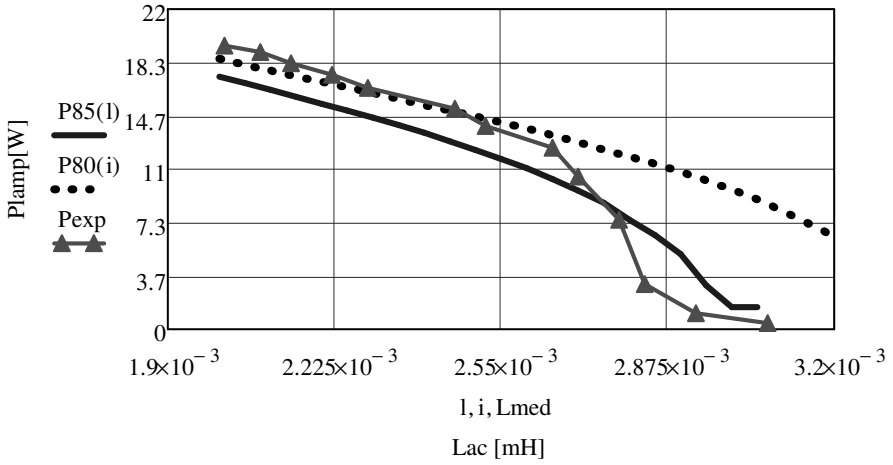

Estimation of the resonant current phase

$$j := \sqrt{-1}$$

$$Ze(L,C,R,f) := \frac{R\cdot\left(1 - L\cdot C\cdot\omega(f)^2 + j\cdot\frac{\sqrt{\frac{L}{C}}}{R}\cdot\omega(f)\cdot\sqrt{L\cdot C}\right)}{1 + j\cdot\frac{R}{\sqrt{\frac{L}{C}}}\cdot\left(\omega(f)\cdot\sqrt{L\cdot C}\right)}$$

$$\phi(L,C,R,f) := \arg\left(\frac{1}{Ze(L,C,R,f)}\right)\cdot\frac{180}{\pi}$$

$$\phi LC85_k := \phi\left(L85_k, Cd, rla85_k, 85\cdot10^3\right)$$

$$\phi 85(l) := \begin{cases} 0 & \text{if } l < L85min \\ 0 & \text{if } l > L85max \\ \text{linterp}(L85, \phi LC85, l) & \text{otherwise} \end{cases}$$

$$\phi LC80_k := \phi\left(L80_k, Cd, rla80_k, 80 \cdot 10^3\right)$$

$$Li := 2. \cdot 10^{-3}, 2.05 \cdot 10^{-3} .. 3.07 \cdot 10^{-3}$$

$$Lk := 2. \cdot 10^{-3}, 2.05 \cdot 10^{-3} .. 3.4 \cdot 10^{-3}$$

$$\phi 80(l) := \begin{cases} 0 & \text{if } l < L80min \\ 0 & \text{if } l > L80max \\ \text{linterp}(L80, \phi LC80, l) & \text{otherwise} \end{cases}$$